U.S. DEPARTMENT OF THE INTERIOR

U.S. GEOLOGICAL SURVEY

NATIONAL EARTHQUAKE HAZARDS REDUCTION PROGRAM ANNUAL PROJECT SUMMARIES: XXXVI

VOLUME II

Prepared by Participants in

NATIONAL EARTHQUAKE HAZARDS REDUCTION PROGRAM

Compiled by

Muriel L. Jacobson

The research results described in the following summaries were submitted by the investigators in September 1994 and cover the period from October 1993 through October 1, 1994. These reports include both work performed under contracts administered by the Geological Survey and work by members of the Geological Survey. The report summaries are grouped into the four major goals of the National Earthquake Hazards Reduction Program.

Open File Report No. 95-210

The data and interpretations in these progress reports may be reevaluated by the investigators upon completion of the research. Readers who wish to cite findings described herein should confirm their accuracy with the author.

EARTHQUAKE HAZARDS REDUCTION PROGRAM

CONTENTS - VOLUME II

Goal II - Evaluating the potential of future earthquakes

Where are future earthquakes likely? How large will they be? How often will they occur? When will they occur? Where are future earthquakes unlikely?

Goal III - Predicting the effects of earthquakes

During an earthquake of a certain magnitude, how severely and for how long will the ground shake? Where will hillsides slide, and flatlands fissure and crack? On what types of ground will earthquake damage be concentrated? Which faults will offset the Earth's surface? By how much? Which coastlines will be elevated or submerged? Where will destructive sea waves be generated? What losses to structures are expected?

Goal IV - Using research results

What new hazard reduction strategies become possible as under- standing of earthquake phenomena advances? What scientific information is needed and can be furnished to practitioners in the engineering, land-use planning and emergency managements communities? How can such information be most effectively communicated to these practitioners?

SEISMIC WAVE MONITORING AT PARKFIELD, CALIFORNIA

T.V. McEvilly, P. Johnson, M. Antolik, R. Clymer
Seismographic Station, University of California, Berkeley, CA 94720
and
E. Karageorgi, R. Nadeau, J. Peterson
Earth Science Division, Lawrence Berkeley Lab, Berkeley, CA 94720
Phone: 510-642-4494 (TVM), FAX: 510-486-5686, E-Mail: tom@seismo.berkeley.edu

Award 14-08-0001-G2160; Program Element: II.7

INTRODUCTION

Two programs of seismic wave analysis continue: Earthquake recording with the high-resolution seismic network (HRSN), begun in December, 1986, and controlled-source monitoring with HRSN begun in June, 1987.

The HRSN (Figure 1) consists of ten, 3-component, borehole seismometers surrounding the 1966 Parkfield epicenter. The data-acquisition system features digital telemetry with 125-Hz bandwidth and 16-bit resolution, and can operate in external-trigger (i.e., controlled-source) or event-trigger (earthquake) modes. Low-gain recorders with similar parameters, on loan from the IRIS PASSCAL instrument pool, are operating at five of the sites in parallel with the telemetry system. Network characteristics are summarized in Karageorgi *et al.*, 1992.

INVESTIGATIONS

1) Microearthquakes.

Local microearthquakes of magnitude about -0.5 to about +1.8 are routinely recorded on scale by the high-gain, telemetered system, extended to near M5 at the five low-gain sites. Studies are underway in source scaling, failure processes, fault zone structure, and material properties within the Parkfield nucleation zone.

Using advanced inversion techniques which make use of the high frequency content of the microearthquake data, we have developed 3-dimensional P- and S-wave velocity models for the area (Michelini and McEvilly, 1991). These models provide a map of fault zone structure at a scale of about 1 km, and have resulted in a substantial improvement in hypocenter location precision. Relocation of all events using the 3-D velocity model has revealed the highly clustered nature of Parkfield earthquakes (Nadeau *et al.*, 1994a,b). The cluster locations expose the fine structure of the fault-zone failure process (Figure 2). The individual cluster events, coherent to 50 Hz and beyond, also provide sequences of repeated near-identical sources throughout time with which to observe changes in wave propagation properties in the fault zone.

2) Controlled-source monitoring with HRSN.

From June, 1987 through December, 1994, the HRSN has been illuminated 50 times with S-waves of three polarizations at seven source positions throughout the study zone, using a shear-wave Vibroseis source, in an on-going, long-term monitoring program (Figure 1). This includes special recordings during and after the $M4^{+}$ earthquake sequences and associated alerts of 1992 and 1993. Analysis techniques to view changes in travel time, attenuation, S-wave polarization and frequency content in large amounts of data have been developed and are applied to the entire data set. We have discovered and continue to monitor significant anomalies in travel time and frequency content occurring in a zone south of Middle Mountain.

This work was reviewed by Karageorgi, *et al.*, 1992. Data reduction is accomplished at the Center for Computational Seismology (CCS) in the Earth Sciences Division of the Lawrence Berkeley Laboratory (LBL).

DATA COLLECTED

We have nearly completed the considerable task of putting the 1987-1994 microearthquake data base into a consistent and correct format (R.N., J.P., T.V.M.). Problems with pick consistency, channel assignments, amplitudes, time code interpretation, data gaps, and format have been dealt with. The data set at L.B.L. is archived in SEGY format. The final results are to be placed on the Berkeley regional mass-store in the first half of 1995. A total of approximately 4500 events are presently in the archive.

Three vibrator data sets have been collected and the data reduced in this project year. Data after routine processing (edit, stack, correlation, gather by source site) are archived in SEGY format on magnetic tape.

RESULTS

Earthquake Studies:

Event analysis: Local Parkfield events are now picked and located with the 3-D model within a month of occurrence. This effort is presently current through November, 1994.

Characterization and Analysis of Microearthquake Clustering (R.N): Using a modification of the similar event characterization method of Aster and Scott, 1993, we have characterized event similarity for the 1987-92 Parkfield HRSN data set, and established our definition of similar event clusters at Parkfield. Results (Figure 2) show that 63% of the earthquakes occur in a relatively sparse distribution of small clusters estimated to be less than 20 meters in radius. Within these clusters, virtually identical small earthquakes occurred with a regularity that can be described by the statistical model used previously in forecasting large characteristic earthquakes. Sympathetic occurrence of microearthquakes in nearby clusters was observed within a range of about 200m at communication speeds of 10 to 100 cm/s. The rate of earthquake occurrence increased significantly during the study period, as did the ratio of deep to shallow events, but the fraction of clustered events decreased (Figure 3). This work is reported in a paper recently accepted for publication by Science Magazine(Nadeau *et al.,* 1994b).

Coda Q Study: A detailed study of temporal variation of coda Q in the Parkfield region using clustered events, cooperative with R. Aster of the New Mexico Institute of Technology, has been completed and submitted to BSSA (Antolik, *et. al,* 1994). The method of Aki and Chouet (1975) was applied to 21 of the event clusters spanning a seven year period. The high degree of similarity between clustered earthquakes at Parkfield permit extremely stable estimates of the spectral ratio, and thus it is possible to tightly constrain the variations of coda Q. Results preclude any variation in Q^{-1} outside of 5 parts in 10^4 at the 95% confidence level.

Temporal Variations in Fault-Zone Properties: We are presently searching for clusters with the greatest similarity of waveforms. We will then continue to search for temporal variations in travel time, polarization, and attenuation (Nadeau *et al.*, 1994c).

Seismicity Studies: A study of the role of fault-zone fluids in microearthquake clustering at Parkfield has been submitted to JGR (Johnson and McEvilly, 1994). The data are consistent with a model in which microearthquake clusters and confined sequences occur in localized cells of fluctuating elevated pore-fluid pressure that occupy only 1-2% of the fault surface but account for most of the microseismicity. These cells may be imbedded in a fault zone that is stronger in the less active intercellular regions.

Controlled-Source Studies (EK):

The final working data sets for analysis are "time gathers": one source into one receiver gathered across calendar time, producing 720 files, each containing, at present, 50 similar traces on most paths. The time gathers are then examined for variations in waveform parameters.

Most displays show only seasonal variations in various properties (travel time, amplitude, spectral properties), due to very near-surface moisture changes under the vibrator (Clymer and McEvilly, 1981).

However, paths in the vicinity of source site 2, south-west of the 1966 epicenter, show a prominent travel-time anomaly that began in mid 1988, and continues through late 1994 (Figure 4). There was a prominent change of character in 1993, but previously anomalous paths remain anomalous, and stable paths remain stable. Temporal variations in travel time appear to correlate with significant seismicity features, such as the larger events in 1992 and 1993. Variations in frequency spectra and polarization angle also correspond to the significant seismicity features.

Analysis of the data from a two-dimensional source array at source site 2 provides estimates of the horizontal slowness and azimuth of the anomalous phases, defining the mode of propagation. Regardless of the path orientation, P and S phases appear to be redirected, leaving the source preferentially toward the north-west. However, later phases tend to leave the source in a south-south-east direction. Anomalous arrivals fall in both categories. The apparent velocities of the later phases are relatively high, implying steep incidence ant deep propagation for the anomalous waves.

References

Antolik, M.., R. M. Nadeau, R. C. Aster and T. V. McEvilly, 1994. Differential analysis of coda *Q* using similar microearthquakes in seismic gaps, Part 2: Application to seismograms recorded by the Parkfield High Resolution Seismic Network, Bull. Seism. Soc. Am., (submitted).

Aster, Richard C. and Jennifer Scott, 1993. Comprehensive characterization of waveform similarity in microearthquake data sets, *Bull. Seis. Soc Am.*, **83,** 1307.

Clymer, R.W., and T.V. McEvilly, 1981. Travel time monitoring with VIBROSEIS, *Bull. Seism. Soc. Amer*, **71**, 1902-1927.

Johnson, P.A. and T. V. McEvilly, 1994. Seismicity at Parkfield and the possible involvement of fault-zone fluids, J. Geophys. Res. (submitted).

Karageorgi, E., R. Clymer and T.V. McEvilly, 1992. Seismological studies at Parkfield. II. Search for temporal variations in wave propagation using Vibroseis, *Bull. Seism. Soc. Am.*, **82,** 1388-1415.

Michelini, A., and T.V. McEvilly, 1991, Seismological studies at Parkfield: I. Simultaneous inversions for velocity structure and hypocenters using cubic B-splines parameterization, *Bull. Seismol. Soc. Am.*, 81, 524-552.

Nadeau, R., M. Antolik, P. Johnson, W. Foxall and T.V. McEvilly, 1994a. Seismological studies at Parkfield: III. Microearthquake clusters in the study of fault-zone dynamics, *Bull. Seis. Soc. Am,* **84**, 247-263.

Nadeau, R., W. Foxall and T. V. McEvilly, 1994b. Periodic recurrence and spatial clustering in characteristic microearthquakes on the San Andreas fault, Science (accepted for publication).

Nadeau, R., E.D. Karageorgi, and T.V. McEvilly, 1994c. Fault-zone monitoring with repeating similar microearthquakes: A search for the Vibroseis anomaly at Parkfield, Seismological Research Letters, **65**, 69. (abs.)

Publications:

Antolik, M.., R. M. Nadeau, R. C. Aster and T. V. McEvilly, 1994. Differential analysis of coda Q using similar microearthquakes in seismic gaps, Part 2: Application to seismograms recorded by the Parkfield High Resolution Seismic Network, Bull. Seism. Soc. Am., (submitted).

Daley, T.M. and T.V. McEvilly, 1990. Shear wave anisotropy in the Parkfield Varian Well VSP, *Bull. Seism. Soc. Am.*, **80**, 857-869.

Foxall, W., A. Michelini, and T.V. McEvilly, 1993, Earthquake travel time tomography of the Southern Santa Cruz Mountains: Control of fault rupture by lithological heterogeneity of the San Andreas fault zone, *J. Geophys. Res.*, 98, 17691-17710.

Johnson, P.A. and T. V. McEvilly, 1994. Seismicity at Parkfield and the possible involvement of fault-zone fluids, J. Geophys. Res. (submitted).

Johnson, P.A. and T.V. McEvilly, 1994. Fluids and faulting: Suggestive evidence and crucial tests at Parkfield, in *Proceedings of Workshop LXIII: The Mechanical Involvement of Fluids in Faulting,* U. S. G. S. Open-File Report **94-228**, 39-71.

Karageorgi, E., R. Clymer and T.V. McEvilly, 1992. Seismological studies at Parkfield. II. Search for temporal variations in wave propagation using Vibroseis, *Bull. Seism. Soc. Am.*, **82,** 1388-1415.

Michelini, A. and T.V. McEvilly, 1991. Seismological studies at Parkfield: I. Simultaneous inversion for velocity structure and hypocenters using B-splines parameterization, *Bull. Seism. Soc. Am.*, **81**, 524-552.

Nadeau, R., M. Antolik, P. Johnson, W. Foxall and T.V. McEvilly, 1994.a Seismological studies at Parkfield: III. Microearthquake clusters in the study of fault-zone dynamics, *Bull. Seis. Soc. Am,* **84**, 247-263.

Nadeau, R., W. Foxall and T. V. McEvilly, 1994b. Periodic recurrence and spatial clustering in characteristic microearthquakes on the San Andreas fault, Science (accepted for publication).

Ph. D. Theses:

Michelini, A., Fault Zone Structure Determined Through the Analysis of Earthquake Arrival Times, 1991.

Foxall, W., Fault-Zone Heterogeneity as a Controlling Factor in the Dynamic Behavior of the San Andreas Fault in Central California, Ph.D. Thesis, Univ. Calif., Berkeley, 1992

Papers Presented on Parkfield Research in 1994

1994 SSA Meeting, Pasadena:

Aster, R.C., G. Slad, R. Nadeau, and T.V. McEvilly. Quantitative estimation of coda stability in the Anza and Parkfield Seismic gaps, Seismological Research Letters, **65**, 35. (abs.)

Karageorgi, E.D., T.V. McEvilly, and R. Clymer. Update on fault-zone monitoring with vibroseis at the Parkfield, California prediction experiment, Seismological Research Letters, **65**, 70 (abs.)

Nadeau, R., E.D. Karageorgi, and T.V. McEvilly. Fault-zone monitoring with repeating similar microearthquakes: A search for the Vibroseis anomaly at Parkfield, Seismological Research Letters, **65**, 69. (abs.)

1994 European Seismological Commission General Assembly, Athens:

Karageorgi, E.D., and T.V. McEvilly, Parkfield prediction experiment: Monitoring with repeated Vibroseis sources, Proceedings of the 24th General Assembly of the European Seismological Commission, 1995.

McEvilly, T.V., Parkfield prediction experiment: Monitoring methods using microearthquakes, Proceedings of the 24th General Assembly of the European Seismological Commission, 1995.

1994 Fall AGU Meeting, San Francisco:

Aster, R., M. Antolik, R. Nadeau, T. McEvilly, 1994. Differential analysis of coda Q using similar microearthquakes in seismic gaps., EOS, **75** (supplement), 454.

Karageorgi, E.D., T.V. McEvilly, and R. Clymer, 1994. Parkfield prediction experiment: Update on monitoring with repeated vibroseis sources, EOS, **75** (supplement), 471.

Nadeau, R., W. Foxall, and T.V. McEvilly, 1994. Periodic occurrence and spacial clustering in characteristic microarthquakes on the San Andreas fault, EOS, **75** (supplement), 469.

Johnson, P.A., L.R. Johnson, J. Peterson, and T.V. McEvilly, 1994, Body wave moment tensor inversion of Parkfield borehole data, EOS, **75** (supplement), 435.

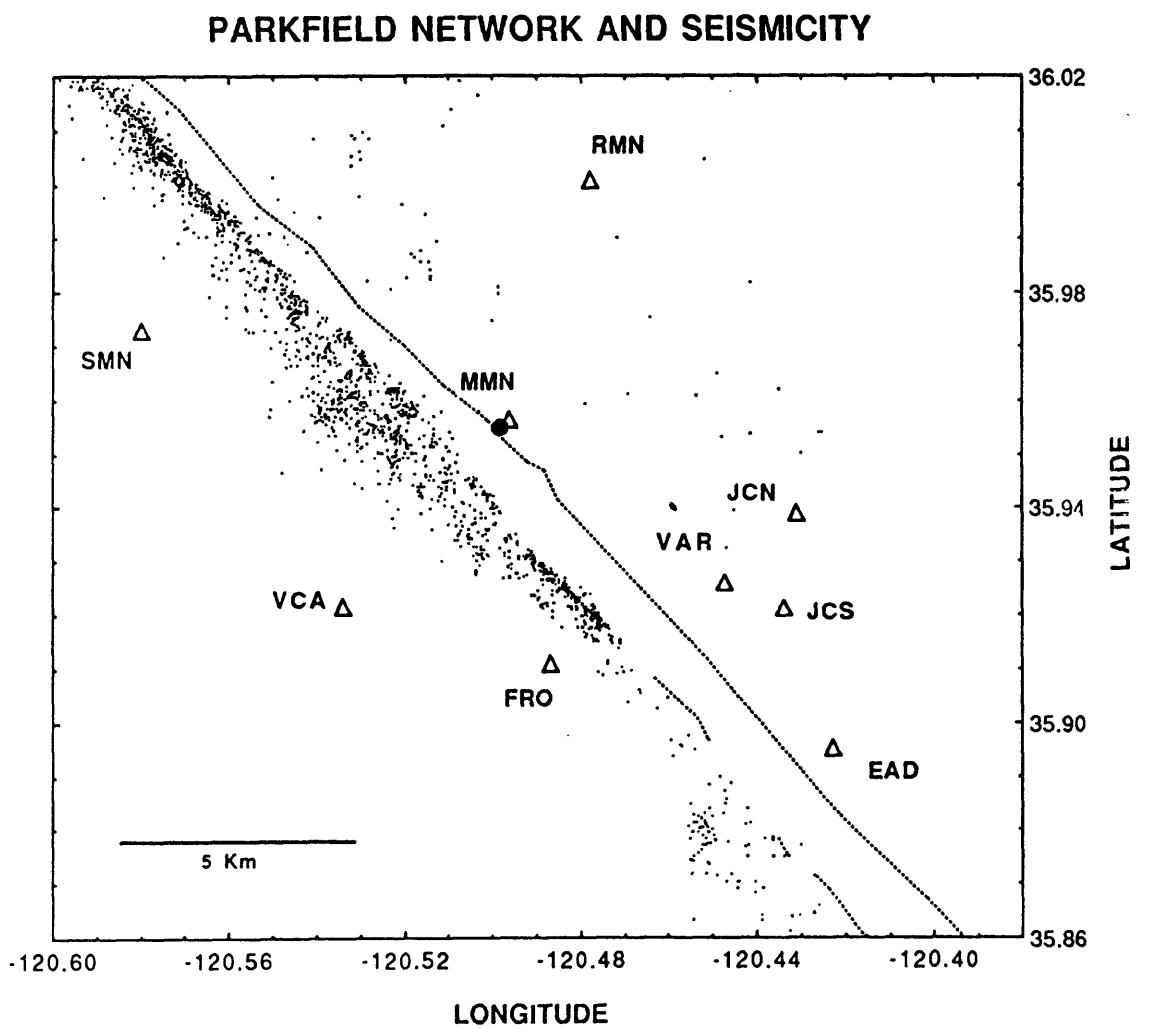

Figure 1. Location map showing the Parkfield borehole seismometer network (open triangles) and microearthquake seismicity (dots) for 1987 to mid-1994. The closed circle near site MMN marks the epicenter of the 1966 Parkfield earthquake. The dotted line is the San Andreas fault trace.

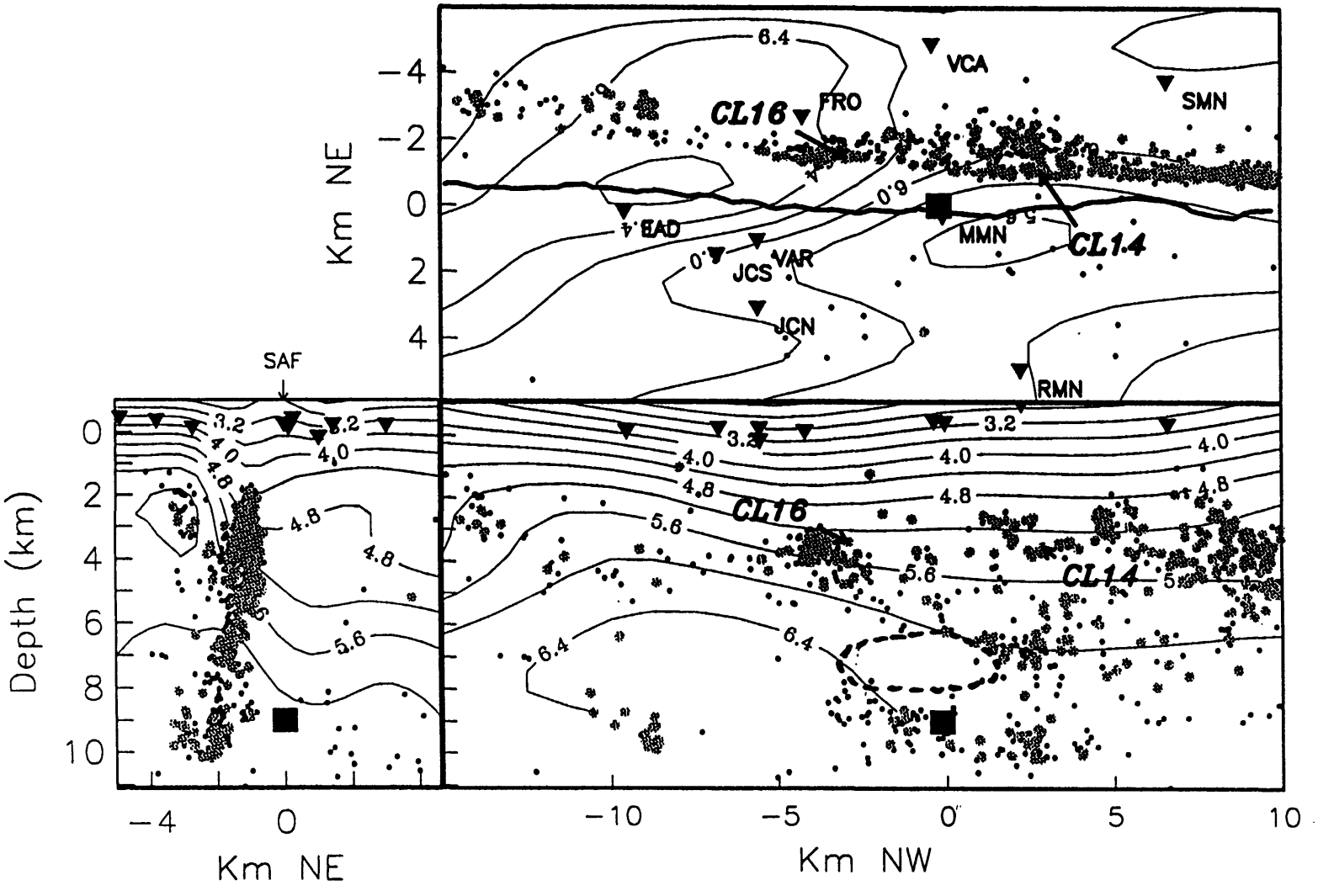

Figure 2. Sections through the 3-D velocity model for Parkfield showing the 294 cluster locations (large dots), background seismicity (small dots), 1966 main shock (large square) and recording stations (small triangles) projected on to the fault plane. The upper rectangle is in plan view, the rectangle directly below is a cross section along the San Andreas fault, and the smaller rectangle to the left is a cross section perpendicular to the fault. Vp contours and Vp/Vs anomaly location (dashed contour) are shown.

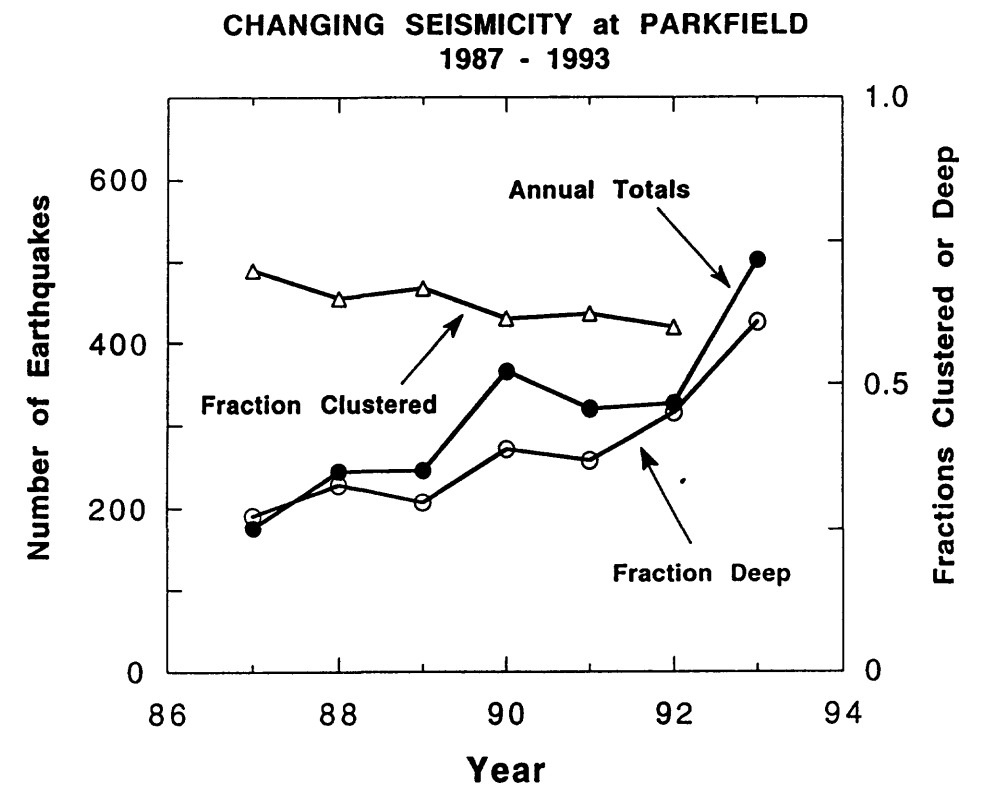

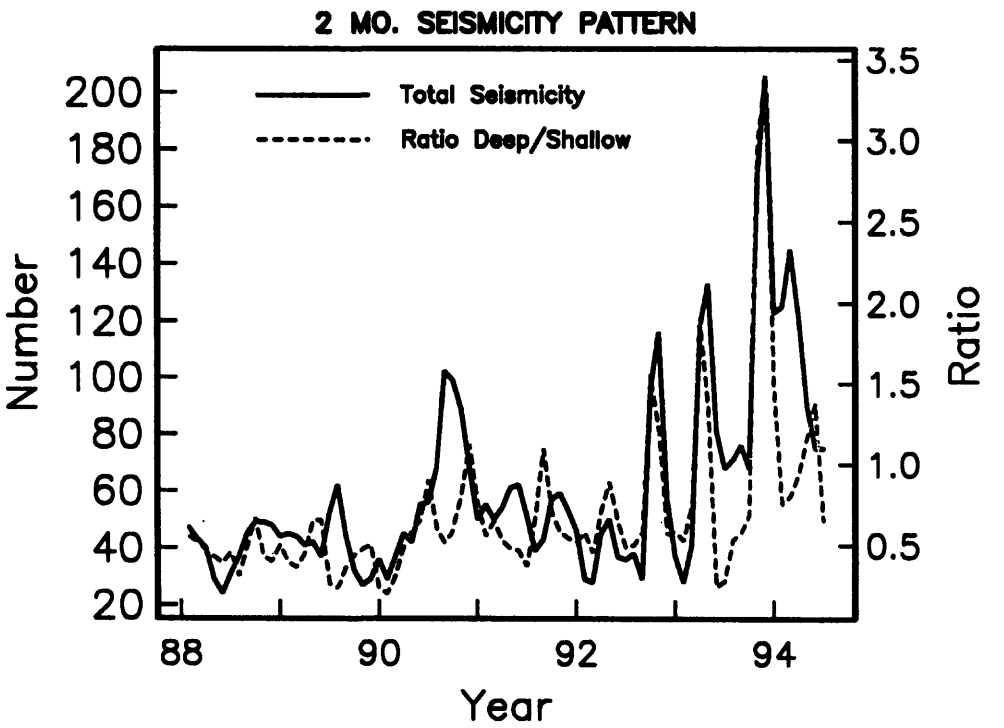

Figure 3. -Upper) Changes in seismicity by year. The annual earthquake count increased substantially over the 1987-1992 period, while the fraction of the total that are clustered events decreased through the analysis period. The fraction of the total activity deeper than 5 km increased significantly. The mode of slip in the fault zone is changing, involving more earthquakes in the deep nucleation zone. -Lower) Two-month seismicity (two-month moving window, moved in one-month increments).

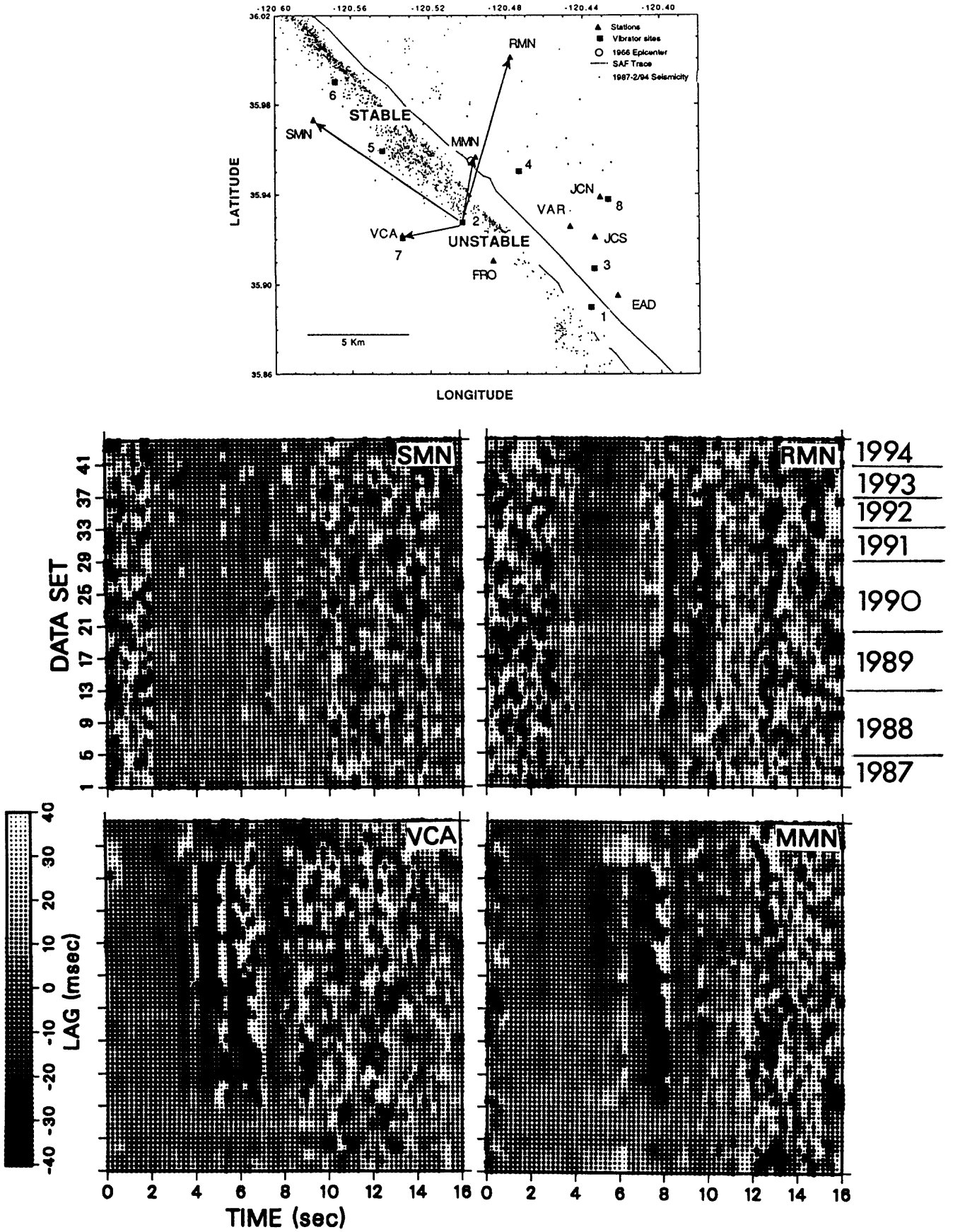

Figure 4. Travel-time variations relative to a reference trace (arbitrarily chosen, here in mid-1988) measured across the repeated 16-sec seismograms in a moving window for several paths from vibrator site two.

BAY AREA DIGITAL SEISMIC NETWORK

T.V. McEvilly, R.A. Uhrhammer, P. Johnson, R. Clymer,
Seismographic Station, Dept. of Geology & Geophysics and
Earth Sciences Division, Lawrence Berkeley Laboratory
University of California, Berkeley, CA 94720
510-642-4494 (TVM); 510-486-5686 (FAX), tom@perry.berkeley.edu

Award 14-08-0001-G2122; Element II.7

Goals

The purpose of the Hayward Fault Network (HFN) in the San Francisco East Bay is to provide high resolution, high frequency (1000 samples per second), wide dynamic range (24-bit digitization), 3-component, on-scale seismic data for earthquakes of magnitude $0 < M < 7.0$ for detailed studies of the Hayward fault. From our experience managing the Parkfield High-Resolution Network, with similar dimensions to the HFN, we believe we can accomplish this goal even in a noisy urban environment, given carefully designed sensors and deep borehole emplacement.

The HFN is a joint effort with the USGS. The network as envisioned will consist ultimately of 24-30 stations, 12-15 each north and south of the San Leandro seismic gap, managed respectively by UCB and USGS. Other sites are being drilled by the State of California Transportation Department (CALTRANS) and instrumented by the Lawrence Livermore National Laboratory (LLNL) at the major Bay Area bridges. Sensors designed and constructed at UCB/LBL are being installed in the entire network. Recording and telemetry equipment will differ between north and south, but the resulting data will be shared in near real time and archived with CALNET data in common format at the Northern California Earthquake Data Center at Berkeley, also operated jointly by UCB and the USGS, and will thus be made promptly available to the research community.

Six-component borehole sondes, with three channels of acceleration and three of velocity, were installed in 1993 in four holes of opportunity at depths of up to 600 feet along the northern Hayward fault. Identical downhole sensor packages were provided to Malcolm Johnston of the USGS for colocation in dilatometer boreholes on the southern Hayward fault, and to Larry Hutchings at LLNL for installation in boreholes drilled by CALTRANS at three piers of the Dumbarton bridge. Site information is specified in Table 1.

The central data acquisition and control platform is a SPARCstation10, already in place. The Quanterra field recorders, once installed, will communicate with the central computer over 38 kb ADN phone lines. There will then be central event detection and other network controlling decision-making.

The HFN data will also be available in real-time to Project REDI (Rapid Earthquake Data Integration). REDI is being developed at UCB to provide clients with near real-time information on significant earthquakes from on-line analysis of telemetered signals from northern California seismographic stations.

1994 Accomplishments

Station Operation. During the past fiscal year we have operated the network of four borehole seismometers on the northern Hayward fault that were installed in 1993. As a temporary system, RefTek Model 72-A07 24-bit event recorders borrowed from the UCB Seismographic Station and Lawrence Berkeley Laboratory have operated independently at each site, recording on DAT tape. The central-site acquisition and control workstation (SPARCstation 10) reads the DAT tapes from the field recorders.

At site BRIB, the sensor cable was recently irretrievably damaged down-hole (while trying to install another instrument). One of the new sondes (described below) will be installed at this site.

New Seismometer Installations. We have had several sensor failures in the original sondes. The sonde at the UC Stadium (site UCSB) was retrieved and cut open: Water had clearly penetrated the sensors. Subsequently, we convinced Wilcoxin Research to produce a hermetically sealed version of their accelerometer, we re-engineered the sonde, purchased heavy-duty, deep-submersion cable, and filled the sonde with an improved epoxy potting material.

The accelerometers also failed at site BBEB, at the east end of the Bay Bridge in Oakland (Figure 1). It will be replaced with one of the new Bay Bridge installations described below, probably BBE2 on Yerba Buena Island.

With funding support from the Electric Power Research Institute (EPRI), the USGS, and LLNL, several of the new sondes are being constructed. One has been installed at HFN site UCSB. The others are being installed cooperatively with LLNL in holes of opportunity being drilled into bedrock under San Francisco Bay by the CALTRANS Bridge Safety Program. The first three have been used already at the Oakland-San Francisco Bay Bridge (Figure 1, sites with prefix "BBE"). In the short term, recording there will be accomplished with LLNL RefTek

event recorders. The remaining sondes will be installed at the Carquinez, Richmond-San Rafael, and San Mateo bridges.

Recording/Telemetry Equipment. Five Quanterra Model Q4124 data platforms have now been delivered, equipped with a new operating system (called Ultrashear) especially developed for HFN to meet the needs of a centrally-controlled network. The major addition is full two-way communication between the remote units and the central computer, via 38.4 kb ADN phone lines. Recording parameters can be changed remotely without disrupting the remote station's operation. Network triggering and data recovery are controlled by the central computer. Further, the platforms feature four, 24-bit 1000 sps data channels, and multiple data streams. The innovations appear to be quite attractive, and may be implemented in the Quanterra recorders of the Berkeley Digital Seismic Network.

One of the new Quanterra platforms was recently installed at site UCSB, with one of the new sondes (described above), and the first ADN phone service to the central computer. First indications are that all components are operating well. Figure 2 shows the M5 Parkfield earthquake of December 20, 1994, as recorded with the new equipment at UCSB.

TABLE 1. Hayward Fault Network Station Information

Site	Latitude (deg N)	Longitude (deg W)	Surface Elevation (meters)	Instrument Depth (m)
Northern sites (UCB):				
BBEB	37.821596	122.329751	-30.8	182.9
UCSB	37.871947	122.251676	94.7	167.6
RFSB	37.916080	122.336104	-27.3	91.4
BRIB	37.918863	122.151695	222.2	108.8
Southern sites (USGS):				
GARS	37.645448	122.011278	339.5	120.6
CHAS	37.743318	122.096570	225.5	118.5
MILS	37.540266	121.887595	343.5	155.3
SUNS	37.642966	121.940231	499.2	123.5
COYS	37.562894	122.096694	-23.1	136.8
Dumbarton Bridge (LLNL/USGS/EPRI/CALTRANS):				
PIER1	37.4976	122.1289	-31.3	0, 71.6, 228.0
PIER27	37.5056	122.1156	-31.3	182.9
PIER44	37.5106	122.1114	-31.3	0, 62.5, 157.9
San Francisco-Oakland Bay Bridge (LLNL/USGS/EPRI/CALTRANS):				
Pier E2 (Y.B. Is)	37.8140	122.3589	-28.6	61.9
Pier E7	?	?	-39.6	135.2
Pier E17	37.82065	122.33631	-35.9	159.7

Notes:
- All coordinates are with respect to WGS84 Datum (equivalent to NAD83). To convert to the NAD27 datum, corrections are +0.000069 deg latitude (8m), and -0.001083 deg longitude (95.2m)
- Elevations are height above WGS84 ellipsoid. To convert to mean-sea-level elevation, add 31.4m.
- Locations of UCB and USGS sites were obtained by GPS survey (carrier phase), accurate to better than 1 m..
- Dumbarton Bridge and Bay Bridge E2 Locations are from 7.5' topographic maps, accurate to ±15m.
- Bay Bridge E17 location is by real-time differential GPS measurement, accurate to ±5m
- UCB site BRIB is colocated with USGS dilatometer site RRCS.
- The east and west ends of the Dumbarton Bridge are equiped with sensors at three depths. The deepest instrument at all three sites is 100 feet into bedrock.

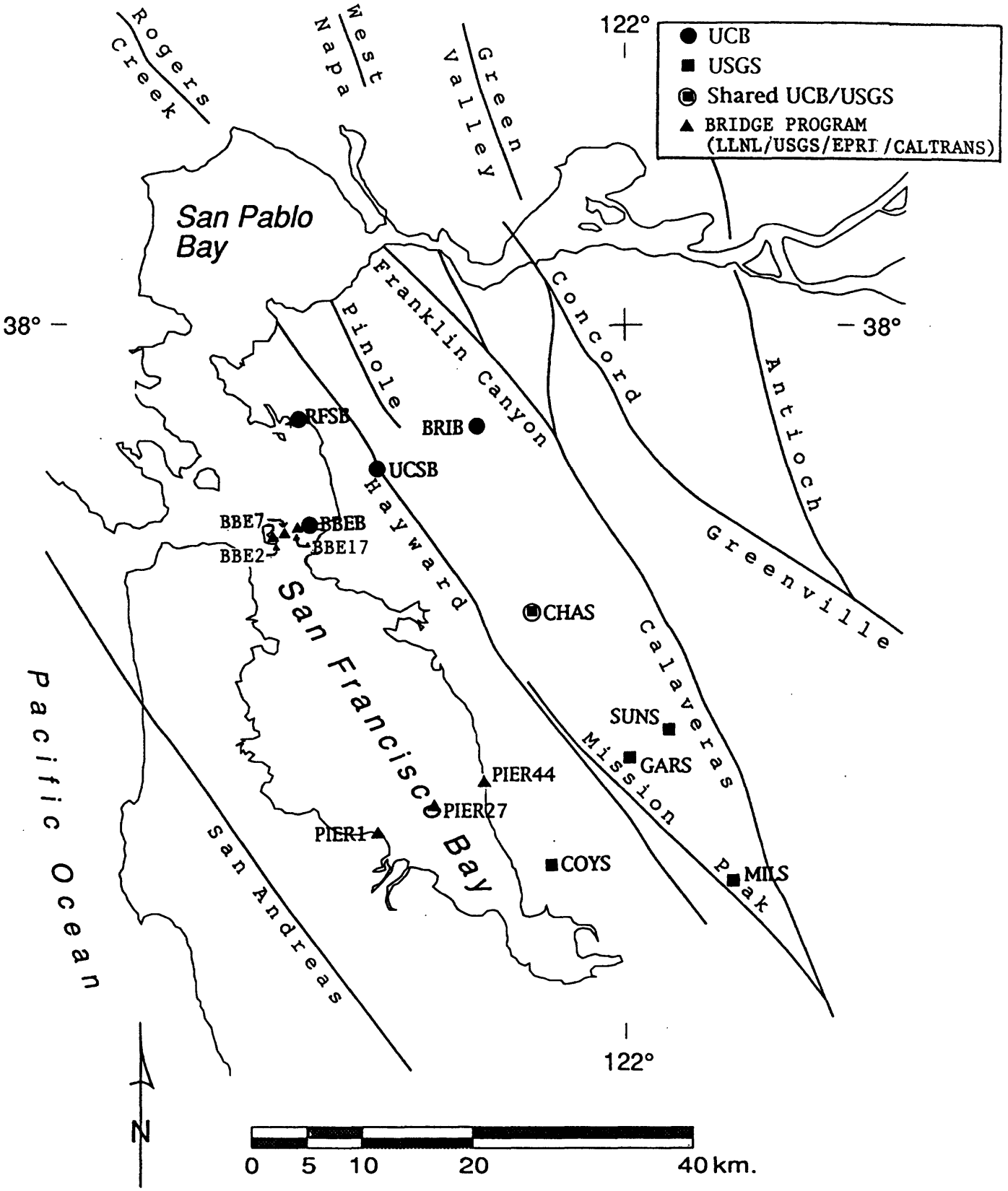

Figure 1. Hayward Fault Digital Network.

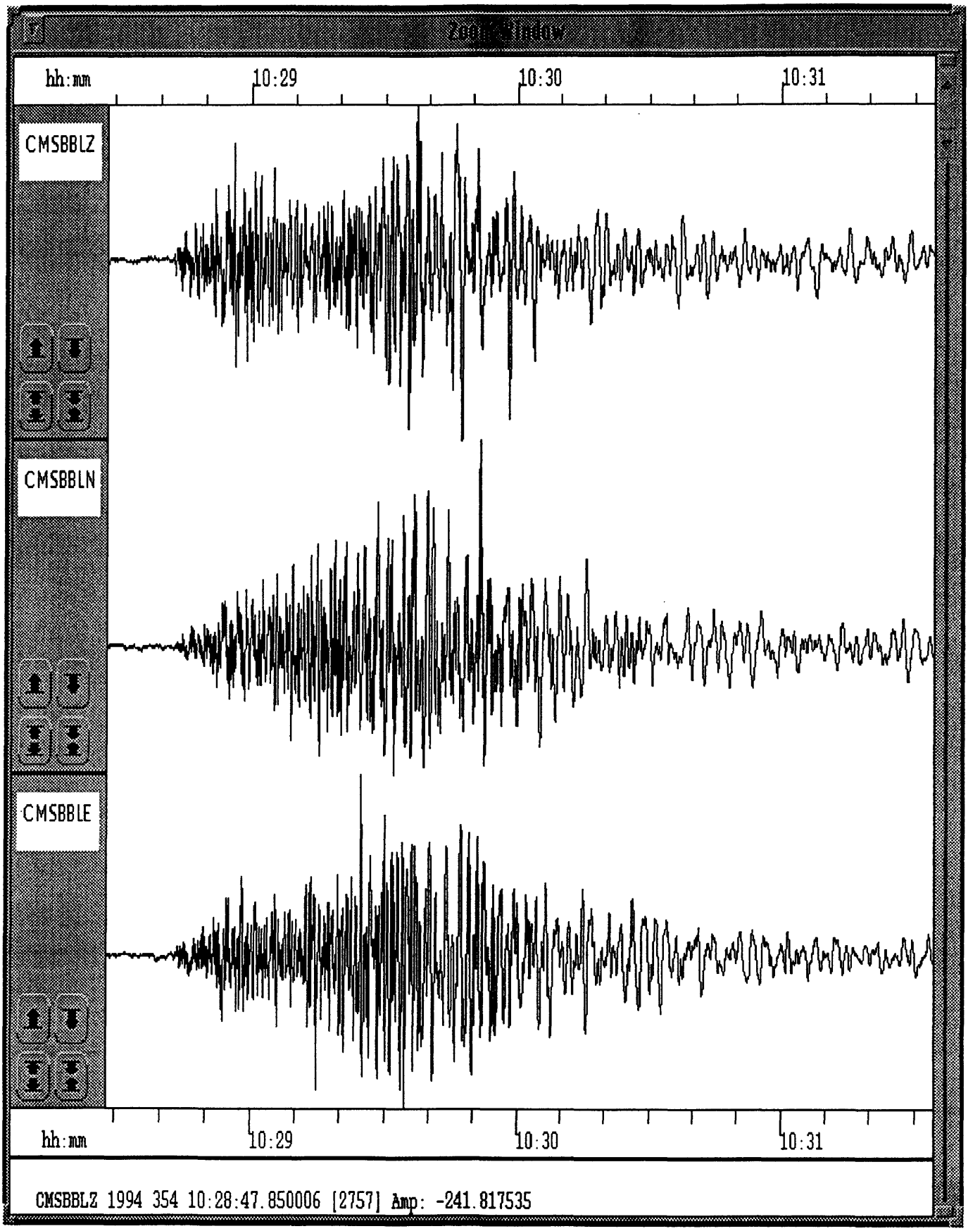

Figure 2. Parkfield M5 earthquake of December 20, 1994, as recorded at HFN site UCSB with full telemetry and recording systems in place.

Geologic and tectonic framework, Mendocino Triple Junction
5-9540-70420

R. J. McLaughlin
U. S. Geological Survey, Branch of Western Regional Geology, MS 975
345 Middlefield Road, Menlo Park, CA 94025
8 (415) 329-4945; Fax No: 8 (415) 329-4936

INVESTIGATIONS UNDERTAKEN:

(1) Continue digitization in ARC/INFO and preparation of interpretive texts for publication at 100 K scale, maps of geology and structure of the onshore-offshore Mendocino Triple Junction region

(2) Write report on structural implications of Miocene marine accretionary prism rocks exposed onshore immediately north of Cape Mendocino.

RESULTS:

(1) Geologic maps of the Cape Mendocino and Eureka 100 k quadrangles and adjacent offshore area, along with structure sections and text were returned to senior author (McLaughlin) for revision following technical review. Report is to be forwarded to BWTR in December 1994.

(2) The Geology of Garberville 100 k quadrangle was digitized and underwent editing by authors (McLaughlin, Blake, Irwin). Structure sections are to be constructed and the quadrangle submitted for technical review in January, 1995.

(3) A composite map of geology and seismicity of the offshore and onshore Cape Mendocino region was derived from the digital Cape Mendocino, Eureka, and Garberville 100 k quadrangles. Earthquakes were color-keyed by depth, and magnitudes keyed by symbol size. Map was produced in cooperation with D. Oppenheimer and M. Magee and presented as part of a poster session in October 1994 GSA National Meeting.

(4) In collaboration with other U. S. G. S. co-authors and with K. Aalto and G. Carver, Humboldt State University, wrote and submitted to *Tectonics*, paper on uplifted and deformed Miocene accretionary prism north of Cape Mendocino.

REPORTS PUBLISHED:

Aalto, K. R., Carver, G. A., Dunklin, T. (Geology Dept., Humboldt State University, CA), Barron, J. A., Sliter, W. V., and McDougall, K., Uplifted Neogene accretionary wedge, Humboldt County, CA: Abstracts with Programs, Geological Society of America, v. 26, no. 2, p. 33.

Magee, Marion (Stanford), McLaughlin, R. J., and Oppenheimer, D. (U. S. G. S., Menlo Park), 1994, Relationship of recent onshore and near-shore seismicity to the structural framework of the Mendocino Triple Junction: Abstracts with Programs, Geological Society of America, v. 26, no. 7, p. A146.

Submitted for publication consideration in *Tectonics*: Aalto, K. R., McLaughlin, R. J., Carver, G. A., Barron, J. A., Sliter, W. V., and McDougall, K., Uplifted Neogene margin, southernmost Cascadia-Mendocino Triple Junction region, California: 13 manuscript pp., 12 figs. - with journal 11/94.

THE ROLE OF MEAN DEPTH OF BACKGROUND SEISMICITY IN RUPTURE INITIATION

Award Number 1434-94-G-2388

Stephen R. McNutt and Max Wyss

Geophysical Institute
University of Alaska Fairbanks
903 Koyukuk Drive
P.O. Box 757320
Fairbanks, AK 99775-7320

phone: (907) 474-7131, fax: (907) 474-5618, email: steve@deus.gi.alaska.edu

Program Element II.2

INVESTIGATIONS UNDERTAKEN

We are studying the mean and quartile depths of the seismicity within and near the source volumes of moderate and major earthquakes in California and Alaska. It has previously been shown that the pattern of increased mean depth of seismicity preceded the ruptures of some mainshocks along the San Andreas fault system. We are developing the tools to test for this pattern for a larger number of cases. We are also integrating the mean depth work with other ongoing work to evaluate systematic errors and completeness of earthquake catalogs.

We developed several tools as part of the Matlab-based software package ZMAP (Wiemer and Zuniga, 1994). ZMAP has been developed at the Geophysical Institute UAF to investigate seismicity rate changes as a function of space, time, and magnitude. Since these questions are closely related to changes in mean depth, we added tools to ZMAP that expand the analyses to address changes in mean depth.

We are now able to interactively (1) decluster a catalog and work with either the complete catalog, the declustered catalog or just the clusters (2) display mean depth curves for selected areas (3) calculate the significance of mean depth changes based on one or more statistical tests, and (4) display mean depth and mean depth changes as a function of space and time.

RESULTS

Results were sparse while we were in the stage of developing the necessary research tools. Nevertheless, we have made a preliminary study of seismicity preceding three earthquakes

in central California to date: 1975 Coyote Lake (ML=5.9), 1984 Morgan Hill (ML=6.2), and 1989 Loma Prieta (ML=7.0). We used the catalog for 1967-1994 from the Northern California Earthquake Data Center. Loma Prieta data are given below as an example.

A map of seismicity prior to the Loma Prieta earthquake is shown as Figure 1. The polygon outlines the approximate rupture area which was also our search area for possible depth anomalies. A depth versus time plot for seismicity prior to the mainshock is shown as Figure 2. Note the cluster of deep pre-shocks at the right of the figure. Both figures 1 and 2 display only hypocenters with vertical errors of 1.5 km or less. We studied the depth error distribution and found that approximately 80 percent of the events had depth errors of 1.5 km or less. We somewhat arbitrarily chose 1.5 km as an error cutoff to preserve resolution. The distribution of depth errors (Fig. 4) is approximately log normal. Depth error does not appear to be a function of depth (Fig. 4), but we found that depth error decreases as a function of magnitude (Fig. 5). Presumably this occurs because larger earthquakes have more impulsive arrivals.

We plot mean depth as a function of time in Figures 6 and 7 using two different window lengths. For each case the deepest mean depth occurs at the right edge of the plot and includes the pre-shocks and foreshocks to the Loma Prieta mainshock. The standard error bars on the plots are large, however, and we will be using additional statistical tests to measure the significance of these possible depth anomalies as we complete our analyses.

We have also made significant progress in identifying changes in the reporting characteristics in earthquake catalogs, by developing a method by which we can measure the degree of stretching (or compression) that the magnitude scale may have undergone as a function of time (Zuniga and Wyss, 1995). Times of magnitude shifts or stretches signal times of changing procedure in the data analysis or in the network configuration. If apparent changes in mean depth should be found at times of inadvertent magnitude scale changes, it would be likely that the depth changes are also not real. Thus, we will check the stability of the reporting of earthquakes for any times at which we may find changes in the average depth, using our new tools for this purpose.

The question of how to assess the correlation of a mainshock with a proposed precursor anomaly has also been addressed (Wyss, 1995; Wyss and Allmann, 1995). We propose a statistical estimate of the performance reliability of a precursor, in an area of heterogeneous probability for mainshocks. The problem we may face is the following: We may wish to test whether observed instances of increased mean depth correlate with nearby mainshocks by chance, or whether these are cases of precursors connected to the mainshocks, in an area where the probability of a mainshock occurring varies strongly as a function of space. We designed and tested a method which will take into account a different local probability for each target area, and then estimates the probability that in n attempts m successes (correlations) were observed.

Now that the software tools have been developed, we will complete the temporal analysis of the 15-20 moderate and major earthquakes listed in our proposal. Using the new ZMAP

features, we will also undertake spatial analyses that were not identified in our proposal, but which we feel may be equally important. We note that a six month extension was granted for this work.

REPORTS PUBLISHED

Wiemer S. and R. Zuniga, ZMAP - a Software Package to analyse Seismicity, EOS, Trans. Amer. Geophys. Union, Vol. 75, No. 44, p. 456, 1994

Wyss, M., Inaccuracies in seismicity and magnitude data used by Varotsos and coworkers, Geophys. Res. Lett., 22, submitted, 1995.

Wyss, M., and A. Allmann, Probability of chance correlations of earthquakes with predictions in areas of heterogeneous seismicity rate: the VAN case, Pageoph, 143, submitted, 1995.

Zuniga, R., and M. Wyss, Inadvertant changes in magnitude reported in earthquake catalogs: Influence on b-value estimates, Bull. Seism. Soc. Amer., 85, submitted, 1995.

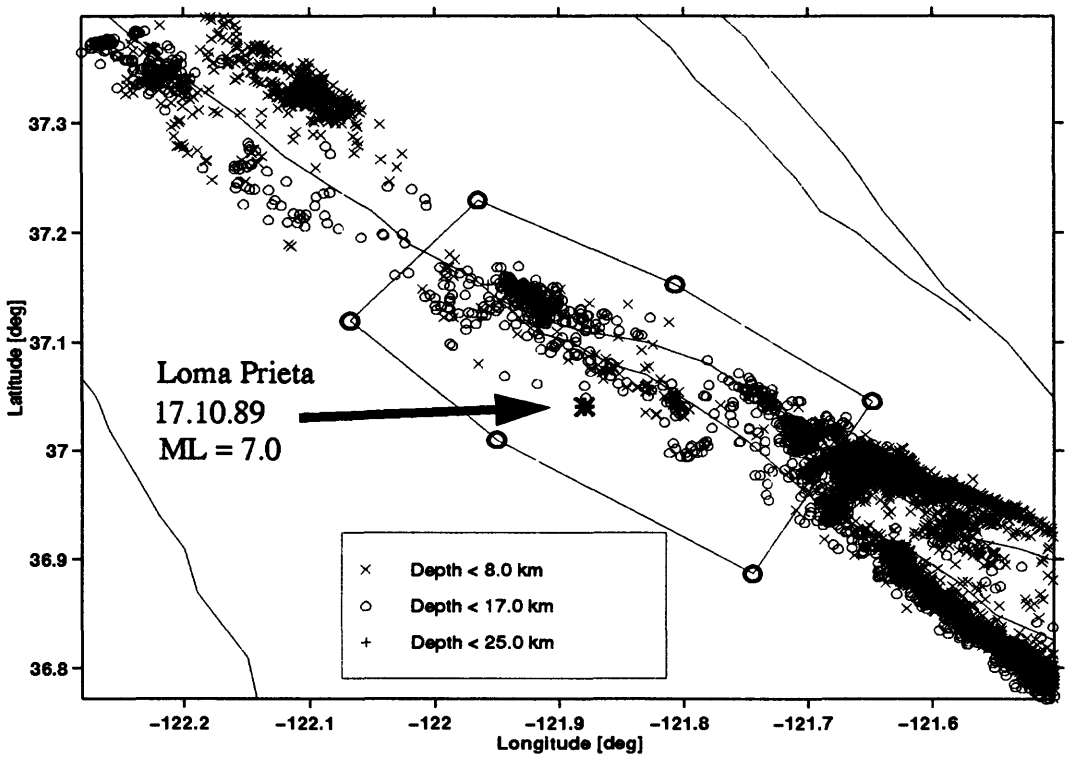

Figure 1: Map of the seismicity prior to the Loma Prieta (ML= 7.0) earthquake. The epicenter location is marked by a star. The polygon indicates the approximate rupture area. All events with a depth error smaller 1.5 km in the period 1.1. 68 to 16.10.89 are shown.

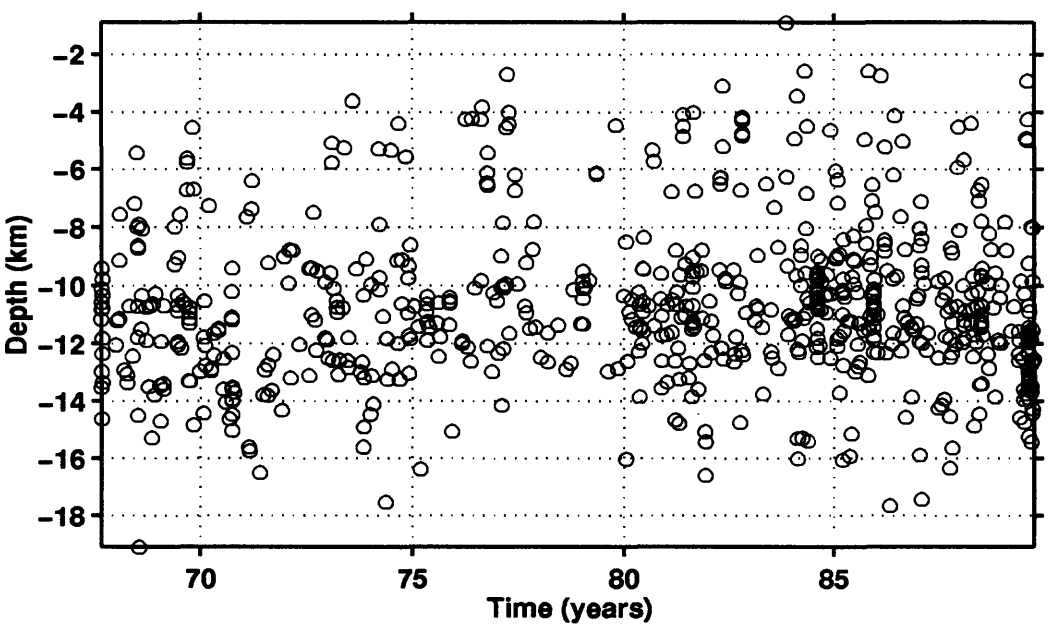

Figure 2: Seismicity in the rupture area outlined in Figure 1 as a function of time and depth. Note the deep foreshocks prior to the Loma Prieta mainshock.

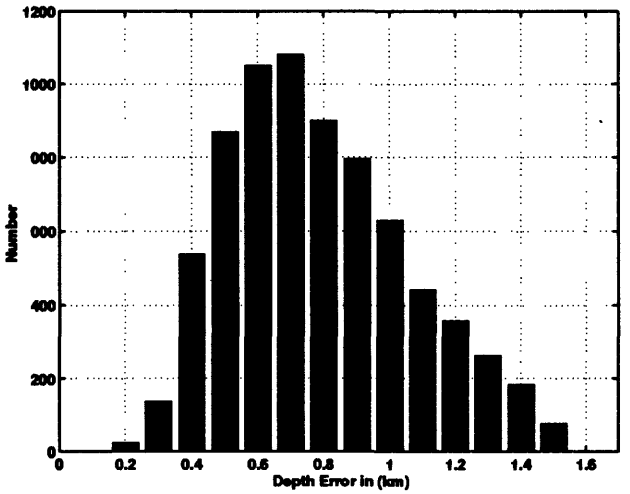

Figure 3: Histogram of depth error for all earthquakes shown in Figure 1. The distribution is approximately log normal.

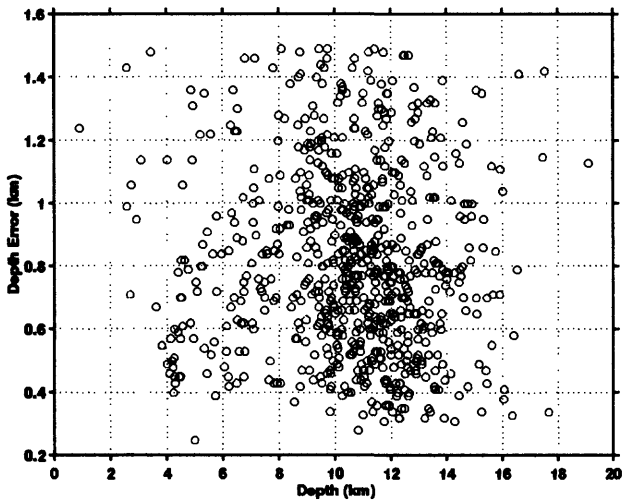

Figure 4: Plot of the depth error as a function of depth for all earthquakes within the rupture area (Figure 1). No correlation between depth and depth error can be observed.

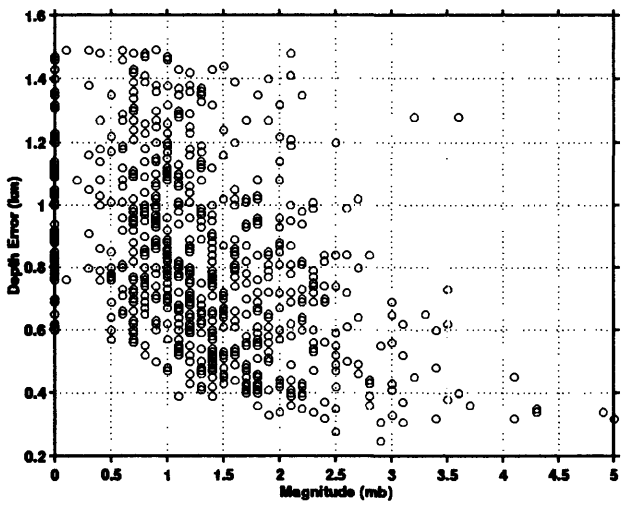

Figure 5: Plot of the depth error as a function of magnitude for all earthquakes within the rupture area (Figure 1). Depth error and magnitude show an inverse correlation.

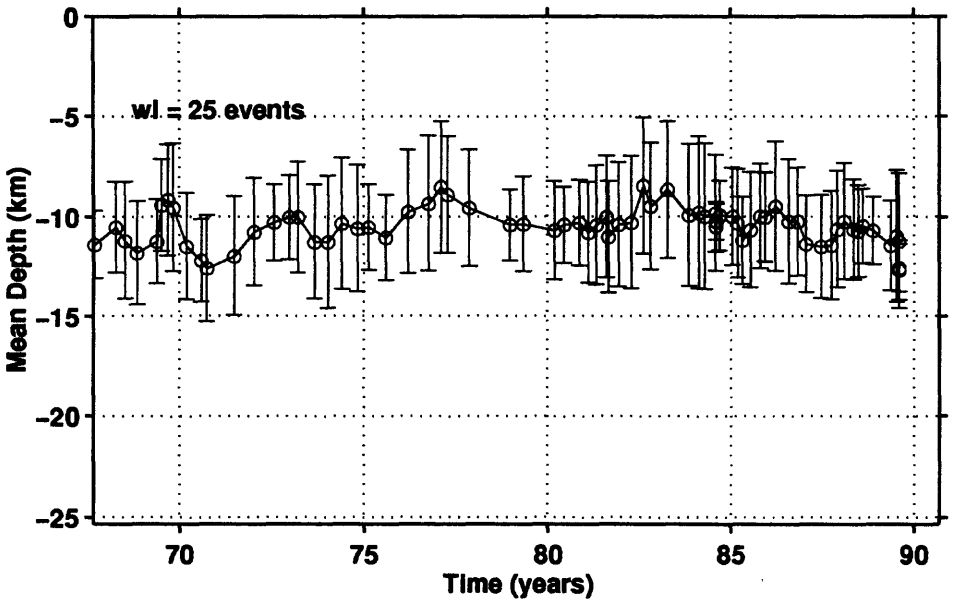

Figure 6: Mean depth as a function of time. A sliding window with a length of 25 earthquakes was moved over the entire time series with a step width of 10 earthquakes. The length of the error bar is one standard deviation of the depth distribution for the 25 earthquakes. Note the decrease in mean depth prior to the Loma Prieta mainshock. This decrease is due to the deep pre-shocks and foreshocks.

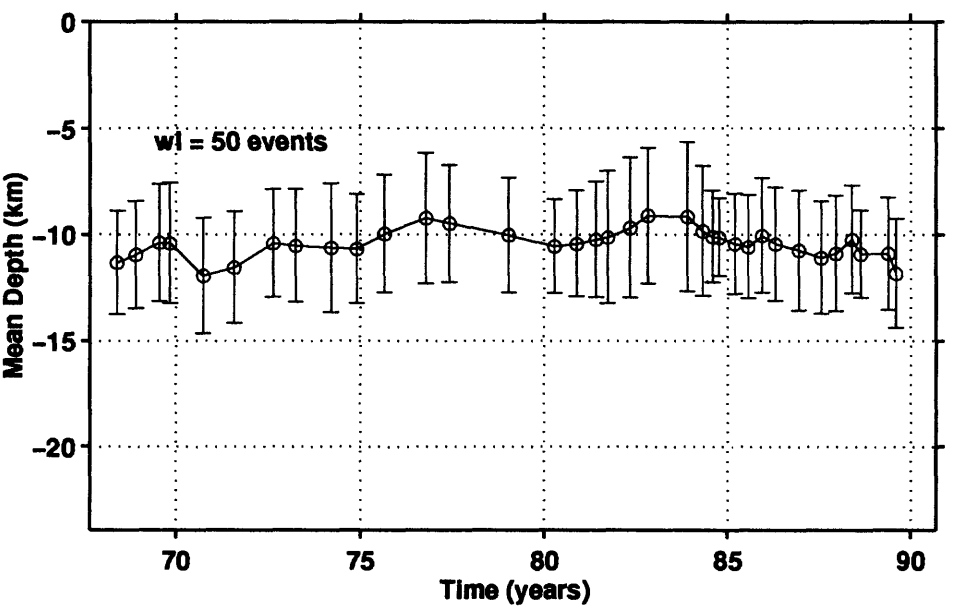

Figure 7: Same as Figure 6, but with an averaging window length of 50 earthquakes moved in steps of 20 earthquakes over the time series.

Experimental Tilt and Strain Instrumentation

9960-12126

C.E. Mortensen
Branch of Earthquake Geology and Geophysics
U.S. Geological Survey
345 Middlefield Road, MS 977
Menlo Park, California 94025
(415) 329-4856
Program Element II

Investigations

1. There are currently 159 Data Collection Platforms (DCP's) that transmit a variety of data to the Direct Readout Terminal (DROT) and the backup Direct Readout Ground Station (DRGS) in Menlo Park. Seventy-five of these DCPs transmit data at 10-minute intervals on two exclusively assigned random channels, which are being utilized under a special agreement with NESDIS. The remainder of the DCPs report at standard 3 or 4-hour intervals as assigned by NESDIS. This system transmits data from all types of low-frequency instruments including dilatometers, creepmeters, strainmeters, water-level meters, magnetometers, tiltmeters, and related measurements. One of the first DCP's installed has been in continuous operation, with no repairs and little maintenance, for more than 3700 days. Maintenance of this network will be transferred to another project in FY 95.

2. Networks of tiltmeters, creepmeters and shallow strainmeters have been maintained in various regions of interest in California. A network of tiltmeters located at seven sites monitors crustal deformation within the Long Valley caldera. Roger Bilham of the University of Colorado and Jon Beaven of Lamont-Doherty installed a very long baseline tiltmeter in Long Valley. This project provided three DCP's to collect the data and return it to Menlo Park via GOES satellite. We also monitor the data received to keep track of deformation within the caldera, comparing results frequently with the USGS tiltmeter array.

3. Creepmeters located along the Hayward, Calaveras and San Andreas faults between Berkeley and the Parkfield area are maintained in cooperation with the Fault Zone Tectonics project. A shallow strainmeter is located near Parkfield, while observatory type tiltmeters and strainmeters are sited at the Presidio Vault in San Francisco, and a tiltmeter is installed in the Byerly Seismographic Vault at Berkeley. Data from these instruments are telemetered to Menlo Park via the GOES satellite. These functions will be transferred to other projects in FY 95.

4. Water-level meters in wells located in Parkfield and the Mojavi region were maintained in cooperation with the Water-level Monitoring Project. This function will be transferred to that project during FY-95.

Results

1. Provided regional monitoring of crustal deformation (tilt) in the Long Valley caldera, Mammoth Lakes, CA.

2. Conducted maintenance activities for various instrumentation arrays in Parkfield and throughout the S.F. Bay region.

NEHRP:PN--COMPONENT: II.5

PALEOSEISMOLOGY OF COASTAL OREGON

9950-15133

ALAN R. NELSON

Branch of Earthquake and Landslide Hazards
U.S. Geological Survey, MS 966
Box 25046, Denver, CO 80225
(303) 273-8592; anelson@gldvxa.cr.usgs.gov

INVESTIGATIONS

The magnitude and recurrence times of past great earthquakes along the Cascadia continental margin are important issues in seismic hazard assessment in the U.S. Pacific Northwest. Some argue that the most recent subduction-zone earthquake had a magnitude of 9 (e.g., plate-boundary rupture >500 km long), similar to the 1964 earthquake in Alaska, and that such an event is typical of the Cascadia subduction zone. Others, citing analogies with historic earthquakes in other suduction zones, suggest that a segmented margin with more frequent magnitude 8 earthquakes (e.g., 100-to-300-km-long ruptures) is more plausible. Recurrence times are also uncertain, with some scientists arguing for average repeat times for M>8 earthquakes of 300 years, and others pointing out that evidence for more than two great earthquakes in the past few thousand years is not widely documented. High-precision ^{14}C dating of trees killed by sudden subsidence at four coastal sites do not rule out an earthquake rupture that may have extended from central Washington to Humboldt Bay, California, about A.D. 1690-1710. Our more recent study of correlative buried soils, which we dated with the means of eight marsh-plant AMS ^{14}C ages, does not rule out synchronous subsidence at seven sites along 440 km of the Oregon and Washington coast. Such ages are consistent with either a magnitude 9 earthquake or a series of magnitude 8 earthquakes after A.D. 1650.

The question of whether or not the most recent subduction-zone earthquake was a giant earthquake of magnitude 9, as well as the magnitude and recurrence of earlier earthquakes, is difficult to address because so little paleoseismological work has been completed in the southern half of the Cascadia zone. Precisely dated trees in Humboldt Bay are 530 km south of the nearest other site with dated trees. The only site with precisely dated marsh plants in central and southern Oregon is on the Coquille River, 260 km north of Humboldt Bay. Most paleoseismicity studies along the Cascadia margin have focused on the extensive marshes in northern Oregon, southern Washington, or in the Humboldt Bay region. Such marshes are not found along the steep, rocky coast of the southern part of the subduction zone. Furthermore, the paleoseismic record in the southern Cascadia forearc may be more complex than the record farther north because the active fold and thrust belt extends on land in this region—coseismic uplift or subsidence of coastal sites in the belt may or may not be synchronous with great earthquakes on the plate boundary.

To deal with the question of the magnitude of the most recent great earthquake and to begin to decipher the complex paleoseismic record of southern Oregon we are taking a new approach in a cooperative study with colleagues in California (Harvey Kelsey, Humboldt State) and Oregon (Eileen Hemphill-Haley, PMG)—one that emphasizes field mapping and precise dating

of tsunami deposits and accompanying land-level changes in adjacent but *contrasting* environmental settings. Unlike earlier work in more northerly marshes, we will collect independent types of evidence of great earthquakes in both brackish-water estuaries and nearby freshwater coastal lakes. An important aspect of the tsunami investigation will be estimating the inundation level (a crude measure of tsunami magnitude) of the most recent and possibily earlier tsunamis. Through detailed stratigraphic and laboratory studies we hope to answer the following questions:

- Did the tsunami generated by the most recent great earthquake in southern Washington and northern Oregon also strike the southern Oregon coast?
- How large was this earthquake; in other words, how far south in Oregon did coseismic land-level changes extend and what was the inundation level of its attendant tsunami?
- How can deposits from local or regional tsunamis be distinguished from the deposits of large storms or floods in southern Oregon?
- Did locally generated tsunamis accompany older great earthquakes in southern Oregon?
- Were the older tsunamis as large as the most recent one?
- Did parts of the coast abruptly rise or fall during any of these earthquakes?
- What is the relation of the timing of older earthquakes to those inferred from the tidal-marsh records of northern Oregon, southern Washington, and the Humboldt Bay region?

RESULTS

Results from the initial lake-coring phase of the project suggest tsunami deposits from repeated great earthquakes may be preserved in low-lying lakes along the southern Oregon coast. From a platform suspended between two canoes, we collected 2-to-6-m-long cores from two or three sites in each of four coastal lakes between Cape Blanco and the Coquille River using a Livingston piston corer. Several small rivers that cross this coastal plain flow into lakes at their downstream ends where sandy barriers block their mouths. We selected lakes with different water-level elevations, surface areas, barrier heights, distances from the coast, and drainage basin sizes along a 40-km segment of coast to see how these factors affect the recoverable sediment record. Most cores could be pushed 2.5-3.0 m into lake sediment before bottoming in unconsolidated medium to coarse sand. These sites were on the oceanward side of the lake, yet far enough from lake-shore dunes to minimize the deposition of wind-blown sand.

The stratigraphy in three of the four lakes (Floras, Croft and Bradley Lakes) consisted of silty clay and clayey gyttja interrupted by sandy intervals. In all lakes, lacustrine sediment apparently overlies dune sand (2-4-ka) that predates the rise of the lakes to their current levels. Sediment in the two deeper lakes (Floras Lake and Bradley Lake) consisted of well-laminated silty clay and clayey gyttja; some of these laminae may be varves. Water at these core sites is deep enough (10 m) that bottom waters do not turn over seasonally. The anoxic, possibly saline, bottom water apparently prevented bioturbation, which would disturb sediment laminae.

In most cores, the sandy intervals that may be tsunami deposits are capped by woody debris consisting of detrital leaves, conifer needles, fragments of herbaceous and woody plant roots, and sticks. AMS ^{14}C ages on some of the most fragile materials (those least likely to be reworked), such as the deciduous tree leaves in cores from Bradley and Floras Lakes, provide ages for the times of sand deposition in each core. The five ages obtained so far suggest unusual events of sand deposition at about 0.3 ka, 1.0 ka, and 1.6 ka (e.g., Fig. 1). The youngest and oldest times of sand deposition match the ages of the two most widespread buried marsh soils farther north in Oregon that have been inferred to record regional coastal subsidence during great earthquakes.

The two Bradley Lake cores (B and C on Fig. 1) show three periods of sand deposition, which correlate between cores. Angular clasts of well-laminated lacustrine clay are enclosed in the middle sand, indicating that flow velocities were fast enough to erode the lake bottom prior to sand deposition. Core B did not penetrate totally through the third (deepest) sand, but the complete recovery of this interval in the more distal core (C) shows it was deposited during four sediment pulses. Each pulse consists of medium sand fining upward to very fine sand or silty sand. The period between pulses was apparently too short for silt to settle out of the water column and form laminae before the next pulse occurred. Preliminary diatom analysis shows that core C sediments are dominated by freshwater diatoms, but that there was an incursion of rare but well preserved planktonic marine diatoms just above the sand at 84 cm. The occurences of these delicate planktonic species in samples overwhelmingly dominated by lake species suggests the diatoms were washed into the lake. If a tsunami carried the sand into the lake, it must have reached an elevation of at least 8 m (Fig. 1).

REPORTS

Atwater, B.F., Nelson, A.R., Clague, J.J., Carver, G.A., Yamaguchi, D.K., Bobrowsky, P.T., Bourgeois, Joanne, Darienzo, M.E., Grant, W.C., Hemphill-Haley, Eileen, Kelsey, H.M., Jacoby, G.C., Nishenko, S.P., Palmer, S.P., Peterson, C.D., and Reinhart, M.A., Summary of coastal geologic evidence for past great earthquakes at the Cascadia subduction zone: *Earthquake Spectra*, (in press).

Bradley, L-A. and Stafford, T.W., Comparison of manual and automated pretreatment methods for AMS radiocarbon dating of plant fossils, *Radiocarbon,* (in press).

Jennings, A.E., Nelson, A.R., Scott, D.B., and Aravena, Juan-Carlos, Marsh foraminiferal assemblages in the Valdivia estuary, south-central Chile, relative to vascular plants and sea level, 1994, *Journal of Coastal Research*, v. 10, (in press).

Kelsey, H.M., Witter, R.C., Nelson, A.R., and Hemphill-Haley, Eileen, 1994, Repeated abrupt late Holocene environmental changes in south coastal Oregon--Stratigraphic evidence at Sixes River marsh and Bradley Lake: *Geological Society of America, Abstracts with Programs*, v. 26, no. 7, p. A-524.

Nelson, A.R., A geologic history of South Slough, *in* Caldera, Melody, and Giles, Marty, eds., *A History of South Slough, Coos Bay, Oregon*: (chapter 1 in a popular history book; in press).

Nelson, A.R., and Kashima, Kaoru, 1993, Diatom zonation in southern Oregon tidal marshes relative to vascular plants, foraminifera, and sea level: *Journal of Coastal Research*, v. 9, p. 673-697.

Nelson, A.R., Shennan, Ian, and Long, A.J., Identifying coseismic sea-level changes in tidal-wetland stratigraphic sequences in the Cascadia subduction zone of western North America: (Branch approval 6/28/94; submitted to *Journal of Geophysical Research*).

Nelson, A.R., Jennings, A.E., and Kashima, Kaoru, Foraminiferal and diatom evidence for the size and rate of rapid late Holocene sea-level changes on the south-central Oregon coast, USA: (Branch approval 8/94; submitted to *Geological Society of America Bulletin*).

Nelson, A.R., Atwater, B.F., Bradley, L-A., and Stafford, T.W., 1994, AMS ^{14}C correlation of subsided wetland soils using rooted-herb and detrital samples in the Cascadia subduction zone: *Geological Society of America, Abstracts with Programs*, v. 26, no. 7, p. A-522.

Nelson, A.R., Kelsey, H.M., Hemphill-Haley, Eileen, and Witter, R.C., 1994, A potential record of tsunamis generated by great earthquakes along the southern Cascadia subduction zone[abs], *in* Proceedings of the Workshop on Paleoseismology:*U.S. Geological, Survey Open-File Report no. 94-568*, p. 134-136.

Personius, S.F., 1993, Age and origin of fluvial terraces in the central Coast Range, western Oregon: *U.S. Geological Survey Bulletin* 2038, 56 p.

Personius, S.F., Kelsey, H.M., and Grabau, P.C., 1993, Evidence for regional stream aggradation in the central Oregon Coast Range during the Pleistocene-Holocene transition: *Quaternary Research*, v. 40, p. 297-308.

Personius, S.F., Late Quaternary stream incision and uplift in the forearc of the Cascadia subduction zone, western Oregon: (Branch approval 11/18/94; submitted to *Journal of Geophysical Research*).

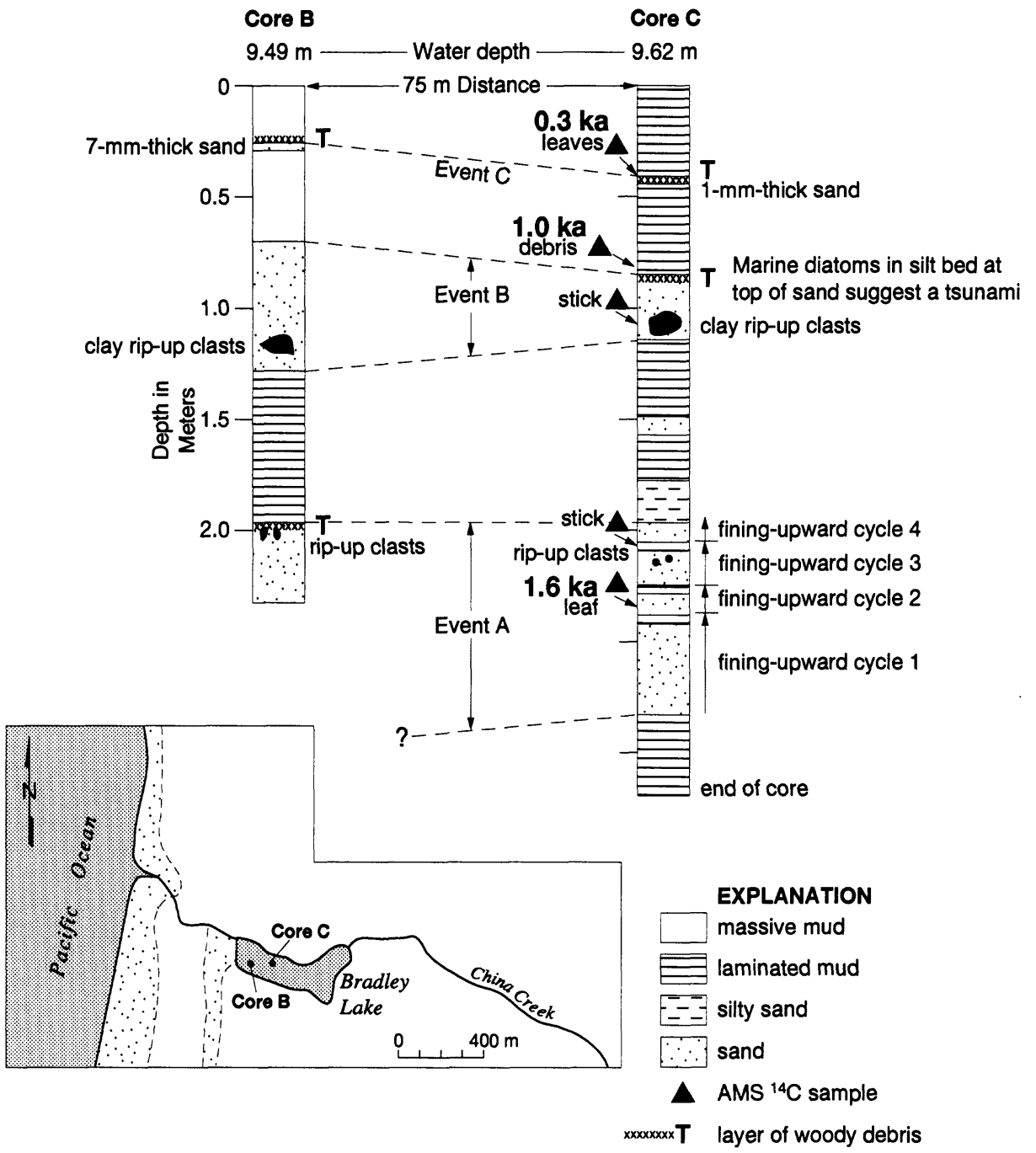

Figure 1. Simplified stratigraphy in two cores from Bradley Lake showing AMS ^{14}C ages and correlation of three sand beds labeled events A, B, and C. The elevation of Bradley Lake is 5.5 m and the dune that forms the west edge of the lake is about 5 m high. A tsunami capable of depositing sand in the lake would probably have had a runup elevation of at least 8-10 m.

GEOARCHAEOLOGIC AND PALEOSEISMIC INVESTIGATIONS OF THE SAN GREGORIO FAULT, SEAL COVE, CALIFORNIA

Grant Award # 1434-93-G-2275

Jay Stratton Noller, Gary D. Simpson, Stephen C. Thompson, and William R. Lettis
William Lettis & Associates, Inc., 1000 Broadway, Suite 612, Oakland, CA 94607
(510)832-3716v; (510)832-4139f;wla@netcom.com

Mark G. Hylkema
Caltrans, 111 Grand Avenue, Oakland, CA 94623-0660
(510)286-5613v; (510)286-5600f

Element II: Evaluating Earthquake Potential

The San Gregorio fault is the largest fault in the San Francisco Bay area whose slip rate and recency of activity are unknown. The fault is the primary structure west of the San Andreas fault in central California. The fault lies primarily offshore but comes onshore at two locations: Point Año Nuevo and Seal Cove. The San Gregorio fault clearly deforms and offsets late Pleistocene marine terraces. Based on these offset terraces, Weber and Lajoie (1979) reported a right lateral slip rate of 6 to 16 mm/yr. Recently collected offshore seismic reflection data, however, suggest that the San Gregorio fault may be part of a family of west-vergent listric thrust faults. These two disparate interpretations have significantly different implications for the role of the San Gregorio fault in the tectonic setting of the San Francisco Bay area. Kelson and others (1992) assumed a right-lateral slip rate of 7±1 mm/yr for the San Gregorio fault, which fits well with the rate of relative plate motion in the Bay area. Lettis and others (1994) interpreted the San Gregorio fault to be the northern part of a near-coastal system of strike-slip faults including the San Simeon and Hosgri faults to the south.

In the Seal Cove-Half Moon Bay area, the San Gregorio fault is morphologically well expressed by a sharp east-facing escarpment. The relative sense of vertical movement is up-on-the-west, which is inconsistent with the interpretation of west-vergent thrust or reverse faulting for the San Gregorio fault.

We selected a site with high potential for revealing the character of late Holocene deformation on the San Gregorio fault in James Fitzgerald Marine Reserve. At this location, the fault transects a prominent archaeological site on a gently sloping to flat bluff-top near the modern sea cliff. The archaeological site is offset by the fault providing an excellent opportunity to constrain the late Holocene slip rate and timing of most recent activity on the fault.

Our preliminary studies at the site included detailed mapping, hand auger borings, archaeological test pits, and a paleoseismic trench. Based on an array of 130 shallow borings at 5- to 1-m spacing, the northern margin of the archaeological site appears to be offset right laterally approximately 9 to 11 meters. We use this offset margin as a piercing line from which to measure fault slip rate. The perimeter of the site was defined by the presence or absence of "midden" debris: shell, bone, chert and other artifacts from prehistoric coastal human occupation. Borehole samples were collected at 10- to 20-cm intervals within the organic horizon. Samples containing a qualitatively determined 5% or greater midden concentration were interpreted to be within the boundary of the site. Midden debris of less than 5% concentration was interpreted to be on the site fringe, largely influenced by on-going bioturbation and erosion. Radiocarbon age estimates from shells and the artifact assemblage within the

midden suggests the presence of a Middle Period component (1 to 2 ka). The range of slip rate offered from these preliminary age estimates is about 4.5 to 11 mm/yr on the northern onshore reach of the San Gregorio fault. We hope to refine this slip rate based on further detailed study of the archaeological site.

Three active traces of the San Gregorio fault were identified in our paleoseismic trench excavated near the southeast boundary of the archaeological site. The fault traces appear to bound a small graben containing ponded middle Holocene alluvial deposits. The ponded deposits have been deformed by multiple surface rupturing earthquakes. At least two events have occurred since inception of cultural deposition at the site, as evidenced by displacement of midden-bearing strata. Preliminary data suggest that the most recent event occurred approximately 650 years ago.

References Cited

Kelson, K.I., Lettis, W.R., and Lisowski, M., 1992, Distribution of geologic slip and creep along faults in the San Francisco Bay region, in Borchardt, G., and others, eds., Proceedings of the Second Conference on Earthquake Hazards in the San Francisco Bay Area: California Department of Conservation, Division of Mines and Geology Special Publication 113, p. 31-38.

Lettis, W.R., Hanson, K.L., Weber, G.E, and Noller, J.S., 1994, The San Gregorio/Hosgri fault system, California - An evaluation of the style and rate of Quaternary deformation: Journal of Geophysical Research, in review.

Weber, G.E., and Lajoie, K.R., 1979, Late Pleistocene rates of movement along the San Gregorio fault zone, determined from offset marine shoreline angles, in Weber, G.E., Lajoie, K.R., and Griggs, G.B., eds., Coastal tectonics and coastal geologic hazards in Santa Cruz and San Mateo Counties, California: Field Trip Guide for Cordilleran Section of the Geological Society of America, 75th Annual Meeting, p. 101-111.

Recent Reports and Publications

Noller, J.S., Lightfoot, K., Simpson, G.D., Thompson, S.C., Lettis, W.R., Kelson, K.I., and Hylkema, M.A., 1994, Use of geoarchaeological techniques in paleoseismic investigations of the San Andreas and San Gregorio faults, California: Part I [abs.]: Geological Society of America Annual Meeting, Seattle, WA, Abstracts and Program.

Lightfoot, K., and Noller, J.S., 1994, Use of geoarchaeological techniques in paleoseismic investigations of the San Andreas and San Gregorio faults, California: Part II [abs.]: Geological Society of America Annual Meeting, Seattle, WA, Abstracts and Program.

Simpson, G.D., Noller, J.S., Thompson, S.C., Lettis, W.R., Lightfoot, K., and Hylkema, M.A., 1994, Use of geoarchaeological techniques in paleoseismic investigations of the San Andreas and San Gregorio faults, California: Part III [abs.]: Geological Society of America Annual Meeting, Seattle, WA, Abstracts and Program.

Thompson, S.C., Noller, J.S., Simpson, G.D., Hylkema, M.A., and Lettis, W.R., 1994, An offset archaeological site constrains Holocene tectonic displacement of the San Gregorio fault, California[abs.]: Geological Society of America Annual Meeting, Seattle, WA, Abstracts and Program.

PALEOSEISMIC AND GEOARCHAEOLOGIC INVESTIGATIONS OF THE NORTHERN SAN ANDREAS FAULT, FORT ROSS, CALIFORNIA

Grant Award # 1434-94-G-2474

Jay Stratton Noller and Gary D. Simpson
William Lettis & Associates, Inc., 1000 Broadway, Suite 612, Oakland, CA 94607
(510)832-3716v; (510)832-4139f;wla@netcom.com

Kent Lightfoot
Department of Anthropology, University of Calitornia, Berkeley, CA 94702
(510)642-1309v; (510)643-8557f

Element II: Evaluating Earthquake Potential

Introduction

The purpose of our studies (1990-present) at the Archae Camp site at Fort Ross along the Sonoma Coast in northern California is two-fold: (1) develop an independent record of past earthquakes on the northern San Andreas fault, including the timing of past earthquakes and average slip rate for the late Holocene; and (2) develop and refine techniques related to the application of archaeology to paleoseismology. At Archae Camp, we are addressing the issues of (1) the history of surface-rupturing events on the North Coast segment of the San Andreas fault; (2) the relationship of the 1906 event (e.g., amount of slip) with past events; (3) the character of other fault parameters (e.g., slip rate, slip per event); (4) the application of archaeological techniques to paleoseismic studies; and (5) the segmentation of the North Coast segment of the San Andreas fault.

Our research program on the northern San Andreas fault involves concurrent archaeological and paleoseismic investigations (Noller and others, 1993). The archaeological study provides the means to palinspastically reconstruct the boundaries and subzones of an archaeological site, thereby providing estimates of cumulative slip over specific time intervals. Paleoseismic trenching provides data to assess fault location and estimate the number of large-magnitude earthquake events during the same time interval. By combining the results of these approaches we can deduce the average slip per event and determine whether the northern San Andreas fault only breaks in 1906-size events (i.e. characteristic recurrence model) or also breaks in smaller magnitude events (i.e. poisson recurrence model).

Study Area

The Archae Camp site at Fort Ross State Historic Park was selected as the location for this study on the basis of: (1) documented surface rupture and offset during the 1906 San Francisco earthquake (Lawson and others, 1908), including a fence offset by 3.7m during the 1906 event that is still present at the site; (2) a prominent, well-defined archaeological site lies astride the 1906 rupture trace; (3) surface rupture during 1906 was concentrated on a single strand through the archaeological site; (4) the local prehistoric record of human occupation spans the past 5,000 to 8,000 years, providing a potential paleoseismic record of earthquakes on the San Andreas fault since the middle Holocene; (5) the site is located halfway between two other detailed paleoseismic study sites on this segment of the San Andreas fault (90 to 100 km to Olema and Point Arena, respectively); and (6) the archaeology of the site has been studied previously.

Methods
Paleoseismic trenches were excavated by backhoe across the San Andreas fault to reveal the subsurface character of the fault and the deformation of adjacent bedrock, sediment and soil units. Exposed structural and stratigraphic relations were logged and described.

We are currently testing the applicability of archaeological techniques to the definition of temporally constrained piercing lines across faults. Potential piercing lines we are assessing at Fort Ross include the archaeological site boundary, features within the archaeological site complex (e.g., house structures), and gradients in the concentration of artifacts (e.g., chipped stone refuse) or phosphorous (e.g., bone and human waste). Ages of the offset ethnostratigraphic units are based on (1) radiocarbon age estimates on charcoal and buried soil; (2) obsidian-hydration age estimates on obsidian artifacts; and (3) the local archaeological chronology.

Trench Investigations
At this location, the fault zone consists of a single trace expressed by a single southwest-facing topographic scarp, linear troughs, ridges, and closed depressions. The depressions are filled in part by sediment shed from the scarp across the fault trace and in part by colluvial deposits from the opposite slope, and ponded sediment. We excavated four parallel trenches across the San Andreas fault at Archae Camp. The trenches expose structural relations and displaced strata that enable us to assess the number and timing of late Holocene surface ruptures at the site. Three of the trenches (ACT-1, -2, and -3) extend from the main archaeological site, across the fault scarp and into the linear depression southwest of the fault. The fourth trench (ACT-4) was excavated across a prominent "mole-track" near the offset fence. Trenches ACT-1 and ACT-2 were excavated in 1991 across the fault. A third trench (ACT-3) is located within the swale about 15 m upslope of trenches ACT-1 and ACT-2. Both trenches ACT-3 and ACT-4 were excavated in September 1994.

Event Recognition and Dating
On the basis of stratigraphic and structural relations exposed in the four trenches, we currently identify six and possibly seven late Holocene surface-rupture events on the North Coast segment of the San Andreas fault at Archae Camp. Distinct surface-rupture events are defined on the basis of distinct upward fault terminations, scarp-derived colluvial deposits, fissure fills, and cross-cutting stratigraphic relations.

We currently are working out the sequence of events exposed in the new trenches, ACT-3 and ACT-4. Trench ACT-3 displays four distinct fault splays or groups of splays that are each truncated by a distinct colluvial unit. Each of these upward fault terminations is interpreted to represent a single surface-rupturing event. We are currently describing this trench and working on sampling of materials for dating. Trench ACT-4 displays a "flower-structure" that truncates colluvial units on a northeast-facing hillslope near the offset fence. The "mole-track" of the 1906 event is still evident in the upper trench profile. Events are recognized by truncated colluvial deposits and a fault-scarp derived colluvial wedge. As with Trench ACT-3, we are currently describing this trench and working on sampling of materials for dating.

Archaeological Investigations
The archaeological phase of our study focuses on the Archae Camp site (California registered site no. CA-SON-670), an areally extensive, multi-component archaeological deposit. Previous archaeological excavations show that the 4000 m^2 site was continuously occupied by Native Americans for more than 3,000 years. The site is located on a wide, side-hill bench between the fault and Fort Ross Creek, and is transected by and offset along its western margin by the fault.

Archae Camp Stratigraphy

The Archae Camp site has had repeated prehistoric occupations of significant duration. The deepest excavated levels at the site contain artifacts dating to the Middle Archaic (3,000 - 1,000 B.C.)(Stillinger, 1975; Lightfoot and others, 1991), although Lower Archaic period (6,000 - 3,000 B.C.) occupations have not been ruled out. Archaeological materials are dominantly stone artifacts, including shouldered lancelote points and other projectile points, bifaces, choppers, fire-cracked rocks, and net weights. Bone, shells, and other faunal material are rare at this site.

The Archae Camp site consists of a long-use-duration midden deposit that drapes over and down the southwest-facing fault scarp, and is limited to an approximate 50-m width along and parallel to the northeast side of the fault. The concentration and age-distribution of buried obsidian artifacts in the main site adjacent to the fault show a relatively confined locus of Upper Archaic site materials encompassed by a wider distribution of Lower and Upper Emergent artifacts. The artifact concentrations are truncated on the southwest by the fault. Historic surficial site materials extend into the adjacent swale, across the 1906 rupture of the fault.

Cultural materials are concentrated at restricted locations and depths in the swale west of the main site. The southeastern boundary of this concentration is coincident with that of the main site. Thickness of artifact-bearing strata within the swale increases to the northwest, well beyond the main site. Northwest along the swale, at the latitude of the northern margin of the main site, the swale strata contain cultural materials buried at a depth of about 50 cm. The assemblage of artifacts in this unit are of Upper Archaic to Lower Emergent affinity.

Farther to the northwest, a relatively deeply buried deposit of older obsidian and chert lithic artifacts is present at depths of 70 to 120 cm. This concentration of materials is bounded on the northeast by the fault and extends more than 10 m to the southeast from the fault. Along the fault, the swale site extends about 23 m farther to the northwest of the northern margin of the main site. Obsidian artifacts in this concentration have hydration-rind thicknesses indicative of Middle to Upper Archaic, and Lower Emergent periods. Scattered older artifacts were recovered farther to the north end of this concentration.

The archaeological materials within the swale, especially those located tens of meters northwest of the main site, are interpreted to represent offset archaeological detritus from the main site. Through successive displacement events during the past 2,500 years on the fault, the swale deposits containing the artifacts were displaced northwestward from the main archaeological site.

Matching Offset Archaeological Sites

We use cultural materials of the Archae Camp site to define piercing lines across the fault. Our approach to mapping these piercing lines involved (1) defining the limit of contiguous site materials and (2) identifying unique features within the site boundaries. With the former method, the site boundary was determined by excavation of test pits and boreholes at selected locations through the site. For the latter method, we established an orthogonal array of excavations and mapped piercing lines on the basis of several key indicators, including the density of index artifacts and the limit of the anthropic soil horizon.

Matching of piercing lines across the fault is made on the basis of correlating age and assemblage of artifacts of the main site with artifacts southeast of the fault. Because the two sites provide at least two pairs of piercing points to match, there is a high potential for measuring the amount of slip along the fault since the time of inhabitation.

Slip-Rate Estimates

We estimate rate of slip along the northern San Andreas fault by measuring the distance that the cultural materials of the swale deposits have been offset from the main site. Our preferred piercing lines across the fault are defined (1) (in map view) by the northwestern boundaries of these two Lower Emergent archaeological units, and (2) (in the plane of the fault) by the loci of Middle to Upper Archaic artifacts within the northwestern part of the main site and the swale. The northwestern site boundary is chosen because it represents the leading edge of the distribution of cultural artifacts, and because the southeastern boundaries of the extent of cultural materials on either side of the fault are poorly constrained.

On the basis of data obtained from the surface and subsurface excavations, we prepared a plot of the distribution of artifacts adjacent to the fault. The maximum possible range of projections of the northwestern site boundaries to the fault result in a resolution of less than five meters . Using our preferred northwestern boundaries, this site component has been offset by about 23 m. Radiocarbon and obsidian-hydration age estimates provide an age range of A.D. 620 and 800 for the deposits containing the artifacts, thus yielding a preliminary slip rate of 17-19 mm yr^{-1}.

In a fault-parallel section we have plotted the distribution of artifacts and their concentration within two meters of the fault. With this projection, a single concentration of Middle to Upper Archaic artifacts is present on either side of the fault, except that they are displaced right-laterally by 26 m. These artifacts are included in a younger unit estimated to 1,150 to 1,330 years old, providing a preliminary slip-rate estimate of 19-22 mm yr^{-1}.

References Cited

Lawson, A.C., 1908, The California earthquake of April 18, 1906: Report of the State Earthquake Investigation Commission, v. 1, The Carnegie Institution, Washington, D.C.

Lightfoot, K., Wake, T., and Schiff, A., 1991, The archaeology and ethnohistory of Fort Ross, California. Volume 1: Introduction: Contributions of the University of California Archaeological Research Facility 49.

Noller, J.S., Kelson, K.I., Lettis, W.R., Wickens, K.A., Simpson, G.D., Lightfoot, K., and Wake, T., 1993, Paleoseismic and geoarchaeologic investigations of the northern San Andreas fault, Fort Ross State Historic Park, California: Final Technical Report, U.S.G.S. NHERP Grant # 14-08-0001-G2076, 17 pp.

Stillinger, R., 1975, A preliminary analysis of Sonoma S.D.A.-1 (CA-SON-670). Report on file, MS# s-6295, Northwest Information Center, Sonoma State University.

Recent Reports and Publications

Noller, J.S., Lightfoot, K., Simpson, G.D., Thompson, S.C., Lettis, W.R., Kelson, K.I., and Hylkema, M.A., 1994, Use of geoarchaeological techniques in paleoseismic investigations of the San Andreas and San Gregorio faults, California: Part I [abs.]: Geological Society of America Annual Meeting, Seattle, WA, Abstracts and Program.

Lightfoot, K., and Noller, J.S., 1994, Use of geoarchaeological techniques in paleoseismic investigations of the San Andreas and San Gregorio faults, California: Part II [abs.]: Geological Society of America Annual Meeting, Seattle, WA, Abstracts and Program.

Simpson, G.D., Noller, J.S., Thompson, S.C., Lettis, W.R., Lightfoot, K., and Hylkema, M.A., 1994, Use of geoarchaeological techniques in paleoseismic investigations of the San Andreas and San Gregorio faults, California: Part III [abs.]: Geological Society of America Annual Meeting, Seattle, WA, Abstracts and Program.

PALEOSEISMIC LIQUEFACTION STUDIES - - CENTRAL U. S. AND PACIFIC NORTHWESTERN U. S.

9950-14185
9950-13185

Stephen Obermeier
Branch of Earthquakes and Landslide Hazards
MS 922, U. S. Geological Survey
Reston, Virginia 22092
703-648-6791

The purpose of this project is to determine where prehistoric earthquake shaking has been strong enough to cause liquefaction, as evidenced by the formation of liquefaction-induced features. The threshold magnitude for significant liquefaction is about M 6. Relict liquefaction-induced features normally take the form of sand- or sandy gravel-filled dikes and sills. These features commonly are preserved in abundance in the geologic record.

Field searches for relict liquefaction features were conducted mainly in two regions during 1994: (1) the states of Ohio and Illinois in the central U. S., and (2) the states of Oregon and Washington in the Pacific Northwestern U. S.

CENTRAL U. S.

Background

Illinois, Indiana, and Ohio have had many small and slightly damaging earthquakes during the 200 years of historic record. Large parts of these states have extensive alluvial lowlands, which range in age from late Wisconsinan to modern. The alluvium is commonly sand-rich, and the ground-water table has been high throughout much of the Holocene. Altogether, the region has many places that have been conducive to formation of liquefaction features during the previous several thousand years. Sediments conducive since early Holocene time are much less common, but still occur in many widespread locales; the valleys are so wide that the laterally cutting streams have not had the opportunity to remove the dikes.

The approach to locating dikes has been to search eroding banks of streams. During the previous three years, hundreds of prehistoric dikes have been found in southern Indiana and Illinois; evidence for a very strong earthquake (M about 7.5) about 6,100 years ago, centered near the Wabash River of Indiana-Illinois, has been found (Obermeier et al., 1993; Munson et al., 1994). In addition, evidence for several other prehistoric earthquakes has been found in the southern half of Indiana (Munson et al., 1994) and the southern one-third of Illinois (Obermeier, unpublished data). The Indiana earthquakes are reasonably constrained in terms of ages and epicentral regions. In Illinois, though, much more work is required.

West-central Ohio has had at least 40-felt earthquakes since

1875, centered about the town of Anna. The largest of these, in 1937, had an estimated magnitude of 5.5. This magnitude is about the same as the largest historic earthquake in the Wabash Valley of Indiana-Illinois, where evidence for many prehistoric earthquakes exceeding magnitude 5.5 has been found. Thus, there seemed the possibility that much larger prehistoric earthquakes had struck near Anna.

Investigations and Results

More than 50 km of stream banks throughout southwestern Illinois and central Illinois were searched from a canoe. Many dikes have been located through the Kaskaskia River valley. All the largest dikes have ages of thousands of years. Some have widths exceeding 30 cm. Some large dikes are within 40 km of St. Louis, Missouri. A few of the smaller dikes may have originated during the 1811-12 New Madrid earthquakes, but the majority are probably at least mid-Holocene in age on the basis of severity of weathering of sediment in the dikes and radiocarbon ages of source sediments. Field evidence to support an earthquake origin of the dikes is very strong.

I was also involved in investigation of dikes discovered by researchers of the Illinois State Museum, who are funded by a grant from the NEHRP program. Most of the combined effort was in central Illinois at a site on the Sangamon River. At this site there are dikes exceeding 30 cm in width that probably formed in early Holocene time. Preliminary field evidence to support an earthquake origin appears strong.

In western Ohio, more than 100 km of stream banks were searched in the vicinity of the town of Anna. A canoe was used to search portions of the Auglaize, Great Miami, Stillwater, and St. Mary's Rivers and Loramie Creek. Portions of the Scioto and Little Scioto Rivers in north- central Ohio were also searched, as were widely scattered sand and gravel pits which contained thick glaciofluvial deposits and had high water tables. The amount and quality of outcrop was generally not very good; still, there was adequate outcrop to express some confidence that the region has not experienced an earthquake above magnitude M 7 the past several thousand years. However, the paucity of outcrop did not exclude the possibility of earthquakes of lower magnitudes.

Reports Published

Obermeier, Martin, Frankel, Youd, Munson, Munson, and Pond, 1993, Liquefaction evidence for strong Holocene earthquakes in the Wabash Valley of southern Indiana-Illinois, with a preliminary estimate of magnitude: U. S. Geological Survey Prof. Paper 1536.

Obermeier, Bleuer, Munson, Munson, et al., 1991, Evidence of strong earthquake shaking in the lower Wabash Valley from prehistoric liquefaction features: Science, v. 251, p. 1061-1063.

Hajic, Obermeier, Munson, Wiant, Tankersley, and Garniewicz, 1994, Distribution and dating of prehistoric earthquakes in

southwestern Illinois: (abstract) 1994 GSA Annual mmeeting, Seattle, p. A-190.

PACIFIC NORTHWESTERN U. S.

Background

Coastal Washington has been almost devoid of historic earthquakes. The only occurences have been scattered small events. Atwater (1992) estimated that great earthquakes have occurred twice the past two thousand years on the basis of geologic evidence for episodes of sudden coastal submergence. One episode took place about 300 years ago and less constrained evidence indicates another episode took place 1,400 to 1,900 years ago. The earthquakes were interpreted to have originated by subduction of the oceanic plate (Juan de Fuca) beneath the continental plate (North American). To test the great earthquake hypothesis, I initiated a search for relict liquefaction features.

In 1991 the search was mainly in coastal Washington, in the Chehalis and Humptulips River valleys. No definitive liquefaction evidence was found that could be associated with subduction earthquakes, although dikes probably from other tectonic sources were discovered. Therefore in 1992 a search was initiated in the Columbia River valley, and numerous dikes associable with the subduction earthquake of 300 years ago were found. Fieldwork in 1993 extended the region of previously discovered dikes in the Columbia River valley and in the Chehalis Valley. In 1994 the field effort was extended into the Willamette Valley in Oregon. Purpose of searching that valley was based on proximity to the coast; the valley is centered about 80 km from the coast and therefore should have been close enough to the seismic source to record strong shaking from great subduction earthquakes, providing that liquefiable sediments were present.

Investigations and Reports

The search in 1994 centered on the Calapooia River, located about 10 to 30 km east of the town of Corvallis. This river was selected because of the abundance of moderately thick, clean sands that have been laid down in the region. About 30 km of the river was searched from a canoe. At least 6 km of fresh outcrop was exposed.

Small dikes of probable earthquake-liquefaction origin were discovered at seven widely scattered sites. All dikes penetrate host sediments that are nearly identical in terms of stratigraphy (a weathered clay overlain by a thick silt). Therefore, all dikes are suspected to have formed at the same time. The dikes are highly weathered near their tops, so the dikes could not have formed during the earthquake of 300 years ago, and probably not during any earthquake 1,400 to 1,900 years ago. A local seismic source is plausible, but inadequate outcrop has been searched to define the pattern of dike sizes and thereby a source region.

Samples of sand were collected at widely spaced sites as a means to estimate relative density of sands that occur along the

Calapooia River. Thereby a lower limit of shaking can be calculated for liquefaction of the sands. Prof. S. Dickenson of Oregon State Univ.is doing the relative density measurements.

Results of a preliminary engineering study to assess the strength of seismic shaking in the Columbia River valley during the subduction earthquake of 300 years ago are given in U. S. Geol. Survey Open-File Report 94-589.

Reports Published

Obermeier, 1994, Preliminary limits for the strength of shaking in the Columbia River valley and the southern half of coastal Washington, with emphasis for a Cascadia subduction earthquake about 300 years ago: U. S. Geological Survey Open-File Report 94-589.

Obermeier, 1994, Use of liquefaction features for paleoseismic interpretations: U. S. Geological Survey Open-File Report 94-663.

Dickenson, Obermeier, Roberts, and Martin, 1994, Constraints on earthquake shaking in the lower Columbia River region during late-Holocene time: Proceedings of the Fifth U. S. National Conference on Earthquake Engineering, vol. 3, p. 313- 322.

Obermeier, Atwater, Benson, Peterson, Moses, Pringle, and Palmer, 1993, Liquefaction about 300 years ago along tidal reaches of the Columbia River, Oregon and Washington: EOS, Transactions of the American Geophysical Union, v. 74, no. 43, p. 198.

Palmer, Dickenson, Roberts, and Obermeier, 1993, Results of a reconnaissance geotechnical survey along the lower Columbia River: EOS, Transactions of the American Geophysical Union, v. 74, no. 43, p. 199.

Moses, Obermeier, and Palmer, 1993,Liquefaction along the Chehalis and Humptulips Rivers, Washington: EOS, Transactions of the American Geophysical Union, v. 74, no. 43, p. 201.

Moses, Palmer, and Obermeier, 1994, Gravel liquefaction as an indication of prehistoric ground shaking in western Washington: (abstract), 1994 Geol. Soc. Am. annual meeting, Seattle, p. A-253.

References Cited

Atwater, 1992, Geologic evidence for earthquakes during the past 2,000 years along the Copalis River, southern coastal Washington: Journal of Geophysical Research, v. 97, no. B2, p. 1901-1919.

Munson, Munson, and Bleuer, 1994, Late Pleistocene and Holocene earthquake-induced liquefaction in the Wabash Valley of southern Indiana: U. S. Geological Survey Open-File Report 94-176, p. 553-557.

Variations in Electrical Properties Induced by Stress Along the San Andreas Fault at Parkfield, California

Grant 14-08-0001-G1357

Stephen K. Park
Tien Chang Lee
Institute of Geophysics and Planetary Physics
University of California
Riverside, California 92521

(909)787-4501

Introduction

Fluctuations of resistivity are monitored with telluric currents in Parkfield. The array uses grounded telephone lines as dipoles (Figure 1). The analysis was discussed in Park [1991]. We look at daily fluctuations of the telluric coefficients relating Dipoles 1 through 6 to the reference dipoles of Dipoles 7 and 8. Thus, we are looking at relative variations, rather than absolute ones. Changes in the telluric coefficients are directly related, albeit through the response of a complex, heterogeneous earth, to changes of resistivity.

Discussion of Data

Results of the analysis for 1994 for Dipoles 1 through 6 are shown in Figures 2 through 7. The fluctuations of the telluric coefficients are projected onto directions perpendicular (P1 in each frame in Figures 2-7) and parallel (P2 in each frame) to the San Andreas fault. As a measure of data quality, the coherency (bottom plot in each frame) between the observed and predicted signals on each dipole is shown. A coherency of 0.998 is equivalent to a fractional noise level of 6%. These projections are further smoothed with a nine day running average which is weighted by the inverse of the square of the coherency (which is a measure of the relative noise). The error bars for each daily point are standard errors calculated from this running weighted average. Based on fluctuations of the projections for all of 1988 and 1989, standard deviations for the daily projections were calculated. The 95% confidence intervals (approximately 2σ) are shown with dashed lines in Figures 2 through 7.

There are several gaps in the data that are due to system problems or noise levels above the level required to yield a coherency of 0.998 or better. Traditionally, the latter problem is manifested on Dipoles 2, 5, and 6 and is due to noise from the electrode at Lc (Figure 1). Gaps on all of the dipoles during the first 80 days of the year and between days 300 and 325 are due to an intermittent noise source on the telephone line to Hr resulting from precipitation. The other major gap in the data occurred between days 210 and 232 on dipoles 2, 5, and 6 due to telephone line problems on the line to Lc. All other gaps are the result of noisy data.

Significant deviations can be identified in one of two ways. First, points which lie outside the 95% confidence intervals can be significant. Second, fluctuations with nonoverlapping error bars may be important. For example, the only significant variations seen so far this year occurred on dipole 4 (Figure 5) between days 180 (June 29) and 207 (July 26) and between days 238 and 280 (August 26 - October 7). Both of these fluctuations are

particularly important because they occur on a dipole that has been very stable for the past 6 years. Hence, a fluctuation of 1% is a large variation for dipole 4. Note that these fluctuations are also very clear in the unsmoothed projections (Figure 8). This dipole terminates on a pressure ridge of the San Andreas fault near Harlan Ranch and straddles a portion of the fault zone just south of Parkfield (Figure 1). Simulation of the observed signal with a 3-D resistivity modeling program is planned for the near future. At this time, we have no explanation for this signal because other monitoring arrays in the region did not observe any temporally coincident anomalies.

Other Results

Analysis of formal errors for the processing used to generate the projections shown in Figures 2-8 has been completed, and these errors are usually smaller than the scatter in the projections between adjacent days. Tentatively, this result suggests that the scatter is not due to noisy data as we had assumed. Another possible source of scatter is a bias from the polarization of the magnetic source. Variations in preferential polarization from day to day may result in slightly different daily estimates of the telluric coefficients. More stable results are obtained if daily projections are smoothed as shown in Figures 2-7. This smoothing may effectively eliminate any bias due to source polarization. We are currently testing if this is the source of the scatter, and will modify the processing accordingly if needed.

Conclusions

Two significant fluctuations have been seen on a normally stable dipole in the past year. These fluctuations were small (1-2%), and lasted from 27 to 42 days each. They were not accompanied by any unusual signals on other monitoring arrays or by seismic activity. Three-dimensional resistivity modeling will determine whether realistically small changes of resistivity could result in the observed fluctuations.

Reports Published

Park., S.K., Seismoelectromagnetic effects, Invited review paper for 12th Induction Workshop, August 7-13, 1994, Brest, France, 41 ms. pgs.

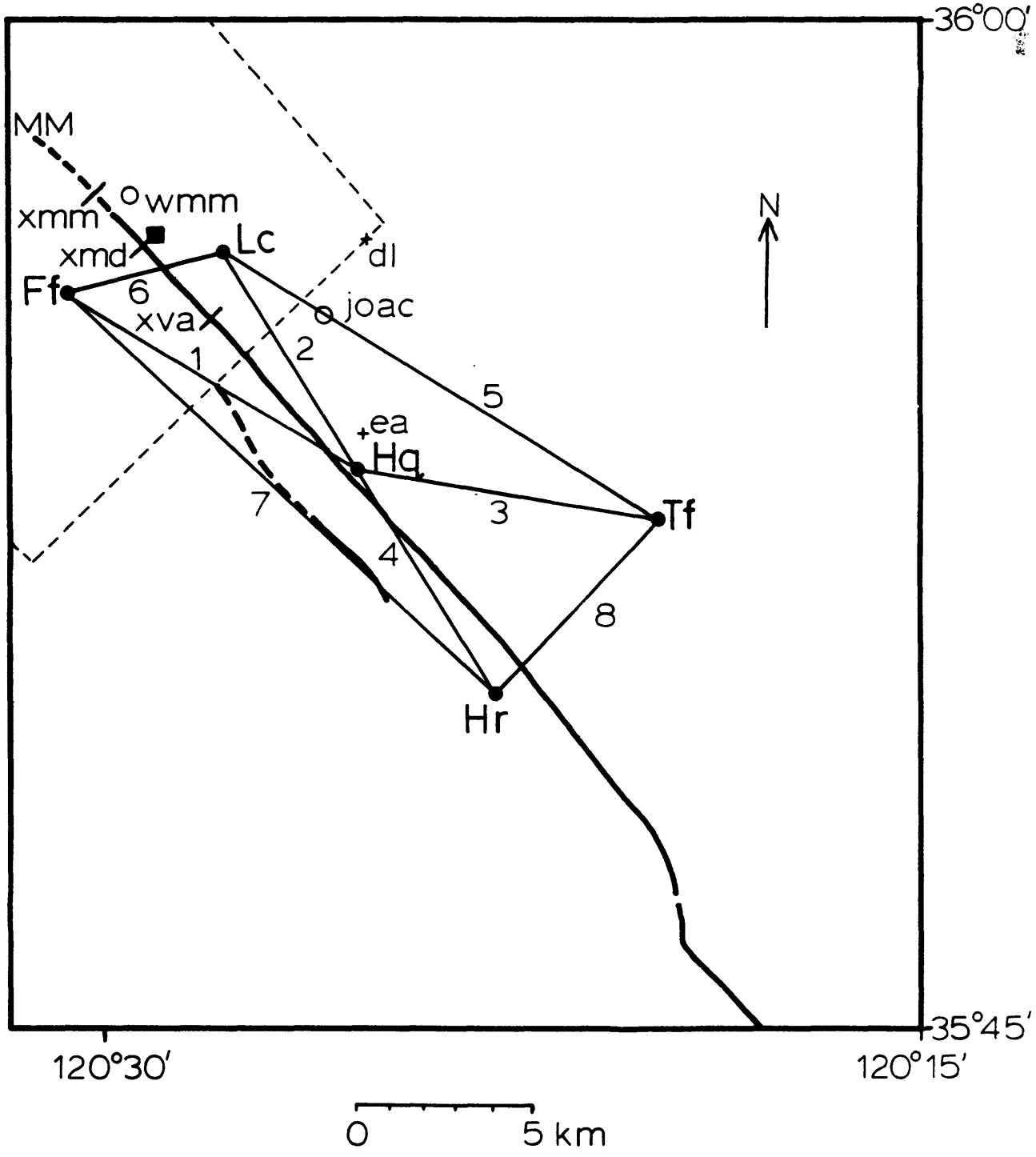

Figure 1 - Telluric monitoring array in Parkfield. Electrodes are marked with dots and electronically created dipoles are shown with lines.

Figure 2 - Residual analysis for Dipole 1 for 1994. The first plot is the projection of the residual on the major eigenvector with a scale of +2% to -2% and the second is the projection on the minor eigenvector with a scale of +5% to -5%. Coherencies are between the signal predicted using the telluric coefficients and the measured signals are shown between .998 and 1.000. 95% confidence intervals are shown with dashed line on the projection plots.

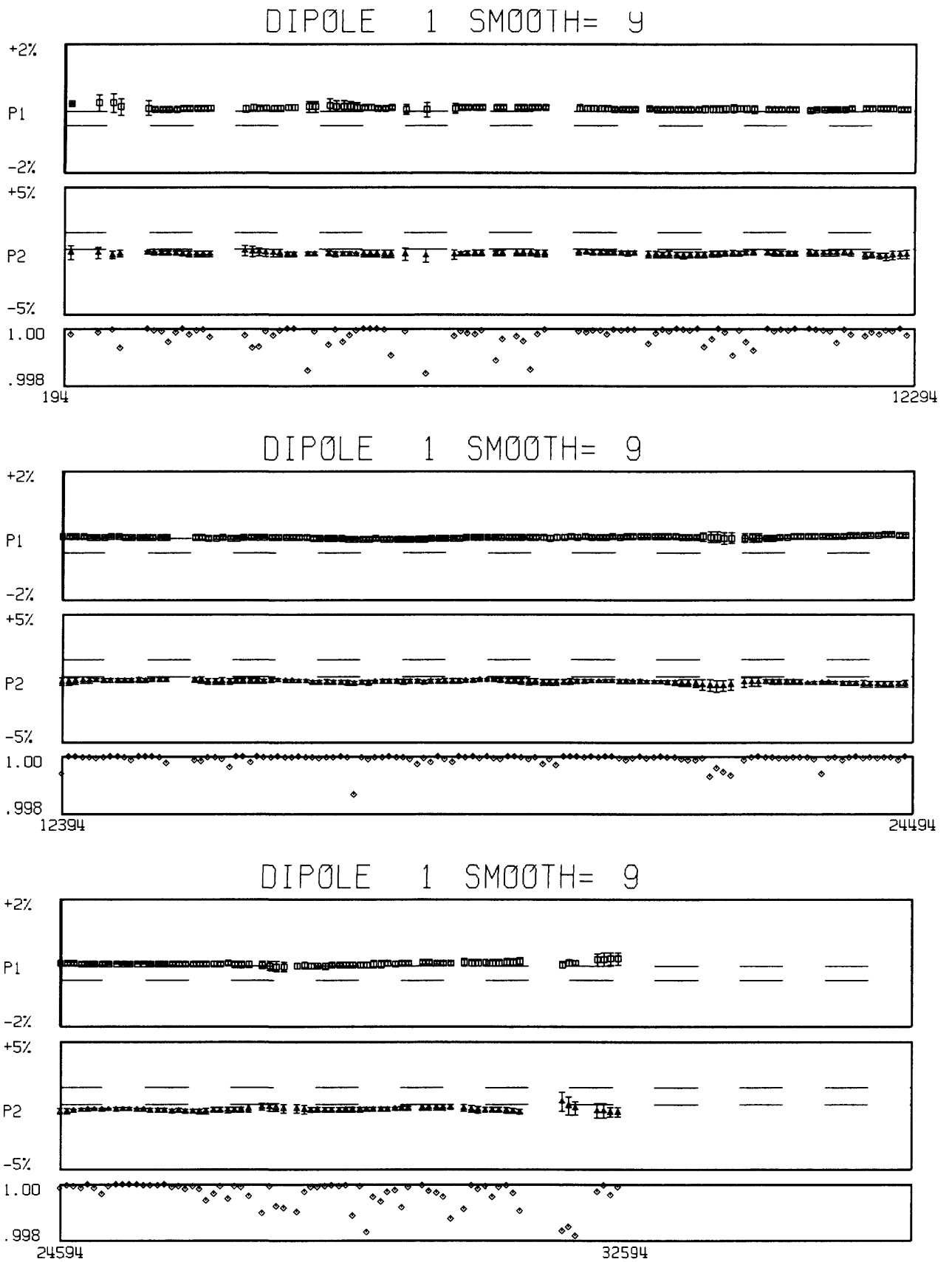

Figure 3 - Residual analysis for Dipole 2 for 1994. See caption of Figure 2 for explanation.

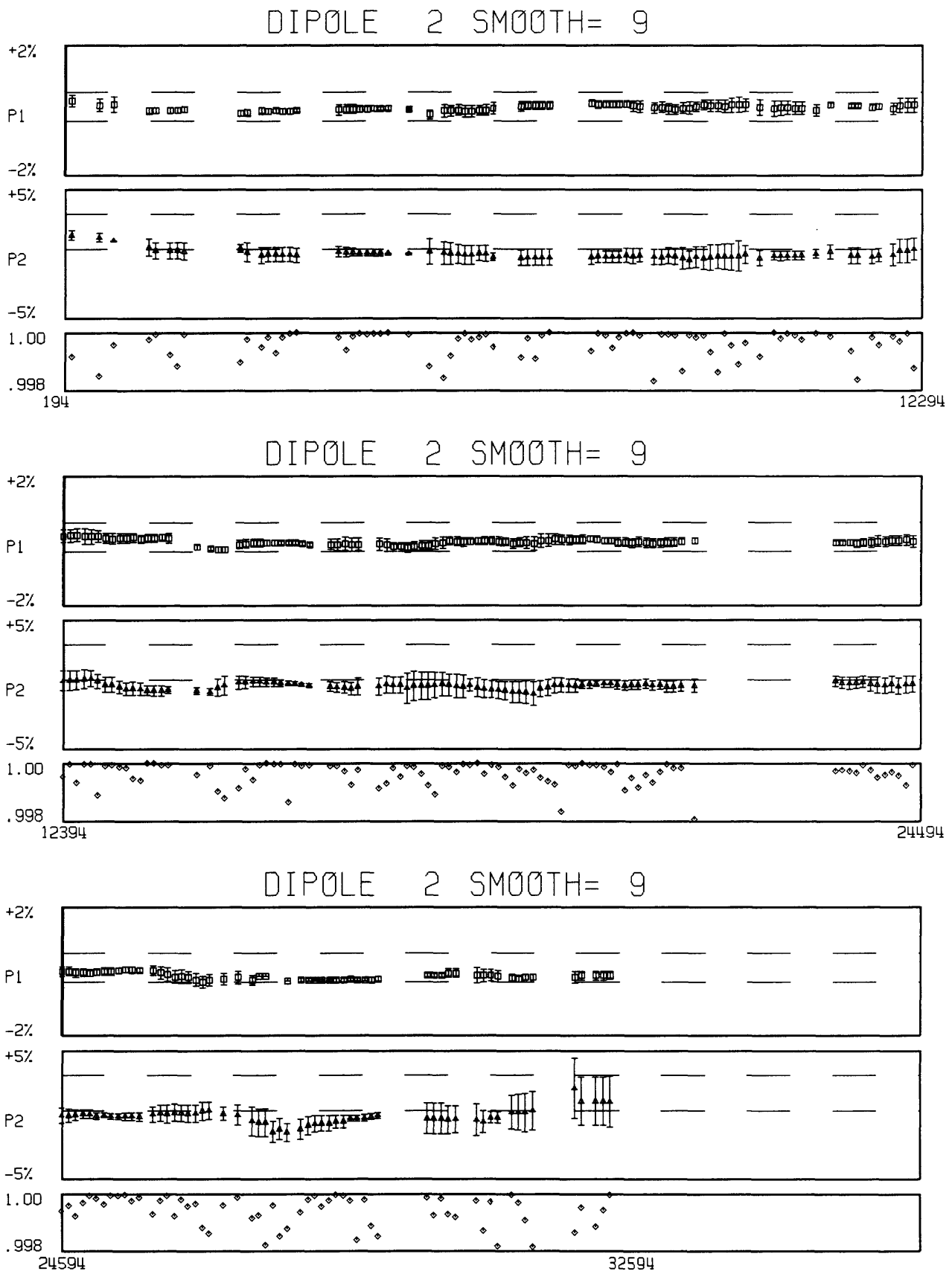

Figure 4 - Residual analysis for Dipole 3 for 1994. See caption of Figure 2 for explanation.

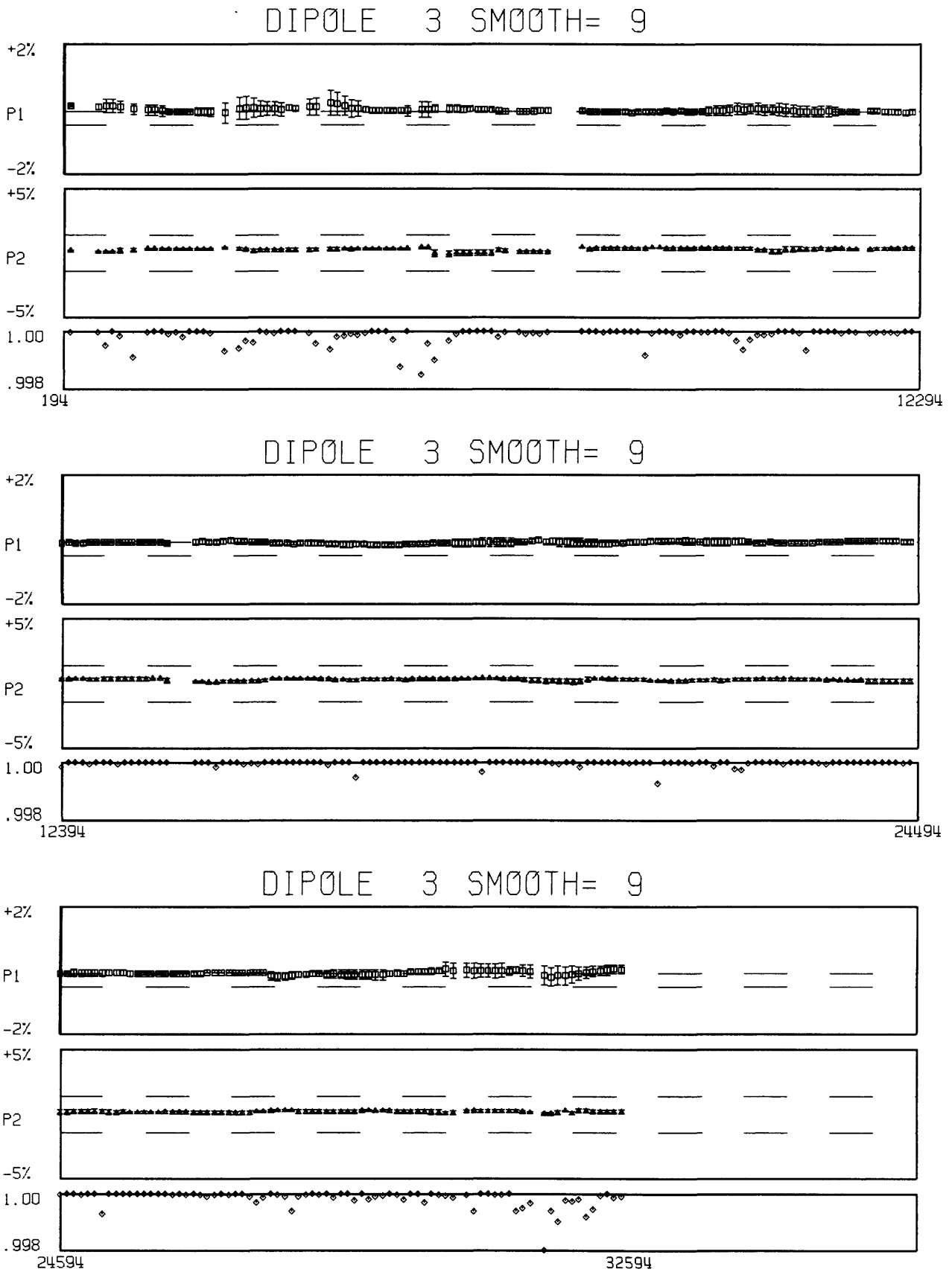

Figure 5 - Residual analysis for Dipole 4 for 1994. See caption of Figure 2 for explanation.

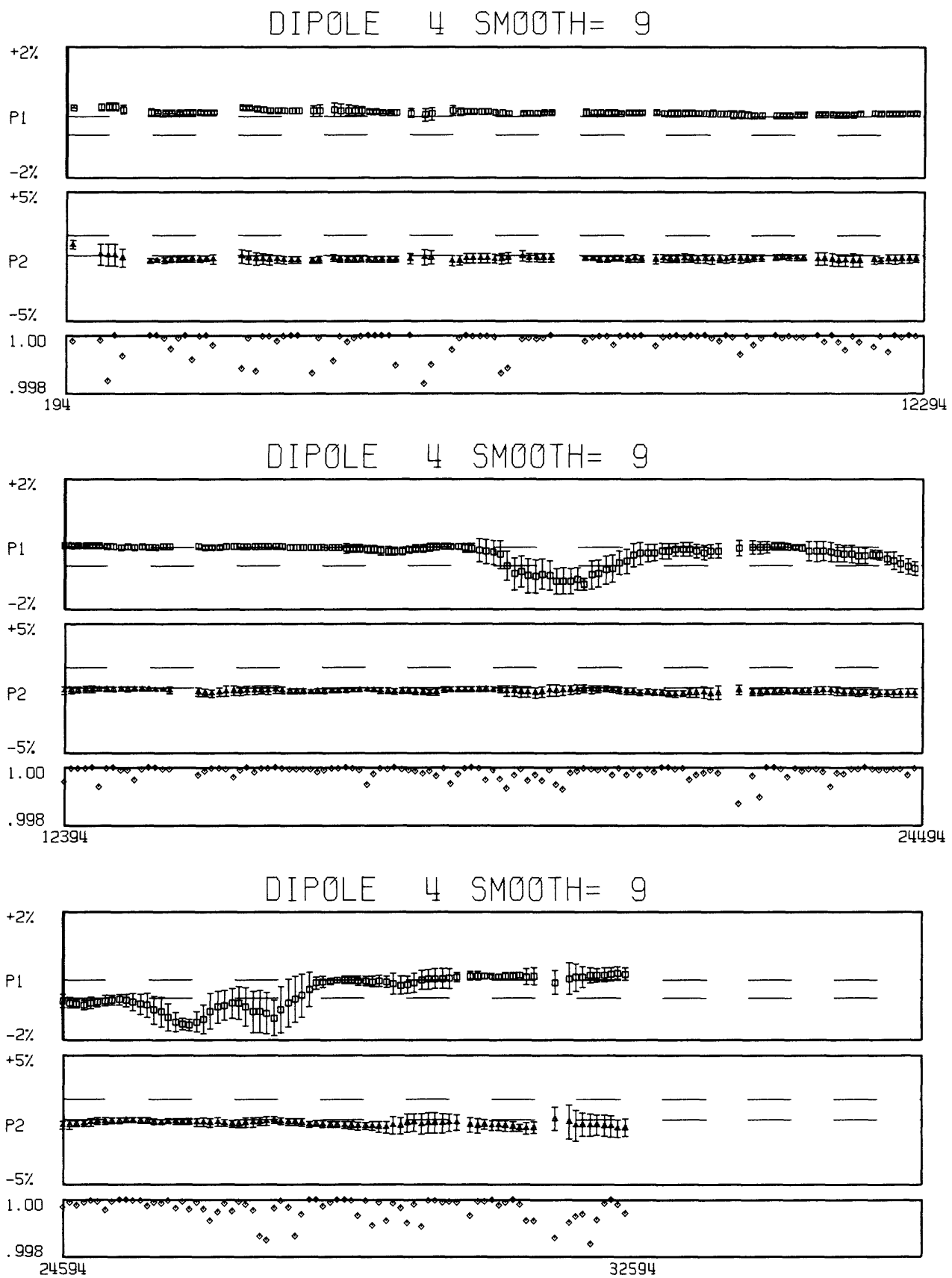

Figure 6 - Residual analysis for Dipole 5 for 1994. See caption of Figure 2 for explanation.

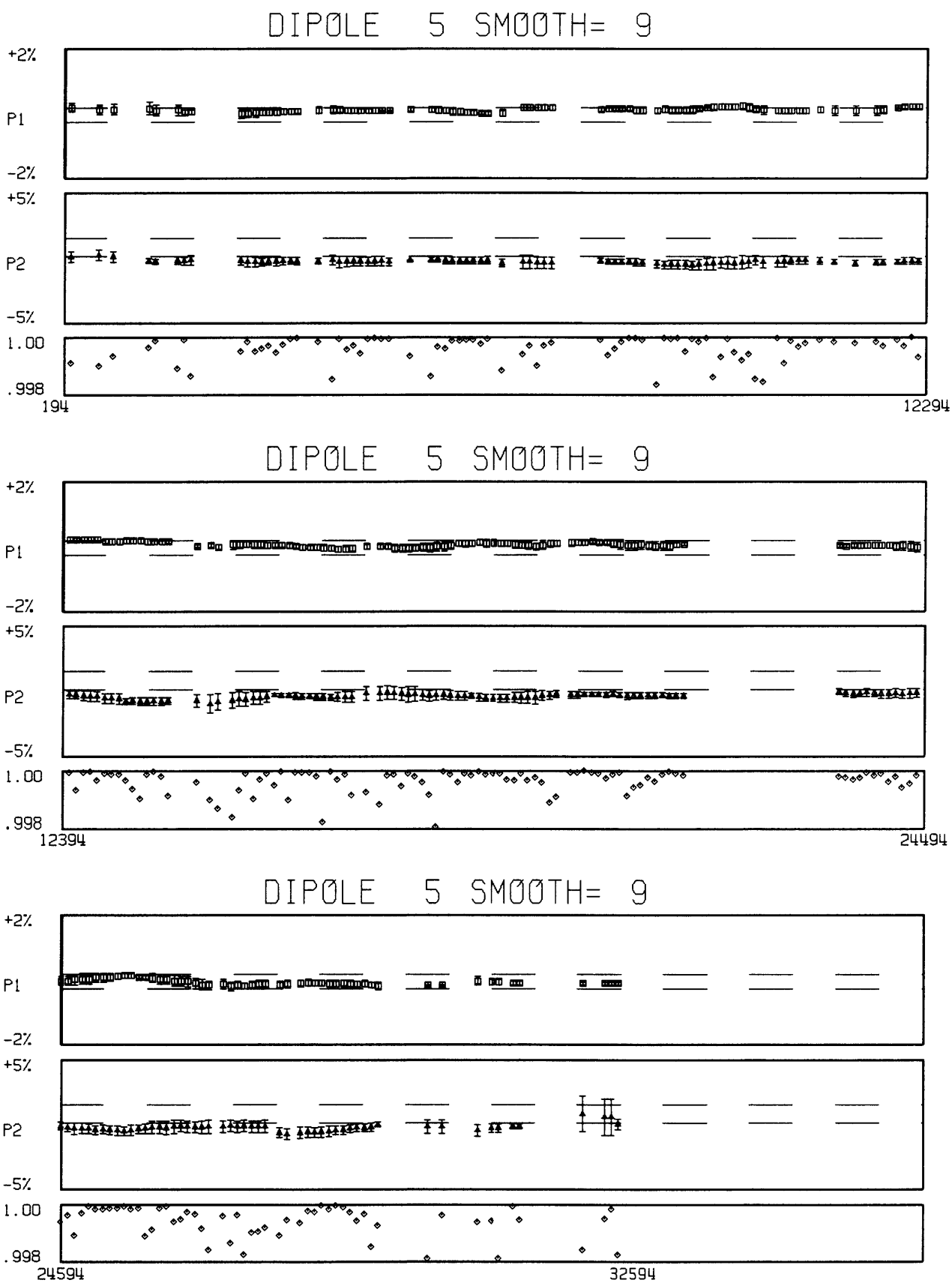

Figure 7 - Residual analysis for Dipole 6 for 1994. See caption of Figure 2 for explanation.

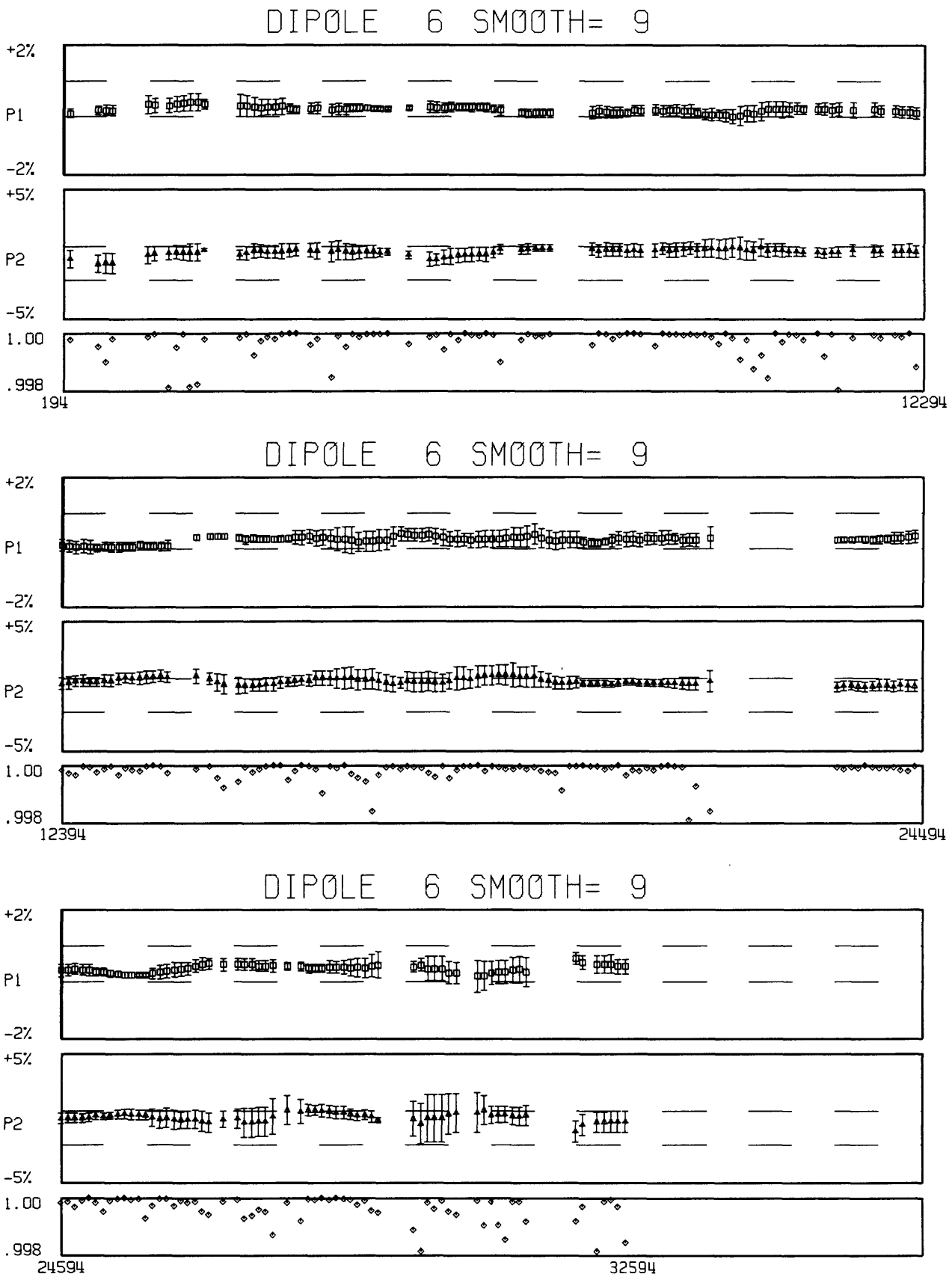

Figure 8 - Unsmoothed projections for Dipole 4 for 1994. Error bars for the projections are determined from noise levels estimated with the coherency which are propagated through the analysis procedure. Note that the scatter between daily projections is larger than the errors.

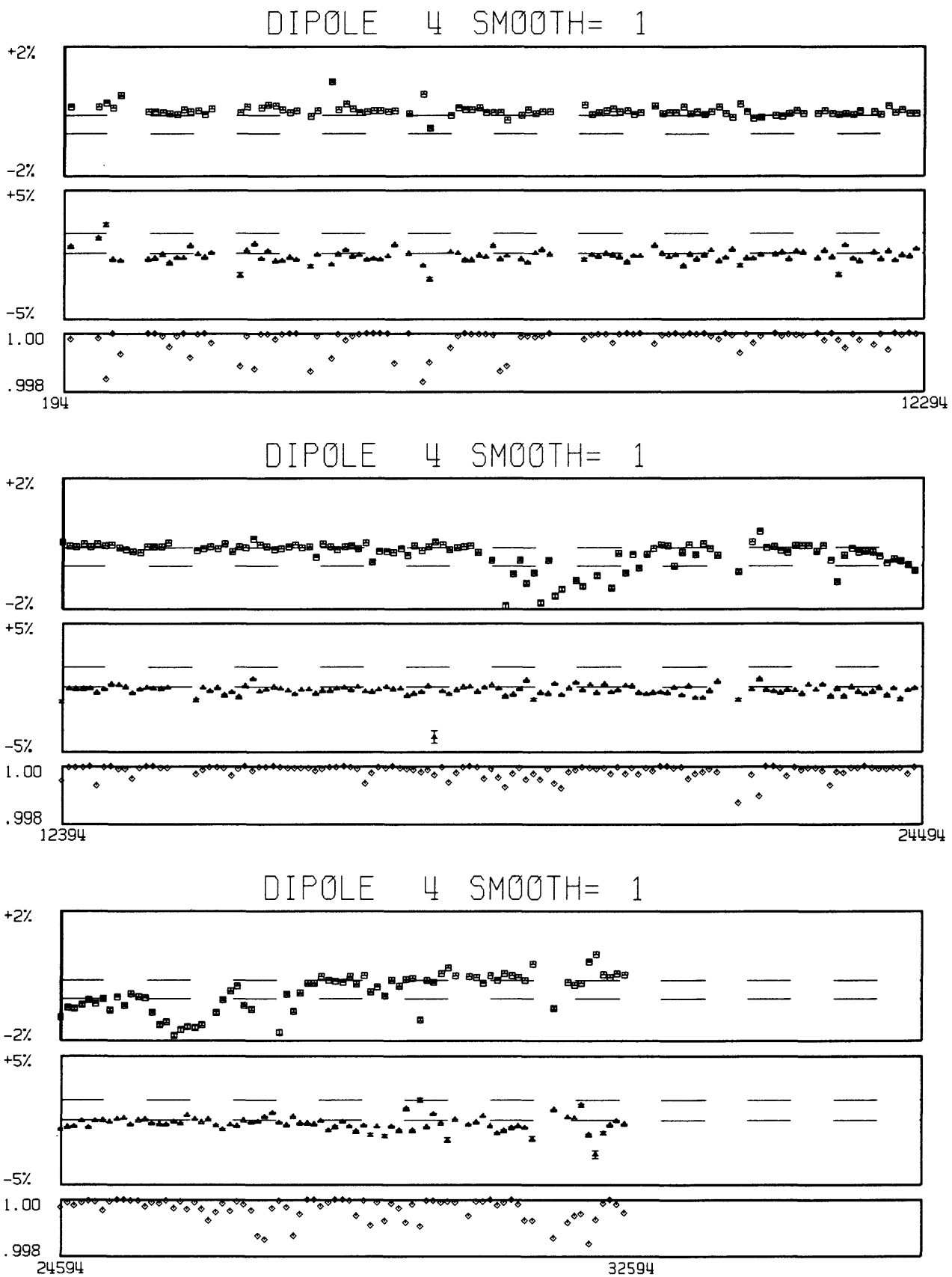

Post-seismic fault creep on the Foothills thrust system following the 1989 Loma Prieta earthquake

Grant # 1434-94-G-2447

Program Element II

David D. Pollard
Department of Geological and Environmental Sciences
Stanford University
Stanford, CA 94305
415 - 723-4679
dpollard@pangea.stanford.edu

Roland Bürgmann and Paul Segall
Department of Geophysics
Stanford University
Stanford, CA 94305
415 - 723-5485
roland@pangea.stanford.edu

Problem

Following the 1989 Loma Prieta earthquake, we repeatedly measured relative displacements along two profiles across the San Andreas fault system using the Global Positioning System (GPS). The observed horizontal displacement rates within a radius of ~20 km from the epicenter differed significantly from those measured in the two decades preceding the earthquake. Fault parallel velocities significantly exceeded those measured between 1970 and 1989. More surprisingly, the GPS data indicate convergence normal to the San Andreas fault and leveling data show a zone of uplift near Loma Prieta (Bürgmann et al., 1990, 1993). The site velocities in excess of the secular rates can be explained by a combination of aseismic reverse slip on a fault in the Foothills thrust belt northeast of the San Andreas fault and strike-slip on the Loma Prieta rupture (Bürgmann et al., 1992, 1993). Savage et al. (1994) argue that a model involving deep shear below the Loma Prieta rupture and post-seismic collapse of the rupture zone fits the Loma Prieta profile data.

Distinguishing between these models is critical for assessing seismic hazard in the region, since these faults may be capable of producing M6-7 earthquakes close to the densely populated Santa Clara valley. There is abundant evidence that the Foothills thrust system was active through the Quaternary as indicated by offset young alluvial deposits and soil horizons (McLaughlin, 1990). Bürgmann et al. (1994) find that average slip rates of 2-3 mm/yr are required on the underlying thrust system to achieve the ~1 mm/yr uplift rates suggested by their analysis of geologic, geomorphic and geodetic data.

Investigations

The existing network geometry did not permit a unique determination of fault-slip geometry and slip rate as only few benchmarks (7 sites) were affected by the post-seismic

anomaly. In April and May of 1994 we reoccupied a 26-station GPS network near the epicenter that was last surveyed in March and April of 1990 by the National Geodetic Survey (NGS) and Stanford University to better define the source of the post-seismic strain anomaly. The NGS data from 1990 were collected with TI-4100 instrument whereas our group employed Trimble 4000 SDT receivers. In 1994 Trimble 4000 SSE receivers were used to occupy the network. At the same time, the Crustal Deformation project of the U.S.G.S. reoccupied the two San Andreas crossing profiles using Ashtech LD-XII receivers. The data were analyzed with the Bernese version 3.5 GPS processing software.

Results

Figure 1 shows total displacements between 1990 and 1994 of sites within ~30 km from the epicenter. The displacement vectors and their 95% error ellipses are shown relative to site LP1_ on Loma Prieta peak.

The results indicate that anomalous contraction is centered northeast of the San Andreas along the Foothills thrust belt. Slip on the modeled thrust fault should cause uplift in the hanging wall, with maximum uplift located near Loma Prieta, which subsided by about 10 cm during the earthquake.

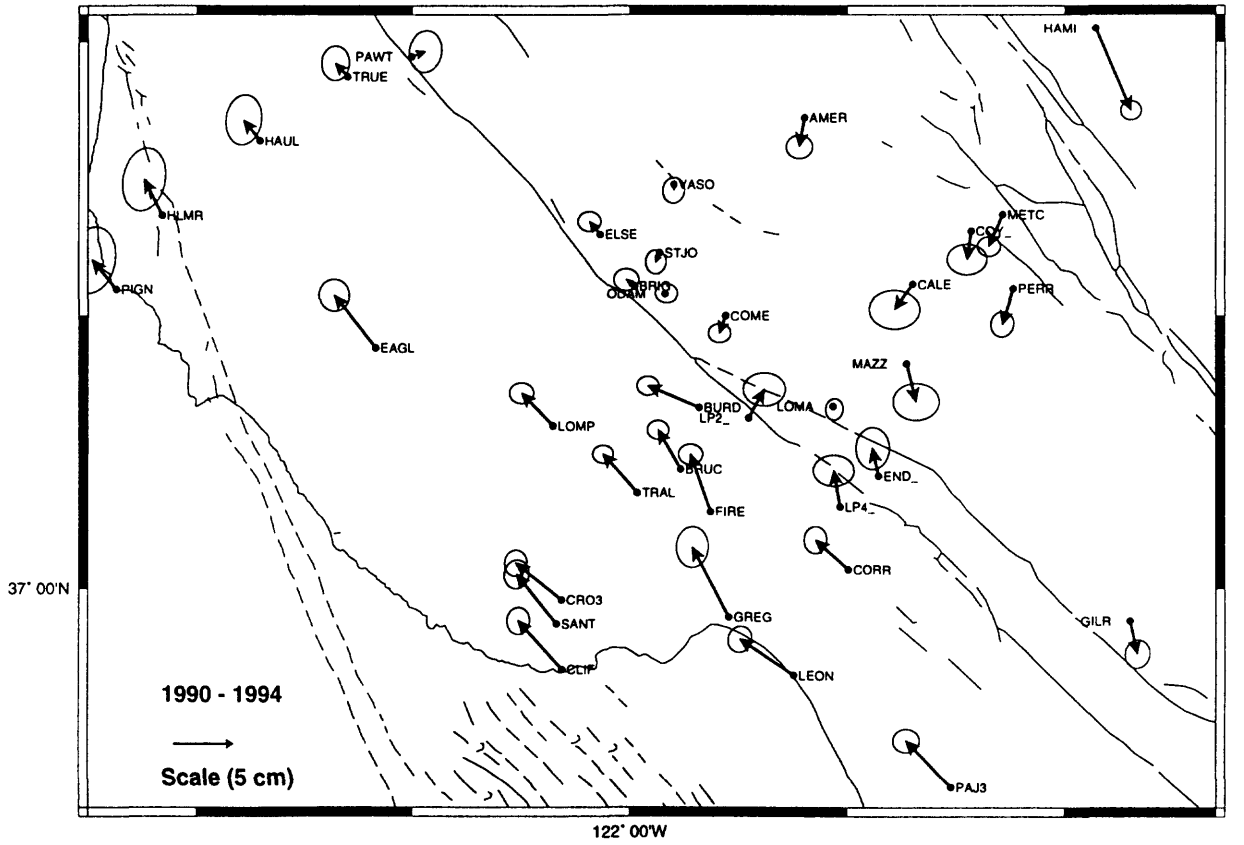

Figure 1. Total displacements between 1990 and 1994 from GPS measurements near the Loma Prieta earthquake rupture. Note the contraction northeast of the San Andreas fault.

These rates greatly exceed geologic estimates of long-term uplift (Bürgmann et al., 1994). Significant post-seismic vertical displacements in the area are not apparent in the GPS data, but may be masked by the ~ 3 cm error associated with 1990 GPS height measurements. The data help constrain the location and magnitude of post-seismic creep. Future work will focus on formally inverting the combined data set for time-dependent slip on actively creeping fault planes.

References

Savage, J.C., Lisowski, M., and Svarc, J.L., 1994, Postseismic deformation following the 1989 (M = 7.1) Loma Prieta, California, earthquake, *J.Geophys. Res.*, v. 99, p. 13,757-13,7765.

Bürgmann, R., Segall, P., Liu, L., Lisowski, M., Prescott, W.H., and Svarc, J.L., 1990, The search for postseismic strain diffusion northwest of the October 17th, 1989, Loma Prieta rupture zone using repeated GPS measurements, *EOS Transactions AGU*, v. 71, p. 1455.

Bürgmann, R., Segall, P., Lisowski, M., and Svarc, J.L., 1992, Rapid aseismic slip on the Berrocal fault zone following the Loma Prieta earthquake, *EOS Transactions AGU*, v.73, p.119.

Bürgmann, R., Segall, P., Lisowski, M., Marshall, G., Stein, R., and Svarc, J.L., 1993, Post-seismic uplift of the southern Santa Cruz Mountains following the Loma Prieta earthquake, *EOS Transactions AGU*, v.73, v. 74, p. 106.

Bürgmann, R., and Segall, P., 1993, Late Cenozoic uplift of the southern Santa Cruz Mountains and its relationship to the active deformation cycle in the San Francisco Bay Area, *GSA Abstracts with Program*, v. 25, no. 6, p. 242-243.

Bürgmann, R., Arrowsmith, R., Dumitru, T., and McLaughlin, R., 1994, Rise and fall of the southern Santa Cruz Mountains, California, from fission tracks, geomorphology, and geodesy, *J. Geophysi.Res.*, v. 99, p. 20,181-20,202.

Bürgmann, R., Segall, P., Lisowski, M., and Svarc, J.L., 1994, Strain development subsequent to the 1989 Loma Prieta earthquake, *U.S.G.S. Prof. Paper 1550D, in press.*

Reports

Bürgmann, R., Segall, P., Lisowski, M., and Svarc, J.L., 1994, Five years of post-seismic strain following the Loma Prieta earthquake, *EOS Transactions AGU, in press.*

Bürgmann, R., Segall, P., Arrowsmith, R., and Dumitru, T., 1994, Slip rates and earthquake hazard along the Foothills thrust belt in the Southern Santa Cruz Mountains, *GSA Abstracts with Program*, v. 26, no. 7, p. 191.

Bürgmann, R., Arrowsmith, R., and Dumitru, T., 1994, Slip Rates and Earthquake Hazard Along the Foothills Thrust Belt in the Southern San Francisco Bay Area, *USGS Open File Report, p. 31-33.*

Quaternary Chronostratigraphy and Deformation History, Los Angeles Basin, California

9960-11426, 9960-12426

Daniel J. Ponti
Branch of Earthquake Geology and Geophysics
U.S. Geological Survey
345 Middlefield Road MS 977
Menlo Park, CA 94025
(415) 329-5679
email: dponti@isdmnl.wr.usgs.gov
Program Element: II

Investigations

1. Post-earthquake investigations of ground deformation following the 1994 Northridge earthquake (9960-11426).
2. Paleoseismic investigations of ground fractures in Potrero Canyon and Granada Hills produced by the Northridge earthquake (9960-11426).
3. Historical re-evaluation of 1906 surface faulting in the southern Santa Cruz Mountains in light of the 1989 Loma Prieta earthquake (9960-12426).

Results

1. The Northridge earthquake of January 17, 1994 produced no evidence for primary surface rupture. Nevertheless, this was a very important earthquake geologically. Although the observed zones of ground deformation are localized, and the displacements are small, permanent ground deformation in these areas was responsible for a significant amount of structural and infrastructure damage. If there is a lesson to be learned from the Northridge earthquake, it's that even concealed faults can produce concentrated zones of surface displacements and that small amounts of ground deformation, regardless of the origin, poses a significant hazard in an urban setting. In order to understand the nature of these features, this project led the effort in coordinating USGS post-earthquake investigations concentrated on large scale mapping and shallow subsurface investigations in Granada Hills and in Potrero Canyon.

   In Granada Hills, at the northern edge of the San Fernando Valley, an E-W trending zone approximately 5 km long and several hundred meters wide contains a complex array of pavement cracks, extensional graben, contractional deformation in the form of pavement humps and tented sidewalks, and laterally offset curbs. This zone occurs along the surface projection of the concealed Mission Hills fault and nearly abuts the westernmost end of the surface rupture zone produced by the 1971 San Fernando earthquake. It is associated with a significant amount of building and infrastructure damage. In many instances, the ground deformation has displaced foundation slabs and caused spectacular ruptures of water and gas mains. Over most of the zone, the cracks appear to be surficial and resulted from decoupling of the pavement from the ground below; nearly all of the observed compressional deformation appears to be the result of pavement decoupling and pounding of curb and sidewalk slabs during strong shaking. Significant deformation in natural ground is dominantly extensional and appears to be

localized within Holocene alluvium in a region approximately 1 km in length, centered just north of the intersection of Balboa Blvd. and Rinaldi St., and also within Miocene bedrock about 1/2 km west of I-405. Extensional graben oriented both NE-SW and NW-SE exhibit vertical displacements of as much as 20 cm; some of these zones overlie buried stream channels. The deformation zone is also characterized by extension of as much as 60 cm, with the principal extension direction generally following the local topographic gradient (downslope). Several N-S and E-W streets in the vicinity of Balboa Blvd. show lateral offsets of as much as 30 cm; detailed surveys of laterally offset streets suggest that deformation extends no more than perhaps 6-15 m below the surface. Post-earthquake surveying has also not revealed any evidence of afterslip in this zone. Strong ground shaking, resulting in lurching and differential compaction, appears to be the principal cause of the ground cracks in Granada Hills. However, the localization of the zone above the Mission Hills thrust suggests that the ground failures may be a response to seismic focusing or tectonic deformation associated with the fault.

Normal faults and associated minor thrust faults are observed on the margins of alluvial fill in Potrero Canyon, an E-W trending valley, located along the north flank of the Santa Susana Mountains. Ground deformation in this valley appears to be the cause of nearly two dozen ruptures in a 12" natural gas pipeline and numerous waterline breaks. The south-dipping thrust faults observed here occur at the approximate surface projection of the causative fault, which lead to speculation that these features may represent primary rupture. Our investigations indicate that primary faulting did not occur here. The dominant displacements in Potrero Canyon occur on a series of discontinuous high-angle normal faults that flank both the north and south margins of the valley and extend for approximately 3 km. A few localized occurrences of sand blows in the valley fill indicate that liquefaction has also occurred. The geometry of these extensional fissures suggest that the alluvial fill has subsided toward the valley center as much as 60 cm and shifted westward (downstream). These displacements probably result from lurching and differential settlement due to strong ground motions, although we cannot yet rule out the possibility that the fractures may in part be related to secondary bending-moment or flexural-slip faulting in response to coseismic folding of the underlying bedrock. Small, low angle, south-over-north thrust faults, with displacements typically less than 15 cm, occur on the south margin of Potrero Canyon only and are commonly found a few meters north of the normal faults. Trenches reveal that many of these features are surficial and detach at the base of the surface soil, although others appear to join with or cut the high-angle faults and may trend into underlying bedrock. No afterslip has been observed. Additional zones of normal faults at the mouth of Tapo Canyon, 6 km to the west, and bedding-plane reverse (possible flexural-slip) faulting in the Saugus Fm. at Stevenson Ranch , 8 km to the east, suggest that this earthquake may have produced a zone of fault-related warping along a significant portion of the north flank of the Santa Susana Mountains.

In addition to the two regions we have studied in detail, intense zones of pavement cracks, spalled and extended curbs, and tented sidewalk slabs have also been observed within a 25 square km area of Northridge and Reseda, in the epicentral region. Most of these features appear to be shaking related damage from pavement and slab decoupling, but several extensional grabens that displace natural ground have been reported from this region. At present, we have not been able to discern any pattern to these displacements consistent with tectonic deformation. The region is considered to have a high liquefaction potential, but there is little evidence of widespread liquefaction in this area. One possible explanation for this deformation zone is that it resulted from dry compaction of buried stream channel and alluvial fan deposits that contain loosely consolidated sands.

2. Paleoseismic investigations in both Potrero Canyon and Granada Hills have been ongoing since shortly after the earthquake. Two trenches across the normal faults on the south side of Potrero Canyon show evidence of at least two prior displacement events; the most recent of which occurred about 1000 years ago. Some of the minor fissures observed in the alluvium do

trend into the underlying Pico Fm. bedrock where they form small N-dipping shear zones oriented subparallel to bedding, but we have not yet been able to expose bedrock below the principal zone of fissuring. Whether tectonic or shaking-induced, these trenching investigations should provide the elapsed time, or recurrence interval since the last time this area has experienced comparable ground motions.

In Granada Hills, three trenches have been excavated and logged across a significant zone of tension cracks that cross Balboa Blvd.. These trenches, which are cut into late Holocene sheet wash and alluvial channel sediments, show that the 1994 displacements across the fractures decrease with depth. This relationship indicates that slip did not propagate to the surface from depth, but rather, the cracks formed by compaction or differential shear within the surface soil mass. There is some suggestion of a prior displacement event deep in one of the trenches, but the evidence for a prior earthquake in the exposed section is not compelling. Pending additional radiocarbon control, it appears that this exposed section may be too young to have experienced the last earthquake recorded in Potrero Canyon.

3. Our historical investigations in of the 1906 earthquake in the Santa Cruz Mountains area continued in 1994 with investigations of the Wrights tunnel deformation. The abandoned Wrights railroad tunnel, which was built across the San Andreas fault zone, was offset and damaged during the 1906 earthquake. A plot produced following the 1906 earthquake showing post-earthquake measurements made in the tunnel has been interpreted as evidence of a broad (1.5 km) zone of tectonic deformation beneath Summit Ridge. We believe, however, that this interpretation is incorrect. The plot of the tunnel shows deformation measured from a reference line, the significance of which is not explained either on the published figure or in the accompanying discussion. Our research reveals that the engineers who constructed the plot assumed that the tunnel portals had not been offset relative to each other. If they were correct, then the reference line represents the original alignment of the tunnel and the broad zone of deformation implied by the plot could not have been tectonic; any tectonic deformation across the fault zone would have offset the portals, even after elastic rebound is taken into account. If, as we believe, there was tectonic offset across the fault in 1906, the reference line must represent the *new* alignment of the portals after reconstruction and the apparent broad zone of deformation becomes an artifact of the difference between the old and new tunnel alignments. We have modeled the position of the deformed tunnel, assuming tectonic offset on a 10-km-deep fault in an elastic half-space, and find the model to be in excellent agreement with the measurements recorded on the plot. We find that offset across the entire fault zone was 1.7-1.8 m, and that distributed deformation of between 0.2-0.7 m (based on 1906 measurements of between 1.1 m and 1.5 m on the principal fault plane) was confined to within only a few hundred m of the main fault. This implies that surface fractures reported on the crest of Summit Ridge in 1906 (and, by analogy, in 1989) did not significantly deform the tunnel, and may not be of significant tectonic origin.

Reports

Hecker, S., Ponti, D. J., Garvin, C. D., and Hamilton, J. A., in press, Characteristics and origin of ground deformation in Granada Hills and Mission Hills during the January 17, 1994 Northridge earthquake: *in* Seiple, R., ed., California Division of Mines and Geology Special Publication.

Hecker, S., Ponti, D. J., Garvin, C. D., Sharp, R. V., Hamilton, J. C., Powers, T. J., Fumal, T. E., Rymer, M. J., Prentice, C. S., Cinti, F. R., and Schwartz, D. P., in press, Ground deformation in Granada Hills and Mission Hills resulting from the January 17, 1994 Northridge earthquake: U.S. Geological Survey Open-File Report.

Ponti, D. J., Schwartz, D. P., Hecker, S., and Fumal, T. E., 1994, Ground deformation in Potrero Canyon and Granada Hills: Keys to recurrence of Northridge-type blind-thrust earthquakes?: EOS, Transactions of the American Geophysical Union, v. 75, p. 176.

Prentice, C. S., and Ponti, D. J., 1994, The Wrights tunnel is NOT an example of a broad shear zone: a re-examination of the documentation of the tunnel deformation associated with the 1906 earthquake: EOS, Transactions of the American Geophysical Union, v. 75, p. 343.

U.S. Geological Survey Staff, 1994, Ground deformation in Granada Hills from the January 17,1994 Northridge earthquake: Seismological Research Letters, v. 65, n. 1 (Northridge earthquake supplement), p. 33.

U.S. Geological Survey Staff, 1994, Ground deformation in Potrero Canyon from the January 17, 1994 Northridge earthquake: Seismological Research Letters, v. 65, n. 1 (Northridge earthquake supplement), p. 34

USGS and SCEC, 1994, The magnitude 6.7 Northridge, California, earthquake of 17 January 1994: Science, v. 266, p. 389-397.

REGIONAL VARIATIONS IN REELFOOT - ROUGH CREEK RIFT GEOMETRY AS STRUCTURAL CONTROLS ON NEW MADRID SEISMICITY

9450-10091

Christopher J. Potter
Branch of Sedimentary Processes
U.S. Geological Survey
Denver Federal Center, MS 939
Denver, CO 80225-0046
Phone (303) 236-3282; FAX (303) 236-0459; cpotter@sedproc.cr.usgs.gov

Investigations undertaken:

This study tests a hypothesis that the locus of the contemporary New Madrid seismic zone corresponds to a segment of the Cambrian Reelfoot - Rough Creek-Rome rift system that had a unique cross-sectional geometry when compared with other parts of the 1000-km-long Cambrian rift system. The hypothesis was based on my reconnaissance examination of available seismic reflection data, and alternative interpretations (relative to those published by McKeown and others, 1990) for some key reflection profiles across the Blytheville arch. Previous workers have recognized that the Cambrian Reelfoot rift provides structural control, in some sense, for the contemporary New Madrid seismic zone, but the precise nature of this structural inheritance is not clear (Hamilton and McKeown, 1988). I am undertaking an extensive examination of conventional seismic reflection and other subsurface data to investigate the regional along-strike variation in the geometry (rift segmentation) of a 400-km-long part of the Cambrian rift system in Arkansas, Missouri, Tennessee, Kentucky and Illinois. The goal of this project is to provide a detailed understanding of inherited structural control of the New Madrid Seismic Zone, through an enhanced understanding of the three-dimensional geometry of the Cambrian rift.

Results:

Analyses of seismic reflection data and a review of drill hole data have resulted in minor modifications of the original hypothesis, while confirming its fundamental aspects. The preliminary hypothesis was that the geographic pattern of New Madrid seismicity is controlled by the presence of a medial Cambrian graben (now "inverted" by late Paleozoic reverse faulting), and by the along-strike transition from this medial graben to a half-graben style that characterized adjacent Cambrian rift segments to the southwest and northeast. Instead, the reflection data show that a regional alternating-half-graben style continued through the entire Reelfoot-Rough Creek-Rome rift system, and that in the vicinity of the Blytheville arch there was a deep narrower medial graben superimposed on this broad half-graben pattern.

An anomalous thickness (up to 6.1 km) of Cambrian clastic sediment accumulated in this 20-km-wide medial graben. I interpret late Paleozoic thrust or reverse fault inversion of this graben to form the Blytheville arch. This interpretation is based on a well-defined footwall cutoff of near-basement reflections, and contrasts with the diapiric inversion proposed by McKeown (1990). Taylor and others' (1991) biostratigraphic work in deep wells shows a normal Cambrian stratigraphic section in the Blytheville arch, rather than the disrupted section that would be predicted by the diapiric model.

Major Cambrian accommodation zones bounded the southwest and northeast ends of the medial Cambrian graben (in northeastern Arkansas and southeastern Missouri - northwestern Tennessee, respectively; fig. 1). Reflection profiles near the southwest end of the RFR (eastern

Arkansas, western Tennessee)show an along-strike change in Cambrian rift geometry, from one dominated by a medial graben to one of simple half-grabens that appear to change tilt direction along the rift axis with no pronounced axial thickening. The present depth to basement in these half-grabens may be as great as 9 km. The accommodation zone at the northeast end of the medial graben is not well-imaged by reflection data.

Knowledge of the contemporary regional stress field (Zoback, 1992) and precise location of earthquakes (Chiu and others, 1992) implies that the northeast trending arm of seismicity that corresponds to the trend of the Blytheville arch (fig. 1) represents dextral strike-slip faulting, and the northwest-trending, southwest-dipping zone of seismicity that crosses the north end of the Blytheville arch represents reverse faulting. In the context of the present study, the northeast trending zone of strike-slip seismicity may be inherited from the intensely faulted deep medial graben. The northwest-trending zone may be inherited from the Cambrian accommodation zone that bounded the northeast end of the Cambrian medial graben. According to this interpretation, the northernmost part of the New Madrid Seismic Zone, which trends northeast (fig. 1), is localized along a half-graben-bounding border fault, northeast of the part of the rift that contains the deep medial graben. Thus, the New Madrid epicentral pattern may be inherited from a very specific along-strike transition in Cambrian rift geometry. Unfortunately, seismic data are not available in the Cambrian rift immediately northeast of the New Madrid Seismic Zone. However, in the area of the dogleg bend that links the Reelfoot rift and Rough Creek graben (fig. 1), the rifting style is clearly one of alternating half-grabens without a medial graben (Potter and others, in press).

Reports from this study:

Potter, Christopher J., 1993, Along-strike variations in the structure of the Reelfoot - Rough Creek rift system -- Implications for New Madrid seismicity (abs.): Geol. Soc America Abs. Prog., v. 25, no. 6, p. A-409.

Potter, Christopher J. and Drahovzal, James A., 1994, The regional configuration of the Cambrian Reelfoot-Rough Creek-Rome rift system (abs.) , *in* Ridgley, J.L., Drahovzal, J.A., Keith, B.D., and Kolata, D.R., eds., Proceedings of the Illinois Basin Energy and Mineral Resources Workshop, U.S. Geological Survey Open File Report 94-298, p. 34-35.

Potter, C. J., Goldhaber, M.B., Heigold, P.C., and Drahovzal, J.D., in press, Structure of the Reelfoot - Rough Creek rift system, Fluorspar Area fault complex, and Hicks Dome, southern Illinois and western Kentucky -- new constraints from regional seismic reflection data: U. S. Geological Survey Professional Paper 1538-Q, 50 ms. pages, 7 figs., 1 plate.

Other references cited:

Chiu, J.M., Johnston, A.C., and Yang, Y.T., 1992, Imaging the active faults of the central New Madrid seismic zone using PANDA array data: Seismological Research Letters, v. 63, p. 375-393.

Hamilton, R.M., and McKeown, F.A., 1988, Structure of the Blytheville arches in the New Madrid Seismic Zone: Seismological Research Letters, v. 59, no. 4, p. 117-121.

McKeown, F.A., Hamilton, R.M., Diehl, S.F., and Glick, E.E., 1990, Diapiric origin of the Blytheville and Pascola arches in the Reelfoot rift, east-central United States: Relation to New Madrid seismicity: Geology, v. 18, p. 1158-1162.

Taylor, M.E., Collins, D.S., Palmer, A.R., Repetski, J.E., 1991, Upper Cambrian biostratigraphic correlations in the Reelfoot Basin, northwestern Arkansas: Program with Abstracts, Louis

Unfer, Jr. Conference on the Geology of the Mid-Mississippi Valley. Southeast Missouri State Univ., Cape Girardeau, MO, 5 p.

Zoback, M.L., 1992, First- and second-order patterns of stress in the lithosphere -- The world stress map project: Journal of Geophysical Research, v. 97, p. 11,703-11,728.

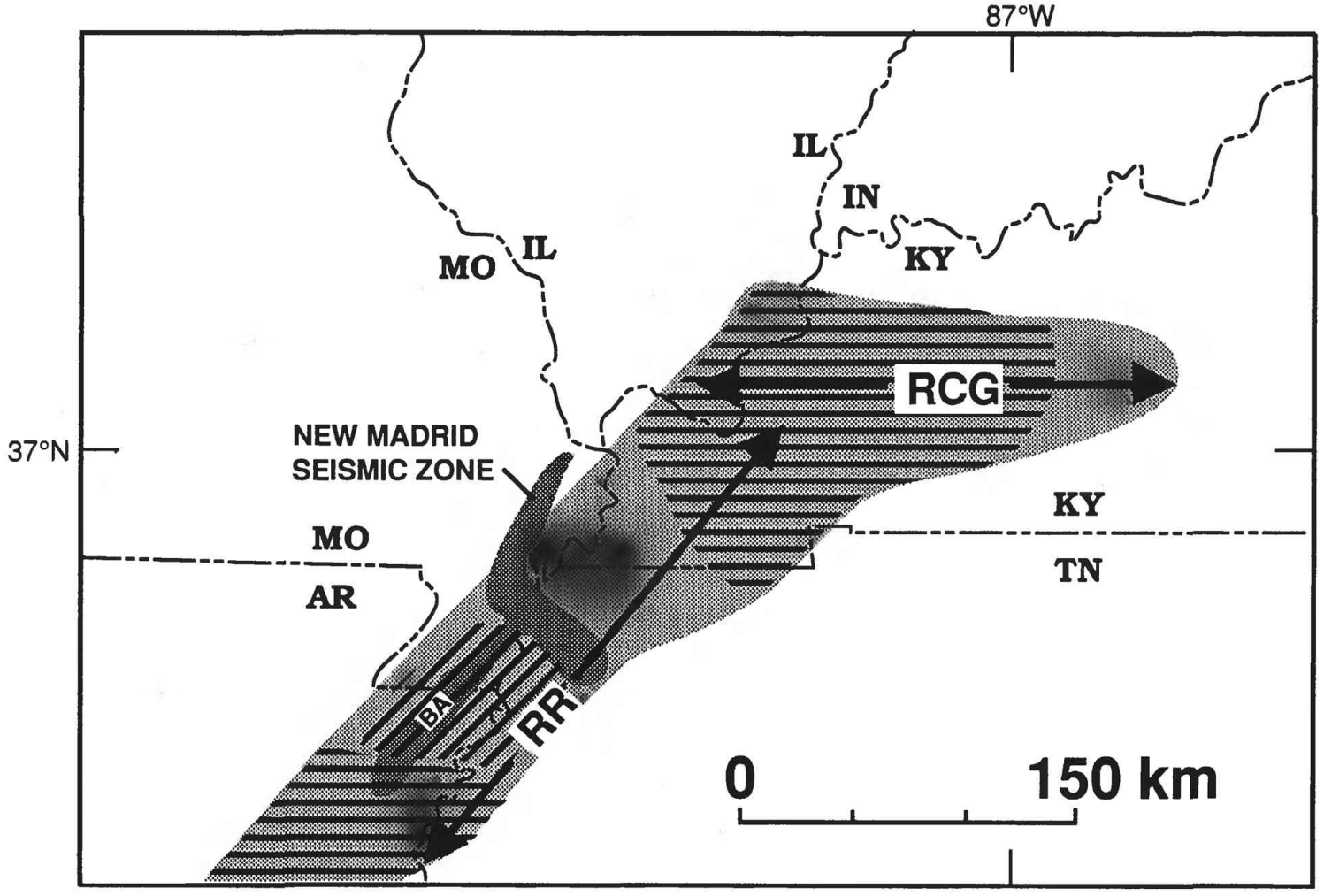

Figure 1: Generalized diagram showing the along-strike variation of structural patterns within the Reelfoot - Rough Creek rift system. The contemporary New Madrid seismic zone is shown in dark stipple; the Cambrian Reelfoot - Rough Creek rift system is shown in a lighter stipple. RR, Reelfoot rift; RCG, Rough Creek graben; BA, Blytheville arch. Horizontally ruled pattern denotes parts of the rift system characterized by major half-grabens with alternating directions of polarity. Diagonally ruled pattern denotes the part of the Reelfoot rift characterized by a deep medial graben superimposed on broad alternating half-graben geometry. The transitions between diagonal ruling and horizonatal ruling represent accommodation zones in the Cambrian rift.

Crustal Geophysics of Seismically Active Regions

9950-10475, 9950-13275, 9950-14275

Thomas L. Pratt, Project Chief
Other Investigators: Meridee Cecil, Jack Odum, William Stephenson, Robert Williams

Branch of Earthquake and Landslide Hazards
U. S. Geological Survey
School of Oceanography WB-10
University of Washington
Seattle, Washington 98195
206-543-7358
tpratt@ravenna.ocean.washington.edu

INVESTIGATIONS:

During FY 1994 we: 1) acquired high-resolution seismic reflection data across a fault zone in the New Madrid, Missouri area that was suspected to have caused the "waterfalls" during one of the 1811-1812 earthquakes; 2) developed a new model to explain the geometry and history of faults in the Puget Sound region; and 3) tested our ability to determine the response of near-surface materials to seismic energy using a controlled seismic source.

RESULTS:

New Madrid. The most exciting part of our New Madrid work was the acquisition of two high-resolution seismic reflection profiles across the southward projection of a fault believed to have caused the "waterfalls" seen on the Mississippi River during the 1811-1812 earthquake sequence. Examination of existing data led us to develop a thrust-fault model for motion on the north-trending, central segment of the New Madrid seismic zone (Pratt, 1994). The model predicts that a north-trending thrust fault should reach the surface near and south of the town of New Madrid, Missouri, and indeed four seismic reflection profiles that cross the feature show a fault zone with about 40 m of up-to-the-west vertical motion.

Our new data crossed the southward projection of the fault zone to test whether it continued or shifted to the west to form Reelfoot scarp, as we suspected. Surprisingly, the new data imaged a fault zone with the opposite sense of vertical displacement (Odum and others, 1994). We have either delineated a second fault or detected a change in apparent offset in the original fault. Further profiling in FY 1995 should resolve the issue and test the validity of our current model for rupture of the 1811-1812 fault zones.

Puget Sound. Initial interpretation of the 845 km of industry seismic reflection data that we purchased last year has led to a radically new interpretation of the faults in the Puget Lowland area. Our interpretation is that the Seattle fault and other northwest-trending structures are part of an extensive thrust sheet that is moving northward. The work has produced the first comprehensive model for the geometry and formation of crustal faults

in the region, which allows for estimates of the total shortening, slip rates, and rupture planes for earthquakes in the region. The results are described in a paper that has been submitted to Tectonics (Pratt and others, submitted; Pratt and others, assorted abstracts).

In addition to interpreting the seismic reflection data, we have undertaken potential field modeling and forward modeling of the thrust sheet motion. The potential field work has demonstrated that the major gravity anomalies in the Puget Lowland area result from changes in the depth to the Crescent Formation caused by thrust structures. The boundary element modeling of the thrust sheet motion is providing initial estimates of the partitioning of strain between different fault strands and predicting topographic effects from hypothetical earthquakes rupturing specific faults (Stephenson and Pratt, 1994). The modeling will eventually be used to estimate the effects of future earthquakes and to better define the faults that ruptured during past events.

Site Response. We undertook a pilot study to see whether we could determine the near-surface site amplification of seismic waves by near-surface materials. The intent is to develop a quick, reliable way of mapping the expected shaking levels during a future earthquake throughout a city or other critical area without waiting to passively record aftershocks or other earthquakes.

The technique, tried in the city of Santa Cruz, CA, used weight drop and elastic wave generating devices to put measured amounts of seismic energy into the ground. The resulting ground motion, which should vary according to the near-surface impedance structure, was measured on low-frequency seismometers in a radial array placed around the source. Initial results show a correlation between measured ground motion and the site amplification measured at the same sites during aftershocks of the Loma Prieta earthquake (Williams and others, 1994). Analysis is continuing, but it is hoped that the technique eventually will be useful for estimating the amount of shaking that a building should be able to withstand if built at a specific site.

REPORTS PUBLISHED:

Papers:

Odum, J.K., Luzietti, E.A., Stephenson, W.J., Shedlock, K.M., and Michael, J.A., High-resolution shallow seismic-reflection surveys of the northwest Reelfoot rift boundary near Marston, Missouri, USGS Professional Paper, in press.

Park, S.K., Pendergraft, D., Stephenson, W.J., Shedlock, K.M., and Lee, T.C., Deliniation of intrabasin structure in a dilational jog of the San Jacinto fault zone, Southern California, Geology, in press.

Pratt, T.L., How old is the New Madrid seismic zone?, Seismological Research Letters, September, 1994.

Stephenson, W.J., Rockwell, T.K., Odum, J.K., Shedlock, K.M., and Okaya, D.A., Seismic reflection and geomorphic characterization of the onshore Palos Verdes fault zone, Los Angeles, California, Bulletin of the Seismological Society of America, in press.

Williams, R.A., Luzietti, E.A., and Carver, D.L., High-resolution seismic imaging of Quaternary faulting on the Crittenden County fault zone, New Madrid seismic zone, northeastern Arkansas, Seismological Research Letters, in review.

Williams, R.A., Pratt, T.L., Stephenson, W.J., and Odum, J.K., Seismic surveys for earthquake hazard reduction in the New Madrid seismic zone, northeastern Arkansas, The Leading Edge, in press (January 1995 issue).

Abstracts:

Pratt, T.L., How old is the New Madrid seismic zone?, 1993, Geological Society of America Annual Meeting, Abstracts with Programs, v. 25, p. A-198.

Pratt, T.L., Johnson, S.Y., Potter, C.J., and Stephenson, W.J., 1994, The Puget Lowland Thrust Sheet, Geological Society of America Annual Meeting, Abstracts with Programs, v. 26, p. A-187.

Pratt, T.L., Johnson, S.Y., Potter, C.J., and Stephenson, W.J., 1994, The Puget Lowland Thrust Sheet, Seismological Society of America Annual Meeting Abstracts, March, 1994, Pasadena.

Pratt, T.L., Johnson, S.Y., Potter, C.J., and Stephenson, W.J., 1994, The Puget Lowland Thrust Sheet, EOS, v. 75, Fall 1994 Annual Meeting Supplement, 621.

Stephenson, W.J., and Pratt, T.L., 1994, Preliminary results from boundary-element modeling of the Puget Lowland thrust sheet, Washington, EOS, v. 75, Fall 1994 Annual Meeting Supplement, 621.

Williams, R.A., Pratt, T.L., Cranswick, E., Carver, D.L., Worley, D.M., and Lee, W.H.K., 1994, Preliminary site response in Santa Cruz, California, using controlled seismic sources, EOS, v. 75, Fall 1994 Annual Meeting Supplement, 447.

Odum, J.K., Stephenson, W.J., Shedlock, K.M., Pratt, T.L., Collins, D.S., Rhea, S.B., and Williams, R.A., 1994, Possible faults associated with the February 7, 1812 earthquake-induced Mississippi River waterfalls near New Madrid, Missouri, Geological Society of America Annual Meeting, Abstracts with Programs, v. 26, p. A-173.

I. NORTHERN SAN ANDREAS FAULT SYSTEM: PALEOSEISMIC AND SLIP-RATE STUDIES IN NORTHERN CALIFORNIA
II. PALEOSEISMIC INVESTIGATIONS ALONG THE CARIBBEAN-NORTH AMERICAN PLATE BOUNDARY (SEPTENTRIONAL FAULT ZONE), DOMINICAN REPUBLIC

9960-12406, 9960-10406

Carol Prentice
Branch of Earthquake Geology and Geophysics
U. S. Geological Survey,
345 Middlefield Rd, MS 977
Menlo Park, CA 94025
415-329-5690; cprentice@isdmnl.wr.usgs.gov
NEHRP II.5

Investigations

1) Geological investigations of the San Andreas and related faults in northern California to determine timing of prehistoric earthquakes and average Quaternary slip rates. 2) Historical investigations of the behavior of the San Andreas fault in the Loma Prieta region in 1906. 3) Work towards production of a map showing recently active traces of the San Andreas fault along the San Francisco peninsula. 4) Investigations of the Septentrional fault in the Dominican Republic to determine timing of prehistoric earthquakes and slip rate.

Results

1) Studies of excavations at sites along faults of the San Andreas system in northern California are being pursued to determine timing of prehistoric earthquakes and fault slip rates. Excavations across the North Coast segment of the San Andreas fault near Manchester, California, exposed a sequence of faulted fluvial deposits. Radiocarbon dates on charcoal samples collected from these deposits will constrain the age of an associated offset fluvial terrace riser, allowing estimation of a minimum slip rate for this fault segment. Radiocarbon dates will also constrain the age of one prehistoric earthquake at this site Sites with high potential for yielding paleoseismic and slip-rate information are being evaluated along the peninsula segment of the San Andreas fault. A test excavation at a site in Portola Valley failed to provide any useful paleoseismic data; this preliminary excavation has ruled this site out as a candidate for further study. Additional sites are being evaluated.

2) Historical investigations of the 1906 earthquake in the Loma Prieta area allow comparison of the effects of the 1906 earthquake in this region with the effects of the 1989 earthquake. In this region in 1906, as in 1989, many large ground cracks occurred in the Summit Road and Skyland Ridge areas. Three specific localities in the Summit Road area were documented well enough in 1906 to make detailed comparisons with 1989: 1) the Wright's tunnel, 2) the Morrell Ranch, and 3) the Blacksmith shop at Burrell. Interpretation of newly discovered and previously known documents related to the Wright's tunnel show that, contrary to common belief, offset of the tunnel was not distributed over a broad zone. Analysis of the 1906 tunnel data shows that 1.7-1.8 m of offset occurred across a relatively narrow San Andreas fault zone. Left-lateral offset was documented (off the main trace of the San Andreas fault) across two fractures in 1906 near the Morrell ranch; newly discovered historical documents verify that these are the same two fractures that ruptured with smaller amounts of left-lateral offset in 1989. The

fractures in 1906 were longer and more damaging. A significant fracture was photographed in front of the Blacksmith shop at Burrell in 1906. Historical research shows the exact location of this fracture and shows that nothing comparable occurred here in 1989. Virtually no surface rupture occurred along the San Andreas in 1989; careful study of historical documents strongly suggests that surface rupture did occur in 1906, though none of the reported values of offset is reliable. This historical research has added to the understanding of 1906 ground rupture in the Loma Prieta region. These studies indicate that fault behavior in 1989 was significantly different than in 1906, but that off-fault ground ruptures were similar, but larger, in 1906.

3. A collaborative project (with Tim Hall of Geomatrix and Bob Wright of Harlan-Tait) to produce a digital strip map showing recently active fault traces along the San Francisco peninsula has been initiated.

4. The Septentrional fault is located offshore of Puerto Rico and represents a significant seismic hazard to the island. Studies along the Septentrional fault on shore in the Dominican Republic, west of Puerto Rico, have yielded data constraining the date of the most recent earthquake along the major North American-Caribbean plate-boundary fault. The most recent earthquake occurred between 760 and 840 years ago. The amount of slip produced by this earthquake was determined: about 5m of left-lateral and 2m of vertical slip, suggesting this earthquake was > M7.5. Evidence for earlier earthquakes was collected; the timing of these events will be constrained by the results of radiocarbon dating of samples now in progress. In addition, offsets of about 40m and 55m were measured on stream terrace risers that cross the fault. Radiocarbon dates of the terrace sediments, now in progress, will allow estimation of the slip rate of the Septentrional fault.

Reports

Prentice, C.S., and Ponti, D.J., 1994, The Wrights tunnel is NOT an example of a broad shear zone: a re-examination of the documentation of the tunnel deformation associated with the 1906 earthquake, [abs.]: EOS, v. 75, no. 16, p. 343.

Prentice, C. S., Mann, P., Pena., L. and Burr, G., 1994, Timing and size of the most recent earthquake along the Central Septentrional fault, Dominican Republic, in Prentice, C.S., et al., eds., Proceedings of the Workshop on Paleoseismology, USGS Open-File Report 94-568, pp. 158-160.

Prentice, C.S., Schwartz, D.P., and Yeats, R.S., eds., Proceedings of the Workshop on Paleoseismology, USGS Open-File Report 94-568, 210 p.

Prentice, C.S., and Ponti, D.J. 1906 and 1989 coseismic ground fractures in the Santa Cruz Mountains. Contribution to the USGS Loma Prieta Professional Paper.

Prentice, C. S., Mann, P., Pena., L. and Burr, G., 1993, Paleoseismology of the North American—Caribbean strike-slip plate boundary in the Dominican Republic, Hispaniola, [abs.]: EOS, v. 74, no. 43, p. 435.

Three-Dimensional Modeling of Crustal Deformation in the Cascadia Subduction Zone

1434-94-G-2428

Mark A. Richards[1] and David Verdonck[2]

[1]Dept. of Geology and Geophysics
University of California
Berkeley, CA 94720
ph: 510-642-8560
fax: 510-643-9980
e-mail: markr@seismo.berkeley.edu

[2]Geophysics Program, AK-50
University of Washington
Seattle, WA 94720

Program Element II

Investigations Undertaken

The objective of this research is to develop three-dimensional models of interseismic deformation that can explain crustal deformation data obtained from geodetic studies of the Cascadia subduction zone. These data show that vertical deformation in the Coast Ranges of Oregon, Washington, and northern California is not consistent with any simple 2-D model of deformation due to a locked subduction zone thrust fault (e.g., Savage, 1983), and they imply that coupling in Cascadia is highly non-uniform (Mitchell et al., 1994). In order to investigate first-order effects of 3-D fault geometry (e.g., a finite-length locked zone), we have applied a straightforward analytical model of a buried rectangular fault to vertical leveling and tide-guage data along the southern segment of the Cascadia margin. A very simple model, with strong seismic coupling between the Mendocino Triple Junction and the central Oregon coast, explains the geodetic data remarkably well. Comparing our model uplift rates to geological observations of rapid coastal subsidence events (Atwater, 1987; 1992; Clarke and Carver, 1992; Kelsey et al., 1993), we infer a plausible repeat time of about 200-300 years for earthquakes of magnitude M_W >8.5 along this segment of the Cascadia subduction zone. The next logical phase of this investigation is to apply similar modeling techniques to the horizontal strain data from several geodetic networks, which, although more sparse than the vertical data, will provide important consistency checks on the proposed model of main thrust segmentation.

Results

A tectonic map of the Cascadia subduction zone is shown in Figure 1. First-order leveling data and tide-guage data from the coastal region have been analyzed and published by Mitchell et al. (1994). These data, which span a time period of more than 60 years, demonstrate that almost the entire Cascadia coastline is being uplifted from the Mendocino Triple Junction (MTJ) in northern California to the Olympic Peninsula in Washington. Although we attributed this uplift to strong interseismic coupling on the main thrust fault, we also concluded that a zone of weak coupling exists in the region surrounding Newport, Oregon (~44-46° N latitude). Here we use a simple 3-D dislocation model of a locked

thrust fault segment between the MTJ and central Oregon to explain the uplift data from the southern portion of Cascadia.

The data modeled are shown as open circles in Figure 2. Error bars represent an estimate of about 1mm/yr uncertainty in uplift rate characteristic of the processed leveling data used by Mitchell et al (1994). Figure 2a shows a N-S run along the coastline, while Figures 2b-e show E-W survey lines across the Coast Ranges. These data show (1) that there is a general trend of landward tilting in the Coast Ranges (Reilinger and Adams, 1982) and (2) that coastal uplift attenuates as the MTJ is approached toward the south and as Newport is approached toward the north.

Our 3-D model is illustrated in Figure 3. We assume that the Cascadia thrust dips at an angle of about 11°, as indicated by seismic studies in northern California (Verdonck and Zandt, 1994) and southern Washinton (Weaver and Baker, 1988). We assume that convergence occurs in the direction N65°E at a rate of 45 mm/yr (Riddihough, 1984; Demets, et al., 1990). We model a locked fault plane 465 km long along strike and 75 km long down-dip, as indicated by the darker shaded region in Figure 3. The lighter shaded region indicates a transitional continuation of this planar fault in which the slip deficit decreases from the maximum (dark region) to zero (unshaded region) over a distance of 125 km.

The surface displacements are calculated from the analytical dislocation model of Okada (1985) for a finite rectangular fault buried in an elastic half-space. Elastic strain is assumed to accumulate at a constant rate due to a steady increase in the slip deficit along the locked zone and transitional zones. The model shown is a "best fitting" model (L1 norm <0.4 mm/yr), derived by varying the dimensions of the locked and transitional zones in forward models. The contours in Figure 3 give the calculated uplift rate in mm/yr, plotted "on-land." The solid lines in Figure 2 give the model uplift rate at each survey point analyzed by Mitchell et al. (1994), and it is readily seen that the model explains the main features in the data: (1) The uplift is bounded to the north and south due to our choice of the dimensions of the locked zone. (2) The general trend of landward tilting is predicted successfully, along with the near-absence of tilting near Newport. Note that even though Arcata is near the end of the locked region, it experiences a high uplift rate due to its proximity to the trench.

The model presented is by no means unique, and additional model parameters could obviously improve the fit. Also, we have so far ignored any transient behavior due to, e.g., viscous relaxation in the mantle. Nevertheless, the fit to the data is remarkable given the simplicity of the model, and it reinforces our earlier conclusion that the uplift data imply a distinct locked fault segment between Newport and the MTJ (Mitchell et al., 1994). The model is also reasonably consistent with geological observations of rapid subsidence events along the Cascadia coast. If it is assumed that about 0.5 meters of interseismic uplift is required to produce geologically detectable co-seismic subsidence, then, given an interseismic interval of about 200-300 years, our model can also explain a number of observations: Observed rapid subsidence events in the South Slough of Coos Bay (Nelson, 1992), lack of subsidence events in eastern Coos Bay and northward at the Umpqua River near Reedsport and at the Suislaw River near Florence (Nelson, 1992), rapid subsidence events at Cape Blanco (Kelsey et al., 1993) and at Mad River Slough near Arcata (Clarke and Carver, 1992). Our model explains this variability in terms of (1) the finite length of the model locked zone and (2) the variation in distance between coastal sites and the Cascadia trench (see contours in Figure 3).

If the entire fault segment modeled fails in a single event, with an interseismic interval of 250 years, then the resulting seismic moment release is about 1.7×10^{29} dyne-cm and the moment magnitude is M_W=8.8. If only one quarter of this zone ruptures, with the same time interval, it would still result in a M_W=8.4 earthquake, with disastrous consequences for coastal Oregon and northern California. Further tests of our model should result from more extensive geological studies of the distribution and timing of rapid subsidence events

along the Cascadia coastline. However, a test can also be perfomed using horizontal strain data collected from several geodetic networks that span the region (e.g, MTJ, coastal Oregon, Columbia River). In particular, the contour lines for uplift in Figure 3 imply a "refraction" of the horizontal strain axes as one approaches the ends of the hypothesized locked zone. Fortunately, new strain networks have been established in these regions that are just beginning to yield high precision results (Mark Murray and Mike Lisowski, pers. comms.), and we plan to use our 3-D model to address these new data.

Reports Published

Verdonck, D., 1994, Three-dimensional model of vertical deformation at the southern Cascadia subduction zone, western United States, *Geology*, in press.

Verdonck, D., 1994, Seismic coupling and earthquake potential of the southern Cascadia subduction zone, GSA Abstracts with Programs, *26*, A-524.

References Cited

Atwater, B. F., 1987, Evidence for great Holocene earthquakes along the outer coast of Washington State, *Science*, *236*, 942-944.

Atwater, B.F., 1992, Geologic evidence for earthquakes during the past 2000 years along the Copalis River, southern coastal Washington, *J. Geophys. Res.*, *97*, 1901-1919.

Clarke, S.H. and G.A. Carver, 1992, Late Holocene tectonics and paleoseismicity, southern Cascadia subduction zone, *Science*, 255, 188-192.

Demets, C., R.G. Gordon, D.F. Argus, and S. Stein, 1990, Current plate motions, *Geophys. J. Int.*, *101*, 425-478.

Kelsey, H.M., R.C. Witter, and M. Polenz, 1993, Cascadia paleoseismic record derived from Late Holocene fluvial and lake sediments, Sixes River Valley, Cape Blanco, south central Oregon, *EOS Trans. AGU*, 74, 199.

Mitchell, C.E., P. Vincent, R.J. Weldon, II, and M.A. Richards, 1994, Present-day vertical deformation of the Cascadia margin, Pacific Northwest, U.S.A., *J. Geophys. Res.*, *99*, 12257-12277.

Nelson, A.R., 1992, Holocene tidal-marsh stratigraphy in south-central Oregon -- Evidence for localized sudden submergence in the Cascadia subduction zone, in *Quaternary Coasts of the United States: Marine Lacustrine Systems, Soc. Sed. Geol. Special Pub. 48*, 287-301.

Okada, Y., 1985, Surface deformation due to shear and tensile faults in a half-space, *Seism. Soc. Am Bull.*, *75*, 1135-1154.

Reilinger, R. and J. Adams, 1982, Geodetic evidence for active landward tilting of the Oregon and Washington coastal ranges, *Geophys. Res. Lett.*, *9*, 401-403.

Riddihough, R., 1984, Recent movements of the Juan de Fuca plate system, *J. Geophys. Res.*, *89*, 6980-6994.

Savage, J.C., 1983, A dislocation model of strain accumulation and release at a subduction zone, *J. Geophys. Res.*, *88*, 4984-4996.

Verdonck, D. and G. Zandt, 1994, Three-dimensional crustal structure of the Mendocino triple junction region from local earthquake travel times, *J. Geophys. Res.*, in press.

Weaver, C.S., and G.E. Baker, 1988, Geometry of the Juan de Fuca plate beneath Washington and northern Oregon from seismicity, *Seism. Soc. Am. Bull.*, *78*, 264-275.

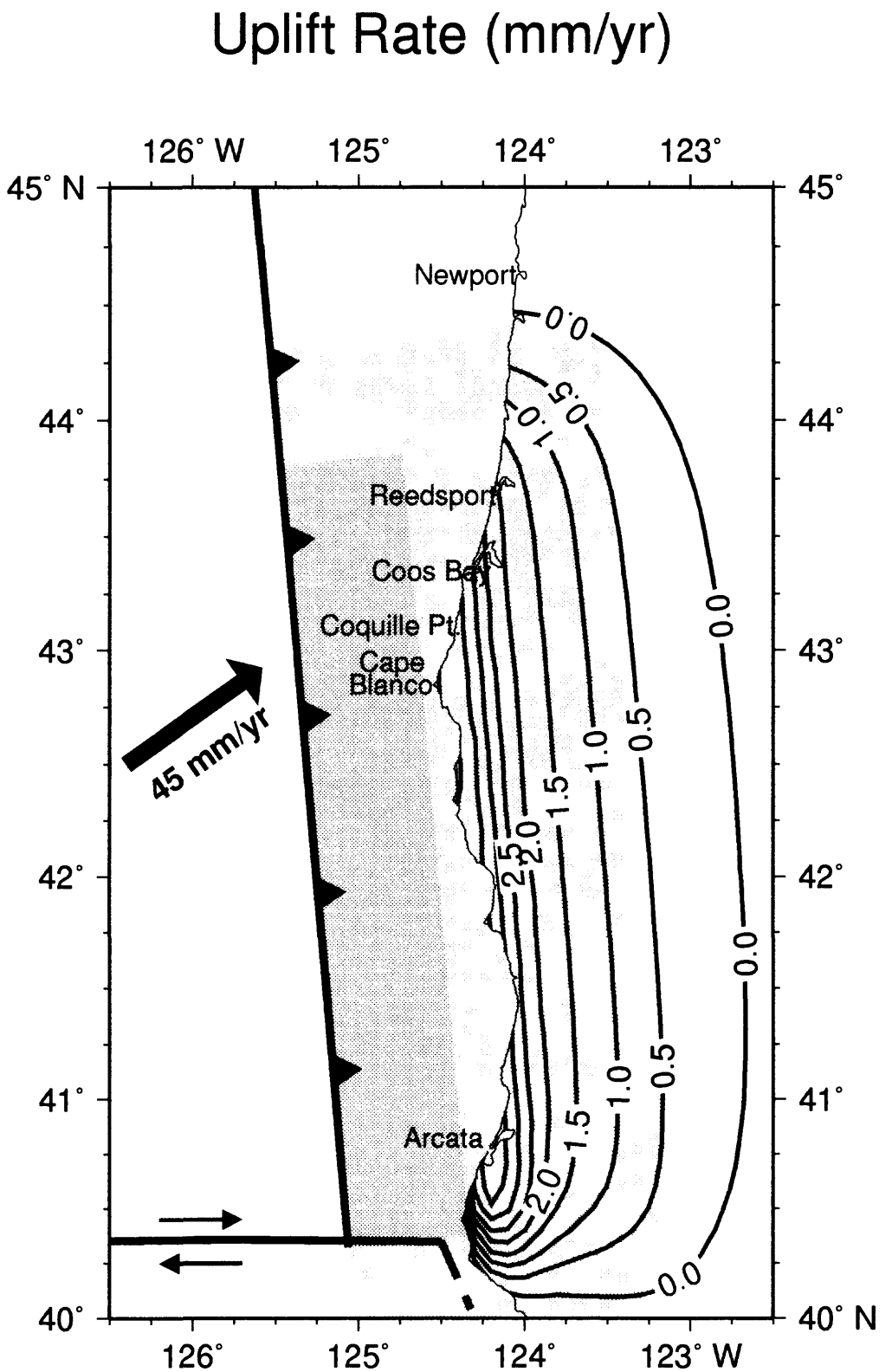

Figure 3: Contour map of uplift rates predicted by model for northern California and central and southern Oregon. Contour interval is 0.5 mm/yr. To determine model prediction for coseismic subsidence multiply uplift rate by earthquake repeat time (assuming complete elastic rebound). Dark shaded region represents fully locked part of the subduction interface. Light shaded area is transition region where slip deficit decreases from being equal to plate convergence rate in fully locked region to zero in unshaded region.

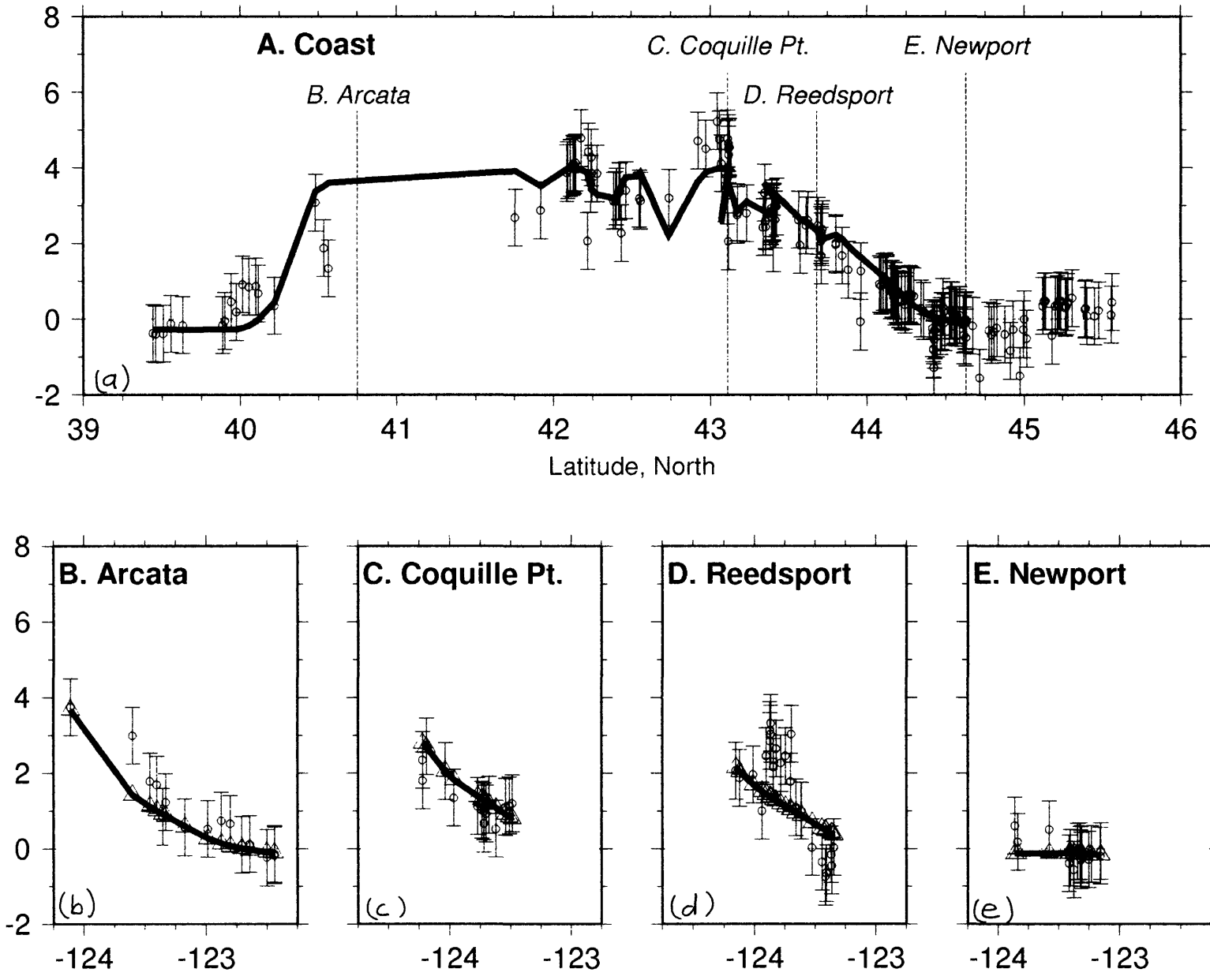

Figure 2: Uplift rates for western Oregon and northwestern California. Open circles are uplift rates determined by Mitchell et al. (1994), with assigned errors of 1 mm/yr. Solid lines give model estimates for uplift rate at each survey point. (a) North-south survey line along Oregon coast. Dashed lines show approximate location of east-west lines. (b) Survey line east from Arcata, California. (c) Survey line east from Coquille Point, Oregon. (d) Survey line east from Reedsport, Oregon. (e) Survey line east from Newport, Oregon.

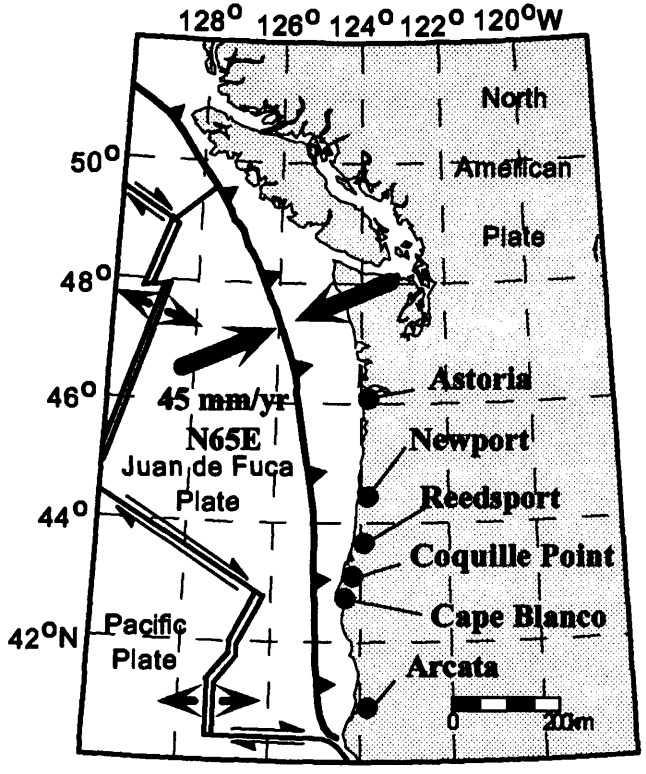

Figure 1: Tectonic map of the Cascadia subduction zone.

Stress Modeling of the New Madrid Seismic Zone

Award Number: 1434-94-G-2465

Program Element II.2

Randall M. Richardson
Department of Geosciences
University of Arizona
Tucson AZ 85721
(602) 621-4950 (Office)
(602) 621-2672 (Fax)
Internet: rmr@geo.arizona.edu

INVESTIGATIONS:

1. Finite element modeling of local stresses associated with dense rift pillows in the lower crust beneath the New Madrid Seismic Zone (NMSZ).

2. Analysis of stress data in the NMSZ for comparison with modeling and with other data for stable North America.

RESULTS:

1. We have modeled the state of stress around the NMSZ using both linear and nonlinear viscoelastic finite element models to determine whether the magnitude and pattern of stress produced locally by the support of the rift pillow may significantly contribute to the total present-day stress field and to the occurrence of intraplate seismicity. These models were run for a loading time of 100 m.y. to account for any relaxation and transfer of stress since the last reactivation of the rift in the mid-Mesozoic. Results indicate that the nonlinear viscoelastic model with rheological stratification based on composition and temperature agrees well with the observed deformation within the seismic zone and with estimates of regional stress magnitudes. The model predicts a maximum compression of 30 to 50 MPa above the rift pillow in the center of the rift axis. Results of the modeling indicate that stresses from the load of the rift pillow may still be present in the upper crust even after 100 m.y., and thus play a significant role in present-day seismicity and deformation of the NMSZ.

2. We have analyzed the available intraplate stress indicators for the NMSZ, and found a 10°-20° clockwise rotation in the direction of $S_{H_{max}}$ (maximum horizontal compression) near the rift axis. If the magnitude of local compression predicted by the nonlinear model produces this observed clockwise rotation, the magnitude of regional compression is a factor of one

to two times the magnitude of local compression and consistent with an origin due to ridge push forces. The addition of the local stress associated with rift pillow, however, results in an approximately 30% reduction in the resolved maximum horizontal shear stress. Thus, while the stress associated with the rift pillow can rotate the stress field into an orientation favorable for failure, reduction in the resolved shear stress requires a separate mechanism for strength reduction.

Reports:

Abstracts:

Zoback, M.L., M.D. Zoback, A.J. Crone, M.N. Machette, and R.M. Richardson, Processes and Patterns of Intraplate Seismicity, *Geol. Soc. Am. Abstracts with Programs , 26* , A332, 1994.

Papers:

Zoback, M.L., and R.M. Richardson, Stress Perturbation and Intraplate Seismicity Associated with Ancient Continental Rifts, *J. Geophys. Res.* , in review.

Grana, J.P., and R.M. Richardson, Tectonic Stress within the New Madrid Seismic Zone, *J. Geophys. Res.* , in review.

Kinematics and Dynamics of Strain Accumulation in the Adirondacks

Grant 1434-94-G-2472

Steven W. Roecker
Department of Earth and Environmental Sciences, Rensselaer Polytechnic Institute,
Troy, NY 12180
Tel: (518) 276 6773 Fax: (518) 276 8627
e-mail: roecker@harold.geo.rpi.edu

John Beavan
Lamont-Doherty Earth Observatory of Columbia University, Palisades, NY 10964
Tel: (914) 365 8882 Fax: (914) 365 8150
e-mail: beavan@lamont.ldeo.columbia.edu

Program Element: II.3

Investigations

The principal objectives of this project are to investigate the current state of deformation within, and the structure of the crust and upper mantle beneath, the Adirondack Mountains of New York. The current state of deformation will be assessed through a Global Positioning System (GPS) geodetic experiment that will reoccupy monuments from surveys conducted 1, 39, 63, and 100 years ago. The structure of the crust and upper mantle will be investigated through the analysis of teleseismic data collected from a year-long deployment of 4 broadband seismometers in different parts of the Adirondacks. These seismic data will be used to determine the shear wave velocity structure beneath the stations from receiver function analysis, and upper mantle anisotropy from splitting of SKS arrivals, both of which will provide valuable clues about the existence (or lack thereof) of any anomalously hot region beneath the mountains. Additional information about the ambient stress field can be obtained from recordings of local and regional earthquakes .

To this point we have concentrated on tasks necessary for the field investigations, which will commence in 1995. These tasks include (1) cataloguing and re-analysis of the triangulation measurements of Verplank Colvin during the Adirondack surveys of the late 19th century, (2) reconnaissance of summits in the Adirondacks for sites suitable for reoccupation by GPS receivers, (3) cataloguing and re-analysis of the leveling line data taken across the Adirondacks in 1931, (4) reconnaissance of benchmarks from the 1931 leveling survey suitable for reoccupation by GPS receivers, (5) identification of suitable areas for deployment of broadband sensors.

Results

1. We have recovered an appropriate subset of Colvin's observations from the archives of the Department of Energy Conservation of New York and from the library of the New York State Museum.

2. Several of Colvin's triangulation measurements have been re-analyzed to provide accurate relative positions between summits in the Adirondacks.

3. Based on the data recovered, twenty of the summits identified as theoretically useful for reoccupation were climbed and evaluated for appropriateness for further GPS work. Of the summits reached by field parties, five are considered "ideal" (those with easily identifiable bench marks and good horizon), another five had evidence of previous occupation but were not unambiguous, and the remainder had no or poor evidence of previous occupation. Fortunately, the five identified are in key locations and therefore can be used to carry out the proposed field work.

4. Site descriptions of all the bench marks occupied during the 1931 leveling campaign have been obtained, and two areas, one at the edge of the Adirondacks, near Utica, NY, and one near the high peaks, near Tupper Lake, were identified as potentially useful sites for reoccupation. A preliminary reconnaissance trip to these sites turned up at least two monuments in bedrock that

would be useful for further GPS measurements. An additional trip to record data at these sites will occur in the near future.

5. Suitable areas for deployment of broadband sensors have been identified in the southeastern (near Lake George) and northern (near the high peaks region) Adirondacks. Other sites in the northwestern and southwestern regions are still under negotiation.

Ongoing Investigations

At this point we have done sufficient reconnaissance and other background work to begin the collection of new data. Seismic and geodetic data collection will begin as soon as equipment from the agencies involved (UNAVCO and IRIS) become available. In the meantime, we will continue to re-analyze existing geodetic data sets and conduct further field reconnaissance.

FLUID PRESSURE AND EARTHQUAKE GENERATION

9960-10216, 9960-11216, 9960-12216

Evelyn Roeloffs, Eddie Quilty
Branch of Earthquake Geology and Geophysics
U.S. Geological Survey
5400 MacArthur Blvd.
Vancouver, WA 98661
Tel. (206)696-7912 Internet: evelynr@pwavan.wr.usgs.gov
Program Element II

INVESTIGATIONS

1. The project collects digital ground water level data in Parkfield, California, as part of the Parkfield earthquake prediction experiment. Ground water level data are also collected at two wells in the Mojave Desert in southern California.

2. The project investigates the hydrologic effects of earthquakes as well as reports of hydrologic earthquake precursors.

RESULTS

Figure 1 is a map of the Parkfield, California ground water monitoring network. A new site at Halliburton Ranch was added during FY1994. Figure 2 shows the data collected during FY1994. Of special interest are the earthquake-related water level rises in the Bourdieu Shallow well at the northern end of the network, shown in Figure 3. These water-level changes are too large to be attributed to the static volumetric strain fields of the earthquakes that produced them, and must be the result of dynamic stresses and strains carried by seismic waves. The responses to earthquake of magnitude less than 5 suggest that seismic waves with periods less than 10 seconds are involved in producing the water-level response. The data demonstrate that sustained coseismic water level changes can be produced at distances of several hundred kilometers from an earthquake.

Figure 4 is a map showing the locations of wells in the Mojave Desert, and Figure 5 shows the data collected during FY1994. The Northridge earthquake produced a coseismic water level drop in the Crystalaire well, shown in Figure 6.

Compilation was completed of an open-file report summarizing all known hydrologic effects of the 1992 Landers, California earthquake. Figure 7 shows the volumetric strain field of the earthquake, together with ground water observations in southern California.

Project personnel responded to the Northridge earthquake by investigating reports of post-seismic discharge changes and compiling data on other hydrologic effects. Of particular potential importance is the report of a pre-earthquake stream discharge increase in the Southern Pacific Spring in Millard Canyon. This anecdotal report is considered potentially significant because it resembles reports of pre-earthquake streamflow changes preceding the 1989 Loma Prieta, California, earthquake, as well as a published report of a discharge increase preceding an earthquake in Japan.

PUBLICATIONS

Galloway, D., Laczniak, R., Reiner, S., Unger, R., and Roeloffs, E., Sustained aquifer fluid-pressure changes in Ash Meadows, Nevada, in response to the Northridge earthquake, Supplement to *EOS, Trans. Am. Geophys. Union, 75*, 171, 1994.

Quilty, E., and E. Roeloffs, Water level observations in the east San Francisco Bay area, California, U.S. Geological Survey Open-File Report OF94-418, in press, 1994.

Quilty, E.G., W.Danskin, C.D.Farrar, D.L.Galloway, S.N.Hamlin, E.A.Roeloffs, M.L.Sorey, and D.E.Woodcock, Hydrologic effects of the 17 January 1994 Northridge earthquake, Supplement to *EOS, Trans. Am. Geophys. Union, 75*, 171, 1994.

Roeloffs, E., and Langbein, J., The earthquake prediction experiment at Parkfield, California, *Reviews of Geophysics, 32*, 315-336, 1994.

Roeloffs, E., and Quilty, E., Water level and strain changes before and after the 1985 Kettleman Hills, California, earthquake, in press, *Pure and Applied Geophysics*, 1994.

Roeloffs, E., and E. Quilty, Groundwater level changes near Parkfield, California, caused by recent earthquakes, Supplement to *EOS, Trans. Am. Geophys. Union, 75*, 471, 1994.

Roeloffs, E.A., Poroelastic techniques in the study of earthquake-related hydrologic phenomena, submitted to *Advances in Geophysics*, 1994.

Roeloffs, E.A., W.R. Danskin, C.D. Farrar, D.L. Galloway, S.N. Hamlin, E.G. Quilty, H.M. Quinn, D.H. Schaefer, M.L. Sorey, and D.E. Woodcock, Hydrologic effects associated with the June 28, 1992 Landers, California, earthquake sequence, to appear as U.S. Geological Survey Open-File Report, 1994.

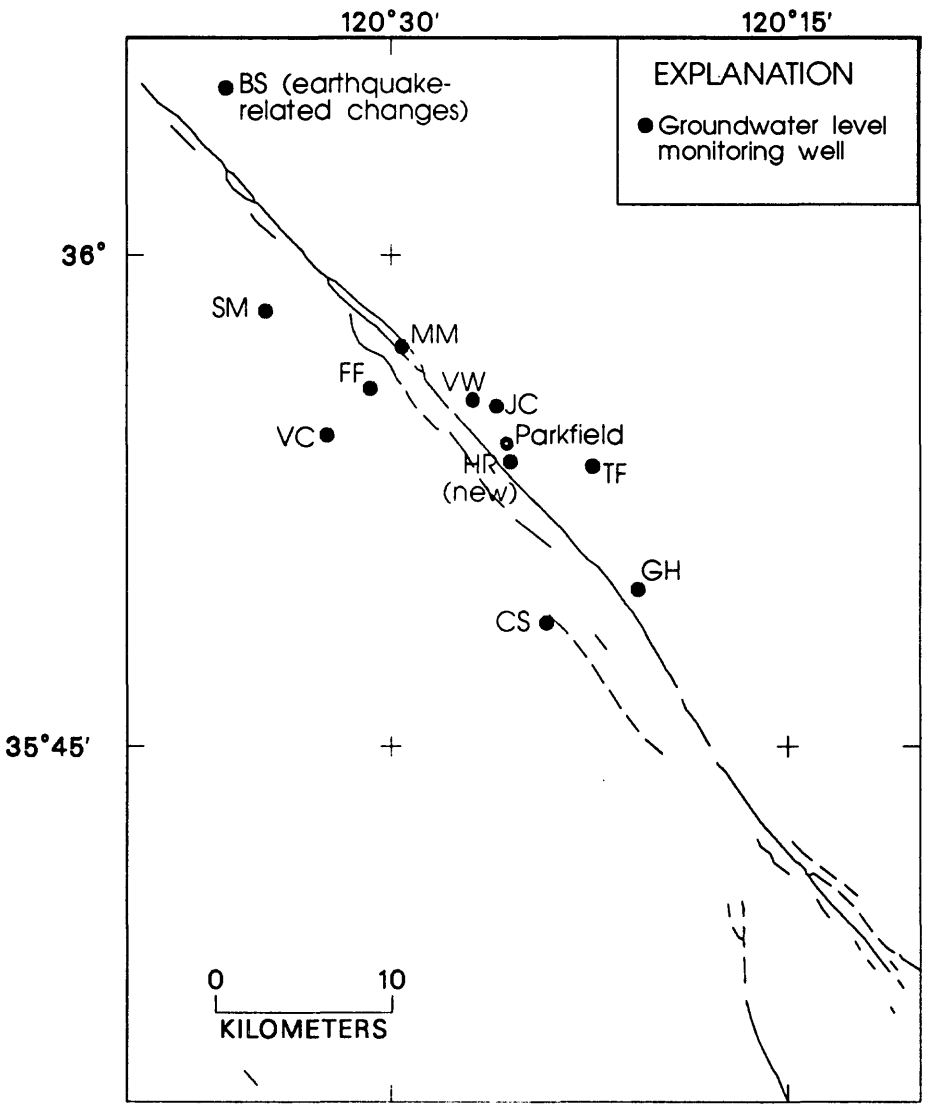

Figure 1. Map showing the Parkfield groundwater level monitoring network, including the new site at the Halliburton Ranch (HR).

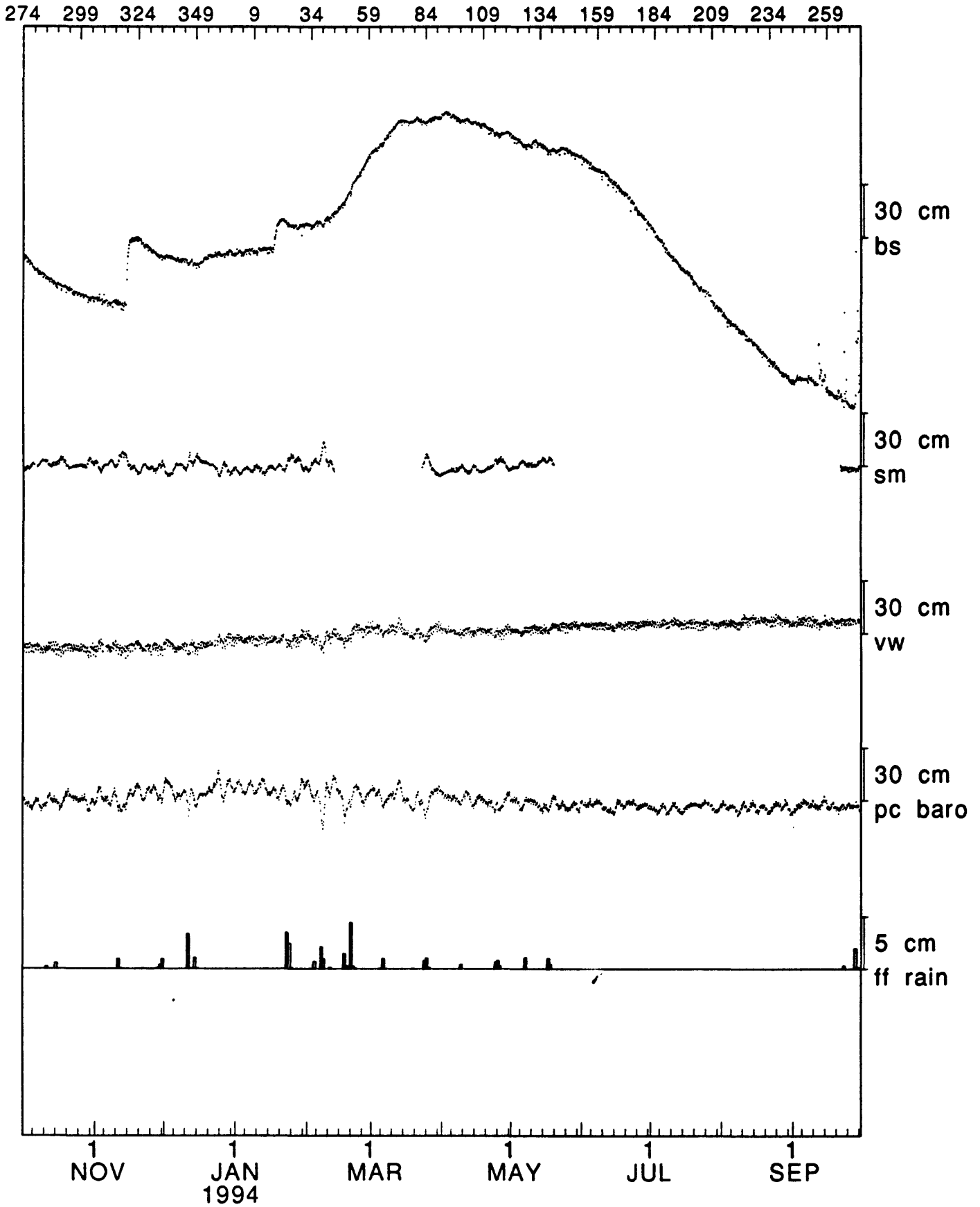

Figure 2. (a) Water level, barometric pressure, and rainfall records for wells near Parkfield, California. Hourly values are plotted for water level and barometric pressure. Water level is in centimeters above an arbitrary datum. Barometric pressure is in centimeters of water with respect to an arbitrary datum. Bars indicate total rainfall in a 24 hour period. Site names are indicated at right.

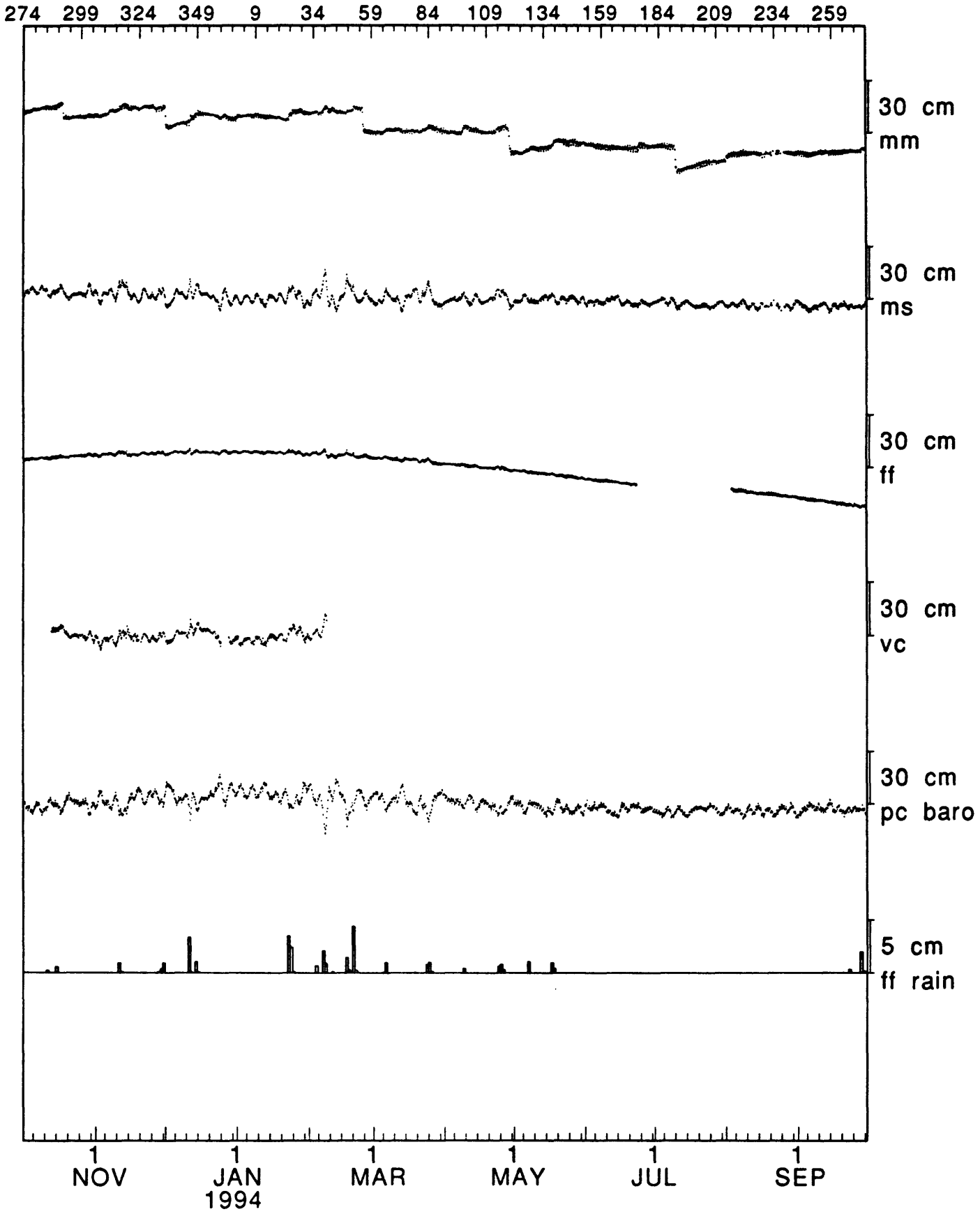

Figure 2. (b) Water level records for Parkfield, plotted as in Figure 2(a).

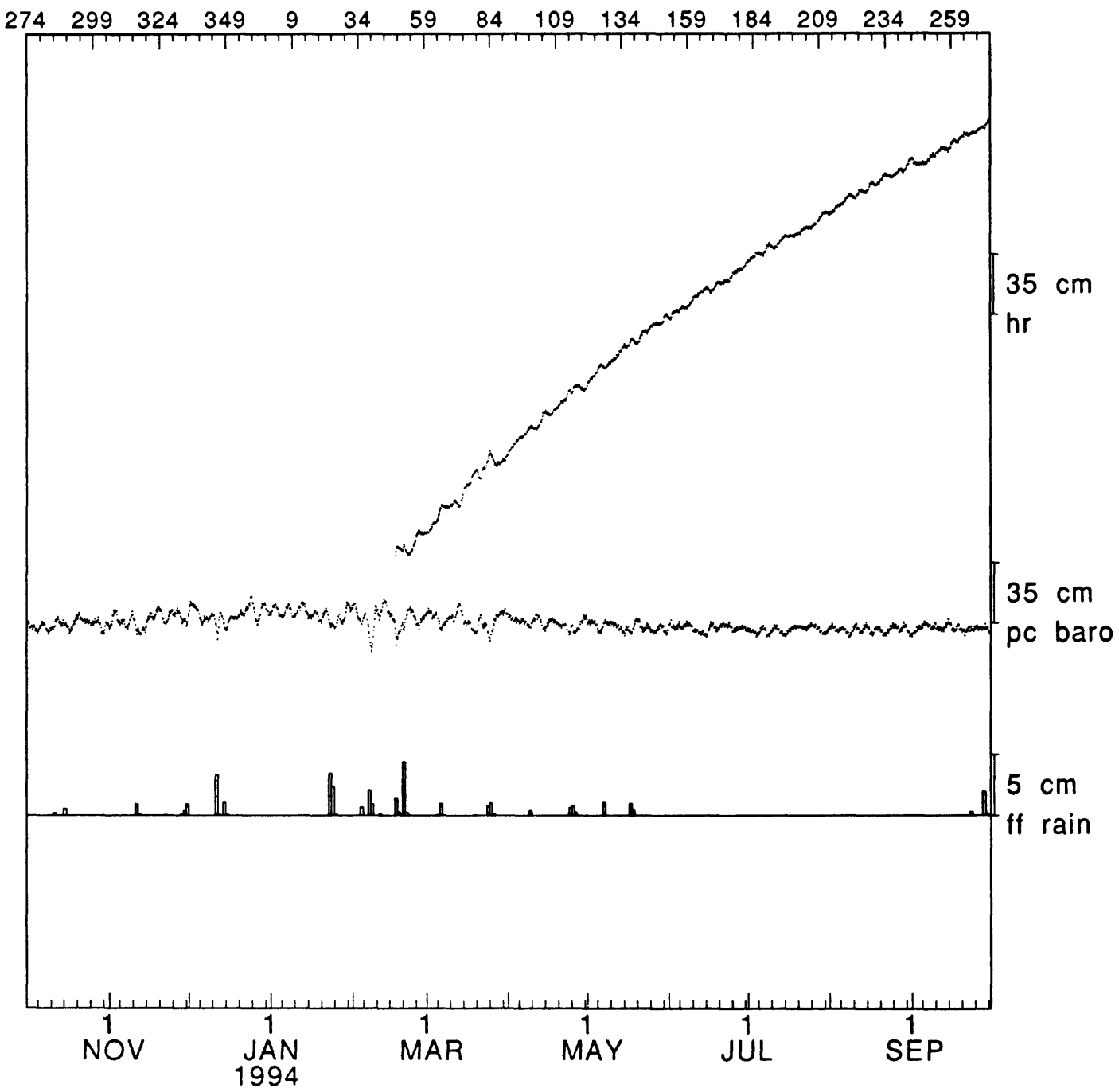

Figure 2. (c) Water level records for Parkfield, plotted as in Figure 2(a).

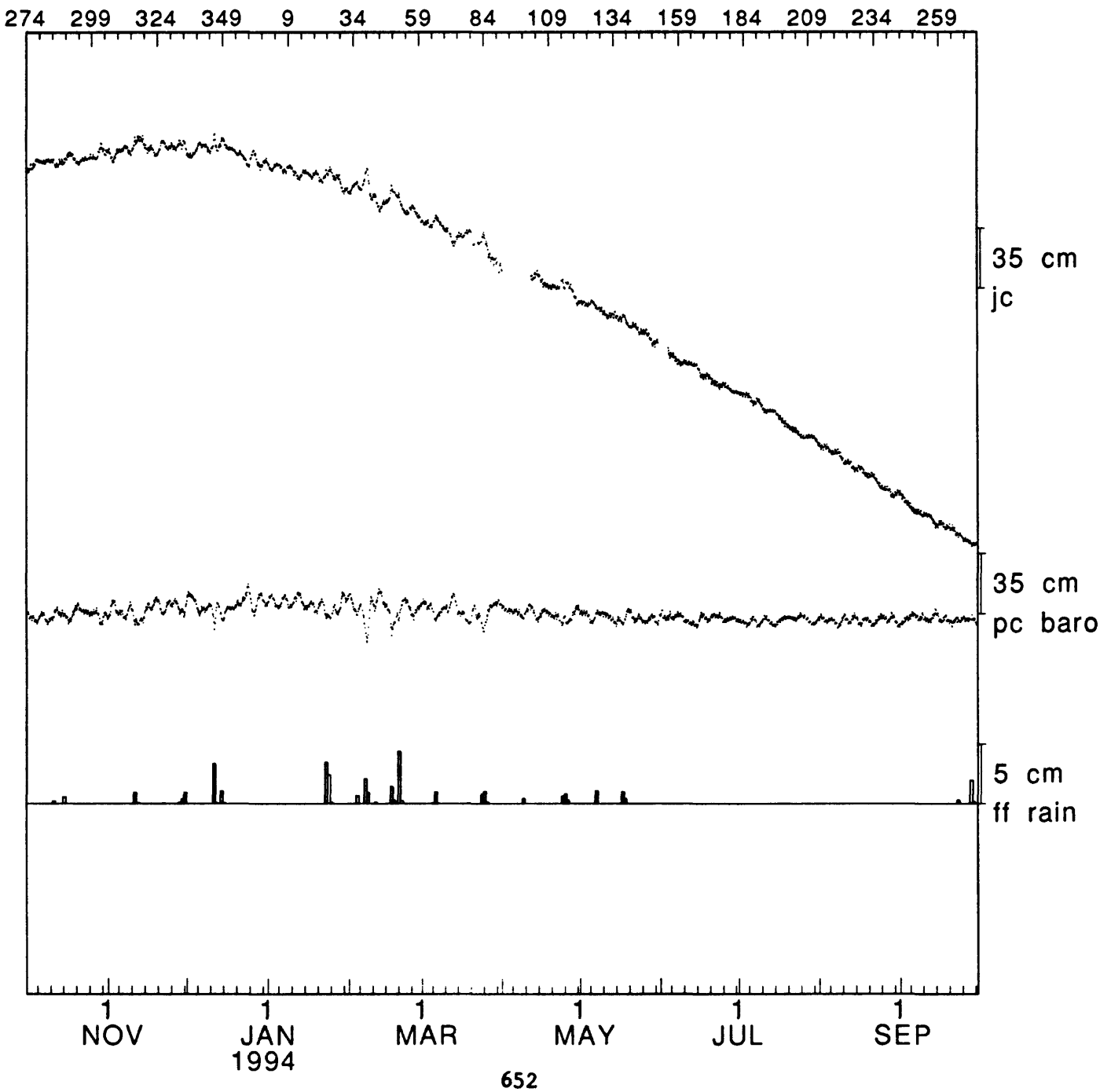

Figure 2. (d) Water level records for Parkfield, plotted as in Figure 2(a).

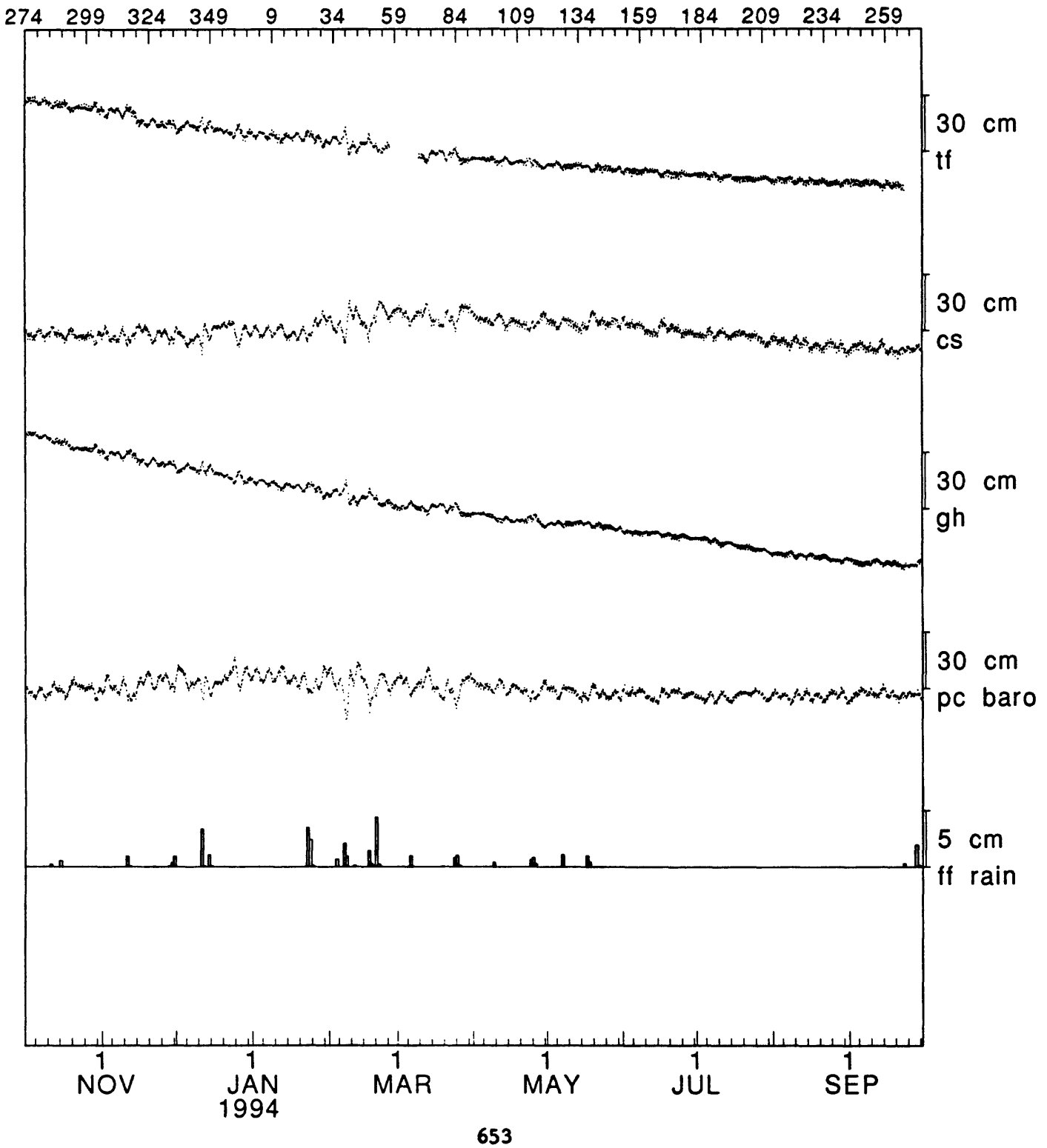

Figure 2. (e) Water level records for Parkfield, plotted as in Figure 2(a).

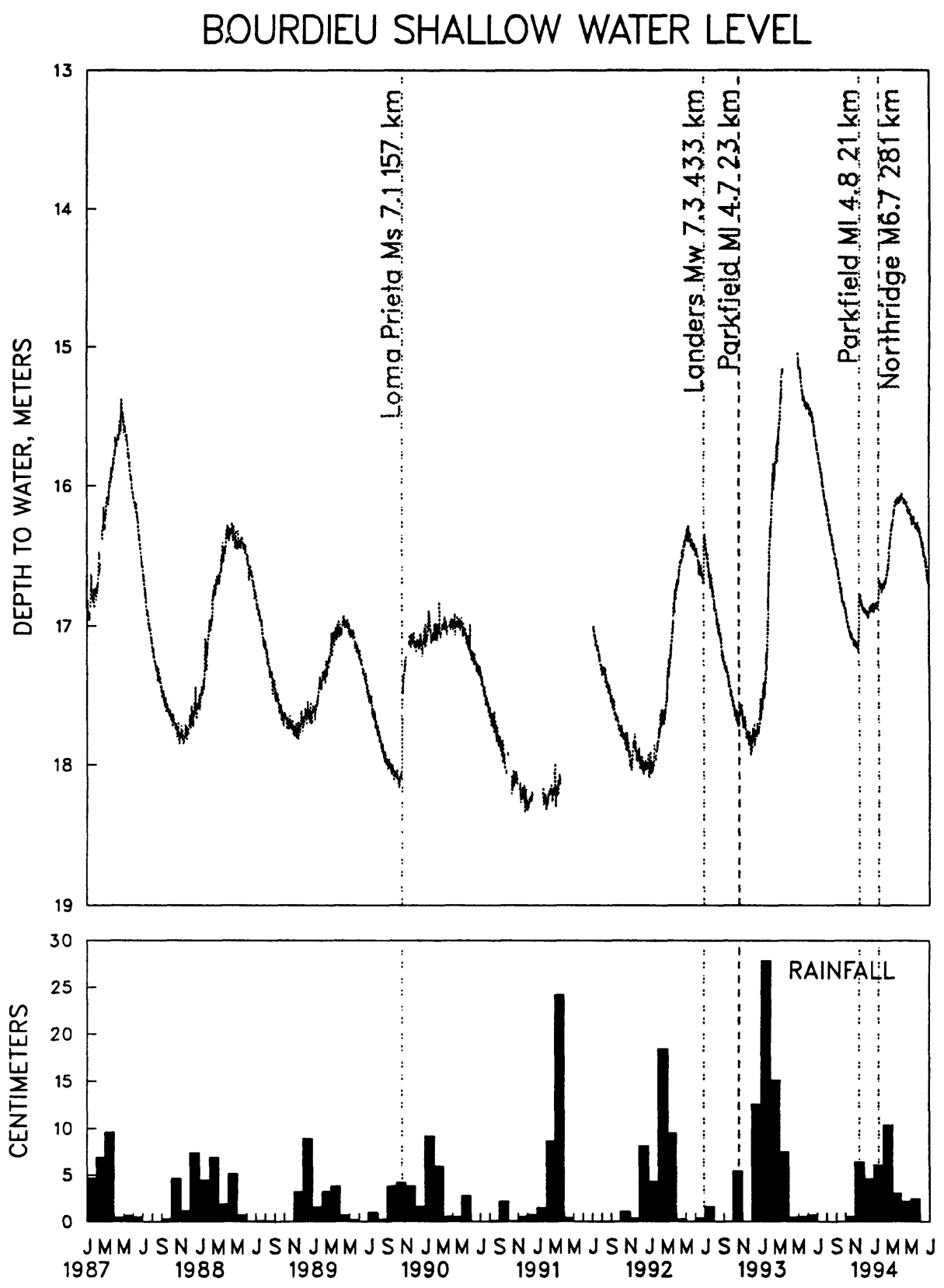

Figure 3. Water level, barometric pressure, and rainfall at the Bourdieu Shallow well near Parkfield, California, marked to show earthquake-related changes following five recent California earthquakes.

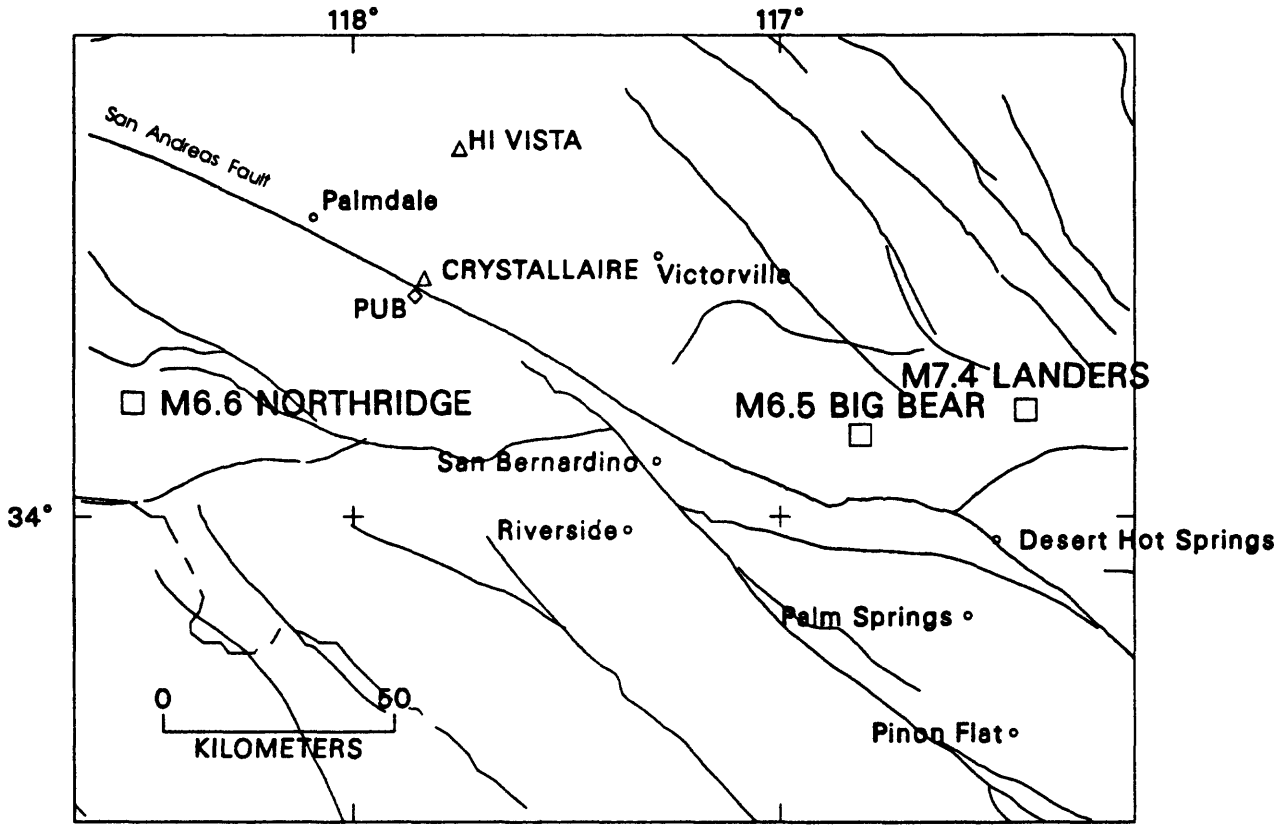

Figure 4 Map showing locations of the Hi Vista and Crystallaire wells, as well as the Punchbowl dilatometer (PUB).

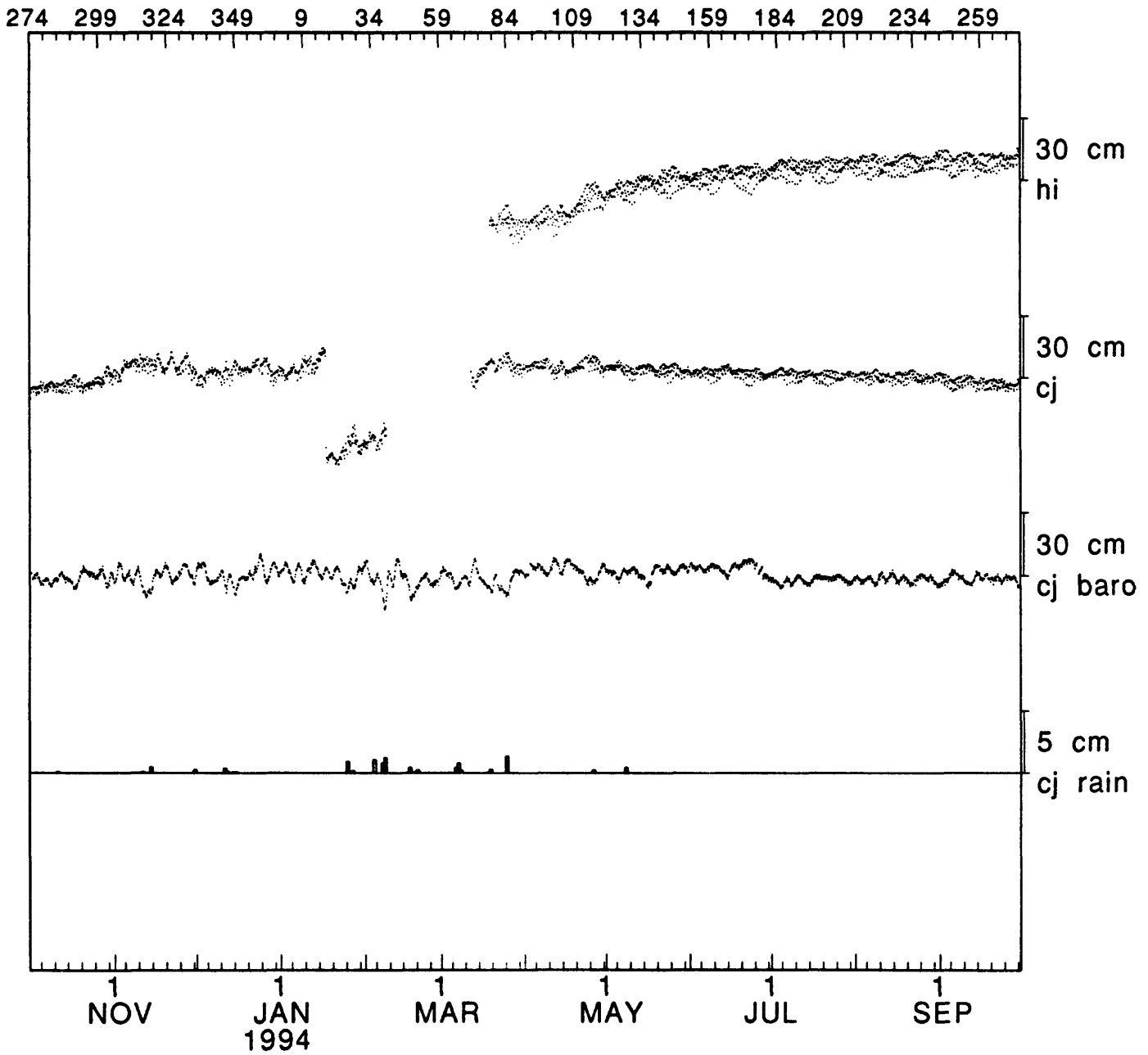

Figure 5. Water level, barometric pressure, and rainfall records for wells near in the Mojave Desert, California. Hourly values are plotted for water level and barometric pressure. Water level is in centimeters above an arbitrary datum. Barometric pressure is in centimeters of water with respect to an arbitrary datum. Bars indicate total rainfall in a 24 hour period. Site names are indicated at right.

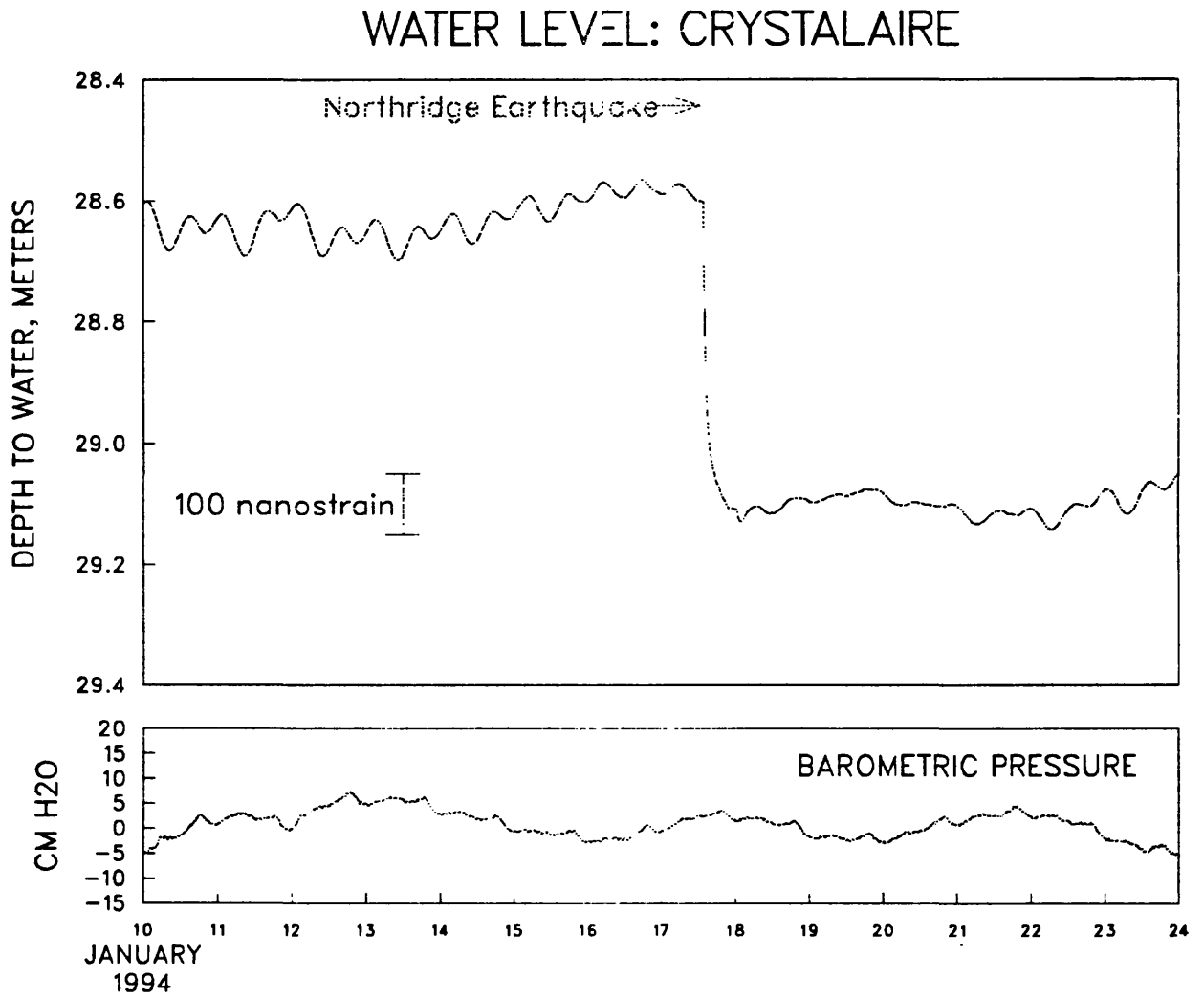

Figure 6. Water level and barometric pressure at the Crystalaire site in southern California, showing a coseismic water level drop in response to the Northridge earthquake on January 17, 1994.

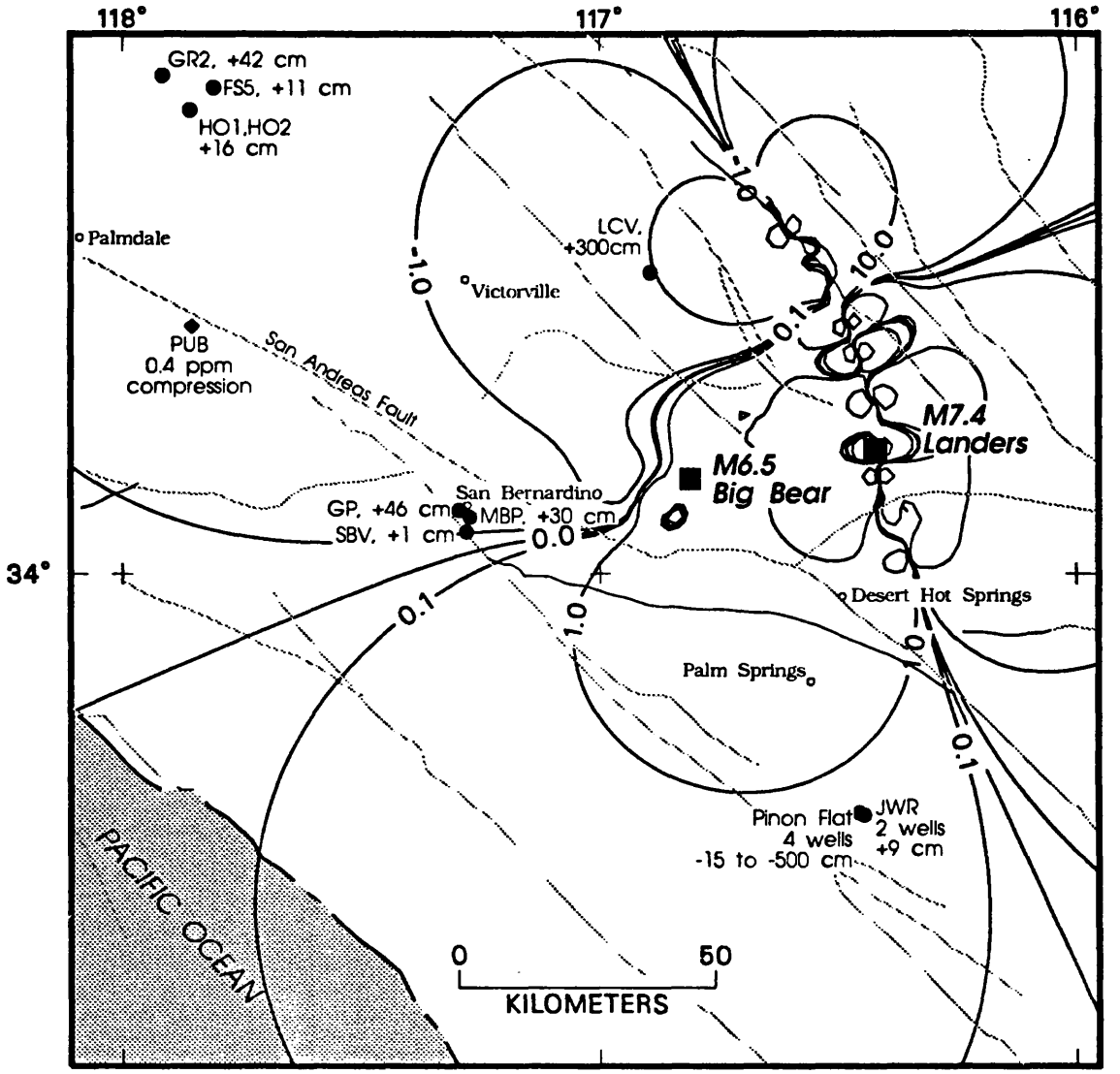

Figure 7. Location of observation wells in southern California where a response to the Landers earthquake was documented. Each site is labeled with the direction and magnitude of the water level change that took place immediately after the earthquake. Contours of calculated volumetric strain, in ppm (microstrain) are shown as solid black curves, with extension positive. Faults are shown as solid gray lines. PUB denotes the Punchbowl borehole strainmeter. Pinon Flat denotes an instrument cluster that includes 4 observation wells; see Wyatt et al. (*Bull. Seismol. Soc. Am., 84*, 768-779, 1994) for details.

OPERATION OF THE JOINT UCB/USGS DATA CENTER

AWARD NUMBER: 1434-94-G-2387

BARBARA ROMANOWICZ AND DOUGLAS NEUHAUSER
SEISMOGRAPHIC STATION
UNIVERSITY OF CALIFORNIA AT BERKELEY
475 McCONE HALL
BERKELEY, CALIFORNIA 94720-4760

SUMMARY

The Northern California Earthquake Data Center (NCEDC) is serving as on-line archive and distribution facility for waveform and catalog data of the Northern California Seismic Network (NCSN) operated by the U.S. Geological Survey and Berkeley Digital Seismic Network (BDSN) operated by the U.C. Berkeley Seismographic Station. These data serve as basis for many research projects relevant to NEHRP goals in the Bay Area and more generally central and Northern California. We have also recently started archiving data from the newly established Bay Area Regional Deformation Network (BARD) of continuous GPS receivers. Plans exist for archiving other data sets, such as Hayward Fault Surveillance Network, strong motion data, Berkeley analog tape collection. The data are accessible to outside users through Internet, and recent "traffic" has demonstrated the usefulness of the Data Center as a service to the seismological community. The current capacity of the NCEDC mass-storage device (300 GBytes) will be reached by the end of 1994.

PROJECT DESCRIPTION

The Northern California Earthquake Data Center (NCEDC) was initiated in late 1991, as a joint project of the Berkeley Seismographic Station (BSS) and the U.S. Geological Survey at Menlo Park, to serve as "on-line" archive for a variety of digital data pertaining to central and northern California earthquakes and related phenomena, and that form the basis of research towards NEHRP goals. The NCEDC is located at U.C. Berkeley, operated jointly with the USGS, and has been accessible to outside users in the scientific community through INTERNET since mid-1992 (Bogaert et al., 1992; Romanowicz et al., 1994).

The primary goal of the Data Center is to provide a stable archive for parametric and digital waveform data from two regional networks: the Northern California Seismic Network (NCSN) operated by the USGS and the Berkeley Digital Seismic Network (BDSN) operated by the BSS (figure 1). The collection of NCSN digital waveform data dates back to 1984, that of the BDSN to 1987. Phase I of the project has two components. One is to transfer these collections from 9 track tapes to the NCEDC optical mass-store device, in order to 1) "save" the collections, doomed by the limited lifetime of the magnetic media and 2) make them easily accessible to users both at the respective institutions and in the community at large. The other is to establish a mechanism for archiving current data as they are produced, in a timely fashion. Such an on-line archive represents a tremendous improvement over previously available data distribution procedures. Data from both NCSN and BDSN were accessible until recently to only a privileged handful of courageous users. Projects that involved the analysis of large quantities of waveform data were practically unrealizable, certainly not on a timely basis.

Phase I is well underway. Current data are being collected, archived (figure 2) and made accessible as soon as they are available. We have completed the loading of 88% of the total waveform collection and expect to finish dealing with the back-log before the end of 1994 (figure 3).

In the meantime, the NCEDC has open its doors to other datasets, effectively entering Phase II of the project. Namely, we have started archiving data from continuously monitored GPS receivers in central and northern California (BARD network). There are currently 8 operational sites and several more are planned in 1994-95. We are currently archiving the data from 4 sites owned and operated by UC Berkeley (3 sites) and LLNL (1 site) and have implemented an automatic electronic transfer procedure from Menlo Park to archive the data from 4 sites operated by the US Geological Survey. Archival of other datasets (Hayward Fault surveillance network, strong motion data, digital data from other seismic and geodetic networks and electromagnetic data), is being currently initiated.

The usage of the Data Center by users outside of UC Berkeley demonstrates the success of the project (figure 4). We currently (10/94) have 280 external (non-UCB) accounts at the Data Center, 40 of which are for members of the USGS. The existence of the Data Center gets widely advertised through a publication in EOS (Romanowicz et al., 1994). A bulletin-board for exchange of comments and suggestions with users is being made available at the NCEDC.

The rationale for locating the NCEDC at UC Berkeley stems from several circumstances. The upgrade of the Seismographic Station facilities, initiated in 1991, through funding from the University of California, has provided opportunities for cost-sharing and created a situation where motivated scientists interact with energetic technical staff, to oversee the timely availability of high quality data. This cooperative program has also created a communication link between scientists at the two institutions involved. Such interaction was previously missing and it is fair to say that the NCEDC plays a similar role, although not as formally recognized, to that of the Data Center for the Southern California Earthquake Center (SCEC).

CURRENT STATUS OF THE DATA CENTER

Hardware

The primary computer system for the Data Center is a SUN SPARCstation with a mass storage system for digital waveform data, magnetic disks for volatile parametric data, and associated peripherals. The mass storage hardware consists of a Sony juke box which provides 300 GBytes of WORM (Write Once) storage. The juke box contains 2 drives and controllers, storage for 50 6-GB platters, and a robotic mechanism for automatically loading and unloading platters from the drives. The juke box is controlled by AMASS software, which schedules the platters and controls the drives and robotics, and provides a cached multi-user UNIX file system for all files on the jukebox. The mass storage system is accessible by all users on the host computer as well as other UNIX systems at the Berkeley Seismographic Station using NFS (Sun's Network File System). The system has approximately fourteen GBytes of magnetic disk which are used for storing parametric information such as seismic event catalogs and phase information, station coordinates and instrument responses, and for staging data to be stored on the jukebox. Several 4 and 8 mm tape drives are used to import data to the data center.

Available data

- NCSN Data

The NCSN (figure 1) records more than 550 components of short-period seismic data from 425 sites in central and northern California and western Nevada. All of the NCSN parametric data, such as earthquake locations, phase information, and first motion focal mechanisms, are available at the NCEDC from 1967 through the present. This location catalog is comprised of about 350,000 earthquakes of magnitude (M) > ~ 1.0 and contains information on origin time, location, magnitudes, and solution uncertainty. The phase catalog consists of arrival times and magnitude information for individual stations, and the focal mechanism catalog contains more than 37,000 fault plane solutions for events that have at least 25 P-first motions. The parametric data are updated once a day via Internet and can be retrieved as ASCII information, or in their native "CUSP" format.

The Data Center provides random access to digital seismograms from more than 100,000 local and regional earthquakes recorded by the NCSN since 1984. These data are available in CUSP, AH and SAC formats. The NCSN waveform data have so far been transferred from Menlo Park to the Data Center by tape. We expect to begin transferring the seismograms each night via Internet shortly. Figure 3 shows the current status of loading of this data collection.

- U.C. Berkeley broadband data

The UC Berkeley event catalog from 1910 to the present and the phase files from 1984 to the present are archived at the Data Center. From 1910 through 1983 the catalog and phase files contain epicenter and/or hypocenter information, magnitude (consistently after 1945), and comments about the events. From 1984 through the present, the catalog and phase files also contain error estimates on locations and depth, phase and amplitude information. We are now starting to report moment magnitude as well as moment tensor information for events of magnitude > 4.

The BDSN, operated by the UC Berkeley Seismographic Station, has recently been upgraded to very-broadband (VBB) instruments and presently consists of 11 stations distributed across central and northern California (figure 1). These stations are equipped with three component STS seismometers (Wielandt and Streckeisen, 1982; Wielandt and Steim, 1986) as well as three component FBA-23 accelerometers.

Continuous and triggered 24-bit digital broadband datastreams packaged in Quanterra data loggers are received at the Seismographic Station headquarters through continuous telemetry. These data-streams, available at the Data Center as soon as they come in, are first temporarily stored on disk, and then archived on the mass-store after they have passed through quality control procedures, within 2 to 10 days on average. All continuous and triggered data from 1991 to the present, starting with two broadband stations in 1991 and expanding to the current 11 stations, are available through the Data Center. They are stored in Mini-SEED format. Digital 16-bit data from 3 pre-existing broadband stations (BKS, MHC and SAO), for the time period 1987-1991, originally archived on PC-readable optical disks in a variety of formats, have been converted to mini-SEED format and are being loaded on the mass-store.

Software

The Data Center provides utilities to search and select event, phase and focal mechanism information from the USGS and UCB earthquake catalogs. Table I lists these utilities. It is committed to providing its waveform data in standard exchange formats. The UCB digital broadband and strong motion data can currently be retrieved based on station/channel/time selection criteria in either full SEED volume format or Mini-SEED format. The NCSN waveform data can be retrieved on an event basis in AH-XDR or SAC format as well as its native CUSP format. A CUSP-SEED translator, jointly funded by the USGS and Incorporated Research Institutes for Seismology (IRIS), is under development and is expected to be available in mid-1994.

Accessing the Data

To obtain accounts and access NCEDC through Internet, follow these instructions:

1. Use telnet to connect to brkseis20.berkeley.edu. Depending on your local computer configuration, you may have to use the Internet address of the machine instead of the hostname:

telnet brkseis20.berkeley.edu
or telnet 128.32.146.106

2. Login to special account "bulletin", using password "board"

3. Select the option to request an account. You will be prompted for information about your name, address, institutional affiliation, e-mail address, and phone number. You should be contacted within 2 working days with your account information. If you do not hear by then, contact the administrator.

References

B. Bogaert, D. Neuhauser A. Walter and B. Romanowicz (1992) The USGS/UCB Northern California Seismic Data Center, EOS Trans. AGU, 73, 371.
B. Romanowicz, B. Bogaert, D. Neuhauser and D. Oppenheimer (1994) Accessing Northern California Earthquake Data, EOS Trans AGU,
E. Wielandt and G. Streckeisen (1982) The leaf spring seismometer: design and performance, Bull. Seism. Soc. Am., 72, 2349.
E. Wielandt and J. Steim (1986) A digital very broadband seismograph, Ann. Geophys. 4B, 227.

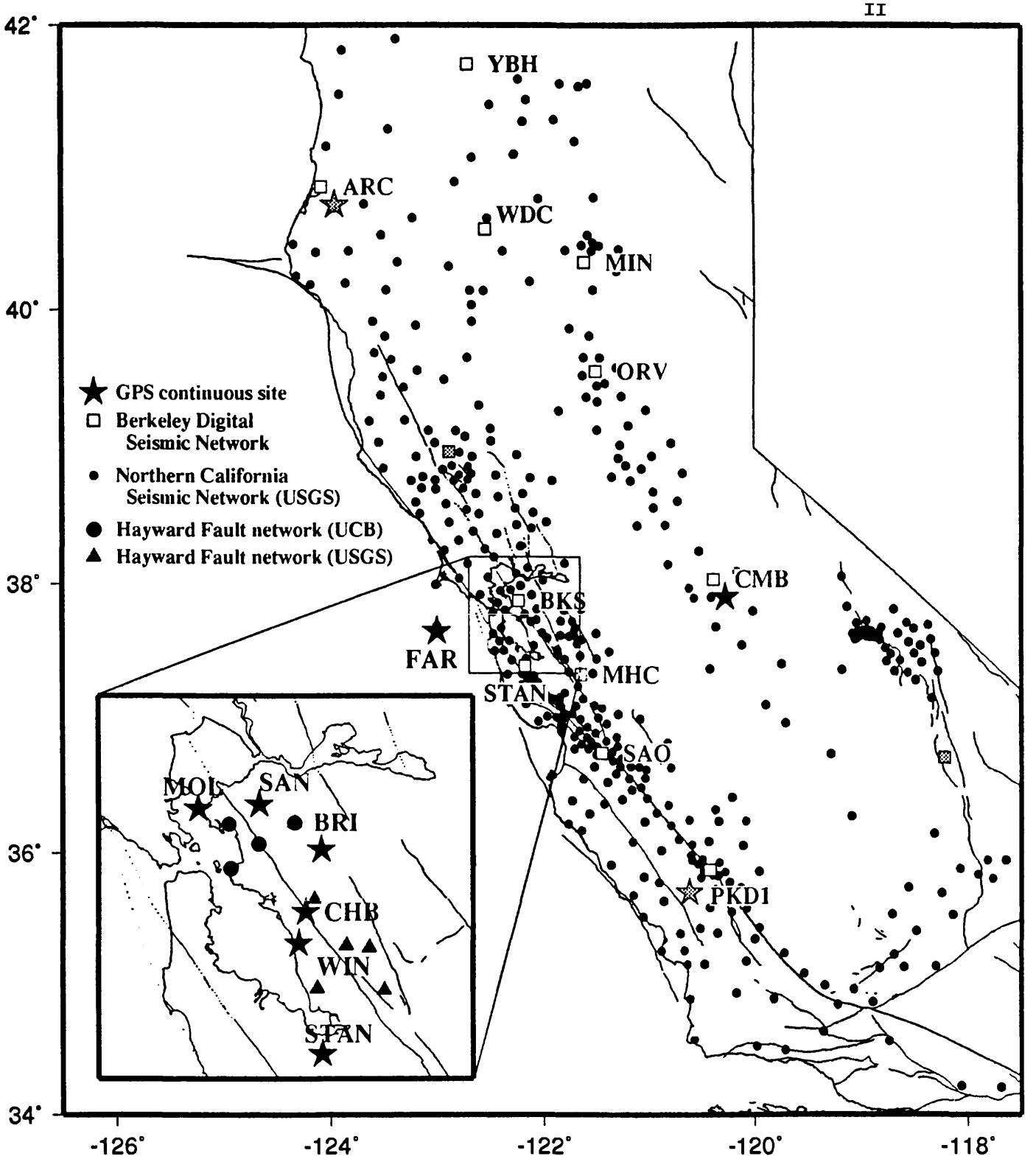

Figure 1. Distribution of stations of the NCSN and BDSN networks. For the BDSN, open symbols indicate operational stations, shaded symbols are currently planned. The distribution of GPS continuous sites (BARD) is also shown, with filled and shaded stars indicating operational and planned stations respectively.

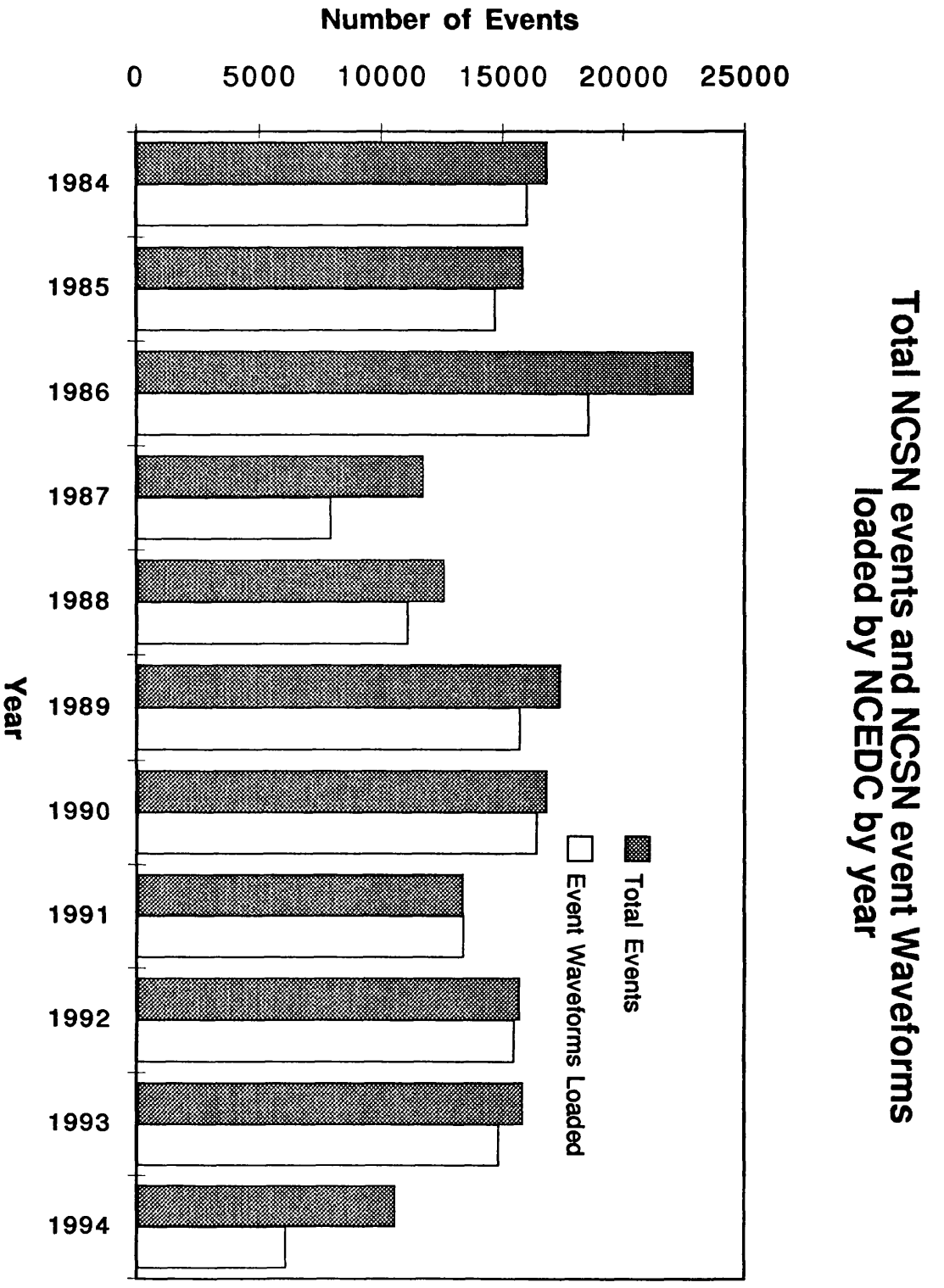

Figure 2. Comparison of total number of events acquired by NCSN for each year to the number of events loaded on NCEDC through October 1994. Data from prior years must be copied from NCSN archive tapes before being sent to the data center.

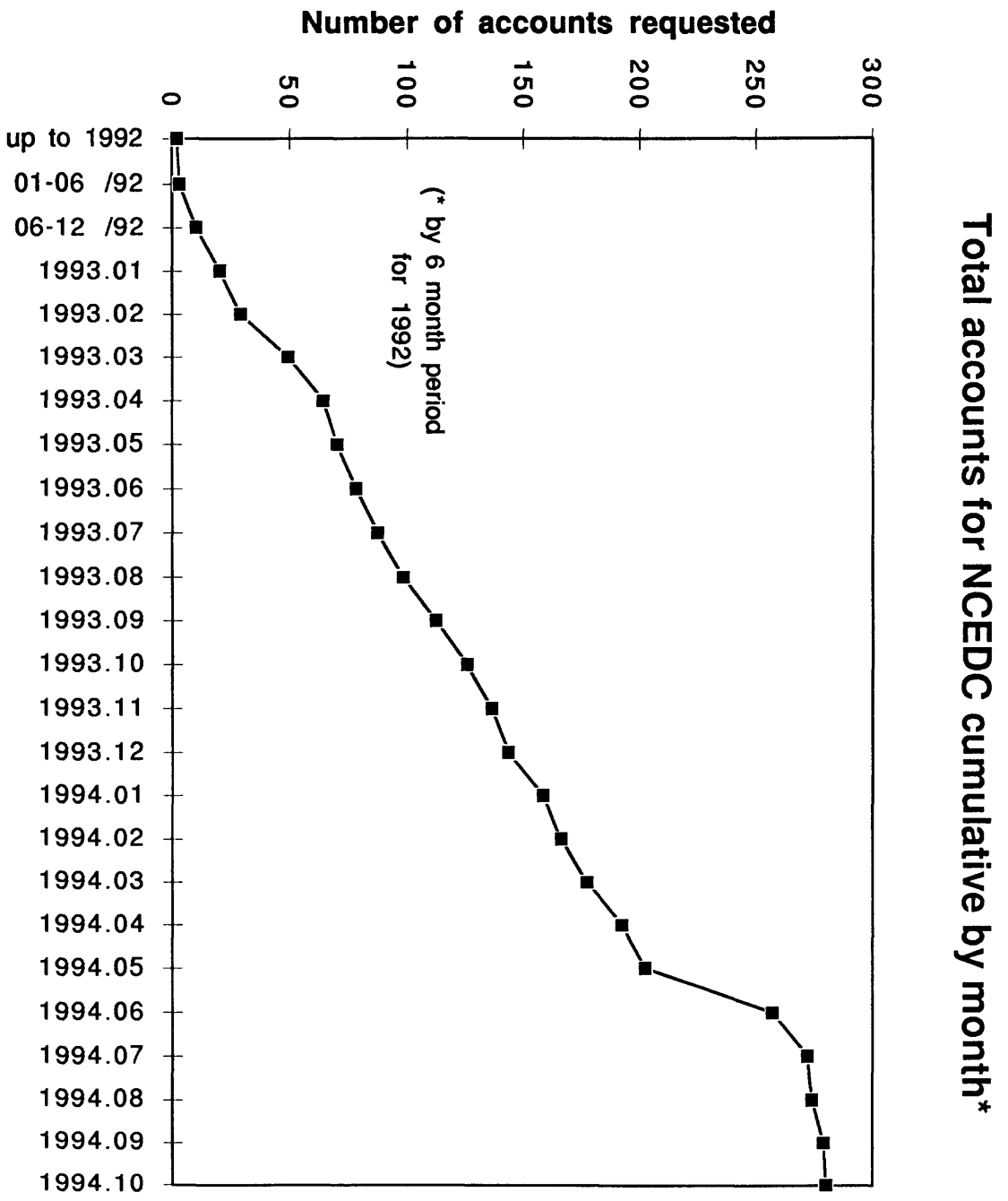

Figure 3. Cumulative number of external user accounts established on the data center form its inception through October 1994. Totals do not include any UCB accounts

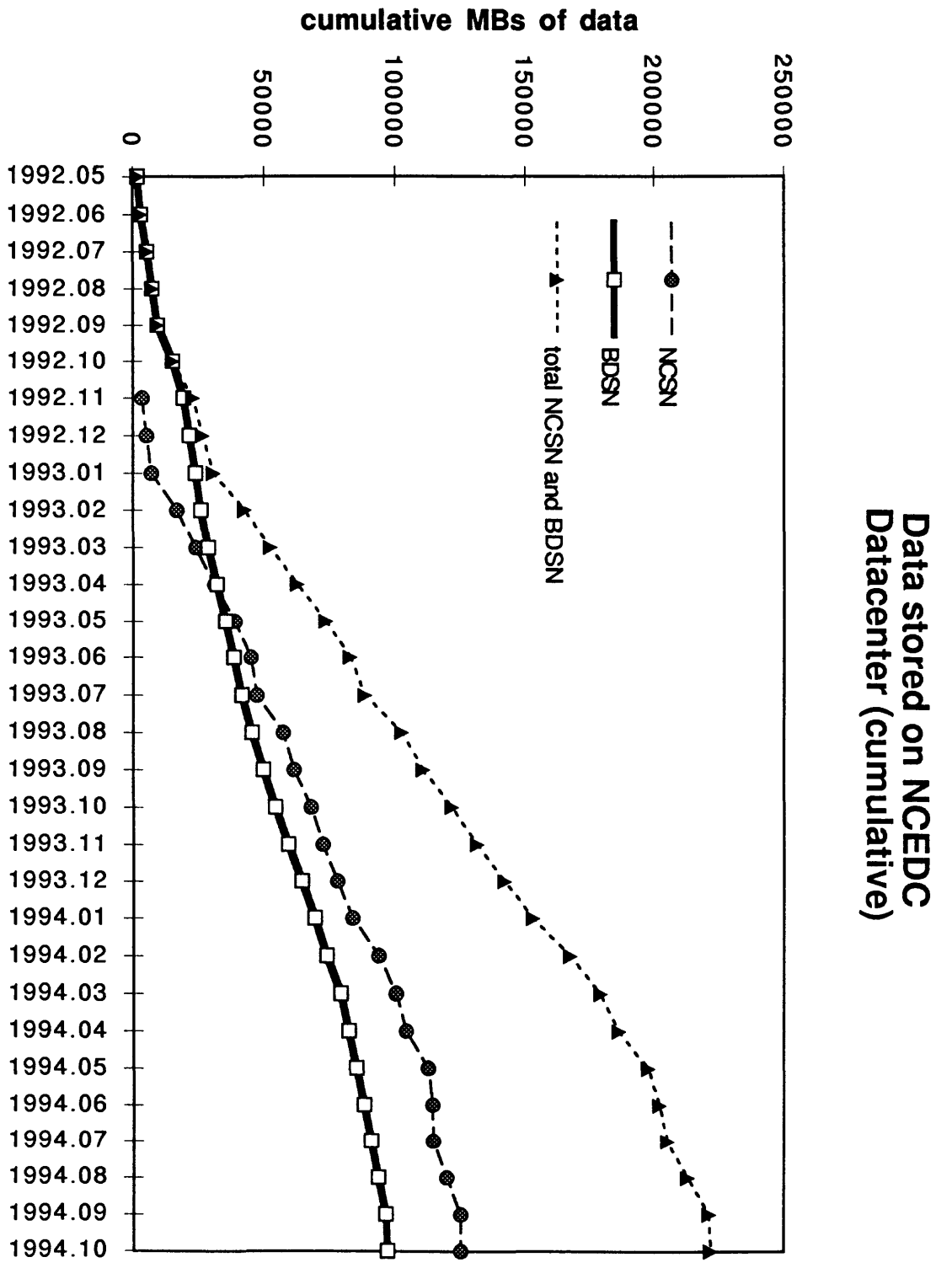

Figure 4. Monthly breakdown showing the cumulative amount of data stored on the data center since inception for BDSN and NCSN data. The rapid rise of NCSN data in 1993 represents the loading of prior years data as well as current data.

Collaborative Proposal (UCB & UCSD): Northern California Permanent GPS Network

Award Number: 1434-94-G-2411

Barbara Romanowicz and Richard W. Clymer

Seismographic Station
University of California at Berkeley
475 McCone Hall
Berkeley, California 94720-4760

SUMMARY

This grant has served to partially support the establishment of a network of permanent GPS receivers in northern and central California, BARD (Bay Area Regional Deformation). The receivers and resources are being pooled between the University of California at Berkeley (UCB, four receivers), Lawrence Livermore National Laboratory (LLNL, one receiver), and the U.S. Geological Survey (USGS, four receivers, previously installed). During the period covered by this grant, three permanent receivers have been installed at Columbia (CMBB), Farallon Islands (FARB) and Tiburon (TIBB). The site at Tiburon is temporary. Data acquisition and archiving has also been initiated at UC Berkeley. The data are available over Internet through the NCEDC (Northern California Earthquake Data Center).

PROGRESS REPORT

The establishment of a permanent regional GPS network in northern California (BARD- Bay Area Regional Deformation) is well underway. Eight stations are now operating in a cooperative effort of the Seismographic Station at U.C. Berkeley, the United States Geological Survey (USGS) in Menlo Park, LLNL and Trimble Navigation (Figure 1). The USGS began operating and maintaining two Ashtech codeless receivers in September 1991 at Chabot and Winton across the central Hayward fault. The USGS, in cooperation with Trimble, also began operating two Trimble P-code receivers in October 1993 at Molate and Nunez across the northern Hayward fault. The Seismographic Station at U.C. Berkeley installed four permanent Ashtech P-code receivers within the past year (one owned by LLNL, the other 3 by UC Berkeley), with partial funding from the USGS-NEHRP program. Two of these sites, at Briones near the Hayward fault and at Columbia in the Sierra foothills, are collocated with broadband stations of the Berkeley Digital Seismic Network (BDSN). The third site was installed in January 1994 on the Farallon Islands with permission from the National Wildlife Refuge, and a radio link was established with the U.C. Berkeley campus to allow daily retrieval of data. Data from the other sites are also retrieved daily via telephone lines. The eighth site was recently installed at Tiburon, on the northern bank of the Bay.

The data from all these sites generally are of high quality and are measuring relative horizontal positions at the 2-5 millimeter level. Preliminary results from data processing at the USGS include several years of solutions for the Chabot-Winton line and several months of solutions for other pairs of stations including Briones, Columbia, Farallon,

Molate and Nunez (Figure 2).USGS used GIPSY and high-precision IGS orbits to process data from the BARD array and three Rogue receiver sites in California (Quincy, Vandenberg, and Goldstone). Figure 3 shows the results for the components of the 30-km Briones-Winton baseline and the baseline lengths of the other baselines with respect to Briones. For baselines 8-180 km long, the rms scatter is 2-5 mm in length, 2-4 mm in north, 2-6 mm in east, and 12-24 mm in vertical, with scatter depending only very weakly on baseline length.

This permanent network serves three main objectives:

1) The configuration of these eight sites is particularly well suited to study the plate boundary affecting the San Francisco Bay Area. Questions to be addressed are, among others, the width of the deformation zone in this region, as well as the partitioning of stress among major faults in this part of the plate boundary. In particular, the Farallon site now allows the collection of data on the western side of the North-American/Pacific plate boundary on a much more frequent basis than provided by the yearly surveying done until now due to logistical difficulties of access to the Islands. In the event of a large Bay Area earthquake, data will be available from this unique site before, during and immediately after its occurrence.

2) The concentration of five sites in the immediate vicinity of the Hayward Fault serves to monitor the secular strain accumulation across this high risk fault (USGS Working Group, 1990). In the aftermath of the Loma Prieta earthquake, this fault is the subject of particular concern, because of the documented occurrence of two previous pairs of magnitude ~7 earthquakes, one on the San Andreas fault and one on the Hayward Fault (1836-1838; 1865-1868). We expect to observe 10-20 mm of deformation across the Hayward Fault within 2 years of monitoring, well above the horizontal accuracy of continuous GPS measurements (4-5 mm). From this we hope to estimate the rate of strain accumulation along the fault as well as constrain the depth of near-surface creep. This will significantly lower uncertainties regarding the seismic potential of the Hayward Fault.

3) With two additional U.C. Berkeley sites to be installed at the south (Parkfield) and north (Arcata) ends of northern California, and combined with PGGA in southern California, BARD will extend the size of the region spanned by permanent GPS arrays to the entire State, providing a means to link up with other GPS networks planned in the Pacific Northwest. In addition to establishing a consistent regional reference framework along the entire North America-Pacific plate boundary and Cascadia subduction zone, these permanent arrays will facilitate and help to coordinate the less frequent, but spatially denser, high-precision GPS surveys conducted by a growing number of agencies and academic institutions, including the USGS, the National Geodetic Survey, Caltrans and county surveyors.

Two of the permanent GPS sites are collocated with broadband seismographic stations of the Berkeley Digital Seismic Network. The combination of the two networks allows us to monitor ground motion in the frequency band 10 Hz to DC. If a large earthquake occurs on the Hayward Fault, the San Andreas fault near Parkfield or in the vicinity of the Mendocino Triple Junction, this combination of data can be used to study pre-seismic deformation (if any), temporal distribution of near surface deformation during and after the event, and determination of the depth extent of rupture. While traditional (non-continuous) geodetic surveys provide denser spatial coverage, they miss the critical first hours during and after seismic events.

Data archival and distribution

In addition to installation of four sites by the Seismographic Station in the past year, procedures have been established at U.C. Berkeley to archive the data in the Northern California Earthquake Data Center (NCEDC, Romanowicz et al., 1994) and make them available to the community. We have been assisted in this task by Dr. Yehuda Bock and the PGGA staff at UCSD and the archival system and software is the same as that used by PGGA, providing standardization across the two California permanent networks. The procedures for archiving data from the four receivers operated by the USGS have been established. They involve electronic transfer of data from Menlo Park to the U.C. Berkeley Seismographic Station.

The Northern California Earthquake Data Center archives continuous GPS data from the Bay Area Regional Deformation (BARD) network in both RINEX and the native binary format of the GPS receiver. Recent data is available in both RINEX and native binary formats, while older data is available in RINEX format only.

The BARD data is available from the NCEDC system via anonymous ftp, and is therefore accessible to anyone connected to the Internet.

host:	quake.geo.berkeley.edu (128.32.146.106)
account:	anonymous
password:	<your-email-address>
directory:	/pub/gps

The BARD continuous data is organized into daily directories. For example, all RINEX data for day 120 of 1994 is located in the directory:

/pub/gps/rinex/1994/1994.120

The RINEX files are archived in UNIX compressed format, but they can be automatically uncompressed by the NCEDC ftp server upon retrieval.

FIGURE 1:

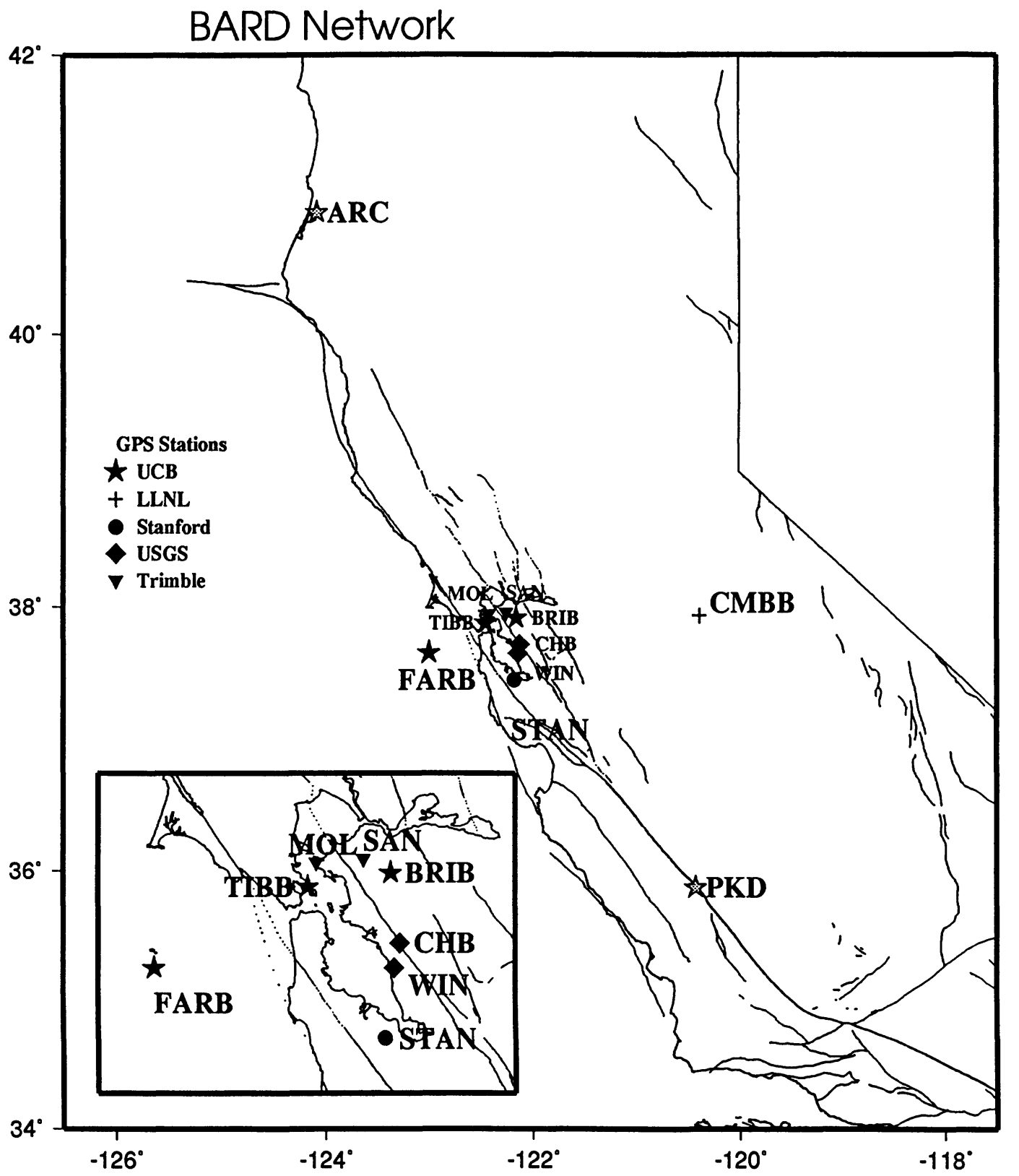
BARD Network
42°
40°
38°
36°
34°
-126°
-124°
-122°
-120°
-118°
GPS Stations
UCB
LLNL
Stanford
USGS
Trimble
ARC
MOL
SAN
TIBB
BRIB
CHB
WIN
FARB
STAN
CMBB
PKD

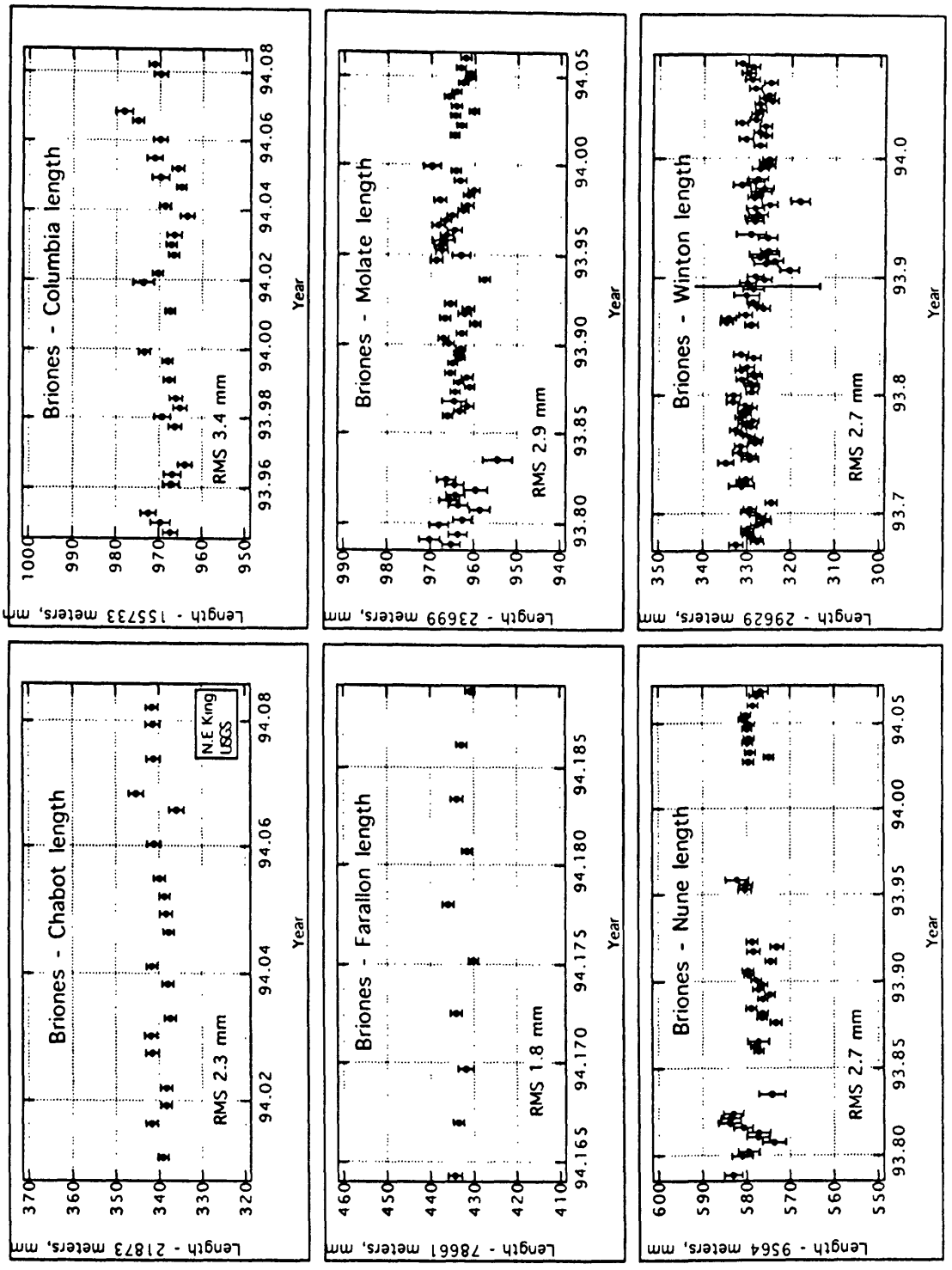

Figure 2. Baseline lengths versus time from Briones to Chabot, Columbia, Farallon, Molate, Nunes, and Winton. Error bars show one standard deviation (formal error) on either side. Since the stations began operating at different times, the time scale is different for each plot.

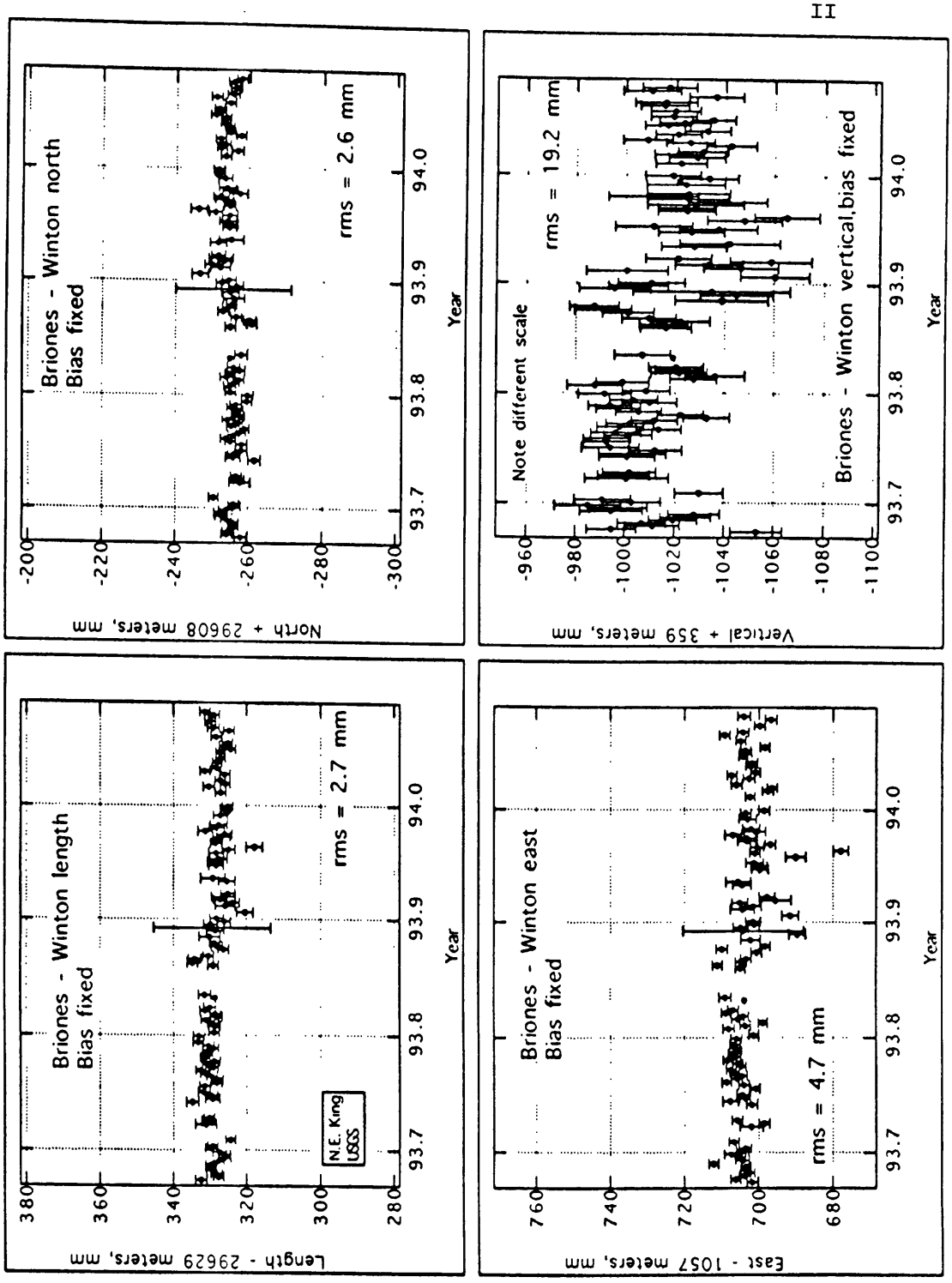

Figure 3.Baseline length and the north, east, and vertical components versus time, for Briones - Winton. Error bars show one standard deviation (formal error) on either side. Each plot also shows the rms scatter about the mean. Note that the ordinate scale is different for the vertical component.

ANNUAL PROJECT SUMMARY

QUATERNARY FAULTING OF THE GREATER MONTEREY AREA, CALIFORNIA

U.S. Geological Survey Grant Award No. 1434-94-G-2443

National Earthquake Hazards Reduction Program, Program Element II: Evaluating Earthquake Potential
Component II.5: Identify Active Faults, Define Their Geometry, and Determine the Characteristics and Dates of Past Earthquakes

Lewis I. Rosenberg
Staal, Gardner & Dunne, Inc.
201 Hoffman Avenue
Monterey, California 93940
(408) 649-2354

Joseph C. Clark
Consultant
Post Office Box 194
Glen Campbell, Pennsylvania 15742
(814) 845-7521

Investigations

1. Detailed investigation and evaluation of Quaternary faults in the greater Monterey area.

2. Determine the subsurface geometry and continuity of onshore faults in the greater Monterey area.

3. Prepare a seismic hazard fault map showing the location and activity of fault segments.

Results

1. Field investigation and air photo interpretation established that late Pleistocene terrace deposits and Holocene colluvium are offset by thrust faults near the city of Monterey, and by through-going near-vertical faults in the town of Carmel, and in Carmel Valley. Seven road cuts exposing these faults were logged in detail. Two radiocarbon dates from colluvium collected along the Sylvan and Hatton Canyon faults indicate movement along the Sylvan thrust within the past 4,900 years, and possible movement along the Hatton Canyon fault within the past 2,100 years.

In addition to late Quaternary faulting, late Quaternary deformation in the region is indicated by three late Pleistocene terrace deposits tilted by as much as 20 degrees and by a tightly folded middle Pleistocene marine terrace deposit.

2. We prepared a subsurface structure contour map on the top of the Monterey Formation for the Seaside and Laguna Seca areas, using approximately 180 water and exploratory well logs. Our field mapping and subsurface analyses reveal that the Seaside, Ord Terrace, and Chupines faults extend from the coast beneath Fort Ord eastward into the Laguna Seca area.

We compiled earthquake data to interpret fault geometry below the depths of well control. D.H. Oppenheimer (USGS) provided us with nineteen focal-mechanism plots of earthquakes in the Monterey and Carmel Valley areas. Although these focal mechanisms are poorly constrained by a lack of offshore seismographs, they indicate right-lateral strike-slip movement on vertical fault planes striking northwest. Interpretation of field mapping, drill hole data, and focal mechanisms suggests that the shorter, discontinuous thrust faults splay off the longer, through-going strike-slip faults.

3. Data collected in this study are being plotted at a scale of 1:24,000 for a seismic hazard map. Rosenberg has met several times with the Monterey County Planning Department to discuss their needs as nontechnical map users.

Our work also will be included on the revised geologic map of the Monterey and Seaside 7.5-minute quadrangles authored by J.C. Clark, W.R. Dupré, and L.I. Rosenberg. This will be submitted to the USGS in December 1994 for review and publication as a MF-series map.

Paleoseismicity Study of the Dover-Foxcroft-Milo, Maine Microseismicity Zone.

1434-94-G-2478
Element II

David C. Roy and John E. Ebel
Department of Geology and Geophysics,
Boston College, Chestnut Hill, MA, 02167.
617-552-3647; Roy@BCVMS.BC.edu.

Martitia P. Tuttle
Department of Geology
University of Maryland, College Park, MD 20742
301-405-1311

Background.

In central Maine, between the towns of Dover-Foxcroft and Milo, there is a 130+ km^2 cluster of persistent felt earthquakes up to magnitude 4.5 in historic times and recorded by the New England Seismic Network (NESN). Microseismic events (magnitudes $\leq$ 1.5), were revealed by a local seismic array established during the summers of 1989-90 (Rea et al., 1989; Doll et al., 1990; Doll et al., 1992). These events occur in a restricted area between the two towns, in Sebec Township, within 7 kms north and 3 kms south of the 085-trending Piscatquis River valley (Fig. 1). There is a 315-degree trend of microearthquake epicenters, extending about 6 km from the 070-striking Harriman Pond Fault (HPF) southeastward to the Piscataquis River at a point where the river makes a sharp bend to follow the trend of the earthquakes. This microearthquake trend seems to form the southwestern limit of the microseisms. A few microearthquake epicenters are aligned parallel, but north of, the HPF at the northern terminus of the microearthquake trend. Microearthquakes also lie to the east of the primary 315-degree trend and extend out northeastward to about 10 km. The microearthquakes all occur at depths less than 2.5 km; most are less than 1.5 km deep. Focal mechanisms from both the larger and smaller earthquakes suggest failures on planes generally parallel to the attitudes of important joint sets observed in surface exposures (Ebel et al., 1991; Foster et al., 1992). The microearthquake data provide circumstantial evidence suggesting that this area could have been the location of at least one strong earthquake (perhaps magnitude 6.0 or greater) in the recent past. The present concentration of moderate and microseismic events in the region could be long-term "aftershocks" following such a large earthquake. Establishing the past occurrence of a major earthquake is the primary focus of the present project. Documentation of a past large equake would greatly enhance our understanding of the seismic hazard in the highly populated coastal region of New England.

Investigations Undertaken.

During the 1994 summer field season an investigation of the glacial and glacial marine sediments within, and nearby, the microseismic zone was undertaken. The field strategy was to carefully examine sand and gravel pits and river cut-banks for liquifaction features and faults that might have been formed by earthquake-induced ground motions. Most of the sand and gravel pits are located in eskers that are notorious for displaying deformation features that are of ambiquous origin and difficult to date. Since the eskers in the region are north-south oriented with southward paleoflows, there are no eskers along the east-west Piscataquis River valley below Dover-Foxcroft (Hanson and Caldwell, 1981; Thompson and Borns, 1985). We examined all pits in the Piscataquis valley upstream from Dover-Foxcroft, pits within 4-6 kilometers north and south of

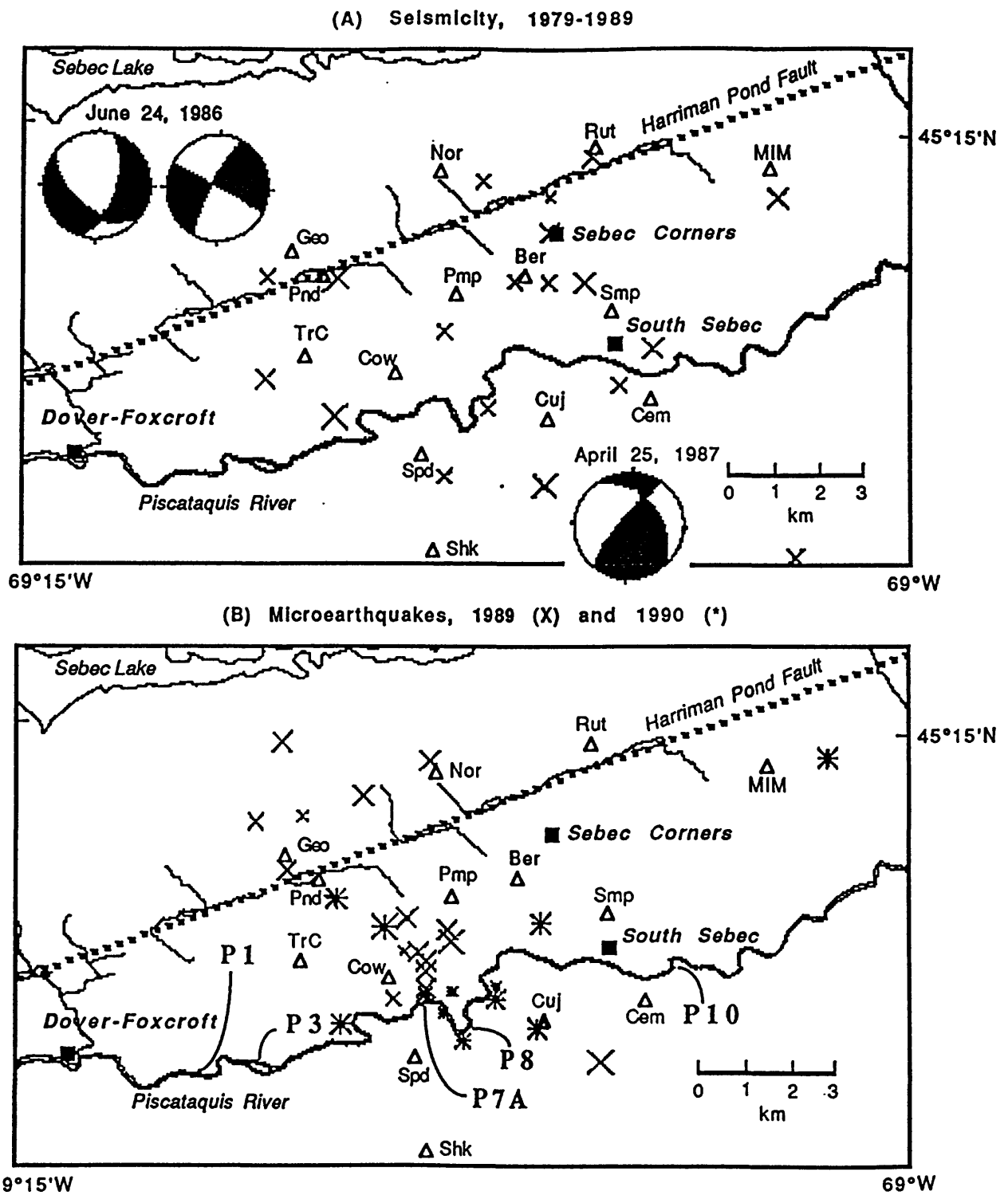

Figure 1. (A) Map of the NESN-recorded seismicity east of Dover-Foxcroft as located by the New England Seismic Network of Weston Observatory. Possible focal mechanism solutions for the June 24, 1986 event (magnitude 2.5) and the April 25, 1987 event (magnitude 3.1) are shown. All of the events have magnitudes above 1.8. (B) Map of the microseismicity recorded by portable stations (triangles) during the summers of 1989 and 1990 (Rea et al., 1991). All of these events have magnitudes less than 1.5. The NESN station MIM is located just southwest of the town of Milo. Cutbank sites (P1, P3, P7A, P8, and P10) are discussed in the text. The bold dashed line in each diagram indicates the trace of the Harriman Pond Fault.

the river between Guilford and Milo, and pits along the Pleasant River northward from Milo. None of the pits displayed features that called for detailed excavation.

The main effort of the field work was the evaluation of the cut banks along the Piscataquis River between Dover-Foxcroft and Milo with special emphasis on the portion of the river that passes through the microseismic zone. The Pleistocene geology of the river valley has been mapped in reconnaisance fashion (with local detail) and is available as open-file reports of the Maine Geological Survey (Hansen and Caldwell, 1981; Hanson et al., 1987) that are compiled and published by the Survey (Thompson and Borns, 1985). Detail studies of the evolution of the Pleistocene and Holocene sediments within the valley have not previously been made. As established by Hanson and Caldwell (1981), the stratigraphy within the valley consists of bedrock overlain, in turn, by glacial-marine clays, silts, and sands of the Pleistocene Presumpscot Formation followed upward by Holocene channel gravels covered by overbank sands and silts. The top of the Presumpscot Formation is mapped at an approximate elevation of 300 ft (91m). The 300 ft. contour crosses the river in Dover-Foxcroft and the inference is made that the upper limit of the post-glacial marine incursion in the Piscataquis valley is at Dover-Foxcroft. Elsewhere in coastal Maine, the basal Presumpscot consists of transgressive sands and gravels formed as sea water progressively flooded the major river vallies and their tributaries. The upper Presumpscot may locally comprise regressive sands, fluvial deposits, lacustrine, and eolian sediments. Thus it seemed possible that the Piscataquis river valley might well contain both Pleistocene and Holocene stratigraphy rich in possibilities for the development of paleoliquifaction features.

Our objective in the Piscataquis valley is to look for liquifaction features in the Pleistocene/Holocene sediments and to access them for liquifiability. In addition, we are looking for structural offsets in the Pleistocene-Holocene contact. In a sense this contact might be used as a "strain gage", or reference surface, to assess post-Pleistocene deformation. Access to this contact and the sediments involved is confined to cut-banks that have been recently eroded by Spring flows or ice-block damage; otherwise the banks are covered by vegetation and slump material. A reconnaisance traverse by canoe of the river between Dover-Foxcroft and Milo produced eighteen cut-bank sites (P1-P18) that display good stratigraphic sections and require a only hand excavation. Most of the sites show only Holocene overbank deposits which were examined for general characteristics of the sediments and possible liquifaction or structural features. More time has been invested on cutbanks with both Pleistocene and Holocene sediments because several of them showed deformational features or abrupt along-strike changes in stratigraphy that might be the result of liquifaction or faults.

Results to Date.

The channel of the Piscataquis River below Dover-Foxcroft is located on the south side of its valley. Along its south bank, the river in many places is excavating hills composed of Presumpscot sediments . Elsewhere along the south bank there are cutbanks in sediments of narrow Holocene flood plains that abut the Pleistocene sediments of the hills beyond. On the north side of the valley, active flood plains are more prominent but vary considerably in width. In places on the north side of the valley there are discontinuous terrace-like surfaces above the active flood plains. These terrace surfaces are of unknown age and stratigraphy but may be related to post-glacial uplift of the valley. Along its north bank, especially in straight reaches, the river is presently excavating Holocene flood plane deposits. Elsewhere, on the inside of bends acretionary scrolls are prograding. Almost all of the sharp bends (especially northward bends) in the river are caused by resistent "headlands" of bedrock and/or Presumpscot sediments. At low water, the cutbanks on the south side of the river reveal in excess of 4 m of Presumpscot sediments. Bedrock outcrops along the shore and outcrops within the river bed are common along the portion of the river we studied. In addition, the bed of the river is composed of a poorly sorted cobble/boulder gravel with local glacially polished bedrock exposed on the bottom. The channel bottom therefore appears quite resistent to further down-cutting in the present flow

regime. Channel widening and flooding seem to be the only ways the river can accomodate extreme discharges.

We conclude that the cut banks of the Piscataquist River display the basal portion of a fine-grained and quiet-water Pleistocene stratigraphy. This basal Presumpscot apparently rests directly on bedrock and is unconformably overlain by Holocene channel gravels and overbank silts and fine sands. We have seen no evidence for a basal transgressive sand facies at the base of the formation. If a basal sand facies was present and overlain by the silts, "blue clays" and fine sands, the formation would present a favorable configuration for the development of liquifaction features. It is possible, however, that the transgressive phase of the formation is present in the bottom of the bedrock valley which may be located to the north of the present river channel. That would mean the Presumpscot stratigraphy we observed along the present channel might be younger than the transgressive phase.

Five sites within, or near, the microseismic zone were excavated because they: 1) contained deformed Presumpscot sediments (P1); 2) showed an abrupt change in the elevation of the Pleistocene-Holocene unconformity along the exposure (P3); 3) contained lensing sand layers in Holocene overbank deposits that might have been caused by successive sand blows (P7A); 4) provided an opportunity to study a Presumpscot section and search for features at a sharp bend in the river along the main microseismic trend (P8); and 5) showed evidence two major along-strike abrupt changes in the Presumpscot and Holocene stratigraphy (P10). A grid of seismic reflection and refraction lines was also accomplished at site P10. At this writing, reduction of the seimic data has not been completed.

Site P1: This north-bank site shows 2.5 m of Presumpscot cohesive clayey silt with thin beds of silty fine-to-medium sand. The Presumpscot sediments are overlain unconformably by a Holocene sequence of coarse gravel (.80 m thick) and overbank silt and fine sand (1.8 m thick). The Presumpscot sand beds are disturbed by a complicated array of folds and faults throughout. As so far excavated, the structures seen in the Presumpscot do not cut the unconformity nor were paleoseismic features observed in the Holocene sediments. Considerably more excation is required at this site to complete the study.

Site P3: This 320 m long site is also on the north-bank of the river oposite a large island in the river. The island appears to have formed when the river shifted most of its flow northward to a new channel. The stratigraphy in this site is similar to Site P1 with 1.7 m of Presumpscot clay unconformably overlain by Holocene gravel and sand (.3 - .8 m) and overbank silt and fine-medium sand (4-5 m). The overbank silts contain pebbles, cobbles, and a boulder scattered vertically and laterally in the flood plain stratigraphy. These "outsized" clasts are interpreted to have been caused by ice-rafting during the Spring break-up. No soft sediment deformation was observed. Of interest at this site was an .8 m "off-set" in the unconformity concealed by a large slump. The offset was revealed to be the result of differential channel erosion along the unconformity and consequent thickening of the basal Holocene gravel.

Site P7A: This site is on the south bank of the river and along the main microseismic epicenter trend. Only Holocene overbank and channel deposits were exposed at this site. Of interest were lenticular median and coarse sand layers of variable thickness that are perched at all levels. The sand beds are interbedded with typical overbank brown silt and fine sand. Some of the sand beds are slightly deformed. Excavation revealed internal lamination and cross-lamination in most of the beds indicating they were transported. No sand dikes or other evidence of sand blows were observed. The exposure is a dissected proximal levee sequence; the only such sequence we have seen so far in cutbanks along the river. Across the river, on the north bank, there is geomorphic feature that strongly resembles a slump mass. This feature is worthy of geophysical exploration and excavation.

Site P8: This site was studied because it is also on the microseismic epicenter trend and brings bedrock and Presumpscot sediments in close proximity. We were specifically looking for faults in the Pleistocene stratigraphy. Much more excavation is required to fully explore the high cutbanks at this site.

Site P10: In many ways this site was the most intriguing exposure we found. It is also the longest exposure at 400+ m (Fig. 2A). Two major excavations were undertaken to explore apparently abrupt changes in stratigraphy that might be caused by faults. The P10A site, located at the southern end the cut, is the longer excavation. It was done to expose a northward change from Presumpscot clay with thin beds of sand to a more northerly stratigraphy showing a sand-delta sequence within the Presumpscot Formation. This transition was shown to be stratigraphic.

The P10B site on the other hand proved to be somewhat more interesting. As illustrated in Figure 2B, there is an abrupt truncation of the delta-sand sequence of the Presumpscot Formation (Unit II) by a sequence of variably mottled gray silts (Unit IV and VI)) and fine sands (units III and V). Cohesive gray Pleistocene silty clay of Unit I underlies Unit II. Units III-VI all contain woody plant material that retains bark and internal structure that suggest a Holocene age, possibly no more than a few hundred years old. Unit IV is the richest in organic matter. The contact between Unit II and the Holocene mottled silts and sands is sharp. Beds in Unit II are little disturbed against the contact as well illustrated by two silty fine sand layers (Fig. 2) that are sharply cut by the contact.. A small "sliver" of disturbed sand is, however, present along the contact just below where the contact appears to cross into overbank deposits (units VII and VIII). Near the waterline at the base of the exposure, gray silt of Unit IV is mixed with sand of Unit II along the contact. Within the overbank deposits there are also discontinuities that may be small erosional surfaces or faults. The origin of these discontinuities is unclear. They may have developed within the overbank deposits at an early time when the change in flood plain elevation was greater than it is today. Below these discontinuities and along the base of the Holocene deposits are downward-projecting "lobes" of tan-rust mottled silt similar to that of Unit VII (Fig. 2B). The origin of the lobes is unknown but Unit VII is tentatively interpreted to be part of an older overbank sequence present to the south at Site P10A. The top of Unit I is present at or just below the low water level all along Site 10. At Site P10B, the top of Unit I-II contact becomes deeper, possibly because of pre-Unit II erosion in the Pleistocene.

We conclude that the contact between Unit II and units IV through VI is a paleochannel of the Piscataquis River. We however did consider the possibility that the contact is the sole of a rotational slump in which the material assigned to units IV, V, and VI rotated downward and away to the north. The auger holes reveal the stratigraphic character of the material to the north of the contact that was largely hidden by modern colluvial cover. The presence of "young" wood, and even leaf debris, within the sediments suggest that they are of late Holocene age.

We believe that the southwestern margin of the present-day backwater (Fig. 2A)is a remnant of the old channel. The movement of the river to its present position appears to have been gradual but the details have not been worked out. The paleochannel was cut into an "old" flood plain where overbank deposits were deposited on eroded (?) Presumpscot sediments. A new flood plain surface has developed, in large part by scroll-bar growth, on the inside of the bend north of P10B. During the development of the new flood plain, the western end of the backwater channel was completely filled by units III-VI. The new flood plain surface is presently .5-1 m lower than the old flood plain surface.

References

Doll, W.E., Rea, C. D., Ebel, J. E., Craven, S. J., and Cipar, J. J., 1992, Analysis of Shallow Microearthquakes in the South Sebec Seismic Zone, Maine, 1989-1990, Seism. Res. Lett., v. 63, p. 557-566.

Doll, W.E., Rea, C.D., Lambrecht, E.F., Craven, S.J., Ebel, J.E., and Cipar, J.J., 1990, Preliminary Results of a Second Season of Microearthquake Monitoring near Sebec (Milo) Maine, Seism. Res. Lett., v. 61, p. 148.

Ebel, J. E., Doll, W. E., Cipar, J. J., Roy, D. C. and Marvinney, R., 1991, Microearthquake activity in the vicinity of Dover-Foxcroft and Milo, Maine, Geological Society of America Abstracts with Programs, v. 23, p. 25.

Figure 2. (A) Locations of sites P10A and P10B (arrows) on the Piscataquis River 1.5 km down stream from the bridge at South Sebec, Maine. The two sketches are from airphotos and illustrate minor changes in the river bend and scroll bar during a twenty-nine-year period. Both photos show minor flooding on the NW shore of the bend and in the back-water down stream and east of the site. Dotted line shows a tree-line that follows a change in flood plain elevation seen in (B). At low water bedrock is exposed at "X". (B) A sketch cutbank exposure at site P10B. The exposure shows a sharp, and north-dipping, contact (solid line) between an upper (?) Pleistocene coarse sand sequence (Presumpscot Formation, Unit II) to the south and Holocene "woody" clayey silt and fine sand (units III-VI) to the north. Overlying the sequences separated by the contact are overbank silts and fine sand (VII and VIII). The stratigraphic units are numbered in order of decreasing inferred age beginning with a cohesive Presumpscot "blue clay" (Unit I). The top of Unit I, where dashed, is inferred to be a Pleistocene erosion surface overlain by Pleistocene deltaic sands and fine gravels (Unit II). Locally, the top of Unit I is interpreted to be a part of the inferred Holocene erosion surface at the base of the III-to-VI sequence (solid contact). Horizontal lines near the top of Unit II are fine sand layers that are truncated by the Holocene erosion contact. Bracketed vertical lines are locations of auger holes. Colluvial cover on the bank is delineated by the hatchered line with hatchers toward the covered areas. Vertical and Horizontal scales are the same.

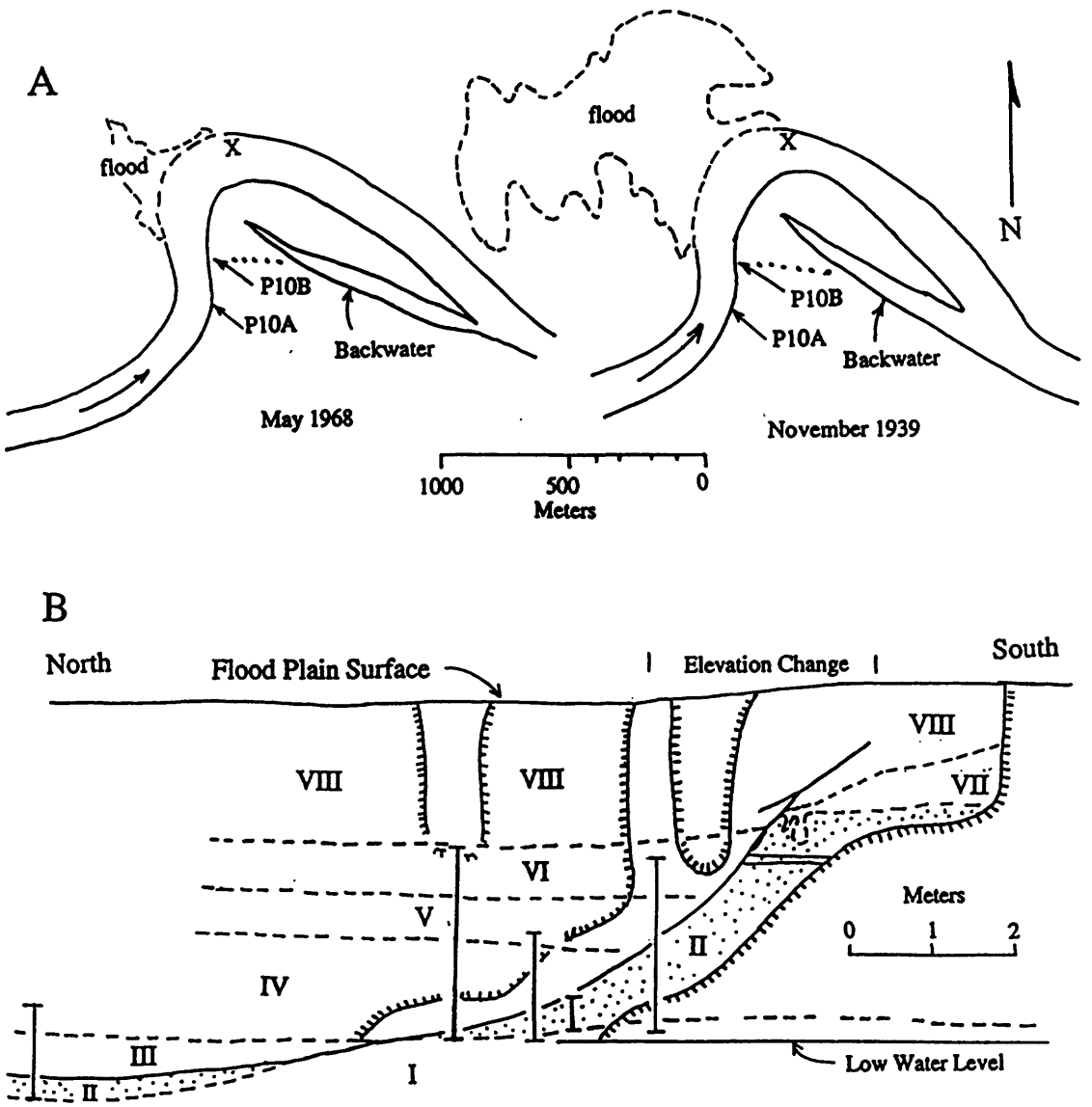

Foster, J. E., Roy, D. C., Ebel, J. E., and Tuttle, M. P., 1992, Faults, joints, liquefaction features, and earthquakes in the Dover-Foxcroft area, Maine, Geological Society of America Abstracts with Programs, v. 24, p. 21.

Hanson, L.S., and Caldwell, D.W., 1981, Reconnaissance Surficial Geology of the Dover Foxcroft Quadrangle, Maine, Maine Geological Survey Open File no. 81-17.

Rea, C. D., W. E. Doll, K. A. Burgger and J. E. Ebel, 1989, Preliminary Results of a Microearthquake Study near Milo, Maine, Seism. Res. Lett., v. 60, p. 145.

Rea, C. D., W. E. Doll, J. E. Ebel, S.J. Craven and J.J. Cipar, 1991, Microearthquake measurements near South Sebec, Maine, 1989-1990, Maine Geological Survey Open-File Report 91-5.

Thomson, W.B., and Borns, H.W., Jr., 1985, Surficial Geologic Map of Maine, Maine Geological Survey.

LATE QUATERNARY FAULTING, SOUTHERN SAN ANDREAS FAULT

9960-11346

Michael J. Rymer

Branch of Earthquake Geology and Geophysics
U.S. Geological Survey
345 Middlefield Road, MS/977
Menlo Park, CA 94025
(415) 329-5649
mrymer@isdmnl.wr.usgs.gov
NEHRP/SC II.5

Investigations

1. Paleoseismic investigation of the East Wide Canyon and Eureka Peak faults, Little San Bernardino Mountains, that had surface slip in association with the 1992 Joshua Tree and Landers earthquakes, respectively.

2. Continued study and mapping of active faults and enclosing geology in the Coachella Valley and Little San Bernardino Mountains.

3. Postearthquake investigation of the 1994 Northridge, California earthquake, with special interest on ground cracks in Potrero Canyon.

Results

1. Trenches across the East Wide Canyon and Eureka Peak faults, both of which experienced surface breakage in 1992, were excavated to determine paleoseismic histories. The East Wide Canyon fault had minor, probably triggered slip (maximum 6 mm right-lateral and 4 mm vertical components of slip) associated with the 1992 Joshua Tree earthquake. Two trenches were hand dug across the East Wide Canyon fault. One trench was cut across a subtle, low scarp. This trench exposed a possible eolian deposit, which abuts the scarp, that overlies Holocene channel gravel. The channel gravels were too coarse and too unconsolidated for worthwhile and safe trenching. A second trench was hand dug in finer-grained materials only 7 m to the south. This trench was 1.5 m deep and revealed evidence of previous seismic slip. Matching silty sand units across the fault trace in the trench walls indicates a prehistoric(?) slip event with a vertical component of slip of about 20 cm; the horizontal component is unknown. Indications of the age of the deposits are minimal because of the dry desert environment; estimation of the age, based on extremely weak soil development, hints at a mid- to late-Holocene age. Lower strata, also of probable mid- to late-Holocene age, mapped in

the trench may indicate an even earlier slip event. In summary, paleoseismic studies in this trench indicate one and possibly a second earthquake in a poorly constrained time frame of mid- to late-Holocene.

The Eureka Peak fault had up to 20 cm of dominantly right-lateral slip with minor amounts (~4 cm) of vertical component of surface faulting associated with the 1992 Landers earthquake. A trench was hand dug across the Eureka Peak fault near the site of largest measured surface slip in 1992. The trench was 2 m deep and clearly showed the 1992 main rupture and a secondary, minor fault plane about 1 m to the east. Interpretation of paleoseismic events in this trench, like the one across the East Wide Canyon fault, showed evidence of at least one and possibly a second pre-1992 surface slip event, and again with a poorly constrained, estimated mid- to late-Holocene age.

2. Geologic mapping of the San Andreas fault zone in the Mecca Hills reveals new age control for mid-Pleistocene deposits. Strata of the upper part of the Palm Spring Formation in the Thermal Canyon quadrangle, where age control consisted of the presence of the Bishop ash bed (identified on the basis of trace-element chemistry of glass shards by A.M. Sarna-Wojcicki), also contains a second, thinner ash bed about 40 m stratigraphically above the Bishop ash bed. This second ash, informally named the ash of Thermal Canyon, was also identified on the basis of trace-element chemistry by A.M. Sarna-Wojcicki. Presence of the ash of Thermal Canyon provides further verification of the identity of the Bishop ash bed and also enables determination of time and rates of tectonic deformation in the Mecca Hills.

3. Widespread surface fractures formed around the margins of Potrero Canyon in association with the 17 January 1994 Northridge earthquake. These fractures are evidence of strong ground motions and the damage potential of a moderately large earthquake. The earthquake-induced effects in Potrero Canyon include surface fractures, liquefaction, and landslides. Vertical displacements across fractures are as great as 61 cm. Surface fractures likely formed by alluvial compaction during strong earthquake shaking; fractures near the alluvium-bedrock contact on both sides of the canyon dip toward the canyon center and a net down-canyon motion of alluvial fill are evidence of a non-fault origin of the fractures. Trench investigations by T. Fumal, T. Powers, and D. Schwartz (see report by D. Schwartz) across several surface fractures showed steeply dipping breaks in a broad zone and, most importantly, evidence of two previous late Holocene episodes of surface fracturing. Timing of the penultimate event using ^{14}C dates on detrital charcoal is about 970–1205 A.D.; an earlier event has an as yet undetermined Holocene age.

Potrero Canyon is located near the up-dip projection of the thrust fault that caused the Northridge earthquake. Observations of compressional fractures along the south side of the canyon led to early speculation that the ground deformation seen here may have been the result of primary tectonic faulting. Surface and trenching investigations indicate that primary faulting did not occur at Potrero Canyon. Relations are consistent with surface displacements resulting from differential settlement and lurching due to strong ground motion with movement

taking place largely along the bedrock-alluvium contact. The distribution and types of earthquake-induced features found in Potrero Canyon are also generally consistent with deformation due to strong ground motion rather than to surface faulting. Specifically, we conclude that the surface fractures likely formed in response to strong shaking that resulted in alluvial compaction. The net down-canyon motion of the alluvial canyon fill supports this model, as does the presence of localized liquefaction, pipe breaks, and better developed crack sets on the western (down-gradient) sides of ridge spurs.

The significance of surface fractures formed in Potrero Canyon is readily apparent when considering the rapid urban expansion of the region. Potrero Canyon demonstrates the severe effects resulting from strong ground motions during a moderate-sized earthquake. In this light, understanding the cause and recurrence of the Potrero Canyon surface fractures and related earthquake-induced effects is a critical element in determining the earthquake hazards of the region.

Reports published

Rymer, M.J., Sarna-Wojcicki, A.M., Powell, C.L., II, and Barron, J.A., 1994, Stratigraphic evidence for late Miocene opening of the Salton Trough in southern California: Geological Society of America Abstracts with Programs, v. 26, no. 2, p. 87.

Rymer, M.J., 1994, New geologic mapping and stratigraphic and structural relations along the San Andreas fault zone in the Coachella Valley, southern California: Geological Society of America Abstracts with Programs, v. 26, no. 2, p. 87.

Rymer, M.J., Powell, C.L., II, Sarna-Wojcicki, A.M., and Barron, J.A., 1994, Late Miocene stratigraphic and paleogeographic setting of Garnet Hill in the northwestern Salton Trough, southern California: Pacific Section, Society of Economic Paleontologists and Mineralogists, in press.

Element II

Quaternary Tephrochronology in the Western Region in Support of Earthquake Hazards Reduction Studies

9540-70020

Tephrochronology Project (Western Region, Menlo Park)
A. M. Sarna-Wojcicki, C. E. Meyer, and Elmira Wan
Branch of Western Regional Geology,
MS 975; 345 Middlefield Road
Menlo Park, CA 94025;
Tel.: 415 329-4930; FAX: 415 329-4936; e mail: asarna@isdmnl.wr.usgs.gov

Investigations

The Tephrochronology project provides stratigraphic correlation and age control to studies of active faults and neotectonics in the Western Region by means of chemical analysis and numerical age dating of tephra (volcanic ash and tuff layers). New (N) or continuing (C) studies are with:

1. Michael Rymer and Bob Sharp (BEGG, Menlo) on the geologic structure, transpression, and neotectonics of the San Andreas Fault in the Salton Trough, California, using the Bishop ash bed and other tephra layers as chronostratigraphic markers (C).
2. Marith Reheis (BCRG, Denver) on Neogene displacement of the Fish Lake Valley Fault Zone, the northern extension of the Furnace Creek Fault Zone in eastern California and western Nevada, and late Neogene tectonics of Fish Lake Valley (C).
3. Richard Madole and Robert Schuster (GRA, Denver), on the age and paleoseismic significance of the Ribbon Cliff landslide of the Columbia River, central Washington, as it relates to the location of the epicenter of the North Cascade earthquake of December 14, 1872 (C).
4. Earl Brabb (BWRG, Menlo) and Davey Jones (Univ. of Calif., Berkeley), on the age and correlation of Neogene tephra layers, for age control in tectonic and chronostratigraphic studies of the eastern San Francisco Bay area (C).
5. Robert Fleck (BIG) and Malcolm Pringle (formerly of BIG, Menlo) on laser-fusion $^{40}Ar/^{39}Ar$ dating of late Neogene tephra layers as chronostratigraphic horizons in the western U.S. (C)
6. Dan Ponti (BESG) on potential problems in evaluating activity on blind thrust faults using benthic foram biostratigraphy in the northern Los Angeles basin (C).
7. Ray Weldon (Univ. of Oregon) and Silvio Pezzopane (USGS, Denver) on tephrochronologic age constrains for neotectonic displacements in the Summer Lake area, southeastern Oregon (C).
8. With Anna Buising and Dean Richesin (Cal State, Hayward) and Alan Bartow (BWRG, Menlo) on age constraints on deformed upper Cenozoic strata, east-central Coast Ranges, Calif. (C).

9. Jim Yount (BWRG, Carson City) and Dave Harwood (BWRG, Menlo) on upper Quaternary stratigraphy and deformation of Mohawk Valley, northeastern Calif. (C).

10. With Emilio Herrero-Bervera, Chuck Helsley (SOEST-Univ. of Hawaii), Robert Negrini (Cal. State, Bakersfield), Mike McWilliams (Stanford Univ.), Brent Turrin (BWMR, Menlo), Julie Donnelly-Nolan (BIGP, Menlo), and others on the age, correlation, and identity of a paleomagnetic episode in the Brunhes Normal Chron. (C).

Results (refer to corresponding numbers, above)

1. (a). Report on mid-Quaternary faulting and deformation along the southern San Andreas Fault in the Mecca and Indio Hills, using the Bishop ash bed as a chronostratigraphic marker, is close to completion (Rymer). (b). Both the Bishop ash bed (759 ±2 ka) and the overlying ash of Thermal Canyon, also present in the Borrego Badlands (Sharp), have now been identified in the Mecca Hills; both ash beds are correlated to the recently-drilled Owens Lake core OL-92, where the age of the ash of Thermal Canyon is estimated to be ~740 ka from a sedimentation-rate curve developed for the core (Jim Bischoff, BEMG, George Smith, BSP).

2. Neogene and Quaternary tephra layers have been collected from Deep Springs Valley, east-central Calif., and are being analyzed in order to provide information on the neotectonics of this area, the site of a recent M ~6 earthquake. The rate of Holocene displacement of the Furnace Creek-Fish Lake Valley fault zone, determined by stratigraphy, tephrochronology, and ^{14}C analysis, continues to be debated by Marith Reheis (BCRG) and Warren Hamilton (BGP), with consensus in sight.

3. A report on the Ribbon Cliff, Wash., landslide has been accepted by the Bulletin of the Seismological Society of America. This report documents the timing of landsliding and shows that the slide is a polygenetic landform that has moved at least twice before the 1872 earthquake, but probably also in 1872.

4. New laser-fusion $^{40}Ar/^{39}Ar$ age on a tuff in the Contra Costa Formation, exposed near Lafayette, in the Berkeley Hills, is 6.25 Ma, as determined by Bob Fleck (BISO). We had correlated this tuff with the ~6 Ma Roblar Tuff, but previous conventional K-Ar analyses yielded an older age of 8 Ma. The new date confirms the age and identity of this unit, which is an important stratigraphic and structural datum for determining the long-term strain on and across the San Andreas Fault system in the San Francisco Bay Area.

5. A report on a new, precise laser-fusion $^{40}Ar/^{39}Ar$ age on the Bishop ash bed, and a revised age on the Matuyama-Brunhes (M-B) Chron boundary, is finished and is being submitted to *Earth and Planetary Research Letters.*

The new age for the Bishop ash bed, 758 ±1.2 ka, is based on ~120 individual determinations of individual sanidine crystals or groups of a few small crystals, and is precise (±0.3%). This result provides a new constraint on the M-B boundary of 772.4 ±1.7 ka, in reasonable agreement with recent data reported from others but more precise. The M-B boundary is an important chronostratigraphic datum that is used as a reference level in numerous geologic studies, including neotectonics.

6. Cores drilled for the Los Angeles MetroRail subway system along Wilshire Blvd. encounted dipping sandstones (part of a fold related to a detachment fault at depth?) estimated to be ~0.7 to 2.5 Ma, based on benthic foraminifers, but 4.4 to 6.0 Ma based on two independent lines of evidence from tephra and diatom assemblages. These finding have important implications for interpretations of the rates of subsurface deformation, such as blind thrusts and detachment faults and folds in this region.

8. See results in vol. XXXV (II), p. 633. Report in prep. as MS Thesis.

9. We have undertaken the study of a suite of tephra collected by Jim Yount and David Harwood from upper Quaternary lake, marsh, and fluvial beds in Mohawk Valley, a faulted half-graben in the northern Sierra Nevada. The suite of ~12 tephra layers range in age from the ~400,000 yr-old Rockland ash bed to the 6850 yr-young Mazama ash bed, and provide age control to this stratigraphic/neotectonic study.

7 and 10. We have determined the age of a paleomagnetic event in the Brunhes Normal Chron, and correlated it among five sites, from Pringle Falls, Ore., on the north, to Long Valley Caldera, Calif., on the south, over a distance of ~700 km using the "Orange set" of ash beds. The event, possibly an aborted reversal, is bracketed between ages of ~140 and ~190 ka by means of plateau step-heating $^{40}Ar/^{39}Ar$ ages on plagioclase. This magnetic event thus cannot be the Blake event, as previously proposed, but is more likely the Jamaica or some other event. It correlates well with the marine oxygen-isotope stage 6. A report on these results has been accepted by JGR. The "Orange ash beds" are being used by Silvio Pezzopane at Summer Lake, Ore., to constrain the time of movement on late Quaternary faults in this area.

Reports (funded wholly or in part by EQHRP)

Herrero-Bervera, E., Helsley, C.E., Sarna-Wojcicki, A.M., Lajoie, K.R., Meyer, C.E., Negrini, R.M., McWilliams, M., and Liddicoat, J.C., Age and correlation of a paleomagnetic episode in the western U.S. by $^{40}Ar/^{39}Ar$ dating and tephrochronology: the Jamaica, Blake, or a new polarity episode? Accepted by *Journal of Geophysical Research.*

Madole, R.F., Schuster, R.L., and Sarna-Wojcicki, A.M., Ribbon Cliff landslide, Washington, and the earthquake of December 14, 1872. Through review. Accepted for publication, *Bulletin of the Seismological Society of America.*

Negrini, R., Erbes, D., Roberts, A., Verosub, K., and Sarna-Wojcicki, A., 1993, Total paleomagnetic vector record of repeating waveforms initiated by the Summer LakeII/Pringle Falls/Long Valley excursion. In EOS, v. 74, no. 43, p. 218.

Negrini, R.M., Erbes, D.B., Roberts, A.P., Verosub, K.L., Sarna-Wojcicki, A.M., and Meyer, C.E., Repeating waveforms initiated by a ~150 ka geomagnetic excursion in western North America: Implications for field behavior during polarity transitions and subsequent secular variations. Accepted by *Journal of Geophysical Research..*

Pringle, M.S., Sarna-Wojcicki, A.M., and Wijbrans, J., Age of the Bishop Tuff, east-central California, and the Matuyama-Brunhes boundary. Through technical review; for submittal to *Earth and Planetary Sciences.*

HYDROGEN AND OTHER NON-RADON GEOCHEMICAL MONITORING

Project # 9970-70087

Motoaki Sato
Branch of Lithospheric Processes
U.S. Geological Survey, MS-959, Reston, VA 22092
Phone:(703) 648-6766; Fax:(703) 648-6789; E-mail: msato@lithos.er.usgs.gov

INVESTIGATIONS

Anomalous increases of hydrogen gas (H_2) in soil, deep-wells, and springs before damaging earthquakes have been reported in several countries. Our project mainly aims at confirming these observations by using continuous monitoring devices at multiple sites. H_2 is virtually absent in normal air (<0.5 parts per million by volume), and tends to be consumed (for hydrogenation), rather than generated, by biomass. However, it is easily generated by chemical reactions of water-rich fluids with ferrous rocks near the base of the brittle crust, where damaging earthquakes commonly occur. H_2 is the lightest and fastest gas and hardly soluble in water. So it is most likely to be the first gas that escapes to the surface from such depths, should dilation of a fault zone occur.

Soil hydrogen concentration is monitored by using a specially-designed fuel-cell sensor at a depth of about 1.5 meters in a column of coarse sand located at or near a fault trace. The depth provides a near-constant temperature environment to the sensor, and the sand column buffers barometric fluctuations while facilitating degassing of soil gas. An isolation amplifier is inserted between the sensor output and the telemetry unit to prevent possible ground-loop noise during heavy rain. There are four soil hydrogen monitoring sites in the Hollister area and seven in the Parkfield area along the San Andreas and Calaveras faults (**Fig. 1**). Duplicate sensors are installed 17 meters apart at five sites in the Parkfield area. All these sites are adjacent to creep-meters to share the satellite-relayed telemetry system.

In addition, parameters related to pumped well water, such as ionic conductivity, dissolved CO_2 and dissolved H_2, used to be monitored at two wells in Parkfield, one drilled into the San Andreas fault zone and the other about 500 meters from the fault. This activity has been suspended because funding for maintenance was cut off two years ago.

RESULTS

Soil Hydrogen

Telemetered soil hydrogen data from 9 sites are compositely plotted as time-series in **Fig. 2** (from 1 October 1993 to 1 October 1994). The data from the Shore Road and San Juan Bautista are eliminated because of erratic behavior of the sensor signals which was probably caused by corroded solder joints. The cumulative rain data recorded at Middle Mountain

are also shown at the top of the figure.

There were a few minor signal changes that were not explainable in terms of rain or instrumental problems. The clearest anomaly occurred between 27 August 1994 and 2 September 1994 at the Twisselman Ranch site, although the magnitude was less than 20 telemetry counts (50 ppmv H_2) as shown in **Fig. 3**. This site had not shown any anomaly for at least 4 years, although the telemetry was interrupted relatively briefly several times. Time-wise, the anomaly preceded and vanished soon after the M_w 7.2 earthquake of 1 September 1994 at 15:15 UT that occurred west of Mendocino (40.3°N, 125.8°W). The correlation could be fortuitous because this was the only site that showed an anomaly during this period. The two sensors at Gold Hill recorded concerting changes during this period, but these changes were also recorded by the creep-meter XGH1, and were most probably caused by telemetry repair work. The many peaks recorded by the Gold Hill #2 sensor were caused by rain for unknown reason because correlation with heavy rain is extremely high.

Another possible anomaly was recorded by the Work Ranch #2 sensor in early February in the form of a sharp increase of a very small magnitude (20 ppmv), followed by depression of the baseline by about the same magnitude. The baseline eventually recovered to the previous level by July, but started adding barely perceptible cyclic changes of roughly 2-week-long periodicity. The reason is not clear. The Work Ranch #1 sensor recorded no changes. This sensor is probably non-functional. Corroded solder joint of the sensor cable is suspected.

The sudden drop in the record that occurred in early December of 1993 at Taylor Ranch #1 sensor was due to the dying mercury battery for biasing the signal to positive voltage. This was anticipated because the same thing happened to the sensor #2 earlier. Both sensors would record larger changes even though the batteries are dead.

In summary, the soil hydrogen data in the FY 1994 period did not indicate major fluid activities in the Parkfield area, even at the time of the second A-level alert issued in mid-November of 1993. The small but discrete peak recorded at the Twisselman site in late August 1994 was an intriguing event. According to the past experience, the magnitude of anomalies prior to a $M > 6$ in the Parkfield area should at least be several hundred ppmv at multiple sites in the area.

REPORTS PUBLISHED

None.

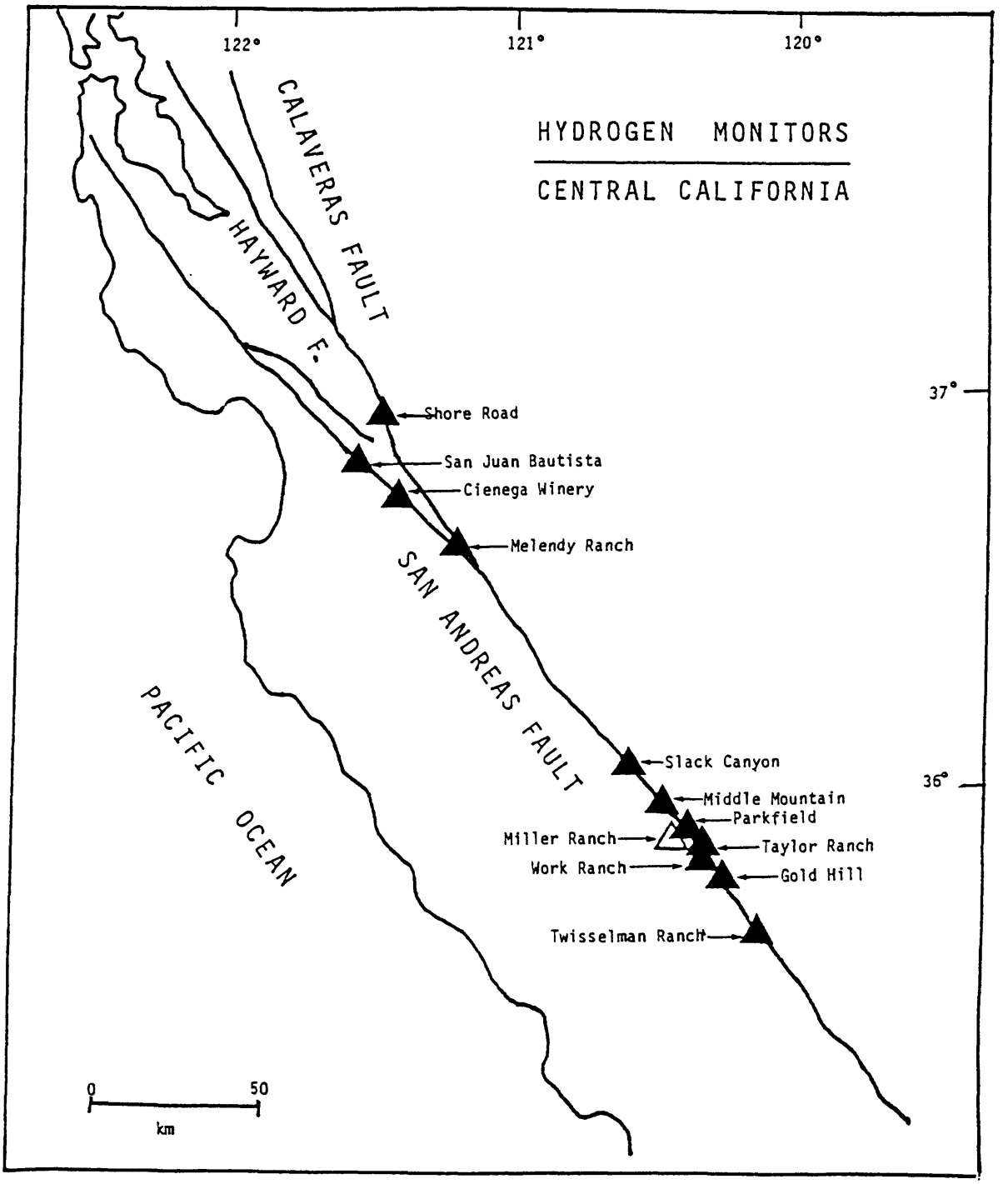

(FIG. 1) A map showing the locations of soil hydrogen monitoring sites in central California (filled triangles). The Wright Road site is no longerin operation. The Miller Ranch site is for water geochemistry only.

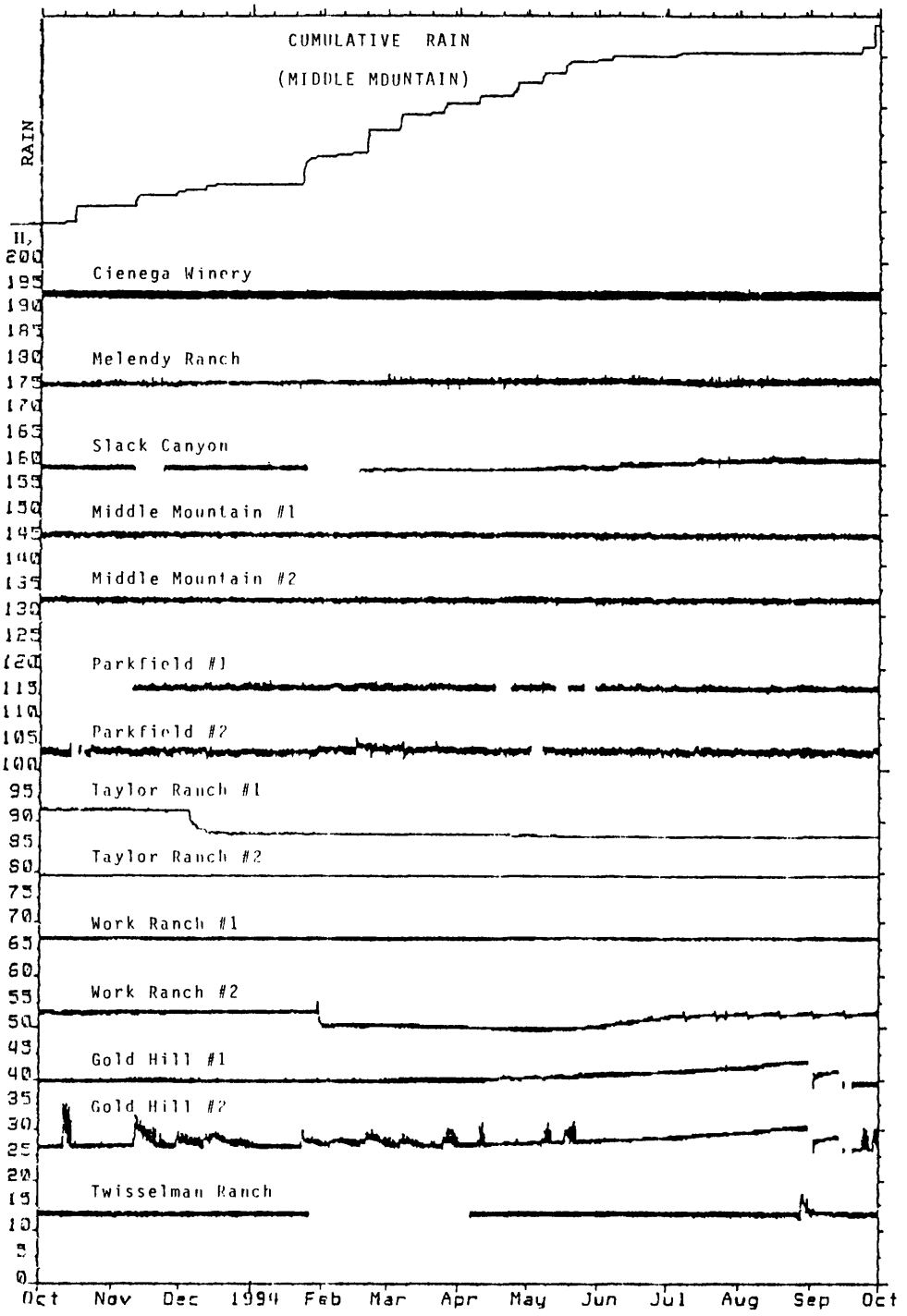

(Fig. 2) Soil hydrogen data recorded in central California between 1 October 1993 and 1 October 1994. The hydrogen concentration scale (vertical axis) is in parts per million by volume divided by 10 (ppmv/10). The plots are composite and the relative levels of H$_2$ are arbitrary. The top trace is cumulative rain monitored at Middle Mountain.

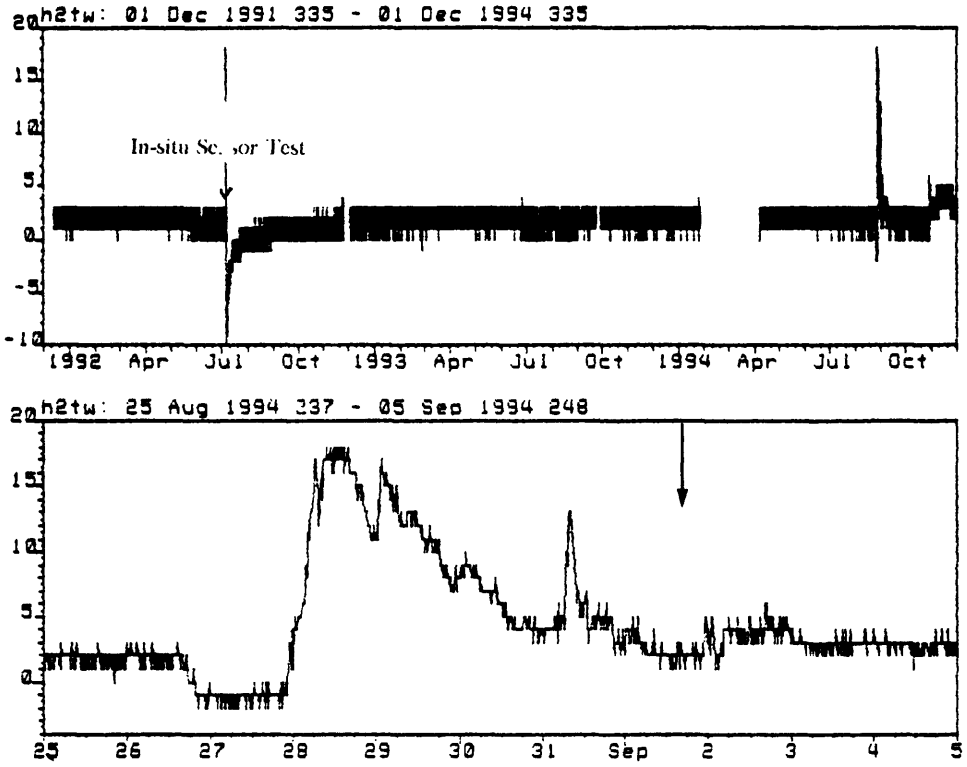

(Fig. 3) The soil hydrogen data recorded at the Twisselman Ranch site. Top: From 1 December 1991 to 1 december 1994. Bottom: From 25 August 1994 to 5 September 1994, where down arrow indicates the time of M 7.2 earthquake off Mendocino. The vertical axes are hydrogen concentration in telemetry counts (10 counts = 25 ppmv).

Surficial and Bedrock Geology in the Midcontinent Mississippi Valley and in the New Madrid Seismic Zone

9510-10210
A. Schultz and R.W. Harrison
U.S. Geological Survey
MS 928, Federal Center, Reston, VA 22092
(703) 648-6501
Fax-1-703-648-6953
Program Element II

Investigations Undertaken

During FY 1994, our investigations were a continuation of research on the tectonic framework of the Midcontinent. Our activity concentrated on characterizing deformation along the Ste. Genevieve fault system in Missouri and the complexly faulted Thebes Gap area in southeast Missouri and southern Illinois. Work consisted of synthesis and analysis of data collected in FY 1993, and the gathering of new field data.

Field work included geologic mapping of the Thebes 7.5-minute quadrangle, Illinois and Missouri, core drilling adjacent to the escarpment at the southern margin of the Benton Hills, southeast Missouri, and field checking areas in and around the Coffman and Minnith quadrangles. The drilling was part of ongoing cooperative research with the Missouri Division of Geology and Land Survey on the nature and timing of deformation along the English Hill and Commerce faults.

Data evaluation consisted of preparation of geologic maps with structural cross sections for the Coffman, Minnith, and Thebes 7.5-minute quadrangles, Missouri, logging and sampling core drilled in FY 1993 and 94, clay analysis of core material, and palynologic analysis of stratigraphic intervals.

Results

Ste. Genevieve fault system

Details of our investigations on the Ste. Genevieve fault system in Missouri are still forthcoming, however, some preliminary observations can be outlined:

1) The system can be characterized as consisting of braided fault strands, generally with high-angle dips and many different strike directions (northwest and east-west dominant).

2) The system has had a complex history, which along different segments has involved both right-lateral and left-lateral strike-slip faulting, high-angle reverse faulting, and extension faulting.

3) One period of faulting occurred after deposition of the St. Laurent Formation (Middle Devonian) and prior to deposition of

Lower Mississippian strata. This deformation was predominantly left-lateral strike-slip faulting along northwest-trending segments and extensional along east-west segments. Total horizontal movement is thought to be a couple thousand feet or less; faulting appears to have been nearly contemporaneous with eruption of the nearby Avon diatremes.

4) At least two episodes of faulting involve Upper Mississippian formations; one episode resulted in high-angle reverse faulting along east-west trends and right-lateral oblique-slip faulting along northwest trends; a second episode resulted in normal faulting along northwest trends and right-lateral oblique slip on east-west trends. Although there is no upper time constraint on these two episodes, they are thought to represent foreland deformation associated with the Ouachita and Alleghany orogenies.

5) Recent weak seismic events in the area of investigation that have been recorded by the monitoring network of the Saint Louis University reveals that most earthquakes in the area are probably not related to movement along the Ste. Genevieve fault system. When plotted on a magnetic anomaly map, most epicenters are found to lie in proximity to steep, linear gradients interpreted as buried faults in the Middle Proterozoic basement other than the Ste. Genevieve system. Field investigations have discovered a previously unidentified northwest-striking zone of cataclastic shears in the Cambrian Lamotte Formation directly over one of these linear magnetic gradients. This shear zone is on strike with a previously mapped fault to the southeast and is en echelon to mapped faults to the northwest. The Avon diatremes are localized along the shear zone. Also, a major drainage divide closely follows the shear zone and fault extensions for more than 45 km.

Thebes Gap-Benton Hills area

Our work in the Thebes Gap-Benton Hills area of southeast Missouri and southern Illinois has resulted in a better understanding of the tectonic history of the New Madrid region. Just 45 km north of the New Madrid seismic zone, rocks in this area are the closest exposures to the seismic zone available for structural analysis. It is also an area of recent moderate seismicity.

Field investigations have documented numerous north-northeast- and northeast-striking strike-slip faults, and associated folds and transtensional grabens. Movement has been dominantly right lateral, but an episode of left-lateral movement (thought to be related to the Ouachita orogeny) has also been recognized.

Perhaps the most important result of our investigations is the identification of a relatively major period of deformation that occurred in the Neogene or Early Pleistocene. Faults active during this period have been found surrounding the northern margin of the Mississippi embayment in southeast Missouri, southern Illinois, and western Kentucky. Analysis of kinematic indicators shows that this widespread event occurred under stress conditions remarkably similar to those active today, ie. east-northeast-directed maximum

horizontal stress.

Preliminary results of our drilling along the southern escarpment of the Benton Hills, coupled with seismic reflection profiles produced by the USGS's Branch of Geologic Hazards and Missouri Division of Geology and Land Survey, suggest that the scarp is fault related and that it was probably produced during the Neogene or Early Pleistocene event. The age range is a result of uncertainties in the age of Mounds Gravel, the youngest deposit involved in faulting. At many places, undeformed Pleistocene loess is known to overlie faults that offset Mounds Gravel.

Another result of our drilling has been a refinement of Late Cretaceous stratigraphy and related tectonic implications for the northern Mississippi embayment. At the base of the Cretaceous section beneath the McNairy Sand, our drill holes penetrated 20-25 ft of organic-rich, silty to sandy marine clay overlying 24-30 ft of gravel, sand, and clay. The upper unit has not been previously identified in the northern Mississippi embayment. Lithologic similarities and a Late Campanian age determination from palynologic evidence indicate that this upper unit is correlative to the Coffee Sand of western Tennessee and northern Mississippi. This correlation extends the occurrence of Late Campanian Seas into the northernmost portion of the Mississippi embayment. The absence of Late Campanian deposits in the New Madrid, extreme northwestern Tennessee, and western Kentucky strongly suggest uplift and erosion prior to deposition of the Maastrichtian McNairy Sand in this region.

The gravel deposits which underlie Coffee Sand in our drill holes have traditionally been regarded in southern Illinois and western Kentucky as equivalent to the Cenomanian Tuscaloosa Formation. However, palynologic evidence from our cored sections indicate that these deposits are Middle Campanian in age and thus are much too young to be correlative to the Tuscaloosa Formation. Investigations are presently being undertaken to determine the extent of the Campanian gravels and their tectonic implications.

Reports Published

Harrison, R.W., and Schultz, Art, 1994, Strike-slip faulting at Thebes Gap, Missouri and Illinois: Implications for New Madrid tectonism: Tectonics, v. 13, no. 2, p. 246-257.

Schultz, A., and Harrison, R.W., 1994, Geologic map of the Minnith 7.5-minute quadrangle, Ste. Genevieve and Perry Counties, Missouri: U.S. Geological Survey Open-File Report 94-421, scale 1:24,000.

Harrison, R.W., and Schultz, A., 1994, Geologic map of the Coffman 7.5-minute quadrangle, Ste. Genevieve County, Missouri: U.S. Geological Survey open-File Report 94-419, scale 1:24,000.

Harrison, R.W., and Nelson, W.J., 1993, Is the present-day

seismicity in the Midcontinent a renewal of an older Neogene tectonic event? (abs.): Geological Society of America, Abstracts with Programs, v. 25, no. 6, p. 479.

Hoffman, David, Palmer, J.R., Harrison, R.W., Odum, J.K., Stephenson, W.J., and Williams, S., 1994, Faulting associated with the southeastern escarpment of the Benton Hills, Scott County, Missouri (abs.): Geological Society of America, Abstracts with Programs, v. 26, no. 1, p. 8.

Seismological Investigations and Tectonic Interpretation of the April, 1992 Cape Mendocino Earthquake Sequence

Award No. 1434-94-G-2494

Susan Y. Schwartz
Earth Sciences Department, University of California
Santa Cruz, California 95064
ph: (408) 459-3133; FAX: (408) 459-2127; email: sschwartz@earthsci.ucsc.edu

Investigations

1) Rupture process of the April 25, 1992 Cape Mendocino, CA earthquake using long-period surface waves, broadband body waves and strong ground motion recordings.

2) Determination of source parameters of aftershocks of the Cape Mendocino earthquake from inversion of local P, SH, and SV amplitude ratios and broadband waveforms.

3) Determination of uniform stress tensor in vicinity of Cape Mendocino from inversion of focal mechanism solutions.

Results

1) Rupture process of the April 25, 1992 Cape Mendocino, CA earthquake

The April 25, 1992, M_W=7.1, Cape Mendocino earthquake occurred in the tectonically complex region of the northward migrating Mendocino Triple Junction (Figure 1). Here, where the Pacific, North America, and Gorda plates meet, seismic activity is greater than in any other region in the contiguous United States. Many large earthquakes have occurred in this region and have concentrated almost exclusively within the Gorda Plate. Most of the smaller magnitude events locate along the Mendocino Fracture Zone or within the Gorda Plate or overlying North American Plate. Few, if any events have occurred along the Gorda-North America thrust boundary. The faulting mechanism of the 1992 Cape Mendocino earthquake (Dziewonski *et al.*, 1993) is consistent with underthrusting of the Gorda Plate beneath the North American Plate and may represent the first historic, damaging event to rupture the southern Cascadia subduction zone from Cape Mendocino to Vancouver Island. Using the extensive set of ground motion data for this earthquake, including strong-motion, body wave, and surface wave data, we have performed a detailed study of its source process over a broad range of frequencies. We have obtained source parameters for this event, including focal mechanism, hypocentral depth, source duration, seismic moment, and the spatial and temporal distribution of slip on the fault exploiting both the broadband and long-period seismic data.

Long-period surface wave analysis

Long-period (150-280 s) Rayleigh and Love waves from the GSN, GEOSCOPE, and IDA networks were analyzed to determine the faulting duration, centroid depth, and moment tensor of the 1992 mainshock. We use a moment tensor spectral inversion method originally developed by Kanamori and Given (1981) and later modified by Romanowicz and Guillemant (1984) and Zhang and Kanamori (1988) to isolate the duration estimate from the depth and moment tensor estimate and by Velasco *et al.* (1992) to optimize the centroid location and stabilize the moment tensor determination. During the first step of this procedure, Rayleigh and Love wave spectra are inverted for the best trapezoid source duration at several different periods utilizing a suite of different phase velocity models for propagation corrections. The second step solves for a point source depth and the moment tensor utilizing both amplitude and corrected phase information and assuming various models for global attenuation and the source velocity. Our best

solution is for a source duration of 20 s, a depth of 15 km, a seismic moment of .31 x 10^{27} dyne-cm and strike= 330°, dip=15°, and rake=90°.

Broadband body wave and strong motion analysis

Broadband body waves, with their higher frequency content, can further constrain details of the earthquake rupture. We studied the body waves from the Cape Mendocino mainshock to obtain first-order source parameters to compare with those obtained from surface wave analysis and to determine the spatial distribution of slip on the fault plane. We inverted P and SH displacements for the hypocentral depth, moment tensor, and source time function of this event assuming a point source. Our results of depth=8-18 km, seismic moment=.18-.20 x 10^{27} dyne-cm, strike=330°, dip=13°, and rake=70° compare well with those determined from the surface wave analysis. However, the source duration from the body waves is about 9 s compared with the 20 second duration obtained with the long-period surface waves. The fit of this model to the P wave displacement waveforms is shown in Figure 2.

A point source for the Cape Mendocino mainshock may not be adequate to fit the teleseismically recorded P and SH waves. Figure 2 indicates that P waveforms at azimuths to the west and northwest are not well fit by our point source solution. Source finiteness is also indicated by both the aftershock distribution and results of an empirical Green function deconvolution procedure (Velasco *et al.*, 1993) which suggest that this earthquake ruptured up-dip in a westerly direction. We performed a finite fault inversion using the broadband body waves to determine the distribution of slip on the fault plane. Figure 3a shows the grid along which strike slip (Figure 3b) and dip slip (Figure 3c) displacements are determined. The results indicate two patches of concentrated slip; one a few km updip and west of the hypocenter and the other downdip and north of the hypocenter. We are in the process of including strong-motion recordings (strong-motion stations are indicated with triangles in Figure 3a) in conjunction with teleseismic displacement waveforms to more precisely determine the slip distribution of the mainshock.

2) Source parameters of aftershocks of the Cape Mendocino, CA earthquake

Source parameters of aftershocks of the April 25, 1992 Cape Mendocino, California earthquake are determined from a grid search inversion of P, SH, and SV amplitude ratios recorded by a small local network of three-component broadband and short-period stations. The inversion procedure consists of: computing synthetic seismograms for three fundamental fault orientations for all source receiver pairs over a range of source depths; calculating the complex envelopes of the seismograms to determine peak amplitudes of P, SH, and SV waves; combining the fundamental fault amplitudes for all possible values of strike, dip and rake, at 10° increments; and determining the best fault orientation and depth as the one that yields the smallest misfit between observed and synthetic P/SH, P/SV, and SV/SH amplitude ratios. The ambiguity in the sense of motion on the nodal planes, arising due to the use of amplitude ratios, is resolved by examining P-wave polarities. Source parameters for the largest events (M>3.4) are also determined by inversion of broadband displacement waveforms using a similar grid-search technique. Comparable results were obtained using both broadband waveforms and amplitude ratios. Focal mechanism solutions for aftershocks of the 1992 Cape Mendocino earthquake reveal that although the mainshock was associated with underthrusting of the Gorda Plate beneath the North American Plate, 70% of the 38 largest aftershocks indicate that these events result from motion between the Gorda and Pacific plates.

For each event, amplitude ratios from four to ten stations were inverted for the best fault plane orientation and depth using locations determined by the U.S Geological Survey and a simple crustal velocity model. The resulting focal mechanisms are shown in three different depth ranges in Figure 4. The majority of aftershocks in the depth range between 0 and 12 km are most likely located in the crust of the North American plate, since published velocity models have the top of the Gorda plate at depths below 15 km in this region (Smith *et al.*, 1993; Verdonck and Zandt, 1994). In this depth range, the fault plane solutions display a large variety, however, most solutions have north-south, nearly horizontal pressure axes. North-south, horizontal pressure axes also dominate the fault plane solutions determined for events in the depth range between 15 and 22 km (Figure 4), but there is more consistency in the orientation of the nodal planes for events in this depth range. Seven out of ten events have one nodal plane that dips to the south-southeast with a slip vector between 160° and 180°. If we interpret this plane to be the fault plane,

the motion on this plane suggests underthrusting of the Gorda Plate beneath the Pacific Plate. The observed slip direction of 160°-180° is consistent, however more southerly, than the expected motion between the Gorda and Pacific Plates. Supporting evidence for southward displacement of the Gorda Plate in this region comes from a southeastward trending gravity anomaly that Jachens and Griscom (1983) have interpreted as the south edge of the Gorda Plate. Based on the geometry of the gravity anomaly, Jachens and Griscom (1983) conclude that the southern edge of the Gorda Plate trends east-west far offshore and begins to bend southward within about 30 km of the triple junction, passing beneath the coast about 20 km south of Cape Mendocino. This geometry is consistent with the southeast trend of aftershocks below 15 km which come onshore at a coincident location as the gravity anomaly. There is no evidence of convergent motion between the Gorda and Pacific Plates along the Mendocino Fault farther to the west, suggesting that the rigid Pacific Plate prevents southward displacement of the Gorda Plate and the convergent motion is fully accommodated by internal deformation within the Gorda Plate. Towards the triple junction where the Pacific Plate ends, it is reasonable to assume that the convergent motion will be accommodated by southward displacement of the Gorda Plate.

The focal mechanisms in the depth range between 23 and 35 km show the most consistency. These events form a tight northwest-southeast linear trend parallel to the events in the 15-22 depth range. They all have one nodal plane parallel to this alignment which we interpret as the fault plane (Figure 4). The motion across this plane is right lateral, consistent with this fault being the near shore extension of the Mendocino Fault. This provides further evidence for the southward bend of the southern edge of the Gorda Plate as the Mendocino Triple Junction is approached. A schematic, interpretive diagram of the Gorda-Pacific plate geometry deduced from these fault plane solutions is shown in Figure 5. Near the Gorda Rise where the Gorda Plate is young and buoyant and the Pacific Plate is old and acts as a buttress, the convergent motion between the Gorda and Pacific Plates is manifested as internal deformation within the Gorda Plate. As the Cape Mendocino Triple Junction is approached, the Gorda Plate has cooled a bit and the buttressing effect of the Pacific Plate is diminished at its terminus, allowing the convergent plate motion to be taken up as southeast directed underthrusting of the Gorda Plate beneath the Pacific Plate at depths between about 15 and 25 km. Below this depth motion between the Gorda and Pacific Plates occurs as right lateral shear along the clockwise rotated, Mendocino Fault. The southeast convergence of the Gorda Plate relative to the Pacific Plate produces a tongue of southward dipping Gorda Plate beneath North America (Southern 'Drag" of Gorda Plate in Figure 5). This south dipping section of Gorda Plate has been imaged seismically by Niazi and Karageorgi (1992) as a zone of relatively high velocities dipping south-southeast extending from Humboldt Bay to south of Punta Gorda. Verdonck and Zandt (1994) also seismically image a south flexing (6°-12°) Gorda Plate in this region that appears to end abruptly near Punta Gorda (Figure 4), allowing only a small amount of underthrusting of the Gorda Plate beneath the Pacific Plate.

3) State of Stress at the Cape Mendocino Triple Junction

We are now in the process of combining our aftershock focal mechanism solutions with other well-determined fault plane solutions for earthquakes near the Cape Mendocino Triple Junction to determine the best-fitting uniform stress tensor using the method of Gephart and Forsyth (1984). Our preliminary results confirm that a northerly, nearly horizontal principal stress direction is compatible with over 60 fault plane solutions obtained for this region. In the presence of our best stress tensor, the resolved shear stress on the 1992 Cape Mendocino fault plane is very low. This suggests that the southern-most section of the Cascadia subduction zone near the triple junction is weak. The weak nature of the San Andreas Fault has been recognized for some time (Lachenbruch and Sass, 1980); however the strength of other major fault zones is still in question. Our preliminary results are intriguing, but further work that we will perform in the next several months is needed for their confirmation.

References

Dziewonski, A.M., G. Ekstrom, and M.P. Salganik, 1993. Centroid-moment tensor solutions for April-June, 1992, Phys. Earth. Planet Inter., 77, 151-163.

Gephart, J.W., and D.W. Forsyth, An improved method for determining the regional stress tensor using earthquake focal mechanism data: Application to the San Fernando sequence, 1984. J. Geophy. Res., 89, 9305-9320.

Jachens, R. C. and A. Griscom, 1983. Three-dimensional geometry of the Gorda Plate beneath northern California, J. Geophys. Res., 88, 9375-9392.

Kanamori, H., and J.W. Given, 1981. Use of long-period surface waves for rapid determination of earthquake source parameters, Phys. Earth. Planet. Int., 27, 8-31.

Lachenbruch, A.H., and J.H. Sass, 1980. Heat flow and energetics of the San Andreas fault zone, J. Geophys. Res., 85, 6185-6223.

Niazi, M., and E. Karageorgi , 1992. Irregular geometry of the Gorda subduction and deep structure of the Eel River basin determined from teleseismic P delays, Tectonophysics, 201, 209-228.

Romanowicz, B.A., and P. Guillemant, 1984. An experiment in the retrieval of depth and source mechanism of large earthquakes using very long-period Rayleigh wave data, Bull. Seismol. Soc. Am., 74, 417-437.

Smith, S.W., J.S. Knapp, and R. McPherson, 1992. Seismicity of the Gorda Plate and an eastward jump of the Mendocino Triple Junction, J. Geophys. Res., 98, 8153-8171.

Velasco, A.A., C.J. Ammon, and T. Lay, 1993. Recent large earthquakes near Cape Mendocino and in the Gorda Plate: Broadband source time functions, fault orientations and rupture complexities, J. Geophys. Res., 99, 711-728

Verdonck, D., and G. Zandt, 1994. Three-dimensional geometry of the Mendocino Triple Junction, J. Geophys. Res., in press.

Zhang, J. and H. Kanamori, 1988. Source finiteness of large earthquakes measured from long-period Rayleigh waves, Phys. Earth Planet. Int., 52, 56-84.

Publications

Schwartz, S.Y., Source parameters of aftershocks of the 1991 Costa Rica and 1992 Cape Mendocino, California earthquakes from inversion of local amplitude ratios and broadband waveforms, Bull. Seismol. Soc. Am., submitted, 1994.

Hagerty, M.T. and S.Y. Schwartz, Rupture process of the April 25, 1992 Cape Mendocino, California earthquake from long-period surface waves, broadband body waves, and strong-ground motions, in preparation, 1994.

Schwartz, S.Y., Source parameters of local earthquakes from inversion of P and S wave amplitudes, Trans. Am. Geophys. Union, 74, 399, 1993.

Hagerty, M.T., S.Y. Schwartz, and C.J. Ammon, Finite-fault modeling of the April 25, 1992 Cape Mendocino earthquake, Trans. Am. Geophys. Union, 74, 399, 1993.

Hubert, A. and S.Y. Schwartz, State of stress at the Cape Mendocino Triple Junction from inversion of focal mechanisms of the 1992 Petrolia, CA earthquake sequence, Trans. Am. Geophys. Union, 74, 200, 1993.

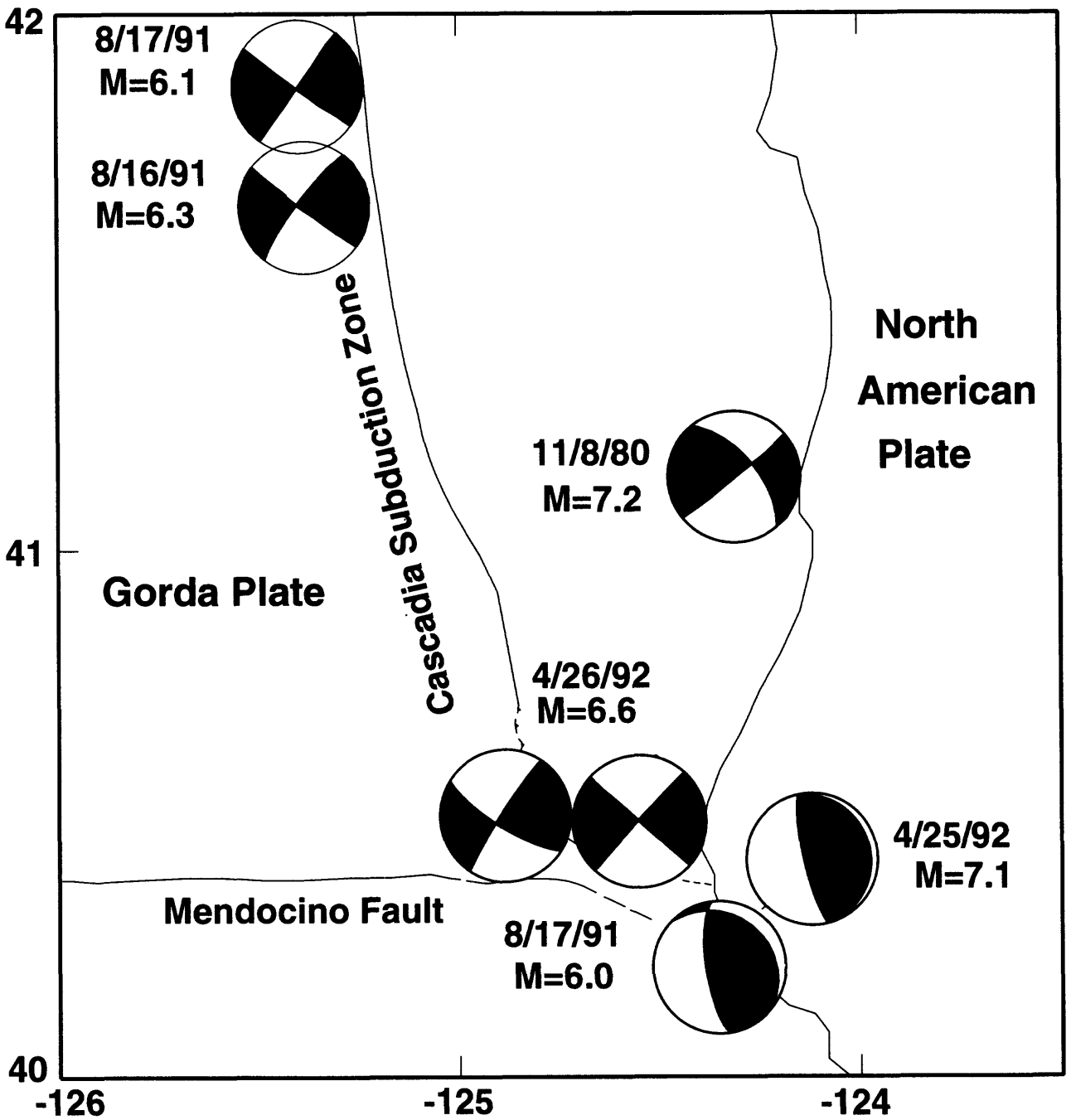

Fig. 1. Map showing location and Harvard CMT solutions for all recent earthquakes with magnitudes greater than 6.0 that occurred in the vicinity of the Cape Mendocino Triple Junction.

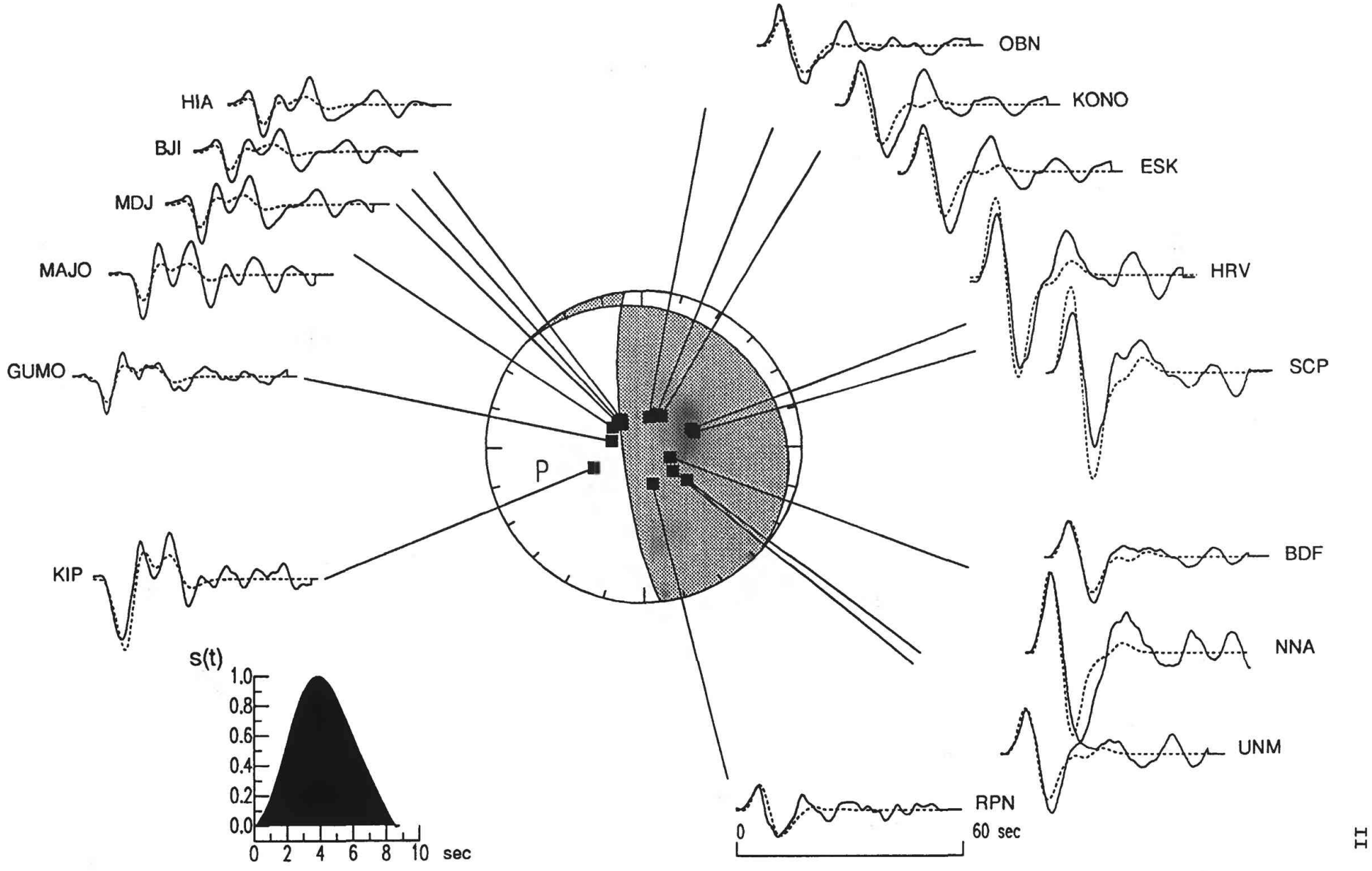

Fig. 2. Focal mechanism, source time function, and P wave data (solid lines) and synthetics (dashed lines) resulting from inversion of broadband P and SH waves for the Cape Mendocino mainshock.

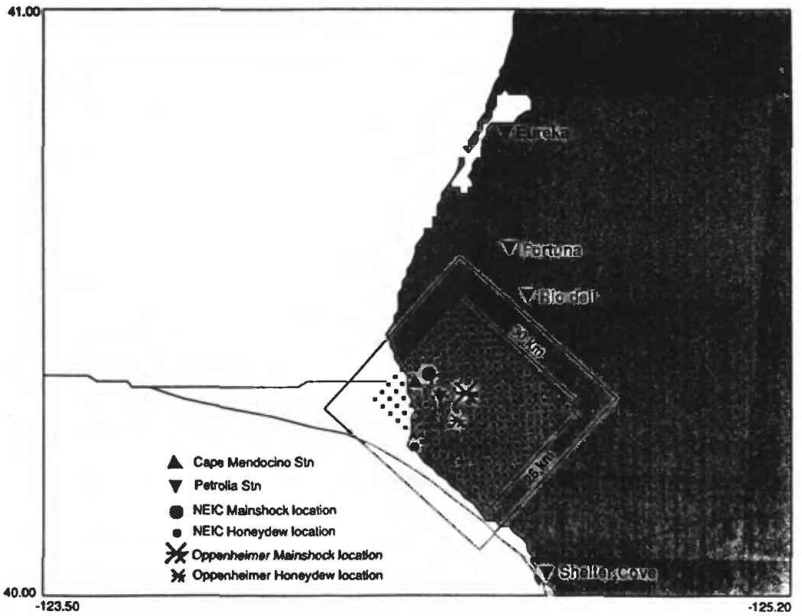

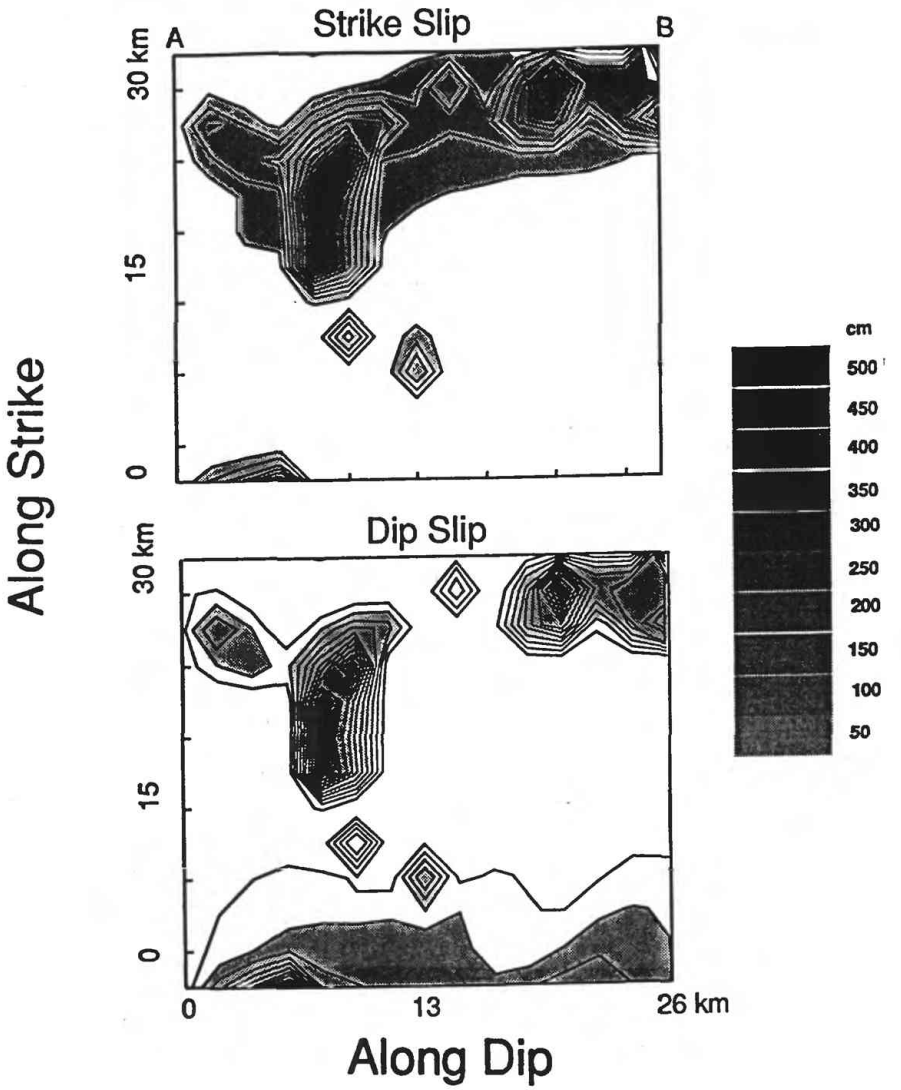

Fig. 3. a) Finite fault grid used in the inversion of teleseismic data for the slip distribution. The USGS mainshock location (large star) and strong motion stations (triangles) whose data will be incorporated into the inversion are indicated. Results of teleseismic finite fault inversion showing amount of strike-slip (b) and dip slip (c) displacement on the fault.

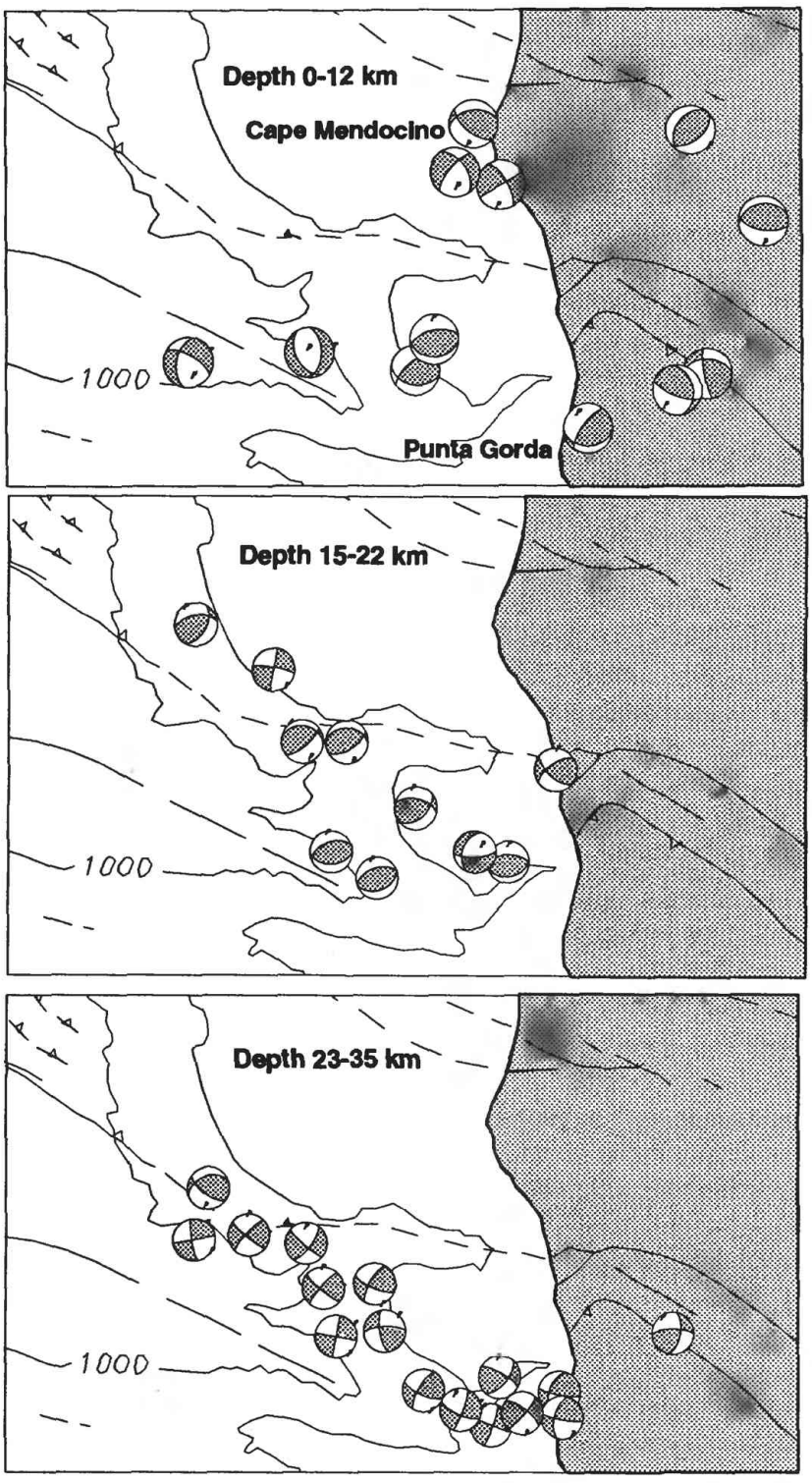

Fig. 4. Focal mechanism solutions for 38 aftershocks of the Cape Mendocino earthquake determined by amplitude ratio inversion. Focal mechanisms are placed at their US Geological Survey locations.

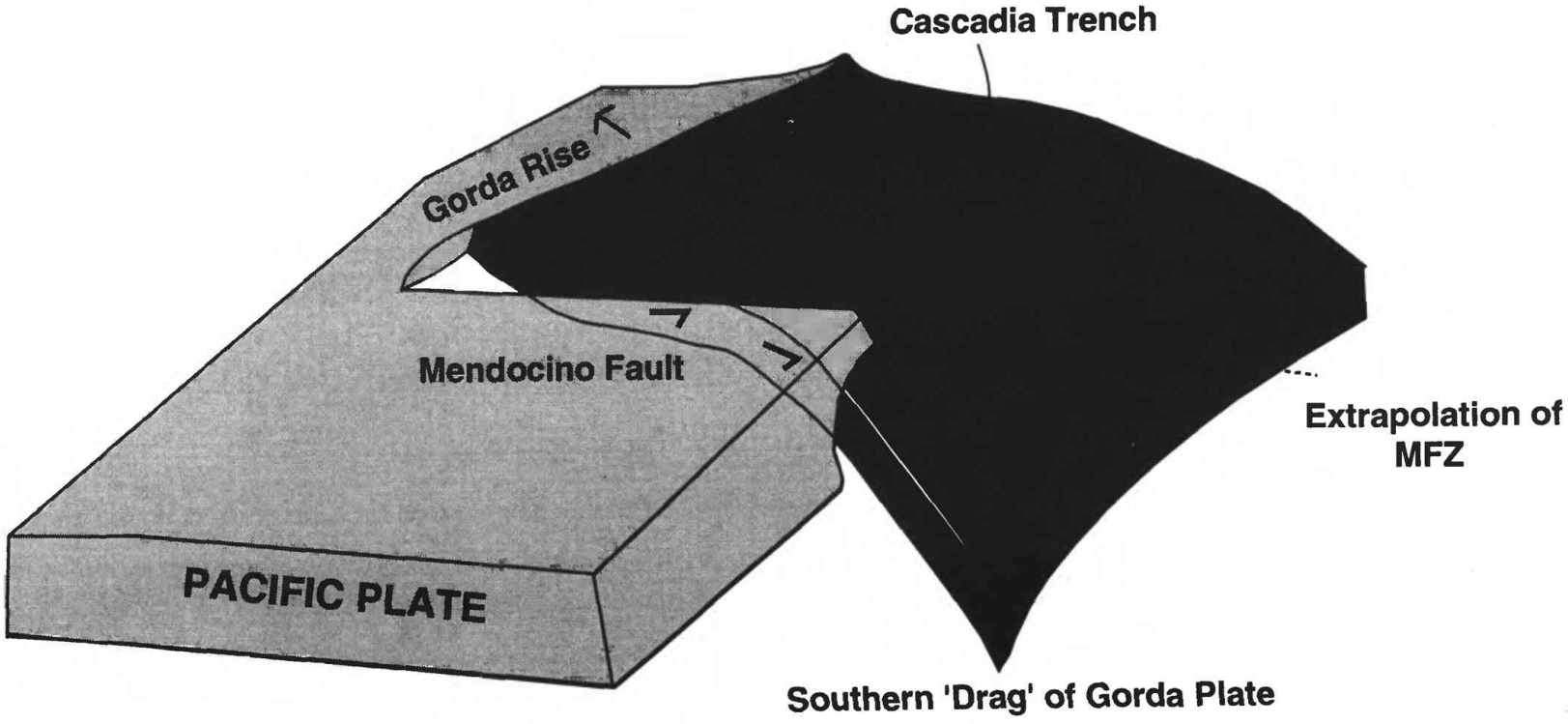

Fig. 5. Schematic interpretation of Gorda-Pacific Plate interactions as determined from focal mechanisms of aftershocks of the Cape Mendocino earthquake. Subduction of the Gorda Plate beneath the Pacific Plate near the Cape Mendocino Triple Junction, produces a tongue of Gorda Plate that extends south of the Mendocino Fault.

SEISMOTECTONICS OF THE CENTRAL UNITED STATES

9905-14010

Eugene S. Schweig, III
U.S. Geological Survey
Center for Earthquake Research and Information
Memphis State University
Memphis, TN 38152
(901) 678-4974; fax (901) 678-4734
schweig@ceri.memphis.edu

Program Element II

INVESTIGATIONS

This project addresses major gaps that currently exist in our understanding of the tectonic setting, seismic source zones, and recurrence intervals of damaging earthquakes in the central U.S., and the integration of surface and subsurface data into seismotectonic models. 1994, the third year of this project, was dedicated mainly to paleoearthquake studies in the New Madrid seismic zone.

RESULTS

The paleoearthquake studies are a collaborative effort with Martitia Tuttle (Lamont-Doherty Earth Observatory) and Yong Li, John Craven, and Michael Ellis (all of the Center for Earthquake Research and Information, the University of Memphis). We have now found seven sites with confirmed pre-1811 liquefaction and at least four sites with probable pre-1811 liquefaction. Details of the sites will be found in Tuttle and Schweig (in press). A summary of the tentative dates of the liquefaction deposits is shown in Table 1 and the locations of the sites are shown in Figures 1 and 2. We have been able to constrain the ages of the liquefaction features through a combination of soil development, radiocarbon ages on wood, charcoal, and soil, and the stratigraphic relationships of the features to Native American occupation horizons and artifacts. Of the confirmed prehistoric liquefaction features in the southern New Madrid seismic zone, we interpret one feature (E-525) as having formed during the Middle Woodland cultural period between A.D. 0 and 500 and five features having formed during the Mississippian cultural period between A.D. 700 and 1600. Of the five Mississippian features, three may have formed during the Early Mississippian period between A.D. 700 and 1200 (E-57, E-560b, and T-101) and the other two features may have formed in the Late Mississippian period between A.D. 1400 and 1600 (E-560a and Y-304). Others we cannot constrain so well but can demonstrate that they are pre-1811. We have also documented two prehistoric sandblows in the northern part of the seismic zone; W-102 formed prior to A.D. 1000 and N-628 formed before A.D. 1500.

Table 1. Tentative Dates of Liquefaction Features

Site	Feature	Archeological Constraint	Radiocarbon Constraint	No. of Events	Date (A.D.)
C-101	Sand blow	≥AD 1400-1670	<AD 1680-1940	1	1811 or 1400-1700
E-525	Sand blow	~AD 0-500	<AD 1220-1390	1	0-500
E-557	Sand dike	≥AD 500-?	<AD ?	1	post 500
E-560	Sand blow a Sand blow b	≤AD 1400-1670 ~AD 800	<AD 1510-1800 NA	1	1300-1670 500-1200
Y-304	Sand blow	≥AD 800-1400	<AD 1400-1630	1	1300-1600
M-801	Sand dikes	NA	>3778-3549 BC	3	pre-1811
T-101	Sand blow	≥AD 700-1670	<AD 1650-1810	1	?
W-102	Sand blow a Sand blow b	NA NA	<AD 1640-1950 <AD 870-990	2	1811 or ? pre-990
N-628	Sand blow	?	<AD 1410-1460	1	pre-1460

Based on these results, it appears that at least two, and probably three, earthquakes large enough ($M \geq 6.4$) to induce liquefaction in the moderately susceptible sediments of the region occurred between A.D. 0 and 1670. One of these events occurred between A.D. 0 and 500; a second event occurred between A.D. 700 and 1200; and a third event occurred between A.D. 1300 and 1670. These results suggest recurrence intervals of hundreds of years for large earthquakes. This is consistent with other paleoseismological studies in the region. It is clear that we must further refine these ages and cover a broader geographic area if we are to determine the significance of these discoveries for seismic hazards. We have submitted an article to Geology on our initial results (Tuttle and Schweig, 1994).

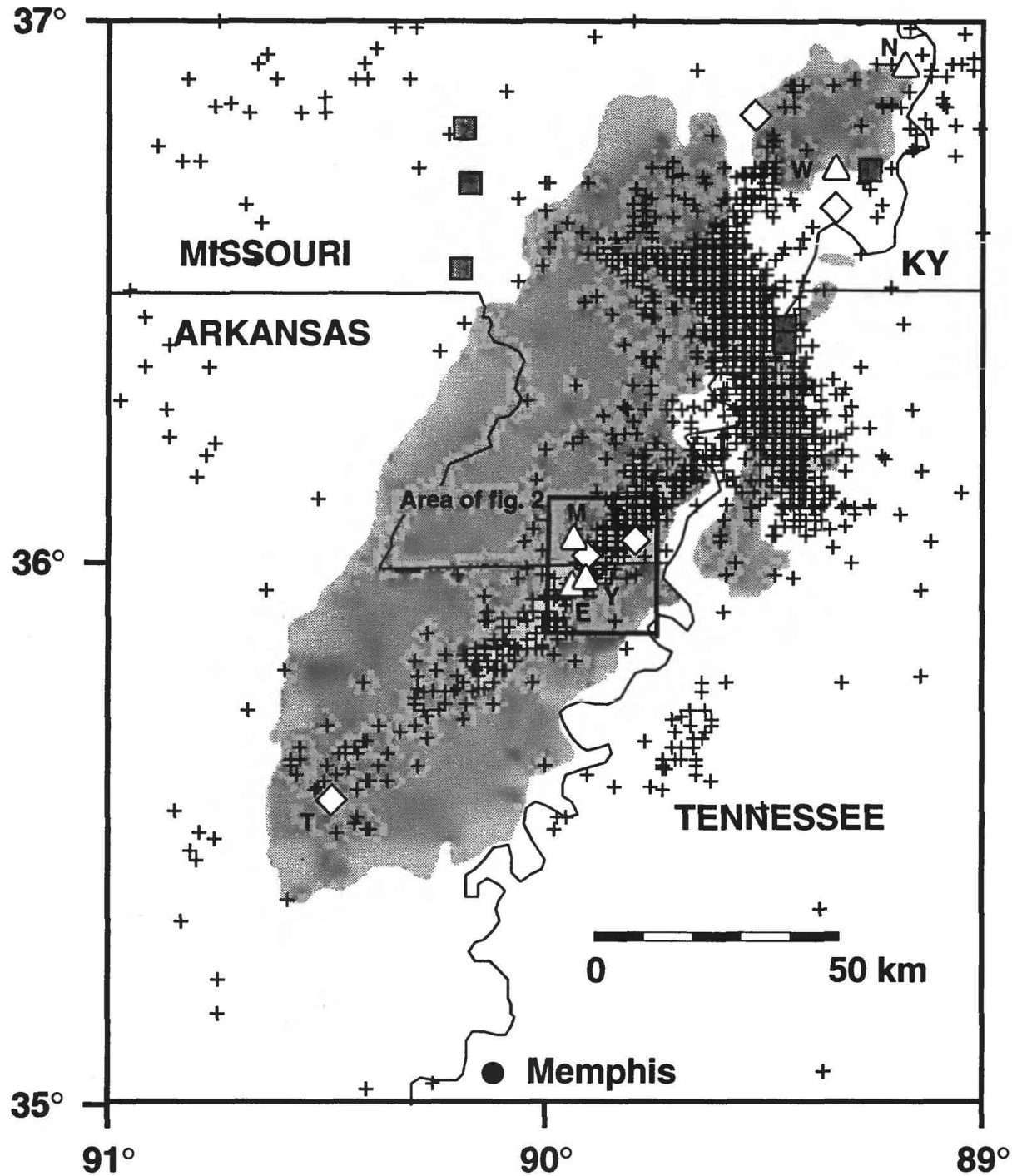

Figure 1: Map of the New Madrid seismic zone. Area of > 1% of area covered by sand blow deposits shown by gray shading (Obermeier, 1989) and locations of recent (1974-1991) seismicity shown by crosses. Gray squares denote sites where other paleoseismic studies have found evidence of pre-1811 liquefaction. Sites where we have found paleoliquefaction features denoted by white triangles; white diamonds are sites where investigations are underway. Y = Y-304, M = M-801, C = C-101, W = W-102, N = N-628, T = T-101 and E = Eaker sites = E-525, 557, and 569.

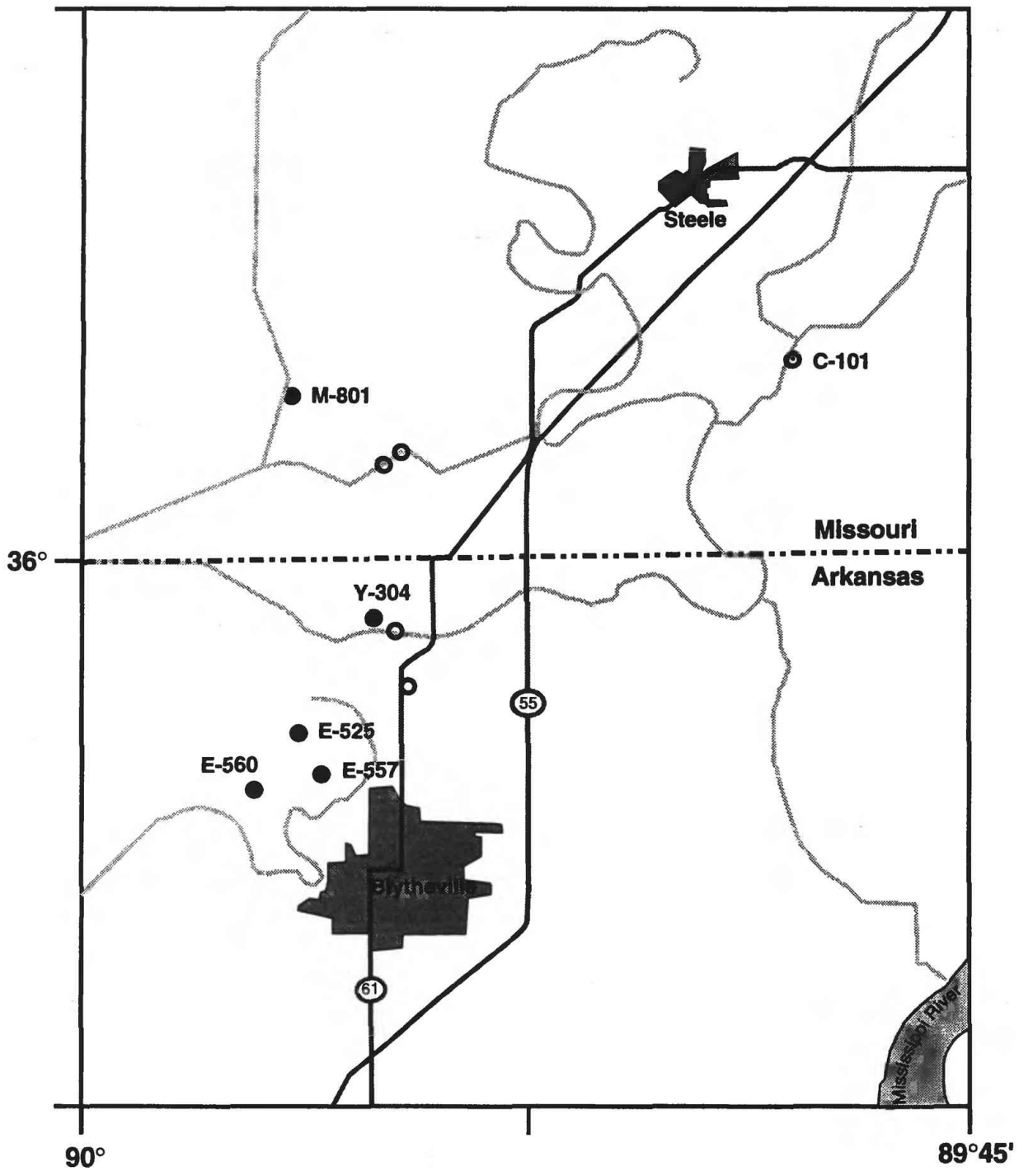

Figure 2: Detailed map of area near Blytheville, Arkansas. Location shown on Figure 1. Sites where we have found paleoliquefaction features denoted by black circles; open circles are sites where investigations are currently underway.

REPORTS:

Craven, J., Yong, L., Schweig, E. S., Ellis, M. A., and Tuttle, M. P., 1994, Paleoliquefaction studies in the New Madrid seismic zone: Journal of the Tennessee Academy of Science, v. 69, p. 46.

Li, Y., Tuttle, M. P., Schweig, E. S., and Ellis, M. A., 1994, New results of paleoearthquake studies in the northern New Madrid seismic zone (abstract): EOS, Transactions, American Geophysical Union, v. 75, supplement to no. 44, p. 452.

Schweig, E. S., and Ellis, M. A., 1994, Reconciling Short Recurrence Intervals with Minor Deformation in the New Madrid Seismic Zone: Science, v. 264, p. 1308-1311.

Schweig, E. S., Ellis, M.., and Tuttle, M., in press, The rate of occurrence of large earthquakes in the New Madrid seismic zone, in Hays, W. W., and Mohammadioun, G., eds., United States-France workshop on assessing earthquake hazards in the central and eastern United States and Western Europe: U.S. Geological Survey Open-File Report.

Schweig, E. S., III, Johnston, A. C., and Johnston, J. S., 1994, Lessons from Northridge, California, and Latur, India, for the Central and Eastern United States (abstract): EOS, Transactions, American Geophysical Union, v. 75, supplement to no. 16, p. 235.

Schweig, E. S., Tuttle, M. P., Li, Y., Craven J. A., Ellis, M. A., Guccione, M. J., Lafferty, R. H., III, and Cande, R. F., 1994, Evidence for Recurrent Strong Earthquake Shaking in the Past 5,000 Years, New Madrid Region (abstract): Geological Society of America Abstracts with Programs, v. 26, p. 26.

Tuttle, M. P., and Schweig, E. S., 1994, Recognizing and dating prehistoric earthquake-induced liquefaction features in the New Madrid seismic zone, central United States, in Proceeding of the Workshop on Paleoseismology (abstract): U. S. Geological Survey, Open-File Report 94-568, p. 186-188.

Tuttle, M. P., and Schweig, E. S., in press, Archeological and pedological evidence for large prehistoric earthquakes in the New Madrid seismic zone, central United States: Geology.

Tuttle, M. P., Schweig, E. S., III, Lafferty, R. H., III, and Guccione, M. J., 1994, Archaeological dating of liquefaction features and seismic events in the New Madrid seismic zone (abstract): Geological Society of America Abstracts with Programs, v. 26, p. A-156-A-157.

Valentine, R., Mirecki, J., Schweig, E. S., 1994, Estimate of historical sedimentation rate in a core from Reelfoot Lake, Tennessee: Journal of the Tennessee Academy of Science, v. 69, p. 46.

VanArsdale, R. B., Williams, R. A., Schweig, E. S., III, Shedlock, K. M., Kanter, L. R., and King K. W., 1994, Preliminary seismic reflection study of Crowley's Ridge, northeast Arkansas: U.S. Geological Survey Professional Paper 1538-C, 16 p.

Van Arsdale, R. B., Williams, R. A., Schweig, E. S., Shedlock, K. M., Odum, J. K., and King, K. W., in press, The origin of Crowley's Ridge, northeastern Arkansas: Bulletin of the Seismological Society of America.

NEHRP Summaries of Technical Reports, v. XXXVI (Submittal date, 12/2/94)

Systems Analysis of Geologic Rate Processes:

SPACE-TIME MODELS AND NONLINEAR DYNAMICS: EARTHQUAKE RECURRENCE PATTERNS AS THE EXPRESSION OF COUPLED TECTONIC OSCILLATORS

9980-13 (VGP Br.)

Herbert R. Shaw
Branch of Volcanic and Geothermal Processes, U. S. Geological Survey
MS-910, 345 Middlefield Road, Menlo Park, CA 94025
(415) 329-5245

Objective: The objective of this project is to develop models that explain the earthquake process in terms of emerging concepts of nonlinear dynamics. Examples of this approach have been given in many previous Technical Reports of NEHRP and in papers cited there (see the entry for this Project in *v. XXXIV* for 1992). The crucial question in the evaluation of earthquake recurrence patterns is spatiotemporal scaling. The present report considers the patterns of epicentral sequences of events (expressed by trajectories drawn between successive events) for chosen intervals of time (hours, days, weeks, months) before and after the Landers main shock of June 28, 1992, and at spatial scales identified by: (1) the immediate vicinity of the Landers main-shock epicenter, involving contiguous portions of the Mojave Desert, Imperial Valley, and San Bernardino Mts., (2) western North America at Longitudes between 100° and 130° W and Latitudes between 20° and 50° N, and (3) the North American quadrant of the Northern Hemisphere at Longitudes between 40° and 180° W and Latitudes between 0° and 80° N, involving the volcanotectonically active Aleutian Islands, Alaska, British Columbia, the western margins of the United States, Mexico, Central America, and northernmost South America, as well as the analogously active regions of central and eastern Mexico, the Caribbean, and those portions of South America that lie above the Equator (principally northern Venezuela and Colombia).

Results: Two aspects of spatiotemporal patterning have been observed: (1) epicentral sequences of events expressed by trajectories drawn between successive events show conspicuous convergences in the vicinities of the respective events Joshua Tree, Petrolia, and Landers, respectively, during periods of days to weeks prior to the main shocks at these sites regardless of spatial scale, and (2) the statistical ratios of numbers of successive events within three subdomains at both the largest and smallest spatial scales tend toward simple fractions that average to the proportions 1/4, 1/2, 1/4. This remarkable result strongly suggests that earthquake triggering mechanisms are globally coordinated at all scales, at least within the three spatiotemporal scales identified above, where the area of the smallest region represented is about 3° on a side. Observations (1) and (2) are both consistent with the idea that nonlinear resonances occurred in the triggering mechanisms of earthquake occurrences during 1992. If such patterns are typical of the longer term behavior of the seismic cycle, then they offer an interesting tool for monitoring the onset of focused earthquake activity over periods of weeks to months prior to major events in California. Spatial nodes of temporal resonances may be characteristic of the earthquake process in California, and such types of nonlinear spatiotemporal organization may even extend to the nature of global seismic signatures.

Development of Automatic Processing Methods for Analysis of Local Network Datasets

Award: 1434-94-G-2454
Program Element: II.2

Peter M. Shearer
Institute of Geophysics and Planetary Physics
Scripps Institution of Oceanography
University of California, San Diego
La Jolla, CA 92093-0225
(619) 534-2260 (office), 534-5332 (fax)
pshearer@ucsd.edu (E-mail)

Investigations

Permanent and portable seismic networks in southern California record a huge volume of high-frequency waveform data from local earthquakes. These records are currently used primarily to pick *P*-waves for determining event locations and focal mechanisms, and to compute magnitudes based on amplitudes and coda decay rates. Even such routine processing is a significant task considering the large number of stations and earthquakes that are involved. Most of the information in the seismograms beyond the first break of the *P*-wave is not used, except for selected events which make up only a small fraction of the total data available. The occurrence of large earthquakes and their aftershocks further strains the capabilities of the system by increasing seismicity rates to many times the background rate.

Our goal is examine these data through development of automatic techniques for processing and stacking local network seismic data which do not require any manual picking of the data. We have focused on two related problems: (1) stacking travel time and waveform data to image primary and secondary seismic phases, and (2) analysis of arrival time patterns in order to identify similar events, and to associate and locate events in the presence of multiple, nearly simultaneous earthquakes, such as typically occur early in afershock sequences.

Results

We have selected 872 events from the ~250,000 events recorded by the Southern California Seismic Network (SCSN) and available through the Southern California Earthquake Center Data Center (SCECDC). Figure 1 shows the SCSN station distribution and the locations for the events that we chose to use. Our goal was to obtain a fairly uniform spatial distribution of earthquakes. This was achieved by dividing the region into 5 km by 5 km cells and searching for the "optimal" event within each cell (generally the largest event, but we excluded those with large location uncertainties and events above m_b = 4.0 where clipped waveforms are a problem).

Figure 2 is a plot of travel time versus range for 31,703 picks obtained from the SCECDC for these events. No corrections are applied for variations in source depth, causing some of the scatter in the *P* and *S* travel time curves. We process these data using software originally designed for analysis of the ~10 million pick database of global picks collected by the International Seismological Centre (ISC). The picks are saved in a compressed binary format (~16 bytes/pick); in this case all event information and picks are stored in a single ~600 kilobyte file and can be read and plotted in seconds.

Figure 3 is an analagous plot of 296,747 picks obtained by our automatic phase picker applied to waveforms from these events stored in the SCEC archives. Our autopicker is based on a simple STA/LTA algorithm and was first developed to study global short-period data (Earle and Shearer, BSSA 84, 366-376, 1994). For the SCEC data, we have modified the picking parameters for the higher-frequency waveforms. The threshold of the trigger was deliberately set very low so as to detect weak phases; this results in a background level of "noise" picks between the major phases.

A comparison between Figures 2 and 3 shows that the autopicker produces many more picks than are available in the handpicked times. The operators appear most concerned with the first-arriving *P*-wave at ranges within about 250 km of the event. They do not routinely pick *S* or *Pg* beyond the *Pn* crossover point. In contrast, the autopick image reveals *Pn*, *Pg* and *S* out to beyond 500 km. A faint *Sn* phase can also be made out in the original of this plot. The agreement in the positions of the travel-time branches between Figures 2 and 3 suggests that the autopicker is producing reasonably accurate arrival times; in the future we plan more detailed comparisons between the picks.

The overall shape of the *P* and *S* travel time curves is determined by the average velocity versus depth profile for these ray paths. Presumably much of the scatter in the times reflects lateral velocity variations which can be explained with three-dimensional velocity inversions. There is clearly potential for using *Pn*, *Pg* and *S* arrival times at ranges beyond 200 km for regional studies of lower crustal and upper mantle velocities—much more information is contained in the archived waveforms than is currently available as travel-time picks.

The Moho reflected phases *PmP* and *SmS* are valuable for constraining Moho depths and lower crustal structure in tomographic inversions. A preliminary analysis of the autopicks from the 872 selected events suggests that clear *PmP* arrivals are fairly rare, but can be seen for certain source-receiver geometries. The clearest example of *PmP* arrivals that we have found so far involves northward propogation from Mojave events between Lancaster and Barstow. Figure 4 shows the event locations and autopick times versus range (the times have been corrected to a consistent source depth of 6 km). The retrograde *PmP* branch is clearly visible following direct *P* by about 1 to 2 s at ranges between 90 and 150 km. For comparison, Figure 5 shows a southeastern path for the same events; in this case no clear *PmP* arrivals are apparent (the scatter in the times is most likely due to lateral heterogeneity in velocity). Note that in these examples *S* is poorly resolved in the autopicked times, obtained almost entirely from vertical component instruments.

Reports

Dinger, K.B. and P.M. Shearer, Results of applying an autopicker to archived waveforms from southern California earthquakes, *EOS Trans. AGU (Fall meeting supplement)*, **75**, 483, 1994.

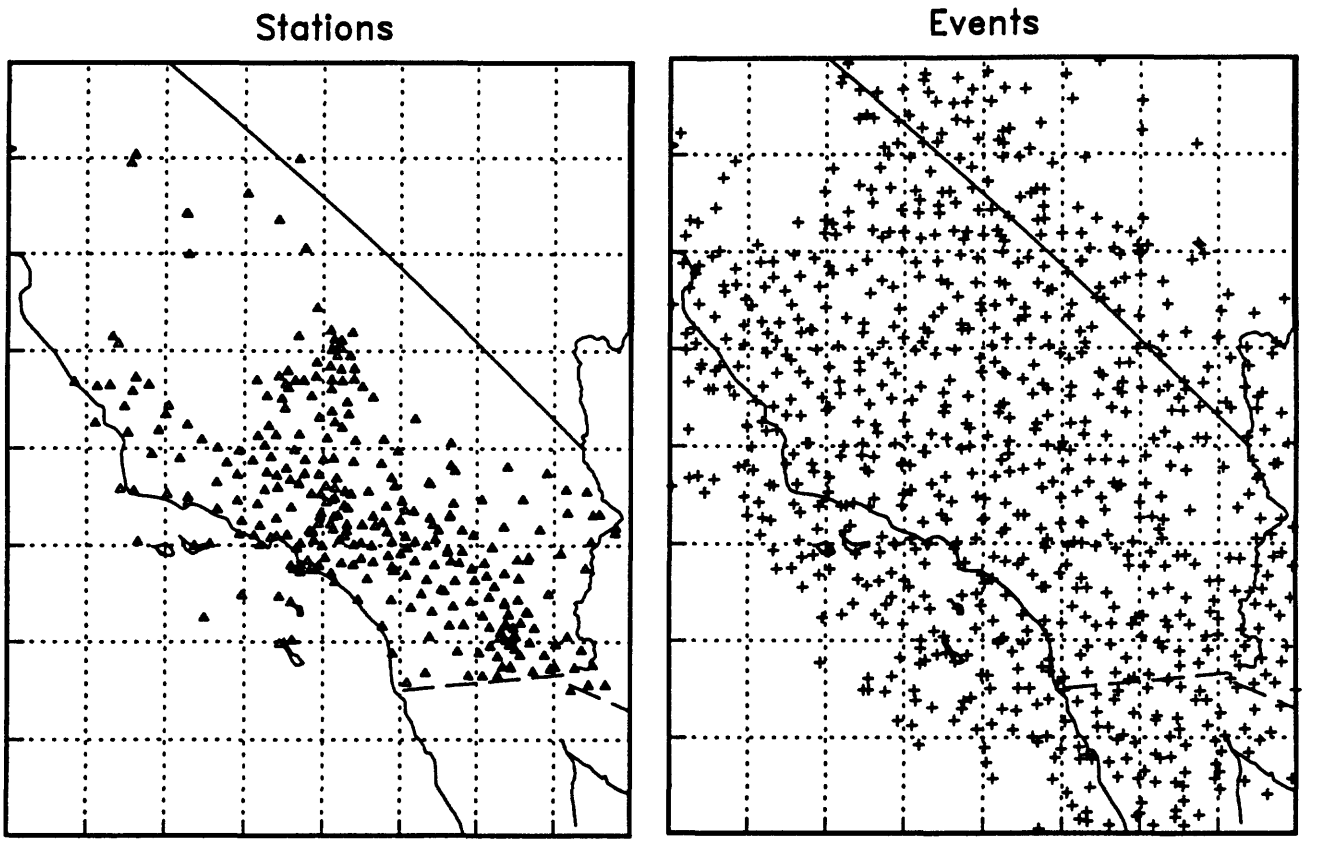

Figure 1. Locations of Southern California Seismic Network (SCSN) stations and 872 selected events from the ~250,000 events in the SCEC database. A reasonably even spatial distribution of events was achieved by searching for the best event within 5 km by 5 km cells.

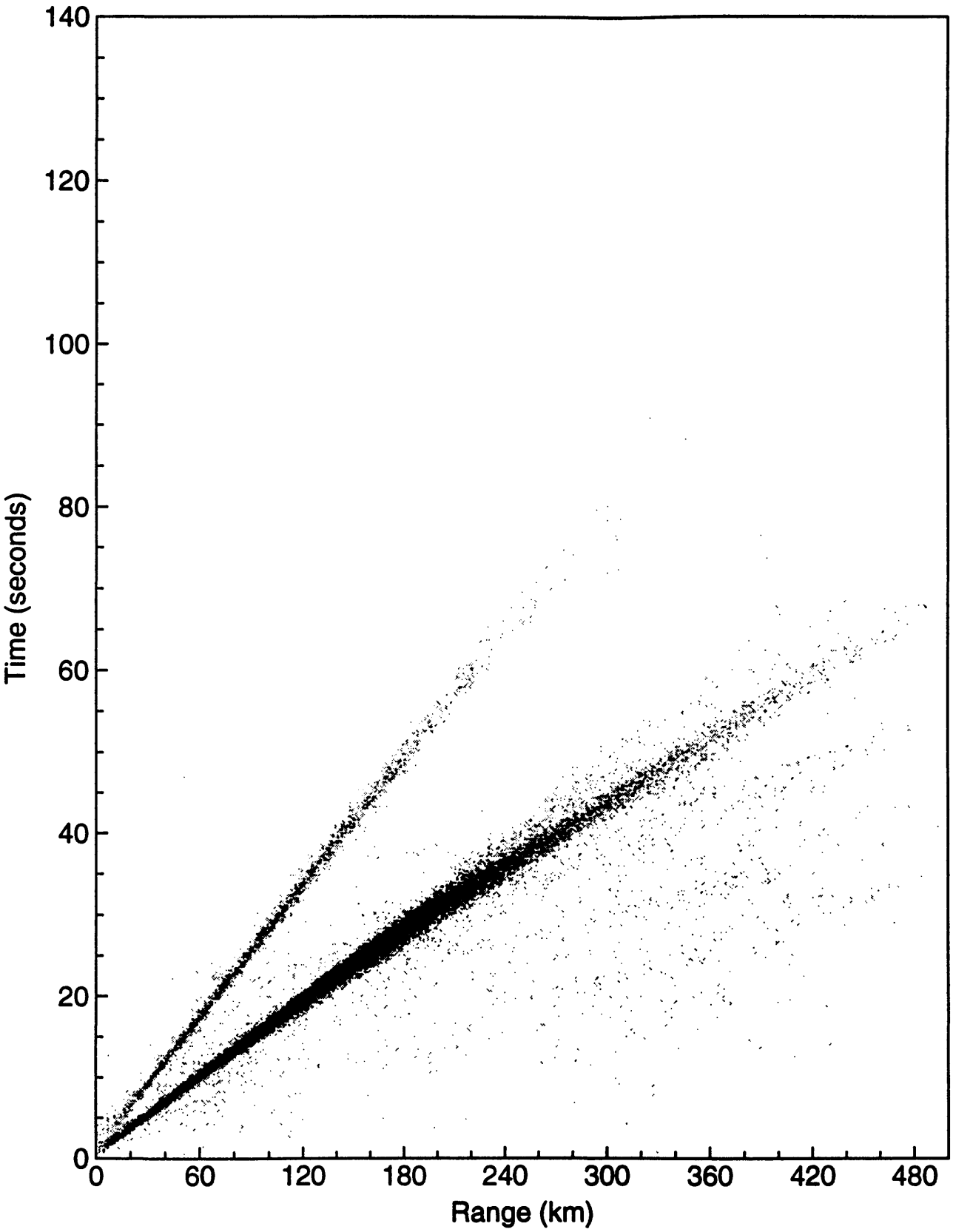

Figure 2. A time versus range plot of 31,703 picks stored at the SCSNDC for the 872 events shown in Figure 1. All source depths are included.

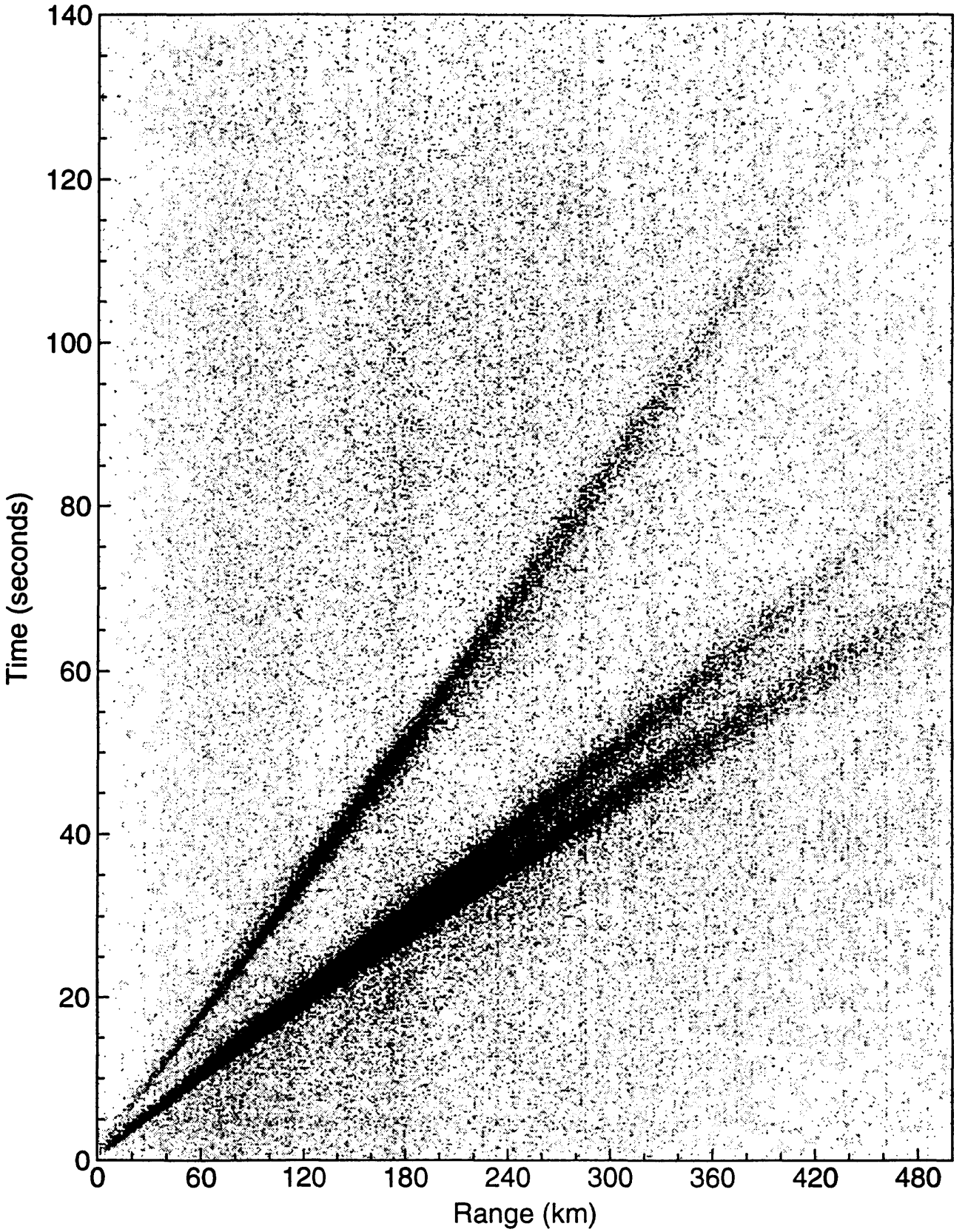

Figure 3. A time versus range plot of 296,747 picks obtained by an automatic picking algorithm applied to records from the 872 events shown in Figure 1. All source depths are included. Note the clearly resolved Pg and Pn branches, and the greater number of picks at ranges beyond about 250 km, compared to the picks in Figure 2.

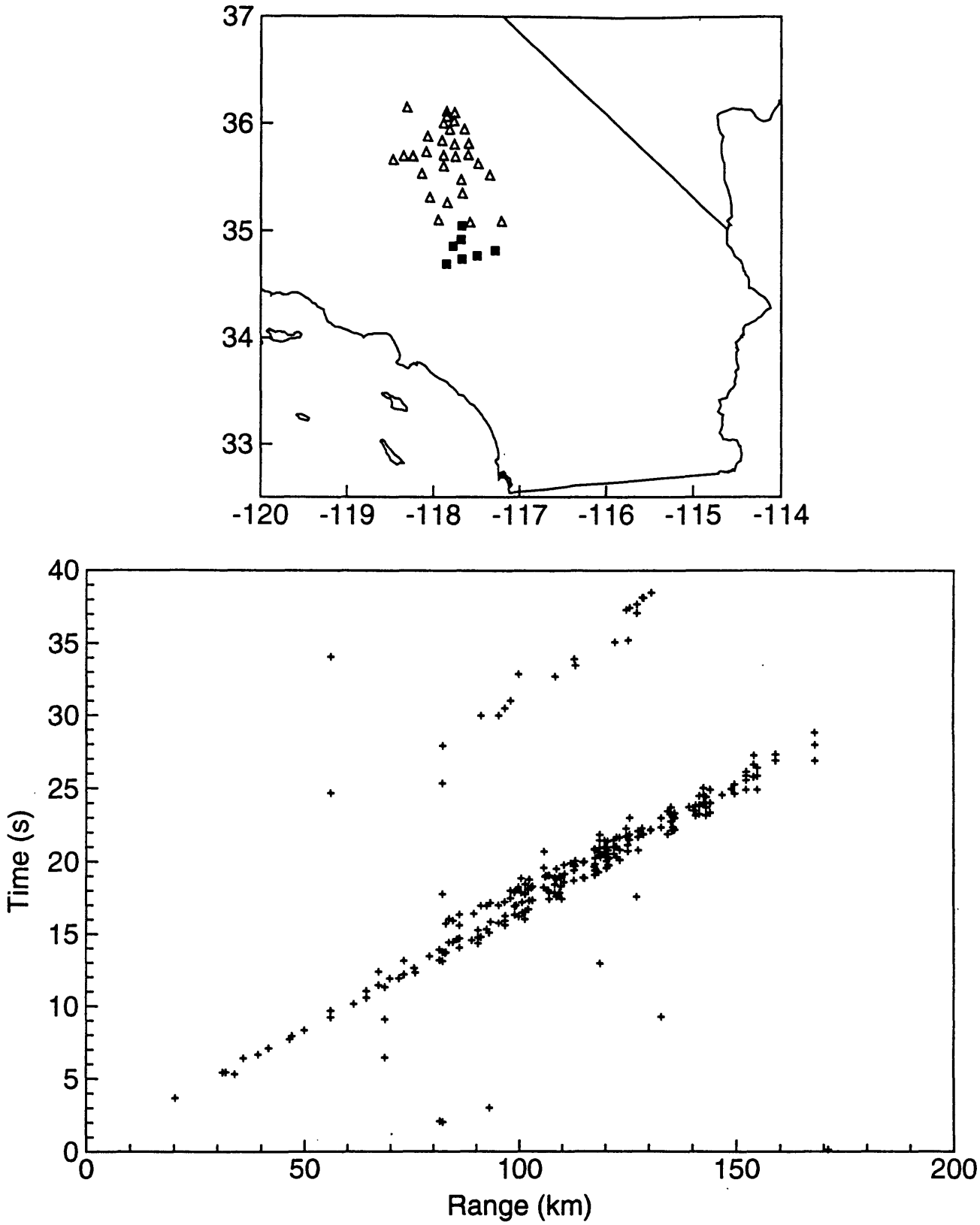

Figure 4. A plot of picks obtained by the automatic picking algorithm for a patch of earthquakes occurring in the Mohave recorded by stations to the north. Note the PmP branch that closely follows P at ranges between 90 and 150 km. The top plot shows the events (solid squares) and stations (triangles).

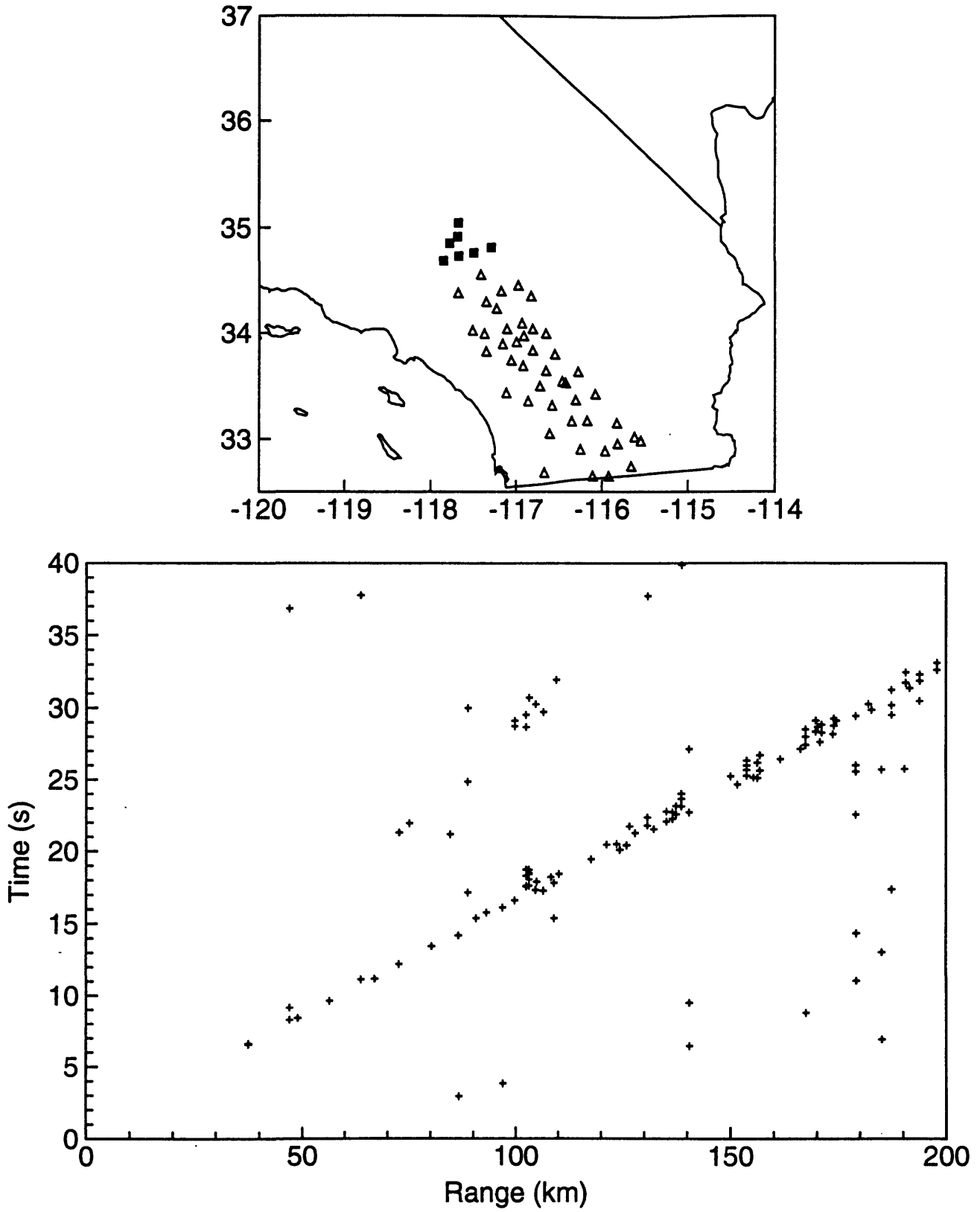

Figure 5. Picks from stations to the southeast of the same patch of earthquakes used in Figure 4. For this source-receiver geometry, PmP cannot be seen.

A LITHO- AND BIOSTRATIGRAPHIC EVALUATION OF THE COSEISMIC SUBSIDENCE AND INTERSEISMIC STRAIN ACCUMULATION IN THE WASHINGTON AND OREGON PART OF THE CASCADIA SUBDUCTION ZONE.

1434-93-G-2317

IAN SHENNAN, JAMES B INNES, MAIREAD RUTHERFORD, FRANCES GREEN, JEREMY LLOYD, KEVIN WALKER, YONGQIANG ZONG & ANTONY LONG

University of Durham
Environmental Research Center
Science Laboratories
South Road
Durham DH1 3LE
United Kingdom

INVESTIGATIONS

Project status

This project commenced May 1993, funded initially for one year, and then received support for a second year. During the first year (May 1993-April 1994) work focused on Johns River, Grays Harbor. This is detailed in the Annual Report submitted summer 1994. The aim of the work at Johns River is to establish sound criteria for the objective identification of coseismic subsidence and interseismic strain accumulation. In the second phase Netarts Bay is also studied, where the evidence for coseismic subsidence in some of the peat-mud couplets is equivocal. This will define the criteria upon which the alternative hypotheses (i.e. aseismic production of peat/mud couplets) can be tested. It is essential that the criteria are defined for **both** the seismic and the aseismic production of peat/mud couplets

Project objectives

The objectives of the full 2 year project are threefold:

1. To establish the relative importance of local and regional processes reflected in the stratigraphic sequences at three selected sites in the PNW: Johns River, Oyster Farm and the south marsh at Netarts Bay.

2. To test the validity of models of interseismic crustal movements through an analysis of the nature of palaeoenvironmental vegetation succession and sedimentation at three sites.

3. To specify criteria that can be used to distinguish peat/mud couplets produced by coseismic subsidence from couplets produced by aseismic processes and to test these criteria.

The two research questions addressed by this project are :

1. Do the alternating peat/mud sequences recorded in the Pacific Northwest reflect earthquake-related events?

2. What is the palaeobotanical evidence for interseismic crustal movements?

RESULTS (since May 1994)

Fieldwork - Johns River, Oyster Farm & South Marsh Netarts Bay

The second year's fieldwork program was designed to complement and build upon the results of the first year's research. It firstly comprised the completion of the detailed taxonomic, ecological and topographic levelling study of the zonation of contemporary vegetation communities at Johns River, Washington, which had commenced during the first year of research in 1993 in order to provide modern analogues for the palaeoecological data. Field survey was then extended to new sites at Netarts Bay in northern Oregon, where the taxonomic and altitudinal zonation of the contemporary marsh vegetation communities were recorded, and a detailed coring survey of the lithostratigraphy of the marsh sediments was completed. Pollen, diatom and foraminiferal analyses of contemporary marsh sediment samples from the Netarts Bay sites are in progress.

Lithostratigraphic Survey

A transect of twenty-one cores was completed at South Marsh, Netarts Bay, running from the *Equisetum* and *Carex* dominated vegetation over sand and shallow peat which fringes the sand dune belt to the west, finishing in the reedswamp and swamp carr communities which fringes the marsh on its landward side. The deeper cores in mid-transect reached depths in excess of four metres and contained a number of buried organic marsh surfaces. These varied in number, but up to six were routinely found. These buried marsh soils (peats) were laterally persistent and draped up the gradient from the centre to the edge of the marsh. Regressive contacts, where peats overlay clastics, were usually gradational. Most of the transgressive contacts where the peats were overlain by clay-silts were abrupt, and in places discrete sand layers capped the peats. Sand layers were also recorded at intervals in the clastic sediments. A few of the transgressive contacts, however, seemed to be more gradational. This stratigraphic survey has served to confirm the general findings of earlier workers at the Netarts Bay site (Darienzo and Peterson 1990). It has also shown that the South Marsh stratigraphy is broadly similar to that from Johns River, and thus comparable. Two full sediment cores were collected from South Marsh, as well as smaller sections of other cores which were of particular interest.

The stratigraphic survey at the third, much smaller site of Oyster Farm has revealed a shallower but similar stratigraphic succession. Rather more of the contacts at Oyster Farm appear to be gradational, although very sharp contacts with capping sand layers are also present. Sediments were collected there by monolith tin from exposed section, supplemented by core samples. Several points along the section were studied to record lateral variability in the sediments.

Contemporary Vegetation

At both Johns River and South Marsh a full taxonomic survey of the modern marsh vegetation has been carried out in order to establish the altitudinal community zonation from low water mark to the transition from high marsh vegetation to the freshwater terrestrial communities beyond. Several marsh vegetation zones have been recognised and these are very similar at both sites, in terms of species composition and altitudinal limits, although significant local variations do occur. In simplified form, they range from exposed unvegetated mudflat, through *Zostera* mudflat, marsh dominated in turn by *Salicornia*, *Carex*, *Triglochin*, Gramineae (e.g. *Distichlis*),

Plantago maritima, *Juncus* and *Potentilla*, and finally to freshwater associations with, for example, *Typha* and *Alnus*. In each zone several characteristic sub-dominant taxa have been recognised. Large numbers of points at the boundaries of these vegetation zones have been levelled relative to national datum (NGVD) to establish their altitudinal variability.

Laboratory Analyses

Contemporary sediments

Samples of surface sediments were collected from within all of the vegetation zones recognised in the vegetation survey at Johns River and South Marsh. These are currently being analysed for pollen, diatom and foraminifera content, as well as for their loss on ignition and particle size characteristics. Thirty contemporary pollen samples from Johns River and twenty-two from South Marsh are nearing completion. These are demonstrating that the pollen assemblages can be related closely to the contemporary vegetation community from which they derive. For example lower marsh surfaces contain abundant Chenopodiaceae (e.g. *Salicornia*) pollen, grasses and *Potentilla* pollen are present in upper marsh sediment, while unvegetated mudflat contains the pollen of better transported, more regional taxa such as *Tsuga* or *Alnus*.

The diatom data are similarly diagnostic, with the salinity profiles of assemblages reflecting closely their position along the altitudinal marsh gradient of the host sample. Polyhalobian forms such as *Cocconeis scutellum* are much more abundant in mudflat samples, whereas upper marsh sediments contain many meso- and oligohalobian forms such as *Achnanthes delicatula* or *Navicula mutica*.

Contemporary samples have been analysed for their foraminiferal content from the Johns River transect. Diagnostic environments have been recognised from the foraminifera relating to the position on the marsh and mudflat transect. For example an assemblage dominated by the species *Trochammina inflata*, but also containing *Trochammina macrescens* and *Haplophragmoides sp.* has been identified from the salt marsh environment. A tidal mudflat assemblage has been identified dominated by *Miliammina fusca*, with minor abundances *of T. inflata* and *T. macrescens*. A lower mudflat/subtidal assemblage was also found characterised by the appearance of *Ammonia beccari var. batavus*, and *Elphidium excavatum*.

Defining the relationship of the contemporary sediments with their contained microflora and fauna has provided a framework for the interpretation of the microfossil assemblages recovered from the sediment cores at the study sites in terms of their palaeoenvironmental meaning, in particular their altitudinal position within the palaeomarsh sequence. This information will be critical in inferring the degree of subsidence experienced during past coseismic events from the biostratigraphic evidence.

Laboratory programme for the rest of the Project (November 1994-April 1995)

Previous work in the area highgrades abrupt and gradual changes, as illustrated by the lithologies and relates these changes to tectonic style and associated sea level fluctuations. The objective of the proposed sampling is to elucidate criteria which may be of use in identification of abrupt v. gradual environmental changes and to relate these as far as possible to sedimentological / tectonic processes. The principal method employed is biostratigraphical.

The proposed work plan through to April 1995 (some of which is already complete and/or underway) is outlined as follows:

Process: Laboratory lithological descriptions of three cores: BH2 (Borehole 2), BH10 (Borehole 10) and OF-1 (Oyster Farm-1).

Status: Completed for Oyster Farm-1. In progress for BH-2 and BH-10. To be completed by Week 50 (mid December).

Process: Sample selection for radiocarbon dating.
Status: To be completed by end Week 2 (mid January)

Process: Biostratigraphical analysis of "300" year old peat from each of three cores. The lower contacts with the peat vary in each of the three boreholes. The analysis is to investigate if the peat deposition may be demonstrated as a synchronous and widespread landward shift in facies and to demonstrate abrupt v. gradual changes within different palaeoenvironments immediately prior to peat deposition.
Status: Samples from OF-1 have already been processed and are currently being analysed. The target deadline for completion of the OF-1 part of this project is Week 52 (end 1994). All samples from BH-2 will be processed by end Week 4, 1995 and for BH-10 by end Week 8, 1995.

Process: To investigate gradual v. abrupt boundaries within the best developed peat successions within BH-2 and BH-10. The objective is to prove the palaeoenvironmental stratigraphy (ie the transition from intertidal mudflat - low salt marsh - high salt marsh), to compare the succession between boreholes, to describe as many differing types of contact as possible.
Status: Processing of samples to be completed by Week 4 (BH-2) and Week 8 (BH-10). Analytical work to be completed by Week 8 (BH-2) and Week 13 (BH-10).

Process: The deepest section sampled is present in BH-2. The basal sand is gradually overlain by a very thin mud which is overlain by a peat, succeeded abruptly by a muddy interval. Sampling is proposed to characterise the nature of this earliest transgressive event.
Status: Processing of samples to be completed by Week 4; Analytical work to be completed by Week 8.

Process: Report production. The data will be integrated, interpreted and written in report format.
Status: To be written and completed from Week 14 - Week 17 (end April 1995).

Publications from the Project to date

Long, A.J. and Shennan, I. (1994). Sea-level changes in Washington and Oregon and the 'earthquake deformation cycle'. *Journal of Coastal Research,* 10(4) 825-838. [offprints not yet received from the publisher]

In preparation (to be submitted in December to *Quaternary Science Reviews*) "A 5000 year record of large earthquakes in Washington, USA" by Ian Shennan, Antony Long, Jim Innes, Yongqiang Zong, Frances Green, Jeremy Lloyd, Mairead Rutherford & Kevin Walker

Conference presentation - Rapid coseismic submergence at Johns river, Washington, presented at the first International Meeting of IGCP 367 "Late Quaternary Coastal Records of Rapid Change", Fort William, Scotland, 13-20 September 1994.

References

Darienzo M.E. and Peterson C.D. 1990 Episodic tectonic subsidence of late Holocene salt marshes, northern Oregon central Cascadia margin. *Tectonics* 9, 1-22.

Low Frequency Data Network

Annual Report - Project Number 9960-12096

S. Silverman
Branch of Earthquake Geology and Geophysics
U. S. Geological Survey
345 Middlefield Road, Mail Stop 977
Menlo Park, California 94025
415/329-4862
silver@thebeach.wr.usgs.gov
Program Element II

Investigations

[1] Real-time monitoring, analysis, and interpretation of strain, creep, magnetic, tilt and other low frequency (sampling rate of every 10 minutes) data within the San Andreas fault system and other areas for the purpose of understanding and anticipating crustal deformation and failure.

[2] Enhancements to satellite-based telemetry system for reliable real-time reporting and archiving of crustal deformation data.

[3] Specialized monitoring, including automated alerts, and display of data relevant to the earthquake program and specific to regions such as the San Francisco Bay area, Mammoth Lakes, and Parkfield.

Results

[1] Data from low frequency instruments in Southern and Central California have been collected and archived using the Low Frequency Data System. During the year measurements from over 100 satellite platforms (most reporting at ten minute intervals) have been received via satellite telemetry and subsequently archived by Low Frequency Network computers for analysis.

[2] The project has operated a configuration of two Sun workstations for use as data archiving, monitoring, and analysis systems. Both workstations receive satellite telemetry in near real-time from a PC-based system which acts as a satellite downlink. Data from the Network are available to investigators in near real-time and software for data display and analysis is available. Tectonic events, such as creep along the fault, can be monitored while still in progress.

[3] The project uses a 1.8 meter satellite receiver dish installed in Menlo Park for retrieval of near real-time surface deformation data from California and South Pacific islands. The GOES geostationary satellite in conjunction with a domestic communications satellite provide the telemetry which makes possible a reliable real-time data collection system. Further expansion of the number of platforms monitored, particularly in the San Francisco Bay area is ongoing.

[4] The project continues to take an active part in the earthquake monitoring activities. Automated alerts for signals which may indicate anomalous tectonic activity notify personnel in near real-time. Data collection and computer operations are automatically monitored for abnormal activity and pages are issued in the event of problems with either.

[5] As part of the Bay Area region study, display facilities have been enhanced to provide improved monitoring and other graphic displays for scientists, the media, and the public. Graphic images of seismicity (updated every 30 minutes) are now available via the Internet (through associated World Wide Web clients). The lobby area has been used extensively by the media for access to data and as a background for interviews, especially after large earthquakes such as the Northridge, January, 1994.

Paleoseismic investigation of the northern Calaveras fault, Alameda and Contra Costa Counties, CA

Award # 1434-93-G-2339

Gary D. Simpson, William R. Lettis
William Lettis & Associates, Inc.
1000 Broadway, Suite 612
Oakland, CA 94607
Tele: (510) 832-3716; FAX: (510) 832-4139; E-mail: wla@netcom.com

Program elements II.3 and II.5

The objective of this study is to develop a paleoseismic site along the northern Calaveras fault where fault slip rate and paleoearthquake timing can be determined. From an initial list of five potential study areas, we conducted preliminary paleoseismic investigations at three sites. These are: the Welch Creek site, in southern Sunol Valley; the Camille Lane site, in Alamo, near the fault's northern termination; and the Vallecitos Ridge site, at the northern end of Sunol Valley.

Of the three sites investigated, the Welch Creek site is by far the most favorable, and thus was studied most extensively. The Camille Lane and Vallecitos Ridge sites were less productive. No fault was encountered at the Camille Lane site in mid- to late-Holocene alluvial fan sediments that cross the projection of the principal geomorphic escarpment north of San Ramon. The lack of faulting at this site supports the interpretation that the northern Calveras fault dies out north of Danville. At Vallecitos Ridge, a Holocene trace of the fault was located, but massive graben-fill sediments were unfavorable for paleoseismic interpretations.

At the Welch Creek site, near the confluence of Alameda and Welch Creeks, the northern Calaveras fault crosses a pair of fluvial terraces and the intervening back-edge. To date, we have excavated four trenches at the site. Two fault-normal trenches were dug to define the location and character of the fault and to assess the preservation of event stratigraphy. Two fault-parallel trenches were excavated, one on either side of the fault, to determine the location and geometry of the terrace back-edge. Results from the Welch Creek site indicate that the northern Calaveras fault has a late Holocene slip rate of between 2 ± 1 mm/yr and 6 ± 1 mm/yr. The range in slip rate values accounts for the uncertainty associated with the lack of age control we have at this time. The slip rate values are based on the offset of the terrace back-edge, whose age we estimate at 5 to 13 ka. Because the maximum age of the back-edge is probably overly conservative, we conclude that the preliminary slip rate is probably more closely approximated by the larger slip rate of 6 ± 1 mm/yr.

At least five, and perhaps as many as seven, paleoearthquakes are recorded at the Welch Creek site. These events are recorded by tilting of the terrace abrasion surface, upward fault terminations, and the presence of colluvial wedges and fissure fills. Timing of individual events, including the most recent event, is unknown at this time.

We are continuing our research of the Welch Creek site in order to address the uncertainties associated with our initial studies. Primarily, we hope to improve age control to constrain the age of the offset terrace back-edge and to date specific event-related deposits. We also hope to constrain the locations of both the fault and terrace back-edge by excavating additional trenches closer to the actual intersection of these features. In addition, we will address the possibility of secondary traces at the site.

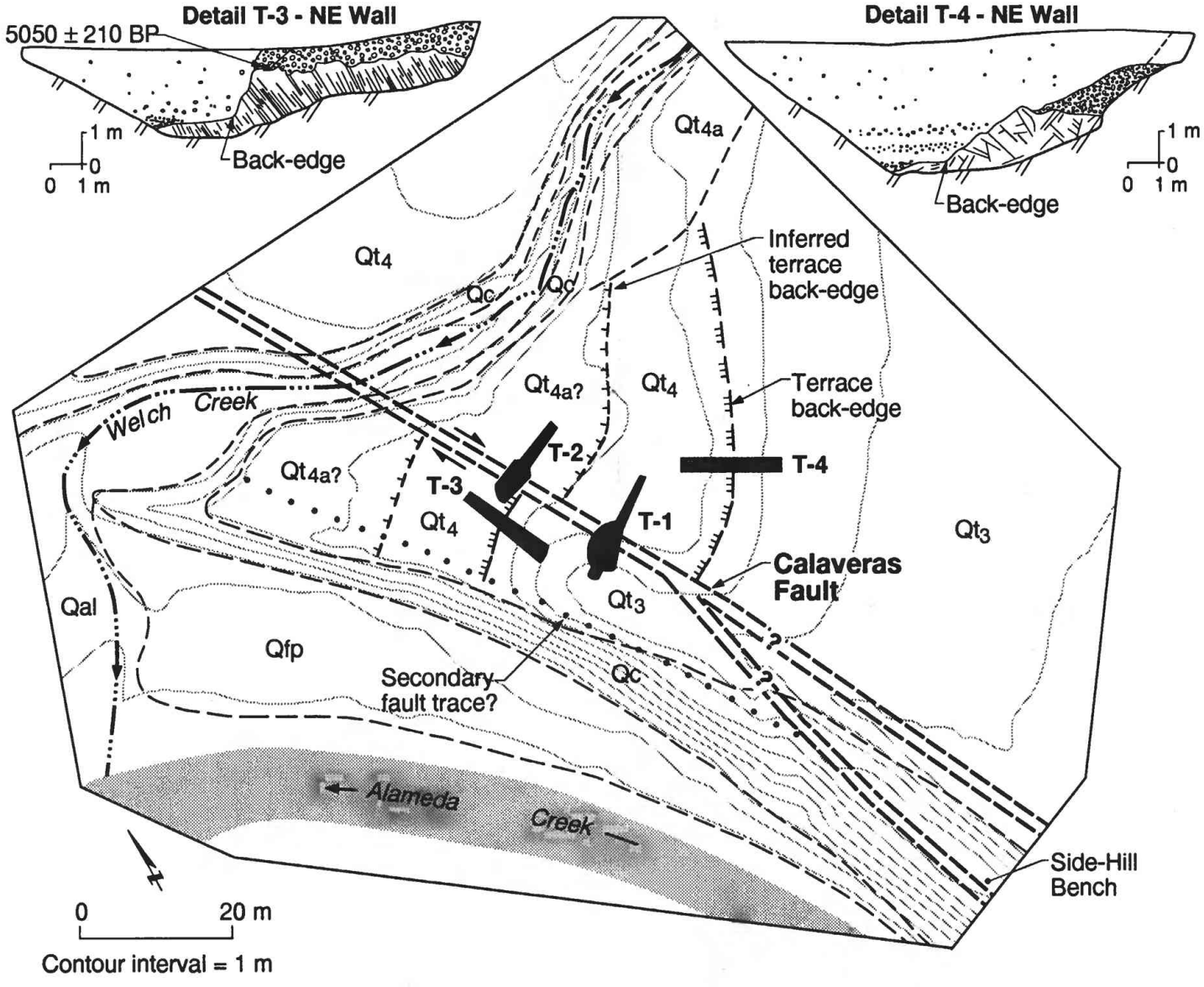

Detailed topographic site map of the Welch Creek paleoseismological study area showing distribution of Quaternary units, location of trenches, and schematic representations of the Calaveras fault and terrace back-edge. Note the presence of the inferred back-edge between terraces Qt $_4$ and Qt $_{4a}$.

Seismicity, Ground Motion, and Crustal Deformation Wasatch Front, Utah, and Adjacent Intermountain Seismic Belt

1434-93-G-2348
Element II. Evaluating Earthquake Potential

R.B. Smith, W.J Arabasz, J.C. Pechmann, and C.M. Meertens*
Department of Geology and Geophysics
University of Utah
Salt Lake City, Utah 84112-1183
801-581-6274 (Tel.); 801-585-5585 (FAX); gg-rbs@mines.utah.edu

Investigations: October 1, 1993 - November 30, 1994

1. GPS surveys of the Wasatch fault zone.
2. Aftershock temporal behavior in the Utah region.
3. Refined analysis of the 1992 M_L 5.8 St. George, Utah, earthquake and its aftershocks.

Results

1. The principal objective of this part of the project is to assess long-term motion across the Wasatch fault zone by surveying benchmarks with the Global Positioning System (GPS), analyzing changes with time, and comparing benchmark locations determined with GPS to those determined from older trilateration and triangulation measurements. The results will be used to model fault induced deformation for the purpose of evaluating the potential for moderate to large earthquakes.

High accuracy GPS surveys were carried out in 1992, 1993, and 1994 across the central, northern, and southern segments of the Wasatch fault, respectively. These surveys occupied a total of 99 benchmarks established as early as the 1940's (Figure 1). To provide ties between the three GPS surveys, 12 of the 1992 sites were reoccupied in 1993 and 22 of the 1992-93 sites were reoccupied in 1994. The 1994 survey included three sites surveyed by the U.S. Geological Survey during their 1992 GPS Basin-Range transect. An additional site was occupied for 3 months in 1994 to maintain continuous tracking during an 88-station HARN (High Accuracy Resolution Network) survey of the state of Utah by the National Geodetic Survey.

The GPS baseline results and variance-covariance files were adjusted using the NGS program DYNAP. The uncertainties in the data ranged from 3 to 5 mm in the horizontal component and 8 to 12 mm for the vertical component. Simultaneous adjustment of the 1992-

*S.J. Hill, L.J. Martinez, and S.J. Nava also contributed significantly to the work reported here.

93 GPS and terrestrial geodetic data indicates NE-SW extension at a rate of 83 ± 15 nanostrain/yr (one sd error bars), corresponding to 6 ± 1 mm/yr over the 70 km-wide network. GPS-GPS results over the 1992-1994 period indicate 78 ± 26 nanostrain/yr or about 5 ± 2 mm/yr of ENE-WSW extension. These rates are comparable to the 4.7 mm/yr of E-W extension measured between eastern Nevada and the U. S. stable interior using Very Long Baseline Interferometry (VLBI) and Satellite Laser Ranging (SLR; Dixon, et al., *Tectonics*, in press). Taken together, the GPS and VLBI/SLR data suggest that the Wasatch fault zone accommodates a major component of eastern Basin and Range extension. Our results provide an important constraint on the strain rate budget controlling earthquakes on the Wasatch fault.

2. We have been systematically studying aftershock temporal behavior and earthquake clustering in the Utah region aimed at (1) having the capability to determine probabilities for strong aftershocks or a larger mainshock when a sizable earthquake occurs (e.g., Reasenberg and Jones, 1989: *Science 243*, 1173-1176) and (2) understanding how space-time variations in aftershock parameters may relate to tectonic processes and stress state. Our modeling to date has been based on the modified Omori relationship $N(t) = K/(t + c)^p$, where N(t) here is the number of events per day at time t after the mainshock, and K, c, and p (designated p* for artificial composite clusters time-shifted to a common mainshock time) are constants. Using aftershock sequences for 11 mainshocks of $4.5 \leq M \leq 6.0$ in the Utah region between 1974 and 1992, we successfully developed a provisional "generic Utah" aftershock model, keyed to the mainshock-independent rate of earthquake production for aftershocks of $M \geq M_m - 3.0$ (Figure 2). Our model parameters, for comparison to those of Reasenberg and Jones for the "generic California" model, are: $a = -2.31$; $b = 0.87$; $p = 0.75$; and $c = 0.02$. Compared to the "generic California" model, the Utah aftershock sequences, on average, decay more slowly and are less "productive" by a factor of 4 to 5 in terms of aftershock rates after 1 day and the cumulative number of aftershocks during the first 30 days. Aftershocks of the 1983 Borah Peak, Idaho, earthquake (M_s 7.3) more closely followed the Utah model. Spatial variations of p and p* in Utah show a tendency for positive regional correlation with surface heat flow, as found by others in southern California.

3. An M_L 5.8 earthquake occurred in SW Utah on September 2, 1992, 8 ± 2 km ESE of the city of St. George. The shock was the largest in the Utah region since 1975 and the largest in the St. George area since 1902. The earthquake caused surprisingly little damage to St. George (population ~28,500) and other nearby communities, although it triggered a massive, destructive landslide 45 km away. No surface faulting was observed. Using the focal depth of 15 ± 2 km determined by others from analysis of teleseismic waveforms, we computed an epicenter of 37° 4.8′ N, 113° 29.2′ W. Our focal mechanism for this earthquake indicates normal slip on a N-striking fault dipping 46° ± 5° E or 46° ± 6° W.

The main shock had no foreshocks ($M_c \geq 2.0$) and remarkably few aftershocks for an event of this size. Only two aftershocks of $M_c \geq 2.0$ occurred, the largest of which was an M_c 2.7 event 8 days after the main shock. To supplement the sparse station coverage provided by regional seismic networks in this area (nearest station 60 km), the University of Utah operated portable seismographs—including 5 telemetered stations and one 3-component digital station—for 6 months following the main shock. Hypocenters of 40 microaftershocks, constrained by

data from the portable seismographs, define a 20-km-long zone extending from 4 to 18 km depth which shallows to the east of the main shock focus. This aftershock distribution implies that the W-dipping nodal plane of the focal mechanism is probably the slip plane. The surface projection of this W-dipping plane lies close to the surface trace of the Hurricane fault—a major W-dipping normal fault with a late-Quaternary slip rate of 0.30 to 0.47 mm/yr which lies along the western margin of the Colorado Plateau. Our data suggest, but do not prove, that the St. George earthquake resulted from buried slip on the Hurricane fault.

On-scale P waves recorded at a distance of 60 km suggest that the main shock rupture was simple and had a length of 0.8 to 5.5 km—much smaller than the length or width of the aftershock zone. Stress drop estimates are poorly constrained but range from moderate to high, with a minimum value of 25 bars. Neither the stress drop of the main shock nor the radiation pattern predicted from our location and mechanism provide any simple explanation for the relatively light damage in the city of St. George.

Reports and Publications

Arabasz, W.J. (1994). Fundamentals of the Wasatch Front's earthquake threat, in *Wasatch Front Seismic Risk Regional Seminar, Seminar 1: Economic Impacts of a Large Earthquake, EERI Regional Seminar Series,* 1-1 - 1-25.

Arabasz, W.J. (1994). Wasatch Front seismicity and expectable strong ground motion, in *Wasatch Front Seismic Risk Regional Seminar, Seminar 2: Earthquake Research and Mitigation, EERI Regional Seminar Series,* 2-1 - 2-40.

Arabasz, W.J. and S.J. Hill (1994). Aftershock temporal behavior and earthquake clustering in the Utah region, *Seism. Res. Lett.* **65,** 32.

Byrd, J.O.D., R.B. Smith, and J.W. Geissman (1994). The Teton fault, Wyoming: Topographic signature, neotectonics, and mechanisms of deformation, *J. Geophys. Res.* **99,** 20,095-20,122.

Martinez, L.J., C.M. Meertens, and R.B. Smith (1994). GPS surveys of the Wasatch fault zone, Utah, *EOS, Trans. Am. Geophys. Union* **75,** *No. 44 (Supplement),* 179.

Nava, S.J., W.J. Arabasz, and J.C. Pechmann (1994). The M 5.9 Draney Peak, Idaho (Idaho-Wyoming border), earthquake of February 3, 1994—a preliminary report, *Program for Northridge Abstracts, the 89th Annual Meeting of the Seismological Society of America.*

Olsen, K.B., J.C. Pechmann, and G.T. Schuster (1994). Simulation of 3-D elastic wave propagation in the Salt Lake Basin, submitted to *Bull. Seism. Soc. Am.*

Pechmann, J.C., W.J. Arabasz, and S.J. Nava (1994). Refined analysis of the 1992 M_L 5.8 St. George, Utah, earthquake and its aftershocks, *Seism. Res. Lett.* **65,** 32.

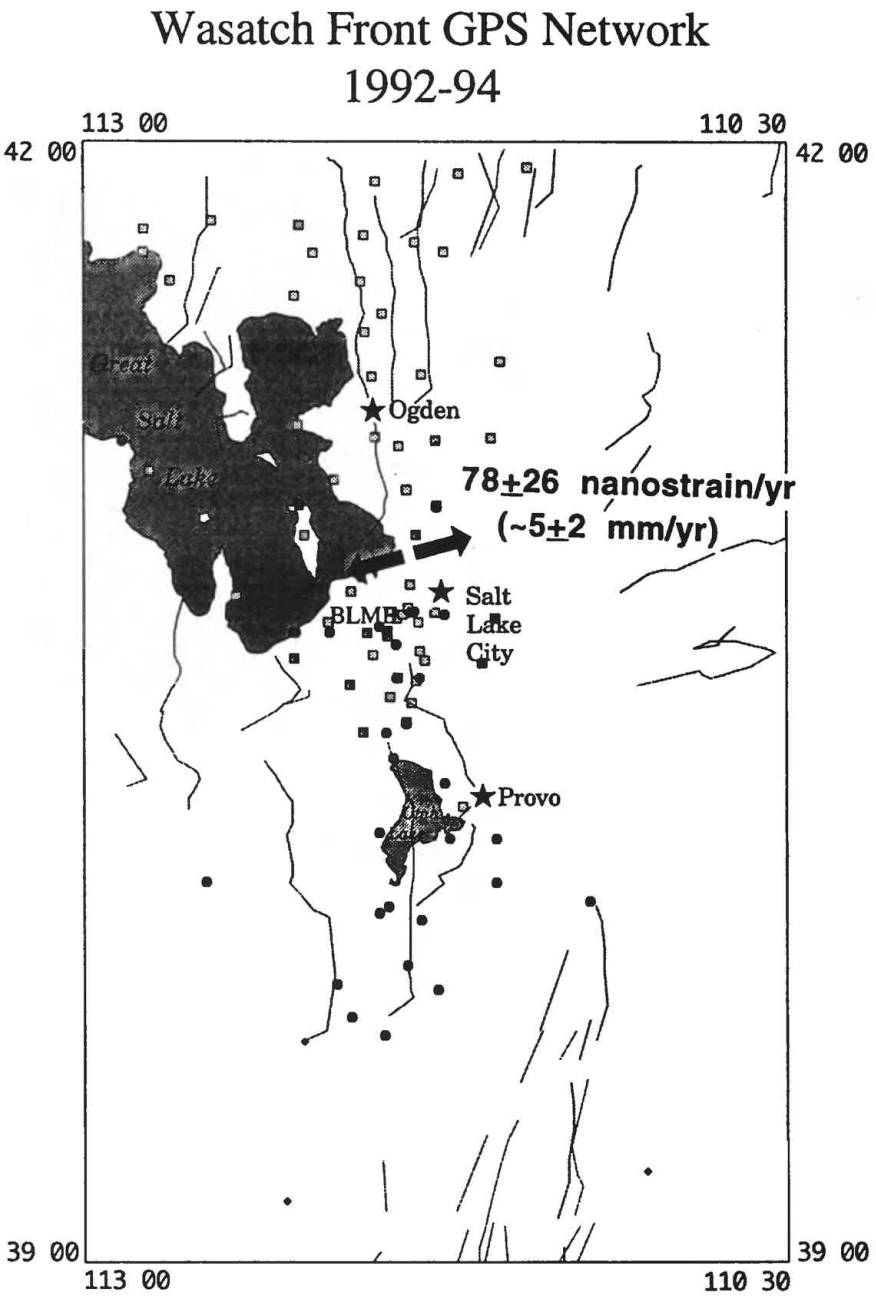

Figure 1. Map of the Wasatch Front, Utah, showing GPS stations and crustal deformation rates. 1992/93 GPS survey = light squares, 1994 GPS stations = medium circles, base station = dark square, USGS Basin-Range GPS profile/1994 GPS stations = dark diamonds. The solid arrow is the measured deformation rate (strain/yr) determined from Dynap processing using 1992-94 GPS-GPS intercomparisons.

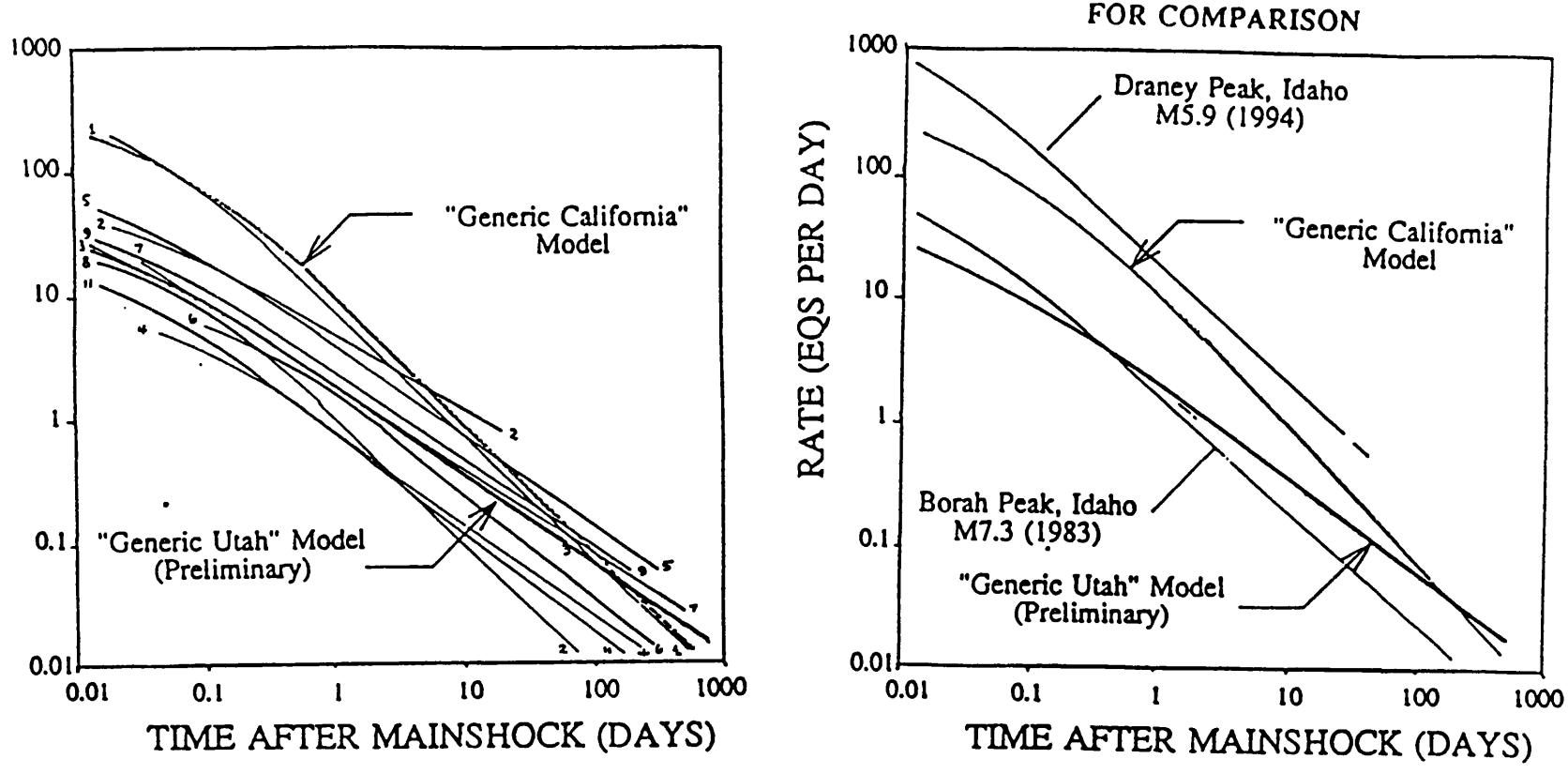

Figure 2. Rate decay and relative productivity of aftershock sequences in the Utah region, normalized to a cutoff magnitude 3.0 units below the mainshock (from Arabasz and Hill, 1994). Left side shows the model fits for a modified Omori rate-decay function for aftershock sequences associated with mainshocks of $4.5 \leq M_L \leq 6.0$ in the Utah region, 1975–1992. A median curve labeled "Generic Utah" model is compared to a similarly derived "Generic California" model of Reasenberg and Jones (1989). On average, the Utah aftershock sequences decay more slowly than the California model and are less "productive" by a factor of 4 to 5 in terms of aftershock rates after 1 day and the cumulative number of aftershocks during the first 30 days. The right side shows model fits for the 1983 Borah Peak and 1994 Draney Peak earthquake sequences compared to the California and Utah models.

SLIP RATE, RECURRENCE INTERVAL, AND BEHAVIOR OF THE CONCORD FAULT AT GALINDO CREEK, CALIFORNIA

1434-94-G-2483

ELEMENT II

David L. Snyder
Rogers/Pacific, Inc.
396 Civic Drive, Pleasant Hill, CA 94523
510-682-7601; Fax 510-682-7605
and
Glenn Borchardt
Soil Tectonics, P.O. Box 5335, Berkeley, CA 94705
510-654-1619; Fax 510-654-4551

Components II.3: "Determine the nature and rates of crustal deformation," and II.5: "Identify active faults, define their geometry, and determine the characteristics and dates of past earthquakes".

Investigations undertaken

This project is a cooperative effort with Christopher J. Wills of the California Division of Mines and Geology. The Concord fault, a right-lateral strand of the San Andreas fault system in the San Francisco Bay Area, is well expressed through the center of the City of Concord by scarps, small hills, a sag pond and a groundwater barrier (Figure 1). A 3-mm/yr creep rate has been measured by Galehouse. This study, north of Galindo Creek, provided the first trenches excavated with the intention of determining the slip rate and recurrence interval of the fault. We chose this site because 1939 air photos show that Galindo Creek crosses the fault at a high angle and had a sharp, right-lateral offset of approximately 20 meters before it was replaced with a concrete-lined channel in 1984. The natural channel is incised into Pliocene bedrock on the northeast and young alluvium is present on the southwest. We focused our investigation on locating older offset channels of Galindo Creek downstream of the fault.

Results

In June 1994, we excavated seven trenches north of Galindo Creek (Figure 2). Three of the trenches crossed the fault approximately perpendicularly and four were approximately parallel to it. The parallel trenches were used to determine the stratigraphic sequence, optain samples for C-14 dating, and to locate and define previous off-set alluvial channels. An off-set stream channel was found approximately 70 meters northwest of the current Galindo Creek channel. Charcoal was collected from the channel and the dates derived from eight C-14 tests indicate that the sediments in the upper 3/4 of the deposit were between 6.92 and 5.66 ka. The maximum slip rate is 13.0 $\pm$ 0.7 mm/yr (90 m/6.92 ky). Because there is a probable bend or "dogleg" in the channel, a much lower slip rate is most probable. The minimum slip rate is 3.8 $\pm$ 0.9 mm/yr (21.5 m/5.66 ky), because the modern channel contains a 21.5 $\pm$ 0.5 meter offset. If no other channel fills lie between the buried and the modern channel, then the youngest charcoal (5.66 ka.) in the buried channel is the maximum age of the offset on the modern channel. Because additional channel fills may be present, further investigation will be necessary. The southwest side of the fault is subsiding relative to the northeast. The vertical slip rate is 0.38 $\pm$ 0.08 mm/yr (2.6 m/6.92 ky.).

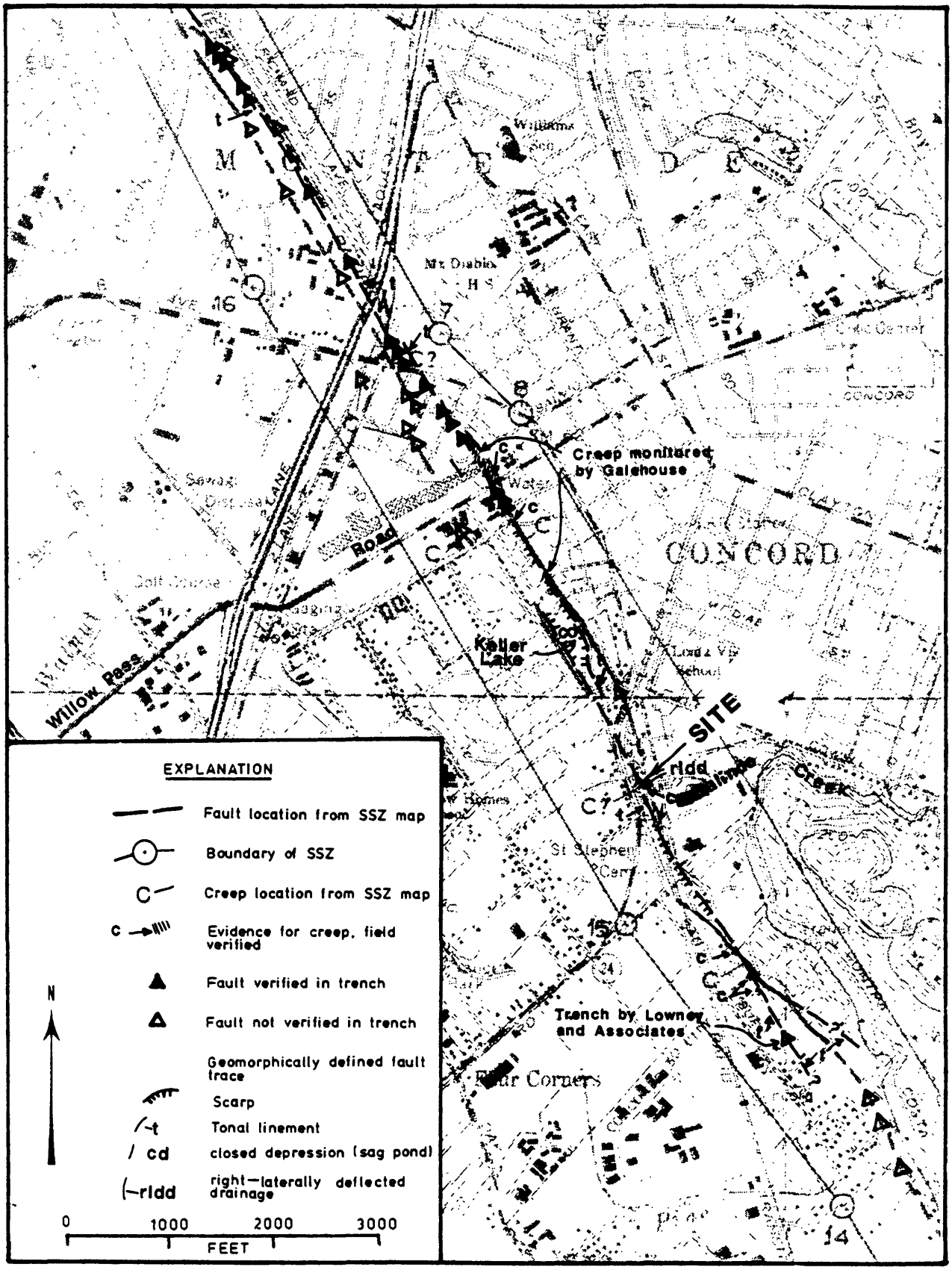

Figure 1. Traces of the Concord fault in central Concord showing Earthquake Fault Zones, creep localitites, localitites where the fault has been located in trenches, or where trenches across a mapped trace have failed to verify a fault, and geomorphic evidence for recently active fault traces.

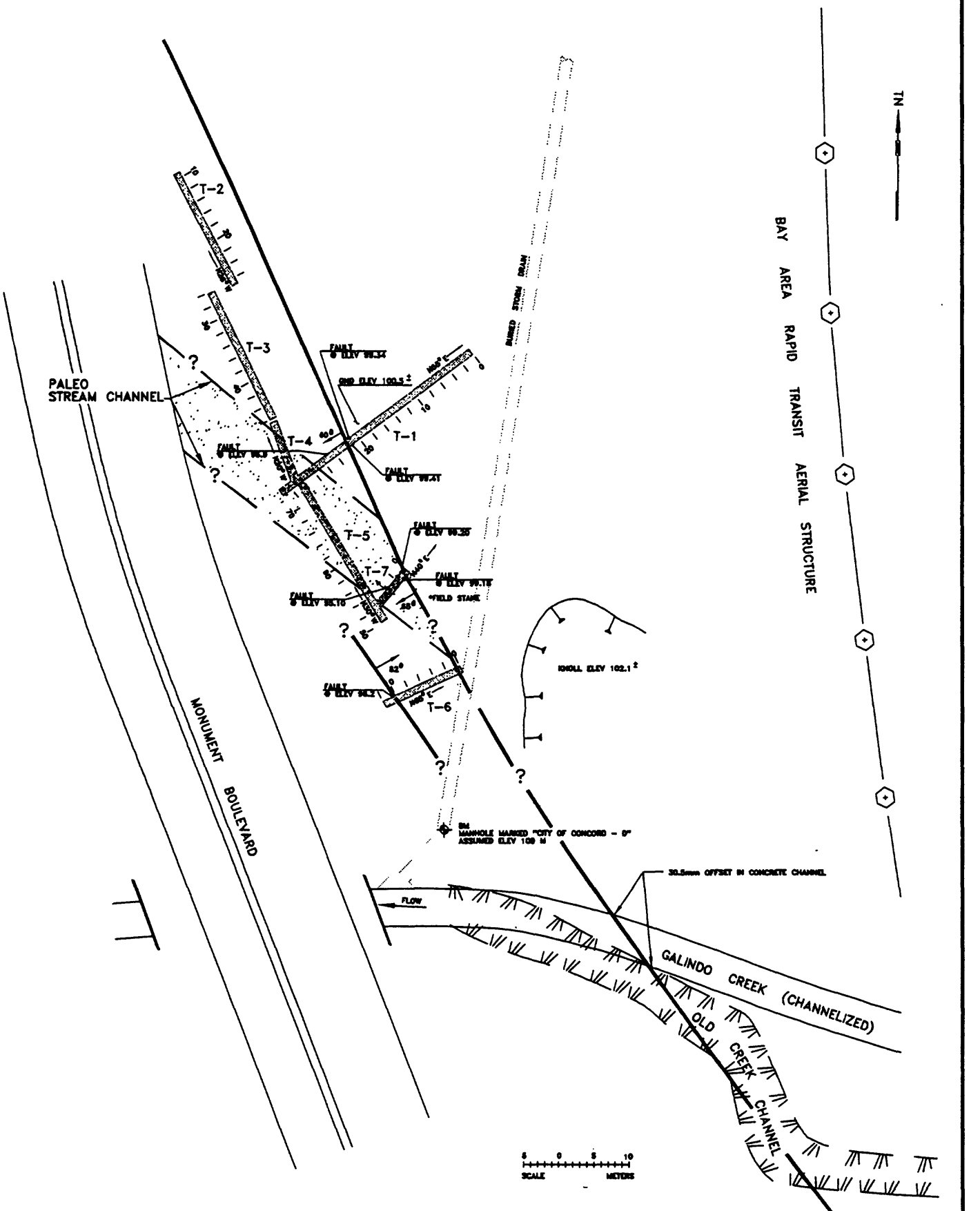

ROGERS/PACIFIC

GEOLOGICAL AND GEOTECHNICAL ENGINEERING

TRENCH LOCATION MAP

CONCORD FAULT SITE

USGS GRANT NO.: 1434-94-G-2483 | FIGURE: 2

CAD FILE: CONCORDS. DWG

The cross fault trenches were used to locate the fault and to research for evidence of recurring earthquakes. These fault-crossing trenches encountered Plio-Pleistocene siltstone bedrock in fault contact with Holocene age alluvium. In addition, in two of the trenches, T-1 and T-7, features that resemble "soil tongues" or fissure fills were encountered. These features were observed at the fault, dipping steeply and widening upward. While their linear extent along the fault may be over 30 meters, the infilling materials vary in grain size in as little distance as one meter. The youngest of these features has sides dipping 50 and 65° southwest, tapers to a point at the 2-m depth, and contains gravelly alluvium similar to but coarser than the material near the current ground surface. Other soil tongues, several of which also widen upwards, underlie the first. If these are true fissure fills, they would represent the first evidence for ground-rupturing earthquakes on the Concord fault. The largest event recorded on the fault was a M5.4 (October of 1955); larger earthquakes will occur.

Reports Published in FY 94

Snyder, David L., Borchardt, Glenn, and Wills, Christopher. J., 1994, Initial paleoseismic study of the Concord fault, California [abs.], EOS, Transactions of the American Geophysical Union, v.75, no. 44, p. 684.

Wills, Christopher. J., Snyder, David L., and Borchardt, Glenn, 1994, Preliminary results of paleoseismic studies of the Concord fault at Galindo Creek, Concord, California [abs.], in Prentice, C.S., Schwartz, D.P., and Yeats, R.S., eds., Proceedings of the Workshop on Paleoseismology: U.S. Geological Survey Open File Report 94-568, p. 200-201.

TECTONIC GEOMORPHOLOGY OF THE MISSISSIPPI VALLEY (OSCEOLA, ARKANSAS TO FRIARS POINT, MISSISSIPPI)

Award No. 1434-94-G-2409
Program Element II.1, II.5

William J. Spitz and Stanley A. Schumm

Resource Consultants & Engineers
A Division of Ayres Associates
3665 John F. Kennedy Parkway
Building 2, Suite 300
P.O. Box 270460
Fort Collins, Colorado 80527
(303) 223-5556

INVESTIGATIONS:

The primary objectives of this investigation are:

1. to identify anomalous reaches of the Mississippi River between Osceola, Arkansas (RM 787) and Friars Point, Mississippi (RM 651), by comparison of river pattern, dimensions, gradient, bed profiles, and water-surface profiles through time,

2. to identify anomalous drainage network patterns on the alluvial plain of the Mississippi Embayment,

3. to identify anomalies along profiles of channels on the alluvial plain,

4. to relate anomalous reaches of the Mississippi River, alluvial plain channels and drainage networks to either known geologic structures, previously unidentified geologic structures, or other factors, and

5. to determine if structural controls have influenced the topography of areas such as Crowleys Ridge, Marianna Gap and escarpment and the Big Creek escarpment.

This investigation deals with those areas encompassed by and in close proximity to the southwestern end of the New Madrid Seismic Zone and includes portions of the Mississippi River and its meanderbelt, the southern parts of the St. Francis Basin, Crowleys Ridge, the Western Lowlands, and the Eastern Lowlands (Figure 1).

RESULTS:

The methods of geomorphic analysis used in this study consist primarily of existing-data compilation and a search for trends and anomalies on topographic, geologic, and soils maps. Plan and profile data for tributary streams, Crowleys Ridge, and valley cross-section data were obtained from USGS 15-minute series topographic maps. Detailed hydrographic survey data for the Mississippi River were used to determine planimetric and cross-sectional

changes between river reaches and through time. Bed-sediment data were used to detect changes of bed material over time and along the course of the Mississippi River. Borehole data were used to determine the variability of bank and floodplain sediments along the river and the occurrence and variability of Tertiary sediments along the river as well as within the valley floor.

Channel profiles for the St. Francis and Little Rivers show a convexity that is coincident with the northwest striking Bolivar-Mansfield Tectonic Zone (BMTZ) and the Blytheville Arch (Figure 1). The amount of apparent deformation is similar to that for the formation of the St. Francis Sunklands (2-3 m) (Guccione and others, 1994). The BMTZ also marks the southwestward shift of older Mississippi River meanderbelt deposits away from the eastern bluff line near Osceola and abrupt course changes and downvalley flattening of channel profiles for the Black and Cache Rivers and Village Creek.

Anomalous geomorphic patterns associated with the northwest trending White River fault zone (WRFZ, Figure 1) (Fisk, 1944) include nearly identical left-lateral salients in the eastern and western bluff lines, the breach and left-lateral offset at the southern end of Crowleys Ridge, and abrupt course changes, anomalous channel patterns, channel profile convexities, and profile steepening of Western Lowland streams within and along the margins of the WRFZ. The WRFZ also appears to have had an effect on development of the Newport Pluton and overlying secondary intrusions and a pluton near the town of Goodwin. These intrusives also appear to have affected the streams that cross them. Steeper valley gradients and an apparent topographic boundary are also associated with the WRFZ.

The Big Creek fault zone (BCFZ, Figure 1) is responsible for vertical offset in upper Tertiary sediments, high escarpments, hummocky topography, disrupted and reversed drainage, and northward sloping topography along the Big Creek and Marianna escarpments (Fisk, 1944; Krinitzsky, 1950). Narrowing and steepening of the valley floor east of Crowleys Ridge and the southern termination of the ridge are attributed to the BCFZ.

Reaches 9, 11, 12, and 13 of the Mississippi River (Figure 1) show anomalous characteristics that are attributed to geologic and tectonic controls. Two small inferred faults and the southeastern margin of the Reelfoot Rift appear to affect the morphology of Reach 9. Deformation along the BCFZ and associated inferred faults appear to control the characteristics of the Mississippi River in Reaches 11 and 12. The intersection of the BCFZ and the WRFZ is controlling the behavior of the downstream end of the St. Francis River and Reach 13 of the Mississippi River.

Valley cross sections were analyzed for anomalous patterns. The westward progression of youthfull terraces and the position of the Black and White Rivers (Figure 1) suggest westward tilting of the Western Lowlands. The position of the Mississippi River between Osceola and Memphis (Figure 1) combined with releveling data and meander migration analyses suggest eastward tilting of the Eastern Lowlands. However, the course of the Mississippi River follows the axis of the Mississippi embayment within the study area, which suggests that subsidence along the embayment axis may be controlling the course of the river as well.

An analysis of the morphologic characteristics and drainage patterns of Crowleys Ridge suggest that the ridge may be fault-bounded along its entire length and cross-cut by several suspected faults. The analyses also indicate that the ridge may be composed of 5 or more structural blocks, some of which show apparent tilting.

We conclude, based on our detailed geomorphic analysis of the valley floor within the Mississippi Embayment, that faulting and deformation may be more extensive than previously thought. The lack of seismicity in the study area does not preclude the existence of tectonism. The large number of coincident geomorphic anomalies along Quaternary and Tertiary features suggest that faulting and deformation may be ongoing and aseismic.

Comparative historical channel banklines and centerlines have been digitized into AutoCADD format and will be submitted to the USGS with the Final Report.

REFERENCES CITED:

Cox, R.T., 1988, Evidence of late Cenozoic activity along the Bolivar-Mansfield tectonic zone, Midcontinent, USA: The Compass, v. 65, p. 207-213.

Guccione, M.J., Miller, J.Q., and VanArsdale, R.B., 1994, Amount and timing of deformation near the St. Francis "Sunklands," Northeastern Arkansas: Geological Society of America Abstracts with Programs, v. 26, no. 1, p. 7.

Fisk, H.N., 1944, Geological investigation of the alluvial valley of the lower Mississippi River: Mississippi River Commission, Vicksburg, 78 p.

Hildenbrand, T.G., Kane, M.F., and Hendricks, J.D., 1982, Magnetic basement in the upper Mississippi Embayment region - a preliminary report; in McKeown, F.A. and Pakiser, L.C. (eds.) Investigation of the New Madrid, Missouri Earthquake Region: U.S. Geological Survey Prof. Paper 1236.

Howe, J.R. and Thompson, T.L., 1984, Tectonic sedimentation and hydrocarbon potential of the Reelfoot Rift: Oil and Gas Journal, v. 82, p. 179-190.

Krinitzsky, E.L., 1950, Geological investigation of faulting in the lower Mississippi Valley: U.S. Army Corps of Engineers Waterways Experiment Station, Tech. Memo. No. 3-311, 50 p.

Schumm, S.A., Rutherford, I., and Brooks, J., 1994, Pre-cutoff morphology of the lower Mississippi River: in Schumm, S.A. and Winkley, B.R. (eds.) The Variability of Large Alluvial Rivers: American Soc. Civil Engineers Press, New York, p. 13-44.

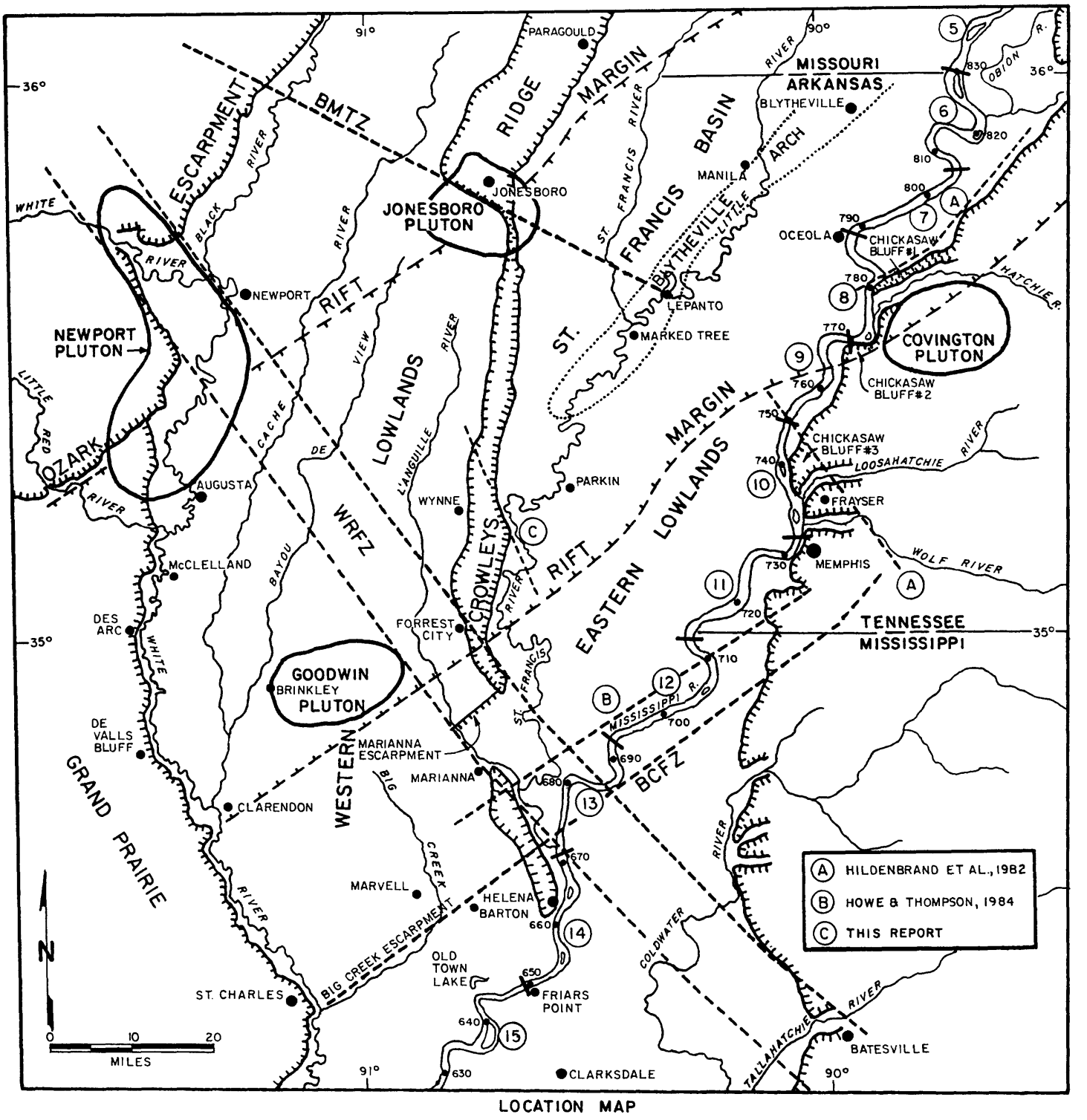

Figure 1. Index map of the alluvial valley of the Mississippi River and major structural features between Blytheville, Arkansas, and Clarksdale, Mississippi. Circled numbers indicate Mississippi River reaches delineated by Schumm and others (1994). Circled letters represent inferred faults within the study area (A: Hildenbrand and others, 1982; B: Howe and Thompson, 1984; C: this study). BMTZ = Bolivar-Mansfield Tectonic Zone (Cox, 1988); WRFZ = White River Fault Zone (Fisk, 1944); BCFZ = Big Creek Fault Zone (Fisk, 1944; Krinitzsky, 1950).

Ground Motion Prediction and Inversion in Realistic Earth Structures
9930-12373

Paul Spudich
Branch of Seismology
U.S. Geological Survey
Mail Stop 977
345 Middlefield Road
Menlo Park, CA 94025

(415) 329-5654 (voice), (415) 329-5163 (fax), spudich@samoa.wr.usgs.gov

Program Element II.5

Investigations Undertaken

The main goal of this project has been to examine the existing seismograms from the 1934 and 1966 Parkfield earthquakes in order to determine how similar the events actually were. Although Bakun and coworkers (1979, 1984, 1985) have already analyzed some of this data, there are several reasons why it is currently opportune to reexamine this data set. First, Mueller (1984) introduced the idea of deconvolution of empirical Green's functions to remove the effects of wave propagation from seismograms so that the source parameters can be retrieved better, i.e. given seismograms from a large and a small shock having similar hypocenters, the small shock seismogram is deconvolved from the large shock. Also, Hartzell (1978) showed that it was possible to simulate a large shock's seismograms by summation of aftershock records. This type of analysis is now available to apply to the 1934 and 1966 main shock records, and it is for this reason that we have retrieved not only the 1934 and 1966 main shock and foreshock records, but also as many other Parkfield-area events as possible. Second, the digitizing process is considerably simplified with the advent of scanners and related software developed at Caltech.

From a scientific standpoint, there are many good reasons to reexamine 1934 and 1966. First, the recent paper by Segall and Du (1993, JGR, 4527) reexamined geodetic data from the 1934 and 1966 shocks and state, " ... the triangulation data allow us to rule out the possibility that the two earthquakes were `carbon copies' as is often stated. The data are unambiguous in that the 1966 event propagated farther to the southeast than did the 1934 event." Despite this assertion, there is still considerable ambiguity in the interpretation of the geodetic data because it cannot distinguish between dynamic slip and quasistatic afterslip, so the geodetic data cannot discriminate between two possible models, called the `complementary' and the `quasi-characteristic' models by Segall and Du. In the former, the 1934 slip distribution is not required to be identical to any part of the 1966 slip distribution, and the geodetic data then suggest that the two events had almost identical moments, but their slip distributions were complementary in space, i.e. 1934 had a lot of slip where 1966 had rather little slip, between Middle Mountain and Gold Hill. In the latter model, the 1934 and 1966 main shocks ruptured dynamically, with identical slip distributions, from Middle Mountain to Gold Hill, and the extra slip in 1966 southeast of Gold Hill occurred as slow afterslip. In this model, the moment of the 1934 event is 60% that of the 1966 event, which may explain why the 1934 event happened only 12 years after the 1922 event. Segall and Du further state, "The only evidence, at this point, that favors the `quasi-characteristic' interpretation is the similarity of the regional wave forms. Since these waveforms have not been modeled in detail, it is, at this point, uncertain what constraint they place on the slip in the two earthquakes."

If this work distinguishes between the complementary and the quasi-characteristic models, then it may either help explain the most problematic feature of the earthquake history at Parkfield, the early occurrence of the 1934 event, or it may clarify one of the fundamental assumptions of the Parkfield prediction experiment, the similarity of earthquakes at Parkfield.

Results of FY94 Activities

This project has collaborated with G.C. Beroza and Martijn Verwoerd of Stanford University to assemble and analyze the available Wood-Anderson (WA) records from the 1934 and 1966 Parkfield main shocks. We have already assembled and photographed the WA records from about 20 Parkfield-area earthquakes, including the 1934 and 1966 main shocks and foreshocks, yielding about 350 separate photographs. These were done for the north and east components of WA stations MHC (Mount Hamilton), TIN (Tinemaha), PAS (Pasadena) and SBC (Santa Barbara) because these stations have the longest continuous historical record. The 1934 and 1966 main shock records and their large foreshock records have been digitized at all stations (where photo quality permits). An example is shown below. A large number of other well-recorded Parkfield area event photos have been scanned and are being digitized by Mr. Verwoerd. Unfortunately, field activities and data analysis caused by the 1994 Northridge earthquake have impeded progress on this project.

Reports Published:

None.

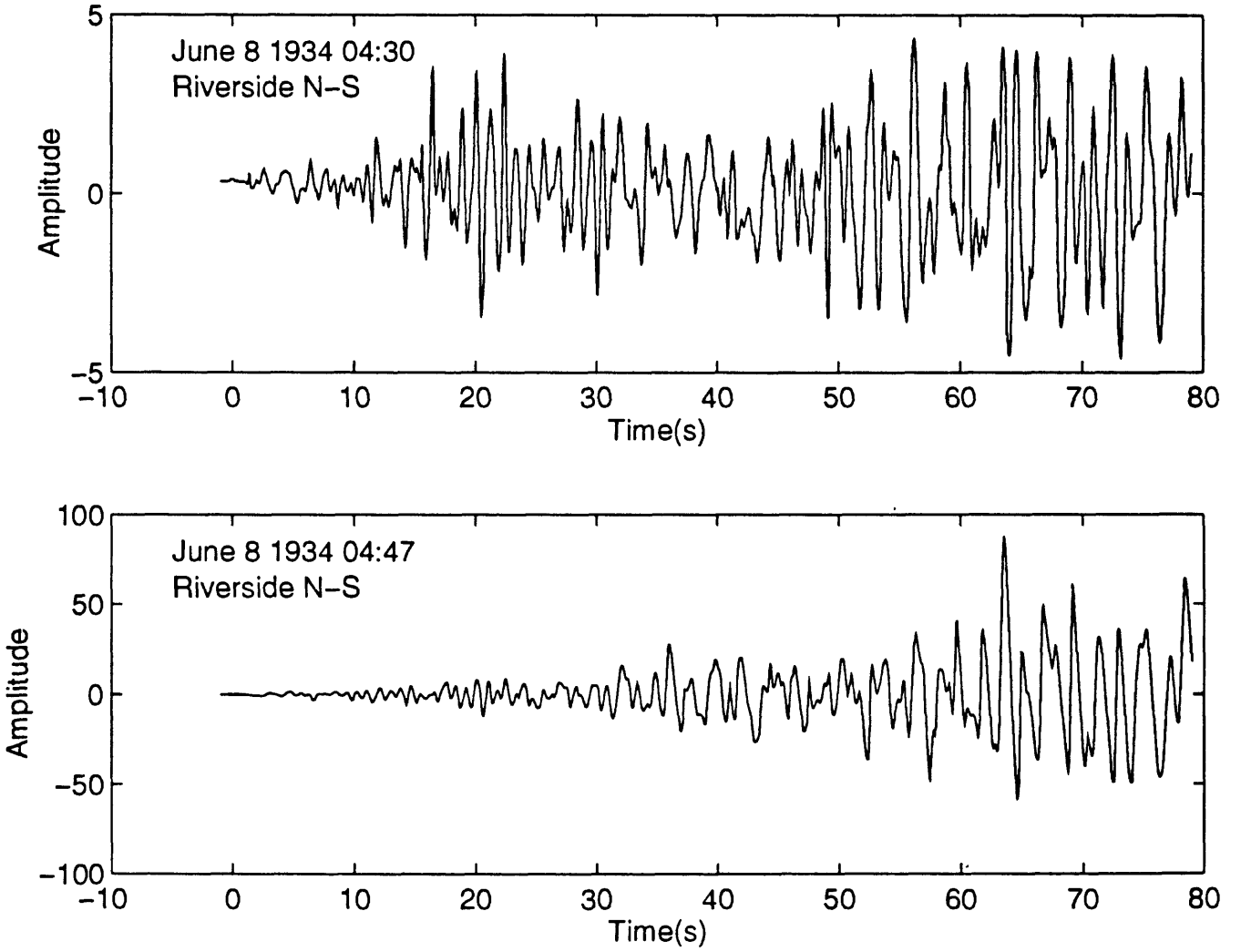

2 Dec 94

Annual Technical Report XXXVI

Modeling and Monitoring Crustal Deformation

9960-10116 Process, Labs, and Theory
9960-11116 Southern California Region
9960-12116 San Francisco Bay Region
9960-13116 Pacific Northwest Region

Ross S. Stein, Wayne Thatcher, Grant A. Marshall, and Kathleen Hodgkinson
Office of Earthquakes, Volcanoes, and Engineering
345 Middlefield Road, MS 977
Menlo Park, California 94025

rstein@isdmnl.wr.usgs.gov

Tel 415 329 4840
Fax 415 329 5163

INVESTIGATIONS

1. We studied how static stress changes accompanying earthquakes can trigger other events, focusing on the Northridge, California, earthquake sequence.

2. We are analyzing the coseismic deformation and stress changes associated with the following large earthquakes: 1952 M=7.3 Kern County (California), 1954 M=6.9 Dixie Valley and M=7.1 Fairview Peak (Nevada), 1971 San Fernando Earthquake (California), and 1992 M=7 Cape Mendocino (California).

3. We have investigated the creation of sea-floor topography at slowly-spreading mid-ocean ridges that is caused by magmatic accretion and surface faulting.

4. We are investigating the thermo-mechanical and seismogenic consequences of ductile shearing and dissipative heating in the sub-seismogenic crust beneath the San Andreas fault system.

RESULTS

Stress Triggering of the 1994 M=6.7 Northridge Earthquake by its Predecessors. The tendency of rocks to fail in a brittle manner is thought to be a function of both shear and confining stresses, commonly formulated as the Coulomb criterion. The Coulomb stress change depends on the geometry and slip of the earthquake, the geometry and sense of slip of the fault or surface of interest, and the effective coefficient of friction. We calculate the Coulomb stress change caused by one earthquake on the rupture surface of a subsequent shock or on a known fault. Such a model of stress transfer implies that earthquakes in 1933 and 1952 increased the Coulomb stress at the site of the 1971 San Fernando earthquake. The 1971 earthquake in turn raised stress and produced aftershocks at the site of the 1987

Whittier Narrows and 1994 Northridge ruptures. The Northridge main shock raised stress in areas where its aftershocks and surface faulting occurred. Together, M≥6 earthquakes near Los Angeles since 1933 have stressed parts of the Oak Ridge, Sierra Madre, Santa Monica Mountains, Elysian Park, and Newport-Inglewood faults by >1 bar. While too small to cause earthquakes, these stress changes can trigger events if the crust is already near failure, or advance future earthquake occurrence if it is not (Stein, G.C.P. King, and J. Lin)

Maps of the Northridge, California, Earthquake Setting, Effects, and Deformation. This set contains three digitally produced 35-mm slides that portray the setting (*slide 1*), effects (*slide 2*), and deformation (*slide 3*) associated with the January 17, 1994, Northridge, California, Earthquake. These slides are intended for both public and professional audiences. The digitally shaded relief was produced from the USGS 1:250,000 scale Digital Elevation Models (DEM) from the Los Angeles East and Los Angeles West quadrangles. Roads are from the USGS Digital Line Graph (DLG) files for the Los Angeles 1:100,000 scale metric quadrangle. Active Faults are from Charles W. Jennings, 1975, Fault Map of California, *California Division of Mines and Geology*. Active Folds are from R. S. Stein and R. S. Yeats, 1989, Hidden Earthquakes, *Scientific American, 260* (6), pp. 48-57. Faults and folds believed to be active during the past million years are depicted (Marshall and Stein).

South End of the Cascadia Megathrust revealed by the 1992 M=7 Cape Mendocino earthquake. We invert geodetic measurements of coseismic surface displacements to determine a dislocation model for the 25 April 1992 **M**=7 Cape Mendocino, California, earthquake. The orientation of the model slip vector, which nearly parallels North America–Juan de Fuca relative plate convergence, and the location and orientation of the model fault relative to the offshore Cascadia megathrust suggest that the 1992 Cape Mendocino earthquake is the first well-recorded event to relieve strain associated with the Cascadia subduction zone. We use data from three geodetic techniques: (1) the horizontal and vertical displacements of 13 monuments surveyed with the Global Positioning System, corrected for observed horizontal secular strain accumulation, (2) section-elevation differences between 29 leveling monuments, and (3) the uplift of 12 coastal sites observed from the die-off of intertidal marine organisms. Maximum observed displacements are 0.4 m of horizontal movement and 1.4 m of uplift along the coast. We use a Monte Carlo approach to estimate an optimal uniform-slip rectangular-fault geometry and its uncertainties. This optimal model resolves 4.9 m of slip on a 14- by 15-km fault that dips 28° SE. The fault extends from 1.5 to 8.7 km in depth and projects to the main-shock hypocenter. The shallowly dipping fault plane is consistent with the observed aftershock locations, and the estimated geodetic moment is 3.1 x 10^{19} N-m, about 70% of the seismic moment. If the 1992 **M**=7 Cape Mendocino earthquake is characteristic for this segment, a comparison of our estimated horizontal-slip vector with plate-convergence rates suggests a recurrence interval of 140 yr, with a 95% confidence range of 100–1000 yr. The coseismic uplift occurred in a region that also has high Quaternary uplift rates determined from marine terrace studies. If repeated ruptures of this southernmost segment of the Cascadia megathrust are responsible for the Quaternary uplift, a comparison of the coseismic uplift with coastal-uplift rates suggests a recurrence interval of 200–270 yr. Thus, comparing horizontal and vertical coseismic deformation to geologic deformation suggests a recurrence interval of 100–300 yr for **M**=7 events at the south end of the Cascadia megathrust (M. Murray, Marshall, and Stein).

Morphology of Slow-spreading Mid-oceanic Ridges Generated by Faulting. Fluctuations in magmatic activity at mid-oceanic ridges perturb the horizontal least principal stress across rift-bounding normal faults, leading to alternating phases of magmatic accretion, which increases valley width, and tectonic extension, which results in the growth of inner rift wall topography. Fine-scale bathymetric surveys and earthquake fault plane solutions show that active normal faults at slow-spreading ridges are moderately-dipping (approximately 45°) planar features throughout the seismogenic oceanic lithosphere. A simple quantitative model that includes flexural deformation of a 10-km-thick elastic plate by slippage on 45° dipping normal faults can match the bathymetric profiles across several slow-spreading ridge segments. Comparison among dip distributions of normal faulting earthquakes at mid-ocean ridges, in the trench-outer rise region, and on continents suggests that most events from these three tectonic environments initiated at dips close to 45°, raising unanswered questions about the mechanical conditions under which the faults originated (Thatcher and Hill).

Thermo-mechanical modelling of ductile deformation beneath the San Andreas fault. We have carried out quantitative 2-D modeling of the bulk flow of a layer of fluid that is driven in a strike-slip sense by constant velocities applied at its boundaries. The fluid has the (linearized) conventional rheology assumed to apply to lower crust/upper mantle rocks, and the temperature-dependence of the effective viscosity of the fluid and the shear heating that accompanies deformation have been incorporated into the calculations, as has thermal conduction in an overlying crustal layer. Two end-member boundary conditions have been considered. In the first, corresponding to a strong upper crust driving a weaker ductile substrate, the ductile layer is deformed by constant velocities applied to its upper horizontal and vertical end bounding surfaces. In the second, the upper horizontal surface is free of horizontal tractions and the fluid layer is driven by constant velocity of its vertical ends, corresponding to a strong ductile layer driving a passive, weak crust. For both boundary conditions, shear heating is concentrated relatively close to the axial plane of the shear zone. The consequence of this concentrated shearing is the development of a narrowly-confined ductile fault zone where earthquake-related displacements will be focused in the post-seismic and inter-seismic intervals of the seismic cycle (W. Thatcher and P. C. England).

Cooperation with Water Resources Division on deformation accompanying geothermal power development in a seismically active site. Long Valley caldera has been the site of unrest in east-central California in the form of seismicity and ground deformation in response to magmatic inflation since 1980. Within this region of uplift, and near the southwestern margin of the resurgent volcanic dome, lies the Casa Diablo geothermal field, under production since 1985 and generating 40 MW of electricity. Analysis of leveling data indicate that the relative subsidence results from reductions in pressure in the shallow production reservoir and reductions in temperature in the underlying reservoir (Marshall).

REPORTS SUBMITTED OR PUBLISHED DURING 1994 (excluding abstracts):

Alpha, T.R., and R.S. Stein, The Northridge, California, Earthquake of January 1994: A computer animation and paper model, *U.S. Geol. Surv. Open-File Rep. 94-214*, 30 p. (1.2 MB Hypercard stack), 1994. Available on Internet at USGS Home Page.

Bills, B.G., D.R. Curray, and G.A. Marshall, Viscosity estimates for the crust and upper mantle from patterns of upper lacustrine shoreline deformation in the eastern Great Basin, *J. Geophys. Res.*, *99*, 22059-22086, 1994.

Bautista, B.C., L.P. Bautista, E.S. Barcelona, R.S. Punongbayan, E.P. Laguerta, A.R. Rasdas, G. Ambubuyog, E.Q. Amin, and R.S. Stein, Relationship of regional and local structures to Mount Pinatubo activity, In R. S. Punongbayan and C.G. Newhall (Eds.), *The 1991-1992 Eruptions of Mount Pinatubo, Philippines*, U.S. Geol. Surv. Prof. Pap., in press, 1994.

King, G.C.P., R.S. Stein, and J. Lin, Static stress changes and the triggering of earthquakes, *Bull. Seismol. Soc. Amer.*, 84, 935-953, 1994.

Langbein, J., D. Dzurisin, G. Marshall, R. Stein, and J. Rundle, Shallow and peripheral volcanic sources of inflation revealed by two-color geodimeter and leveling data from Long valley caldera, California, 1988-92, submitted to *J. Geophys. Res.*, 1994.

Marshall, G.A. and R.S. Stein, 3-Slide Set: Maps of the Northridge, California, Earthquake Setting, Effects, and Deformation: U.S. Geol. Surv. Open-File Rep. 94-442, 1994.

Murray, M.H., M. Lisowski, G.A. Marshall, and R.S. Stein, The 1992 M=7 Cape Mendocino, California, Earthquake: Coseismic Deformation at the South End of the Cascadia Megathrust, submitted to *J. Geophys. Res.*, 40 p., 1994.

Sorey, M.L., C.D. Farrar, G.A. Marshall, and J.F. Howle, Effects of geothermal development on deformation in the Long Valley caldera, eastern California 1985-1993, 13 p., submitted to *J. Geophys. Res.*, 1994.

Stein, R.S., G.C.P. King, and J. Lin, Stress Triggering of the 1994 M=6.7 Northridge, California, Earthquake by its Predecessors, *Science*, 265, 1432-1435, 1994.

Thatcher, W., and D. P. Hill, A simple model for the fault-generated morphology of slow-spreading mid-ocean ridges, *J. Geophys. Res.*, in press, 1994.

Thatcher, W., Microplate versus continuum descriptions of active tectonic deformation, *J. Geophys. Res.*, in press, 1994.

Webb, F.H., M. Bursik, T. H. Dixon, G.A. Marshall, and R.S. Stein, Is Long Valley inflating? Results from one year of continuous GPS measurements, in press., *Geophys. Res. Letts.*, 1994.

Earthquake Geodesy in Southern California

Final Technical Report
Contract # 14-08-0001-G1805
J. Stock and K. Hudnut
Caltech; Seismological Laboratory; Pasadena, CA 91125
Internet: jstock *or* hudnut@seismo.gps.caltech.edu
(818) 395-6938 or (818)583-7232
FAX (818)564-0715 or (818)583-7827
ELEMENT II.2

Summary

This project obtained a large volume of GPS data before and after the 1992 Joshua Tree/Landers/Big Bear earthquake sequence as well as the 1994 Northridge earthquake. The data were therefore of great utility in determining the displacement fields associated with those earthquakes, thus providing data used in several fundamental studies of the earthquake source (e.g., *Bennet et al.*, in press; *Freymueller et al.*, 1994; *Johnson et al.*, 1994; *Hudnut et al.*, 1994; *Hudnut & Larsen*, submitted; *Massonnet et al.*, 1993; *Wald & Heaton*, 1994).

Furthermore, for these earthquakes, the *Hudnut et al.* source models are now incorporated in the National Geodetic Survey's HTDP program (*Snay & Herbrechtsmeier*, 1994), which is widely used among the surveying community. Another example of this project's outreach is that for both earthquakes, we provided the surveying, public works, and engineering communities with early geodetic results soon after the earthquakes occurred. These efforts have helped foster a strong appreciation of earthquake researchers' efforts among these communities in southern California.

The surveys conducted as part of this project in 1990, 1991, 1992 and 1993 provided strong foundations for much future work. The details of these surveys were reported in previous annual technical reports, and in reports written for the surveying agencies.

Surveys Accomplished

The main accomplishments in terms of data collection are best summarized by a rough description of the surveys we completed. All of the work shown derived much of its NEHRP funding from this project. In almost all cases, a large amount of in-kind support was provided by County, City, and other surveying agencies. Some of the work was partially supported by SCEC or the USGS internal program as well.

Southern San Andreas	Nov. 1989	~20 stations	kinematic
Parkfield (Hwy. 46 array)	Nov. 1989	~20 stations	kinematic
Los Angeles Basin	Feb. 1990	~25 stations	static
Southern San Andreas	March 1990	~20 stations	kinematic
Upland Eq. Response	April 1990	~6 stations	static
Southern San Andreas	Oct. 1990	~30 stations	static
Parkfield (Hwy. 46 array)	Oct. 1990	~20 stations	static
Inter-County 1991	March 1991	~70 stations	static
Sierra Madre Eq. Response	June 1991	~10 stations	static
Inter-County 1992	April 1992	~70 stations	static
Joshua Tree Eq. Response	June 1992	~12 stations	static
Landers Eq. Response	June 1992	~25 stations	static
Southern San Andreas	Feb. 1993	~30 stations	static
Inter-County 1993	July 1993	~130 stations	static

A.

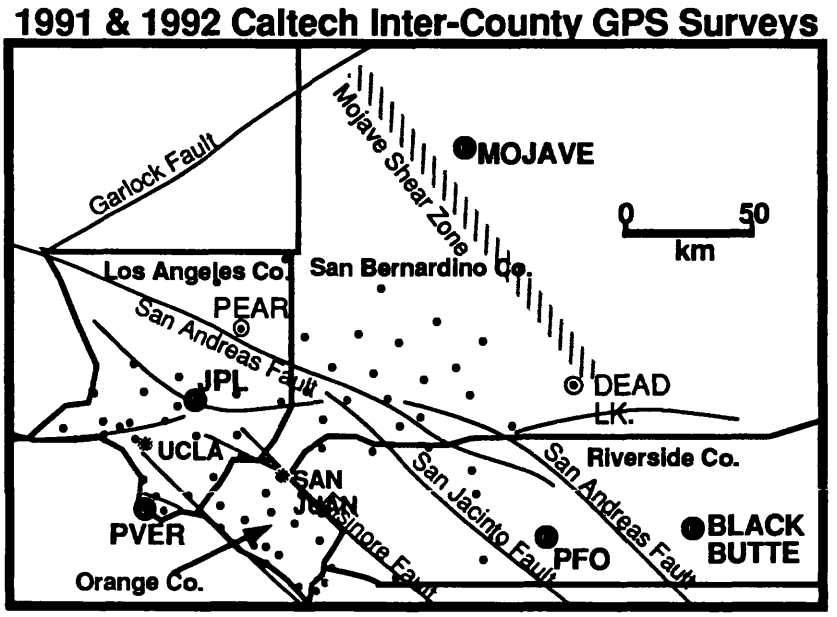

B.

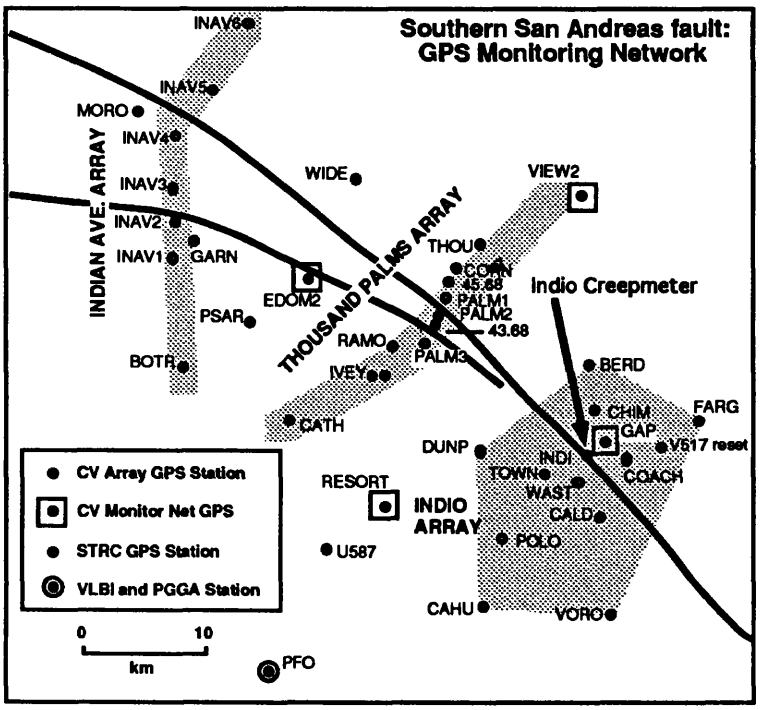

Maps showing stations in the main GPS networks established by this project. Map **A** shows the Inter-County network, as measured in 1991 and 1992. In the 1993 Inter-County survey, an additional 60 stations were measured within the same region. Map **B** shows the Southern San Andreas arrays surveyed by static GPS in 1990 and 1992 (post-Landers).

Scientific Results

The main scientific results of this project relate primarily to the 1992 Landers earthquake sequence. The most significant publication to result from this project was a report summarizing the GPS results as well as other geodetic data, and from these data producing a dislocation model and interpreting aspects of the earthquake source (*Hudnut et al.*, 1994). To represent that paper here, we reproduce a figure from it that perhaps best highlights the scientific contributions of this project.

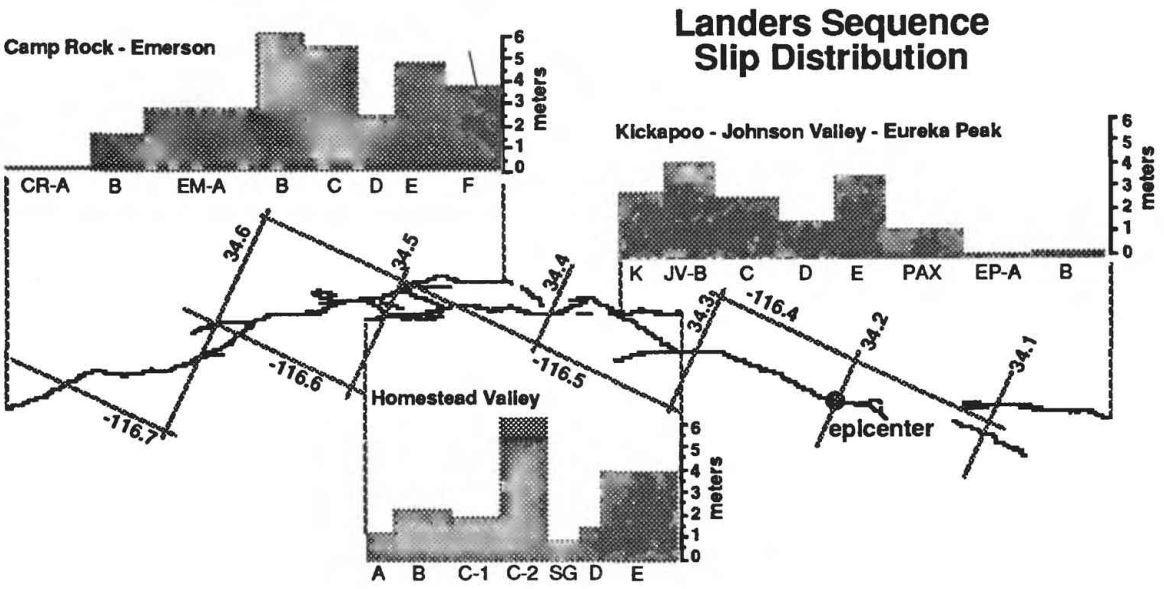

Diagram illustrating the slip distribution determined from geodetic data for the 1992 Landers earthquake. This figure from *Hudnut et al.* (1994) shows one of the main scientific contributions to result from this project.

Ongoing Work

Although this is a final report, we briefly mention here ongoing work that will result in more products from this project over the next year or two. Actually, the original intention of this project was to study interseismic as well as coseismic deformation. We began the GPS surveys with a project in Los Angeles in 1990. The data collected at these stations in 1990, 1991, 1992 and 1993 will provide a useful study of interseismic (and pre-seismic) deformation in the Los Angeles region. Work is in progress (with continuing SCEC and internal USGS support) on the interseismic deformation signals contained in all of the data sets we collected through this project. The 1992 and 1994 events have drawn our resources completely into studying these coseismic signals in as much detail as possible. In the absence of more future earthquakes, we hope to devote more work to investigating the interseismic periods in more detail. The 1990-1994 interval covered by this project was an excellent period to study coseismic signals, yet we do anticipate that data from the Los Angeles region from 1990 through 1993 should allow an interesting interseismic study.

History

This project began in April 1989 with Kerry Sieh as P.I. and Ken Hudnut as Co.-I., under a different name, "Geodetic Measurement of Coseismic Slip and Block Rotation in Southern California." The name was changed to "Earthquake Geodesy in Southern California" after the first year. From 1990 through 1992, Sieh was P.I., and during the

time that Hudnut was a Research Fellow at the Caltech Seismo Lab, this project supported his salary as well as field work on the Inter-County GPS Survey work and GPS surveys on the southern San Andreas fault. Since mid-1992, Joann Stock has been the P.I., and this project supported continuations of the work. Hudnut left the project in August 1992 to work for the USGS (in Pasadena), and maintained a collaborative role. In 1993 and early 1994, Dragana Simic and then later Michael Cline were hired by Caltech as temporary employees to work on data management, data processing, and data analysis. Their work in coordination with Hudnut and the SCEC group based at UCLA made possible two reports to the County Surveying agencies - one report on the 1990 through 1992 Inter-County Surveys, and another on the 1993 Inter-County Survey. Because of the large amounts of in-kind support for the 1990, 1991, 1992 and 1993 Inter-County surveys provided by these agencies, completion of these reports was crucial. Ms. Simic left the project in Sept. 1993 to move to New York, and Mr. Cline left the project for a job with the National Geodetic Survey (as the advisor to the State of New Jersey) in March 1994.

References

BENNETT, R., R. REILINGER, W. RODI, Y. LI, K. HUDNUT
COSEISMIC FAULT SLIP ASSOCIATED WITH THE 1992 M 6.1 JOSHUA TREE, CALIFORNIA EARTHQUAKE: IMPLICATIONS FOR THE JOSHUA TREE - LANDERS EARTHQUAKE SEQUENCE
IN PRESS, J. GEOPHYS. RES.

FREYMUELLER, J., N. E. KING AND P. SEGALL
THE COSEISMIC SLIP DISTRIBUTION OF THE LANDERS EARTHQUAKE
BULL. SEIS. SOC. AMER., V. 84, #3, 646-659, 1994.

JOHNSON, H. O.; D. C. AGNEW, K. W. HUDNUT
EXTREMAL BOUNDS ON EARTHQUAKE MOMENT FROM GEODETIC DATA
BULL. SEIS. SOC. AMER., V. 84, #3, 660-667, 1994.

HUDNUT, K. W., Y. BOCK, M. CLINE, P. FANG, J. FREYMUELLER, K. GROSS, D. JACKSON, S. LARSEN, M. LISOWSKI, Z. SHEN, AND J. SVARC
COSEISMIC DISPLACEMENTS IN THE 1992 LANDERS EARTHQUAKE SEQUENCE
BULL. SEIS. SOC. AMER., V. 84, #3, 625-645, 1994.

HUDNUT, K. W. AND S.C. LARSEN
SLIP DISTRIBUTION OF THE 1992 LANDERS, CALIFORNIA EARTHQUAKE SEQUENCE, DETERMINED FROM GEODETIC DATA
SUBMITTED, JGR

MASSONNET, D., M. ROSSI, C. CARMONA, F. ADRAGNA, G. PELTZER, K. FEIGL, AND T. RABAUTE
THE DISPLACEMENT FIELD OF THE LANDERS EARTHQUAKE MAPPED BY RADAR INTERFEROMETRY
NATURE, V. 364, PP. 138-142, 1993.

WALD, D. J. AND T. H. HEATON
SPATIAL AND TEMPORAL DISTRIBUTION OF SLIP FOR THE 1992 LANDERS, CALIFORNIA EARTHQUAKE
BULL. SEIS. SOC. AMER., V. 84, #3, 668-691, 1994.

SNAY, R. AND E. HERBRECHTSMEIER
THE TDP-H91-CA MODEL FOR HISTORICAL HORIZONTAL DEFORMATION IN CALIFORNIA
MANUSCRIPTA GEODAETICA, V. 19, PP. 180-198

Project Bibliography

*Hudnut, K.W., Faults, in *Encyclopedia of Earth System Science, Volume 2*, Academic Press, Inc., San Diego, p. 219-225, 1992.

*Hudnut, K.W., Geodesy tracks plate motion, *Nature*, v. 355, No. 6362 (20 February), pp. 681-682, 1992.

*Mori, J., K. Hudnut, L. Jones, E. Hauksson, and K. Hutton ('compilers'), Rapid scientific response to the Landers quake, *EOS, Trans. Amer. Geophys. Union*, v. 73, No. 39 (29 September), pp. 417-418, 1992.

*Lindvall, S.C. and K.W. Hudnut, Field guide to the area of maximum displacements along the 1992 Landers earthquake rupture, *in "Landers Earthquake of June 28, 1992 - San Bernardino County, California,"* Assoc. Engin. Geol. (So. Calif. Sect.), pp. 33-38, Oct. 10, 1992.

Bock, Y., D. Agnew, P. Fang, J. Genrich, B. Hager, T. Herring, K. Hudnut, R. King, S. Larsen, J.-B. Minster, K. Stark, S. Wdowinski, and F. Wyatt, Detection of crustal deformation related to the Landers earthquake sequence using continuous geodetic measurements, *Nature*, v. 361, No. 6410 (28 January), pp. 337-340, 1993.

*Sieh, K., L. Jones, E. Hauksson, K. Hudnut, D. Eberhart-Phillips, T. Heaton, S. Hough, K. Hutton, H. Kanamori, A. Lilje, S. Lindvall, S. McGill, J. Mori, C. Rubin, J. Spotila, J. Stock, H.K. Thio, J. Treiman, B. Wernicke, and J. Zachariasen, Near-field investigations of the Landers earthquake sequence, April to July, 1992, *Science*, v. 260, pp. 171-176, 1993.

*Bodin, P., R. Bilham, J. Behr, J. Gomberg, and K. Hudnut, Slip triggered on southern California faults by the 1992 Joshua Tree, Landers, and Big Bear earthquakes, *Bull. Seis. Soc. Amer.*, v. 84, #3, 806-816, 1994.

*Hudnut, K. W., Y. Bock, M. Cline, P. Fang, Y. Feng, J. Freymueller, X. Ge, K. Gross, D. Jackson, M. Kim, N. King, J. Langbein, S. Larsen, M. Lisowski, Z. Shen, J. Svarc and J. Zhang, Co-seismic displacements of the 1992 Landers earthquake sequence, *Bull. Seis. Soc. Amer.*, v. 84, #3, pp. 625-645, 1994.

Johnson, H. O., D. C. Agnew, K. Hudnut, Extremal Bounds on Earthquake Moment from Geodetic data, *Bull. Seis. Soc. Amer.*, v. 84, #3, 660-667, 1994.

Bennett, R., R. Reilinger, W. Rodi, Y. Li, K. Hudnut, Coseismic fault slip associated with the 1992 M 6.1 Joshua Tree, California earthquake: Implications for the Joshua Tree - Landers Earthquake Sequence; in press, *J. Geophys. Res.*

Hudnut, K. W. and S. C. Larsen, Slip distribution of the 1992 Landers, California earthquake sequence, determined from geodetic data, submitted to *J. Geophys. Res.*, 1994.

Peltzer, G., K. Hudnut, and K. Feigl, Analysis of coseismic displacement gradient using Radar Interferometry: new insights into the Landers Earthquake; in press, *J. Geophys. Res.*

Reports:

*Hudnut, K. W., The Inter-County Surveys. 25 pgs. 4/15/93. (Report to surveying community in So. Calif. on results of the 1991 & 1992 Inter-County GPS surveys).

*Hudnut, K. W., Inter-County 1993 Survey Progress Report. 6 pgs. 11/11/93. (Progress report to surveying community in So. Calif. on results of the 1993 Inter-County GPS survey).

*Cline, M., Inter-County 1993 Survey: NGS Software Adjustment Report. Dec. 6, 1993 (amended March 14, 1994).

*Hudnut, K. W. and M. H. Murray, Preliminary GPS Results of the USGS: The Northridge Earthquake. January 26, 1994. (included copy of the report we sent out on internet on Jan. 25, 1994)

(* copy accompanying this report)

Using compressive growth structure for estimating slip rates, potential earthquake magnitudes, and recurrence intervals on buried thrust faults in the northern Santa Barbara Channel, CA.

1434-92-G-2192

John Suppe, Enrique Novoa, Karl Mueller, and Maribeth Price
Princeton University
Princeton, NJ 08544
(609) 258-4119
(609) 258-1274 FAX
John@wanda.princeton.edu
Program Element 2.1

Investigations Undertaken:

Our research in the Santa Barbara Channel region is centered on determining the rates and recency of dip slip along active blind thrust faults by axial surface mapping and kinematic analysis of compressive growth structure. Products of this work allow us to determine the lateral distribution of slip along these faults, and their lateral propagation rates. These studies have fundamental long term value for seismic hazard assessment in this region by providing primary information for determining earthquake magnitude and recurrence. We are also working to develop new methods for determing the paleoseismic record of blind thrusts by integrating studies of high resolution growth sedimentation with kinematic modeling of folding processes at earthquake recurrence timescales. Work on active folds in the Transverse Ranges, Los Angeles Basin and Ventura Basin indicate that many folds record numerous paleo folding "events" related to blind thrust earthquakes.

Results:

Arc/Info Database: Our long-term efforts in the Santa Barbara Channel to map compressive growth structure is focused on compiling and digitizing a database of over 400 industry seismic reflection profiles in the Arc/Info format. Approximately 200 of these lines are new for 1994; these tighten our existing coverage in the central and northern Channel areas, and provide new data further to the east.

Axial Surface Mapping and structural contouring: Axial surface mapping and structure contour plots, using this new data, indicate that the south-vergent Channel Islands thrust terminates in the central channel, south of the city of Santa Barbara (Figure 1). Deep levels of shortening in the eastern channel appear to be accommodated along a newly identified north vergent thrust, although at slower rates than in the eastern Channel. We term active folds developed above bends in this blind thrust the Western Deep Trend (Figure 2).

Axial surface mapping in the eastern Santa Barbara Channel indicates that the Pitas Point blind thrust extends to the longitude of Pt Conception, where its long-term slip rate of 1.3mm/yr is similar to that in the east. The slip budget along this fault decreases to the east, indicating its younger shortening history there. The geometry of the related Blue Bottle fold trend changes dramatically along strike. In the eastern channel the Pitas Point thrust ramp is steeply inclined, where it reactivates a Miocene normal fault(Figure 3). The amplitude of this fold is much less pronounced in the western channel, where the causative blind thrust ramp cuts gently upsection to the south. Axial surface mapping of the Hondo trend indicates that slip is transferred southward to

the Pitas Point thrust in the eastern channel from a north-dipping blind thrust ramp near the coastline. This ramp is active, based on compressive growth structure.

High Resolution Seismic Reflection Profiling: In addition to our mapping of deep structure using industry seismic, we have completed other studies to determine the recency of slip along active blind thrust ramps in the Santa Barbara Channel. In pursuing this, we have acquired, processed and interpreted 140km of high resolution seismic reflection data with Dan Francis of Cal State University, Long Beach in the central and western Santa Barbara Channel. These efforts are part of a pilot, high-resolution seismic survey of active folds funded by the Southern California Earthquake Center to test the feasibility of doing paleoseismology in the offshore environment. Our study focussed on imaging Late Quaternary deformation across active folds which we had previously mapped using the dense array of industry seismic reflection profiles.

Our results indicate that near surface sediments have been folded along active axial surfaces along both the Blue Bottle and Oakridge fold trends. We have coordinated this work with a recent Ocean Drilling Project borehole in the central Santa Barbara Channel in an effort to determine the age of deformed sediments imaged in the high resolution seismic profiling. Velocity measurements of core taken during drilling of the borehole, coupled with our data suggest that sediments as young as 25 ka are folded. Folding near the ODP borehole is associated with the newly mapped extension of the Pitas Point thrust in the western Santa Barbara Channel. Late Quaternary folding is also apparent on the 3.5Mhz data along the active, synclinal axial surface associated with the Channel Islands Thrust in the western Channel.

Future Work

Future efforts to define the recency and magnitude of paleoseismic events in the Santa Barbara Channel and the long term kinematic evolution of blind thrust faults there will utilize continued mapping and analysis of industry seismic data, in addition to ultra high resolution seismic reflection profiling.

ARC/INFO based structure contour maps

We will develop new ARC/INFO based structure contour maps of key time horizons, integrated with three dimensional fault geometry. These maps result from a structural integration of petroleum seismic profiles, well data, balanced cross sections, and earthquake hypocenters and focal mechanisms. The maps will be available as structure contour maps, TIN surfaces, and possibly other formats. The value of these maps is to a) insure a fully integrated and self consistent subsurface fault topology using all available data, b) document geometric fault segmentation in 3D and c) provide digital fault geometries for modeling strong motion, stress transfer, and geodetic deformation. These maps are based on our extensive seismic grids in the Santa Barbara Channel and allow us to develop a fully self-consistent time horizons within these basins. The value of these high resolution maps is that they provide a consistent time framework for long-term slip rates on blind thrusts within these basins.

3D structural analysis.

Efficient structural mapping in Arc/Info requires the establishment of considerable computer infrastructure of software and hardware capable of handling petroleum seismic and well data, surface geology, and earthquake data in a georeferenced 3D environment. We have made a major effort to establish such an environment, major elements of which are complete. We have developed an Arc/Info capability for storing and displaying seismic shot-point data and for using that data in mapping axial surfaces, faults and stratigraphic horizons. We are waiting for delivery of a large format (40 inch) roll scanner which will allow efficient and rapid digitizing of faults,

horizons, axial surfaces, and structural data on paper seismic lines and geologic maps. In spite of Arc/Info's enormous power and wide adoption in the planning community, it has some significant limitations in geophysical and structural uses because it is a 2D database. For this reason we have made a major push in the last six months and obtained the very powerful and topologically rigorous GOCAD 3D earth modeller and 2D and 3D Geosec balancing software. We are now starting to develop capabilities to use this software to fully incorporate earthquake hypocenters and focal mechanisms, petroleum seismic and well data, and surface geology directly into 3D TIN surface models and maps of major blind thrust faults.

Ultra high resolution seismic reflection studies

Our pilot 3.5 MHz study this past year has demonstrated the feasibility of imaging very young sediments deformed by active folding associated with blind thrust faults in marine environments. Recent advances in ultra-high resolution seismic reflection profiling of active faults in San Fransisco Bay and in the Sea of Japan indicate that even better results are possible, particularly at water depths less than 200 m. The resolution of the system used in these studies optimally images beds as thin as 10cm. We will undertake continued profiling of active folds with other researchers in the shallow waters of the eastern Santa Barbara Channel in 1995, in an effort to image event stratigraphy associated with individual folding events.

Reports Published

Mueller, K.J., and Suppe, J., 1994a, New methods for determining the paleoseismic history of blind thrust faults: Geological Society of America Abstracts with Programs, V. 26, No. 7, p. 314.

Mueller, K.J., and Suppe, J., 1994b, Paleoseismology of blind thrusts through analysis of their fault-related folds: International Lithosphere Commission Workshop on Paleoseismology: U.S. Geological Survey Open File Report No. 94-568.

Mueller, K.J., Price, M., Shaw, J., and Suppe, J., 1994, 46 kilometer westward lateral propagation of the Channel Islands Thrust in the last 1 Ma revealed by axial surface mapping, Santa Barbara Channel, California (abs): American Assoc. Petroleum Geologists Bulletin, V. 78, No. 4, p. 671.

Novoa, Enrique, John Shaw, and John Suppe, 1994, Structural transect across the Eastern Santa Barbara Channel (Western Transverse Ranges) California [Abs.]: American Association of Petroleum Geologists Bulletin , v 78, n. 4, p. 672.

Shaw, J. H., Hook, S. C. and Suppe, J., 1994, Structural trend analysis by axial surface mapping. Amer. Assoc. Petroleum Geol. Bull., v. 78, p. 700-721.

Shaw, J. H., and Suppe, J., 1994, Active faulting and growth folding in the eastern Santa Barbara Channel, California. Geol. Soc. America Bull., v. 106, p. 607-626.

Shaw, J. H., and Suppe, J., submitted, Earthquake hazards of active blind-thrust faults under the central Los Angeles basin, California. Journal of Geophysical Research.

Suppe, J., Shaw, J.H., and Novoa, E., 1994, Active deformation in the complex foreland basins of the Transverse Ranges, California, Geologie Alpine, Ser. Spec. No. 4, p. 100-101.

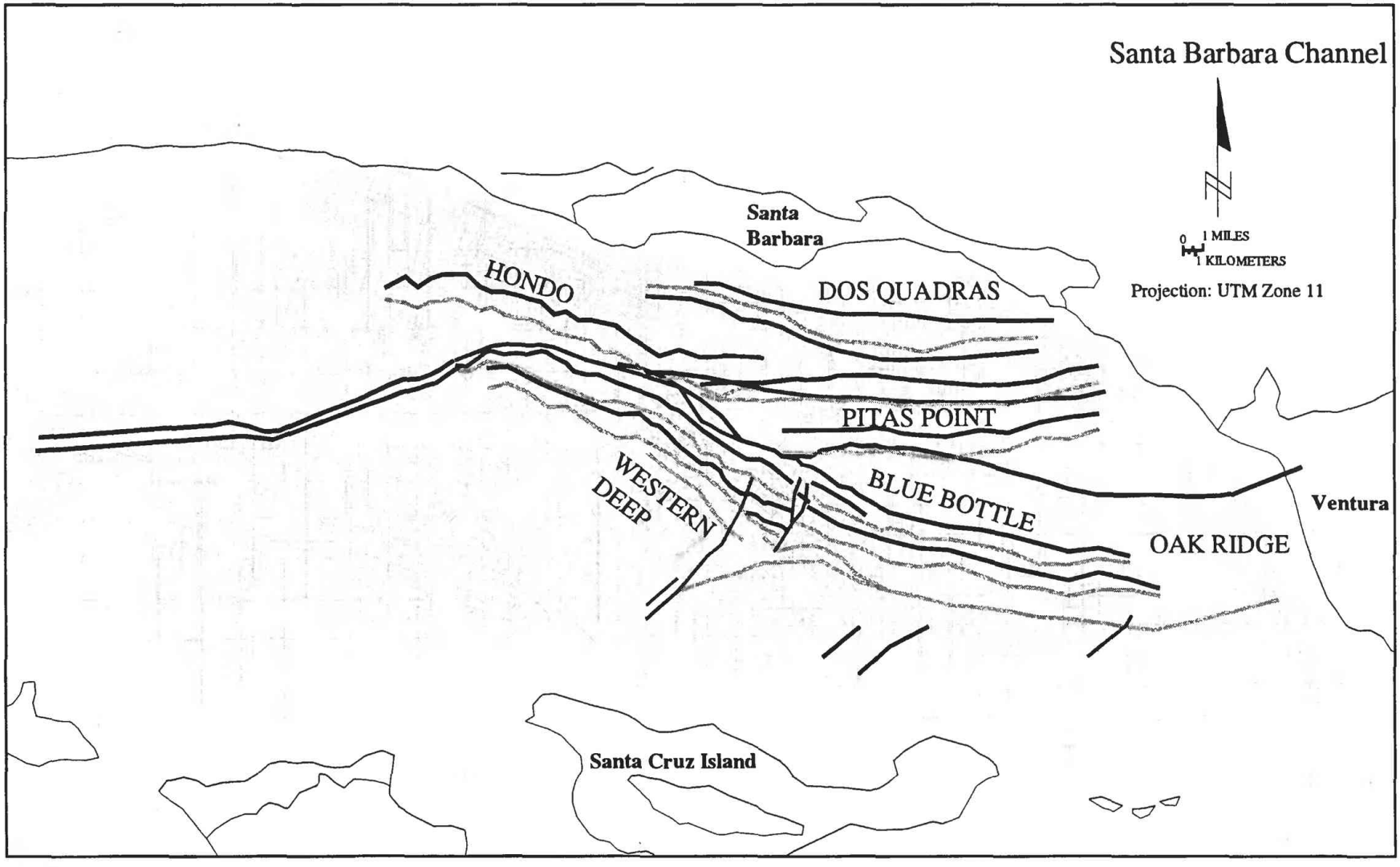

Figure 1. Regional map of the Santa Barbara Channel area showing our seismic data coverage and the active fold trends present there. Active axial surfaces are marked as dark bold lines; these represent the locus on active folding of the sea bottom along each trend. Inactive axial surfaces marked in grey record the initial positions of active axial surfaces at the onset of fold growth; they record limb width which we then relate to underlying fault slip using fault-related folding and growth theory. Thin grey lines represent digitized locations of seismic reflection profiles in our database.

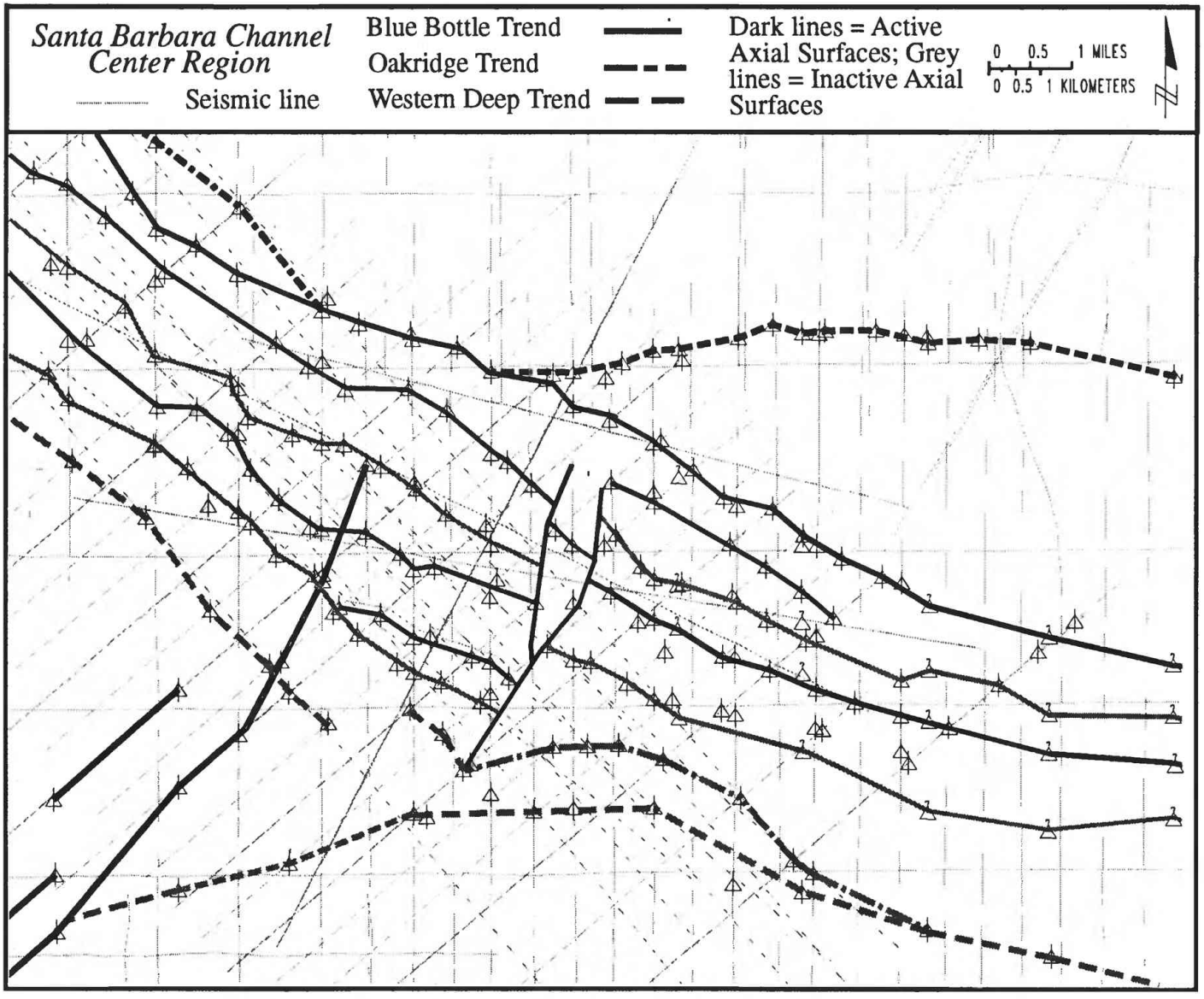

Figure 2. Detailed map of a segment boundary along the Blue Bottle fold trend in the central Santa Barbara Channel. Note that this also may be a boundary between other fold trends developed by slip on deeper blind thrust fault ramps at depth such as the Western Deep and Oakridge trends. We use information from our mapping of fold trends to develop kinematically reasonable subsurface maps of blind thrust faults throughout the Santa Barbara Channel.

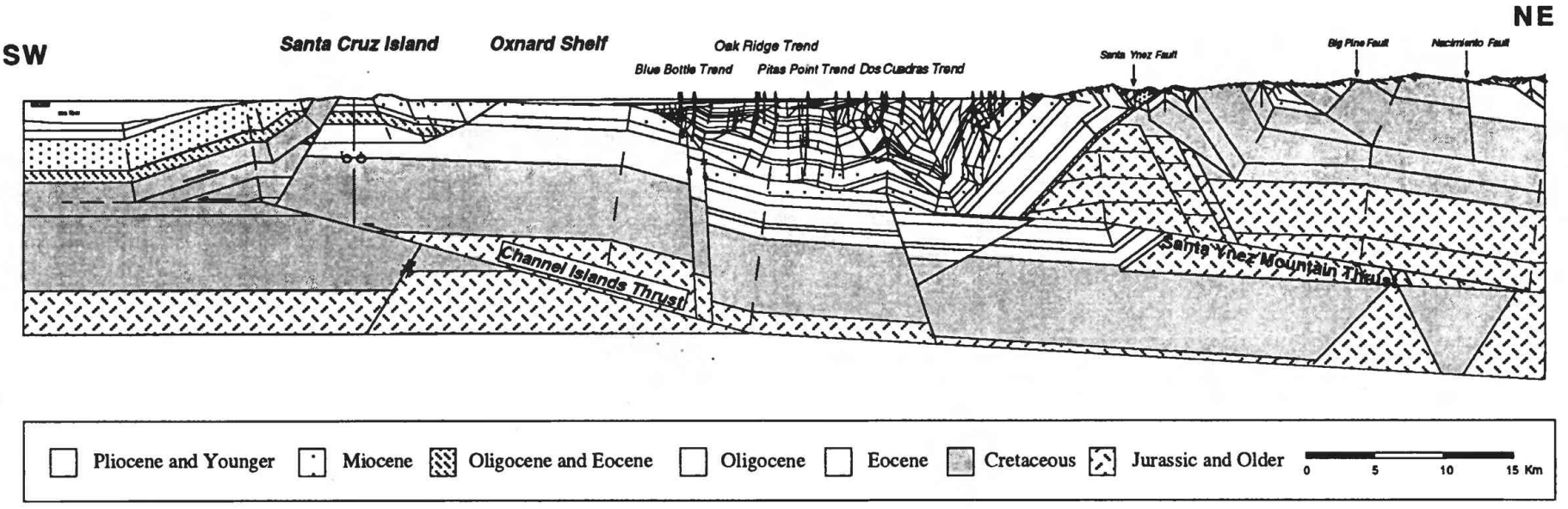

Figure 3. Balanced structural cross section across the eastern Santa Barbara Channel from Novoa (work in progress) and Shaw et.al., (1994) that defines the geometry and kinematic links between active folds and blind thrusts in the region. The cross section compiles data from industry seismic reflection lines, wells, geologic maps and bathymetry. The dominant structures in the region include; 1) the active, south vergent Channel Islands thrust and related Oak Ridge fold trend; and 2) the Santa Ynez Mountain thrust and associated active folds. These folds include the Dos Cuadras trend, a complex wedge and backthrust structure, the Pitas Point trend, a simple anticline, and the Blue Bottle trend, a fold developed above a steep thrust ramp with a history of structural inversion.

INFLUENCE OF THE SOUTHERN WASHINGTON CASCADES CONDUCTOR ON VOLCANISM AND TECTONISM

Project Number 9980-04028

Donald A. Swanson
U.S. Geological Survey
Department of Geological Sciences AJ-20, University of Washington, Seattle, WA 98195
(206) 553-5587 (voice and fax) e-mail: donswan@geology.washington.edu
Program Element II

Investigations undertaken

Those parts of the Purcell Mountain and Packwood 7-1/2-minute quadrangles lying south of the Cowlitz River (fig. 1), astride the approximate eastern edge of the Southern Washington Cascades Conductor (SWCC; Stanley and others, 1987, 1990, 1992), were mapped geologically at a scale of 1:24,000. (R.B. Moore, Branch of Volcanic and Geothermal Processes, U.S. Geological Survey, Denver, is completing mapping in these quadrangles north of the river. In addition, parts of the Hamilton Buttes, Randle, and Blue Lake (Swanson, 1993) quadrangles were field checked and modified where necessary. In addition, mapping in the Packwood Lake quadrangle was started. An open-file map, including cross-sections and a 31–page descriptive and interpretative text, was open-filed for the East Canyon Ridge quadrangle (Swanson, 1994a).

This work is part of an ongoing cooperative effort with Roger Ashley and Russell Evarts (Branch of Western Mineral Resources, U.S. Geological Survey, Menlo Park) and R.B. Moore to define the development of the Cascade Range along an east-west research corridor in the Mount St. Helens-Mount Adams-Mount Rainier area (fig. 1). The SWCC, an anomalous electrical conductor at intermediate depth within the crust, underlies that part of the research corridor between Mount St. Helens and Mount Adams. One goal of the cooperative effort is to compare and contrast volcanism and tectonism above the SWCC with that beyond the limits of the SWCC.

Improved understanding of the nature and influence of the SWCC is important in order to define and evaluate earthquake hazards in the area. The western margin of the SWCC coincides with the St. Helens seismic zone (Weaver and Smith, 1983; Grant and others, 1984; Grant and Weaver, 1986), which "could, under certain assumptions, be capable of generating a magnitude 7.0 earthquake" (Weaver and Smith, 1983, p. 10,380). The northeastern margin of the SWCC includes a north-northwest-trending zone of seismicity near Mount Rainier (Weaver and Malone, 1987; Stanley and others, 1987) and the epicentral area of the 1981 Goat Rocks earthquake (magnitude 5.0; Zollweg and Crosson, 1981; Weaver and Smith, 1983).

Six days were devoted to paleomagnetic sampling of selected volcanic and intrusive rocks, in cooperation with Jon Hagstrum (Branch of Isotope Geology, U.S. Geological Survey, Menlo Park). Thirty-four sites, with approximately 340 cores, were studied for the purposes of assessing the relative ages of folding and to evaluate further the amount of tectonic rotation these Tertiary rocks have experienced. Hagstrum worked up the paleomagnetic data obtained inn FY93, and we prepared an abstract for the 1994 Fall AGU meeting (Hagstrum and Swanson, 1994).

R.C. Evarts and I prepared a guide for the field trip that we led for 22 people attending the Annual Meeting of the Geological Society of American in Seattle in October 1994 (Evarts and Swanson, 1994).

Results

The Purcell Mountain and Packwood quadrangles south of the Cowlitz River contain a suite of volcanic rocks ranging in age from latest Eocene or earliest Oligocene to Quaternary (probably middle to late Pleistocene). Fluvial volcanic sandstone and diamictite (mostly of lahar origin) dominate the 3–4–km–thick Tertiary section exposed in the quadrangles; andesitic and basaltic andesitic lava flows, andesitic and dacitic

pyroclastic flows, and minor dacitic and rhyolitic lava flows and domes, are locally present. These rocks were intruded by numerous andesitic and microdioritic sills and then folded along a north-northwest-trending anticline (the Castle Butte anticline) that diagonally crosses the area. Dips on the flank of the anticline are as high as 50°, and the fold has a structural amplitude of at least 3 km.

The folding probably took place before about 12 Ma, the approximate age (from zircon fission-track counts) of a suite of hornblende andesite-dacite and hornblende diorite-quartz diorite dikes and sills that intrude the section farther south. This hornblende-bearing suite—the Kidd Creek suite of Marso and Swanson (1992)—forms a subvolcanic complex with a large radial dike swarm (Swanson, 1990, 1991) centered in the northeast part of the McCoy Peak quadrangle. The pattern of the radial dikes, and their systematic subvertical orientation, indicate that they were intruded after folding, which produced dips of 30–50° (in places, possibly disturbed by faulting, even 85°). The paleomagnetic samples obtained by Hagstrum and me in FY93 and worked up in FY94 confirms this interpretation (Hagstrum and Swanson, 1994). The paleomagnetic data and associated field observations, combined with stratigraphic evidence and scanty K-Ar ages obtained by others, suggest that folding was confined to a narrow time window between 18 Ma (possibly 15.6 Ma) and 12 Ma.

Quaternary lava flows of andesite and basaltic andesite unconformably overlie the folded Tertiary rocks in the northeastern part of the Packwood quadrangle. These valley-filling flows were erupted from vents associated with Goat Rocks volcano in the Goat Rocks Wilderness along the crest of the Cascades. These flows have normal paleomagnetic polarity and are probably younger than about 780,000 yrs. They are not detectably folded or faulted.

No evidence of active faulting was found in the quadrangles. However, many small shear zones, generally north-northwest striking, cut the Tertiary rocks. These shears typically have indicators of dextral slip (subhorizontal slickensides on appropriately stepped surfaces). The northwest to north-northwest strike of most of the shears is similar to that of the fold axes in the mapped quadrangles. Perhaps both can be accounted for in a transpressional setting.

Large landslides are common. One lake (Hager Lake south of Packwood) and several marshes formed as a result of slides. This situation is similar to that in the Hamilton Buttes quadrangle described in last year's report. Bob Schuster (Branch of Geologic Risk Assessment, U.S. Geological Survey, Denver) and I looked for drowned trees for possible dating but found none. Schuster has one age from nearby landslide-dammed Packwood Lake that suggests temporal correlation with earthquakes that shook the Puget Sound area (Schuster and others, 1992). This year Pat Pringle (State of Washington), Schuster, and I drilled several auger holes in one landslide-dammed marsh to use Mount St. Helens ash deposits to bracket the age of sliding; this slide was probably too old to correlate with the 1200-year event. We suspect that at least some of these slides have been triggered by other earthquakes but need ages to test this hypothesis.

Straight sections of the Cowlitz River cut across the fold grain and suggest fault control. However, three observations, made together with R.B. Moore and N.G. Banks, indicate that there has been little or no significant faulting along the Cowlitz. One is that a thick (more than 100 m), distinctive diamictite apparently continues northward along strike across the Cowlitz valley from Goat Dike in the Packwood quadrangle onto Davis Mountain in the Purcell Mountain quadrangle. A second piece of evidence is that a belt of silicic (mainly rhyolitic) rocks mapped south of the river in the Purcell Mountain quadrangle has an apparent counterpart north of the river. The third piece of evidence is that fold axes project across the river with no recognizable change in pattern. There still may be some faulting or shearing along the river valley; some shears can be seen in exposures near the edge of the alluviated valley floor. Such features could have been favorable sites for differential erosion to form the valley. But, the field evidence now suggests that no major fault or faults follows the valley.

To summarize, work in the Purcell Mountain, Packwood, and adjacent quadrangles has found several features unusual for the southern Washington Cascades. Dextral shear is pervasive throughout all of the quadrangles mapped, though not of notable magnitude along individual shears, and may together with the

folds indicate a transpressional regime. Numerous landslides could have been triggered by earthquakes. Folding appears to have been confined to a short time interval centered about 15 Ma. Continued study of the several quadrangles already completed, and of those targeted for future work, will address these issues.

Reports

Evarts, R.C, and Swanson, D.A., 1994, Geologic transect across the Tertiary Cascade volcanic arc, southern Washington, *in* Swanson, D.A., and Haugerud, R.A., eds., 1994, Geologic field trips in the Pacific Northwest: 1994 Annual Meeting, Geological Society of America, Seattle, Washington, p. 2H-1–31.

Hagstrum, J.T., and Swanson, D.A., 1994, Paleomagnetism of the Miocene intrusive suite of Kidd Creek: implications for the timing of deformation in the Cascade arc, southern Washington: Eos, American Geophysical Union, Transactions, v. 75, no.44, p. 198–199.

Swanson, D.A., 1994a, Geologic map of the East Canyon Ridge quadrangle, southern Cascade Range, Washington: U.S. Geological Survey Open-File Report 94-591, 31 p., map scale 1:24,000.

Swanson, D.A., 1994b, Coeval volcanism and subsidence about 36 million years ago in the Cascade arc, southern Washington: Geological Society of America Abstracts with Programs, v. 26, no. 7, p.A-113.

References Cited in addition to the new reports

Grant, W.C., and Weaver, C.S., 1986, Earthquakes near Swift Reservoir, Washington, 1958–1963: seismicity along the southern St. Helens seismic zone: Bulletin of the Seismological Society of America, v. 76, p. 1573-1587.

Grant W.C., Weaver, C.S., and Zollweg, J.E., 1984, The 14 February 1981 Elk Lake, Washington, earthquake sequence: Bulletin of the Seismological Society of America, v. 74, p. 1289-1309.

Marso, J.N., and Swanson, D.A., 1992, The intrusive suite of Kidd Creek: a middle Miocene magmatic event in the Cascade arc of southern Washington: Geological Society of America Abstracts with Programs, v. 24, n. 5, p. 67.

Schuster, R.L., Logan, R.L., and Pringle, P.T., 1992, Prehistoric rock avalanches in the Olympic Mountains, Washington: Science, v. 258, p. 1620–1621.

Stanley, W.D., Finn, Carol, and Plesha, J.L., 1987, Tectonics and conductivity structures in the southern Washington Cascades: Journal of Geophysical Research, v. 92, p. 10,179-10,193.

Stanley, W.D., Mooney, W.D., and Fuis, G.S., 1990, Deep crustal structure of the Cascade Range and surrounding regions from seismic refraction and magnetotelluric data: Journal of Geophysical Research, v. 95, p. 19,419-19,438.

Stanley, W.D., Gwilliam, W.J., Latham, Gary, and Westhusing, Keith, 1992, The southern Washington Cascades conductor—a previously unrecognized thick sedimentary sequence?: American Association of Petroleum Geologists Bulletin, v. 76, p. 1569–1585.

Swanson, D.A., 1990, Trends of middle Tertiary dikes in and north of the Dark Divide Roadless area, southern Washington Cascades: Eos, Transactions of the American Geophysical Union, v. 71, p. 1144.

____, 1991, Geologic map of the Tower Rock quadrangle, southern Cascade Range, Washington: U.S. Geological Survey Open-File Report 91-314, scale 1:24,000, 26 p.

____ 1993, Geologic map of the Blue Lake quadrangle, southern Cascade Range, Washington: U.S. Geological Survey Open-File Report 93–297, scale 1:24,000, 34 p.

Weaver, C.S., and Malone, S.D., 1987, Overview of the tectonic setting and recent studies of eruptions of Mount St. Helens, Washington: Journal of Geophysical Research, v. 92, p. 10,149-10,154.

Weaver, C.S., and Smith S.W., 1983, Regional tectonic and earthquake hazard implications of a crustal fault zone in southwestern Washington: Journal of Geophysical Research, v. 88, p. 10,371-10,383.

Zollweg, J.E., and Crosson, R.S., 1981, The Goat Rocks Wilderness, Washington, earthquake of 28 May 1981: Eos, Transactions of the American Geophysical Union, v. 62, p. 966.

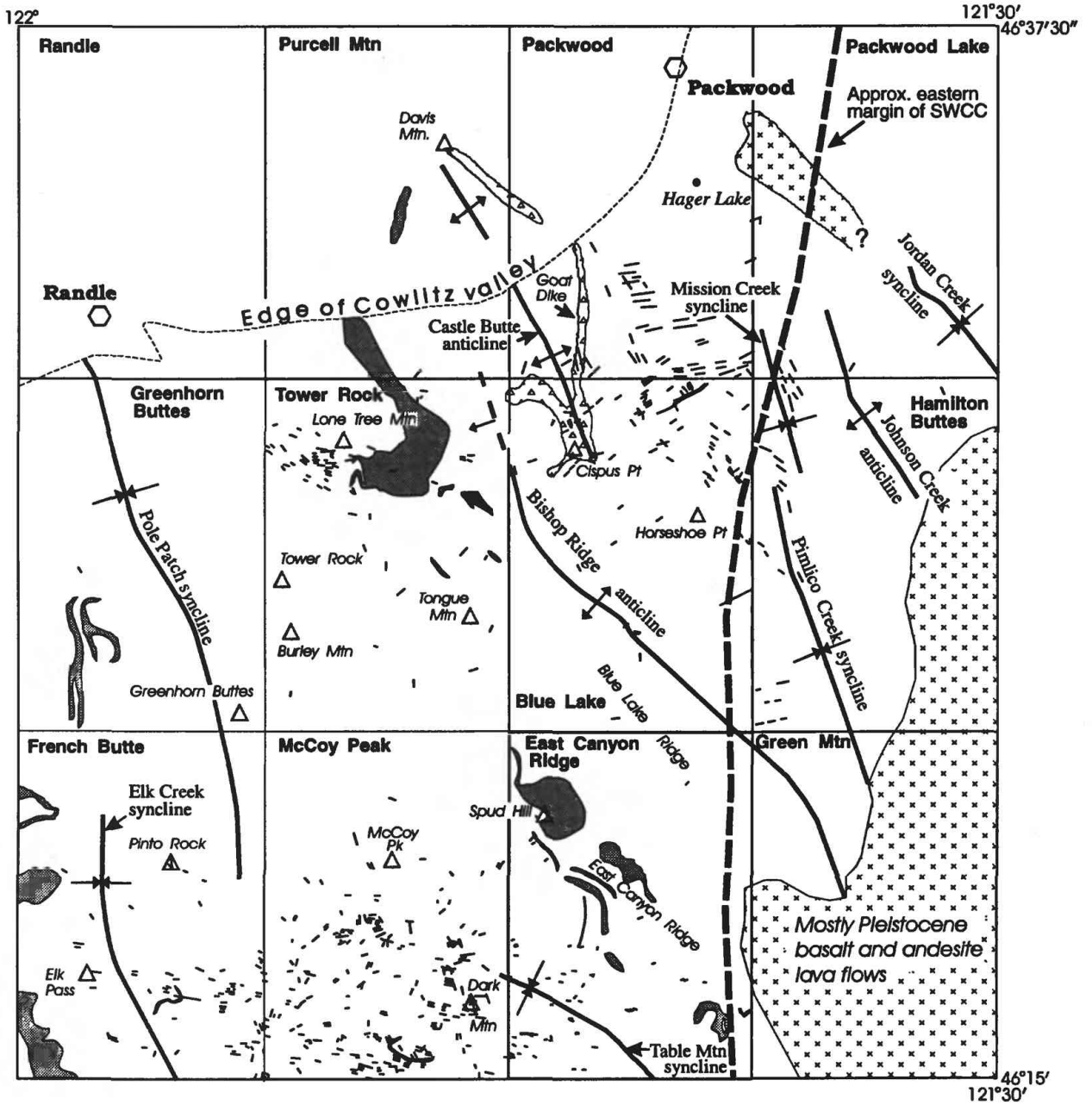

Figure 1. Map showing locations of Purcell Mountain and Packwood quadrangles and other quadrangles being mapped in the southern Washington Cascades relative to the eastern edge of the Southern Washington Cascades Conductor (SWCC). ▬, silicic rocks; ▲▲▲▲, distinctive diamictite; ×××××, Quaternary volcanic rocks. Short lines are andesite dikes. Geology north and west of Cowlitz River is diagrammatic and designed to show interpreted northward continuations of folds, silicic rocks, and distinctive diamictite, as shown me by R.B. Moore. See text for discussion.

Nearfield Geodetic Investigations of Strain across Faults in Southern California

1434-93-G2290

Arthur G. Sylvester
Department of Geological Sciences, and Institute for Crustal Studies
University of California, Santa Barbara, California 93106-9630
(805) 893-3156; arthur@magic.ucsb.edu

Program Element: II, Component II-3

INVESTIGATIONS

The long-term, fixed purpose of this investigation is to search for and monitor the spatial and temporal nature of nearfield displacement across active and potentially active faults. Thus, we document pre-, co- and post-seismic displacement and aseismic creep, if any, especially where seismographic, paleoseismic, and geomorphic evidence indicates current or recent fault activity. The geodetic arrays range in length from 300 m to 7000 m and are intermediate in scale, therefore, between the infrequent, regional geodetic surveys traditionally done by the National Geodetic Survey, and point measurements by continually recording instruments such as creepmeters, tiltmeters, and strainmeters. All leveling is done according to First Order, Class II standards, and horizontal surveys are done to First Order standards.

We concentrated on four main tasks during 1994: 1) establish and survey new leveling lines across the Sierra Madre frontal fault; 2) resurvey the CDMG geodetic array across the Cucumonga fault at the mouth of Day Canyon; 3) establish and survey a leveling line across a growing fold in Quaternary gravel above an area of abundant aftershocks of the 28 June 1992 Landers 1992 earthquake (M=7.3); and 4) resurvey of all of our trilateration arrays established across surface ruptures related to the 28 June 1992 Landers earthquake to search for continued afterslip. We also resurveyed 20 leveling arrays and 5 trilateration arrays, and we spent several days in the 1994 Northridge earthquake area searching futily for surface ruptures of tectonic origin that might yield measurements of post seismic slip.

RESULTS

1) We established and surveyed a 2 km-long leveling line across the Sierra Madre frontal fault at the mouth of Big Tujunga Wash in Sunland. The line consists of 28 permanent bench marks. The position of this array is critical to understanding the mechanics of the fault in its future surface rupture events, because it is located at the boundary between the San Fernando and Sunland-Tujunga segments of the fault. Its addition to our growing galaxy of nearfield leveling lines in southern California enhances our coverage of the Sierra Madre frontal fault. Indeed, we also resurveyed our other lines across fault in 1994 following the 1994 Northridge earthquake and detected no significant vertical height changes within the lines.

2) We retrilaterated and releveled the geodetic array of 20 bench marks that the California Division of Mines and Geology established across the Cucumonga fault in 1975. Whereas the leveling revealed one bench mark, located on a power stanchion, had a height change of 10 mm in 19 years, the heights of all others had not changed more than 2 mm in the same time (Fig. 1). A permissive case may be made that the height difference increased 4 mm across one of the main and youthful fault traces, but it is hazardous to assert that the height change is tectonic, let alone to postulate its cause. Every line length that we measured with a Wild TC2000 total station distance meter increased in almost direct proportion to their length, when compared to CDMG measurements made with a Tellurometer. We have no reason to doubt the TC2000 measurements, because the instrument was checked and adjusted by the manufacturer the day before the resurvey, and it has always yielded comparable results when tested against competing instruments (e.g., Sylvester, et al., 1993). Similarly, we lack any reason to doubt the Tellurometer data for much the same reasons. We are temporarily baffled, because if the length differences were real and tectonic, rather than nontectonic or surveying blunders, then we should have expected that the fault crossing lines would have shortened, and the fault-parallel lines should have remained unchanged. We suspect some undetected reflector constant is the culprit for our inability to analyze critically the results of the two trilateration surveys. Judging solely from the leveling results, I concluded that displacement has *not* occurred across faults in the Day Canyon segment of the Sierra frontal fault zone since 1975.

3) We placed a 3 km-long, northeast-trending line of 56 permanent bench marks across an anticline in the center of the Nebo 7 1/2' quadrangle, 5 km northwest of Barstow in the Mojave Desert. The

anticline, whose surficial limbs of Quaternary gravel dip 45°, is situated over a robust, isolated zone of small to moderate magnitude earthquakes that commenced and persisted after the 1992 Landers earthquake. The anticline probably represents a fault propagation fold over a thrust fault at the end of one of the northwest-striking strands of the Calico fault whose surface trace lies one kilometer east of the leveling line. Future repeated surveys, compared to the tectonic first order survey acquired in summer 1994 ought to reveal when and how fast the fold is growing, if at all. Judging from the fold growth history of the youthful Ventura Avenue anticline (Rockwell et al., 1988), one may postulate that the Nebo fold ought to grow slowly now relative to its initial growth that has already tilted the limbs 45°.

4. We observed no afterslip during 1994 (or 1993) within any of our arrays across the surface ruptures of the Landers earthquake (Sylvester, 1993), even in the array across the Burnt Mountain fault, south of Yucca Valley. That array accumulated nearly 45 mm of afterslip in the time from five days after the earthquake to the middle of summer 1993, but it ceased completely as of January 1994

REPORTS PUBLISHED

Sylvester, A. G., in press. Nearfield vertical displacement in the creeping segment of the San Andreas fault, central California, 1975 to 1994. Tectonophysics.

COSEISMIC(?) RIGHT-LATERAL STRIKE SLIP IN EASTERNMOST VENTURA BASIN FOLLOWING THE 1994 NORTHRIDGE EARTHQUAKE

In our quest to measure post seismic slip, we searched for surface ruptures of tectonic origin in the days following the 17 January 1994 Northridge earthquake. Of those we saw, save one, we concluded with Ponti et al., (1994) that all could be adequately explained by nontectonic mechanisms. About 8 km west of the junction of Hwy 126 with I-5, however, about 3 km north of Potrero Canyon, and 100 m north of Hwy 126 at the mouth of San Martinez Grande Canyon, Aaron Martin (ICS-UCSB) found a zone of fractures on 23 January. We looked at them on February 6 and observed a 1 m-wide zone of left-stepping, en echelon fractures striking east-west that locally and clearly displayed unequivocal right-lateral offsets of 10 cm. The fracture zone cut the alluvial fan at the mouth of the canyon. From the canyon we traced the zone of fractures about 250 m each way where it was present at the base of a sharp break in slope that we presumed was the ancient river bank, now enhanced and steepened by the farmer's bulldozer. On subsequent reflection, we regard the break in slope as a previously unmapped, degraded fault scarp. West of the canyon the zone extended at a low angle into Hwy 126 which had been freshly patched, precluding tracing the fractures farther or determining their offsets. To the east the zone followed the base of an abrupt and steep slope at the base of which the fractures cut a buried concrete irrigation pipe so effectively that the pipe was rendered useless, subsequently dug up, and completely replaced. We duly reported the presence of the fracture zone to the appropriate USGS and CDMG field investigators, but alas, the fractures were obliterated by heavy rain before the mappers could inspect and map them more systematically than we. We concluded that the fractures were tectonic, even though we tried hard to make a case for an origin by lurching of the farmer's field toward the Santa Clara River, It is noteworthy that the right lateral sense of slip supports the observation (Donnellan et al , 1994) of 40 mm postseismic right lateral displacements in the Ventura basin.

References Cited

Donnellan, A., G. A. Lyzenga, and B. H. Hager, 1994. GPS measurement of postseismic deformation associated with the Northridge earthquake. EOS, Trans. Am. Geophys. Un. 74 (44), p. 166.

Ponti, D. J., D. P. Schwartz, S. Hecker, T. E. Fumal, 1994. Ground deformation in Potrero Canyon and Granada Hills: Keys to recurrence of Northridge-type blind-thrust earthquakes? EOS, Trans. Am. Geophys. Un. 74 (44), p. 176.

Rockwell, T. K., E. A. Keller, and G. R. Dembroff, 1988. Quaternary rate of folding of the Ventura Avenue anticline, western Transverse Ranges, southern California. Geological Society of America Bulletin 100, 850-858.

Sylvester, A. G., 1993, Investigation of nearfield postseismic slip following the Mw 7.3 Landers earthquake sequence of 28 June 1992, California. Geophysical Research Letters 20, 1079-1082.

Sylvester, A. G., R. Bilham, M. Jackson, and S. Barrientos, 1993. Aseismic growth of Durmid Hill, southeasternmost San Andreas fault, California. Journal of Geophysical Research 98, 14,233-14243.

Figure 1. HEIGHT CHANGES -- DAY CANYON -- 1977 TO 1994

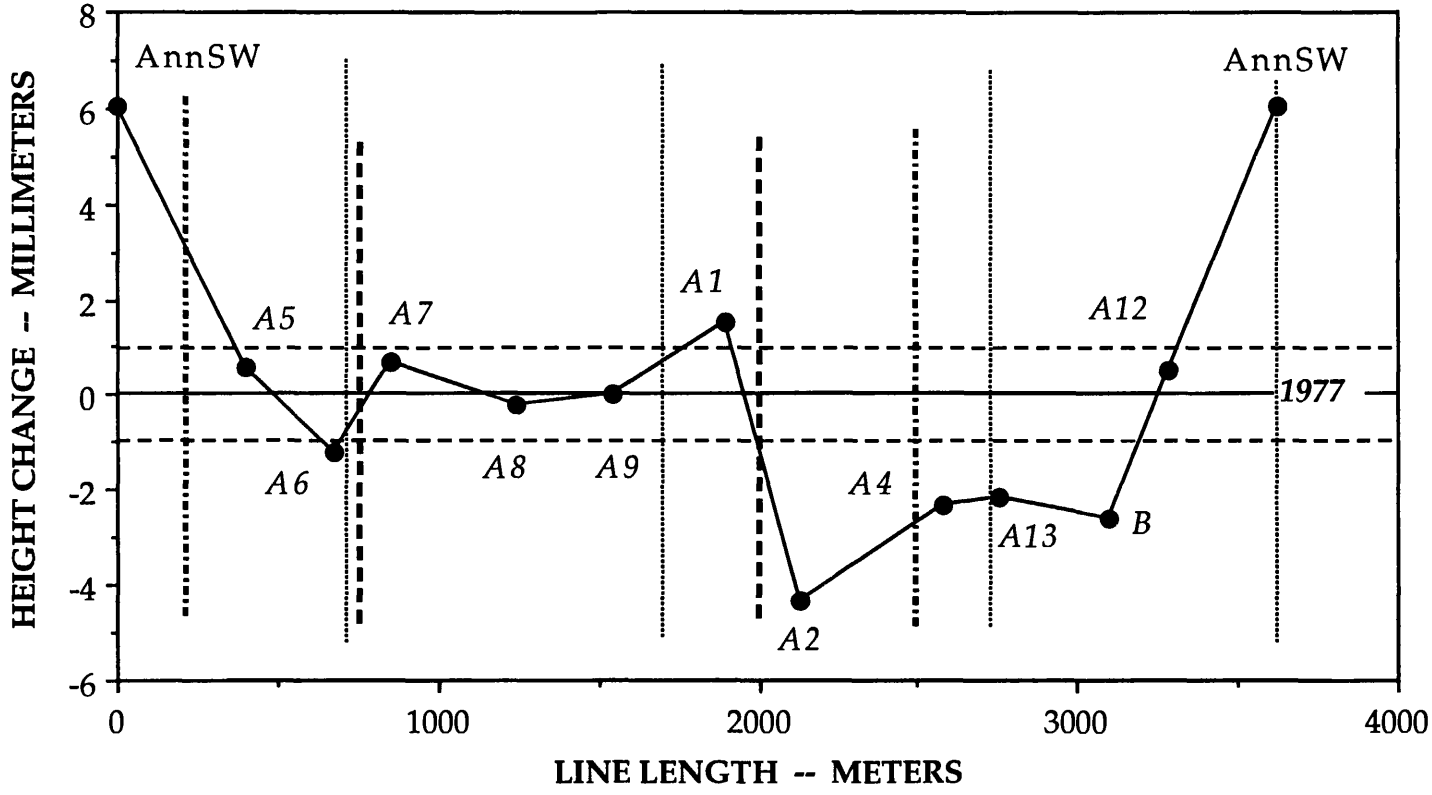

Figure 1. Height differences among permanent bench marks across Sierra Madre frontal fault system, Day Canyon, Rancho Cucumonga, from 1977 to 1994. Bench marks were established and surveyed by the California Division of Mines in Geology in 1977 as a 4-sided array having the form of an irregular parallelogram. Thus the parallelogram shape has been unfolded and depicted here as a line with the common point of the line in the array being bench mark AnnSW. Fold lines are depicted by light vertical dotted lines. Bench mark AnnSW is at the SE corner, A13 is in the SW corner, A1 is in the NW corner, and A7 is in the NE corner. Heavy dashed vertical lines are the positions of two, east-west striking faults through the array, and the pattern of the dash is the same for each fault. Bench mark A9 in the center of the east-west part of the line in the mountain block is arbitrarily held fixed, and one standard deviation of uncertainty (0.07 ppm) of bench mark heights in the 1994 survey is contained within the vertical dimension of each black dot. Horizontal dashed lines indicate the uncertainty to one standard deviation (1.0 ppm) in the 1977 survey. Bench mark AnnSW is located on the corner of a concrete power stanchion and may be unstable. The mountain side-up displacement of about 6 mm between A1 and A2 is matched by about 2 mm mountain side-up displacement between A7 and A8 across the same fault. One may say that the displacements occurred between 1977 and 1994, but it cannot be stated that the displacements are tectonic or nontectonic in origin, and it would be meaningless to assign a slip rate to this fault based on these data.

Postglacial Offset Along the Seattle Fault

1434-94-6-2467

Robert M. Thorson
Department of Geology and Geophysics, University of Connecticut
354 Mansfield Road, Storrs CT 06269
Phone, 203-486-1396; FAX 203-486-1383; EM thorson@uconnvm.uconn.edu
Program Element II.5

Investigations

Our major objective was to re-examine and verify the Pleistocene shoreline features previously used to estimate surface displacements across the Seattle Fault, and to search for additional geological features that would further constrain the neotectonic displacements suggested by earlier studies. We focussed on the Kitsap and Olympic Peninsulas north of Belfair and south of the Hood Canal bridge, with a particular interest in Bainbridge Island and the Poulsbo area. Our work proceeded in the following stages: (1) We searched for candidate sites (coastal terraces, spits, deltas, etc.) by applying geomorphic criteria to existing geological and topographic maps. (2) We examined available aerial photographic coverage on file at the Map Library of the University of Washington, and at the Washington State Department of Ecology, concentrating on false-color images at the scale of 1:12,000, and on shoreline-survey oblique color coastal photos at variable scales. (3) We visited 26 candidate sites in the field, inspecting the surface for distinctive lanforms, searching for exposures, hand-drilling shallow boreholes, and surveying their elevations using the nearest available vertical datum. (4) We revisited all of the delta localities (n=14) used to establish the uplift pattern north of Tacoma. At four of these localities (Belfair, Eldon, Fulton Creek, Brinnon) we attempted to trace the former lake stage away from the large deltas onto the adjacent forested slopes. (5) In an attempt to find additional evidence for subtle water-plane features, we performed a continuous traverse of Point Monroe, Bainbridge Island, from 100 meters elevation to sea level. We selected this area because conditions for the creation and recognition of paleo-shoreline features were ideal.

Owing to the expected difficulty of finding additional, recessional paleo-shoreline features, we extended our investigations to include an additional glaciolacustrine datum (the top of the Lawton Clay), which was protected from glacial erosion by the overlying advance outwash (Esperance Sand). Using borehole data from the archive at the Seattle Engineering Department, we attempted to characterize the floor of this paleo-lake with enough resolution in order to recognize surface offsets of tectonic origin. We restricted our search to the eastern side of Eliot Bay and Puget Sound within the City of Seattle, concentrating on the areas near West Point and Alki Point

We inspected all of the available drilling records (>1000), selecting 263 for additional analysis. For each of these records, the elevation (or range thereof) of the lithologic contact was identified idependently of location and elevation, and ranked according to its quality. Filtering the data set for quality control produced a residual of 136 points where all three coordinates (X,Y,Z) were sufficiently well constrained to be useful in our analyses.

Results

Our most significant result was the independent confirmation of the general glacioisostatic record developed more than ten years ago from regional evidence. Such confirmation, based on the discovery of geological features at two additional field localties, upgrades the utility of the Pleistocene shoreline method for neotectonic investigations. The first new locality at Squamish Harbor contained field evidence for a transgressive beach associated with Glacial Lake Bretz. This transgressive (onlap) sequence lies unconformably above older lacustrine deltas, and requires, paradoxically, that the water levels in Puget Sound were rising during a time of rapid isostatic uplift. This could occur only if glacially impounded meltwater drained over an uplifting spillway in the direction of the tilt gradient (northward). The second critical locality is a 200-m long roadcut along Highway #3 near Lofall that bisects a sandy depositional terrace near the mouth of Big Valley, a north draining spillway that regulated the level of Lake Bretz west of Hood Canal. Faults, fluidization pipes, and liquefied horizons in the exposure require an episode of pervasive sediment disturbance caused by the upward escape of overpressured water that occurred during the transition to a lower lake level but prior to subsequent stablization of the shoreline, possibly also transgressive in character. Features from both localities indicate that a substantial drop in water levels was associated with a switch to northerly drainage when the ice front remained active, and when isostatic uplift was rapid. This stratigraphic evidence is supported by the altitudinal zontation of dozens of small valleys cut within the Esperance Sand, and which appear to have been caused by the headward propagation of gullies associated with transient, accelerated groundwater flow during the lake drawdown.

All of the remaining candidate sites (n=14) were investigated in the field. Although none were exposed clearly enough to exhibit diagnostic sedimentary structures, their morphological similarity to the Lofall exposure, their similar apparent age, their broad range in elevation (20-40 m), and their gradational boundaries suggest that most are local accumulations of sand that were derived from the former lake margin, and reworked to a position below wave base during the transition from the high to low lake levels, a fall of approximately 64 m. This interpretation is supported by the regional distribution of the terraces, which are most extensive where the magnitude of lake-level lowering reached a maximum. Although we had originally hoped that each terrace would provide an elevation constraint for uplift, the scatter

in elevations and the apparent absence of a meaningful pattern precluded their use as neotectonic reference points, our original objective.

During our reconnaissance, we discovered a new delta control point near the head of Lynch Cove in the southern part of the project area that exposed a topset-foreset contact similar to, but less dramatic than, those used to reconstruct the dominant isostatic pattern. Its contact elevation of 20.4 m +/- 2 m (relative to the Lake Bretz datum) lies directly on the uplift trend between the Belfair and McKenna Falls deltas, reinforcing the previous interpretation of differential uplift near Bremerton, and apparently precluding significant, non-isostatic, localized displacements crossing Lynch Cove.

Arguably, the most potentially important result of our investigation involves extension of the water-plane method to the lake floor through use of the Lawton Clay/Esperance Sand contact. The sources of error in such an analysis are many, and involve the original field measurements, accurate location of the borehole in the field, accurate plotting by public works, the correct stratigraphic interpretation, unrecognized displacements caused by landsliding, topographic irregularities on the former lake floor, (especially along its bounding edge), differential compaction and/or crustal dislocation during the loading hemicycle, and finally, postglacial displacements relevant to neotectonism. Our preliminary conclusions are: (1) much of the variance in elevation of the datum is strongly correlated with surface elevation (r=0.83), which, in turn, is correlated with pre-Vashon surface elevation. (2) The contact, like the accordant pattern of hilltops, is generally horizontal, indicating that isostatic adjustments post-dated lake formation, and are fully recovered. (3) Local variability in the attitude of the contact is real, substantial, and probably higher than for recessional points, suggesting that block-tilting (and/or folding) occurred as a direct consequence of loading. The implication of these preliminary results is that ice-sheet loading obscures the effects of "tectonic" deformation to such a degree that it minimizes the neotectonic value of Quaternary deposits older than the last ice advance.

Reports Published

Thorson, R.M., 1994 [*abstract*] Obscuring the dichotomy between Quaternary tectonics and glaciology in the Puget Sound-Georgia Strait Depression. GSA Annual Meeting, Abstracts with Programs, Seattle, WA, p. 187.

In preparation:

Thorson R.M., and Swaim, M., A Transgressive Pleistocene beach in Puget Sound. *Quaternary Research.*

Thorson, R.M., The role of wet-based ice sheets in modulating long-term tectonic stresses.*Geology*.

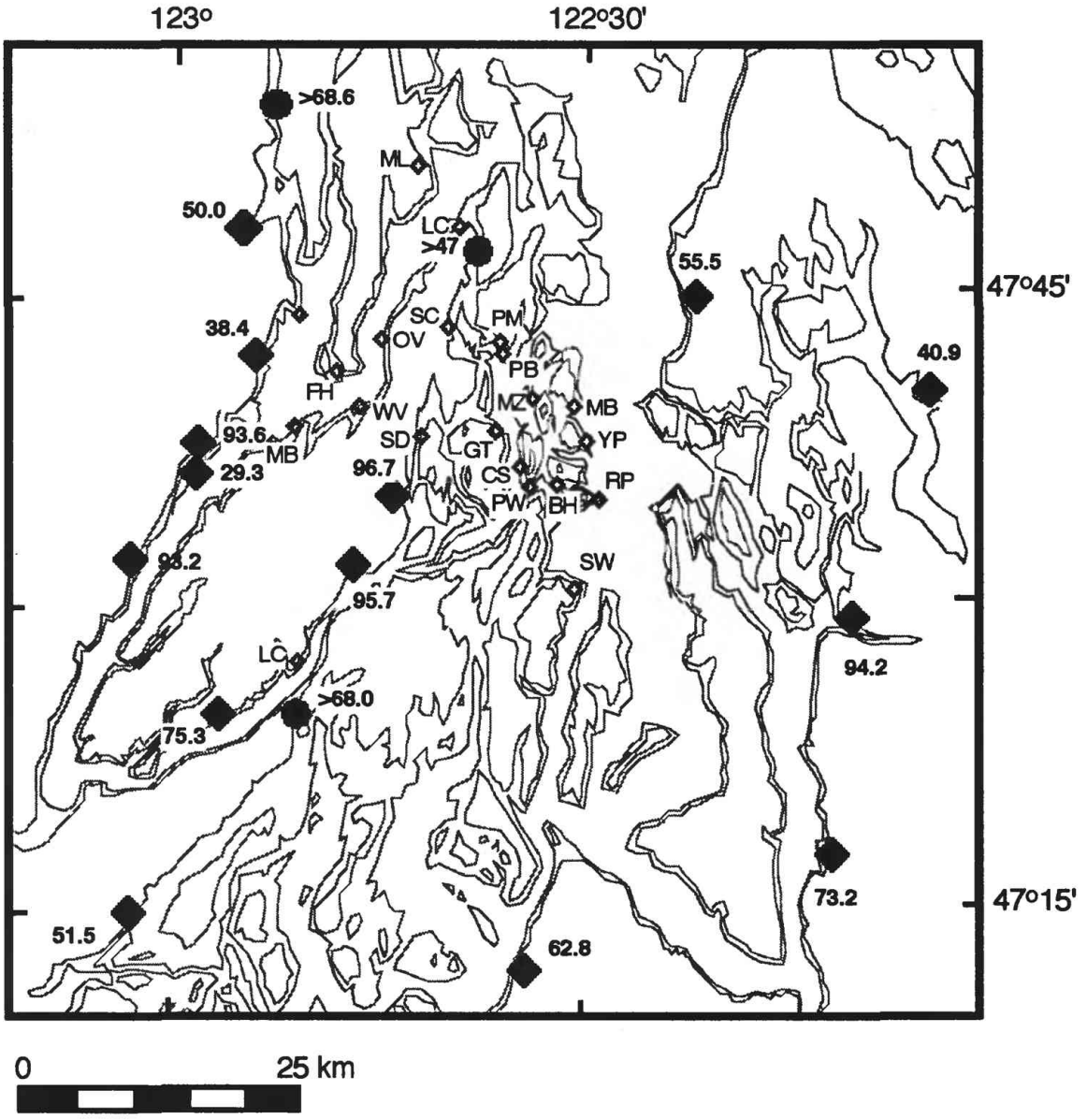

Figure 1. Base Map of study area showing location of lacustrine control points from Thorson (1989) normalized to the Lake Bretz datum (large squares, elevation in meters) and additional control points examined during this study (small open squares; abbreviations not described). Shorelines shown are those of Lake Russell, Lake Bretz, and present.

Basic Earthquake Hazards Studies in Hawaii

Award No. 1434-94-G-2488
Clifford H. Thurber and Clifford G. Munson
Department of Geology and Geophysics
University of Wisconsin-Madison
Madison, WI 53706
608-262-6027, FAX 608-262-0693, email clifft@geology.wisc.edu
Program Element NI

Investigations undertaken

We are analyzing 3-component digital seismic data recorded by the 1990 PASSCAL experiment (Project ALOHA) and the USGS strong motion array to investigate attenuation, peak ground acceleration (PGA), and site response characteristics on the Island of Hawaii. At present, knowledge of attenuation, PGA, and site response in Hawaii is quite limited. The current project directly addresses this knowledge gap. We model attenuation using the approach of Anderson, Hough, and coworkers, with a site component and a distance-dependent path component for the spectral decay parameter We are employing a new nonlinear least squares method that includes estimates of parameter uncertainties to determine "optimal" and "constrained" estimates of the spectral decay parameter (κ) using microearthquakes in south-central Hawaii (magnitude up to about 3) from the PASSCAL data and larger earthquakes (moment magnitude up to 6.8) island-wide from USGS strong motion data. We are also working to derive a PGA versus distance and magnitude relation for Hawaii using strong motion data and the multiple-regression approach of Joyner and Boore [1993, 1994]. The regression model includes a site term for strong motion stations on ash. The third component of our work involves multiple methods for estimating site response, including shallow seismic profiling, spectral ratios, a generalization of Nakamura's horizontal-to-vertical spectral ratio method, and microearthquake receiver function modeling. The result of these efforts will be the first thorough analysis of attenuation, peak ground acceleration, and site response in Hawaii for the purposes of earthquake hazard evaluation.

Results

Our derived values for the spectral decay parameter (κ) for Hawaii are plotted as a function of epicentral distance in Figure 1, along with values for Imperial Valley and Pinyon Flat from Anderson [1986]. Our values for κ overlap those for Imperial Valley. In particular, the site terms for Hawaii and Imperial Valley are comparable and are significantly greater than that for Pinyon Flat. However, unlike the Imperial Valley values, the Hawaii κ values do not show a significant increase with increasing epicentral distance. This implies that the bulk of the attenuation takes place in the near surface. This finding is consistent with the results of Munson et al. [1993] that the anisotropy causing observed shear wave splitting in southern Hawaii is also mainly restricted to the near surface (uppermost 4 km or less). The high attenuation values are also consistent with the strong shear wave velocity anisotropy observed [Munson et al., 1993].

We derive a horizontal PGA predictive equation for the island of Hawaii using the Joyner and Boore [1993 and 1994] two-step linear regression method. Our data set consists of 56 horizontal PGA values from 13 events (Figure 2) including six subevents of the 1975 Kalapana main shock (moment magnitudes M_w = 6.1, 6.1, 6.1, 6.4, 6.8, and 6.6), the 1983 Kaoiki event (M_w = 6.5), and two 1989 South Flank subevents (M_w = 6.1 and 6.0). Epicentral distances vary from 0 to 98 km and event depths vary from 8 to 16 km. We use records from instruments triggered before the S-wave arrival. Moment magnitudes and additional earthquake source parameters are determined by a theoretical fit to the observed Fourier spectra using the method of Anderson and Humphrey [1991]. Our resulting equation is

$$\log PGA = 0.910 + 0.286\,(M_w - 6) - 6.792 \times 10^{-3}\, r - \log r + 0.422\, G_{HC}$$

where PGA is in units of g, $r = (d^2 + h^2)^{1/2}$ with d = fault distance and h = average depth, and G_{HC} is 1 for Hamakua Coast ash sites and 0 otherwise. The standard deviation for our attenuation curve ($\sigma_{\log Y} = 0.182$) is comparable to that of Joyner and Boore [1981] ($\sigma_{\log Y} = 0.260$) and Boore et al. [1993] ($\sigma_{\log Y} = 0.205$). Klein [1994] modifies the Boore et al. [1993] attenuation curve to approximately fit the Hawaii PGA data by shifting the curve upwards by a factor of 1.2. Our attenuation curve decays more gradually than this modified Boore attenuation curve for distances less than 20 km while beyond 20 km our curve decays much more rapidly. Figure 3 (a to c) shows the fit of our curve to data from 3 events and (d) a comparison of our curve to those of Boore and Klein (that is, modified Boore). Three Quaternary ash sites on the Hamakua coast display horizontal PGA amplifications as high as 4.8 relative to lava sites, generating a significant site term in our attenuation curve.

Work on site response is in progress. We are taking a multi-faceted approach to the problem of site response estimation. Pseudo-acceleration response spectra (PARS) for three events are shown in Figure 4 (a to c) along with a summary plot in Figure 4d comparing average spectra on lava to that on two ash areas (Hamakua Coast and Wood Valley). Site response variations are clearly substantial, especially the short period amplifications at Hamakua Coast sites, as discussed above. Ongoing efforts include using a generalization of Nakamura's method (horizontal to vertical single-station spectral ratios), microearthquake receiver functions, and forward modeling of spectra to investigate the role of the very shallow structure in site response. Shallow seismic profiling at strong motion station sites was carried out in the summer of 1994 to test these estimates of shallow structure. Initial results indicate a good correspondence between profile structure and prior estimates of the structure.

References

Anderson, J. G., Implication of attenuation for studies of the earthquake source, in Earthquake Source Mechanics, AGU Monograph 37, 311-318, 1986.

Anderson, J. G. and J. R. Humphrey, A least-squares method for objective determination of earthquake source parameters, Seismol. Res. Lett. 62, 201-209, 1991.

Boore, D. M., W. B. Joyner, and T. E. Fumal, Estimation of response spectra and peak acceleration from western North American earthquakes: An interim report, USGS Open File Rep. 93-509, 72 pp., 1993.

Joyner, W. B. and D. M. Boore, Peak horizontal acceleration and velocity from strong-motion records including records from the 1979 Imperial Valley, California earthquake, Bull Seismol. Soc. Am 71, 2011-2038, 1981.

Joyner, W. B. and D. M. Boore, Methods for regression analysis of strong-motion data, Bull Seismol. Soc. Am 83, 469-487, 1993.

Joyner, W. B. and D. M. Boore, Methods for regression analysis of strong-motion data, ERRATA, Bull Seismol. Soc. Am 84, 955-956, 1994.

Klein, F. W., Seismic hazards at Kilauea and Mauna Loa volcanoes, Hawaii, USGS Open File Rep. 94-216, 94 pp., 1994.

Munson, C. G., C. H. Thurber, and Y. Li, Observations of shear wave splitting on the southeast flank of Mauna Loa volcano, Hawaii, Geophys. Res. Lett. 20, 1139-1142, 1993.

Reports Published:

Munson, C. G., and C. H. Thurber, Spectral modeling of Hawaiian earthquakes: source parameters, attenuation, and site response, Seismol. Res. Lett. 65, 34, 1994.

Munson, C. G., C. H. Thurber, and A. D'Silva, A peak-ground-acceleration predictive equation for Hawaii, EOS, Trans. Am. Geophys. Un. Suppl. 75, 448, 1994.

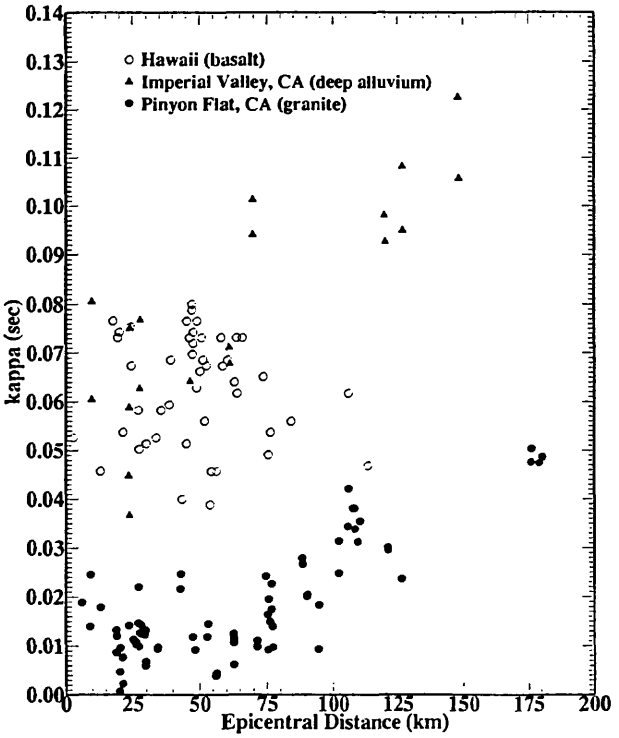

Figure 1. Spectral decay parameter (κ) values as a function of distance for Hawaii (open circles) compared to Imperial Valley (triangles) and Pinyon Flat (filled circle) values from Anderson [1986]. The Hawaii values substantially overlap the Imperial Valley values.

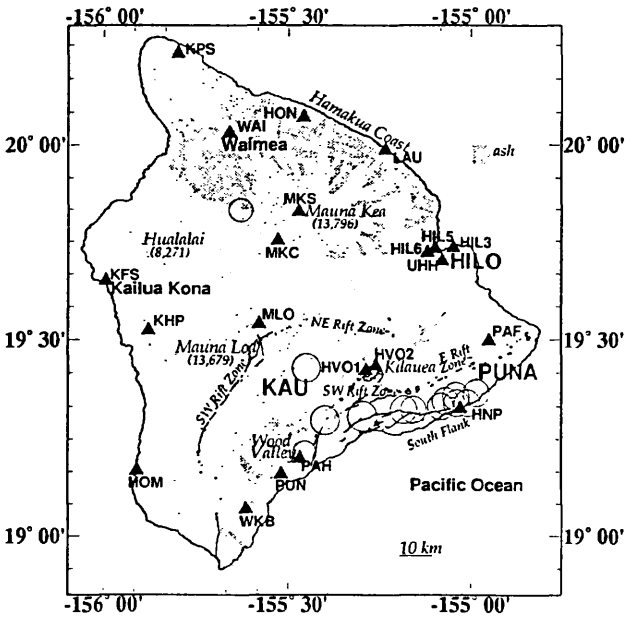

Figure 2. Location map for Hawaii showing events (open circles) and strong-motion stations (solid triangles) used in the PGA analysis. Areas of significant ash thickness are shaded.

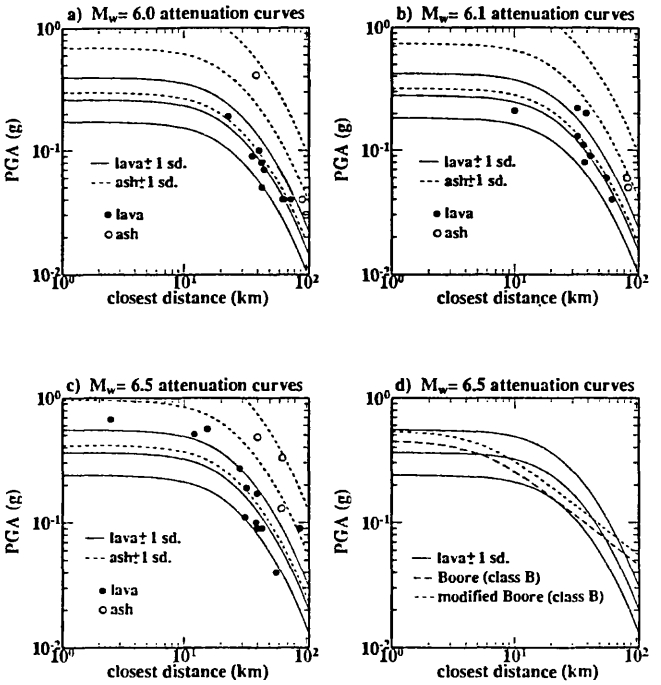

Figure 3. (a-c) Fit of data from 3 events to our PGA versus distance curves, showing both lava (solid) and ash (dashed/open) predicted and observed values. (d) Comparison of our PGA curve to the Boore and Klein (modified Boore) curves for $M_W = 6.5$.

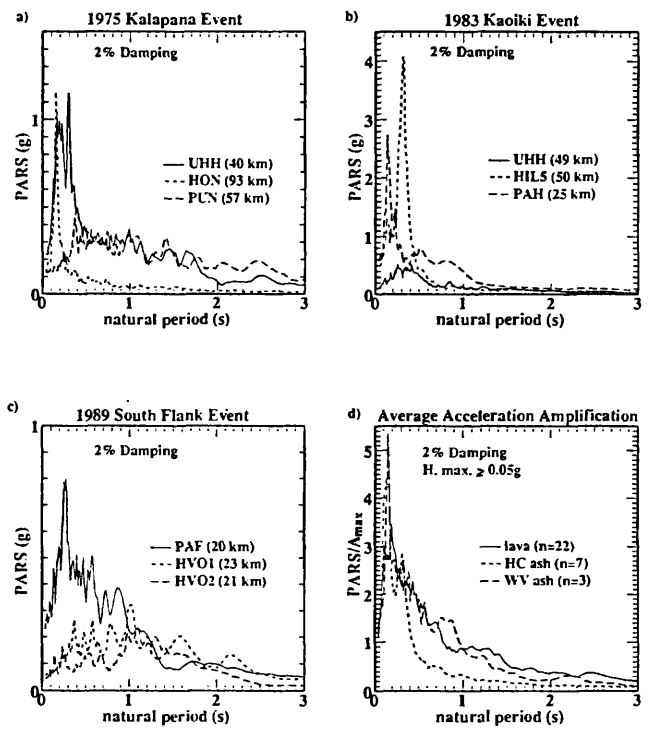

Figure 4. (a-c) Pseudo-acceleration response spectra (PARS) for three events, and (d) summary plot comparing average spectra on lava to that on two ash areas (Hamakua Coast and Wood Valley).

CHARACTERIZING SEISMICITY AND ITS GEOLOGICAL ASSOCIATION IN NORTHEASTERN NORTH AMERICA WITH RELATIVE LOCATION AND EMPIRICAL GREEN'S FUNCTIONS

Contract no. 1434-94-G-2421

M. Nafi Toksöz
Massachusetts Institute of Technology
Earth Resources Laboratory
42 Carleton Street
Cambridge, Massachusetts 02142
(617)-253-7852
FAX: (617)-253-6385
email: nafi@erl.mit.edu
Program Element II.2

1. INVESTIGATIONS

The goal of this study is to analyze the seismograms of earthquakes in the Charlevoix Seismic Zone (CSZ) of Quebec in order to characterize faulting in that region. Two approaches are used to achieve this goal. In one approach, the Empirical Green's Function (EGF) method is applied to earthquake doublets and multiplets in the CSZ to derive a relative source time function (STF) for the larger events of earthquake pairs (*e.g.*, Hartzell, 1978; Mueller, 1985). The STF is analyzed to determine source parameters (*e.g*, Li and Thurber, 1988; Mori and Frankel, 1990) including seismic moment, fault length, stress drop, rupture directivity, and rupture velocity. The rupture directivity is combined with the P focal mechanism of the larger event of a pair to ascertain which nodal plane is the probable fault plane (*e.g.*, Frankel *et al.*, 1986; Mori, 1993). Waveform correlation and a relative event location technique (*e.g.*, Jordan and Sverdrup, 1981; Poupinet *et al.*, 1984; Ito, 1985) are employed to identify the doublets and multiplets appropriate for the EGF analysis. In a second approach, the waveform correlation and relative event location methods are applied to waveform data to relocate seismicity in the CSZ. The purpose of the relocation effort is to search for well defined spatial patterns of hypocenters which may delineate the orientation and dimensions of active faults.

CHARLEVOIX SEISMIC ZONE AND NETWORK DATA

The Charlevoix Seismic Zone (CSZ) is defined as a 90 x 30 km rectangle located along the St. Lawrence River (Figure 1a) in southern Quebec and is among the most seismically active areas in eastern North America (Buchbinder *et al.*, 1988). Historically, the CSZ has been the location of several large earthquakes (Smith, 1962). The largest instrumentally recorded earthquake of this group occurred on March 1, 1925 with m_b = 6.5 (Stevens, 1980; Ebel *et al.*, 1986; Bent, 1992). The latest potentially damaging earthquake (m_b = 5) occurred on August 19, 1979 (Hasegawa and Wetmiller, 1980).

The waveform data used in this study were recorded by the Charlevoix Telemetered Network (CLTN) operated by the Canadian Geological Survey (CGS). The Geophysics Division of the CGS provided access to their database and the computer programs necessary to convert the waveform data from their in-house format to SAC. The CLTN consists of six three-component stations located in groups of three each along the northwest and southeast shorelines of the St. Lawrence River (Figure 1a). These stations are situated parallel to the general northeasterly strike and bound the seismicity of the CSZ (Buchbinder *et al.*, 1988). The CLTN is a short-period local network which was modernized in November 1987 to include digital recording at a rate of 80 sps and three-component instruments with automatic gain control to insure a wide dynamic range of 126 dB (Munro, personal communication). The wide dynamic range of the instrument allows recording of seismic waveforms of M0-5 earthquakes on scale at local distances and is especially suitable for the EGF analysis.

2. RESULTS

Eleven earthquakes were analyzed using the EGF method. Applying the cross-correlation analysis and relative event location technique to digital waveform data from the CLTN, we identified two multiplets and two doublets in the CSZ (Figure 1b) with M = 0.2 to 4.4. Previously, Wetmiller and Adams (1990) had identified two earthquakes (M_{bLg} = 4.3, 4.4) as a doublet, both of which occurred in March 1989 about 47 hours apart. Since the M_{bLg} 4.3 event was followed by two smaller aftershocks with similar locations, we defined this group of four events as a multiplet. Waveforms of the four events with magnitudes ranging from 0.2 to 4.4 show a striking similarity, with the maximum amplitude of the largest event exceeding that of the smallest by a factor of about 1000. The waveform similarity suggests that the multiplet has hypocenters very close to each other and very similar focal mechanisms. In addition to CLTN data, P first motion data from two regional networks (Figure 1a), the Eastern Canada Telemetered Network (ECTN, operated by the Canadian Geological Survey) and the New England Seismic Network (NESN, jointly operated by the Weston Observatory of Boston College and the Earth Resources Laboratory of MIT), were used to constrain the P focal mechanisms for the four largest earthquakes ($M_{bLg} \geq 3.3$) of the four groups of events in the study. SH focal mechanisms were also generated for these four events, which were found to be completely consistent with the P focal mechanisms. To insure the larger earthquakes and the EGF events in each group (Figure 1b) had similar focal mechanisms, we checked the P and SH polarities for the eleven earthquakes with the CLTN data, and found the P and SH polarities for events in the same group were the same with only one exception. The P wave polarity of the 920310 event (see Figure 4), which is projected close to one of the P wave nodal planes for station A21, differed from those of the two small aftershocks, reflecting slight differences in the focal mechanisms of the mainshock and aftershocks.

Figure 2 illustrates the EGF deconvolution procedure which we used to extract the relative STFs for larger events of the doublets and multiplets. SH waveforms recorded at station A61 are displayed for the three events in one multiplet (M3.3, M1.6 and M0.2) with spatial separations of less than 250 m (multiplet 3 in inset of Figure 1b) and a similar focal mechanism. The seismogram of the smallest event was used as the EGF and deconvolved from those of the two larger events to obtain the STFs for the larger earthquakes. Three-component S waveforms of the EGF events recorded at four stations were deconvolved from those of the larger events of earthquake pairs to extract the STFs for the larger events. The STFs obtained with different components at the same station are very similar and have only slight differences, suggesting that the assumption of a similar focal mechanism for the two events in the pair is correct. We summed the STFs extracted with three component data at a station and used the stack as an average estimate of the STF at that station. The procedure increases the signal-to-noise ratio for the STFs, and should average out the slight dissimilarity caused by the small differences in location and focal mechanism between the EGF event and the larger event. In the following examples, the STFs are the stacked three-component average.

SOURCE TIME FUNCTIONS AND RUPTURE DIRECTIVITY

Azimuthal variation of the pulse amplitudes and widths of the STFs provide strong evidence for the rupture directivities of five of the earthquakes with magnitudes ranging from 1.2 to 4.4. For a unilaterally propagating rupture (*e.g.*, Ben-Menahem, 1962), the source duration is narrowest in the direction of rupture propagation and widest in the opposite direction. Due to the same effect, the amplitude of the STF in the rupture direction is larger than that in the opposite direction. The poor time resolution (0.0125 s) of our data set precluded obtaining a reliable estimate of the rupture direction from the azimuthal variation of pulse width. Therefore, we used the azimuthal variation of the pulse amplitudes to estimate the rupture direction. STFs of three larger events (M4.3, M1.2 and M4.4) were retrieved using the smallest earthquake (890310-0351, M0.2) of multiplet 4 (inset in Figure 1b) as the EGF event. The STFs of each event recorded at three widely spaced stations show significant azimuthal variations (Figure 3). The amplitudes of the STF pulses for the M4.4 event increase as the azimuth increases (Figure 3d), with the smallest amplitude at station A16 and the largest amplitude at station A64. This amplitude variation indicates that the rupture of the M4.4 event (mechanism on lower right of Figure 3a) is towards station A64 (Figure 3a). For the M4.3

earthquake (mechanism on upper left of Figure 3a), the largest pulse amplitude and the narrowest pulse width of the STF is recorded at station A61 (Figure 3b) and indicates a rupture direction towards the west (Figure 3a). We even observed rupture directivity for the M1.2 event. The amplitudes of the STF pulses observed at stations A61 and A64 are larger than that for station A16 by a factor of 2 (Figure 3c), suggesting that the rupture direction of the earthquake is towards the northwest between stations A61 and A64 (Figure 3a). The rupture velocity for these events ranges from $0.5V_S$ to $0.7V_S$. The rupture directions for the M4.3, M1.2 and M4.4 earthquakes are estimated to be 290°, 300° and 320°, respectively, suggesting that the rupture direction of the earthquake multiplet rotated about 30° clockwise. However, the reason for this apparent rotation of the rupture direction is not yet clear. The rupture directions of the three events are also consistent with the spatial trend of the relative locations of events in multiplet 4 (inset of Figure 1b). Based on the rupture directions and the focal mechanisms of the M4.3 and M4.4 events, we determined that the east-dipping nodal planes were the actual fault planes of the two earthquakes and marked the rupture directions with arrows on these fault planes (Figure 3a). Wetmiller and Adams (1990) also selected the east-dipping planes as favorable fault planes for these events based on seismicity distribution and geological information.

STFs of the 920310-0545 (M3.3) and the 920314-2128 (M1.6) events were extracted from seismic recordings at four stations (Figure 4a). S waveforms of the smallest event (920311-0120, M0.2) in the multiplet were used as the EGFs. The STF of the M1.6 earthquake is a simple pulse with a duration of about 0.05 s, and reveals no rupture directivity as evidenced by the lack of pulse amplitude and width variation at the different stations (Figure 4b). In contrast, the STF of the M3.3 event has two distinct peaks at three of the four stations, suggesting two episodes of rupture with a total duration of about 0.15 s (Figure 4c). Since the M1.6 event is simple with no rupture directivity, we substituted its waveforms for those of the M0.2 event as the EGFs. The STFs of the M3.3 earthquake show no change in relative pulse shape among the four stations (Figure 4d) despite changing the EGF event. This example demonstrates that the STF of a larger event can be successfully retrieved so long as one or more suitable EGF events can be found. Although the STFs of the M3.3 earthquake indicate a rupture direction approximately east-west, the equation used to estimate the rupture direction, by fitting the amplitudes of the STFs to a straight line, is not appropriate for a double event. Therefore, we have to use other information to constrain the rupture direction and the actual fault plane. The relative locations of the two subevents (3-1a and 3-1b of multiplet 3 in the inset of Figure 1b) and the focal mechanism of the first subevent suggest rupturing towards the east with the west-dipping plane being the preferred fault plane. We marked the fault plane with an arrow on the focal mechanism solution of the first subevent in Figure 4a. In this study we have found that even a small earthquake (M~3) may exhibit rupture complexity. The rupture complexities of microearthquakes in Miramichi, Canada (M=3-4.1) and in Reading, Pennsylvinia (January 16, 1994, M=4.6) have also been observed from retrieved relative source time functions (Li *et al.*, 1994).

SOURCE PARAMETERS

We estimated the source parameters for the larger shocks of the doublets and multiplets in the CSZ. The STFs reveal that six of the events are simple with a single pulse ranging in source duration from 0.05 to 0.2 s. One earthquake (Figure 4c) appears to be a double event. The azimuthal variation in amplitude observed in the STFs indicate definite rupture directions for five of the events, including one with magnitude only 1.2. The rupture velocities derived for these events vary from $0.5V_S$ to $0.7V_S$. The source parameters derived from the STFs (seismic moment, fault radius, and stress drop) are summarized in Table 1. For M3.3 to 4.4 events (M_O = 1.4×10^{20} to 5.3×10^{21} dyne-cm), the stress drop estimates range from 24 to 90 bars and the fault radii are from 120 to 330 m. For smaller events with magnitudes 1.2 to 1.8 (M_O = 3.5×10^{18} to 7.2×10^{18} dyne-cm) and the stress drops fall to 2 to 3 bars. Because of the relatively short duration of the STFs of the events and the cubic dependence of the stress drop on the rise time, a small error in the rise time measurement will result in a very large error in the estimate of stress drop (Table 1), especially for those events with smaller magnitudes and extremely short durations (*i.e.*, M1.2-1.8). These large errors reflect the difficulty in making accurate measurements of the stress drops for small events.

We have compared our estimates of source parameters with those obtained by other investigators for earthquakes in the CSZ (Table 1). Boatwright (1994) and Atkinson and Somerville (1994) estimated stress drops of 50 to 70 bars and fault radii of 200 to 350 m for three earthquakes in the magnitude range of 3 to 4.5. These results agree quite well with the source parameters we estimated using the EGF method. In this study we have observed an apparent stress drop increase with earthquake size, similar to some studies by other researchers on earthquakes in northeastern North America (Boatwright, 1994; Shi *et al.*, 1994). However, due to the relatively large error estimates associated with the stress drops we derived for the smaller events and the limited data set, we suggest that further investigation using waveform data of more events with better time resolution (high sampling rate) is required to verify the apparent scaling relationship between stress drop and seismic moment.

CORRELATION OF SEISMICITY WITH FAULTS

We have applied the waveform correlation analysis and relative event location technique to relocate a large number of earthquakes occurring between 1987 and 1993 in the CSZ. Preliminary work has produced good results in specific subregions of the CSZ. Figure 5 shows the improved spatial correlation of the seismicity with some mapped faults along the north shore of the St. Lawrence River after hypocenter relocation. The two northeast trending lineations of relocated hypocenters shown in Figure 5, one along the north shore of the river and the other further to the northwest, appear to be steeply dipping planar features in depth view. 3-D spatial transformations of the entire data set of relocated hypocenters (covering most of the CSZ) show two or more major planar features cutting across the dominant northeast trend of the mapped faults and extending across the river. These seismic features may define cross faults and may correlate with some of the mapped faults striking southeast in Figure 5. This work is ongoing, with more 3-D imaging planned to confirm these apparent features.

3. REFERENCES

Atkinson, G.M. and P.G. Somerville, 1994. Calibration of time history simulation methods, *Bull. Seism. Soc. Am., 84,* 400-414.

Ben-Menahem, A. (1962). Radiation of seismic body waves from a finite moving source in the earth, *J. Geophys. Res., 67,* 345-350.

Bent, A. L. (1992). A re-examination of the 1925 Charlexoix, Quebec earthquake, *Bull. Seism. Soc. Am., 82,* 2097-2113.

Boatwright, J. (1994). Regional propagation characteristics and source parameters of earthquakes in northeastern North America, *Bull. Seism. Soc. Am., 84,* 1-15.

Buchbinder, G.G.R., A. Lambert, R.D. Kurtz, D. R. Bower, F.M. Anglin, and J. Peters (1988). Twelve years of geophysical research in the Charlevoix seismic zone, *Tectonophysics, 156,* 193-224.

Ebel, J.E., P.G. Somerville and J.D. McIver (1986). A study of the source parameters of some large earthquakes of northeastern North America, *J. Geophys Res., 91,* 8231-8247.

Frankel, A., J. Fletcher, F. Vernon, L. Haar, J. Berge, T. Hanks and J. Burne (1986). Rupture characteristics and tomographic source imaging of M_L~3 earthquakes near Anza, southern California, *J. Geophys. Res., 91,* 12633-12650.

Hartzell, S. (1978). Earthquake aftershocks as Green's functions, *Geophys. Res. Lett., 5,* 1-4.

Hasegawa, H.S. and R.J. Wetmiller (1980). The Charlevoix earthquake of 19 August 1979 and its seismo-tectonic environment, *Earthquake Notes, 51,* 23-37.

Ito, A. (1985). High-resolution relative hypocenters of similar earthquakes by cross-spectral analysis method, *J. Phys. Earth, 33,* 279-294.

Jordan, T.H. and K.A. Sverdrup (1981). Teleseismic location techniques and their application to earthquake clusters in the South-Central Pacific, *Bull. Seism. Soc. Am., 71,* 1105-1130.

Li, Y., C. Doll and M.N. Toksöz (1994). Estimates of source time functions an associated parameters using the EGF method for the M=1.5 to 4.5 earthquakes in the Charlevoix, Miramichi, and New Hampshire seismic zones, *Seism. Res. Lett., 65,* 32.

Li, Y. and C.H. Thurber (1988). Source properties of two microearthquakes in Kilauea volcano, Hawaii, *Bull. Seism. Soc. Am., 78,* 1123-1132.

Mori, J. (1993). Fault plane determinations for three small earthquakes along the San Jacinto fault California: Search for cross faults, *J. Geophys. Res., 98,* 17711-17722.

Mori, J. and A. Frankel (1990). Source parameters for small events associated with the 1986 North Palm Springs, California, earthquake determined using empirical Green's functions, *Bull. Seism. Soc. Am., 80,* 278-295.

Mueller, C. (1985). Source pulse enhancement by deconvolution of an empirical Green's function, *Geophys. Res. Lett., 12,* 33-36.

Poupinet, G., W.L. Ellsworth and J. Frechet (1984). Monitoring velocity variations in the crust using earthquake doublets: An application to the Calaveras fault, California, *J. Geophys. Res., 89,* 5719-5731.

Rondot, J., 1979. Reconnaissances geologiques dans Charlevoix-Saguenay. Ministere des Richesses Naturelles, Quebec, DPV-682.

Shi, J., W.Y. Kim and P.G. Richards (1994). Estimation of seismic energy release, stress drop and determination of magnitude, for small regional earthquakes in the Northeastern U.S., *EOS, Trans., AGU, 75, no. 16,* 237.

Smith, W.E.T. (1962). Earthquakes of eastern Canada and adjacent areas 1534-1927, *Pub. Dominion Obs., 26,* 271-301.

Stevens, A. E. (1980). Reexamination of some larger La Malbaie, Quebec earthquakes (1924-1978), *Bull. Seism. Soc. Am., 70,* 529-557.

Wetmiller, R.J. and J. Adams (1990). An earthquake doublet in the Charlevoix seismic zone, Quebec, in *Current Research, Part B, Geological Survey of Canada, Paper 90-1,* 105-113.

4. PUBLICATIONS AND ABSTRACTS

Li, Y., C. Doll, Jr., W. Rodi, and M.N. Toksöz, 1994. Precise relative location of earthquakes for characterizing seismicity and its geological association in the Charlevoix Seismic Zone, Quebec, *Seism. Res. Lett., 65, SSA Abstract 201,* 60.

Li, Y., C. Doll, and M.N. Toksöz, 1994. Estimates of source time functions and associated parameters using the EGF method for the M=1.5 to 4.5 earthquakes in the Charlevoix, Miramichi, and New Hampshire seismic zones, *Seism. Res. Lett., 65,* 32.

Li , Y., C. Doll, Jr., and M.N. Toksöz, 1994. Source characterization and fault plane determinations for M_bL_g = 1.2 to 4.4 earthquakes in the Charlevoix Seismic Zone, Quebec, Canada, submitted to *Bull. Seism. Soc. Am.*

Table 3

Source parameters for earthquakes in the CSZ

Event ID	Magnitude M_N or (M_L)	M_{og} 10^{18} (dyne-cm)	M_o/M_{og}	M_o 10^{19} (dyne-cm)	rise time $\tau_{1/2}$ (ms)	radius r (m)	Stress drop $\Delta\sigma$ (bars)
890915-0216	(0.0)	1.6					
890201-0538	1.8		2.2	0.352	16.7± 7.2	96± 44	1.7 (0.6-10.9)
901102-0427	(0.5)	3.8					
901021-1338	3.3		82	31.16	25.0±12.5	143± 72	46.6 (13.7-381)
920311-0122	(0.2)	1.8					
920310-0545a	3.3		75	13.50	21.9± 6.3	125± 36	30.2 (14.2-83.3)
920310-0545b			90	16.20	25.0±12.5	143± 72	24.2 (7.1-198)
920314-2128	1.6		4	0.720	18.8± 7.2	108± 44	2.5 (0.9 -12.0)
890310-0451	(0.2)	2.0					
890309-0941	4.3		2415	483.0	50.0±12.5	286± 72	90.3 (46.1-216)
890310-0329	1.2		1.8	0.360	16.7± 7.2	96 ± 44	1.8 (0.6-11.2)
890311-0831	4.4		2651	530.2	58.3±19.1	334±109	62.3 (26.7-204)
		*	*	*	*	*	*	
March 1, 1925	m_b = 6.5	Ebel *et al.* (1986)					100 - 300
		Bent (1992)					35
August 19, 1979	m_b = 5.0	Hasegawa and Wetmiller (1980)					50
March 9, 1989	M_N = 4.3	Boatright (1994)				340	50
March 3, 1990	M_N = 3.6	Boatright (1994)				210	69
March 3, 1990	M_N = 3.6	Atkinson and Somerville (1994)					70

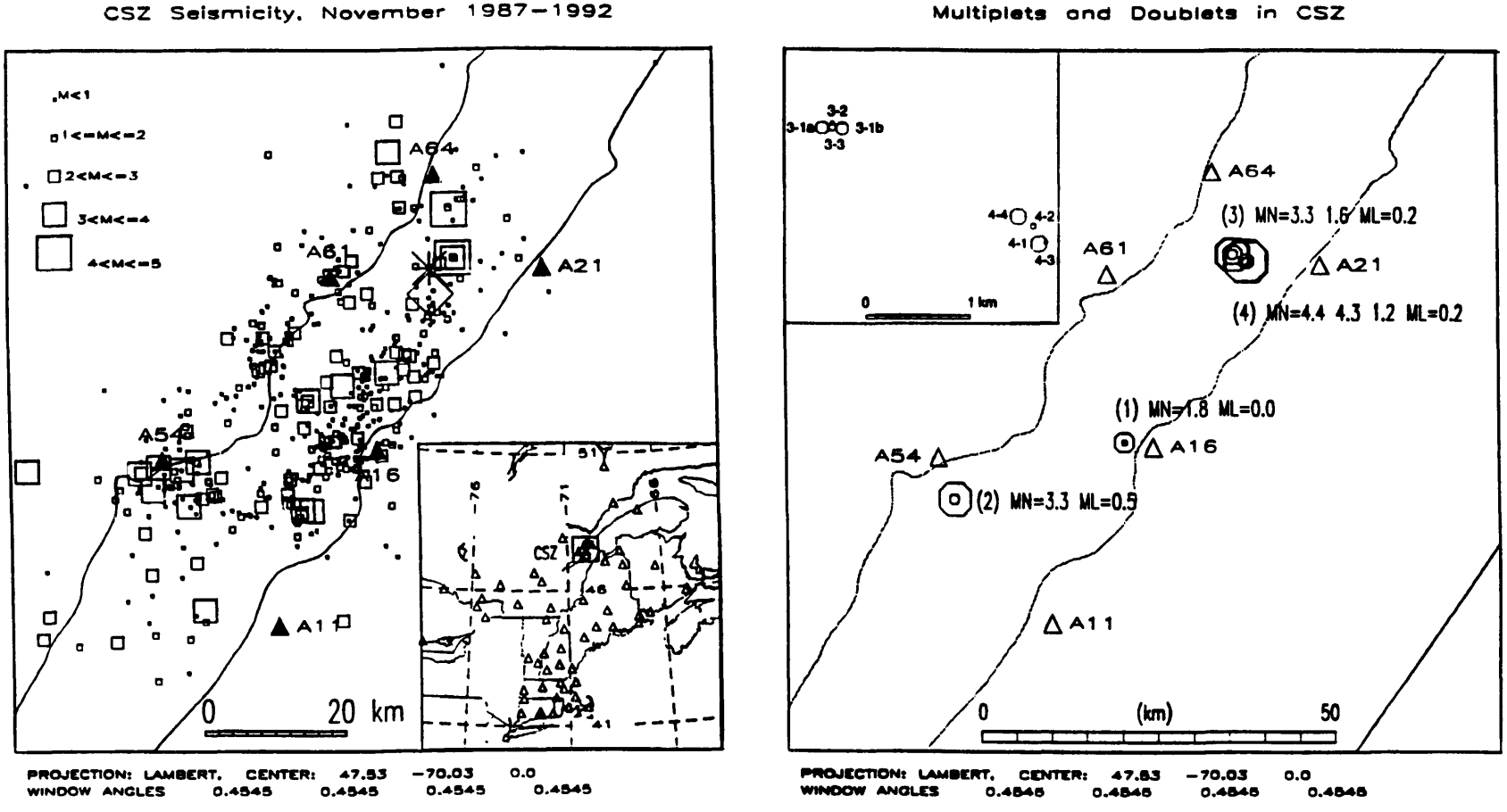

Figure 1: a) Seismicity (squares) of the Charlevoix Seismic Zone (CSZ) in Quebec, Canada for November 1987-1992. The 1925 (m_b=6.5) and the 1979 (m_b=5.0) earthquakes are shown as an asterisk and a diamond, respectively. The filled triangles mark the locations of the CLTN stations. The inset map depicts the location of the CSZ in northeastern North America and the sites of the ECTN and the NESN stations (open triangles), many of which were used to determine the focal mechanisms of the larger microearthquakes studied. b) Epicentral locations (octagons) of the two doublets (pairs 1 and 2) and the two multiplets (groups 3 and 4) analyzed in this study. The inset map emphasizes the close spatial separation among the slave and master events of each multiplet resolved by the waveform cross-correlation and relative event location technique.

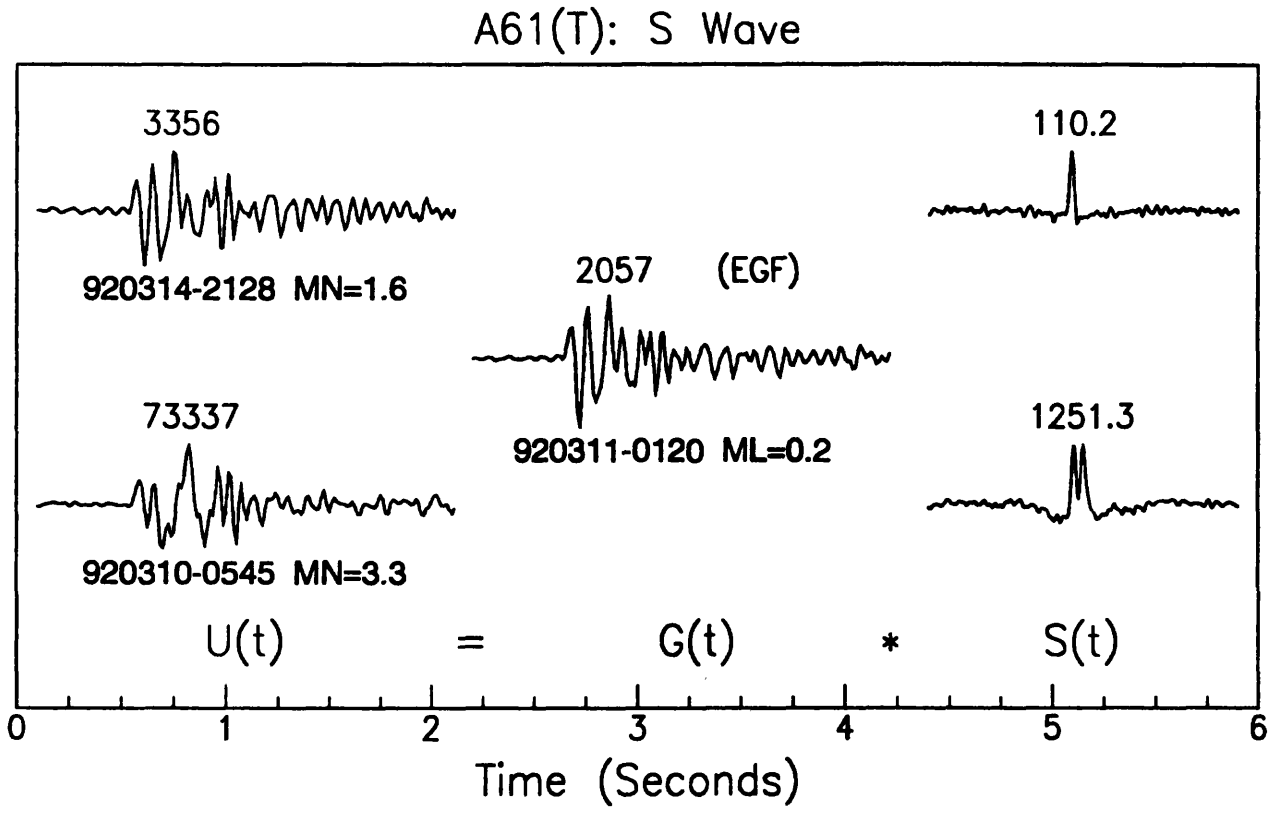

Figure 2: Demonstration of the EGF deconvolution procedure to retrieve the relative STFs of two larger earthquakes of a multiplet consisting of three events. The tangential S waveform of the smallest event is treated as the EGF and deconvolved from the seismograms of the two larger events U(t), to derive the STFs S(t), of the two larger earthquakes. The STF of the M1.6 event (920314-2128) is a simple pulse with a source duration of about 0.05 s. The STF of the M3.3 earthquake (920310-0545) appears to have two peaks, suggesting two episodes of rupture with a total duration of about 0.15 s.

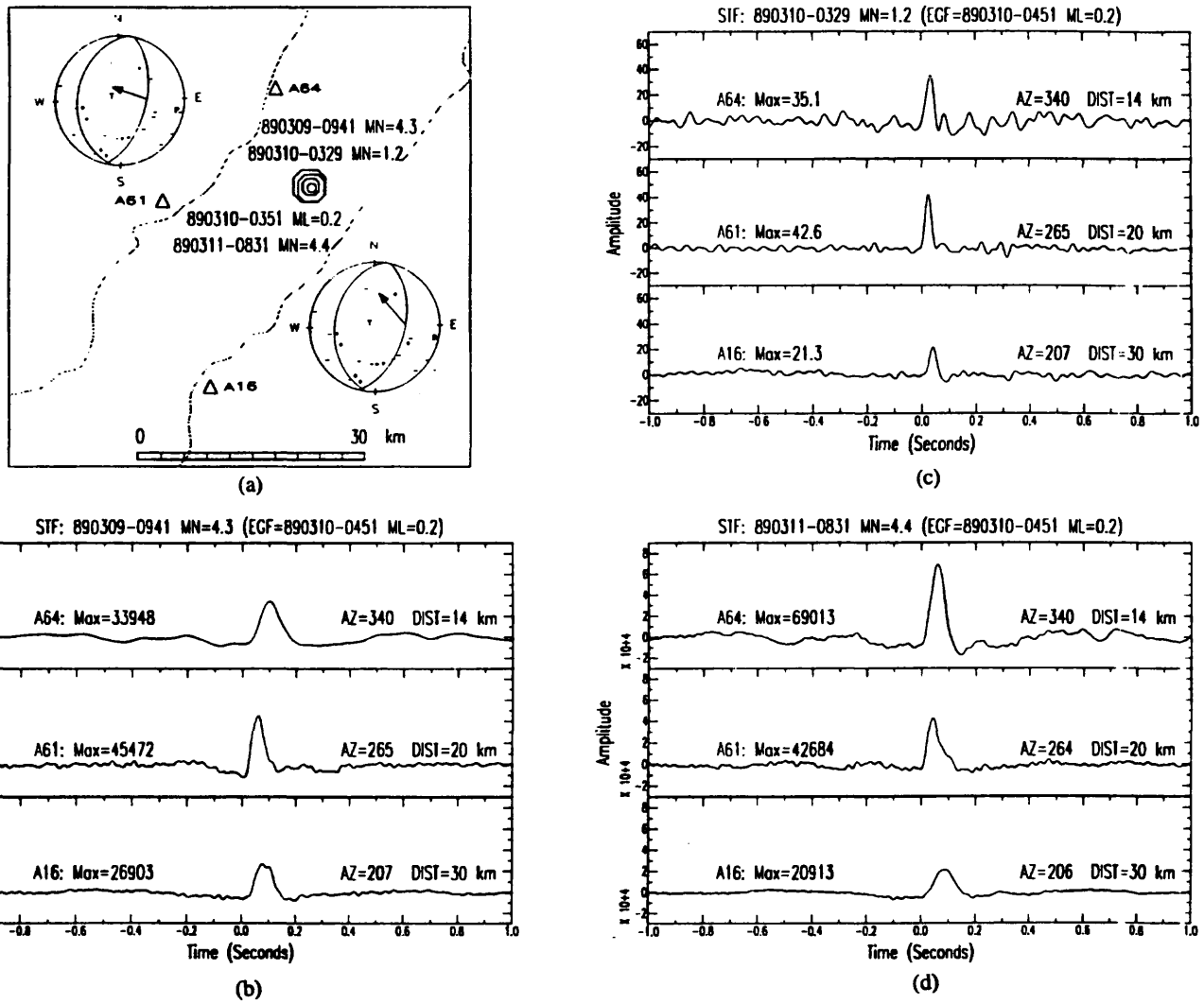

Figure 3: (a) Epicentral location of multiplet 4 (M0.2-4.4) and the focal mechanisms of the two largest events. (b-d) The STFs for the three larger earthquakes recorded at the three stations (triangles) in (a). All three events exhibit a clear rupture directivity revealed by the significant azimuthal variations in pulse amplitude and width of the STFs, indicating a rupture direction approximately northwest. The arrow points from the probable fault plane in the rupture direction on the thrust focal mechanisms of the M4.3 and M4.4 earthquakes in (a).

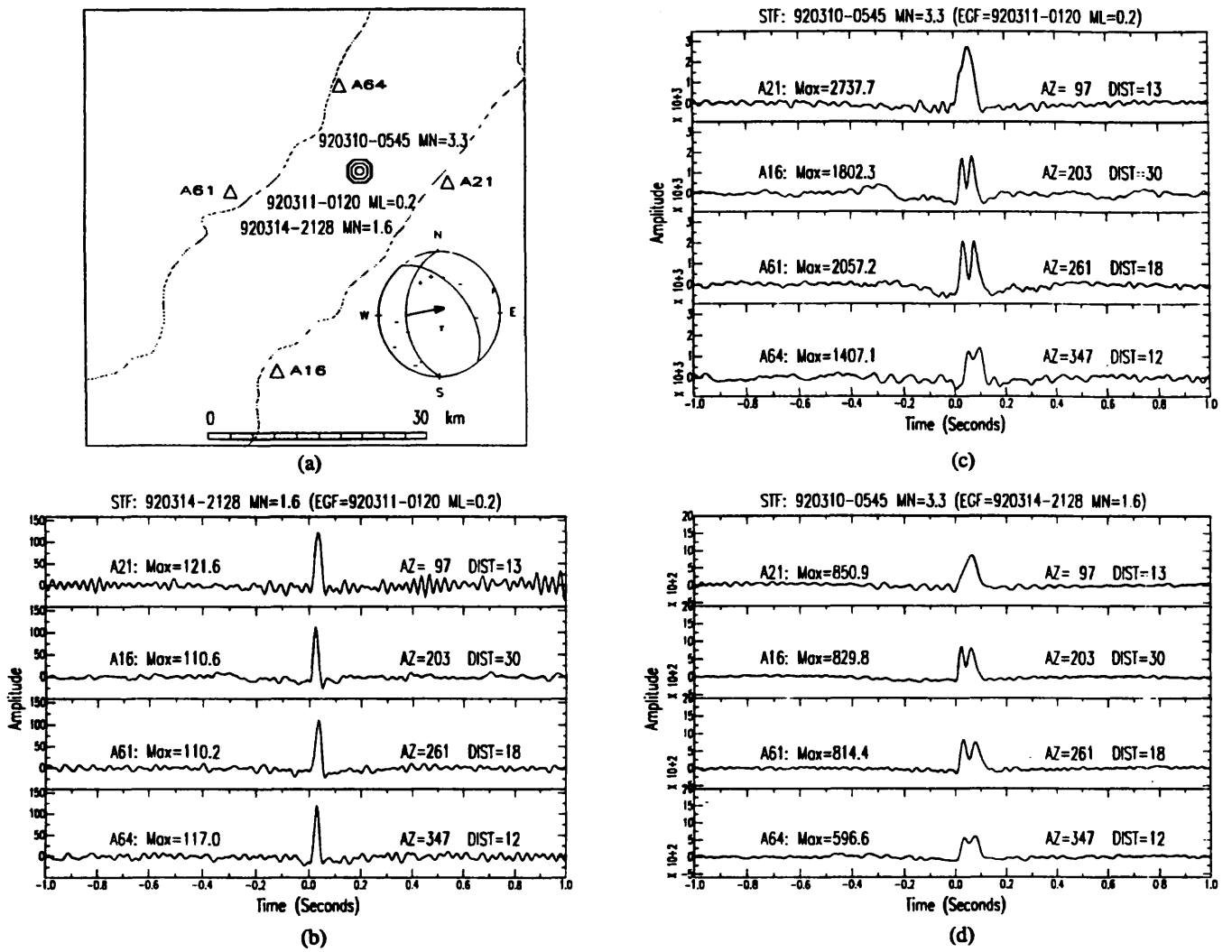

Figure 4: (a) Epicentral location of multiplet 3 (M0.2-3.3) and the focal mechanism of the largest event. (b-d) STFs of the M1.6 and M3.3 events derived at the four CLTN stations (triangles) in (a). The M0.2 earthquake is used as the EGF to retrieve the STFs in (b) and (c). STFs of the M3.3 event were also estimated with the M1.6 event as the EGF in (d). The pulse shape is preserved among the STFs of the four stations when compared to the results obtained using the M0.2 event as the EGF in (c). The azimuthal variations of the STF pulse amplitudes and widths suggest a rupture approximately from west to east. The arrow extends from the probable fault plane on the thrust focal mechanism (first subevent) toward the direction of rupture.

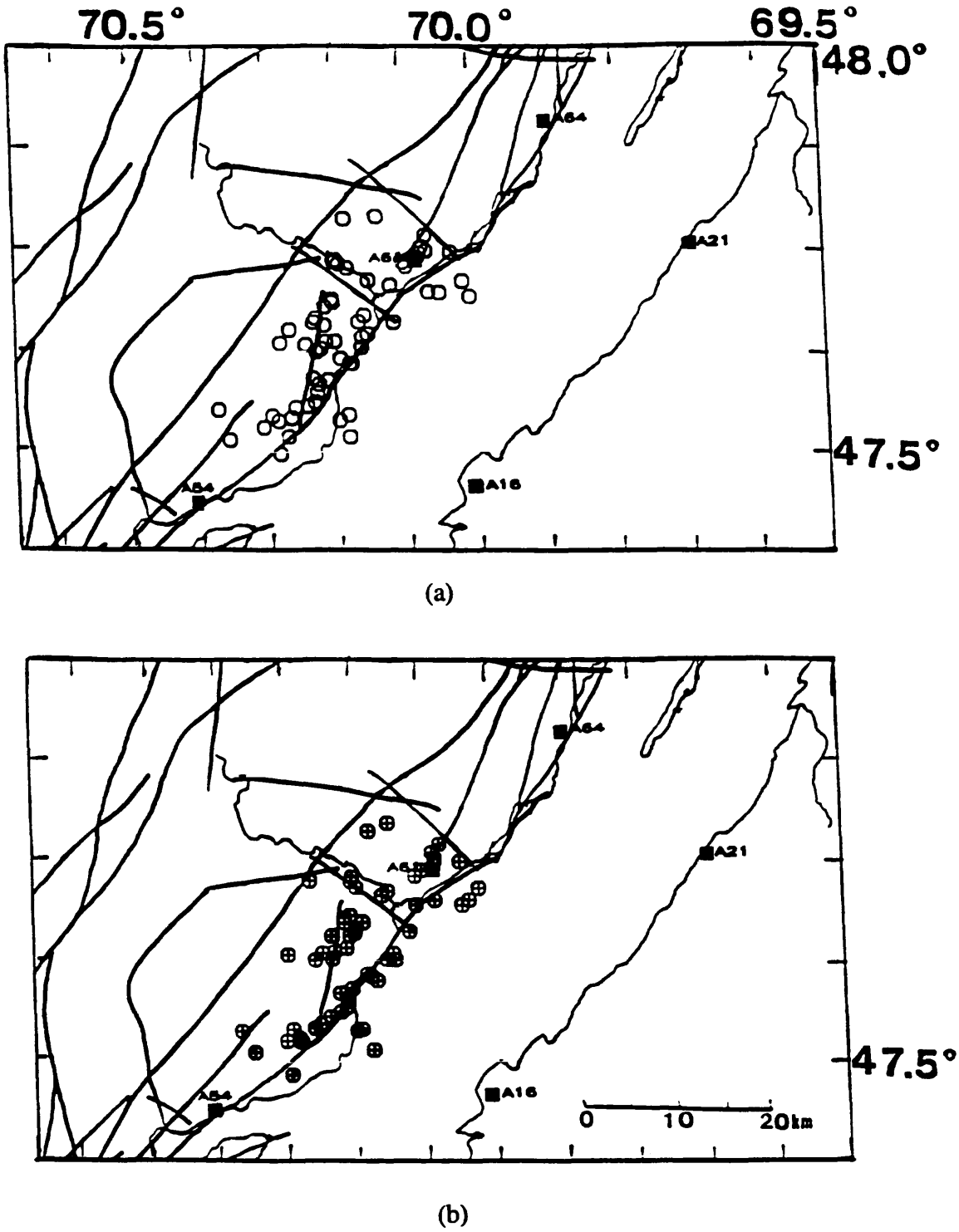

Figure 5: a) Original HYPOINVERSE locations (open octagons), and b) Relative event locations (crossed octagons) of earthquakes superposed on a fault map (Rondot, 1979) of the CSZ. After relocation of the earthquakes, two linear trends of epicenters are more clearly defined striking parallel to the St. Lawrence River and some of the major mapped faults. In particular, the linear trend along the shore of the river shows a strong spatial correlation with an extensive fault striking northeast. The spatial correlation of a few of the epicenters with a southeast trending cross fault, southwest of Station A61, is improved after event relocation.

Collaborative Research (University of Maryland and Branch of Geologic Risk Assessment, USGS): Evidence for Paleoseismicity from Liquefaction Features in the New Madrid Seismic Zone

Agreement No. 1434-93-G-2352

Martitia P. Tuttle
University of Maryland
Department of Geology
College Park, Maryland 20742
(301) 405-1311
mt90@umail.umd.edu

Investigation

Prehistoric liquefaction features in the southern part of the New Madrid seismic zone (NMSZ) are the focus of this project conducted in collaboration with E. Schweig of the U.S. Geological Survey. Robert Lafferty, III of Mid-Continental Research Associates, who first drew our attention to liquefaction sites at Eaker Air Force Base, has provided archeological analysis of artifact assemblages at several sites. Margaret Guccione of University of Arkansas at Fayetteville has provided information on the depositional history of northeastern Arkansas and southeastern Missouri. Marion Haynes of Haynes Farm in Blytheville, Arkansas, has shared his knowledge of sand blows and archeological sites in the area. By using an interdisciplinary approach involving archeology, geology, and pedology, we have been able to identify and date earthquake-induced liquefaction features in an area where they had not been recognized during previous studies (Wesnounsky and Leffler, 1992; and Rodbell and Schweig, 1993).

Field investigations are completed at twelve sites and are currently underway at another four sites (Fig. 1). Because evidence of multiple episodes of liquefaction is often present and because liquefaction events are closely spaced (several hundreds of years) in time, detailed study has been required at most sites. The field investigations include evaluating structural and stratigraphic relations of the liquefaction features, logging trench walls, photographing significant features, describing sediments and also soil characteristics, and collecting samples for various analyses. Archeological analysis and radiocarbon dating are being carried out for most of the sites and pedological analysis is being performed for all sites.

The degree of soil development in near-surface sand blows and dikes first alerted us that some of the features pre-dated the 1811 and 1812 earthquakes. Soil horizons and soil properties, such as rubification (which is an increase in hue redness and in chroma), structure, consistence, and acidity, are known to develop systematically with time (Birkeland, 1984; Harden, 1982). During our site investigations, we are collecting data on soil properties of liquefaction features of different ages and will use this data to construct a soil development index that can

be used to estimate the age of liquefaction features when other dating methods can not be applied.

Native American occupation horizons and features containing artifacts have been very useful in identifying and dating prehistoric liquefaction features. In several cases, sand blows are both overlain and underlain by occupation horizons. Artifacts and charcoal within the occupation layers help to constrain the ages of associated sand blows. Because of the usefulness of Native American occupation horizons, we now focus our searches for prehistoric liquefaction features in areas where Native Americans are likely to have lived (i.e., relatively high and dry areas near bodies of water). Having established that prehistoric liquefaction features do occur in the southern part of the New Madrid seismic zone and having learned where to look and what to look for, we are expanding the area of our search. An understanding of the age distribution of liquefaction will help to estimate the source areas and magnitudes of the prehistoric earthquakes.

Summary of Results

In the southern part of the NMSZ, we have found nine liquefaction features that are demonstrably prehistoric in age and another four features that may predate the 1811-1812 earthquakes (Fig. 1). Radiocarbon dating of the liquefaction features and their stratigraphic relations with Native American occupation horizons have allowed us to estimate when the features formed (see Table 1). Of the nine prehistoric liquefaction features, one feature (E-525) formed during the Middle Woodland cultural period between A.D. 0 and 500 and five features (E-557, E-560a 560b, Y-304, T-101) formed during the Mississippian cultural period between A.D. 800 and 1670. The liquefaction features that formed during the Mississippian cultural period may be the result of more than one earthquake sequence. Features at sites E-560 and T-101 probably formed between A.D. 800 and 1200, whereas features at Y-304, E-560b, and E-557 probably formed between A.D. 1300 and 1670. Additional radiocarbon dating and archeological analysis hopefully will resolve this issue. We can not distinguish the ages of the remaining three prehistoric features (M-801), but know from radiocarbon dating that they formed since 4035 B.C. In addition, we have studied with Michael Ellis and Yong Li of the University of Memphis a site in the northern part of the zone, where a feature formed prior to A.D. 1020 (W-102b). A few examples of prehistoric liquefaction features are presented below.

At site Y-304 (Fig. 2), a sand-blow crater cross-cuts a Native American occupation horizon that contains potsherds, including Varney Red Filmed pottery, typical of the Early to Middle Mississippian cultural periods (A.D. 800 to 1400). The thickness of the occupation horizon suggests that the sand blow formed towards the end of this period. In addition, a Native American pit occurs in the upper part of the sand-blow crater. Archeological analysis of artifacts in the pit indicates that it was utilized also during the Early to Middle Mississippian cultural periods. Radiocarbon dating of charcoal from the base of the pit yielded a conventional age of 455 $\pm$ 110 yr B.P., which corresponds to a 2 sigma calibrated range of A.D. 1300 to 1660. The

archeological analysis and radiocarbon dating together indicate that this sand blow formed between A.D. 800 and 1400 (Table 1).

At site E-560, two stacked sand blows occur between Native American occupation horizons (Fig. 3). The two sand blows are separated by a 10-cm-thick clay layer, indicating that the two sand blows did not formed as a result of the same earthquake. The presence of ceramic artifacts from both the late Woodland (A.D. 500 to 800) and early Mississippian (A.D. 800 to 1200) cultural periods within the buried occupation horizon suggests that the lower sand blow (E-560b) formed during the transition period between the two cultures, about A.D. 800 $\pm$ 100 yr. The development of a late Mississippian (A.D. 1400 to 1670) occupation horizon on the upper sand blow (E-560a) indicates that it formed prior to 1670. Radiocarbon dating of tree roots within cultural pits dug into the upper sand blow is consistent with this maximum age estimate. Therefore, the two sand blows formed between about A.D. 800 and 1670 (Table 1).

At site E-557, clasts of a Native American occupation horizon containing potsherds of both the Woodland and Mississippian cultural periods occur within a large sand dike (Fig. 4). Radiocarbon dating of a piece of charcoal within the top of the dike yielded a conventional radiocarbon age of 490 $\pm$ 60 yr B.P. which corresponds to a 2 sigma calibrated range of A.D. 1320 to 1500. This age probably closely reflects the timing of the event. A portion of the overlying occupation horizon remains intact but dips into the top of the dike. The collapse of overlying material into the dike and the absence of vented sand to either side of the dike suggest that it formed as a result of lateral spreading towards the nearby Pemiscot Bayou. Lenses of sand similar to that filling the dike occur above the disturbed portion of the occupation horizon. During the archeological excavation of the top of the dike, it was observed that the lenses of sand had vented through small round (plan view) conduits in the underlying occupation horizon. The top of the vented sand became the new ground surface after the event. An occupation horizon overlying and developed within the top of the vented sand indicates that Native Americans occupied the site following the event. Artifacts within the occupation horizon overlying the vented sand were also of the Mississippian cultural period. Therefore, this liquefaction feature formed between A.D. 800 and 1670 and probably between A.D. 1320 and 1500 (Table 1).

At site W-102, two sand blows are stacked one on top of the other and feeder dikes of both sand blows are present (Fig. 5). The feeder dike of the upper sand blow clearly cross-cuts the A-horizon of the lower sand blow. The upper sand blow (W-102a) is only 24 cm thick and exhibits only a small amount of soil development in its top 10 cm. The lower sand blow (W-102b) is 150 cm and is characterized by a 37-cm-thick A-horizon. The small amount of soil development within the upper sand blow suggests that it may have formed during the 1811-1812 earthquake sequence. Radiocarbon dating of charcoal collected above the sand blow yielded a conventional age of 240 $\pm$ 60 yr B.P., which corresponds with a 2 sigma calibrated range of A.D. 1510 to 1950. This date is consistent with an 1811-1812 origin, but does not rule out

an earlier age. In contrast, the thick A-horizon developed in the lower sand blow indicates that this sand blow pre-dates the 1811-1812 New Madrid earthquakes. Radiocarbon dating of a soil sample from the top of this A-horizon yielded a conventional age of 1,140 ± 60 yr B.P., which corresponds to a 2 sigma calibrated range of A.D. 770 to 1020. Therefore, the lower sand blow formed prior to A.D. 1020 (Table 1). Additional radiocarbon dating on soil collected below the sand blow may help to constrain its age.

Field investigations are currently underway at two sites near the Missouri-Arkansas state line and at a third site about 40 km to the southwest (white diamonds on Fig. 1). A brief account of preliminary observations at these sites follows. At the site in Missouri, *en echelon* sand blows, that may be related to the Bootheal Lineament, bury an occupation horizon that contains ceramic artifacts of the Woodland cultural period. Away from the sand blows, the upper part of the occupation horizon also contains potsherds of the Mississippian cultural period. The age relation of the sand blows to the different cultural components of the occupation horizon is uncertain at this time. Development of a 28-cm-thick A-horizon suggests that the sand blow is prehistoric. Organic samples associated with the sand blows have been collected for radiocarbon dating.

At the nearby site in Arkansas, a paleosol with *in situ* trees are exposed about 3 m below the present ground surface in a large borrow pit. Sand blow deposits are seen overlying the paleosol in several locations within the borrow pit. Feeder dikes of the sand blows are also exposed. Two of the tree trunks are buried by sand blow deposits. The trees did not develop adventitious roots in the sand blow deposits suggesting that the trees were killed by the event. The paleosol and sand blow deposits are overlain by interbedded clayey silts and sands. A fairly thick A-horizon has developed in the upper-most deposit of cross-bedded sand. Given the amount of deposition above the sand blows and soil development within the overlying profile, the buried sand blows are certainly prehistoric and may predate other prehistoric liquefaction features documented in the area. A sample taken from one of the trees buried by a sand blow will be submitted for high precision radiocarbon dating.

At the other site in Arkansas currently under investigation, several surficial sand blows are characterized by 15 to 30-cm-thick A-horizons. The thick A-horizons suggest that the sand blows are prehistoric. The sand blows bury organic-rich A-horizons. A feeder dike of one of the sand blows cross-cuts a Native American fire pit. Charcoal samples from the fire pit and from the upper part of the soil buried by one of the sand blows have been collected for radiocarbon dating.

Based on field observations and archeological and radiocarbon analyses, it appears that at least two, and possibly three, earthquakes large enough ($M \geq 6.4$ according to Obermeier, 1989) to induce liquefaction in the moderately susceptible sediments of the region occurred between A.D. 0 and 1670. One of these events occurred between A.D. 0 and 500. A second large event, and possibly a third, occurred between A.D. 800 and 1670. Additional analyses of samples collected at the

study sites, as well as investigations conducted at other liquefaction sites in the area, may help to resolve this issue.

A paleoearthquake chronology is beginning to emerge for the southern part of the NMSZ that appears to be similar to the chronology developed for the northern part of the zone (Russ, 1982; Saucier, 1991; and Kelson et al., 1994). This suggests that large, possibly great, earthquakes occur fairly frequently (every few hundred to a thousand years) in the NMSZ. Although much work remains to determine the timing, magnitude, and location of prehistoric earthquakes, our interdisciplinary approach is yielding valuable new data that contributes to the assessment of earthquake hazards in the central United States.

References Cited

Birkeland, P. W., 1984, Soils and geomorphology, Oxford University Press, New York and Oxford.

Harden, J. W., 1982, A quantitative index of soil development from field descriptions: Examples from a chronosequence in central California, Geoderma, vol. 28, p. 1-28.

Kelson, K. I., G. D. Simpson, C. C. Haradan, W. R. Lettis, R. B. VanArdsdale, and J. B. Harris, 1994, Multiple Holocene earthquakes along the Reelfoot fault, Central New Madrid seismic zone, Proceedings of the Workshop on Paleoseismology, U.S. Geological Survey Open-File Report 94-568, p. 92-93.

Obermeier, S.F., 1989, The New Madrid earthquakes: An engineering-geologic interpretation of relict liquefaction features, U.S. Geological Survey Professional Paper 1336, 114 p.

Russ, D. P., 1982, Style and significance of surface deformation in the vicinity of New Madrid, Missouri, *in* McKeown, F. A., and Pakiser, L. C., eds., Investigations of the New Madrid, Missouri, earthquake region, U.S. Geological Survey Professional Paper 1236, p. 94-114.

Saucier, R. T., 1991, Geoarchaeological evidence of strong prehistoric earthquakes in the New Madrid (Missouri) seismic zone, Geology, vol. 19, p. 296-298.

Rodbell, D. T., and E. S. Schweig, 1993, The record of seismically-induced liquefaction on late Quaternary terraces in northwestern Tennessee, Bulletin of the Seismological Society of America, vol. 83, p. 269-278.

Vaughn, J. D., 1991, Evidence for multiple generations of seismically induced liquefaction features in the Western Lowlands, southeast Missouri, Seismological Society of America, Annual Meeting, 63rd, Eastern Section, Program with Abstracts, p. 67.

Vogel, J. C., A. Fuls, E. Visser, and B. Becker, 1993, A simplified approach to calibrating 14C dates, Radiocarbon, vol. 33, p.73-86.

Wesnousky, S. G., and L. Leffler, 1992, The repeat time of the 1811 and 1812 New Madrid earthquakes: A geological perspective, Bulletin of the Seismological Society of America, vol. 84, p. 1756-1785.

Publications

Li, Y., M. P. Tuttle, E. S. Schweig, and M. A. Ellis, 1994, New results of paleoearthquake studies in the northern New Madrid seismic zone, EOS, Transactions, American Geophysical Union, vol. 75, no. 44, p. 452.

Schweig, E. S., M. Tuttle, Y. Li, J. A. Cravin, M. A. Ellis, M. J. Guccione, R. H. Lafferty, III, and R. F. Cande, 1993, Evidence for recurrent strong earthquake shaking in the past 5,000 years, New Madrid region, central U.S., EOS, Transactions, American Geophysical Union, vol. 74, no. 43, p. 438.

Tuttle, M. P., E. S. Schweig, and R. H. Lafferty, III, 1993, Archaeological constraints on the age of a prehistoric sand blow in northeastern Arkansas, EOS, Transactions, American Geophysical Union, vol. 74, no. 43, p. 438.

Tuttle, M., E. Schweig, and N. Barstow, 1993, Preliminary evidence of prehistoric earthquakes in the New Madrid seismic zone, central United States, EOS, Transactions, American Geophysical Union, vol. 74, no. 16, p. 281.

Tuttle, M., E. Schweig, R. Lafferty, and R. Cande, 1993, (invited), Evidence of repeated strong ground shaking in the New Madrid seismic zone, *in* Monteleone, S., ed., Transactions of the Twenty-First International Water Reactor Safety Information Meeting, U.S. Nuclear Regulatory Commission, NUREG/CP-0132, p. 17-5 to 17-6.

Tuttle, M. P., E. S. Schweig, R. H. Lafferty, III, and M. J. Guccione, 1994 (invited), Archaeological dating of liquefaction features and seismic events in the New Madrid seismic zone, central United States, Abstracts with Programs, Geological Society of America, vol. 26, no. 7, p. A-156-157.

Tuttle, M. P., and E. S. Schweig, 1994, (invited) Recognizing and dating earthquake-induced liquefaction features in the New Madrid seismic zone, central United States, Proceedings of the Workshop on Paleoseismology, U.S. Geological Survey Open-File Report 94-568, p. 186-188.

Tuttle, M. P., and E. S. Schweig, submitted, Prehistoric liquefaction features: Lessons learned in the New Madrid seismic zone, central United States, Journal of Geophysical Research.

Tuttle, M. P., and E. S. Schweig, submitted, Archeological and pedological evidence for large prehistoric earthquakes in the New Madrid seismic zone, central United States, Geology.

Table 1. Approximate Dates of Liquefaction Features and Events

Site	Feature	Archeological Constraints[1]	Radiocarbon Constraints[2]	Event	Date (A.D.)
C-101	sand blow	≥ 1400-1670	> AD 1410-1630 < AD 1660-1950	1 or 2	1811 or 1400-1600
E-525	sand blow	~ AD 0-500	< AD 1050-1410	4	0-500
E-557	sand dike	~ AD 500-1670	~ AD 1320-1500	2	1300-1670
E-560a	sand blow a	≤ AD 1400-1670	< AD 1460-1955	2 or 3	800-1670
E-560b	sand blow b	~ AD 800-1200	< AD 1460-1955	3	800-1200
M-801	3 sand dikes	not available	> 4035-3360 BC	1, 2, 3, 4	1811 & > 4035 BC
T-101	sand blow	~ AD 500-1200	< AD 1520-1950	3	500-1200
W-102a	sand blow a	not available	< AD 1510-1950	1 or 2	1811/12 or > 1020
W-102b	sand blow b	not available	< AD 770-1020	3 or 4	< 1020
Y-304	sand blow	~ AD 800-1400	< AD 1300-1660	2	800-1400

[1] Based on artifacts assemblages, primarily ceramics from the Woodland and Mississippian cultural periods.

[2] Based on the Pretoria calibration procedure (Vogel et al., 1993), two sigma calibrated ranges of conventional radiocarbon ages.

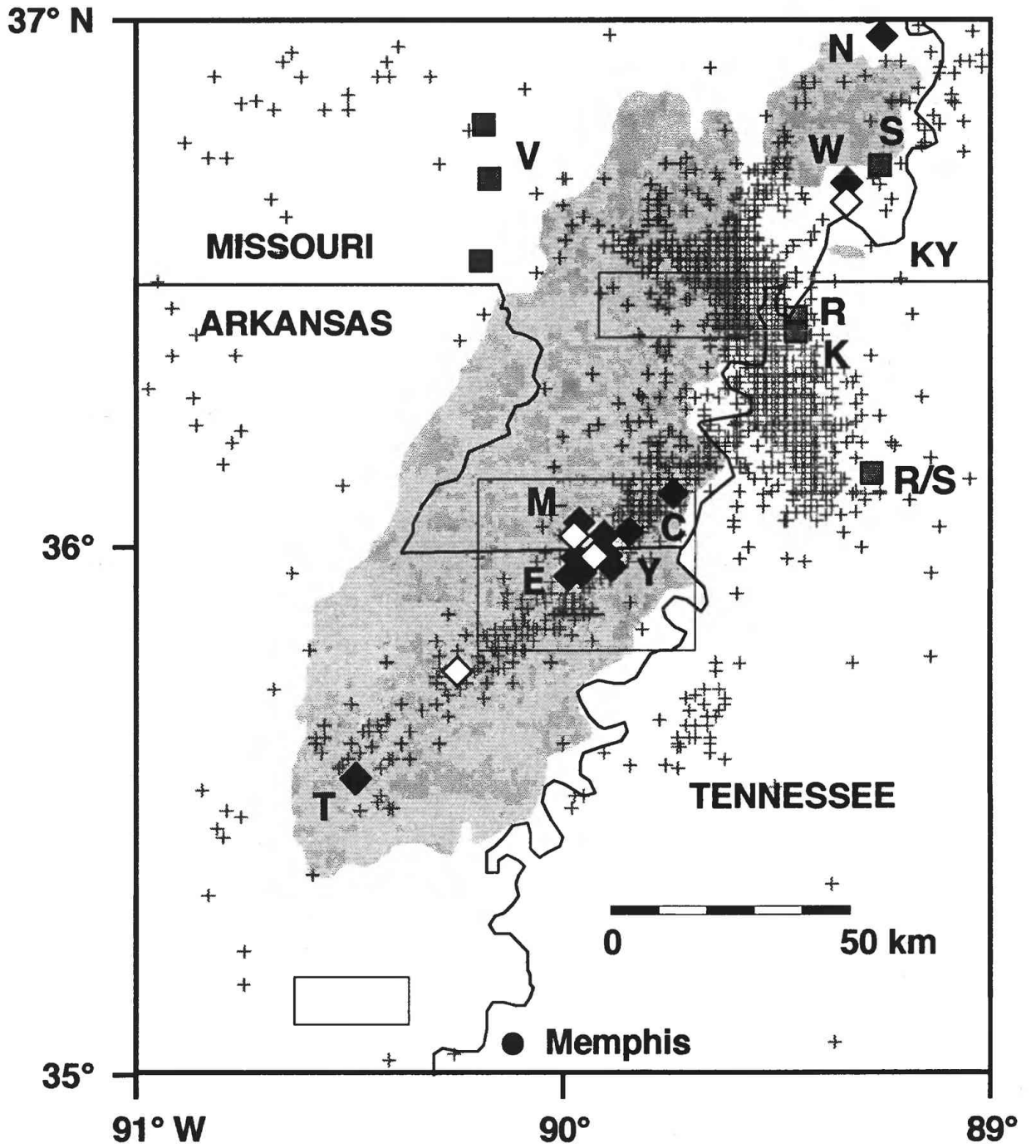

Figure 1. Map of the New Madrid seismic zone (excluding southern Illinois) in the central United States. Crosses indicate locations of recent (1974-1991) seismicity. Gray shading represents >1% of area covered by sand-blow deposits (Obermeier, 1989). Study sites denoted by black diamonds and labeled C = C-101, E = E-525, E-557, and E-560, M = M-801, T = T-101, W = W-102, and Y = Y-304. Sites where investigations are currently underway denoted by white diamonds. Sites of other paleoseismic studies indicated by gray squares and labeled R = Russ (1982), K = Kelson et al. (1994), RS = Rodbell and Schweig (1993), S = Saucier (1991), and V = Vaughn (1991). Study areas of Wesnousky and Leffler (1992) outlined by boxes.

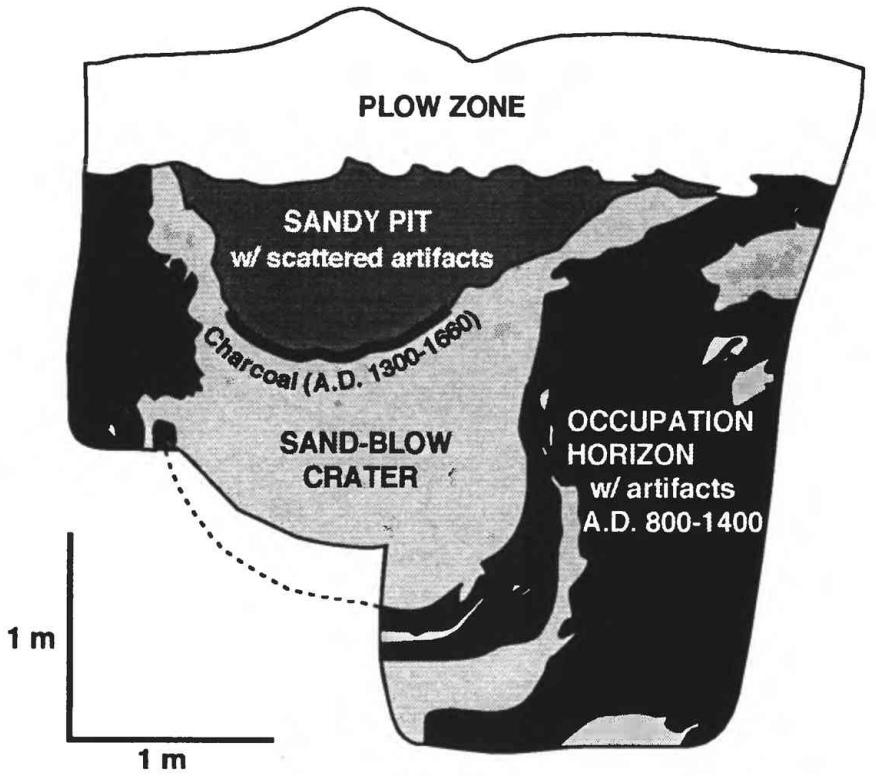

Figure 2. Log of trench wall at Yarbro-304 (Y on Fig. 1). Prehistoric sand-blow crater cross-cuts thick Native American occupation horizon containing artifacts. Feeder dike below crater not shown. In addition, pit containing artifacts and charcoal occurs in upper part of sand-blow crater. This sand-blow crater formed between A.D. 800 and 1400.

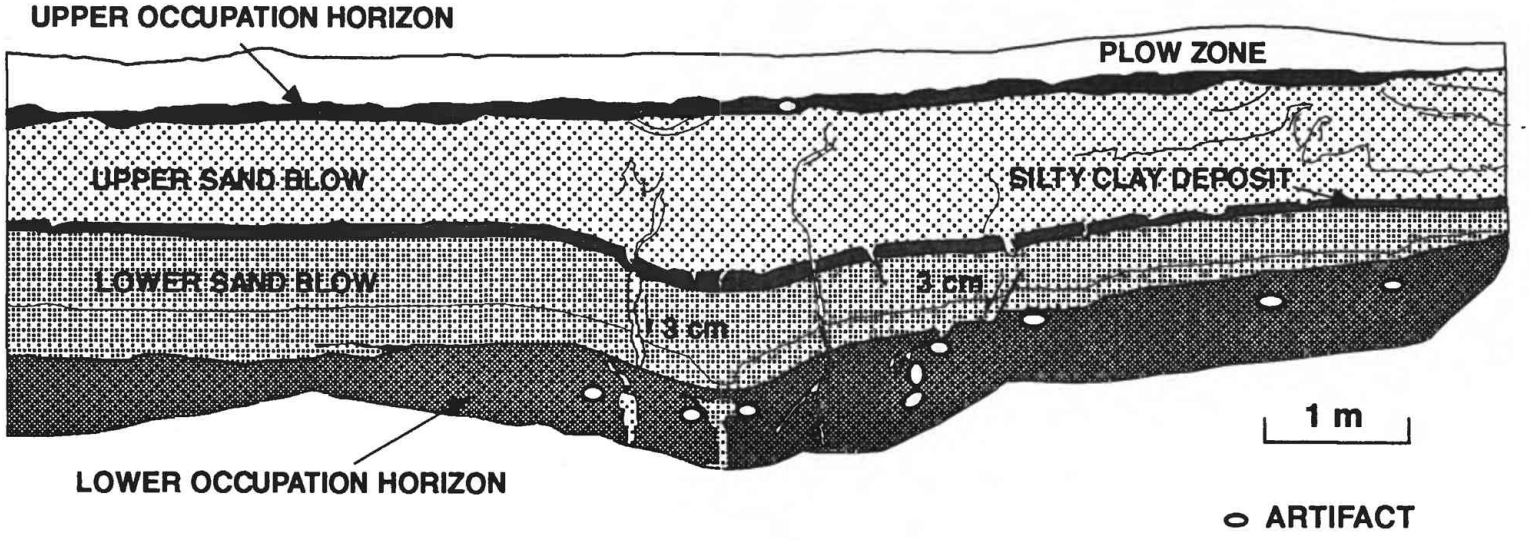

Figure 3. Log of trench wall at Eaker-560 (near E on Fig. 1). Two stacked sand blows are found between Native American occupation horizons containing artifacts. These sand blows formed between A.D. 800 and 1670 and may represent two different earthquake sequences.

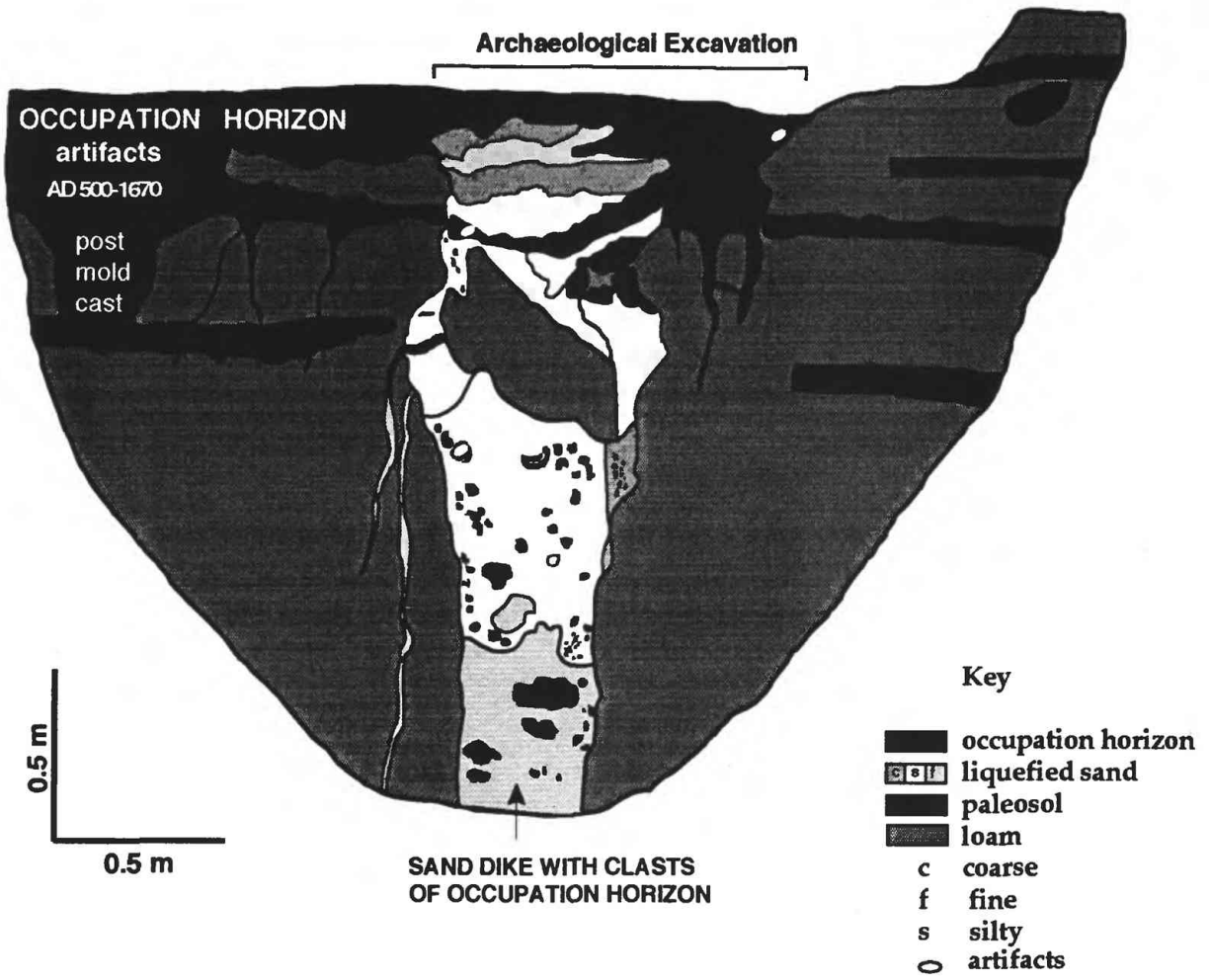

Figure 4. Log of trench wall at E-557 (also near E on Fig. 1). Clasts of Native American occupation horizon containing artifacts collapsed into fissure partially filled from below by a sand dike. An occupation horizon is also developed in the top of the vented sand above the fissure. This liquefaction feature formed between A.D. 800 and 1670.

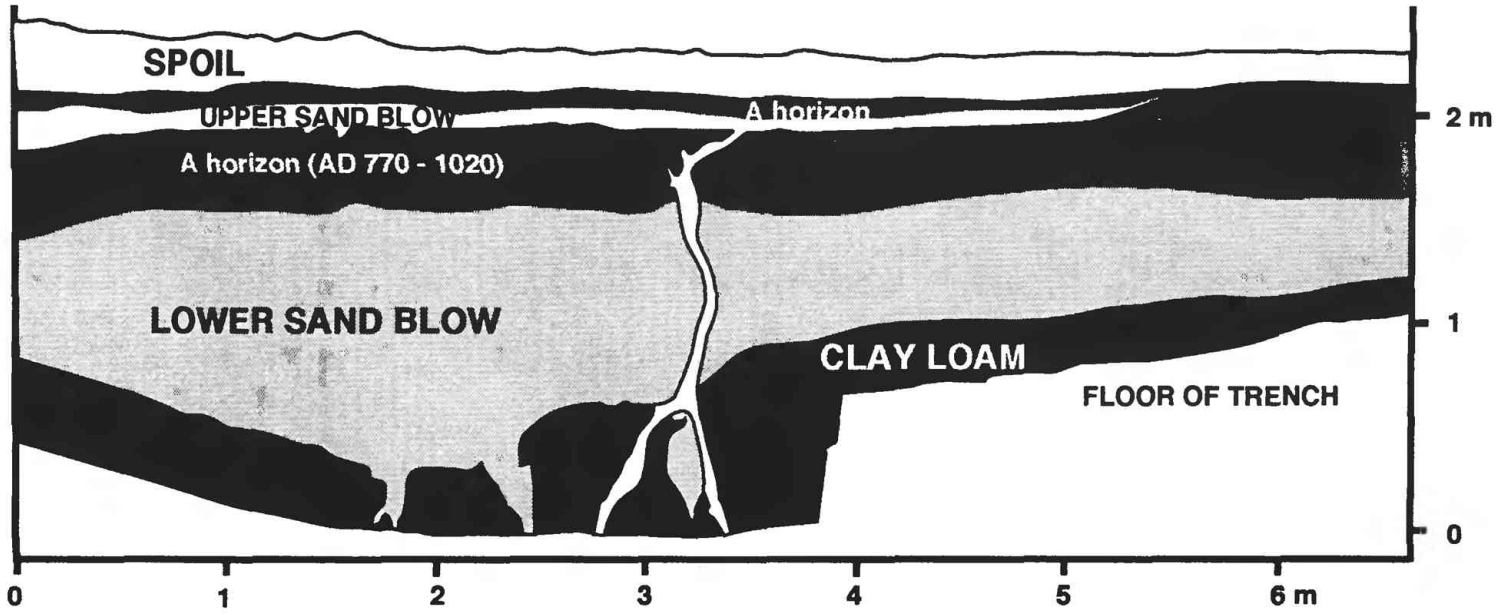

Figure 5. Log of exposure at site W-102 (W on Fig. 1). Two stacked sand blows and their associated feeder dikes are exposed. Radiocarbon dating of the A-horizon developed in the lower sand blow indicates that it formed prior to A.D. 1020.

Kinematic Interpretation of the 1992 Landers, California, Earthquake Aftershocks Using Micropolar Continuum Theory

Award Number 1434-94-G-2463

Principal Investigators:
Jeffrey R. Unruh, William Lettis & Associates, Inc., 1000 Broadway, Suite 612, Oakland, CA 94607 (ph: 510-832-3716; email: wla@netcom.com)
Robert J. Twiss, Department of Geology, University of California, Davis 95616 (ph: 916-752-1860; email: twiss@geology.ucdavis.edu)

in collaboration with
Egill Hauksson, Seismological Laboratory, California Institute of Technology, Pasadena

Program Elements: I.1; I.2; II.1; II.4

Investigations Undertaken

The goal of this study is to use micropolar continuum theory (Twiss et al., 1991; 1993) to interpret the coseismic deformation field in the central Mojave block associated with aftershocks of the 1992 Landers earthquake. This approach allows us to compare the strain rate field expressed by patterns of seismic P and T axes directly to coseismic strains determined by inversion of geodetic data. Using this approach, we seek to: 1) test the hypothesis that focal mechanisms can be used directly to infer the seismogenic deformation field; 2) test the hypothesis that micropolar continuum theory gives us the means to constrain the kinematics of block rotations within seismogenic shear zones from the aftershock focal mechanisms; and 3) interpret the tectonic significance of the Landers earthquake for accommodating distributed Pacific/North American plate motion in the Eastern California Shear Zone (ECSZ).

The theoretical basis for applying micropolar continuum mechanics to the analysis of earthquake focal mechanisms is described in detail by Twiss et al. (1993). The coseismic slip is necessarily in the direction of the maximum resolved rate of shear on the fault plane. Assuming that micropolar theory provides the appropriate kinematic model, we can infer the following information from the distribution of aftershock P and T axes: (1) the orientations of the principal strain rates ($d_1 > d_2 > d_3$; d_1 extensional); (2) a scalar deformation parameter **D** that is formed by a ratio of the differences between the magnitudes of the principal strain rates; and (3) a scalar net vorticity parameter **W** that represents the difference between the continuum vorticity and the vorticity of rotating blocks within the deforming region (Twiss et al., 1991; 1993). For this study, we adopt a restricted kinematic model in which the axial net vorticity vector is assumed to be parallel to the intermediate principal strain rate axis (Twiss et al., 1993).

Earthquake data used in this study were provided by Egill Hauksson of the California Institute of Technology. Data consisted of focal mechanisms for the 1992 Joshua Tree and Landers earthquake sequences, as well as background seismicity in the Mojave block between 1981 and 1991 (Hauksson et al., 1993; Hauksson, 1994). We subdivided the focal mechanisms into groups, each associated with a geometrically defined segment of the surface fault. For aftershocks that occurred on blind structures with no surface expression, such as the Joshua Tree sequence and the Big Bear aftershocks, we defined fault segments on the basis of alignments of epicenters that define a distinct trend or orientation. We calculated seismic P and T axes from focal mechanisms using the algorithm PTFROMDAT, and displayed the results on equal-area, lower hemisphere Kamb contour plots using Allmendinger's STEREONET 4.7-IIa. For most subsets of the data, the contour plots reveal well-defined P and T maxima, which we interpret as evidence that the group of aftershocks reflects a homogeneous deformation. Visual inspection of the initial Kamb

contour plots also revealed examples where the P and T axes did not form well-defined maxima. In each of these cases, we redefined the fault segment boundaries until the P and T axes in each group formed well-defined maxima on a Kamb-contour plot.

We used a grid-search algorithm (PTGRDSRCH) to find the best-fit reduced strain rate tensor and net vorticity vector for each group of P and T axes. The algorithm creates a five-dimensional user-defined grid for the five model parameters and evaluates the misfit between the model and the observed data at each grid point. Each P and T axis pair defines two possible shear plane-slip line pairs. The algorithm uses a conjugate gradient iterative technique to find the model shear plane-slip direction pair that differs from each observed pair by the minimum possible angle of rotation, and of the two possible pairs, it chooses the pair with the minimum rotation angle to be the best fit to the data. The mean of the cosines of this rotation angle, taken over all the data, defines the misfit of the model to the group of data. We adopt the orientations of the P and T maxima on the Kamb contour plots to be the initial orientations of d_3 and d_1, respectively, in the grid search. The patterns of clustering and girdling of the P and T axes on the contour plots were compared to theoretical P/T plots for different values **D** and **W** in Twiss et al. (1993), and appropriate but restricted ranges of these parameters were chosen for the initial search. The best model found during the initial grid was used as a starting point for the second grid. The analysis proceeded iteratively until the solutions converged on a best-fit orientation of the d_1 and d_3 axes and best-fit values of **D** and **W**, as defined by the maximum mean cosine of the misfit angle.

To compare the seismogenic strain determined from inversion of the aftershock data to coseismic crustal motions in the Mojave block, we inverted GPS and other geodetic data to determine the orientation and magnitude of the horizontal principal strains associated with the Landers earthquake. Data consisted of the magnitude and direction of coseismic station displacements reported by Hudnut et al. (1994). We divided the central Mojave block into a network of triangular cells whose vertices are located at geodetic measurement stations. The horizontal principal strains and the magnitude of the vertical axis rotation for each triangular cell were calculated from the coseismic displacements using GPSTRAIN, a modification of an algorithm provided by Andrea Donnellan of the Jet Propulsion Laboratory (Pasadena, California).

Results

The analysis indicates that the deformation inferred from a micropolar inversion of the 1992 Landers earthquake aftershocks is consistent with the geodetic measurements of the coseismic displacement (Unruh et al., 1994). In the central Mojave block and along the Landers surface rupture zone, d_1 is horizontal NW-SE and d_3 is horizontal NE-SW. In the western Mojave block and in the vicinity of the Big Bear earthquake, d_1 is horizontal E-W and d_3 is horizontal N-S. Inversion of geodetically-measured displacements across the seismogenic zones gives similar results, indicating that the aftershocks accommodated a similar deformation to the main rupture and do not reflect elastic rebound or deformation associated with residual stresses.

The best-fit inversions of the aftershock data give values for **D** that correctly predict transtensional or transpressional deformation along the fault where the kinematics can be checked using independent constraints from surface mapping. The largest non-zero values of **W** are associated with the Johnson Valley fault north of the main shock and with the Kickapoo fault. Detailed mapping in this region following the earthquake revealed that surface faulting occurred within a 2.5 km wide zone along the Kickapoo fault between the Johnson Valley and Homestead Valley faults (Sowers et al., 1994). The majority of the secondary surface faults in this region strike N20E to N50E, oblique to the north-striking Kickapoo fault. The NE-striking faults accommodated both extension and left-lateral slip, and intervening blocks bounded by the faults locally were rotated clockwise (Johnson et al., 1993). Based on the patterns of surface faulting and the values of **D** and **W** obtained from the micropolar inversion, we infer that the kinematics of block rotation are consistent with a pinned block model (Twiss et al., 1993).

Regionally, the aftershock data define two major domains within the central Mojave block: 1) The San Bernardino Mountains, which are characterized by E-W d_1 (extension) and N-S d_3 (shortening); and 2) The central Mojave desert, which is characterized by NW-SE d_1 and NE-SW d_3 . The characteristic d_1 and d_3 orientations for the two domains also are expressed in the 1981-1991 background seismicity, indicating that the secular seismogenic strain has the same geometry as the 1992 coseismic deformation. We interpret the NW-SE orientation of d_1 to be characteristic of the ECSZ, a zone of distributed dextral shear that transfers approximately 22% of the Pacific-North American plate motion from the San Andreas system to the Walker Lane Belt in eastern California. The western boundary of the ECSZ is well-defined by the Landers aftershocks. The location of the eastern boundary is less well-constrained, but appears to extend no farther east than the Pisgah fault, consistent with geodetic determinations of the locus of secular NW dextral shear strain accumulation in the central Mojave block (Sauber et al., 1994).

Results Published

Unruh, J.R., Twiss, R.J., and Hauksson, E., 1994, Local and regional coseismic deformation for the 1992 Landers earthquake aftershocks inferred from micropolar inversion of seismic P and T axes: EOS (Transactions, American Geophysical Union), 1994 Fall Meeting Supplement, v. 75, no. 44, p. 180-181.

Twiss, R.J., and Unruh, J.R., 1994, Kinematics of a contractional strike-slip duplex inferred from inversion of the seismic P and T axes, 1989 Loma Prieta aftershock sequence: EOS (Transactions, American Geophysical Union), 1994 Fall Meeting Supplement, v. 75, no. 44, p. 180.

Unruh, J.R., Twiss, R.J., and Hauksson, E., in preparation, Seismogenic deformation field in the Mojave block expressed by the 1992 Landers earthquake aftershocks: implications for tectonics of the Eastern California Shear Zone

References

Hauksson, E., 1994, State of stress from focal mechanisms before and after the 1992 Landers earthquake sequence: Bulletin of the Seismological Society of America, v. 84, p. 917-934.

Hauksson, E., Jones, L.M., Hutton, K., Eberhart-Phillips, D., 1993, The 1992 Landers earthquake sequence: seismological observations: Journal of Geophysical Research, v. 98, p. 19835-19858.

Hudnut, K., and 16 co-authors, 1994, Co-seismic displacements of the 1992 Landers earthquake sequence: Bulletin of the Seismological Society of America, v. 84, p. 625-645.

Johnson, A.M., Fleming, R.W., and Cruikshank, K.M., 1993, Broad belts of shear zones as the common form of surface rupture produced by the 28 June 1992 Landers, California, earthquake: United States Geological Survey Open-File Report 93-348, 48 p.

Sauber, J., Thatcher, W., Solomon, S.C., and Lisowski, M., 1994, Geodetic slip rate for the eastern California shear zone and recurrence time of Mojave desert earthquakes: Nature, v. 367, p. 264-266.

Sowers, J.M., Unruh, J.R., Lettis, W.R., and Rubin, T.D., 1994, Relationship of the Kickapoo fault to the Johnson Valley and Homestead Valley faults, San Bernardino County, CA: Bulletin of the Seismological Society of America, v. 84, p. 528-536.

Twiss, R.J., Protzman, G.M., and Hurst, S.D., 1991, Theory of slickenline patterns based on the velocity gradient tensor and microrotation: Tectonophysics, v. 186, p. 215-239.

Twiss, R.J., Souter, B.J., and Unruh, J.R., 1993, The effect of block rotations on the global seismic moment tensor and patterns of seismic P and T axes: Journal of Geophysical Research, v. 98, p. 645-674.

FIELD EXPERIMENT OPERATIONS

9930-03

John Van Schaack
Branch of Seismology
U. S. Geological Survey
345 Middlefield Rd. MS977
Menlo Park, CA. 94025
(415) 329 4780; jvs@andreas.wr.usgs.gov
Element II

This project is responsible for a number of activities associated with the Earthquake Hazards Reduction Program: Personnel maintain and operate a number of portable recording systems used in earthquake aftershock studies, install and maintain radio telemetry systems used to transmit network data to the Centers, install new seismic stations for special topical studies, maintain all the VHF, UHF, and microwave radios used in the California networks, and manage all the radio frequencies used by the Office of Earthquakes Volcanoes and Engineering.

Personnel from the project installed 5 standard seismic telemetry stations in the area just North of Northridge immediately following the Northridge earthquake of January 1994. The data is transmitted via radio and U. S. Army Corp. of Engineers Microwave network to Pasadena. These stations will be a permanent part of the Southern California network.

Five 5-day magnetic tape recording systems were also deployed in the Northridge area immediately following the earthquake. These recorders reoccupied sites used in earlier southern California earthquakes. The recorders were operated for about 2 weeks.

We have developed a third memorandum of agreement with the Federal Aviation Administration which allows us to use their microwave facilities for stations near Mt. Shasta.with the data being transmitted to a facility colocated with our microwave network.

We are just beginning to convert all of the VHF radio systems to the new standards required by rechanneling the 162-173Mhz band.These requirements are mandated by the National Telecommunications and Information Agency and must be completed in California by the end of 1999.

Personnel of this project were heavily involved in loading explosives and shooting during the Los Angeles Region Seismic Experiment in southern California in October 1994 as well as installing and operating portable recorders during active experiments in Oregon and Alaska.

The ANZA Network: Data Collection and Analysis

1434-94-G-2480

Dr. Frank Vernon
Institute of Geophysics and Planetary Physics
Scripps Institution of Oceanography
University of California, San Diego
La Jolla, California 92093
Phone: (619) 534-5537
Fax: (619) 534-6354
email: flvernon@ucsd.edu

Investigations: This report covers the progress of the research investigating the Anza-Coyote Canyon seismic slip gap for the period from January through December, 1994. The objectives of this research are: 1) To study the mechanisms and seismic characteristics of small and moderate earthquakes, and 2) To determine if there are premonitory changes in seismic observables preceding small and moderate earthquakes. This work is carried out in cooperation with Tom Hanks, Joe Fletcher and Larry Baker of the U. S. Geological Survey, Menlo Park.

Network status: During the period of this report, ten stations of the Anza Seismic Network were telemetering three component broadband data. The network has a front-end computer which allows the ANZA event data to be available over the INTERNET in near real time. No changes were made to the data logging software. The catalog is complete through December 1994. The complete waveform data will also be loaded to the on-line optical disk storage system by the end of December also. The network ceased operations on December 31,1994 due to a lack of operating funds. All data will be delivered to the IRIS Data Management Center for future distribution.

Seismicity: Since the beginning of 1994, the ANZA network recorded 1354 events of which were large enough to locate and determine source parameters. These events have magnitudes determined by of the Southern California Seismic Network from less than M=1.0 up to the Northridge M=6.8 event. The seismicity pattern in the Anza region is concentrated in two clusters located near the KNW and TRO stations respectively. These clusters have been active for the past 12 years while the ANZA network has been operational. The activity near TRO reached a maximum near the beginning of 1990 and is significantly higher than before 1989. The seismicity off the fault appears to be lower than the levels observed in the middle 1980s. It is also interesting that there is an apparent decrease in activity along the Anza segment of the San Jacinto fault after the Landers earthquake.

Examination of Geologic Effects of the 1964 Great Alaska Earthquake as a Guide to Recognizing Paleoseismic Indicators

Timothy J. Walsh
Washington Division of Geology and Earth Resources
P.O. Box 47007
Olympia, WA
98505-7007
206-902-1450
1434-93-G-2384

Rodney A. Combellick
Alaska Division of Geological & Geophysical Surveys
794 University Ave., #200, Fairbanks, AK
99709
907-474-7147
1434-93-G-2385

Gerald L. Black
Oregon Department of Geology and Mineral Industries 800 NE Oregon St., #28,
Portland, OR 97232
503-731-4100
1434-93-G-2386

ELEMENT II.5

We have observed several hundred clastic dikes resulting from liquefaction in the Portage, Alaska, area during the great Alaska earthquake of 1964. The earthquake (M_w=9.2) caused widespread lateral spreading and submergence in this area, about 85 km from the primary epicenter. Within two decades the submerged surface and vegetation (1964 peat) were buried by up to 2 m of intertidal deposits (Placer River Silt). Lateral migration of stream channels has exhumed many clastic dikes, most of which intersect the pre-earthquake surface through breaks in the 1964 peat. These breaks are probably associated with ground cracks mapped immediately after the earthquake. Clastic dikes observed so far are up to 1.5 m wide and contain predominantly medium to coarse sand and gravel up to coarse pebble size. Source beds are as shallow as 42 cm below the buried pre-earthquake surface. Sand in the upper portion of most dikes was removed to as much as 50 cm below the peat and replaced with silt, probably as a result of postearthquake tidal flooding and deposition of Placer River Silt. Some dikes terminate in sand boils that rest on 1-2-cm of silt overlying the peat . However, preserved sand boils are uncommon and extruded sand was never observed to be more than 10 cm thick but may be as thin as 1-2 grain thicknesses.
grain thickness.

In contrast, along the Knik and Matanuska Rivers at 95 km epicentral distance, mapped ground cracks remain open to 1.3 m depth and 3.7 m width but show no evidence of significant sand injection. Limited excavation suggests that these cracks healed by filling from above and were the loci of minor or no sand extrusion.

In both areas, lateral-spreading damage to the Alaska Railroad was extensive. Differences in ground-crack fillings probably result from differences in depth to liquefied layers and perhaps epicentral distance.

Regional Seismotectonic Studies

9904-13010

Craig S. Weaver
Branch of Seismology
U.S. Geological Survey
at Geophysics Program AK-50
University of Washington
Seattle, Washington 98195
206-553-0627
206-553-8350 fax

Investigations

1. Continued analysis of the seismicity and volcanism patterns of the Pacific Northwest in an effort to develop an improved tectonic model that will be useful in updating earthquake hazard assessments in the region. Particular emphasis on examining the relation between crustal earthquake distributions and evolving models of block tectonics. (Weaver, Yelin, co-authors from Menlo Park, Golden, and Portland)

2. Continued acquisition of seismicity data across the Pacific Northwest, with emphasis on monitoring the Cascadia subduction interface, the Cascade volcanoes, and the Mount St. Helens area including the St. Helens zone. (Weaver, Yelin, Norris, Meagher, with the University of Washington)

3. Study of the Klamath Falls, Oregon earthquake sequence. (Weaver, Yelin, Meagher, Norris with A. Qamar of the University of Washington)

4. Study of seismically recorded rockslides and avalanches on Cascade volcanoes, with particular emphasis on a rockfall on Lassen Peak in September, 1993. (Norris)

5. Study of historical seismicity at Lassen Peak. This project is investigating earthquake swarms that occurred at Lassen Peak in 1946 and 1950. The study seeks to determine the nature of the swarms (rate of occurrence of events greater than magnitude 2.0, variation in S-P times, variations in amplitude ratios) and compare these results with similar parameters determined from better-monitored seismic swarms in the Long Valley area. (Meagher, Norris, Weaver)

Results

Earthquake distribution and block tectonic models. In Blakely et al (see Reports list) the results of a low altitude detailed aeromagnetic survey of the Portland, OR - Vancouver, WA area are presented. The aeromagnetic data clearly indicate the presence of buried, northwest striking faults on both the northeast and southwest sides of the Tualatin Mountains (locally called the Portland or West Hills). The magnetic signature of the fault on the northeast side of the Portland Hills extends southeast of downtown Portland for a distance of 50 km. The magnetic anomaly on the southwest side of the Portland Hills coincides with a previously mapped fault. The aeromagnetic data also provide evidence for a set of apparently disconnected faults on the eastern side of the Portland basin.

The aeromagnetic data image faults at depths of a few kilometers. Contemporary microseismicity occurs at depths of 10 to 25 km. with a near absence of activity at depths less than 10 km. The surface projections of fault planes inferred from earthquake focal mechanisms in the Portland Hills lie well to the east of the surface projections of the shallow structures producing the magnetic anomalies. Thus it is difficult to argue conclusively that the contemporary seismicity is directly connected to the shallow structures that are imaged by the aeromagnetic data.

Despite the current uncertainties in how to interpret the geologic, seismologic and aeromagnetic data in a comprehensive model, the aeromagnetic data are important in that they provide convincing evidence for subsurface faults that may present a seismic hazard. Further investigations are clearly needed.

In the Puget Sound area, we have investigated the relation of crustal earthquakes to the South Whidbey Island fault zone as part of a study coordinated by Sam Johnson (see Reports list). The south Whidbey Island fault represents a segment boundary between two major crustal blocks of very different ages and composition. The fault was active during the Neogene, forming the active boundary between thrust tectonics to the southwest and relative quiescence to the northeast.

The importance of the South Whidbey Island fault to the regional earthquake hazard assessment is under investigation. Only a few earthquakes have been located near the location of the fault zone; no clear relation exists these deep crustal events (below 15 km) and the fault zone. Both the Portland Hills fault and the South Whidbey fault illustrate the problems of linking surface geological and shallow geophysical observations with deeper seismicity.

Outreach Activities. During FY94 we expanded contacts with emergency managers in Oregon and Washington and strengthened our ongoing discussions with the engineering community. The following are some of the highlights of our 1994 contacts:

- Production of Open File Report 94-226B (see publication list). This OFR complements Susan Goter's 1:1,00,000 multicolor epicenter map "Earthquakes in Washington and Oregon, 1872-1993", USGS OFR 94-226A. A copy of map of the earthquake distribution is shown in Figure 1; there has been heavy public demand for both products.
- An address by Tom Yelin to the National Coordinating Council on Emergency Management, Region X. The meeting was held 8/3-5/94 in Portland Oregon. Earthquake hazards in Alaska, Idaho, Washington and Oregon were described and issues surrounding earthquake forecasting and prediction were discussed.
- Yelin helped plan the FEMA-USGS-Idaho Bureau of Disaster Services workshop "Perspective on Earthquakes in Rural Areas", held in Boise, Idaho 10/26-28/94.
- Yelin and Norris traveled to Klamath Falls in January 1994 to deploy temporary seismographs to record renewed aftershock activity there and to participate in public presentations to a total of about 400 people on the continued felt aftershock activity from the M5.9 and M6.0 September 1993 earthquakes.
- Weaver summarized new seismic source results at the Applied Technology Council's Seattle Workshop and at a national meeting during the Fifth International Earthquake Engineering Meeting held in Chicago.
- Weaver addressed the Washington Emergency Managers Association annual meeting, describing the different earthquake source zones in Washington and giving a review of the capabilities of the University of Washington seismic network to provide data in near-real time.

- At the Portland Metro meeting, "When the Earth Moves-Again", Weaver outlined the current understanding of earthquake source zones, the expected maximum magnitude event in each, and gave estimates of the type of ground shaking expected. The bottom line in the Pacific Northwest is that the known past, the period of recorded history since about 1840, is not representative of the region's earthquake hazards and risks.

Reports

Blakely, R.J., R.E. Wells, T.S. Yelin, I.P. Madin and M.H. Beeson, Tectonic setting of the Portland-Vancouver area, Oregon and Washington: Constraints from low-altitude aeromagnetic data, *Bull. Geol. Soc. Amer.*, submitted.

Johnson, S. Y., Potter, C. J., Armentrout, J. M., Finn, C., Pratt, T. L., and C. S. Weaver, The southern Whidbey Island fault, Washington, *Geol. Soc. Amer. Bull.*, submitted.

Norris, R. D., 1994, Seismograms from large rockfalls and avalanches in the Cascades and their implications for seismic detection of hazardous mass movements, *Bull. Seism. Soc. Amer., 84*, in press.

Norris, R. D., 1993, Seismic and field observations of the 26 August 1993 rockfall from Lassen Peak, California (abs), *EOS: Trans. Amer. Geophys. Union, 74*, 649.

Norris, R. D., Meagher, K. L., and Weaver, C. S., The 1936, 1945-47, and 1950 earthquake sequences near Lassen Peak, California: Seismic evidence for active Basin and Range extension in the southern Cascade Range, (in review).

Weaver, C. S., 1994, Work in progress in the Pacific Northwest National Earthquake Hazards Reduction Program Fiscal Year 1994, *U.S. Geol. Surv. Open-File Report 94-154*, 34 pp.

Wong, I.G., J. Unruh, T.S. Yelin and J. Bott, 1994, Crustal seismicity in the Portland, Oregon region and its relationship to the Cascadia subduction zone (abs), *Geol. Soc. Amer. Abstracts with Programs, 26*, A-524.

Yelin, T.S., A.C. Tarr, J.A. Michael and C.S. Weaver, 1994, Washington and Oregon Earthquake History and Hazards, *U.S. Geol Surv. Open File Report 94-226B*, 12pp.

Yelin, T.S., 1994, The September 1993 Klamath Falls, Oregon earthquakes, *Pacific Northwest NEHRP Regional Fact Sheet*, 2pp.

Figure 1: Map of earthquake locations for the years 1872-1993. For the period prior to 1970, only selected largerearthquakes are plotted. For the period 1970-1993 earthquakes with magnitudes of 1.5 or greater are shown. For most areas included on the map, all earthquakes that actually occurred that had magnitudes of 2.5 or greater should be plotted. In a few areas (particularly in the map's southeastern quadrant) a few magnitude 2.5 or smaller earthquakes may have occurred that were not recorded and located by the operators of the region's seismograph networks. This figure was taken from USGS OFR 94-226B. The numbered earthquakes and two and three letter place name abbreviations are discussed and explained in that report; we don't repeat those discussions here.

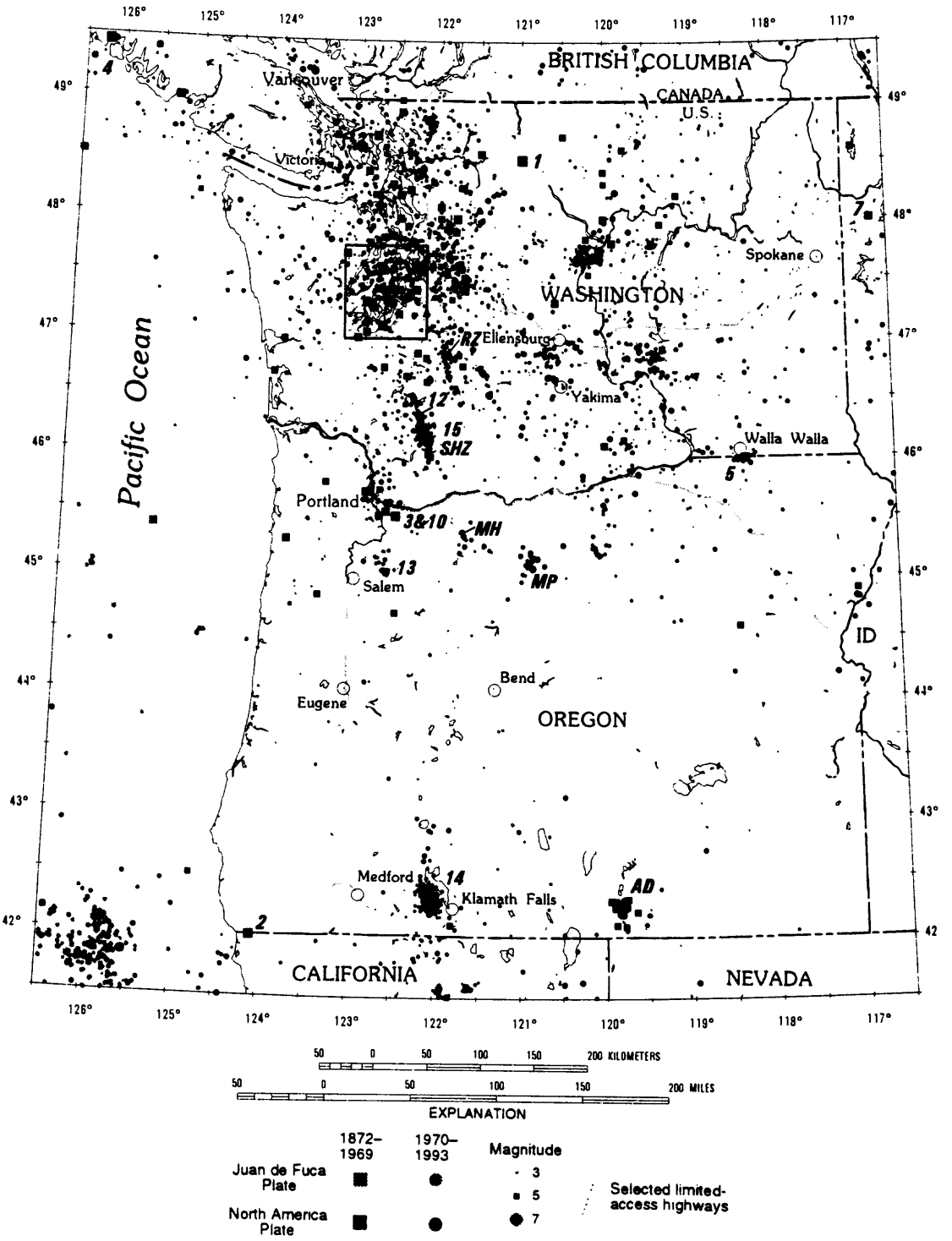
BRITISH COLUMBIA
CANADA
U.S.
Vancouver
Victoria
Pacific Ocean
WASHINGTON
Spokane
Ellensburg
RZ
Yakima
12
15
SHZ
Walla Walla
5
Portland
3&10
MH
13
Salem
MP
ID
Bend
Eugene
OREGON
Medford
14
Klamath Falls
AD
2
CALIFORNIA
NEVADA
1
4
7
126°
125°
124°
123°
122°
121°
120°
119°
118°
117°
49°
48°
47°
46°
45°
44°
43°
42°
50 0 50 100 150 200 KILOMETERS
50 0 50 100 150 200 MILES
EXPLANATION
1872–1969
1970–1993
Magnitude
3
5
7
Juan de Fuca Plate
North America Plate
Selected limited-access highways

Determination of Late Pleistocene - Holocene Slip Rates Along the San Gregorio Fault Zone, San Mateo County, California

Award Number: 1434-93-G-2336

Gerald E. Weber and Jeffrey M. Nolan

Weber, Hayes and Associates
120 Westgate Drive, Watsonville, CA 95076
(408) 722-3580, FAX (408) 722-1159, Email - jweber@earthsci.ucsc.edu

Program Elements: II.3 and LL.5
Determine the Nature and Rates of Crustal Deformation.
Identify Active Faults, Define Their Geometry, and Determine the Characteristics and Dates of Past Earthquakes.

INVESTIGATIONS UNDERTAKEN

The purpose of this study has been threefold: 1) to resolve some of the questions regarding the late Quaternary - Holocene movement history of the San Gregorio fault zone, 2) to locate sites for exploratory trenching and studies to develop late Quaternary slip-rate information, and 3) to resolve the number and ages of wave-cut platforms in the marine terraces on Ben Lomond Mountain. This information will allow a better assessment of the role of the San Gregorio fault zone in the Holocene tectonics of the San Francisco Bay area and the potential for the San Gregorio fault zone to generate large destructive earthquakes in the greater San Francisco - Monterey Bay region.

To accomplish these goals we performed the following:

1. Geologic mapping along the San Gregorio fault zone. Our primary objective was to map Quaternary deposits and faults, however, we also mapped contacts between pre-Quaternary rocks where appropriate. The geologic mapping was combined with extensive aerial photo interpretation and review of the available literature, including consulting reports.

2. Geologic mapping of the marine terraces between Greyhound Rock and Davenport in Santa Cruz County. Our mapping focused on the Davenport, Highway 1, and Greyhound Rock wave-cut platforms within the Santa Cruz marine terrace (Bradley and Griggs, 1976). We measured the elevations of the shoreline angles of these wave-cut platforms and the height of the steps between platforms. We flew the coastal strip to observe and photograph the marine terrace shoreline angles and wave-cut platforms exposed in the high cliffs between Davenport and Greyhound Rock.

3. We examined and prepared a field log of the only exposure of the Davenport wave-cut platform and shoreline angle near the town of Davenport.

4. We performed a gravity survey along Highway 1 across the mouth of Pescadero Creek in an attempt to determine the amount of vertical offset across the Frijoles fault.

RESULTS

Our preliminary interpretations of these data suggest the following:

1. The map of Quaternary faulting along the San Gregorio fault zone (Weber and Lajoie, 1980) requires only minor changes in the fault pattern. However, the trace of the Holocene active portion of the Frijoles fault should be revised. The active fault trace of the Frijoles fault at Point Ano Nuevo branches off of the main trace (Coastways fault) north of Whitehouse Creek.

The Frijoles fault as mapped along the axis of Arroyo de los Frijoles and through the mouth of Pescadero Creek does not appear to be a primary strand of the fault as was indicated by Weber (1980) and Weber and Lajoie (1980). This is based on the relatively minor vertical offset of the Purisima Formation-Pigeon Point Formation contact (Pliocene/Cretaceous) in the vicinity of Arroyo de los Frijoles. Horizontal offset of this contact cannot be determined, but does not appear to be large. The Frijoles fault near the mouth of Pescadero Creek clearly offsets the lowest emergent marine terrace vertically along a series of reverse-oblique fault strands. However, the amount of right lateral movement, once again, cannot be determined.

2. Apparent right lateral offset of stream terraces of Ano Nuevo Creek are consistent with slip rates of 1-3 mm/yr, on the Coastways fault only. The apparent offset of geomorphic features near San Gregorio Creek constrains offset between 3-9 mm/yr, across the major strands of the fault. These slip rates are preliminary.

3. We have located 3 sites for exploratory trenching studies of the Coastways and Frijoles fault strands of the San Gregorio fault zone. These will be investigated during 1995. They include the two areas discussed in #2 above.

4. The marine terrace stratigraphy of Ben Lomond Mountain should be revised as follows:

A) The lowest emergent terrace (Santa Cruz Terrace) contains only one wave-cut platform and shoreline angle (Highway 1), not three as indicated by Bradley and Griggs (1976). The Highway 1 wave-cut platform probably corresponds with the 103 ka (isotope stage 5c) sea-level high stand.

B) The designation of the Greyhound Rock and Davenport wave-cut platforms within the Santa Cruz Terrace as wave-cut platforms formed by separate sea-level high stands is not warranted by field evidence.

1) Only 1 wave-cut platform and shoreline angle are present north of Scott Creek. The Greyhound Rock wave-cut platform appears to be an intertidal bench, not an abrasional platform formed by a separate sea-level high stand.

2) Field evidence for the Davenport wave-cut platform and shoreline angle is weak. The lone field exposure of the Davenport wave-cut platform and shoreline angle at Davenport appears to be a fluvial terrace of San Vicente Creek. Five, twenty five year old, refraction seismic lines across the Santa Cruz marine terrace that show a 7-9 foot high step are, therefore, the sole evidence of the existence of the Davenport wave-cut platform.

Bradley and Griggs, 1976 study of the Ben Lomond Mountain marine terraces has been the basis for numerous subsequent analysis of Pleistocene uplift rates and neotectonics. The presence of 3 wave-cut platforms (each related to a different sea-level high stand) in the Santa Cruz Terrace proved a dilemma to the interpretation of terrace ages and uplift rates. At least 4 different interpretations of terrace ages and uplift rates exist for this terrace sequence. The Greyhound Rock wave-cut platform and shoreline angle are anomalous because of the narrow width of the platform and its absence elsewhere in Santa Cruz and San Mateo Counties.

The recognition of only 1 wave-cut platform and shoreline angle in the Santa Cruz Terrace reduces the ambiguity surrounding platform ages and uplift rates. It suggests the Highway 1 wave-cut platform and shoreline angle of the Santa Cruz Terrace corresponds with the 103 ka sea-level high stand and that the uplift of Ben Lomond Mountain has been constant. Uplift rates vary from about 0.35 m/ka near Santa Cruz to 0.48 m/ka near Greyhound Rock.

5. We have revised slightly the marine terrace stratigraphy west of the San Gregorio fault zone. Interpretations of terrace ages and uplift rates west of the fault zone are incomplete and presently being analyzed.

REPORTS PUBLISHED

We have submitted 2 abstracts to the May 1995 joint meeting in San Francisco of the American Association of Petroleum Geologists, SEPM and Association of Engineering Geologists. We have also submitted a manuscript written jointly with William Lettis and Kathryn Hanson on the evidence for large Quaternary horizontal offsets along the San Gregorio - Hosgri fault zone to the Journal of Geophysical Research. We are presently waiting for notice of acceptance, or rejection, of both the abstracts and the manuscript.

REFERENCES CITED

Bradley, W.C., and Griggs, G.B., 1976, Form, genesis, and deformation of central California wave-cut platforms, Geol. Soc. of Am. Bull., v.87, p.433-449.

Weber, G. E., 1980, Recurrence intervals and recency of faulting along the San Gregorio fault zone, San Mateo County, California, Ph.D. dissertation University of California, Santa Cruz, 204p.

Weber, G.E., and Lajoie, K.R., 1980, Map of Quaternary faulting along the San Gregorio fault zone, San Mateo and Santa Cruz Counties, California, U.S. Geological Survey Open-File Report 80-907, 3 map sheets.

Paleoseismic Study of the Southern Sargent Fault

Award Number: 1434-94-G-2466

Gerald E. Weber and Jeffrey M. Nolan

Weber, Hayes and Associates
120 Westgate Drive, Watsonville, CA 95076
(408) 722-3580, FAX (408) 722-1159, Email - jweber@earthsci.ucsc.edu

Program Elements: II.5
Identify Active Faults, Define Their Geometry, and Determine the Characteristics and Dates of Past Earthquakes.

INVESTIGATIONS UNDERTAKEN

The purpose of this study is to determine the recency of faulting and the movement history of the southern portion of the Sargent fault. As of December 1, 1994 we have opened the first of several trenches on the floodplain of the Pajaro River northwest of Lomerias Muertas in southern San Benito County, California. Work is in progress. We have performed the following:

1. Geologic mapping along portions of the Sargent fault at Lomerias Muertas. This was combined with extensive aerial photo interpretation and review of the available literature, including unpublished and proprietary consulting reports.

2. Excavation of a two, 15 foot deep exploratory trenches across the mapped trace of the southern Sargent fault on the floodplain of the Pajaro River northeast of Lomerias Muertas. One trench collapsed prior to shoring. The second trench is being logged.

3. Fault parallel trenches will be excavated some time in December to try to find piercing points across the fault.

RESULTS

The preliminary results of our logging the initial exploratory trench suggest the following:

1. A fault is clearly exposed in the walls of the trench cutting the late Pleistocene - Holocene sediments of the Pajaro River and Lake San Benito. The fault strikes roughly north 60^0 west and dips 70^0 northeast. This dip was unexpected. The Sargent fault has been characterized as a reverse oblique fault due to the N60^0W strike and the location of the fault in respect to the San Andreas and Calaveras faults.

2. Slickensides on the fault plane indicate that the slip vector is primarily horizontal. The relatively small vertical component of slip is consistent with normal movement. The amount of horizontal slip cannot, as of yet, be determined.

3. The fault offsets sedimentary units approximately 54 cm near the base of the trench, while units near the surface are offset 5 cm. This suggests at least 2 rupture events, probably both within the Holocene.

4. We are continuing to log the existing trench and collecting material for C_{14} dating. Additional trenches will be excavated during December 1994. Work continues.

REPORTS PUBLISHED

We have submitted an abstract to the May 1995 meeting of the American Association of Petroleum Geologists, SEPM and Association of Engineering Geologists. This meeting will be held in San Francisco. We are presently waiting for notice of acceptance, or rejection, of this abstract.

Tectonic Framework and Geology of the San Francisco Bay Region

Carl M. Wentworth and Earl E. Brabb
Branch of Western Regional Geology
U.S. Geological Survey
345 Middlefield Road
Menlo Park, CA 94025
(415) 329-4950 / 5140
cwent@sierra.wr.usgs.gov / ebrabb@isdmnl.wr.usgs.gov

INVESTIGATIONS

The principal activities, which were pursued as part of a larger Regional Geology project that is focussed on the Bay region, included mapping of Quaternary deposits and of bedrock structure and stratigraphy, geologic compilation at 1:24,000 to 1:100,000, development of digital techniques for the compilation and analysis of geologic maps, cooperative work with other projects, and participation in regional program activities.

RESULTS

Contra Costa County geology - Digital compilation of bedrock geology at 1:62500 for the county was completed and released in digital form* as ARC/INFO vector coverages of the 1:62,500 geology and 1:100,000 base layers and a postscript image of the map at 1:75,000 (Graymer, Jones, and Brabb, 1994, and see cc_g1 area on index map). This work was done in cooperation with Jones and Graymer at UC Berkeley and involves major change in both structure and stratigraphy resulting from field checking throughout the County, new microfossil data, and resulting reassignment of stratigraphic identity of many fault-bounded units. This reinterpretation of the area recognizes several contrasting stratigraphic sequences juxtaposed by thrusts and leads to the conclusion that crustal blocks defined by strands of the San Andreas fault system have undergone compression that has shifted these blocks and their boundary faults east relative to North America, which implies that the blocks and their boundary structures are bounded below by an active decollement. (See Jones and others, 1994)

Quaternary deposits of Contra Costa and Alameda County - New mapping of surficial units having distinctive lithology and physical character has been completed at 1:24,000 for both counties and is being compiled at 1:62,500 for standard open-file release. These maps and correlation of units with similar units around Monterey Bay that liquefied in 1906 and 1989 provide a new basis for predicting liquefaction in the East Bay region.

Santa Clara Valley Quaternary - 1:24,000 compilation of new Quaternary mapping in a block of eight 7.5 minute quadrangles (Palo Alto, Mountain View, Milpitas, Calaveras Reservoir, Cupertino, San Jose West, San Jose East, and Santa Teresa Hills: and see area labeled sccq on index map) was completed and released in digital form* as ARC/INFO vector coverages of the 1:24,000 geology and 1:100,000 base layers and a postscript image of the map at 1:50,000 (Helley and others, 1994).

Alameda County bedrock geology - A digital compilation from 1970's mapping and compilation is in hand and work is beginning to address the many problems now recognized in that geology, including serious misidentifications of units and the need to reinterpret structural relations in the light of the thrust pattern now recognized to the north.

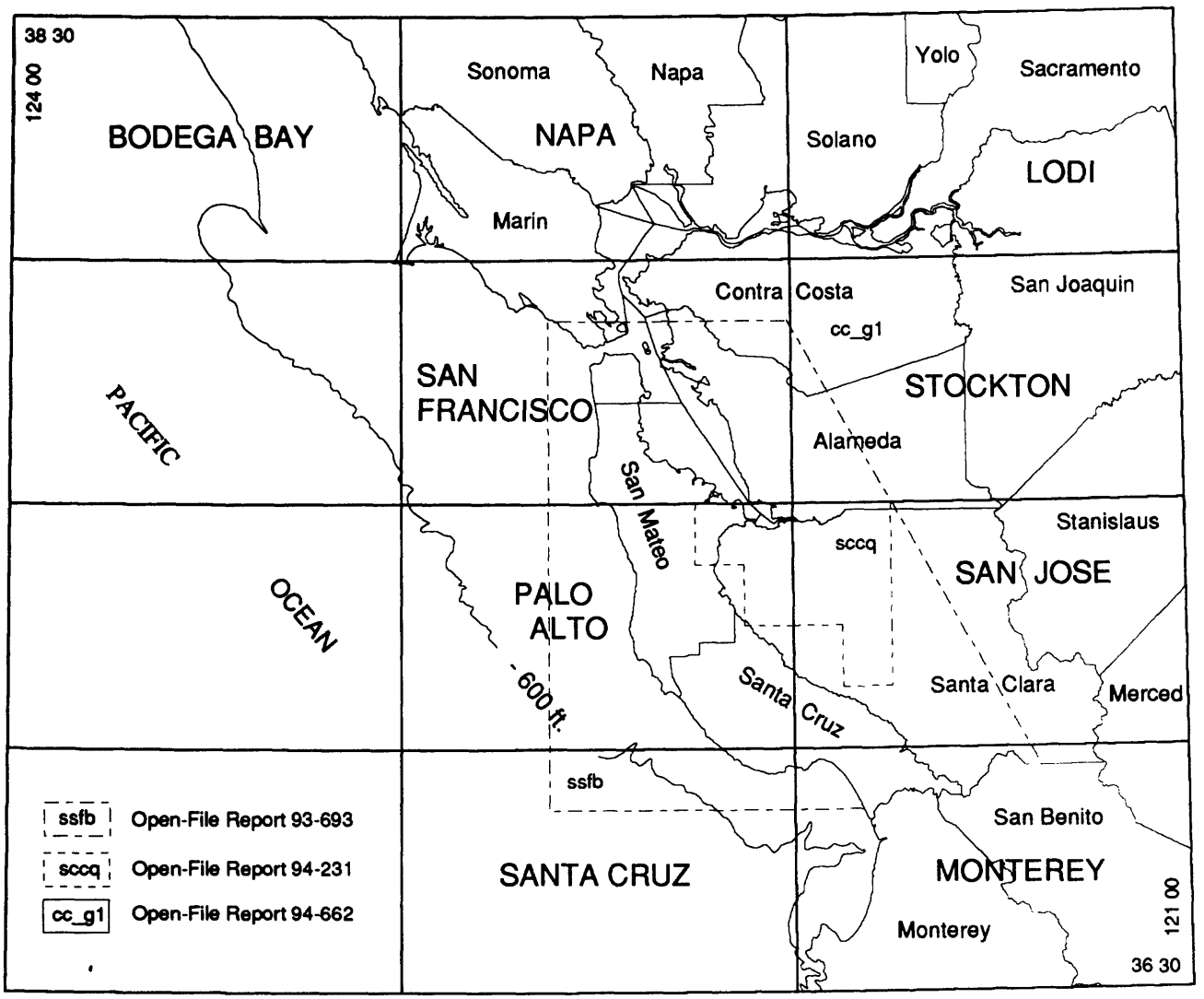

Index Map of the San Fancisco Bay Region, showing areas covered by digital Open-file Reports, 1:100,000 quadrangles, and counties.

Fossil Database - Information on fossil localities in the region (collections, identifications, and interpretations) extracted from the literature and theses has been entered into a standardized database designed to satisfy project and general requirements. About 2,000 localities have been entered, largely by Betty Harrod (now retired) and volunteers Larry Dickerson, John Parker, Mary Bowen, and Earl Brabb, using the Mac-based database program Filemaker Pro.

Industry Fossil Collections - About 12,000 surface samples of microfossils from the greater San Francisco Bay region have been obtained from Shell, Exxon, Chevron, Arco, and Unocal oil companies by Earl Brabb. These consist of picked slides and washed samples, as well as supporting reports and location maps.

Geologic Materials of the southern San Francisco Bay region - Completed and released a 1:125,000 digital database* for the south San Francisco Bay region (see index map, area labeled ssfb with dashed boundary) compiled from three 1970's regional compilations (flatlands deposits - Helley and Lajoie,

hillside materials - Ellen and Wentworth, and Santa Cruz County geology - Brabb). The geology is represented in the database as an ARC/INFO coverage with the unit polygons described in the INFO database table by unit identifier, general lithology, geologic age, and stratigraphic name.

Active Fault Maps - Digitized several fault maps as ARC/INFO coverages. San Andreas fault on the San Francisco Peninsula: Sarna and others, MF 650; Pampeyan, OF 93-684; Brown, MF 355; and relevant CDMG Alquist-Priolo quads; Hayward fault in the East Bay: Lienkamper, MF-2196.

Northridge Ground Motion Maps - In cooperation with Roger Borcherdt and others, prepared maps in ARC/INFO of strong motion stations that recorded the Northridge earthquake and their peak horizontal and vertical accelerations in which the recording stations and peak acceleration values, together with one of many possible contour representations of those values, are shown over a geologic background prepared from the 1:750,000 State geologic map (Wentworth and others, 1994). These maps were open-filed at page size (Wentworth and others, 1994)and used to prepare colored posters.

Bedrock surface beneath the Bay trough - A new map of the southern Bay trough has been prepared by volunteer Walter Hensolt and is being reviewed for release in the USGS Open File.

REPORTS

Helley, E.J., Fitzpatrick, J.A., and Bischoff, J.L., Uranium-series dates on oyster shells from elevated marine terraces of San Pablo Bay, California: U.S. Geological Survey Open-File Report 93-286.

*Helley, E.J., Graymer, R.W., Phelps, G.A., Showalter, P.K., and Wentworth, C.M., 1994, Preliminary Quaternary geologic maps of Santa Clara Valley, Santa Clara, Alameda, and San Mateo Counties, California: A digital database: U.S. Geological Survey Open-File Report 94-231, data resolution 1:24,000.

*Graymer, R.W., Jones, D.L., and Brabb, E.E., 1994, Preliminary geologic map emphasizing bedrock formations in Contra Costa County, Cal;ifornia: a digital database: U.S. Geological Survey, Open-File Report 94-622, map resolution 1:50,000.

Jones, D.L., Graymer, Russell, Wang, Chi, McEvilly, T.V., and Lomax, A., 1994, Neogene transpressive evolution of the California Coast Ranges: Tectonics, v. 13, No. 2, p. 561-574.

Nakata, J.K., Sorg, D.H., Russell, P.C. and others,1993, New radiometric ages and tephra correlations from the San Jose and the northeastern part of the Monterey 1:100,000 map quadrangles, California: Isochron/West, v. 60, p.19-32.

*Wentworth, C.M. 1993, General distribution of geologic materials in the southern San Francisco Bay region, California: a digital database: U.S. Geological Survey Open-File Report 93-693, data resolution 1:125,000, database manager C.M. Wentworth.

Wentworth, C.M., Borcherdt, R.D., Mark, R.K., and Boore, D.M., 1994, Maps of peak horizontal and vertical accelerations recorded for the Northridge, California, earthquake of January 17, 1994 and general geology of the epicentral region: U.S. Geological Survey Open-File Report 94-197.

---

* The digital Open-File reports can be obtained directly over Internet as tar files of ARC workspaces containing the map coverages and associated files, or on tape from Carl Wentworth (call 415-329-4950 to arrange). For Internet access, connect by ftp to sierra@wr.usgs.gov (130.118.37.33), login as anonymous, cd to pub, and look at the READMEs for available documents.

Annual Project Summary

A Collaborative Project (UNR & U of I): Study of Possible Evidence of Paleoliquefaction in Ditch 12 within the New Madrid Seismic Zone

USGS Project Number : 1434-94-G-2395
P.I.: Steven G. Wesnousky
Institution: University of Nevada, Reno
Address: Center for Neotectonic Studies
University of Nevada, Reno 89557
Tel: 702-784-1382
FAX: 702-784-1382
e-mail: stevew@seismo.unr.edu
Program Element: NEHRP-II.2

The great New Madrid earthquakes of 1811-12 were accompanied by extensive liquefaction within the meizoseismal zone. One of us (S.G.W) during the period 1989 through 1991 examined 10's of kilometers of ditch banks within the southern limb of the New Madrid Seismic Zone for evidence of prehistoric liquefaction events. A previous study provided no definitive evidence of widespread paleoliquefaction events during the last 5000 to 10,000 years. The lack of evidence indicating any widespread paleoliquefaction event was the basis to suggest that the return time of great New Madrid earthquakes was greater than the 500 to 1100 year return time that is often quoted on the basis of historical earthquake statistics. However, one of the exposures observed in that study did allow an interpretation whereby a buried sand layer observed along one ditch was vented during an extensive paleoliquefaction and ground subsidence episode about 5000 years ago. Because the understanding of the recurrence behavior of great earthquakes in the New Madrid region is important to understanding both the seismic hazard and rate of intraplate deformation in the New Madrid region, we have commenced a stratigraphic and soils analyses of exposures adjacent to this site to remove the ambiguity attendant to interpretation of possible paleoliquefaction features along this ditch and, by inference, the repeat time of great 1811-12 earthquakes.

The crux of our work rests in observations at what we refer to as Sites 2 and 3, separated by a distance of about 250 meters, along the Ditch No. 12 (Wesnousky and Leffler, 1992). The Ditch No. 12 is located west of Big Lake Wildlife Refuge in Arkansas (The ditch trends east-west, is directly above the southern limb of the New Madrid Seismic Zone, and within the meizoseismal zone of the great 1811-12 earthquakes. Numerous sand-filled breaches are exposed in the topstratum and confirm the pervasive nature of liquefaction along the ditch.

In prior work, we observed Site No. 2 to expose a sand unit interpreted to have vented in 1811-12. The exposure is capped by about 1 m of man-made fill. Beneath the fill is a 1 to 2 meter thick layer of clean fine to medium sand. The sand is fed by a dike at the base of the exposure. Soil development on the sand is marked by a 5-10 cm thick A-horizon and no significant B-horizon. The weak soil profile suggests that the deposit on which it formed is very young, most likely a result of the ejection of the sand to the surface in 1811-12. The internal structure of the ejected sand shows two distinct thin layers of silt and lignite. The thin layers probably represent brief time lapses between episodes of venting and the attendant settling of finer grained, lighter materials. The lack of any soil development or oxidation indicates that the layers were exposed for a very brief time. In contrast to the weakly developed soil on the ejected sand at Site 2, the buried surface on which the ejected sand rests is characterized by a well-developed soil profile, consisting of a 10-15 cm thick A-horizon (2Ab) and a B-horizon (2Bb) which is about 1 m thick. The strong development of the 2Ab-2Bb soil profile suggests that the surface on which the sand ejected was stable for a long period of time prior to being breached by liquefied sand in 1811-12. The buried 2Ab-2Bb profile grades downward into a clean sand which, in turn, rests in sharp contact with another buried surface on which the 3Ab-3Bb soil-

profile is developed. A speculative interpretation is that the 2Ab-2Bb profile is developed on sands ejected at the time of a prehistoric earthquake.

Nearby at Site 3, we also previously obtained radiocarbon dates from wood samples to place direct limits on the age of the topstratum through which the sand vented. The topstratum at this location is very dark clay and sharply interrupted by the intrusion and ejection of very light gray, locally oxidized, very fine to fine grained sand. Again, the weak soil profile developed on the extruded sand, composed of a thin A-horizon and virtually no B-horizon, indicates that it most likely formed since 1811-12. A very well developed soil is present on the surface through which the sand vented, suggesting considerable antiquity and stability to the surface on which it is developed.

Unit 2Ab at Site 3 is a loamy sand which rests in abrupt and irregular contact with the underlying silty loam (2Eb) and loam (2Bb). It may be speculated that the loamy sand (2Ab) was originally vented to the surface during a paleoliquefaction event but, like at Site 2, no evidence for a feeder dike was observed. Large pieces of bark-covered wood were recovered from 2 locations within the lowermost meter of topstratum at Site 3 (Figure 12). The 2 samples have radiocarbon dates of 5090 ± 60 and 11,100 ± 100 C-14 yr B.P., respectively (Beta Analytic Inc.; Lab sample numbers Beta-38311 and Beta-41984). The wood at the base of the topstratum has an age of 11,100 ± 100 C-14 years B.P. Thus, the topstratum represents about 5,000 to 10,000 years of accumulation since abandonment of the surface. Speculatively assuming that unit 2Ab (the loamy sand) was vented onto an earlier surface during a paleoliquefaction event, the exposure would provide evidence for two large earthquakes in about the last 10,000 years, or a return time of about 5,000 years.

In summary, both Site 2 and 3 show a distinct buried surface on which rests a buried sand or loamy sand. It is possible that both (1) the buried sand units were vented in a past liquefaction event and (2) the burial of the surfaces on which the sands rest reflects major subsidence at the time of a great earthquake much like is known to have occurred throughout much of the St. Francis Sunk Lands during the great 1811-12 earthquakes. During September of 1994, we further excavated a number of exposures between Site No. 2. and Site No 3. The exposures provided evidence of a paleovent feeding one of the buried layers of sand. We collected numerous samples of wood that are currently being used to place age constraints on the timing of the paleovent. We will return in Spring of 1995 to further excavate the exposures and examine whether or not we can place limits on the size of the sandlayer which is fed by the paleovent.

Annual Project Summary

Earthquake Frequency Statistics, Seismic Hazard, and the Mechanics of Faulting
USGS Project Number : 1434-94-G-2460
P.I.: Steven G. Wesnousky
Institution: University of Nevada, Reno
Address: Center for Neotectonic Studies
University of Nevada, Reno 89557
Tel: 702-784-1382
FAX: 702-784-1382
e-mail: stevew@seismo.unr.edu
Program Element: NEHRP-II.5

We have been using a global data set of strike-slip faults to examine whether or not (1) the geometrical complexity of fault traces or (2) the shape of the magnitude-frequency distribution along particular faults is a function of the amount of cumulative strike-slip offset recorded by the faults. The motivation for (1) arises from earlier work that suggested, on the basis of a small data set of faults primarily from California, that fault trace complexity decreases as a function of cumulative offset. The motivation for (2) stems from the questions regarding whether or not seismicity along a single fault is described by the Gutenburg-Richter relationship:

$$Log\ n = a\text{-}bM \qquad (1)$$

where n = number of events of magnitude M and a and b are empirical constants. Catalogs of regional seismicity are typically well described by the Gutenburg-Richter relationship (equation 1). The assumption that seismicity on a single fault also satisfies equation 1 implies that there will be numerous lesser-size events in the time interval between the occurrence of the largest earthquakes on a fault. However, a number of studies have reported evidence to suggest that faults tend to generate earthquakes that have a relatively narrow range of magnitudes near the maximum, and that the occurrence of these earthquakes does not follow the log-linear frequency-magnitude relationship of equation 1, a concept now commonly referred to as the characteristic earthquake model of fault behavior. Determining whether it is the Gutenburg-Richter relationship or characteristic earthquake model that describes the seismicity along particular faults is problematic because historical records of seismicity are generally much shorter than the repeat time of the largest earthquake on a fault. However, the recurrence of the largest size events along a fault can be determined independently from geologically determined paleoearthquake histories and fault slip rate data. Thus, in addition to examining the geometrical complexity of strike-slip faults, we have been combining instrumental records of seismicity with interpretation of paleoearthquake and fault slip rate data to examine the shape of the magnitude-frequency distribution for the global data set of strike-slip faults.

We have been limiting our analysis to strike-slip faults that are either (1) located within regional seismic networks, or (2) have been the focus of fault slip rate or paleoearthquake studies, or (3) for which maps of sufficient detail exist to define discontinuities in fault trace that measure a kilometer or greater in width normal to fault strike. The faults considered are located in California, Mexico, New Zealand, Japan, China and Turkey. We define the complexity of a fault trace as the number of observed steps per unit length of fault trace, our definition of a step limited by the scale of available maps to those measuring 1 km or more in width perpendicular to fault strike.

It is only faults located in California, Japan, New Zealand, and Baja Mexico that fall within seismic networks that have been recording for a relatively long period of time. The faults of southern California fall within the CIT-USGS network, which has recorded since 1932 (Given et al., 1987). The faults of northern California are within the USGS-CALNET seismic network, which has been officially recording since 1969. The RESNOR seismic network of northwestern

Baja Mexico has been in operation since 1976. Seismicity in the vicinity of the Japanese faults has been recorded by the Japanese Meteorological Agency network since 1926. The Institute of Geological and Nuclear Sciences (formerly DSIR) has been operating a computerized seismic network in New Zealand since 1964. Slightly different methods are used in each network to estimate magnitude, but the various scales (local magnitude, ML, in southern California and New Zealand, coda magnitude, Mc, in northern California and Baja Mexico, and the Japanese Meteorological Agency magnitude, MJMA, in Japan) generally correlate with moment magnitude.

The tentative results of our analysis are twofold. First, we observe a tendency for fault trace complexity to be a decreasing function of cumulative geological offset. Secondly, when combining estimates of the largest earthquakes along each fault based on fault slip rate and paleoearthquake data with the instrumental record of seismicity, we observe that 90% of the faults show an earthquake frequency distribution in agreement with the Characteristic earthquake model. The faults that show an earthquake frequency distribution like predicted by the Gutenberg-Richter model also show relatively lesser amounts of geological offset, suggesting that the shape of the magnitude-frequency distribution may also be a function of cumulative geologic offset and, hence, fault trace complexity.

A PILOT STUDY OF LATE QUATERNARY SURFACE DEFORMATION, SADDLE MOUNTAINS ANTICLINE, NORTHERN PASCO BASIN, WASHINGTON

Grant No. 1434-94-2392

Michael W. West, P.I.
Alan J. Busacca
Glenn W. Berger
Mark E. Shaffer
Francis X. Ashland

Michael West & Associates, Inc.
8906 W. Bowles Avenue, Suite. 290
Littleton, CO 80123
(303) 972-1537; FAX (303) 972-1549

Program Element II.5: Identify active faults, define their geometry, and determine the characteristics and dates of past earthquakes.

INTRODUCTION

Studies by West and Shaffer (1988, 1989,) in the Yakima fold belt, northern Pasco Basin, disclosed evidence of late Quaternary deformation along the north limbs of two asymmetric, faulted anticlines. Our conclusions regarding evidence for late Quaternary deformation along the north flank of the Saddle Mountains anticline were controversial. The controversy revolved around the following questions:

- Is late Quaternary deformation present on the north flank, Saddle Mountains anticline?
- If so, is the deformation tectonic (coseismic folding and thrust surface rupture) or non-tectonic (landsliding)?
- If the deformation is tectonic, what are the implications for seismic hazard/risk in the Pacific northwest and the seismotectonic evolution of the Yakima fold belt and other active fold-thrust belts?

Our earlier studies left several questions unanswered: (1) the characteristics (age, recurrence interval, tectonic slip/event, slip rate) of late Quaternary movement along thrust faults; (2) the relation of secondary hanging wall deformation to primary thrust movement; (3) the relation of possible syntectonic fanglomerates to recurrent Neogene to late Quaternary development of fold-fault structures; (4) the association of contemporary seismicity with late Quaternary deformation; (5) the tectonic relation (relative age, kinematics) between in-sequence (adjacent) and out-of-sequence anticlines in an active fold-thrust belt; and (6) the seismotectonic hazard posed by late Quaternary deformation in the project area.

As part of our FY 94 NEHRP grant, we addressed Questions 1 and 2 through a combination of geologic mapping and trench exploration. Data generated by our study contributes to an

understanding of: (a) surface rupture parameters and primary deformational features associated with seismogenic folds and reverse/thrust faults; (b) secondary deformational features that may be of value in recognizing active fold-thrusts and obscure rupture patterns along low-angle faults; and (c) seismotectonic hazards near nuclear facilities on the Hanford Reservation and major dams on the Columbia River. We believe important contributions have been made to understanding of earthquake hazard/risk in the Pacific Northwest and the tectonic evolution of fold-thrust structures.

Fold/Thrust Tectonics

The seismogenic potential of active fold-thrusts has been underscored by the Coalinga (M 6.7) earthquake of May 2, 1983 (Stein and King, 1984), the Whittier Narrows (M 5.9) earthquake of October 1, 1987 (Hauksson and others, 1988) and the Soviet Armenia earthquake of December 7, 1988 (Wyllie and Filson, 1989). Most paleoseismological studies, however, focus on normal and strike-slip faults (Hull, 1987) because such faults are easier to recognize and study. As a result, a large body of literature is available regarding interpretation of seismogenic normal and strike-slip faults. Comparable literature relating to active reverse/thrust faults is limited, not because these faults pose less hazard, but because they are more difficult to recognize and interpret. The difficulty in recognizing late Quaternary deformation and confusion with landsliding on the north flank of the Saddle Mountains may be classic examples of this problem -- a problem that persists in spite of various studies conducted for nuclear facilities on the Hanford Reservation, a few kilometers to the south.

Experience gained from the El Asnam earthquake (Philip and Meghraoui, 1983) shows that primary geomorphic expression of seismogenic surface rupture along thrust faults may be irregular and obscure. Secondary extensional faulting in the hanging wall of a reverse/thrust fault may be far more prominent than primary coseismic slip on a low-angle, causative thrust. These secondary extensional features include normal faults, graben, en echelon faults and tension gashes (Philip and Meghraoui, 1983), and fault propagation folds (Avouac and others, 1992). Greater relief on secondary, high-angle extensional structures in the hanging wall will be preserved geomorphically much longer than the primary low-angle fault displacement. Avouac and others (1992), in recent studies of El Asnam surface deformation, concluded that fold and fault patterns are complex, segmented, and evolutionary. They note that normal faults in the hanging wall probably merge with the main thrust fault at depth in the Beni Rached segment. In the Sara El Marouf and Kef El Mes segments, slip along the underlying thrust fault is characterized by fault-propagation folds. Analogs to surface deformation described by Philip and Meghraoui (1983) and Avouac and others (1992) are recognizable on the north flank of the Saddle Mountains.

Regional tectonic Setting - Yakima Fold Belt

The Yakima Fold Belt, a series of subparallel, east-west to northwest-trending, asymmetrical anticlinal ridges separated by shallow synclines, occupies the central and western parts of the Columbia Plateau. In cross section, the anticlinal ridges typically have steep northern limbs and

relatively gentle southern limbs. Studies by WPPSS (1981), Myers and Price (1979) and Reidel (1984) interpret the folds as having developed in response to north-south directed compression.

The Saddle Mountains anticline is an asymmetrical, north-vergent compound upwarp traceable over a distance of 110 km from east-southeast of Ellensburg to about 20 km southeast of Othello, Washington. Fold geometry varies from open to tight along the fold axis, and the axial trace is segmented by changes in fold geometry and cross structures. A south-dipping, reverse/thrust fault with at least 2500 m of displacement (Reidel, 1984) bounds the Saddle Mountains anticline along its north flank. Near the east end of Smyrna Bench, faulting overturns the Saddle Mountains basalts along a fault dipping 40° to the south.

Geologic Evidence for Late Quaternary Deformation

The principal late Quaternary tectonic features in the Smyrna Bench segment are the Smyrna Bench graben and a discontinuous scarp coincident with the inferred trace of Saddle Mountains fault north of the graben (Figure 1). The Smyrna Bench graben can be traced as a distinct geomorphic and structural feature over a length of 13 km. Near the extreme western end, the graben is defined by discontinuous fault strands. In the central and eastern sectors of the graben, faults on both flanks are continuous and define a down-dropped axial block, 300 to 1100 m in width, which can be traced to the eastern end of Smyrna Bench and the structural transition to the Saddle Gap segment.

The primary line of evidence suggesting a late Quaternary origin for the Smyrna Bench graben is disruption of modern stream systems draining the north flank of the Saddle Mountains. In the central and eastern sectors of the graben, each major stream drainage has been disrupted by movement on faults flanking the down-dropped block. Preexisting stream channels can be traced from near the crest of the Saddle Mountains across the graben to the north edge of Smyrna Bench and into the Lower Crab Creek Valley. Down-dropping of the central graben block, however, has beheaded these drainages creating closed depressions (sag ponds) along the channel thalwegs (Figure 1). Alluvial fans are accumulating in the closed depressions on the graben floor. Remnants of these channels on the north flank of the graben have reversed course and flow to the south into the down-dropped block. The graben is a remarkable example of the effect of surface fault displacement on a pre-existing drainage system, and a late Pleistocene to Holocene age for the graben is plausible.

The other significant late Quaternary tectonic feature on Smyrna Bench is a discontinuous topographic escarpment located north of the graben. This escarpment is similar to coseismic surface rupture along the Oued Fodda fault responsible for the El Asnam, Algeria earthquake (M 7.3) of October 10, 1980 (Philip and Meghraoui, 1983). Moreover, the escarpment coincides with the inferred location of the Saddle Mountains fault (Reidel, 1984, 1988).

Bingham, Lonquist and Baltz (1970) invoked massive block-glide movement of Smyrna Bench to explain development of the graben. Their interpretation was an attempt to reconcile extensional faulting in a compressional tectonic environment. The only plausible mechanism was mass movement of Smyrna bench as an intact block toward the north creating a graben along the back side. Sliding was inferred to have taken place in several episodes with the latest slide movement occurring shortly before 12 ka (Bingham, Lonquist and Baltz, 1970).

RESULTS

As part of our NEHRP studies, we excavated two trenches across apparent late Quaternary fault scarps in the Smyrna Bench segment, Saddle Mountains anticline. The objectives of trenching were: (1) to define ages of deformation; (2) to determine the nature of deformation (coseismic folding/faulting vs. non-tectonic landsliding); and (3) to assess implications for seismotectonic hazard.

Trench #1

Trench #1, across the north-bounding scarp, Smyrna Bench graben, exposed both normal and thrust faults (Figure 2). Normal faults in the southern part of the trench juxtapose Miocene and Pliocene bedrock and exhibit throws of 0.7 to >4 m in late Pleistocene to Holocene loesses and paleosols. We identified two significant thrust faults in the northern half of the trench. One fault apparently thrusts Miocene Ellensburg Formation over Pliocene Ringold(?) Formation and a second fault thrusts Pliocene Ringold(?) Formation over Miocene Elephant Mountain Basalt. If the sedimentary unit in fault contact with the Elephant Mountain Basalt is indeed Ringold Formation, then this would indicate that Ringold sediments were initially down-dropped into the Smyrna Bench graben and subsequently thrust over the Elephant Mountain Basalt. The thrust faults displace the basal part of a 100-400 ka petrocalcic soil horizon, and one thrust fault appears to deform but not displace the upper surface of the petrocalcic horizon. A thrust roll scarp in the petrocalcic horizon exhibits 0.6 m of fold shortening and 0.3 m of fault slip (Figure 3).

Significant discrepancies exist between the age and slip on normal faults and thrust faults exposed in the trench. Normal faults exhibit more than 4 m of throw in late Pleistocene to Holocene loesses and paleosols. The maximum slip on thrust faults mapped in the trench is probably less than about 1 m, and latest movement is 100-400 ka. These discrepancies indicate that a younger thrust fault lies north of the graben and Trench #1. This inference is consistent with our interpreted location of the active thrust trace.

Trench #1 is important for the following reasons:

- The tectonic model relating extensional deformation in the hanging wall to reverse movement on an underlying thrust fault is valid.
- The age of latest movement in the graben is Holocene.
- Normal faults and related features exposed in the trench are tectonic in origin; massive block-glide landsliding does not explain graben development and is unlikely.
- The discrepancies between the age and slip on normal faults and thrust faults indicates a younger thrust trace lies north of the graben and Trench #1.

Trench #2

Trench #2 was intended to expose the active thrust trace defined by previous mapping. The target of Trench #2 was an irregular, 5 m high scarp north of the Smyrna Bench graben on or near the inferred trace of the Saddle Mountains fault (Figure 4). The photogeologic expression of this scarp is consistent with coseismic surface rupture on a south-dipping thrust fault.

Trench #2 disclosed a stacked sequence of paleosols in loess overlying a petrocalcic horizon developed on coarse debris fan deposits. The change from debris fan to loess deposition records the truncation of the fan source area by development of the intervening Smyrna Bench graben 100-400 ka. Two small displacement (0.3 m) thrust faults, dipping 20°-30° south, are coeval with petrocalcic soil development but do not displace the uppermost carbonate horizon.

We conclude, based on our 1994 trench and an earlier trench excavated in 1987, that the 5 m high scarp north of the graben is not the active trace of the Saddle Mountains fault as originally postulated. The scarp instead is formed by stacked, wedge-shaped paleosols developed on loess parent material after truncation of the debris fan sedimentation. Each paleosol thins and disappears to the north. One paleosol consists of a heterogeneous mixture of structureless loess and blocks of semi-indurated soil fragments. A large, detached soil block appears to have been "rafted" into place and is now resting on an older paleosol. Localized fractures in the older paleosol under the soil block indicate the possibility that the soil block was deposited dynamically from a position upslope.

We consider the origin of the scarp-forming, stacked paleosols to be problematic. The stacked paleosols may be related to "normal" loess deposition; although, the nature of the process and how a scarp-like feature would develop as a result are not clear. The scarp, in our opinion, is an aggradational not an erosional feature. A possible alternative may be related to "avalanching" of loess from an upslope position. We noted that the loess when disturbed, for example by excavation, tends to flow downslope in a fluid-like state. Fluid flow is a function of the very fine-grained nature of the loess, low natural moisture content, and entrained air. Linear, scarp-like forms commonly developed at the front of flowing loess sheets. On a much smaller scale these loess fronts are indistinguishable from the larger 5 m high scarp. This indicates that the larger scarp could be related to stacking of loess flows from upslope and, moreover, would account for many of the features observed in the trench. A possible means of initiating loess flows would be thrust faulting upslope. If this interpretation is correct, the stacked paleosols represent the medial and distal parts of colluvial wedges north of the active thrust trace. Although this interpretation is speculative, it is consistent with available data and is a valid hypothesis for future research.

Trench #2, due to the relatively great thickness and instability of the stacked paleosols was neither deep enough nor long enough to resolve the origin of the stacked paleosols or the 5 m high scarp. We infer the active thrust trace must lie between the north flank of the graben and Trench #2.

The petrocalcic soil horizon exposed in Trench #2 is significant and, we believe, may be an important marker for assessing the tectonic history of the Saddle Mountains. The petrocalcic horizon is well-developed and mappable across Smyrna Bench. In Trench #2, the petrocalcic horizon shows varying relations to topography and late Quaternary stratigraphy (Figure 4). In the north end of the trench and most of Smyrna Bench, the petrocalcic horizon is developed on gently north-sloping debris fans within 2-3.5 m vertically of the modern ground surface. It is overlain by a single late Pleistocene paleosol (50± ka) and Holocene loess. At the south end of Trench #2,

the petrocalcic horizon is buried by 4 to 5 paleosols and Holocene loess to depth of 6± m. Moreover, the petrocalcic horizon in the trench does not parallel the ground surface from north to south across the 5 m high scarp, indicating the horizon developed under different topographic conditions than exist today and was subsequently buried by wedge-shaped loess sheets. Directly south of Trench #2, the petrocalcic horizon is exposed at a depth of 1-2 m in the normal fault scarp defining the north flank of the graben. If these petrocalcic soil horizons are indeed correlative, then the current topographic and stratigraphic positions are indicators of late Quaternary tectonic deformation and may provide the means to resolve questions raised by the current studies as illustrated in Figure 5.

Conclusions

We conclude that the Smyrna Bench graben is tectonic and related to movement on the underlying Saddle Mountains thrust fault similar to the Oct. 10, 1980, El Asnam, Algeria, M 7.3 earthquake. Graben development began 100-400 ka and continued into the Holocene. Hanging wall deformation over 19-25 km in the Smyrna Bench and Saddle Gap segments of the anticline indicate a maximum earthquake magnitude of 6.9-7.0. Our findings have potentially significant implications for seismic risk to critical facilities, 20± km to the south, on Department of Energy's Hanford Reservation.

REPORTS PUBLISHED

We presented preliminary results of our work in a paper entitled "Paleoseismological Study of Late Quaternary (Holocene) Faulting, Saddle Mountains Anticline, Yakima Foldbelt, Washington" at the geological Society of America Annual Meeting in Seattle, October 23-27, 1994. A short paper entitled "A Pilot Study of Late Quaternary (Holocene) Faulting, Saddle Mountains Anticline, Yakima Foldbelt, Washington" is in preparation for submittal to *Geology*.

REFERENCES

Avouac J.P. and others, 1992, On the growth of normal faults and the existence of flats and ramps along the El Asnam active fold and thrust system: Tectonics, v. 11, n. 1, p. 1-11.

Bingham, J.W., Lonquist, C.J. and Baltz, E.H., 1970, Geologic investigation of faulting in the Hanford region, Washington: U.S. Geological Survey Open-File Rept. 70-27, 104 p.

Hauksson, E. and others, 1988, The 1987 Whittier Narrows earthquake in the Los Angeles metropolitan area, California: Science, v. 239, p. 1409-1412.

Hull, A.G., 1987, Paleoseismic slip at reverse faults in Crone, A.J. and Omdahl, E.M., eds., Proceedings of conference XXXIX -- directions in paleoseismology: U.S. Geol. Survey Open File Report 87-673, p. 262-270.

Myers, C.W. and Price, S.M., eds., 1979, Geologic studies of the Columbia Plateau -- a status report: RHO-BW1-ST-4, Rockwell Hanford Operations, Richland, Washington, 326 p.

Philip, H. and Meghraoui, M., 1983, Structural analysis and interpretation of the surface deformations of the El Asnam earthquake of October 10, 1980: Tectonics, v. 2, n. 1, p. 17-49.

Reidel, S.P., 1984, The Saddle Mountains: the evolution of an anticline in the Yakima fold belt: Amer. Jour. Science, v. 284, p. 942-978.

Reidel, S.P., 1988, Geologic map of the Saddle Mountains, south-central Washington,: Washington Div. Geol. & Earth Res. Geol. Map GM-38.

Stein, R.S. and King, G.C.P., 1984, Seismic potential revealed by surface folding: 1983 Coalinga, California, earthquake: Science, v. 224, p. 869-872.

Washington Public Power Supply System, 1981, WPPSS Nuclear Project No. 2 final safety analysis report, Amendment 18, Chapt. 2.5

West, M.W. and Shaffer, M.E., 1988, Probabilistic and deterministic seismotectonic studies, O'Sullivan Dam and Potholes Reservoir, Washington: Unpub. consultant's report prepared for the U.S. Bureau of Reclamation, Denver, CO, 110 p.

West, M.W. and Shaffer, M.E., 1989, Late Quaternary tectonic deformation in the Smyrna Bench and Saddle Gap segments, Saddle Mountains anticline, Yakima fold belt, central Columbia Basin, Washington (abs.): Geol. Soc. of America, Cordilleran/Rocky Mountain Section Meeting, v. 21, n. 5, p. 157-158.

Wyllie, Jr., L.A. and Filson, J.R., eds., 1989, Armenia earthquake reconnaissance report: Earthquake Spectra, Spec. Supplement, 175 p.

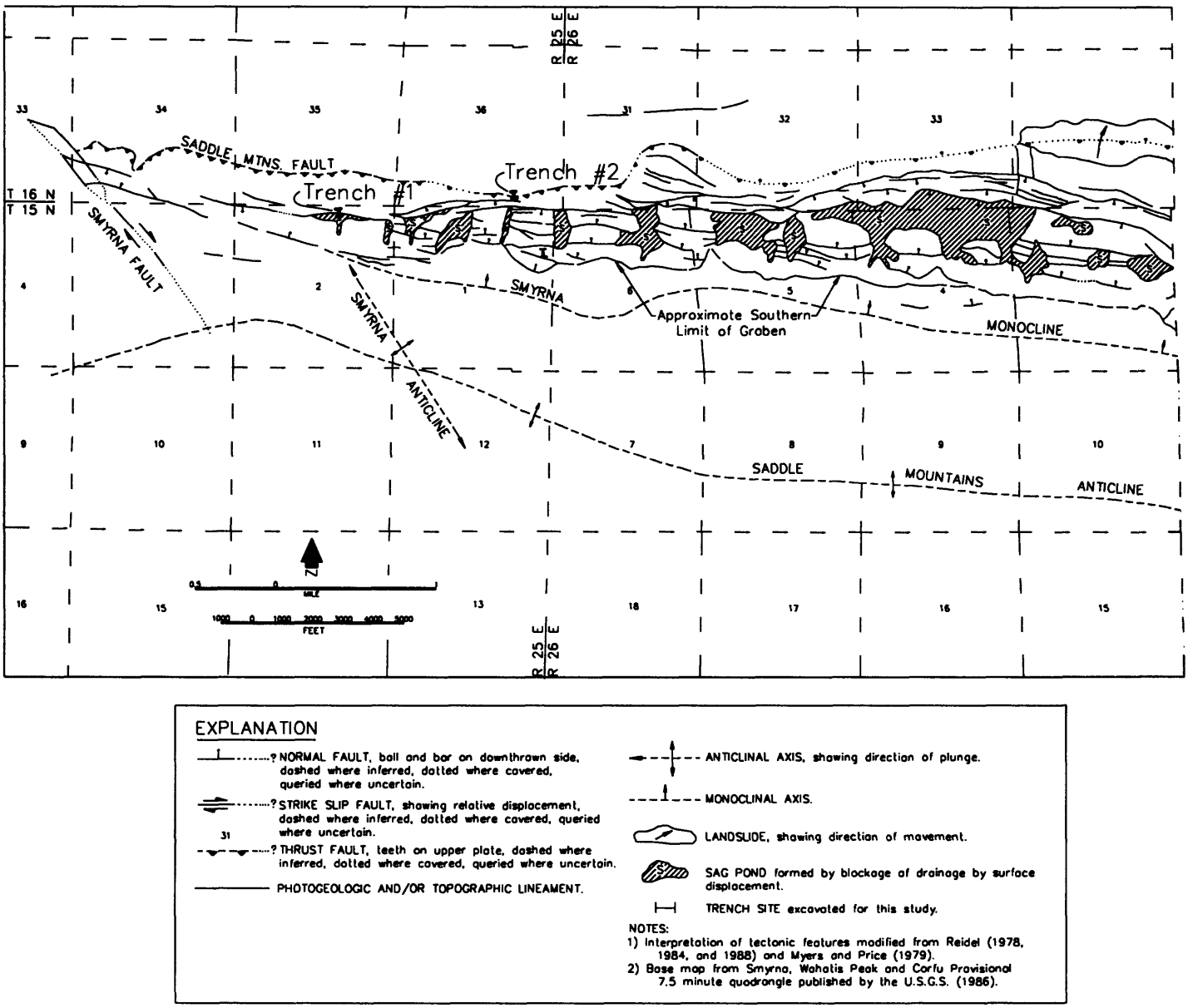

EXPLANATION

- NORMAL FAULT, ball and bar on downthrown side, dashed where inferred, dotted where covered, queried where uncertain.
- STRIKE SLIP FAULT, showing relative displacement, dashed where inferred, dotted where covered, queried where uncertain.
- THRUST FAULT, teeth on upper plate, dashed where inferred, dotted where covered, queried where uncertain.
- PHOTOGEOLOGIC AND/OR TOPOGRAPHIC LINEAMENT.
- ANTICLINAL AXIS, showing direction of plunge.
- MONOCLINAL AXIS.
- LANDSLIDE, showing direction of movement.
- SAG POND formed by blockage of drainage by surface displacement.
- TRENCH SITE excavated for this study.

NOTES:
1) Interpretation of tectonic features modified from Reidel (1978, 1984, and 1988) and Myers and Price (1979).
2) Base map from Smyrna, Wahatis Peak and Corfu Provisional 7.5 minute quadrangle published by the U.S.G.S. (1986).

FIGURE 1 - Tectonic map of the western half of Smyrna Bench, Saddle Mountains anticline, showing the Smyrna Bench graben, Saddle Mountains fault, sag ponds caused by beheading of stream drainages, and trench locations. Trench #1 was intended to explore a normal fault and sag pond on the north flank of the Smyrna Bench graben. Trench #2 was excavated across a 5 m high scarp north of the graben believed to be associated with Saddle Mountains fault.

FIGURE 2 - View of west wall, Trench #1, showing normal fault with 0.9 m of displacement in 100-400 ka petrocalcic horizon, overlying paleosol and Holocene loess. The main graben-bounding normal fault is to the left (south) of this photograph and exhibits at least 4 m of throw in the petrocalcic horizon. A thrust fault juxtaposing different units of either the Ellensburg or Ringold formations is present in the center of the photograph. Maximum slip in pre-petrocalcic horizon Quaternary units appears to be about 0.6 m. The upper surface of the petrocalcic horizon appears to be deformed (broken and bowed upward) but not displaced by this fault. The apparent offsets in the fault planes are caused by a 2 m wide bench between the upper and lower trench walls. The normal fault trends obliquely to the trench walls and is exposed on the lower wall to the left of this photograph.

FIGURE 3 - View of thrust fault and roll scarp in the base of the petrocalcic soil horizon, west wall, Trench #1. The roll scarp represents about 0.6 m of fold shortening and 0.3 m of slip in the fault plane. Lower and to the left (south) of this photograph, the fault thrusts Ellensburg and/or Ringold sediments over Elephant Mountain Basalt. If the sediments are indeed part of the Ringold Formation, an episode(s) of down-to-the-south normal faulting followed by thrust faulting is indicated.

FIGURE 4 - View of west wall of Trench #2 excavated across 5 m high scarp north of the Smyrna Bench graben. Note increasing elevation of the ground surface to the left (south). The 100-400 ka petrocalcic horizon developed on cobble-boulder debris fan deposits is visible as a white band in the lower part of the trench. The depositional environment at the top of the petrocalcic horizon changes abruptly from debris fan to loess deposition and may record truncation of the debris fan source area in the higher terrain to the south by development of the Smyrna Bench graben. The 5 m high scarp is formed by stacked paleosols developed on loesses which thin and pinch out to the right (north). Note the planar nature of the petrocalcic horizon and its divergent position with respect to modern topography, indicating that it has been buried by loess sheets originating to the left (south). The active trace of the Saddle Mountains thrust fault is inferred to lie between the south (left) end of Trench #2 and the north flank of the Smyrna Bench graben as illustrated on Figure 5. A small displacement thrust fault is visible in debris fan deposits in the lower center of the photograph. This fault does not displace the upper surface of the petrocalcic horizon.

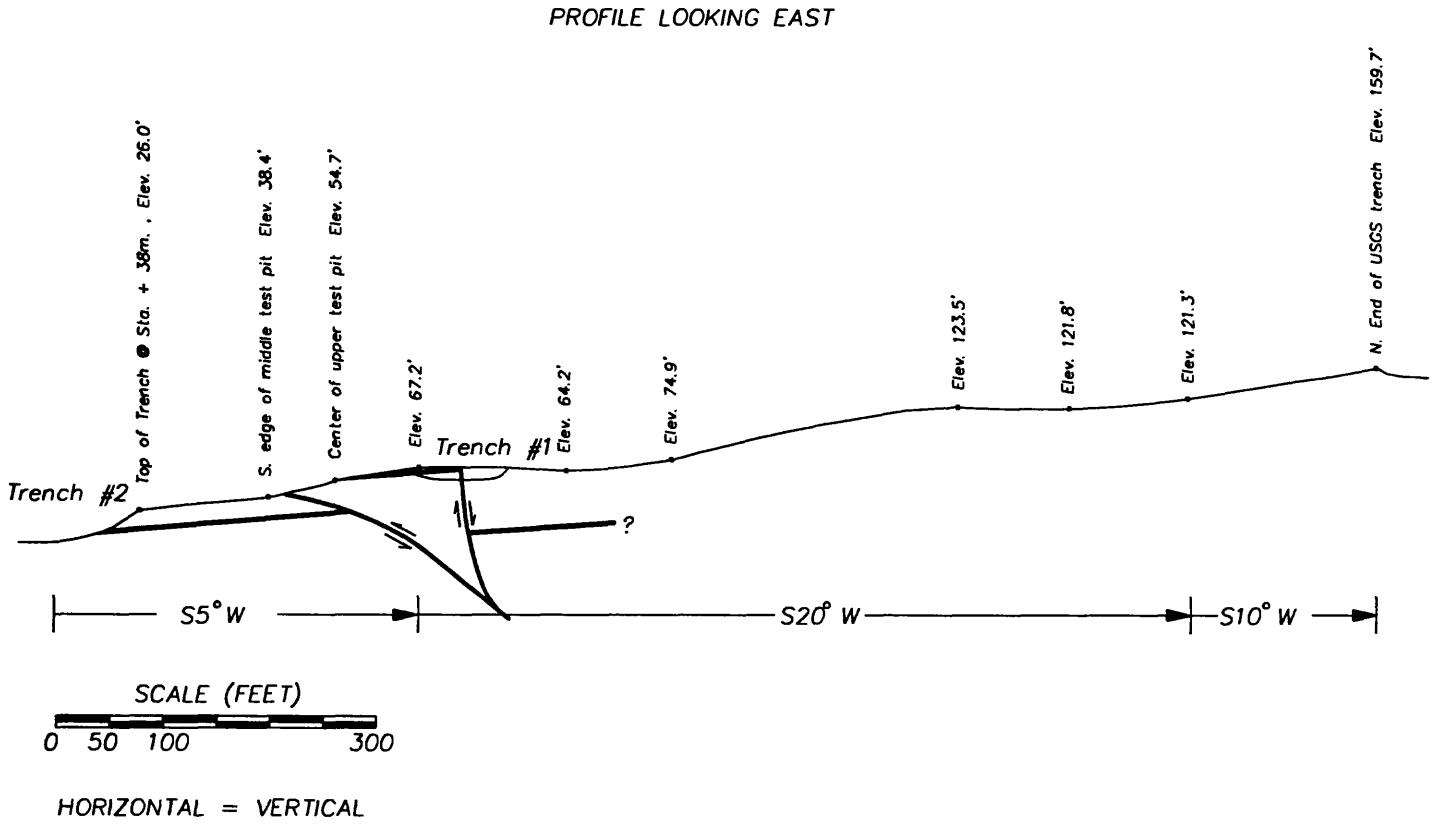

FIGURE 5 - Diagrammatic representation of topographic profile at the Trench #2 site based on hand leveling data. Trench #1 is projected on to the profile at its approximate location with respect to the inferred active thrust trace and the north-bounding fault in the graben. The 100-400 ka petrocalcic horizon is shown in cross-hatched pattern and in the approximate positions defined from trenching and mapping. The elevation of the petrocalcic horizon in the graben is not known. The relative positions of the petrocalcic horizon indicate the presence of an active thrust trace at the approximate location shown. Neither trench, however, crossed the most likely position of the active thrust trace based on 1994 studies. Trench #1, however, crossed the main Holocene normal fault on the north flank of the graben and shows displacement in the petrocalcic horizon exceeding 4 m. Both trenches exposed small displacement (<1 m) thrust faults approximately coeval with the 100-400 ka petrocalcic horizon.

Piñon Flat Observatory: A Facility for Studies of Crustal Deformation

Award Number: 14-08-0001-G1764

Frank K. Wyatt, Duncan Carr Agnew,
Hadley O. Johnson

Institute of Geophysics and Planetary Physics
Scripps Institution of Oceanography
University of California, San Diego
La Jolla, CA 92093-0225
(619) 534-2411 (FAX 534-2332); fwyatt@ucsd.edu

Program Elements: II.3 and II.7

This grant supports the operation of Piñon Flat Observatory (PFO) as a research center for the study of crustal deformation. Through this grant, the U.S. Geological Survey provides a part of the funding needed to run the 160-acre facility and to maintain the reference-standard instruments there. The work done at PFO includes establishing the most reliable record of crustal deformation possible, something attained by operating the best instruments available and by a systematic intercomparison of results from many types of sensors. The result is an accurate record of strain and tilt changes in the area near the observatory, between the active San Jacinto fault and southern San Andreas fault systems; and from this, a better understanding of the mechanics of faulting.

The site continues to be utilized by roughly 20 different research teams. **Figure 1** shows the results of some of their work, namely the record of strain change in the NW/SE direction gotten by three types of measurement over the last 6 years. Two are geodetic measurements, made in the area around PFO by USGS investigators: Geodolite data (collected from 1974 to 1991, though now ended), and two-color EDM data (collected from 1986 to the present, and continuing). The third is the continuous record made by the NW/SE laser strainmeter.

As this figure shows, this strainmeter, like all the other instruments at PFO, operated well during the first half of 1994. We obtained on-scale strain records of the Northridge earthquake, which showed, as we have come to expect, no immediate strain precursor. Strain records from the aftershocks are being analyzed by Dr. Joan Gomberg as part of her research into the triggering mechanism for the many distant events triggered by the 1992 Landers earthquake.

The NW/SE laser strainmeter data in **Figure 1** do show a large rate of strain in late 1993 and early 1994, essentially reversing the large strain seen after the Landers earthquake. These two strains (not, we note, resolvable with the geodetic data) are the largest we have seen since the instrument was fully anchored. While it has been suggested that the second strain change may correlate with a signal seen on the PGGA GPS data in the Los Angeles Basin, this remains speculative; unfortunately, this strain excursion corresponds to the wettest winter in many years in California—the end of a multiyear drought—and we cannot rule out a possible strain response to changes in the water table (though the many wellbores we monitor don't show changes mimicing the strain signal).

From the standpoint of instrument comparison, two points are also evident from this figure. First, the long-term strain rates found by the two sorts of geodetic systems are in fair accord, both being 3×10^{-8} yr^{-1}. This rate, though low (as would be expected for a measurement roughly parallel with the local strike-slip faults) is significantly different from zero, indicating that there is more to the strain

field than simple shear. The laser strainmeter appears to be showing a rate in excellent accord with the long-term geodetic rate. So far as we know, this is the only example of geodetic and continuous data agreeing on a secular rate, and the signal here is a relatively small one. Second, at any period shorter than the secular rate of change, the strainmeter provides a much better measure of strain changes than the geodetic measurements do—and it should be noted that these geodetic measurements, over these distances, have a precision that equals or exceeds GPS. At periods of a few days this advantage is a factor of 10^3 or more, even if the geodetic measurements were made daily.

This record, and several others, were interrupted by a devastating fire in July 1994. Since that time we have been working hard to restore the instruments as quickly as possible. Over the July 4th weekend, the "Palm" fire—officially 19,200 acres, or 30 square miles in all—swept south from near Palm Springs and through the observatory, pushed by strong winds and with a flame front estimated at 50 feet high. The stippled area in **Figure 2** shows the burned-over area at the observatory: more than half the total. Nearly all of the critical buildings were saved (and most of the nearby homes), and we are thus extremely grateful to the fire-fighters; the total cost of fighting the fire was put at $5.8M. The things that were severely damaged were mostly those elements of the site that extended laterally above ground, there being no way to defend these long structures. This meant that some of the power distribution, much of the signal wiring outside the area of the central-recording facilities, and ~35% of the long-base laser strainmeter vacuum pipes were destroyed by the fire. Only a few instrumented vaults were destroyed; unfortunately, these included the vaults containing the Lamont-Doherty longbase fluid tiltmeter. The remainder of the site, away from the areas that were defended by the fire fighters and away from the areas immediately downwind of the defended structures, now has the look of a lunar landscape. Incredible heat is given off as trees and other thick vegetation burst into flames; signal wire, vacuum pipes and the like were partially melted wherever a tree or substantial bush was close by. Many sections of the strainmeter vacuum pipe were softened by the heat and sucked flat by the vacuum inside the pipe.

While almost all instrumentation was off when we first were allowed into the area, (almost two days after the main fire, with small fires still underway in various places around the site), we were, within 24 hours, able to restore power to most of the site, and the power company soon restored power to the mains. By the end of the week phone service was restored and we had finished the work to get the seismic and GPS receivers on line. Both structures that housed the two permanent GPS receivers got singed, but escaped without serious damage. The antennas were in fine shape. Also, and most fortunately, none of the critical components of the long-base systems (the optical/laser/vacuum equipment in the end-vaults) were damaged in the slightest.

The University of California is self-insured, and fortunately has agreed to support reconstruction of the site: total cost about $305,000. We have focused on routing key signals from working instruments to the recording trailer, using undamaged lines. On September 13, 1994 we managed (with a great deal of effort) to get the Northwest-Southeast strainmeter running again. There were enough undamaged sections of vacuum pipe to install them on the NW/SE line and get that instrument back in operation on a temporary basis. Further reconstruction of the strainmeters (the North/South and East/West instruments especially) will require fabricating new vacuum-pipe components and will therefore take more time; we expect to be done with this before June of 1995. These two systems aside, the site is largely restored to operation.

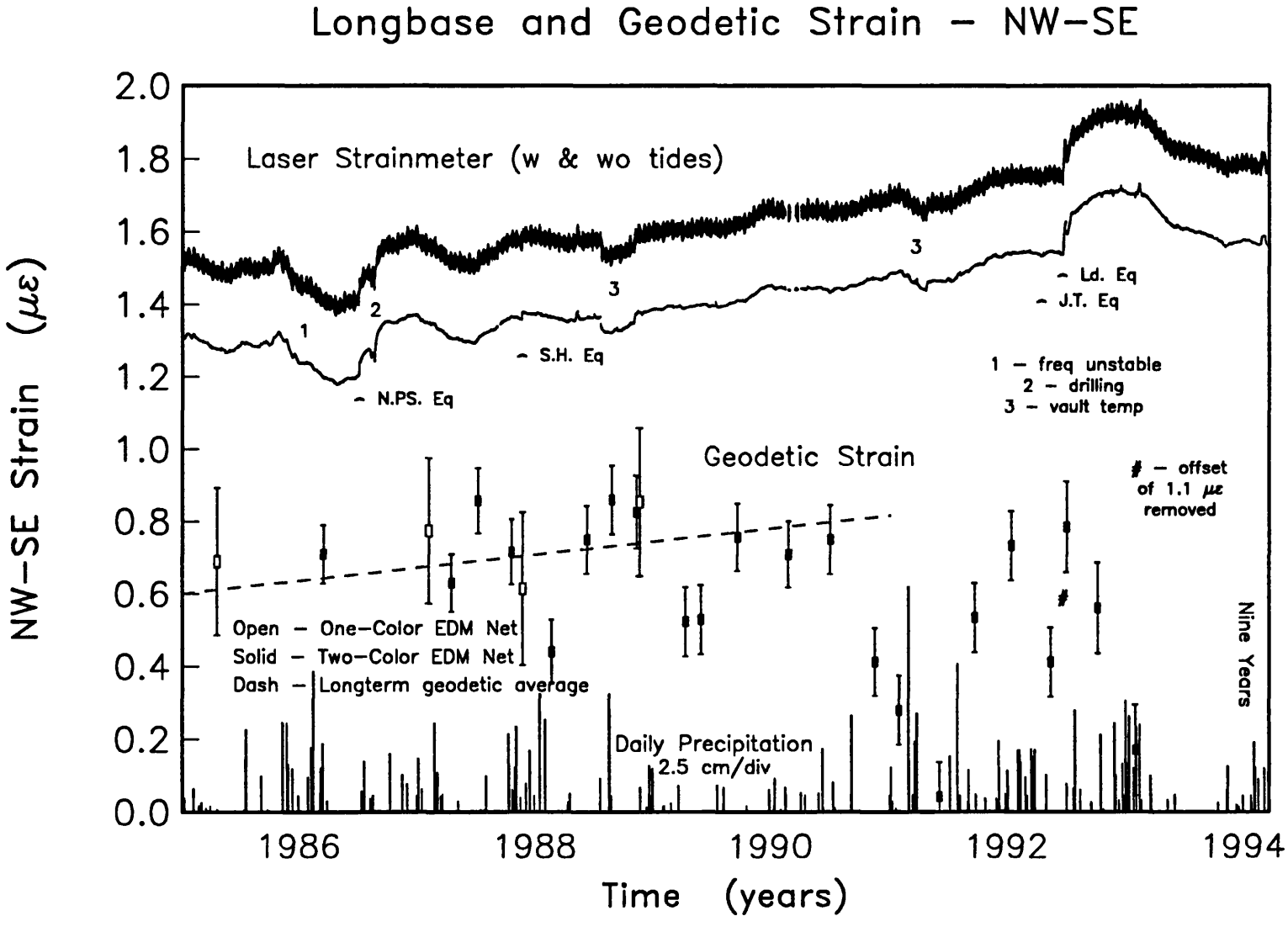
Longbase and Geodetic Strain – NW–SE
NW–SE Strain (με)
2.0
1.8
1.6
1.4
1.2
1.0
0.8
0.6
0.4
0.2
0.0
Laser Strainmeter (w & wo tides)
1
2
3
3
3
– N.PS. Eq
– S.H. Eq
– Ld. Eq
– J.T. Eq
1 – freq unstable
2 – drilling
3 – vault temp
Geodetic Strain
– offset of 1.1 με removed
Open – One–Color EDM Net
Solid – Two–Color EDM Net
Dash – Longterm geodetic average
Daily Precipitation
2.5 cm/div
Nine Years
1986
1988
1990
1992
1994
Time (years)

Figure 1.

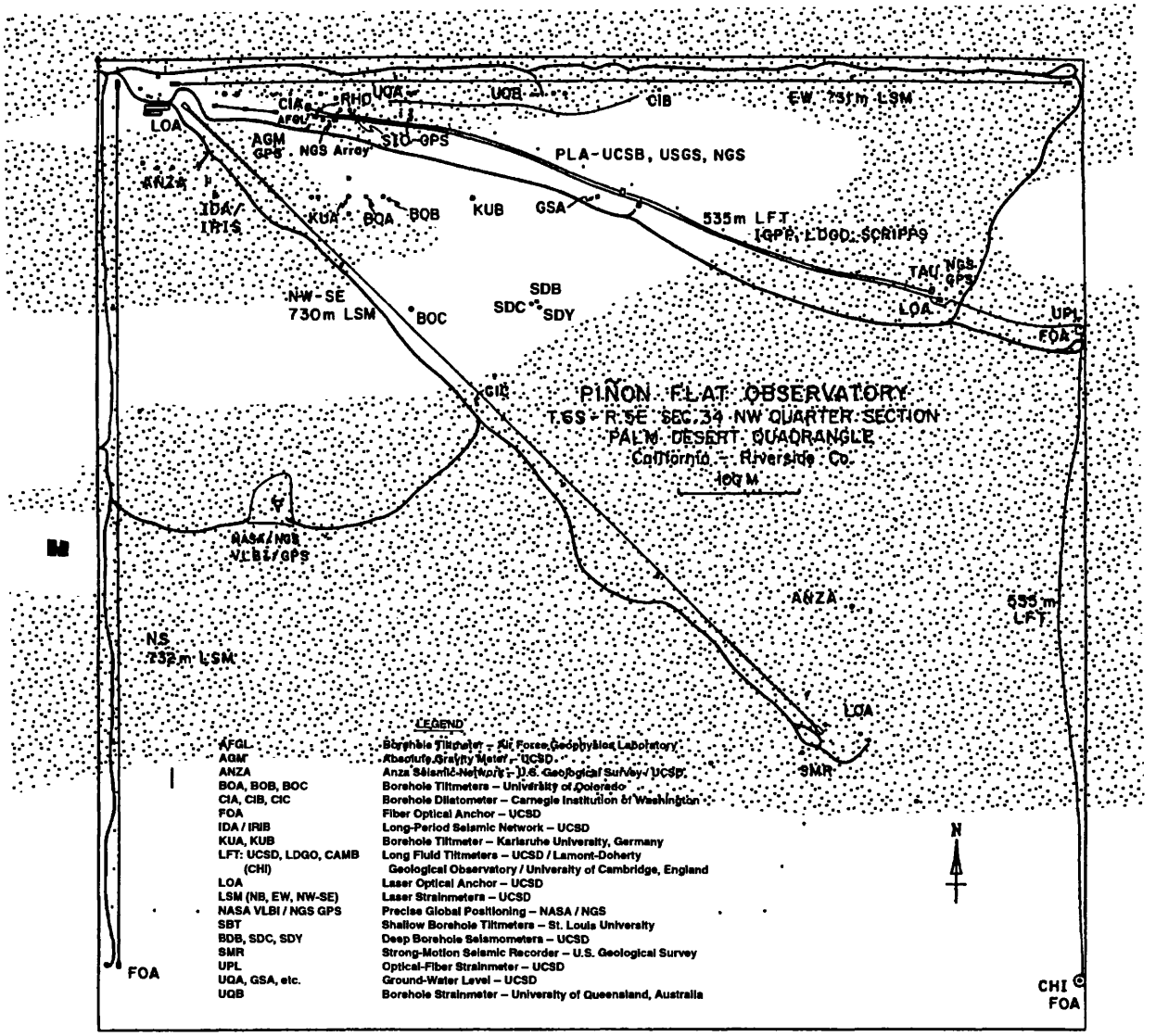
PIÑON FLAT OBSERVATORY
T.6S - R.5E SEC.34 NW QUARTER SECTION
PALM DESERT QUADRANGLE
California - Riverside Co.
1000 M
LEGEND
AFGL Borehole Tiltmeter – Air Force Geophysics Laboratory
AGM Absolute Gravity Meter – UCSD
ANZA Anza Seismic Network – U.S. Geological Survey / UCSD
BOA, BOB, BOC Borehole Tiltmeters – University of Colorado
CIA, CIB, CIC Borehole Dilatometer – Carnegie Institution of Washington
FOA Fiber Optical Anchor – UCSD
IDA / IRIB Long-Period Seismic Network – UCSD
KUA, KUB Borehole Tiltmeter – Karlsruhe University, Germany
LFT: UCSD, LDGO, CAMB (CHI) Long Fluid Tiltmeters – UCSD / Lamont-Doherty Geological Observatory / University of Cambridge, England
LOA Laser Optical Anchor – UCSD
LSM (NB, EW, NW-SE) Laser Strainmeters – UCSD
NASA VLBI / NGS GPS Precise Global Positioning – NASA / NGS
SBT Shallow Borehole Tiltmeters – St. Louis University
BDB, SDC, SDY Deep Borehole Seismometers – UCSD
SMR Strong-Motion Seismic Recorder – U.S. Geological Survey
UPL Optical-Fiber Strainmeter – UCSD
UQA, GSA, etc. Ground-Water Level – UCSD
UQB Borehole Strainmeter – University of Queensland, Australia
N
EW 731m LSM
NW-SE 730m LSM
NS 732m LSM
535m LFT
PLA-UCSB, USGS, NGS
IGPP, LDGO, SCRIPPS
NASA/NGS VLBI/GPS
ANZA
SMR
CHI
FOA
LOA
UPL
TAU
AGM
SIO GPS
IDA/IRIS
KNZA
KUA
BOA
BOB
KUB
GSA
BOC
SDB
SDC
SDY
CIB
CIA
RHO
UQA
UQB
AFGL

Figure 2.

Deformation Monitoring of the Southernmost San Andreas Fault

Award Number: 14-08-0001-G1786

Frank K. Wyatt, Mark Zumberge,
and Duncan Carr Agnew
Institute of Geophysics & Planetary Physics
Scripps Institution of Oceanography
University of California, San Diego
La Jolla, CA 92093-0225
(619) 534-2411 (FAX 534-5332); fwyatt@ucsd.edu

Program Elements: II.3 and II.7

This grant supports the measurement of strain at the southernmost end of the San Andreas fault in the Coachella Valley, using a long-base laser strainmeter (LSM). (A predecessor grant supported operation of an optical fiber experiment to establish if anchoring was possible in the clayey material of the Coachella Valley; this experiment was brought to a successful conclusion in October 1994.) Installation of a long-base strainmeter should be highly enlightening in trying to understand the style of crustal deformation in this tectonically active area—an area posited as the likely epicentral region for a M 8 earthquake—and as transmitted through such poorly consolidated material.

Construction of the long-base instrument at Durmid Hill (hereafter DHL) began in March 1992, and involved a major effort throughout the spring of that year which included building roads and bridges, drilling the anchoring boreholes, excavating the vault pits, trenching, and precise installation and burial of 525 m of PVC vacuum-pipe casing. Work was then brought to a standstill by the combination of responding to the Landers earthquake, by the loss both of our long-time caretaker at Piñon Flat Observatory (PFO), and by the ill-health of our chief engineer, which eventually forced him to go on disability. (Unfortunately, until this was settled, which took a year and a half, we were not permitted to hire other personnel). Work the following winter (1993) was also slowed by the ending of the California drought—at times of rain the area becomes completely impassable because of mud. In the fall of 1992 we began the detailed design of the LSM components—some 65 pages of engineering drawings—basing them on the plans for the earlier LSM's built at PFO. This required about two months of solid effort. Starting in 1993 a capable part-time engineer and undergraduate student carried out the substantial field-assembly work needed to complete the instrument: distribution of power to the site; construction and installation of three vaults; electrical and signal wiring; and preparation and installation of 525 m of vacuum-pipe tubing for the strainmeter itself. Installation of the vacuum system went rapidly and the main vacuum pump was first turned on in January 1994. On the trip to install the optics and electronics (February 3, 1994) the strainmeter was started, and has run well ever since. Though the installation has been delayed, we have come in on budget, with enough remaining dollars to complete the optical fiber anchoring this year; we expect that this system will be in operation by the time of this submission (December 2, 1994).

We have had to make several design choices in installing this instrument, and learned several lessons. A major one is that we now believe that the construction of further instruments of this type should be relatively straightforward, and such instruments, once installed, can run with relatively little maintenance. The results from Durmid Hill have persuaded us that long-base laser strainmeters should be considered as a potential way to monitor strain changes in a variety of locations.

Our initial design goals were:

1. To construct a high-quality long-base strainmeter that would be as low-maintenance as possible. While we can never hope to compete with borehole strainmeters in this area, we hoped to make the systems much simpler and more robust than those at PFO with little loss in quality.
2. To make the instrument as "portable" as possible. Though this may seem an odd word to apply to something so substantial, we have sought in our design to make sure that everything not sunk in the ground could be removed and re-installed elsewhere. If enough data showed a site not to be useful, most of the expensive components could be removed and re-assembled at another site; while this new site would of course have its own preparation costs, these would be much less than the cost of a completely new instrument.

The DHL instrument is identical in principle to the existing laser strainmeters at PFO: a Michelson interferometer with one of its optical arms spanning an extended path, which must be evacuated to remove the effects of variations in the index of refraction of air. By counting interference fringes, the displacement between the two ends is measured continuously. However, the new instrument does differ in a number of ways from what has been done before.

- *Vacuum-pipe burial.* Our most difficult initial decision was whether to run the vacuum pipe above ground, as at PFO, or in a casing in a trench. We decided on the latter, as providing better thermal stability, immunity to vandalism, and certainly much lower maintenance costs; we are happy with this decision, though it meant that it took much more effort to construct the instrument. The vacuum pipe was installed inside a buried PVC casing, being loaded into it from a center shelter. Getting this casing aligned to within a few mm was a very difficult task, especially given the 20-50 mm effects on survey-sightings caused by air temperature gradients. The main lesson we learned was not to attempt to dig the trench floor especially level (almost impossible given the inhomogeneity of the near-surface "rock"), but to simply add sand to produce a uniform bed (in the end, 230 tons, all spread by hand). The casing was initially level to within 5 mm; subsequent measurements have shown 20 mm of settling in spots, but we believe that this will prove to be a one-time, transient effect.
- *End vaults.* For vaults (one at each end and one in the center) we used steel shipping containers embedded in concrete pads and covered over with dirt. This has worked out very well; damaged (but otherwise perfectly usable) containers can be purchased for less than $1000, and with some modest effort made adequately protected against corrosion for their expected life.
- *Vacuum system.* The biggest, and most pleasant, surprise of the whole installation was the behavior of the vacuum system. Despite thorough cleaning and preparation, the vacuum pipes on the four previous instruments (three at PFO and one at Camp Elliott) have, we thought, continued to outgas so much that large vacuum pumps must be kept running constantly to maintain the vacuum. A pump of this class (a reserve pump from PFO) was therefore installed at DHL; since we knew that the pipe had not been cleaned to the same degree as the earlier ones, we expected it to be just adequate. It quickly produced a good vacuum (1 μbar), which remained long after it was shut off. Repeated tests have shown that the system at DHL "leaks" so little that we have been able to maintain the vacuum by simply running the pump for a few hours each month—with substantial savings to our power bill. We still are not entirely sure why we have gotten such good results; we believe that (1) the metal itself, (2) the use of better O-rings (*Viton*), (3) much better finishing of the seals they sit in, and (4) the use of bellows for pipe-length compensation (see below) are the main reasons. Since a single leak in any of the several hundred welds, seals, and joints within the system would prevent this result, our attention to detail has paid off.

- *Pipe-length compensation.* Though the burial of the pipe has reduced the extreme swings in temperature from over 40°C at the ground surface, to 20°C in the ground, there is still an annual cycle. The resulting long-period pipe-length changes are taken up by compensating bellows at each end, as opposed to the automated telescopic joints used at PFO. Using bellows requires anchoring of the end monuments (not available when the PFO strainmeters were first built) since the stretching and compression of the bellows will cause local stresses, but it has removed a complicated and high-maintenance part of the system.
- *Optics and Lasers.* One problem with the PFO strainmeters has been the frequency stability and ease-of-maintenance of the lasers used in the interferometers. The existing PFO lasers are stabilized against a Fabry-Perot reference cavity, checked by occasional comparison with an iodine-stabilized laser. Though this gives very good short-term and long-term stability (and was the only technology available when the instruments were built) it requires a great deal of electronics and frequent measurements by the staff. At DHL we are using a stabilized laser that is produced commercially.

The combination of using bellows and a commercial laser means that instead of an entire rack of electronics, we have one panel for the laser control and another for the fringe counter. The use of bellows, and the quality of the vacuum system, means that the whole vacuum system is completely passive and draws no power, so that the entire LSM can be run off uninterruptible power quite easily—and it does. The strainmeter needs only about 200 W of power (we have also had to install air conditioners, which demand another 150 W, but these do not require uninterruptible power). The only substantial data gaps so far have come from occasional hanging-up of the PC-based datalogger—but the latter problem does not cause any ambiguity in data interpretation. In the (almost) one year of operation to date, essentially no maintenance has been needed; we have more than met our first goal.

Figure 1 shows the data from the DHL laser strainmeter, from the time the laser was turned on. The immediate stability of the data is in notable contrast to the long-term transients expected on borehole instruments as they settle in. The trend seen through day 80 in the data in **Figure 1** actually matches the secular strain rate predicted by a dislocation model. Since the instrument was not yet fully anchored, we have to take this to be a fortuitous coincidence, especially since the rate reversed after day 80 when air-conditioning was begun in the instrument-end vault—with temperatures in the underground vault approaching 100°F and Spring just beginning. Note that the total relative motion over the time shown is only 0.05 mm, a testimony to the intrinsic stability of the end-monuments, anchored (so far) only via the borehole pipes put in for the optical-fiber anchors. While we must await the start of the optical anchoring system to get better results, the data so far certainly argue against the idea that the local deformation is purely inelastic: to accommodate the 25 mm/yr seen geodetically within a 5-km shear zone would imply a strain of -5 $\mu\varepsilon$/yr, far higher than what we see. On the other hand, the strain rate that we see would be consistent with 20 mm/yr of slip going on below 10 km (rather than the 5 km of the model), and 5 mm/yr in a narrower shear zone. Trying to understand how to combine the existing geological, and geodetic data with our strain measurement is something we plan to pursue, both by modelling and by adding further observations.

As usual for high-quality strain data, the earth tides are well recorded. Given the subdued topography of the area, any departures of the observed tides from those expected on the spherical earth (with ocean loading) must be caused by geological inhomogeneities. We might expect these near a fault; and it has long been argued, largely on the basis of enhancements of possible precursory strains in fault zones, that these zones are "soft" (more properly, "more compliant") compared to the surrounding rock, thereby concentrating strain on them. We can now say that this is not true for the San Andreas fault at Durmid Hill. **Figure 2** tells the story (in terms familiar to earth-tidalists): it shows, for the two

best-recorded tides, the complex amplitude of the observed tide compared with that on a spherical earth, at the azimuth of DHL, at DHL and at PFO (in the latter case the "observed" value comes from the three LSM's there). The largest vector is for the elastic earth; the next two are for the loads from the world ocean and for the Gulf of California. The observed values are shown with error bars for DHL (at PFO they are too small to see).

It is clear that the match between observed and theory is about as good (to within 10%) at DHL, in the fault zone, as at PFO, well off it. Indeed, it may turn out to be better at DHL, since the disagreement there for the M_2 tide could well be an inadequate loading estimate for the Gulf of California; we intend to try both better models of the tides there, and loading Green functions that are derived from a more realistic crustal structure, to see what effect they have. Combined with a boundary-element model for the fault zone, to predict the possible distortions around the fault, we should be able to set good limits on the extent to which the fault zone is more compliant at tidal frequencies. (It could be more compliant at longer periods, but this would require a rheology that tended to the less compliant level at tidal frequencies.)

The DHL strain data, also occasionally show pronounced oscillations at periods of about 3 hours, 1.5 hours, and 40 minutes. These signals, and much of the other short-period "noise" in the record (the DHL records are not as nicely sinusoidal as those from PFO), are caused by seiching of the nearby Salton Sea. These seiches were recorded by the water-level gauges set up (under NEHRP sponsorship) by Dr. John Beavan and Dr. Roger Bilham of Lamont-Doherty, and discussed by them in several USGS reports. This water-level project has now been terminated, but we have been working with Dr. Beavan to maintain one of the gauges and a recorder, with which we are monitoring the sea level close to DHL. We hope to combine these sea-level data with the strain data to determine the shear modulus of the crust in this area, since this has the primary influence on the loading Green function; note that this is poorly determined from seismic data. Another, somewhat unexpected source of loading-signals has been the many large freight trains on the nearby railroad track: these cause a brief, but easily noticeable signal of about 10^{-9} ε (filtered out in the usual recordings).

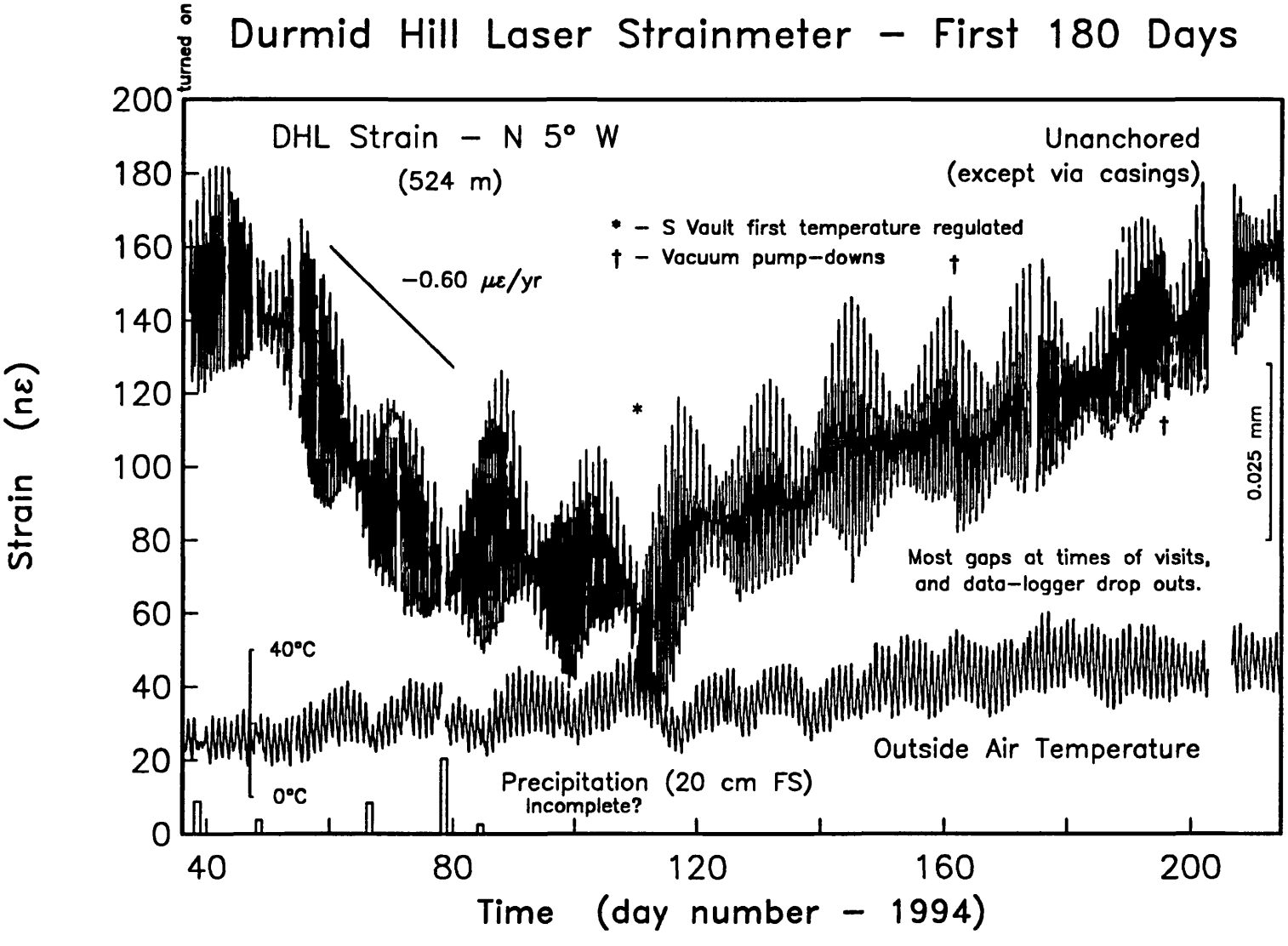
Durmid Hill Laser Strainmeter – First 180 Days
turned on
DHL Strain – N 5° W
(524 m)
Unanchored
(except via casings)
* – S Vault first temperature regulated
† – Vacuum pump–downs
–0.60 με/yr
0.025 mm
Most gaps at times of visits,
and data–logger drop outs.
40°C
0°C
Outside Air Temperature
Precipitation (20 cm FS)
Incomplete?
Strain (nε)
Time (day number – 1994)
200
180
160
140
120
100
80
60
40
20
0
40
80
120
160
200

Figure 1.

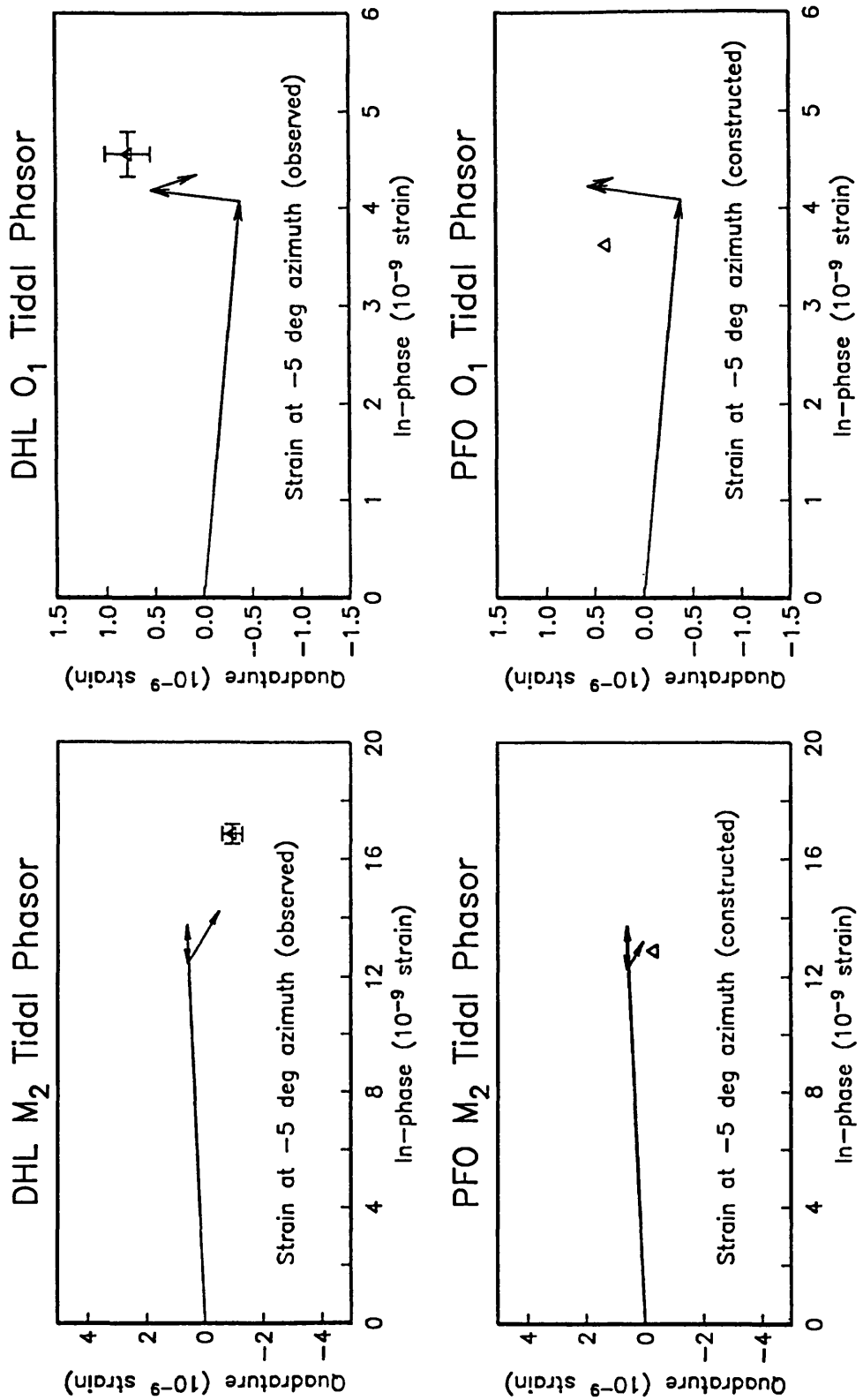
DHL O_1 Tidal Phasor
PFO O_1 Tidal Phasor
DHL M_2 Tidal Phasor
PFO M_2 Tidal Phasor
Strain at −5 deg azimuth (observed)
Strain at −5 deg azimuth (constructed)
In-phase (10^{-9} strain)
Quadrature (10^{-9} strain)

Figure 2.

Segmentation, Slip Rates, and Earthquake Dimensions in the Active Fold-Thrust Belt of Northern Los Angeles Basin, California

Award Number 1434-94G-2492

Robert S. Yeats, Principal Investigator
Department of Geosciences, 104 Wilkinson Hall
Oregon State University, Corvallis, OR 97331-5506
Phone (503)737-1226; fax (503)737-1200
e-mail: yeatsr@bcc.orst.edu
Program Element II.1

Investigations

The subsurface geology between Beverly Hills and Las Cienegas oil fields was completed in spring, 1994 (cf. Hummon et al., 1994; Schneider et al., submitted 1994). The subsurface geology from Beverly Hills to Santa Monica, and to the eastern end of the Las Cienegas oil field is now complete and is being prepared for publication (Tsutsumi et al., 1994, and in prep.). With support from SCEC, our geologic data, including well locations, have been digitized and are now available electronically (see details under Reports Published).

A report on the East Ventura basin (Yeats et al., 1994) covers most of the aftershock zone of the Northridge earthquake. Gary Huftile is updating two cross sections from this study based on the new seismicity data, one east and one west of the Gillibrand Canyon segment boundary. A paper on the Northridge earthquake (Yeats and Huftile, 1994) has been submitted to *Nature*.

In the northern LA fold thrust belt, we have acquired well data east to the Bandini oil field, except for Chevron.

Results

Dip and slip rate on the blind reverse fault bordering the LA trough on the north

The LA trough east of the Newport-Inglewood fault is bounded on the north by a south-facing monocline. The folds (East Beverly Hills, South Salt Lake, Las Cienegas) and reverse faults (Las Cienegas, San Vicente) of the LA fold-thrust belt are secondary structures to

the monocline, which itself is an expression of a reverse fault beneath well depth. Figure 1 is a digitized cross section through the East Beverly Hills anticline illustrating the great increase in thickness southward of post-Delmontian strata from the San Vicente fault to the LA trough, and, in contrast, the great increase in thickness northward of Mohnian (Miocene) strata from the East Beverly Hills syncline to the North Salt Lake fault. Note that strata on the flanks of the monocline (south of East Beverly Hills anticline) increase in dip with increasing age and do not form growth triangles of constant dip, as found on the Compton-Alamitos trend and in the Santa Barbara Channel (Shaw, 1993). Note also that there is almost no separation of the Mohnian-Topanga contact across the San Vicente fault, whereas the separation of the base of the Delmontian is several hundred meters.

Figure 1 shows evidence that Miocene deformation was by extension, including normal-fault displacement on the San Vicente fault. The orientation of this fault is related to Miocene extension. The Delmontian (Miocene-Pliocene boundary) is about the same thickness across the section, indicating a time of little deformation. The Repettian (lower Pliocene) is the first sequence to show thickening toward the LA trough, recording basin inversion from a Miocene trough on the north to a Pliocene-Quaternary trough on the south. Because the San Vicente fault was oriented in a plane of high shear stress during Pliocene contraction, it was reactivated as a reverse fault.

Analysis of growth strata, that is, strata deposited during the time of faulting, allows the determination of the dip of the blind fault. Figure 1 shows that the bedlength of older horizons, say, the base of the Delmontian, is much greater than that of, say, the top of the upper Pico. The difference in bedlength of the older horizon and the younger gives the horizontal shortening between the two horizons. The difference in thickness between the two horizons gives the relative vertical displacement between the two horizons. Figure 2 shows how we use this relationship to determine the dip-slip vector of relative displacement between the LA trough and the crest of the monocline. This vector must be parallel to a line in the blind fault plane. Because the ages of the two horizons are known, the slip rate on the blind fault can be determined. Schneider et al. (1994) determined the dip of the blind fault to be 61° at East Beverly Hills and 62° at Las Cienegas. The long-term dip-slip rate is 1.1-1.3 mm/yr at East Beverly Hills and 1.3-1.5 mm/yr at Las Cienegas. The blind fault lacks a backlimb and is a basement-involved compressive structure as modeled by Narr and Suppe (1994), based on studies in

the Laramide Rocky Mountains. The East Beverly Hills structure is a "rabbit-ear" fold (out-of-the-basin crowd structure) as described for a Wyoming example by Brown (1988).

Figure 3 is a cross section west of the Newport-Inglewood fault (H. Tsutsumi, 1994). Here the LA trough is fairly shallow, and there are five south-facing reverse faults, a more complex structure than east of the Newport-Inglewood fault. The faults are of different ages. Strand A of the Santa Monica fault (SMF) underwent normal separation in the Mohnian, reverse separation in the Delmontian and Repetto, and became inactive prior to the end of the Repetto. The Rancho fault became active in the middle Pico but largely died out before the upper Pico. The northernmost strand of the SMF may be entirely Quaternary; its fault scarp is preserved (Dolan and Sieh, 1992).

Could the Northridge blind thrust have been recognized prior to the earthquake?

The Oak Ridge fault, with a slip rate of 5 mm/yr (Yeats, 1988; 1993) is overridden by the Santa Susana fault in the western Santa Susana Mountains (Yeats, 1987). This was earlier taken as evidence the fault was inactive beneath the Santa Susana Mountains. However, Yeats and Huftile (1994a, b) present evidence that the Northridge earthquake occurred on the eastward extension of the Oak Ridge fault. The Northridge earthquake uplifted both the footwall and the hangingwall of the Santa Susana fault. We proposed (Yeats and Huftile, 1994a, b) that in hindsight (always 20-20), repeated footwall uplift over many Northridge-type south-side-up earthquakes should cause the north-dipping fault to be exposed in the mountains, whereas lack of a south-dipping active reverse fault would cause the north-dipping fault to be exposed at the range front. For example, the Red Mountain fault and part of the San Cayetano fault are underlain by active south-dipping faults (Padre Juan and Sisar-Lion faults, respectively), and their footwalls are uplifted. The San Cayetano fault east of Fillmore, on the other hand, occurs at the range front.

A new cross section by Gary Huftile through the Northridge mainshock shows uplift of the Santa Susana footwall and the general asymmetric shape of the fold controlled by the south-dipping blind thrust. The south flank of the East Ventura basin is the forelimb of this structure. Between the Santa Susana fault and the East Ventura basin is the inactive Pico anticline, which is controlled by a south-vergent Pliocene blind thrust (Yeats et al., 1994). It has been tipped

to the north as part of the broad, asymmetric fold controlled by the Northridge thrust.

References

Brown, W.G., 1988, Deformational style of Laramide uplifts in the Wyoming foreland: Mem. Geol. Soc. America 171:1-25.

Dolan, J.F., and Sieh, K.E., 1992, Tectonic geomorphology of the northern Los Angeles basin: seismic hazards and kinematics of young fault movement, in Engineering Geology Field Trips: Orange County, Santa Monica Mountains, and Malibu: 35th annual meeting of the Association of Engineering Geologists, field trip guide, B20-B26.

Narr, W., and Suppe, J., 1994, Kinematics of basement-involved compressive structures: *American Jour. Sci. 294*:802-860.

Shaw, J.H., 1993, Active blind-thrust faulting and strike-slip fault-bend folding in California: Princeton University PhD thesis, 216 p.

Yeats, R.S., 1987, Late Cenozoic structure of the Santa Susana fault zone: U.S. Geological Survey Prof. Paper 1339:137-160.

Yeats, R.S., 1988, Late Quaternary slip rate on the Oak Ridge fault, Transverse Ranges, California: implications for seismic risk: *Jour. Geophys. Research 93*:12,137-12,149.

Yeats, R.S., 1993, Converging more slowly: *Nature 366*:299-301.

Reports published

Huftile, G.J., and Yeats, R.S., 1994, Cross sections through the aftershock zone of the 1994 Northridge (M_w6.7) earthquake: *EOS Transactions 75*(44) November 1, 1994/supplement, p. 166.

Huftile, G.J., and Yeats, R.S., 1994, Convergence rates across a displacement transfer zone in the Western Transverse Ranges, Ventura basin, California: *Jour. Geophys. Research*, in press.

Hummon, C., Schneider, C.L., Yeats, R.S., Dolan, J.F., Sieh, K.E., and Huftile, G.J., 1994, Wilshire fault: earthquakes in Hollywood? *Geology 22*:291-294.

Schneider, C.L., Hummon, C., Yeats, R.S., and Huftile, G.J., 1994, Structural timing and kinematics of the northern Los Angeles basin, California, based on growth strata: submitted to *Tectonics.*

Tsutsumi, H., Yeats, R.S., Hummon, C., Schneider, C.L., and Huftile, G.J., 1994, Subsurface analysis of the active trace of the Santa Monica fault and the northern extension of the Newport-Inglewood fault zone, Los Angeles basin, California: *EOS Transactions 75*(44), November 1, 1944/supplement, p. 622.

Yeats, R.S., Huftile, G.J., and Stitt, L.T.,1994, Late Cenozoic tectonics of the east Ventura basin, Transverse Ranges, California; *American Association of Petroleum Geologists Bull. 78*:1040-1074.

Yeats, R.S., and Huftile, G.J., 1994a, The Northridge earthquake: what did we know and when did we know it? *EOS Transactions 75*(44), November 1, 1994/supplement, p. 176

Yeats, R.S., and Huftile, G.J., 1994, Oak Ridge fault system and the 1994 Northridge, California, earthquake: submitted to *Nature.*

Digital Availability of Northern LA Basin Data

The well base map, 5 structure contour maps, and a cross section location map constructed by C. Hummon and C.L. Schneider have been digitized and are available to the public by computer through an anonymous FTP file server. By the time this report appears, subsurface data from Santa Monica through Las Cienegas and several cross sections should also be available. Cross sections were created in Deneba Canvas for Macintosh and will be archived in two formats: Macintosh Canvas (.cvs) and either TIFF (.tif) or Drawing Exchange Format (.dxf), allowing a broad range of users access to the information. To access the data:

ftp ava.bcc.orst.edu
login name: anonymous
password [your email address]
cd pub\SCEC

Note: the FTP is case-sensitive. Additional information regarding the archive will be in the Readme file which is automatically displayed when changing into the SCEC directory. Also, to help external users assess data quality, a meta-data file will be included for each GIS coverage which will contain information specific to the file. If there are problems, contact Tony Thatcher at thatchep@bcc.orst edu

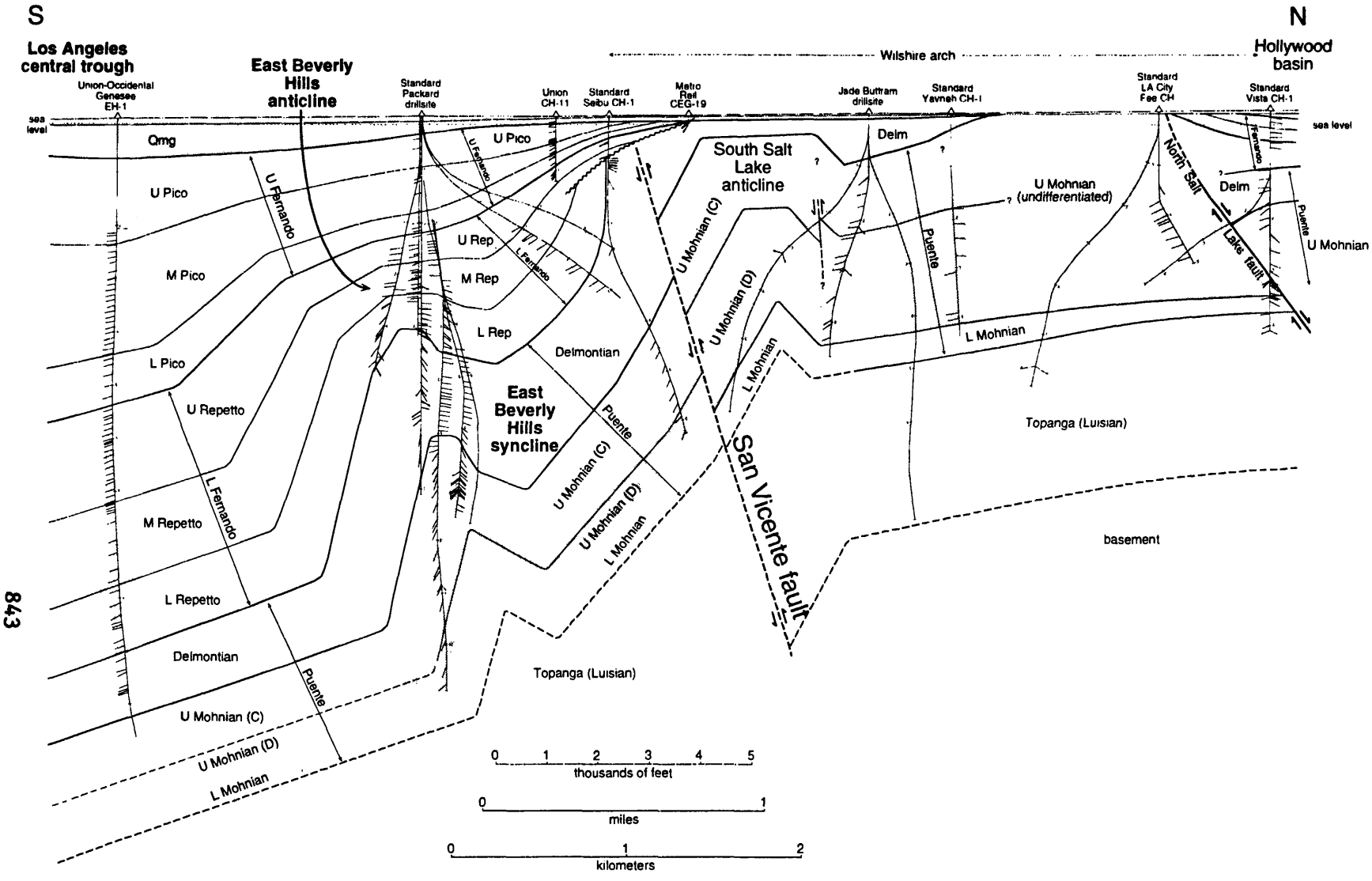
S
N
Los Angeles central trough
East Beverly Hills anticline
Wilshire arch
Hollywood basin
Union-Occidental Genesee EH-1
Standard Packard drillsite
Union CH-11
Standard Seibu CH-1
Metro Rail CEG-19
Jade Buffram drillsite
Standard Yavneh CH-1
Standard LA City Fee CH
Standard Vista CH-1
sea level
Qmg
U Pico
M Pico
L Pico
U Repetto
M Repetto
L Repetto
Delmontian
U Mohnian (C)
U Mohnian (D)
L Mohnian
U Fernando
L Fernando
Puente
U Rep
M Rep
L Rep
East Beverly Hills syncline
South Salt Lake anticline
U Mohnian (undifferentiated)
Delm
North Salt Lake fault
San Vicente fault
Topanga (Luisian)
basement
0 1 2 3 4 5
thousands of feet
0 1
miles
0 1 2
kilometers

Figure 1

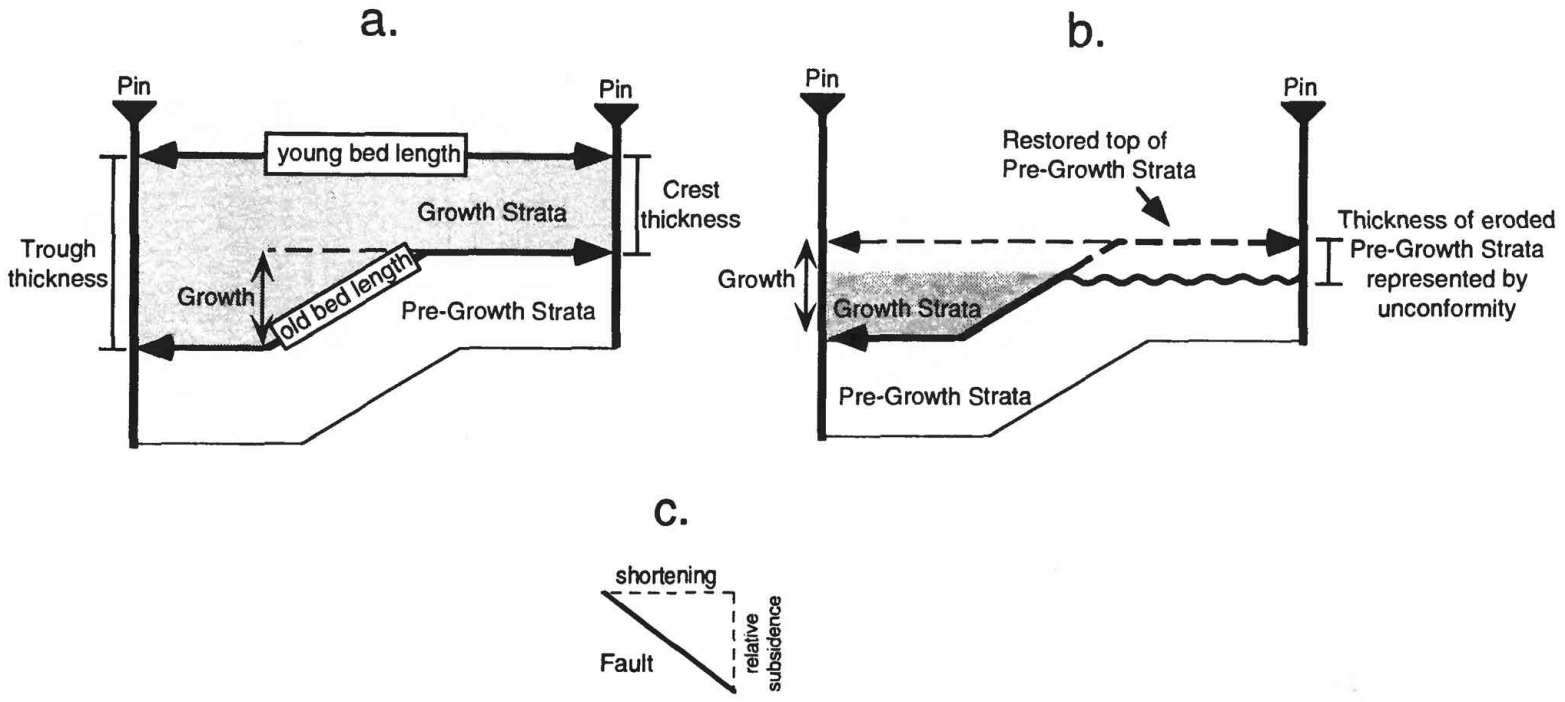

Shortening = old bed length-young bed length.
Relative subsidence = Trough thickness -Crest thickness

$$\text{Fault dip} = \text{Tan}^{-1}\left(\frac{\text{Relative Subsidence}}{\text{Shortening}}\right)$$

Figure 2

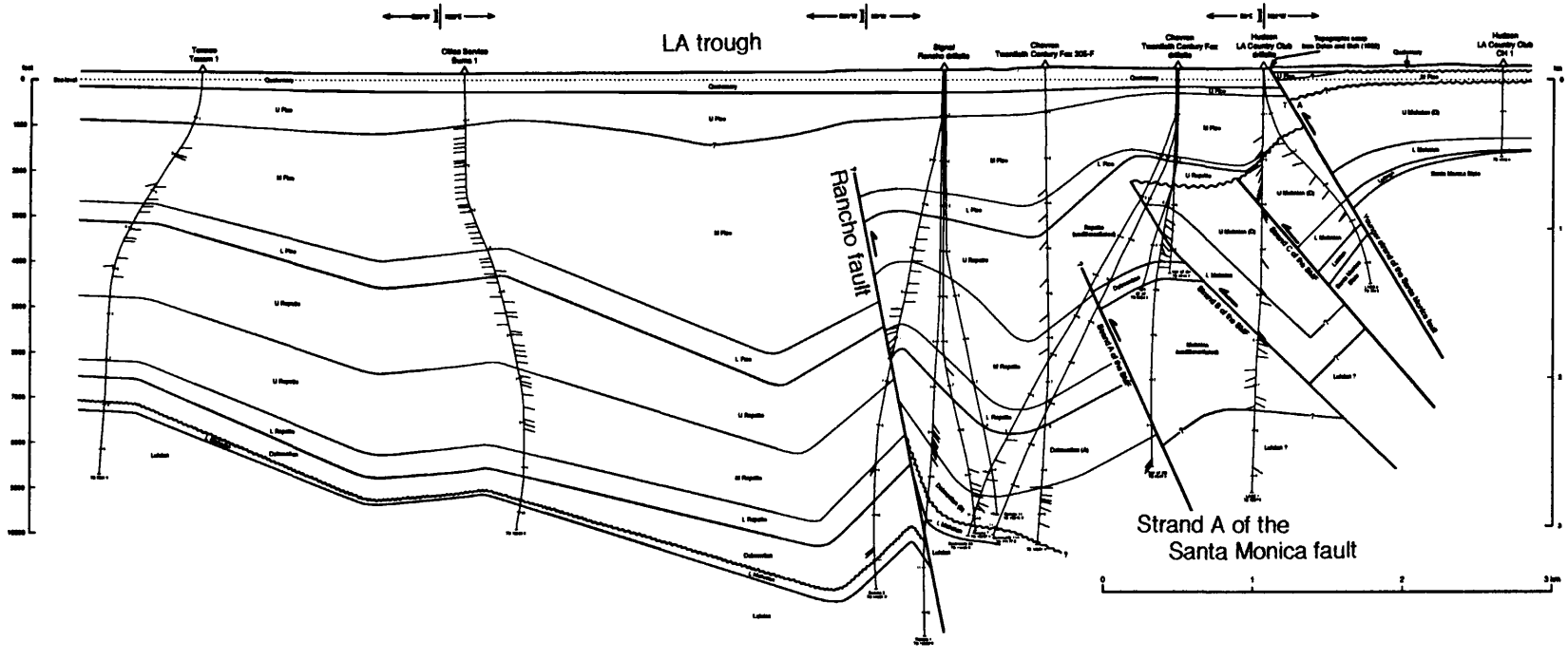

Figure 3

NEHRP

Annual Project Summary

Determination of Crustal Stress State at New Madrid Seismic Zone From Inversion of Earthquake Focal Plane Mechanisms: Implications for Fault Reactivation

Award Number: 1434-94-G-2391

Mark D. Zoback and Marian E. Magee
Dept. of Geophysics, Stanford University
Stanford, CA 94305
(415) 725-9295, FAX (415) 725-7344, zoback@pangea.stanford.edu

We have determined the stress state associated with seismicity in the New Madrid seismic zone using focal mechanisms of earthquakes recorded by the PANDA network (Chiu et al., 1992), a 40 station digital seismograph array which was deployed over 34 months from 1989 through 1992. Focal mechanism solutions for 102 earthquakes located primarily in the center of the zone exhibit reverse, normal, right-lateral, and left-lateral slip on a variety of nodal planes (Figure 1a). The diverse slip directions evident in these focal mechanisms indicate an apparent complexity that is inconsistent with recognized geologic structure and a uniform stress field.

Seismicity in the New Madrid seismic zone is concentrated along several well-defined trends (Figure 1b). Right-lateral strike-slip faulting is indicated along the main NE-SW seismic trend that lies approximately down the center of the late Precambrian/early Paleozoic crustal Reelfoot rift from Marked Tree, AK to Caruthersville, MO. Additional microseismicity in the area is concentrated along a NNW-SSE trending zone from New Madrid, MO to south of Ridgely, TN and a short EW trending zone west of New Madrid. Previous studies (e.g., Zoback and Zoback, 1981; Russ, 1982) suggested that focal mechanisms of regional earthquakes and geomorphic evidence of recently uplifted horst-like block appear to be consistent with a maximum compressive stress acting about 70°- 80°E.

We carefully reviewed each individual first motion focal mechanism and determined that 28 of the original mechanisms determined by Chiu and his colleagues, as well as 43 focal mechanisms that we recomputed using FPFIT (Reasenberg and Oppenheimer, 1985) are reasonably well-resolved with errors in each nodal plane's strike, dip, and rake of less than 10°. We did not use mechanisms for 31 of the original 102 earthquakes because we were unable to either resolve the many inconsistent readings or find an objectively best solution from among many possible solutions. Normal, thrust, and strike-slip faults on a variety of planes are still well represented in the revised data set (Figure 2) and exhibit diverse slip directions that appear to be incompatible with a uniform stress field.

Seventy-one well resolved earthquake focal mechanisms were used to invert for the orientation and relative magnitudes of the principal stresses with the grid-search method of Gephart and Forsyth (1984). We found that a uniform strike-slip stress field with the maximum horizontal stress (S_{Hmax}) is directed N76°E fit the data with a minimum average misfit of 11° (Figure 3).

We tested for a spatially non-uniform stress field over the central region by inversion of the earthquake focal mechanisms located within specific spatial subsets of the overall seismic zone (Figure 4a). The resultant best-fit stress tensors were well within the 68% confidence limit of the best-fit uniform stress tensor for the entire data set, as shown by the 1 sigma contours in Figure 4b. Consequently, we find that no significant stress gradients are required by the data.

From analysis of resolved shear stress on the earthquake planes (Magee and Zoback, 1994), it appears that many of these diverse earthquakes are occurring on planes which require some sort of weakening mechanism (e.g., a lower coefficient of friction, elevated crustal or fault pore pressure) to explain slip under the inferred stress state within the New Madrid seismic zone. The apparently weak planes are pervasive throughout the entire central seismic zone and, although planes well oriented to slip in this stress field appear to result primarily in strike-slip earthquakes, these weak planes are slipping in thrust, normal, and strike-slip earthquakes.

In summary, we have carefully examined the distribution of earthquake focal mechanisms with respect to a best-fitting uniform stress tensor using an established inversion technique (Gephart and Forsyth, 1984; Gephart, 1990) and attempted to determine whether gradients in principal stress directions or relative magnitudes, or variable fault strengths are required to fit the observed slip directions. From our inversion of the focal mechanisms for the orientation and relative magnitudes of the principal stresses we find that these seemingly incompatible focal mechanisms do not require a spatially heterogeneous stress field, but are consistent with a strike-slip stress regime with the maximum horizontal stress direction rotated about 10° clockwise from the regional S_{Hmax} direction for midplate North America (Zoback and Zoback, 1989). The diverse slip directions and faulting mechanisms in the central region of the New Madrid seismic zone appear to indicate a locally weak crust, as well as low and variable fault strengths.

Reports Published

Magee, M. E. and M. D. Zoback, 1994, Complex Earthquake Focal Mechanisms and Regional Stress in the New Madrid Seismic Zone, *EOS, Transactions, American Geophysical Union, 75, 437.*

A paper is in preparation for submission to Bulletin of the Seismological Society of America, co-authored by M. E. Magee, M. D. Zoback, and J. M. Chiu.

References

Chiu, J.M., A.C. Johnston, and Y.T. Yang, 1992, Imaging the active faults of the central New Madrid seismic zone using PANDA array data, *Seism. Res. Lett., 63*, 375-393.

Gephart, J. W., 1990, Stress and the direction of slip on fault planes, *Tectonics, 9*, 845-858.

Gephart, J.W., and D.W. Forsyth, 1984, An improved method for determining the regional stress tensor using earthquake focal mechanism data: Application to the San Fernando earthquake sequence, *J. Geophys. Res., 89*, 9305-9320.

Magee, M. E. and M. D. Zoback, 1994, Complex Earthquake Focal Mechanisms and Regional Stress in the New Madrid Seismic Zone, *EOS, Transactions, American Geophysical Union, 75, 437.*

Reasenberg, P. A., and D. Oppenheimer, 1985, FPFIT, FPPLOT, and FPPAGE: Fortran computer programs for calculating and displaying earthquake fault-plane solutions, *U.S. Geological Survey Open-File Report 85-739*, 109 pp.

Russ, D.P., 1982, Style and significance of surface deformation in the vicinity of New Madrid, Missouri, *in* Investigations of the New Madrid, Missouri, Earthquake Region, F.A. McKeown and L.C. Pakiser, eds., *U.S. Geol. Surv. Prof. Paper 1236*, 95-114.

Zoback, M.D., and M.L. Zoback, 1981, State of stress and intraplate earthquakes in the United States, *Science, 213*, 96-104.

Zoback, M.L. and M.D. Zoback, 1989, Tectonic stress field of the continental U.S. in Geophysical Framework of the Continental United States (L. Pakiser and W. Mooney, eds.), *GSA Memoir, 172*, 523-529.

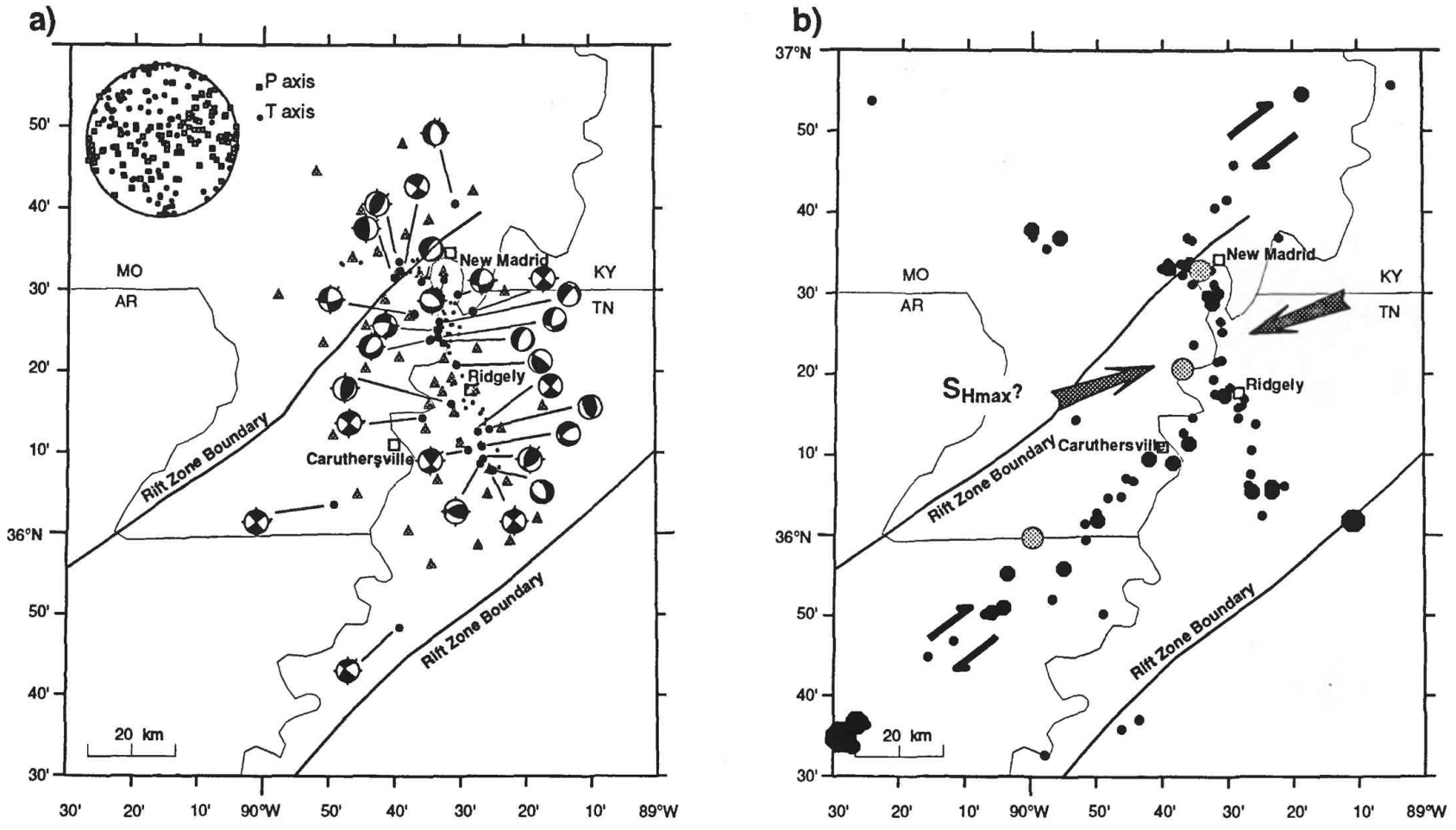

Figure 1. a) Representative focal mechanisms determined by Dr. Chui and collegues for some of the 102 larger earthquakes recorded by the PANDA seismic network. Stations locations marked by gray triangles. P and T axes for 102 earthquake focal mechanisms are plotted on the stereonet, upper left corner, and reflect apparent complexity inconsistent with regional geology and unifiorm stress field shown in 1b. b) Regional map of New Madrid seismic zone. Seismicity (9176-1993) from NEIC catalog shown as blcak dots. Gray filled dots show 1811-1812 M>8 earthquakes. Large arrow shows SHmax direction consistent with focal mechanisms of larger regional earthquakes.

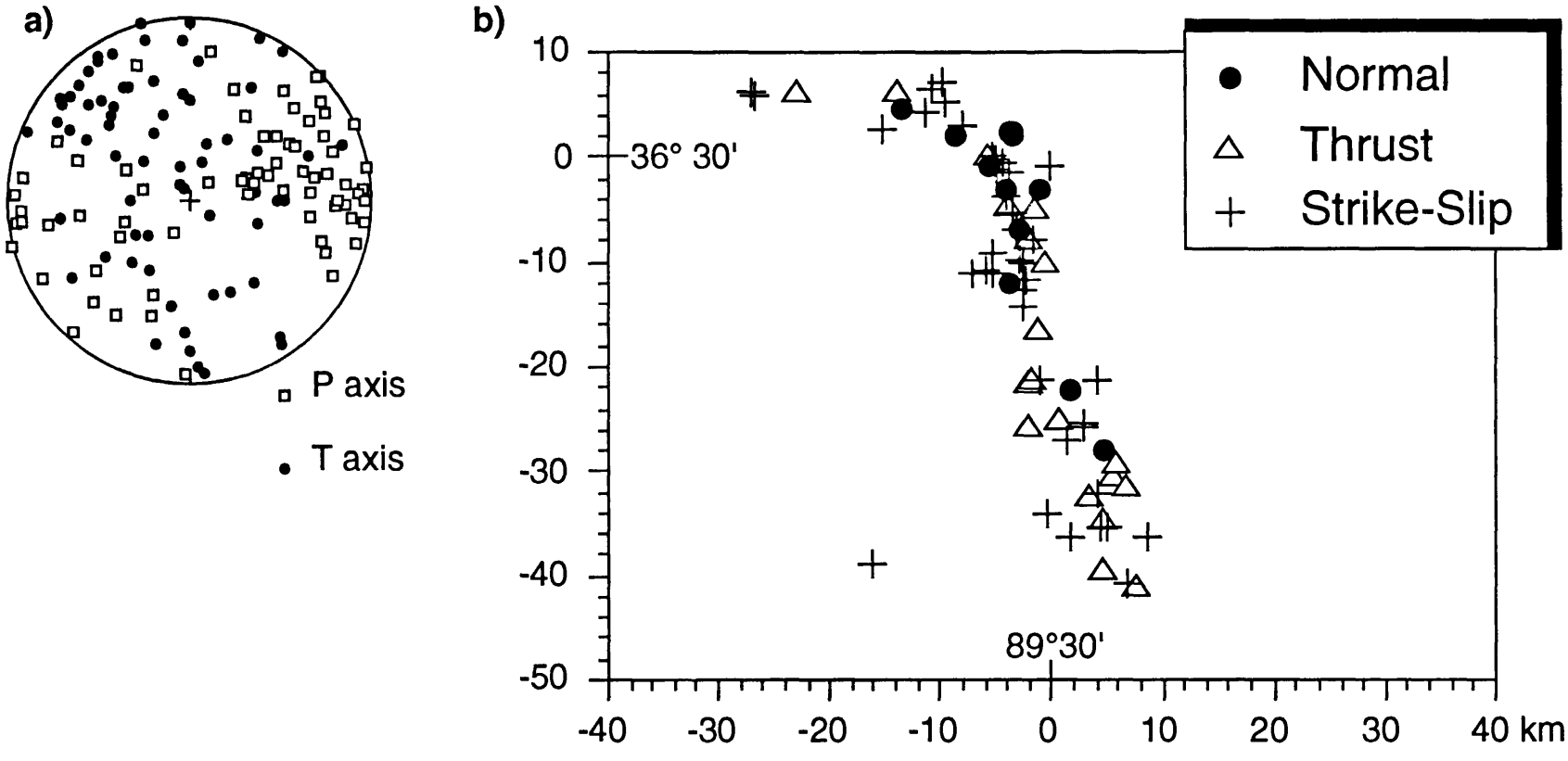

Figure 2. a) P and T axes for final 71 earthquake focal mechanisms used in inversion to determine stress tensor. b) Map of central region, New Madrid seismic zone. Earthquake locations are marcked by symbol indicating faulting style determined by rake of one nodal plane. Note that normal, thrust, and strike-slip earthquakes are occurring throughout the central region.

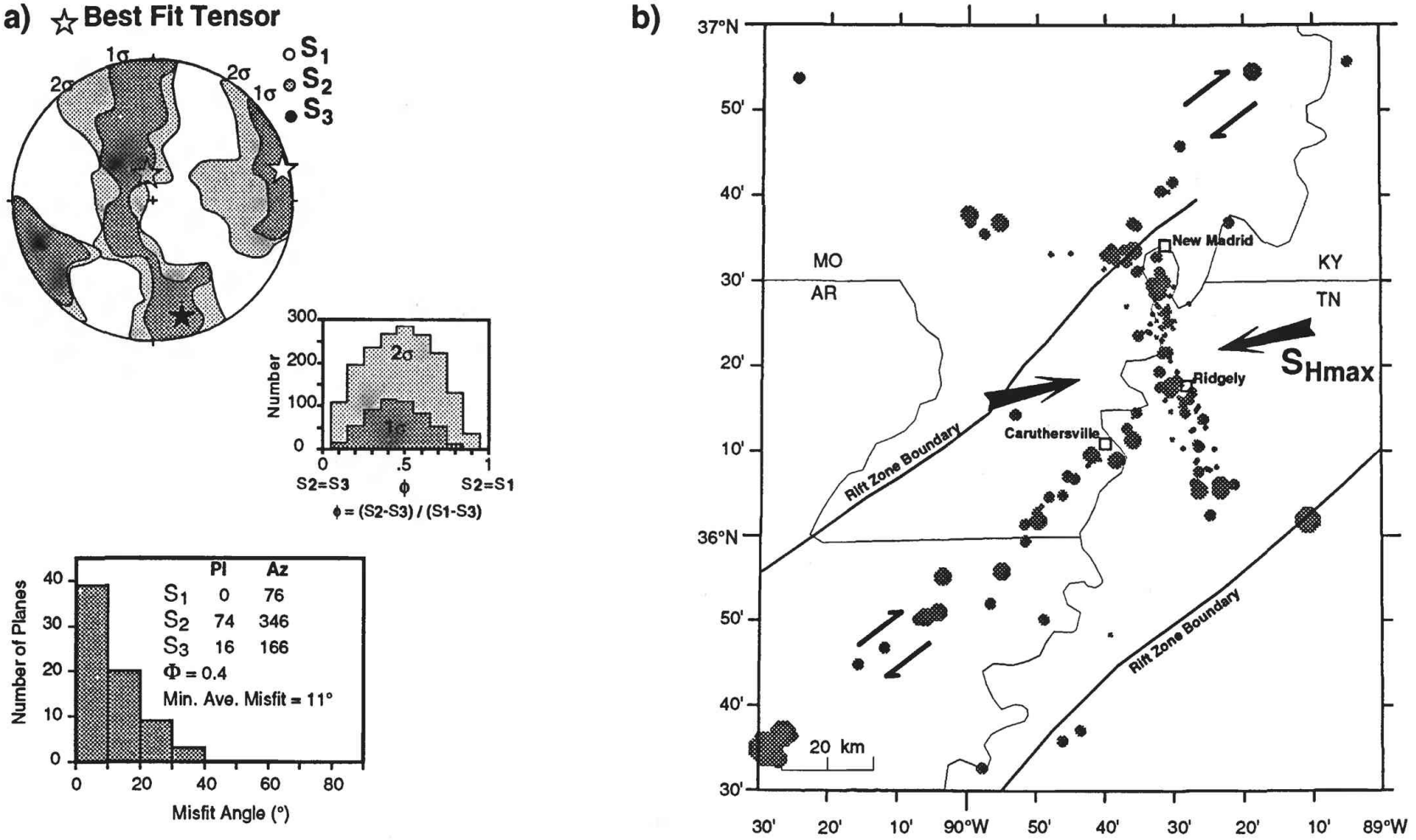

Figure 3. a) Stress inversion results. Stereonet showing 1σ and 2σ contours around best-fitting stress tensor. S_1 and S_3 principal stress directions for the best-fit stress tensor are nearly horizontal, with S_2 approximately vertical. Histogram of ϕ values for model stress tensors indicate that although ϕ is not well constrained, the relative magnitude of S_2 is midway between S_1 and S_3 . Histogram of number of planes versus their misfit angle shows that 85% of the 71 earthquakes have one plane that requires less than 20° of rotation about an appropriate axis to make the observed slip direction consistent with the predicted sense and direction of maximum shear on that plane. b) Map of New Madrid seismic zone showing S_{Hmax} direction with respect to regional structure, regional seismicity, and microseismcity in the cental region.

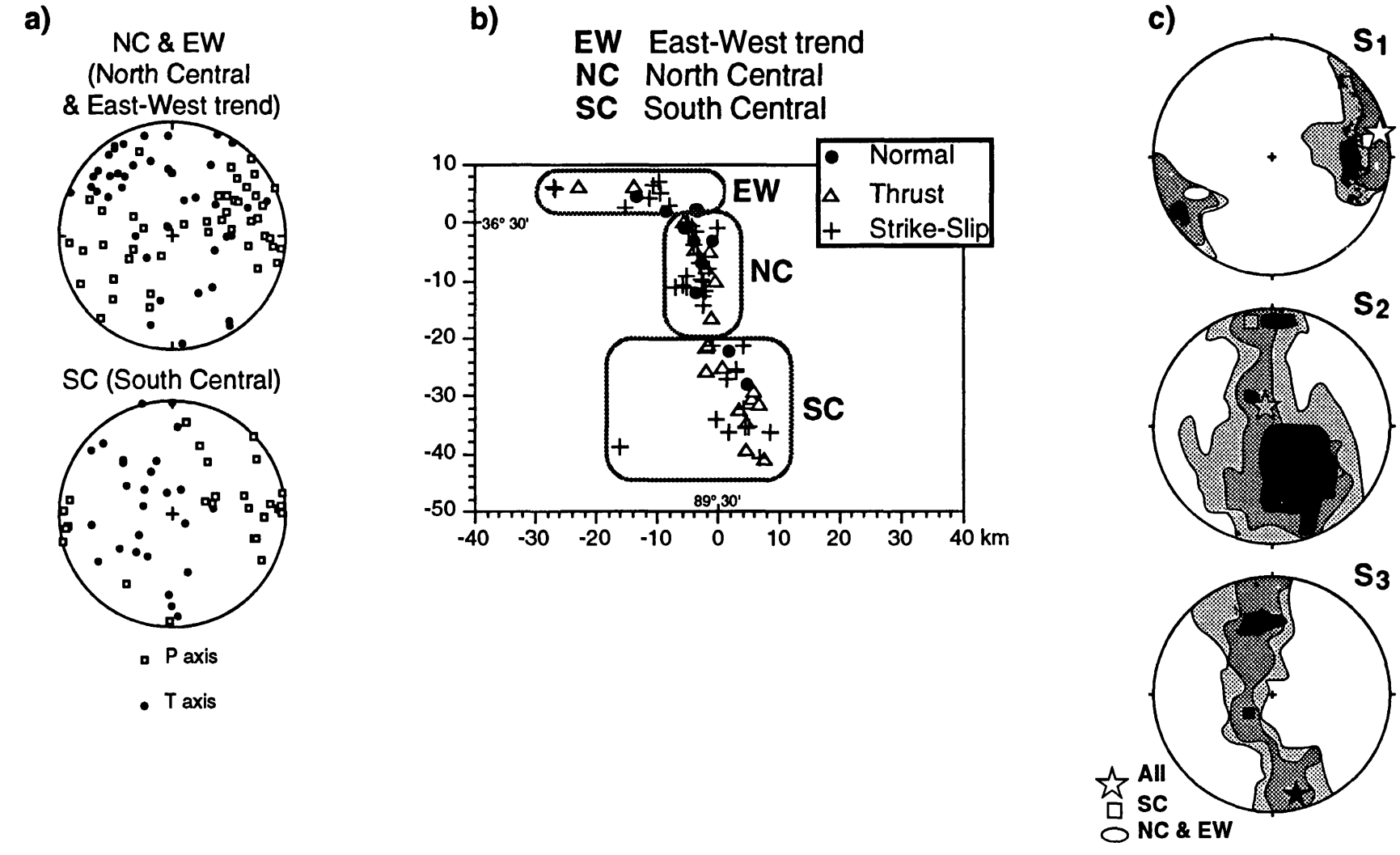

Figure 4. Inversion results for spatial subset. a) Stereonet of P and T axes for earthquakes within subregions designated in b. b) Map showing earthquakes designated by spatial groups. Area shown and symbols as in Fig. 2. NC and EW were inverted together because there were too few earthquakes in subset EW for a reliable result. c) Stereonets of stress tensors determined for each spatial subset shown with the best-fit stress tensor and 1σ, 2σ contours for all 71 earthquakes. Note that each principal direction determined for the spatial subsets is within the 1σ contours of the best-fit solution for the total data set.

SEISMOTECTONICS OF THE SAN FRANCISCO PENINSULA

Mary Lou Zoback
Jean Olson
Seismology Branch
U. S. Geological Survey
345 Middlefield Road, MS 977
Menlo Park, CA 94025
(415) 329-4760
zoback@andreas.usgs.wr.gov

INVESTIGATIONS:

1. Investigation of seismicity within the San Francisco bay block and evaluation of possible fault structures within the basement.

2. Analysis of stress rotation in the vicinity of the Amazonas rift in Brazil and possible causal relationship to intraplate seismicity.

3. Assisted in compilation and review of Menlo Park contributions for the Science paper on the Northridge earthquake produced by OEVE and SCEC.

RESULTS:

1. San Francisco Bay occupies a gentle structural downwarp within the 30 km-wide block bounded by the subparallel San Andreas and Hayward fault zones. This block is characterized by diffuse low-level seismicity. Through-going fault zones within the Bay block were suggested a decade ago on the basis of prominent linear N50-60°W trending aeromagnetic anomalies aligned with mapped onshore shear zones within the Franciscan Formation (Brabb and Hanna, 1982, USGS Map GP-932). Both gravity data and recent high resolution seismic-reflection profiling of Holocene bay mud rule out significant vertical offsets across these proposed fault zones, despite their similarity in strike to thrust faults in the southern San Francisco Peninsula. In contrast to earlier reports of extensive Holocene strike-slip faulting (Mann et al., 1993, EOS, v. 74, p. 693), new high resolution seismic reflection data also appear to preclude any major Holocene strike-slip-related disruption along these fault zones.

Precise relocation of earthquakes indicate that seismic activity within the Bay block generally decreases with increasing distance from the two bounding faults. Most events occur between 6 and 12 km depth (similar to the depth range of the background seismicity along the San Andreas and Hayward faults). Five unusual events located beneath San Francisco were found to have focal depths of ~16km. The most persistently active cluster of seismicity occurs beneath San Francisco

airport (SFO) at about 10 km depth. Reliable fault-plane solutions for 12 of the largest events ($2.0 \leq M \leq 3.0$) within the Bay block indicate oblique strike-slip mechanisms with both normal and reverse components of slip and a distinct contrast in deformation axes between the North and South Bay. South Bay events have NE-trending P-axes consistent with "fault-normal" compression observed on the southern Peninsula, whereas North Bay events have "fault parallel" NW-trending P-axes. Neither the precise relocations nor the fault-plane solutions for the Bay seismicity suggest any clear or convincing association of these events with the postulated N50-60°W trending transbay fault zones; nodal planes for the cluster of seismic deformation beneath SFO are nearly 45° oblique to the trend of the proposed nearby transbay fault zone.

Both the low level of microseismicity and geodetic observations limiting shear strain rates within the Bay block to be less 3 mm/yr suggest that any through-going earthquakes on the bay faults must have very large recurrence intervals. However, fault interaction models suggest another possible mode of deformation of the Bay block related to its unique tectonic setting. Sympathetic slip up to several tens of cm might be occurring on pre-existing N50-60°W trending vertical fault zones within this block in response to stress changes related to major earthquakes on the adjacent segments of the subparallel San Andreas and Hayward faults.

2. The state of stress in the vicinity of old continental rifts is examined to investigate the possibility that crustal structure associated with ancient rifts (specifically a dense rift pillow in the lower crust) may actually modify the regional stress field and increase the likelihood of brittle failure. Both shallow (2.0-2.6 km depth) breakout data and deep (20-45 km depth) crustal earthquake focal mechanisms indicate a consistent N to NNE maximum horizontal compression in the vicinity of the Paleozoic Amazonas rift in central Brazil. This compressive stress direction is nearly perpendicular to the rift structure and represents a ~75° stress rotation relative to a regional E-W compressive stress field in the South American plate. Elastic 2-D finite element models of the density structure associated with the Amazonas rift (as inferred from independent gravity modeling) indicate that elastic support of this dense feature generates horizontal rift-normal compressional stresses between 60-190 MPa, with values of 80-100 MPa probably most representative of the overall structure. The observed ~75° stress rotation constrains the ratio of the regional horizontal stress difference to the rift normal compressive stress to be between 0.25 and <1.0, indicating that this rift normal stress must be between 4 to >1 times larger than the regional horizontal stress difference.

A general expression for the modification of the local horizontal shear stress (relative to the regional horizontal shear stress) is derived. The same ratio of the rift normal compression relative to the regional horizontal stress difference which controls the amount of stress rotation also determines whether the superimposed stress increases or decreases the local maximum horizontal shear stress. The potential for fault reactivation is analyzed considering both the local stress rotation and modification of horizontal shear stress for both thrust and strike slip stress regimes. The results are applied to the present day state of stress in the vicinity of three ancient continental rifts. In the Amazonas rift case, because the observed stress rotation only weakly constrains the ratio of the regional horizontal stress difference to the rift normal compression to be between 0.25 and <1.0, the resultant normalized horizontal shear stress may be reduced (for ratios >0.5) or enhanced (for ratios <0.5). Furthermore, more information is needed to predict how a change in horizontal shear stress directly influences the likelihood of faulting in a thrust faulting stress regime such as in the vicinity of the Amazonas rift.

A rift normal stress associated with the New Madrid rift may be sufficient to rotate the horizontal stress field ~20° clockwise (an orientation very favorable for the observed reactivation

of steep strike-slip faults parallel to the axis of the rift). However, a 20-40% reduction in the local horizontal shear stress accompanies this rotation a suggesting a reduced strength within this dominantly strike-slip seismic zone (relative to the surrounding crust). Sparse and ambiguous stress data suggest that the Mid-Continent rift of the central U. S.may represent an example in which superposition of a rift-normal compressive stress significantly reduces the local horizontal shear stress and hence decrease the likelihood of faulting; this may, in part, explain the marked lack of seismicity associated with this large ancient rift. The modeling and analysis here demonstrate that rift-normal compressive stresses are a significant source of stress acting on the lithosphere which may be a major contributing factor to the association of intraplate seismicity with old zones of continental extension.

REPORTS:

Zoback, M. L., and Richardson, R. M., 1994, Stress perturbation and intraplate seismicity associated with ancient continental rifts: Tectonics, submitted.

abstracts:

Olson, Jean O., Zoback, M.L., Simpson, R. W., and M, 1994, Deformation of the San Francisco bay block?: EOS (Transactions American Geophysical Union), v. 75, p. 683.

Zoback, M. L., Zoback, M.D., Crone, A.J., Machette, M.N., and; Richardson, R. M., 1994, Processes and patterns of intraplate seismicity: Geological Society of America Abstracts with Programs, v. 26, p. 325.

COLLABORATIVE RESEARCH: SITE CATEGORY AND REGION SPECIFIC ATTENUATION RELATIONS FOR LOS ANGLES

1434-94-G-2436
1434-94-G-2452

Keiiti Aki
University of Southern California
Department of Geological Sciences
University Park
Los Angeles, CA 90089-0740
(213) 740-5830, 8801 (Fax)

Walt Silva
Pacific Engineering and Analysis
311 Pomona Avenue
El Cerrito, CA 94530
(510) 528-2821, 2135 (Fax)

A key element in reducing the seismic risk to structures due to ground shaking and soil failure is to better quantify the hazard in terms of expected levels of motion for varying earthquake sizes, distances to the site, and soil foundation conditions. The objective of this project is to produce more accurate predictions of strong ground motions for a variety of site conditions for the Los Angeles region. The results will be available to the engineering and planning communities to assess the seismic design of existing structures and facilities as well as to provide design bases for future construction.

Title: LA Basin Microzonation - Annual Project Summary 1994

Award Number: USGS 1434-94-22646
PI's: Ralph Archuleta, Jamison Steidl, and Alexei Tumarkin
Institution: Institute for Crustal Studies and Department of Geological Sciences, University of California at Santa Barbara
Address: 1140 Girvetz Hall, Santa Barbara, CA 93106
Telephone: (805) 893-8231
Fax: (805) 893-8649
email: ralph, steidl, or alexei@quake.crustal.ucsb.edu
Program Element: III.1 III.2 (predicting the effects of earthquakes)

Investigations Undertaken:

The project objective is to collect seismic data from sites throughout the Los Angeles metropolitan region for seismic hazard analysis. It has long been known that each soil type responds differently when subjected to ground motion from earthquakes. Usually the younger softer soils amplify ground motion relative to older more competent soils or bedrock. Our goal has been to instrument different sites in the Los Angeles area to quantitatively measure this amplification of ground motion and produce a data base of amplification factors. These amplification factors are then used to help distinguish regions where the seismic hazard is greatest due to amplification from the surface geology and sub-surface structure.

The heavy demand for PASSCAL instruments postponed the start date of this project until November of 1994 when the instruments arrived at UCSB. Deployment of the PASSCAL instruments took place in December and January after intensive calibration of the sensors at the Southern California Earthquake Centers (SCEC) Portable Broadband Instrument Center (PBIC) laboratory at UC Santa Barbara.

The 10 PASSCAL instruments were deployed along with 3 SCEC and 2 Caltrans instruments for a total of 15 stations. Figure 1 shows the locations of the 15 stations deployed in December 1994 (solid triangles - 94/95 portable deployment), the locations of the 3 SCEC and 2 Caltrans instruments deployed prior to December 94 in the pilot study supported by UCSB funding and the seismicity recorded at these locations in early 1994.

Many of the sites chosen for deployment in this project are co-located with permanent strong motion stations. In addition to collecting weak motion data at these sites, we will also be able to compare amplification factors derived from weak motion data to those derived from strong motion records. An important question to engineering seismologists is how significant is the non-linear effect on strong ground motion, and at what amplitude level can we expect to see it? The Northridge mainshock and aftershock data recorded by this study, along with the permanent strong motion stations will provide ground motion data with the amplitude range to address these questions.

Results:

As part of the pilot study for this project we had five sites operating from March 93 to January 94 and then we moved four of the five sites after the M6.7 Northridge event. In figure 2 we show the N-S component of motion from the 4 portable digital stations LA00, LA02, LA03, and LA04 (locations shown in Figure 1) for the M6.7 Northridge mainshock and a M5.3 aftershock. Also shown are the response spectra from 0.1 to 10 seconds. The response spectra have been corrected for the geometrical spreading factor only. The long period amplification in the Los Angeles basin can be easily seen in this figure in the period range from 1 to 10 seconds. The LA00 spectra (black) which is our "reference" site located on Cretaceous rock of the Santa Monica mountains has the smallest spectra at these periods as expected. At shorter periods things become more complicated and attenuation and topographic effects as well as path effects from the two different earthquakes may be needed to explain the data.

The extensive data sets collected from the Northridge aftershock sequence by different organizations and agencies are still being compiled. The data collected by UCSB mentioned above represents only one small part of this data set. Once released by SCEC, the complete Northridge data set will be combined with the data that is currently being collected under this project. These data will be analyzed to produce a data base of amplification factors for the metropolitan Los Angeles region.

Reports Published:

Due to the late start date for this project no significant publications have been submitted yet. Although we have accomplished much in the preliminary stages of this project, there is still a great deal of science to be done. Most of the accomplishments to date have been in the data collection phase and we look forward to the scientific analysis and a successful completion of the project in the year to come. Poster presentations of the work in progress took place at the Seismological Society of America annual meeting, Pasadena, CA in April of 1994 and at the SCEC annual meeting, Temecula, CA in September 1994.

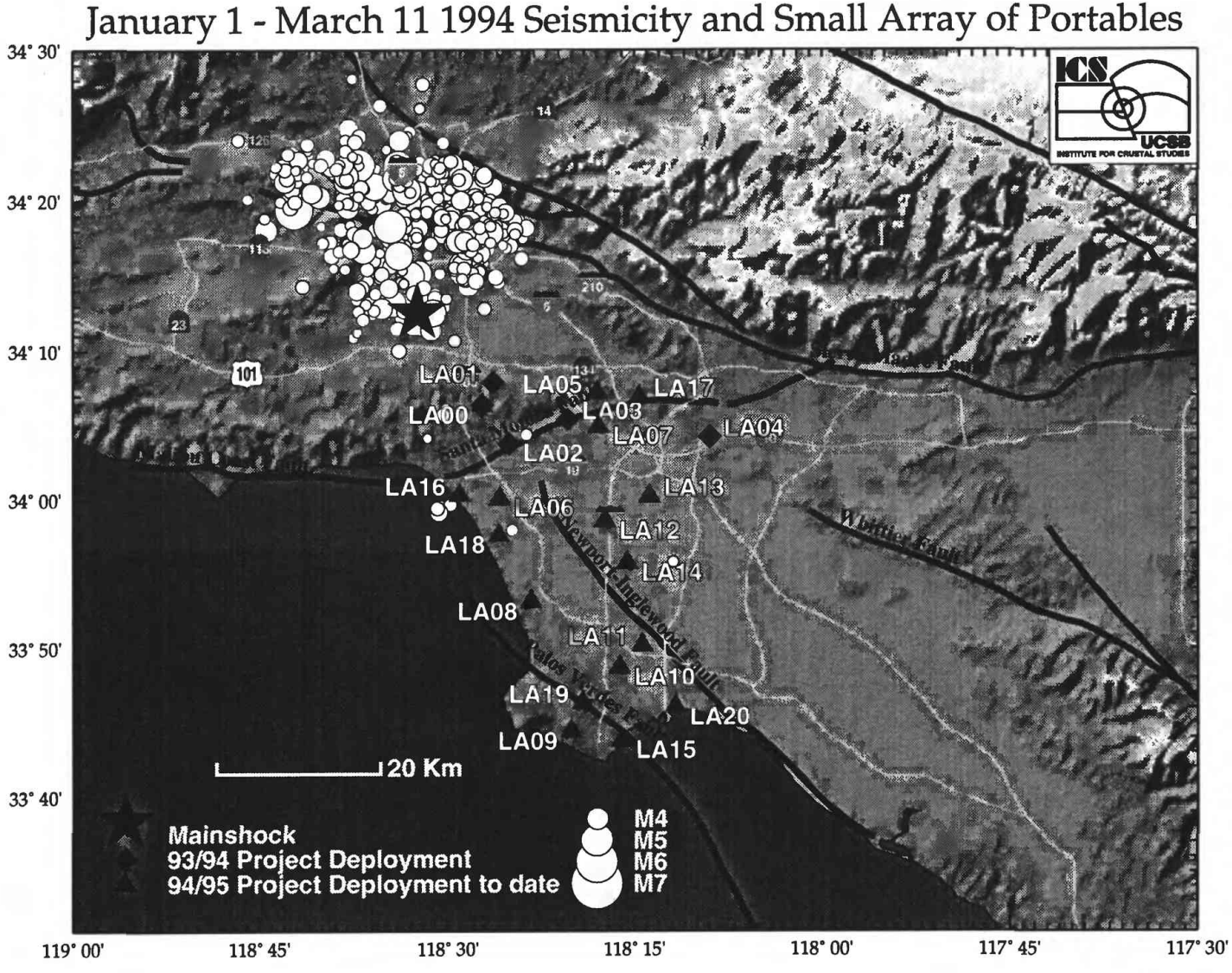
January 1 - March 11 1994 Seismicity and Small Array of Portables
34° 30'
34° 20'
34° 10'
34° 00'
33° 50'
33° 40'
119° 00'
118° 45'
118° 30'
118° 15'
118° 00'
117° 45'
117° 30'
ICS
UCSB
INSTITUTE FOR CRUSTAL STUDIES
LA01
LA05
LA17
LA00
LA03
LA07
LA04
LA02
LA16
LA13
LA06
LA12
LA18
LA14
LA08
LA11
LA10
LA19
LA20
LA09
LA15
20 Km
Mainshock
93/94 Project Deployment
94/95 Project Deployment to date
M4
M5
M6
M7

Figure 1

Northridge 1/17/94 M6.7 and 1/18/94 M5.3 Response Spectra and Acceleration Data

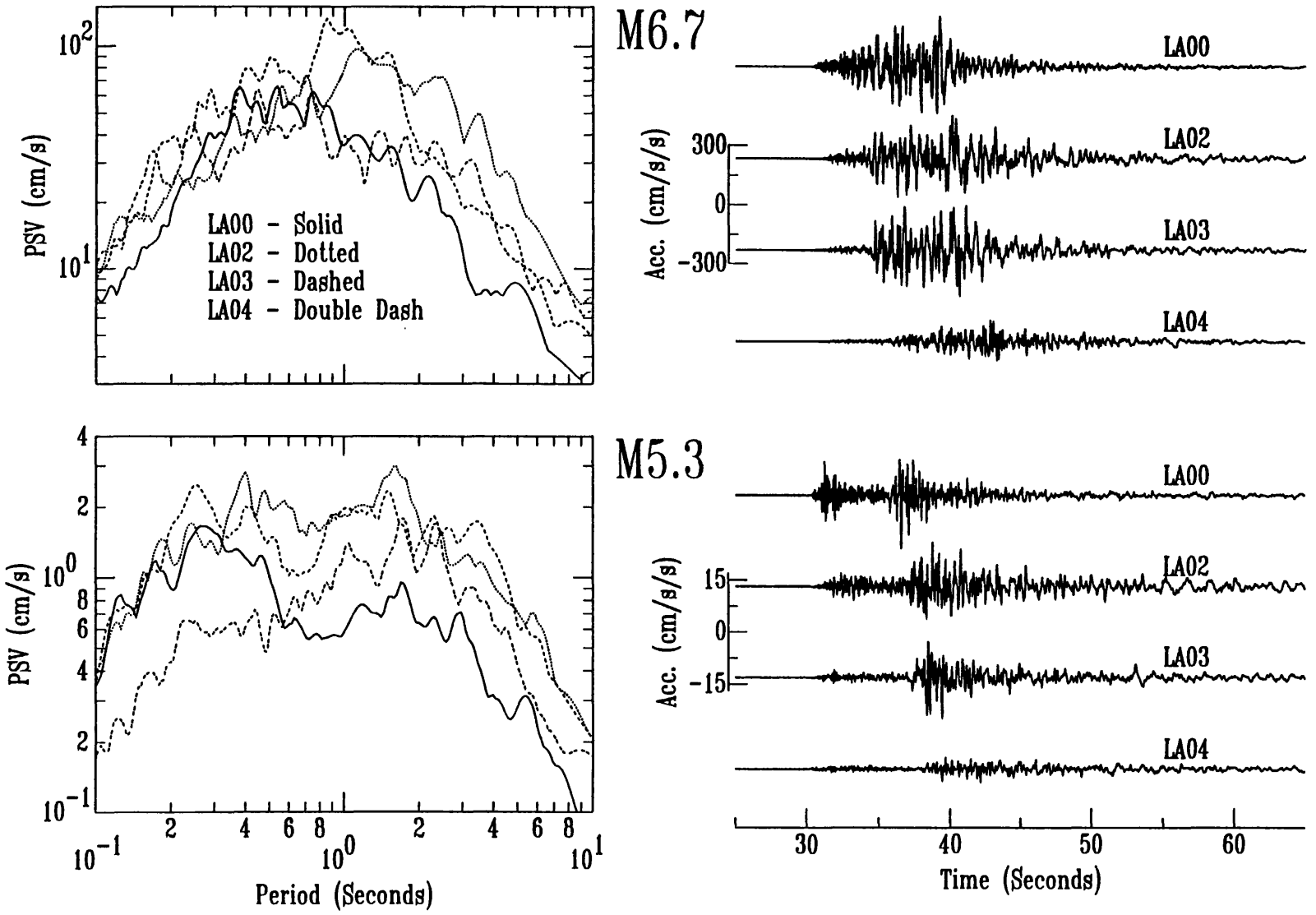

Figure 2

NEHRP 1434-94-G-2419

ATTENUATION AND SOURCE PARAMETERS FOR EARTHQUAKES IN THE PACIFIC NORTHWEST REGION

Gail M. Atkinson

The attenuation and source parameters of earthquakes in the Pacific Northwest region was investigated using data from the Western Canada Telemetered Network (WCTN). The dataset contains over 900 digital records from 57 earthquakes of $3.0 \leq M \leq 7.0$, recorded at 20 hard-rock stations in southwestern British Columbia. Both shallow crustal events and events within the subducting Juan de Fuca plate are represented in the dataset. The instruments allow reliable recovery of Fourier amplitude spectra for frequencies from about 0.5 Hz to 20 Hz.

The Fourier spectral data were analyzed by the method of Atkinson and Mereu (BSSA, 1992, p. 2014-2031), in which a grid search of parameters is performed to determine the best-fit source, path and site terms. Monte Carlo simulations of synthetic databases are then used to assess the significance of the determined parameters. The underlying model equation for the regressions is given by:

$$\tilde{a}(f)_{ij} = E(f)_i \; D(f,R) \; S(f)_j$$

where $\tilde{a}(f)_{ij}$ is the recorded Fourier amplitude spectrum of acceleration of earthquake i at station j, as a function of frequency (f), $E(f)_i$ is the source spectrum of earthquake i, D(f,R) describes the geometric and anelastic attenuation of spectral amplitudes with hypocentral distance (R), and $S(f)_j$ is the amplification of spectral amplitudes at station j. The regression is constrained by the condition that S(f) averages to a factor of unity over all hard rock sites. D(f,R) is allowed to take a variety of forms to allow flexibility in determining both geometric and anelastic attenuation, and possible variation of the functional form over different distance ranges.

Regression of the dataset as a whole showed that the attenuation can be approximated by R^{-1} geometric spreading with anelastic attenuation as given by $Q=380f^{0.39}$ (assuming a shear wave velocity of 3.7 km/s). However the attenuation for shallow crustal earthquakes ($h<10$ km), which occur above the major thrust that underlies the rocks of the Wrangellia terrane, is significantly different than that for other events, namely intermediate-depth ($20<h<25$ km) crustal events and events within the subducting slab ($30<h<65$ km). Therefore the data may be divided into two distinct subsets.

Shallow crustal earthquakes ($h<10$ km) show a trilinear decay of spectral amplitudes, with geometric spreading rates of R^{-1}, R^{0}, and $R^{-0.5}$ in the distance ranges $10<R\leq75$ km, $75<R\leq230$ km and $R>230$ km, respectively. The associated Q model for the shallow

crustal travel paths is given by $Q=174f^{0.58}$. Deeper crustal events (h>15 km) and those within the subducting slab appear to have R^{-1} geometric spreading over all distance ranges, with an associated Q given by $Q=263f^{0.49}$.

The source terms determined from the regressions are relatively insensitive to the shape of the attenuation curve (ie. linear or trilinear); they can be determined to within about 0.1 to 0.2 log units. Table 1 lists the source parameters determined for the study earthquakes. The stress drop is the value required, within the context of the Brune source model, to match the observed high-frequency spectral amplitudes. The moment magnitudes of most events were determined from the long-period level of the source spectrum of displacement. For the largest few events the WCTN data have insufficient bandwidth to determine the long-period level; in these cases published moments were used, or moment was estimated from M_S.

Stress drop increases with magnitude for M<4, probably due to finite bandwidth effects. For M>4, the events show an average constant stress drop of about 35 bars. This is lower than the average California value (about 70 bars), and much lower than the average eastern value (about 150 bars). Stress drops for shallow crustal events appear to be about the same as those for deeper events and events within the subducting slab, although very shallow (h<5 km) earthquakes appear to have low stress drops.

Earthquakes of M<5 are well-matched by the Brune spectral shape. The largest two events (M 6.0 and M 7.0), by contrast, exhibit a clear deficit of spectral amplitudes at f<2 Hz, relative to that expected from the Brune model. This may be due to source complexity.

The shapes of the source acceleration spectra at high frequencies (5<f<20 Hz) are generally flat, with little evidence of kappa or f_{max} effects within this frequency band. In this respect, the hard-rock sites of the WCTN appear to be similar to the hard-rock sites of the ECTN. They do not exhibit the high-frequency decay observed for soil or soft-rock sites in California.

TABLE 1 - Source Parameters of Study Earthquakes

Event	Location (lat.,lon.)		GSC M		depth (km)	Moment M	f_o (Hz)	stress drop (bars)
A840316.A	48.5	-121.7	3.5	MC	2	3.0	4.2	5
A901207.A	49.7	-123.6	3.0	ML	4	3.0	4.6	7
A820513.A	48.7	-123.6	3.0	ML	19	3.1	8.3	55
A870916.A	49.1	-122.7	3.2	ML	4	3.1	4.9	11
A910703.A	49.3	-122.5	3.1	ML	5	3.1	6.4	21
A920517.A	49.8	-124.6	3.0	ML	0	3.1	6.5	21
A880926.A	48.5	-122.6	3.0	ML	11	3.2	4.1	8
A811126.A	47.7	-122.6	3.5	MC	22	3.3	3.0	4

TABLE 1 - cont

A820130.A	48.8	-122.7	3.2	ML	24	3.3	5.9	31
A810822.A	48.6	-126.0	3.0	ML	37	3.3	4.9	17
A890606.A	51.0	-124.5	3.5	ML	5	3.3	4.4	15
A910915.A	48.6	-123.0	3.1	ML	20	3.3	5.0	21
A850228.A	47.5	-122.6	3.5	MC	46	3.3	4.5	17
A830205.A	48.7	-125.4	3.6	ML	37	3.4	4.3	20
A890206.A	48.4	-122.2	3.5	MC	0	3.4	2.5	3
A860302.A	48.7	-124.9	3.0	ML	38	3.5	2.7	6
A800921.A	47.2	-121.9	3.5	MC	6	3.5	4.4	23
A860608.A	49.0	-125.3	3.2	ML	32	3.5	2.6	6
A860906.A	48.7	-125.3	3.5	ML	33	3.6	3.5	18
A890214.A	48.4	-122.2	3.6	ML	1	3.6	2.7	8
A880311.A	47.2	-122.3	3.9	MC	65	3.6	3.7	29
A860210.A	48.4	-122.0	3.7	ML	1	3.6	2.9	12
A870408.A	49.7	-123.6	3.9	ML	3	3.6	4.2	40
A880429.A	50.0	-128.0	3.5	ML	36	3.6	2.5	7
A920313.A	48.3	-122.9	3.5	ML	23	3.6	4.1	30
A881122.A	47.7	-125.5	3.5	ML	60	3.6	3.3	16
A890924.A	50.9	-125.5	3.8	ML	5	3.7	4.4	49
A910219.A	49.7	-122.7	3.9	ML	5	3.7	4.5	65
A830828.A	47.9	-122.9	4.1	MC	51	3.7	4.5	57
A900403.A	48.8	-122.2	3.8	ML	2	3.7	2.0	4
A831031.A	47.3	-123.2	3.7	ML	45	3.7	5.4	107
A891024.A	48.9	-125.2	3.9	ML	37	3.8	3.0	26
A881001.A	50.2	-128.0	3.9	ML	34	3.8	1.9	7
A821002.A	49.6	-127.2	4.2	MB	20	3.8	2.1	8
A811112.A	47.9	-122.4	3.7	MC	26	3.8	3.6	47
A890306.A	48.4	-122.2	4.0	ML	2	3.8	2.4	14
A900414.B	48.8	-122.2	4.0	ML	4	3.8	2.3	11
A800608.A	48.0	-123.1	3.8	ML	52	3.9	2.4	21
A870607.A	49.8	-127.0	3.8	ML	31	3.9	2.3	19
A890618.A	47.4	-122.8	4.1	ML	45	4.1	3.1	75
A900402.A	48.8	-122.2	4.4	ML	1	4.1	1.7	13
A890912.A	49.8	-126.9	4.4	ML	34	4.2	2.0	32
A891224.A	46.7	-122.1	4.4	ML	18	4.2	2.3	50
A820722.A	49.6	-127.9	4.7	MB		4.2	1.3	9
A871207.A	49.3	-127.8	4.7	MB		4.3	0.7	6
A890305.A	47.8	-123.4	4.6	MB	46	4.3	2.0	45
A851027.A	49.3	-127.9	4.7	MB		4.4	1.0	14
A930803.B	51.2	-130.8	4.0	MB		4.5	1.6	39
A900414.A	48.8	-122.2	4.9	ML	2	4.6	1.2	25
A940212.A	49.0	-129.6	5.2	MB		4.7	0.8	11
A930803.C	51.3	-130.3	5.1	MB		4.8	1.0	46
A810214.A	46.4	-122.2	5.1	MB	7	4.8	1.6	111
A900216.A	49.2	-127.6	5.2	MB		4.8	0.6	18
A860616.A	49.4	-127.0	5.2	ML	35	5.1	1.3	100
A940103.A	49.6	-127.0	5.5	ML	28	5.3	1.1	46
A930803.A	51.2	-130.8	6.0	MS		6.0		48
A920406.A	50.7	-130.1	6.8	MS	20	7.0		7

Notes: GSC M is catalogue magnitude. f_o is corner frequency.

EARTHQUAKE INTENSITY MAPS FOR THE MARCH 25, 1993, SCOTTS MILLS, OREGON EARTHQUAKE

Award Number 1434-94-G-2481

Gerald L. Black
Oregon Department of Geology and Mineral Industries
800 NE Oregon Street #28, Suite 965
Portland, Oregon 97232

Investigations

The magnitude 5.6 March 25, 1993 Scotts Mills earthquake was the largest recorded event in northwest Oregon. It was felt over an area extending from Roseburg, Oregon on the south to Seattle, Washington on the north and the Oregon coast on the west to Bend, Oregon on the east.

This study will produce:

1. A digital isointensity map of the felt area at a scale of 1:500,000.

2. A digital isointensity map of the Portland, Or-Vancouver, Wa metropolitan area at a scale of 1:100,000.

3. A digital database of the intensity data.

4. A non-technical report describing the maps and conclusions to be published in Oregon Geology.

Progress

Immediately after the earthquake a questionnaire was published in newspapers throughout the felt area. Over 4,500 responses are on hand at the Oregon Department of Geology Offices (Nearly 3,300 received directly at our offices, 510 responses collected by Dr. Anthony Qamar at the University of Washington., and an additional 700 damage reports from the Oregon Emergency Management Division.).

To date, location information (i.e. street addresses) has been entered into Microsoft Excel spreadsheets for all 4,500 responses. Intensities have been assigned to over 3,500 responses using the Modified Mercalli scale. Software suitable for producing the final digital maps has been purchased and is being used to geocode the location information.

Ground Motion Prediction

9930-10303

David M. Boore

Branch of Seismology
U.S. Geological Survey
345 Middlefield Road, MS 977
Menlo Park, California 94025
(415) 329-5640
FAX (415) 329-5163
Email Address: boore@samoa.wr.usgs.gov
Program Element: III

Investigations

This project uses ground-motion recordings in the development of methods for estimating ground motion in future earthquakes with application to probabilistic seismic hazard maps, building codes, and the design of critical facilities such as dams and nuclear power facilities.

Results

We carried out a number of follow-up studies related to our new equations (Boore *et al.*, 1993) for estimating earthquake ground motion. By examining residuals at sites where downhole shear-velocity measurements were available, we developed an alternative expression for the site effect as a simple function of average shear-wave velocity. The coefficients in that expression were very similar to those found by S. Midorikawa (written communication, 1993) from an analysis of Japanese strong-motion data, as shown in Figure 1. Our analysis of the data included a study of how ground-motion variability depends on magnitude and ground-motion amplitude. We demonstrated that there is no statistically significant difference in the magnitude scaling of ground motion at short and long distances, and we showed that ground motion in reverse slip earthquakes is higher by a small amount on the average than in strike-slip earthquakes.

Reports

Atkinson, G. M. and D. M. Boore (1994). Ground motion relations for eastern North America, submitted to *Bull. Seism. Soc. Am.*

Atkinson, G. M. and D. M. Boore (1994). Empirically-based stochastic ground motion predictions for eastern North America, submitted to *Earthquake Spectra.*

Boore, D. M. and W. B. Joyner (1994). Prediction of ground motion in North America, Proceedings of Seminar on New Developments in Earthquake Ground Motion Estimation and Implications for Engineering Design Practice, ATC 35-1, Applied Technology Council, p. 6-1–6-41.

Boore, D. M., W. B. Joyner, and T. E. Fumal (1993). Estimation of response spectra

and peak accelerations from western North American earthquakes: an interim report, U.S. Geological Survey Open-File Report 93-509, 72 p.

Boore, D. M., W. B. Joyner, and T. E. Fumal (1994). Estimation of response spectra and peak accelerations from western North American earthquakes: an interim report, Part 2, U.S. Geological Survey Open-File Report 94-127, 40 p.

Gibbs, J. F., D. M. Boore, W. B. Joyner, and T. E. Fumal (1994). The attenuation of seismic shear waves in Quaternary alluvium in Santa Clara Valley, California, *Bull. Seism. Soc. Am.*, **84**, 76–90.

Joyner, W. B. and P. Spudich (1994). Including near-field terms in the isochrone integration method for application to finite-fault or Kirchoff boundary integral problems, *Bull. Seism. Soc. Am.* **84**, 1260–1265.

Figure 1. The coefficient that controls the shear-velocity dependence of response spectral amplification, as determined by Boore et al. (1994) from primarily California data and by S. Midorikawa from Japanese data. Also shown are the coefficients proposed by Borcherdt for determining short-period and mid-period amplification factors in building codes; they were determined from Fourier amplitude spectra of recordings from the Loma Prieta earthquake.

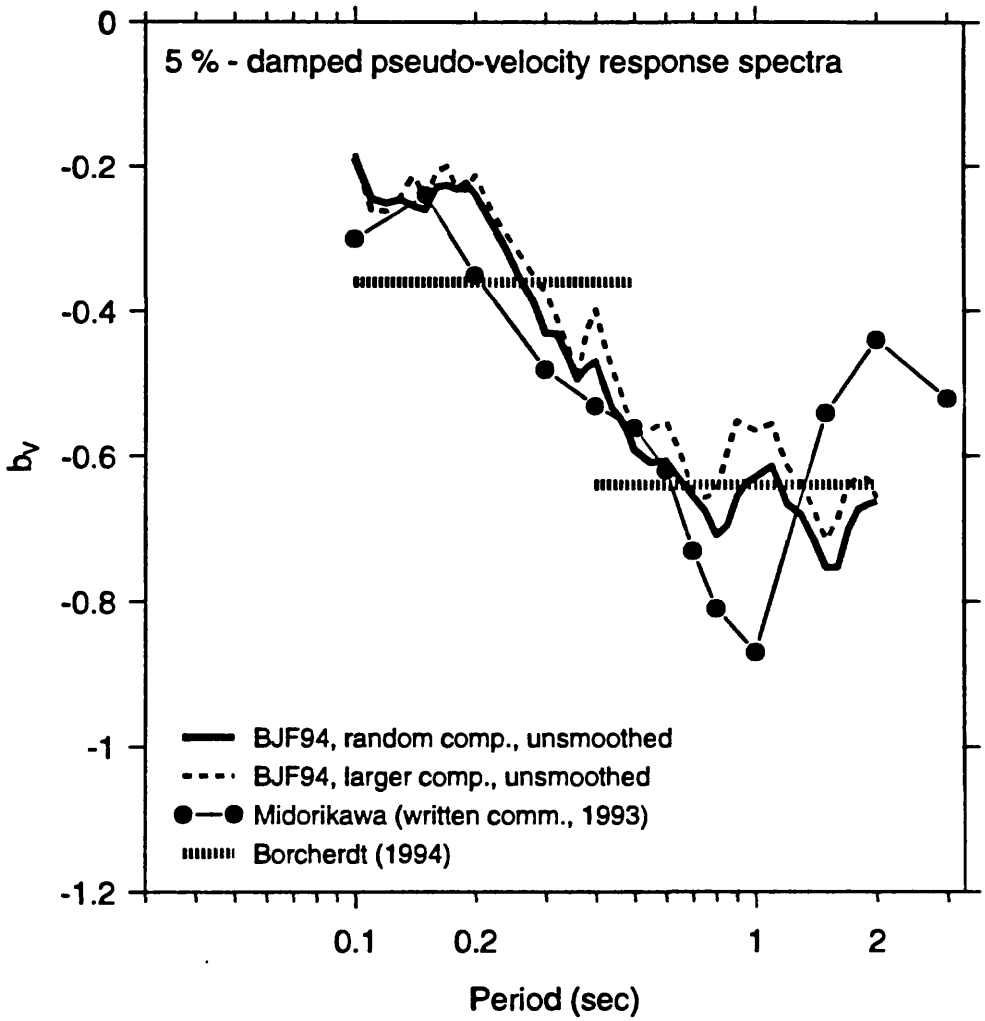

Seismic Response of the Deep Stiff Clay Deposits in the Oakland Area

1434-94-G-2416

Jonathan D. Bray, PI
Susan W. Chang, Graduate Student Researcher
Department of Civil Engineering
University of California, Berkeley
Berkeley, CA 94720
510-642-9843
FAX 510-642-7476
bray@ce.berkeley.edu

INVESTIGATIONS

Damage patterns from the 1989 Loma Prieta Earthquake demonstrated that the seismic response of deep stiff clay deposits can be significant (Sun et al., 1991). At deep stiff clay sites in the Oakland area, peak ground accelerations were amplified by a factor of two to four, and spectral accelerations at some frequencies were amplified by a factor of four to eight (Figure 1). This research program will evaluate the seismic response of deep stiff clay sites in the Oakland area, validate existing analytical procedures with respect to such deposits, and assess the seismic hazards resulting from future earthquake shaking in the heavily populated Oakland area. This project is a continuation of work performed for USGS Project Number 1434-92-G-2177, "Characteristics and Seismic Response of the Deep Old Bay Clay Deposits in the East San Francisco Bay Area."

RESULTS

Preliminary Site Response Analyses

Since the initiation date of this project, preliminary one-dimensional seismic wave propagation analyses using the program SHAKE91 (Idriss and Sun, 1992) have been performed for three of the deep stiff clay sites in the Oakland area. Characterization of these sites was based on the field and laboratory work performed for the previous study (Guha et al., 1993), as well as on the field work conducted by the U.S. Geological Survey. Generalized soil profiles and shear wave velocities at the three sites used in our analyses are shown in Figure 2.

The results of the preliminary one-dimensional seismic wave propagation analyses further suggest that deep stiff clay deposits can produce significant amplification of peak ground acceleration and longer period motions. As shown in Figure 3, the 1-D seismic response analysis for the Oakland Outer Harbor site was able to capture the tendency of this deep stiff clay site to amplify motions. The response spectrum computed by SHAKE91 also fits the general trends of the response spectrum of the recorded horizontal motion, except at frequencies near 1 Hz. It is not know if these discrepancies are due to the characteristics of the input rock motion, the dynamic soil properties chosen for the analyses, three dimensional effects, limitations of equivalent-linear

analyses, or the presence of surface waves.

Further Work

Further work for this research program will include:

- additional one-dimensional site response analyses incorporating the material specific dynamic properties for the Old Bay Clay deposits determined in the previous study (Guha et al., 1993) and refinements to the input motions,
- site response analyses using one-dimensional fully nonlinear codes, and
- site response analyses to estimate the influence of the irregular bedrock topography on the recorded motions.

The analytical models developed from the above work will be employed to develop an overall assessment of the expected behavior of deep Old Bay Clay sites during future design earthquake events.

REFERENCES

Guha, S., Bray, J.D., and Drnevich, V.P. (1993) "Characteristics of the Deep Old Bay Clay Deposits in the East San Francisco Bay Area," Geotechnical Engineering Report No. UCB/GT/93-09, University of California, Berkeley

Idriss, I.M. and Sun, J.I. (1992) "SHAKE91, A Computer Program for Conducting Equivalent Linear Seismic Response Analyses of Horizontally Layered Soil Deposits, Program Modified based on the Original SHAKE program published in December 1972 by Schnabel, Lysmer, and Seed," University of California, Davis

Sun, J.I., Chang, S.W., Bray, J.D., and Mejia, L.H. (1993) "Damage Patterns/Response of Deep Stiff Clay in Oakland," Proceedings from the Third International Conference on Case Histories in Geotechnical Engineering, June 1-4, Volume III, pp. 1611-1616

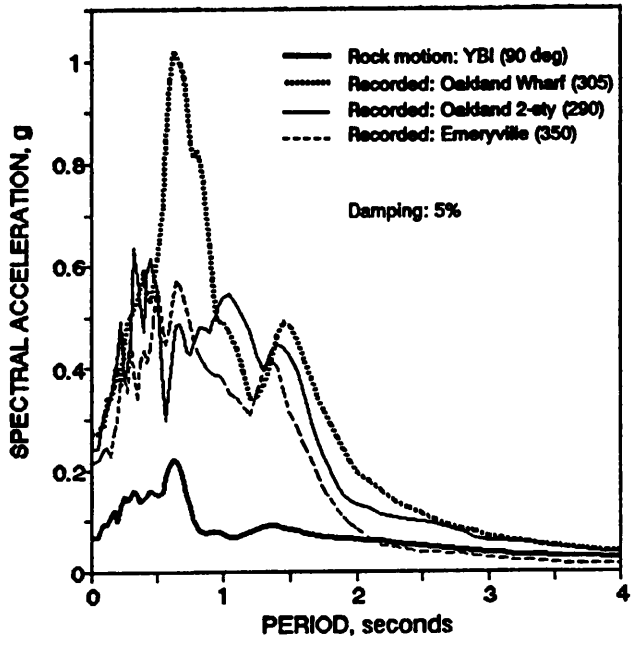

Figure 1: Response spectra for three deep soil sites in the Oakland area (Loma Prieta Earthquake)

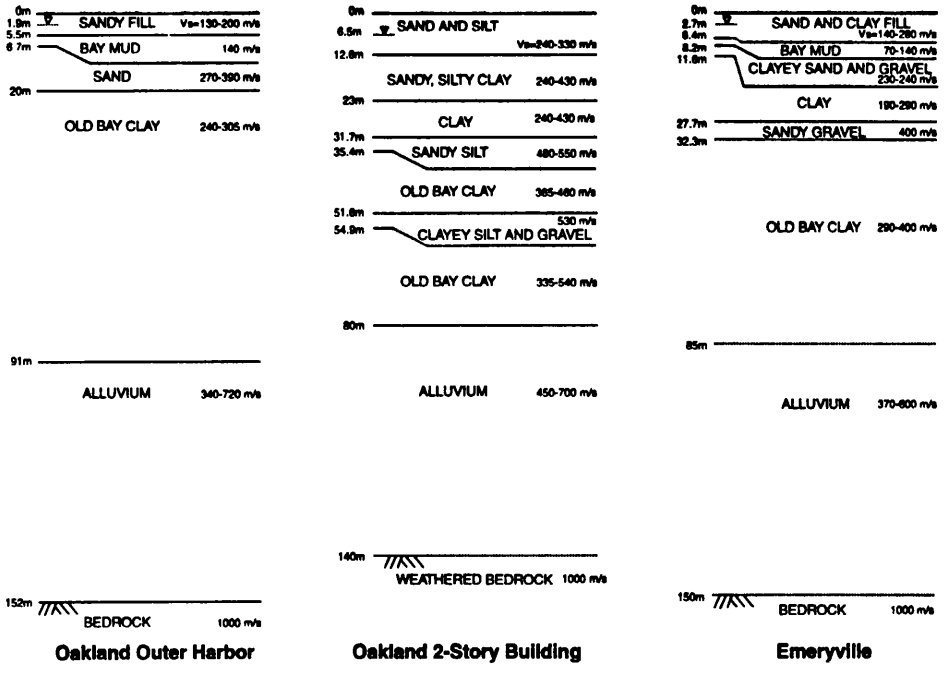

Figure 2: Generalized soil profiles used in dynamic response analyses

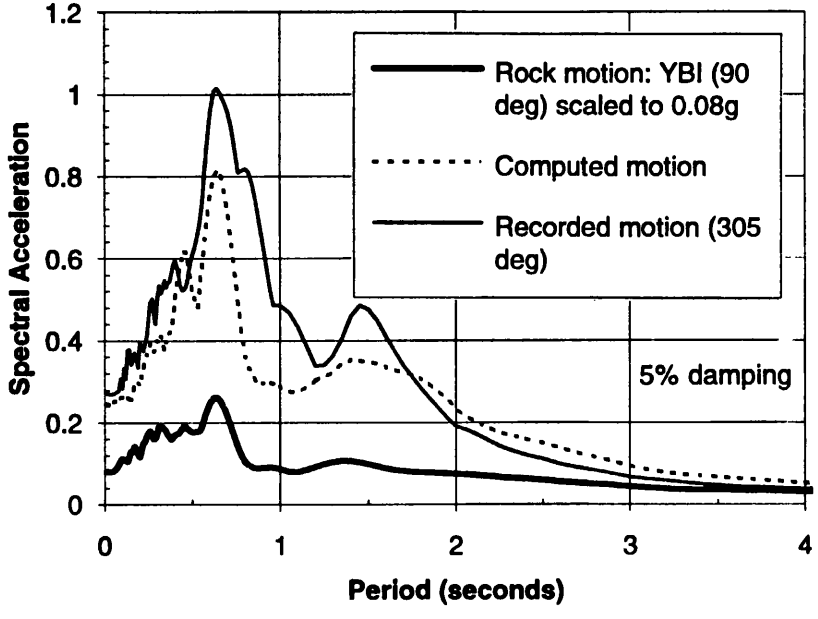

Figure 3: Response spectra from computed and recorded motions at the Oakland Outer Harbor

FAULT ZONE TECTONICS

9960-12086

Katherine S. Breckenridge
Branch of Earthquake Geology and Geophysics
U.S. Geological Survey
345 Middlefield Road, MS 977
Menlo Park, California 94025
(415) 329-4849
E-mail: kate@thepub.wr.usgs.gov

Investigations

[1] Develop new sites for creepmeter network along the Hayward fault in the eastern San Francisco Bay area.

[2] Maintain a network of creepmeters along the San Andreas and Calaveras faults in central California. Monitor data in near realtime to detect changes in fault slip that may be significant in the earthquake cycle. Participate in all Parkfield Prediction Experiment Working Group functions. Maintain long-term database of creepmeter measurements.

[3] Maintain the archive of raw data from Low Frequency instrumentation in California.

Results

[1] The project continues collaboration with Roger Bilham (CIRES) and Jim Lienkaemper (USGS) to develop sites for creepmeters along the Hayward fault in the San Francisco Bay Area. In FY 94 the project developed a new siting strategy for East Bay creepmeters. Initial network plans were based on roughly 10 KM spacing for 7 instruments between San Pablo in the north and Fremont at the southern end of the fault. Since much of the Hayward fault slips at a relatively uniform rate of ~5 mm/year, we have chosen to forego equidistant spacing and instead pursue monitoring near fault-crossing lifelines. In addition to characterizing the rate and nature of slip our goal is to determine how ongoing creep impacts fault-crossing utility lines. Co-locating creepmeters with high priority lines will provide site response information that will be useful to utility companies and emergency officials for developing response plans immediately after moderate and large earthquakes. With satellite telemetry delivering data every 10 minutes we can quickly determine which areas are most affected by surface fault slip. Triggered slip from such an event may continue for months to a few years afterward and creepmeter records will provide an ongoing measure of fault activity for use in long-term maintenance schedules. Although the impact of fault creep as strain on a pipeline is not well understood, continuous monitoring of the fault near a lifeline will allow us to build a set of observations which can be used in testing theories of strain transfer and seismic mitigation. As part of this new focus for monitoring fault creep in the Bay Area, we are interested in providing data to utility companies and emergency planners on an annual basis and ASAP after significant earthquakes.

To activate this change in network design the project has been gathering data on locations of significant fault-crossing lifelines in the East Bay. We are working with Pacific Gas and Electric, Pacific Bell, East Bay Municipal Utility District, San Francisco Water District, and the State of California Division of Water Resources to determine where high priority locations and to assess the suitability of those areas for creepmeter monitoring. Two creepmeters

have been installed in the past year, in Fremont and in the City of Hayward, using a new system of piers based on a vertical steel rod anchored with a tie-back rod. Rods are driven to refusal with as much as 50,000 pounds pressure. At both sites, rods are between 35 and 50 feet deep. Prior generations of USGS creepmeters are based on concrete-reinforced steel piers extending about 3 feet. Initial data show no apparent signal related to pier wobble during precipitation, which is a major factor for creepmeters in Parkfield and Hollister. Thus far 2 episodic creep events of about 1.0 to 1.5 mm have occurred at the Fremont site since July. No episodic creep has been seen from the Hayward site, which is an upgrade of the old Palisade St. creepmeter installed by Bob Nason in 1970. Episodic events are absent from the prior record at that site.

[2] Creepmeters were operational throughout the year, although routine maintenance trips were cut back from 4 to 3 per year in an attempt to economize on field expenses. A major focus of the project this year has been to establish an online tabulation of manual measurements from field sheets for each creepmeter on the satellite telemetry system. These records facilitate comparison between periodic manual readings of micrometers or dial gages and the telemetered datastream, and serve as a basis for corrections applied to the data. For the Parkfield network, 11 of 12 instruments have complete online records for all site visits since 1984, when satellite telemetry was established. Retrospective cleaning has been completed for 9 instruments to verify processing applied by various members of the project over the past 10 years, and to create a file of clean, 10-minute sampled data to complement the daily-sampled dataset produced by the project for long-term rate analysis. Discrepancies and judgement calls are annotated in the field-visit file to serve as a complete log of how data have been processed. For the Hollister network 3 years of field-visit data have been entered. Retrospective analysis and cleaning will commence when the Parkfield data are complete.

Parkfield: Figure 1 shows residual creep for the instruments in the Parkfield network from 1975 to the end of November 1994, with the Coalinga earthquake represented as a vertical bar. An average annual rate, determined by a least squares fit from the beginning of the record, has been extracted from the data. Aside from the strong left-lateral movement seen at X461 in response to slope instability, there have been no unusual signals in the network over the past year.

Hollister: Figure 2 shows residual creep from the Hollister area network with the Loma Prieta earthquake (LPEQ) marked by a vertical bar. Afterslip effects from the quake, obvious at XHR2 and CWC3 though muted at XSJ2, terminated as late as mid-1993. An increase in background slip rate at XSJ2 occurred as a result of a slow earthquake near San Juan Bautista in December 1992. Although an episodic creep event occurred during the sequence, it was characteristic of strain-creep events catalogued by Gladwin and others (JGR, 1994), and we do not associate it with the swarm. However, characteristic strain-creep events at XSJ have not previously included subsequent background rate increases. The 8 month episode from December 1992 to August 1993 more than doubled the rate of creep seen in the preceding year, which we interpret as the creep response to the slow earthquake.

Residual slip data from the Calaveras Fault are shown on the right side of figure 2. Analysis during the past year focused on the strong seasonal transients recorded on XSH1 since the instrument was rebuilt in May 1986, replacing SHR1 which broke during the Tres Pinos earthquake in January 1996. Both the telemetered data (XSH1) and the periodic manual readings (XSH1MIC) are plotted, in addition to dial readings from SHR2 - the original contraction rod adjacent to XSH1. Long-term data for SHR2 are not included, due to the instrument losing zero on 2 occasions in the prior record. However there was good correspondence between slip seen on extension-meter SHR1 and on contraction-meter SHR2 from 1970 to 1984. Data from SHR2 since 1985 have been stable and serve as an additional reference to slip activity at the site. In particular, the strong right-lateral transients seen on XSH1 during the rainy season are absent from SHR2. Indeed most of the signal on XSH1 may be the response of piers to soil moisture conditions. An episodic creep event recorded on XSH1 in August 1993 is also evident on SHR2, although a second event in December 1993 was not

seen by the contraction-meter. Clarifying the operational status of XSH1 is an important part of determining the Loma Prieta slip response on the Calaveras fault. As evident from HLC1 and HLD1, the fault in the town of Hollister is still dormant while north of town the fault may be in a gradual transition from essentially no movement to right-lateral slip.

[3] The collection of raw telemetered data from the Low Frequency Data network is updated and backed-up annually, and is current to April 1994 for the 488 sensors monitoring crustal deformation in California. This archive is the repository for all original telemetry data. Principal Investigators for each of the instrument networks keep separate collections of processed and reduced data for their own research, retrieving data from the Low Frequency Data Archive as necessary for retrospective analyses and to fulfill data requests.

In FY94 a 4 Gigabyte disk drive was purchased to facilitate development of a centralized Parkfield archive. At present, data collected within the USGS as part of the Parkfield Earthquake Prediction Experiment are distributed among several computer systems for processing and analysis. The goal of the Parkfield data disk is to co-locate data from the different instrument networks to facilitate rapid analysis during alert sequences, to make data more widely available to members of the Parkfield Working Group, and to incorporate data collected by scientists in the External Program. Archive development is proceeding slowly due to time constraints imposed by the East Bay creepmeter network expansion.

Reports Published

Gladwin, M.T., Breckenridge, K.S., Gwyther, R.L., and R.H.G. Hart, 1994, Measurements of the strain field associated with episodic creep events on the San Andreas fault at San Juan Bautista, California, *Journal of Geophysical Research* v. 99, no. B3, pp. 4559-4565.

Parkfield Creep: Residuals (in Millimeters)

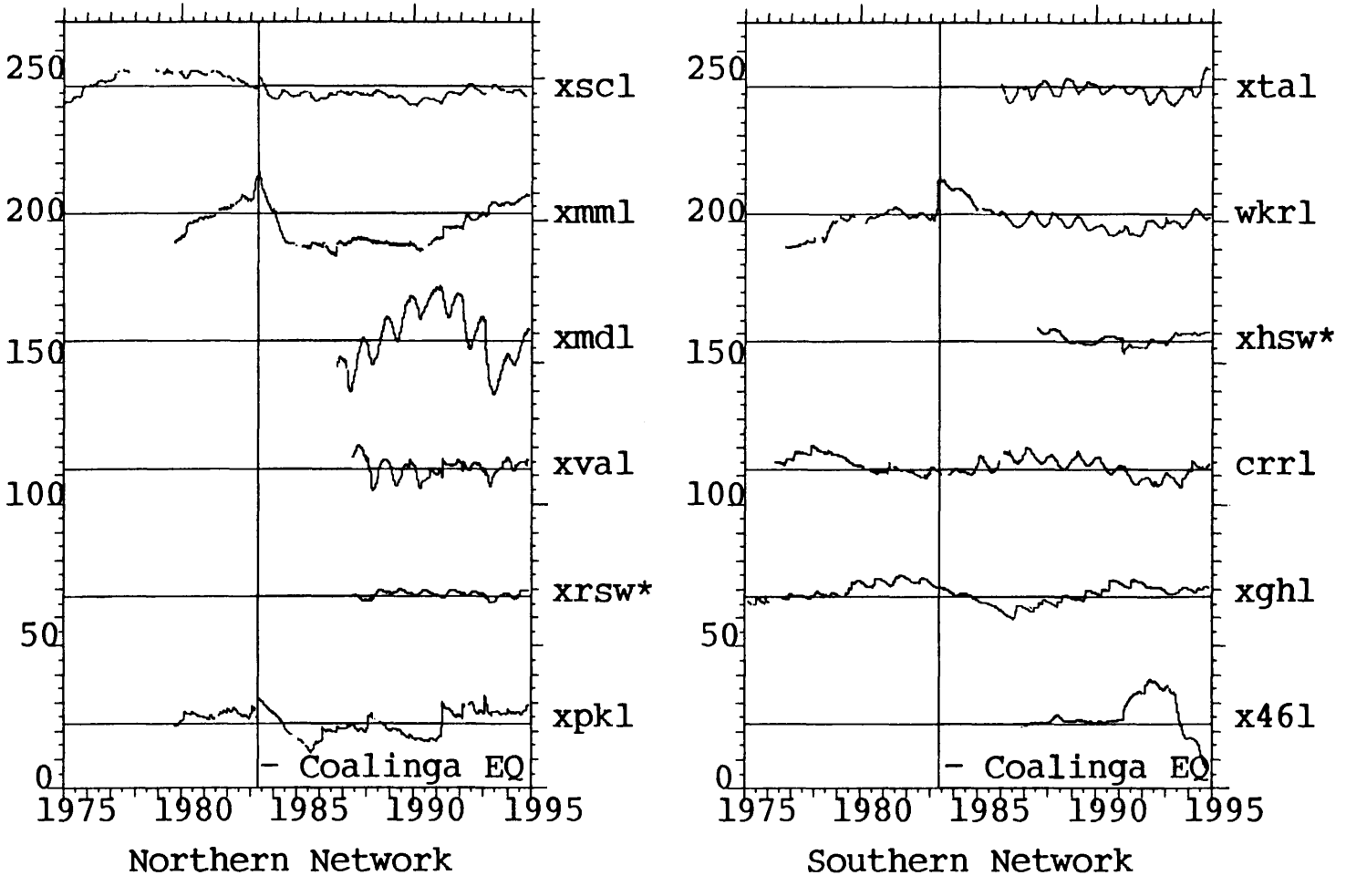

Figure 1

*Southwest Trace

Hollister Creep: Residuals (in Millimeters)

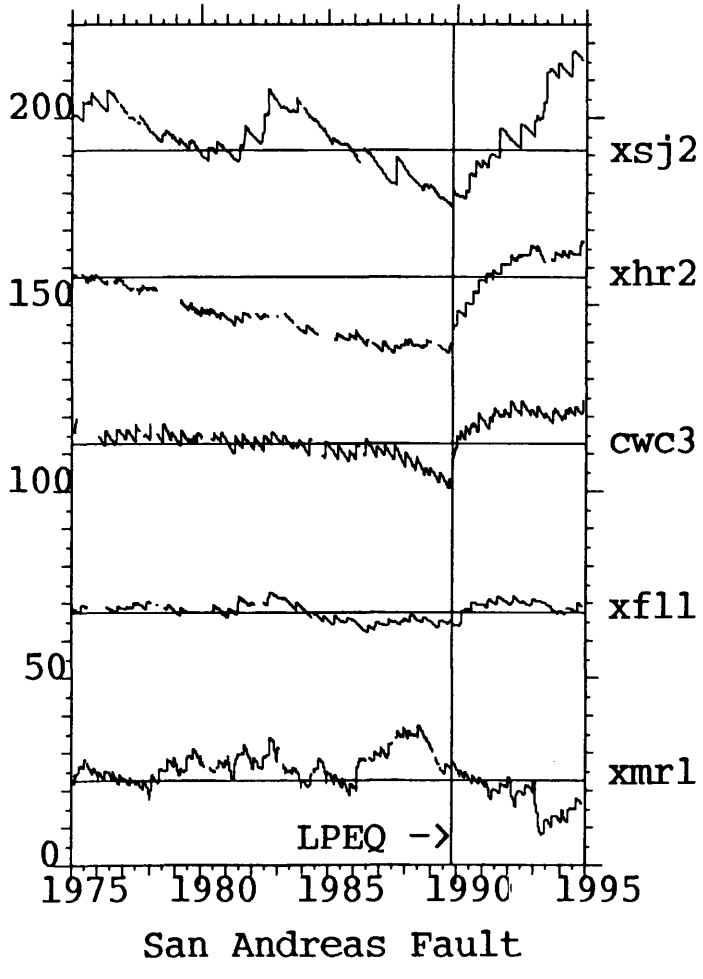

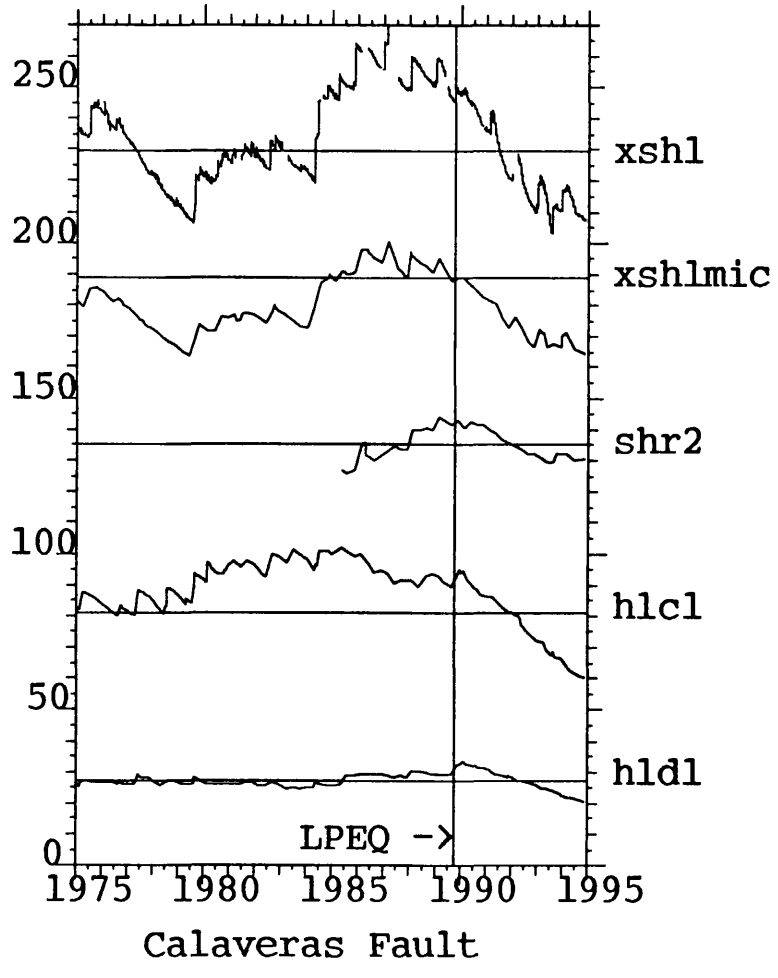

Figure 2

INSTRUMENTATION AND TESTING OF STRUCTURES

9920-10302

MEHMET ÇELEBI

BRANCH OF EARTHQUAKE AND GEOMAGNETIC INFORMATION
U.S. GEOLOGICAL SURVEY
345 MIDDLEFIELD ROAD, MS 977
MENLO PARK, CALIFORNIA 94025
415-329-5623
[e-mail: celebi@samoa.wr.usgs.gov]
[Element III]

Investigations

1. Plans are being carried out to deploy a special purpose strong-motion array to study soil-structure interaction. Essential hardware have been partially purchased with appropriated funds. This particular project will continue into FY95 and FY96. The recommendations developed during a workshop held in 1992 are being followed.

2. The process of selection of structures recommended for strong-motion instrumentation has continued in Memphis (Tennessee), Reno (Neveda), Hawaii and Puerto Rico.

3. Cooperative instrumentation of building in Olympia, Washington and instrumentation of building in Seattle are completed.

4. Cooperative instrumentation plans of the U.S. Court of Appeals Court Building in San Francisco is underway. This building is being seismically upgraded by base-isolation.

5. The majority of the accelerographs planned for the free-field strong-motion network have been deployed in Puerto Rico in cooperation with the University of Puerto Rico (Mayaguez).

6. Efforts have been made to instrument a building in Puerto Rico in cooperation with University of Puerto Rico (Mayaguez) and NIST. The building will be instrumented for both earthquake and hurricane hazard. The instrumentation scheme in another building is being upgraded.

7. Studies of records obtained from instrumented structures during the 1987 Whittier, 1989 Loma Prieta and the 1994 Northridge earthquakes have continued. Journal and conference papers have been prepared. Cooperative project with NIST on low-level amplitude tests of instrumented structures has been completed. Journal and conference papers have been prepared.

8. Plans are being made to convert the wind-monitoring system at Theme Buildings in Los Angeles into strong-motion monitoring system.

Results

1. Papers resulting from study of records obtained from structures are prepared, published in refereed journals and presented in conferences.

2. Invited talks given at conferences, workshops and as outreach.

3. As funds are available, instrumentation efforts continue. Special purpose array for soil-structure interaction studies is in process being realized. Network in Puerto Rico is in operation. Data are being retrieved from instrumented structures during earthquakes.

Reports Published

Çelebi, M., Lysmer, J., and Luco, E., (compilers), 1992, Recommendations for a Soil-Structure Interaction Experiment, (Report based on a workshop held at San Francisco, Ca on February 7, 1992), USGS OFR: 92--295, April 1992.

Çelebi, M., Filimonov, M., and Gorshkov, A., 1993, Application of Pattern Recognition Method (PRM) to Estimate Ground Motions in San Francisco Peninsula, California, USGS OFR 93-398.

Çelebi, M., 1993, [Authored Chapter 3: Strong Motion, Chapter 4: Earthquake Code for Design and Construction, Chapter 6: Industrial Facilities, Chapter 9: Reconstruction, and Contributed to Chapter 1: Introduction and Chapter 5: Buildings], in *Erzincan, Turkey Earthquake of March 13, 1992: Reconnaissance Report*, **Earthquake Spectra**, Supplement to Volume 9, Publication 93-01.

Çelebi, M., 1993, Recovery: The Reconstruction of Erzincan, Turkey, EERI Special Earthquake Report, EERI Newsletter, April 1993.

Çelebi, M., and Brown, R., 1993, Building Damage from the March 13, 1992, Earthquake near Erzincan, Turkey, **Earthquakes and Volcanoes, v. 23, no. 4, 1992.**

Çelebi, M., 1993, Seismic response of two adjacent buildings with downhole and free-field recordings (Part I: Data and Analysis), *Journal of Structural Division*, American Society of Civil Engineers, v. 119, no. 8, pp.2461-2476, August 1993.

Çelebi, M., 1993, Seismic response of two adjacent buildings with downhole and free-field recordings (Part II: Interaction), *Journal of Structural Division*, American Society of Civil Engineers, v. 119, no. 8, pp. 2477-2492, August 1993.

Çelebi, M., 1993, Loma Prieta Response of an eccentrically braced tall building, *ASCE Structures Congress* , Irvine, Calif., April 1993.

Çelebi, M., Phan, L., and Marshall, R., 1993, Dynamic characteristics of five tall buildings during strong and low-level amplitude motions, *International Journal of Design of Tall*

Buildings, John Wiley and Sons, Ltd, March 1993.

Çelebi, M., 1993, Seismic Response of an eccentrically braced tall building, *Journal of Structural Division*, American Society of Civil Engineers, v. 119, no. 4, pp. 1188-1205, **April 1993.**

Çelebi, M., 1993, Site Response Effects Observed During the 1989 Loma Prieta, California and 1992 Erzincan, Turkey earthquakes and Code Implications, **(invited paper)**, 2nd National Conference on Earthquake Engineering, 1-13 March 1993, Istanbul, Turkey.

Çelebi, M., 1993, Reconstruction of Erzincan, Turkey following the 13 March 1993 earthquake, PROC., 25th UJNR Panel on Wind and Seismic Effects, Tsukuba, Japan, May 1993.

Marshall, R. D., Phan, L. T., and Çelebi, M., 1994, Full-Scale Measurement of Building Response to Ambient Vibration and the Loma Prieta Earthquake, Vth U.S. National Conference on earthquake Engineering, July 10-14, 1994, Chicago, Ill.

Phan, L. t., Hendrikson, E. M., Marshall, R. D., and Çelebi, M., 1994, Analytical Modeling for Soil-Structure Interaction of a 6-story Commercial Office Building, Vth U.S. National Conference on earthquake Engineering, July 10-14, 1994, Chicago, Ill.

Çelebi, M., 1994, Identification of site frequencies from building records, (in review), ASCE.

Çelebi, M., 1994, Response Study of a Flexible Building Using Three Earthquake Records, ASCE Structures Congress, Atlanta, Georgia, April 24-28, 1994.

Çelebi,M., 1994, Response Study of a 13-Story Building, Vth U.S. National Conference on earthquake Engineering, July 10-14, 1994, Chicago, Ill.

Çelebi, M., 1994, Free-field motions near buildings, PROC., 10th ECEE, Vienna, Austria, Aug. 1994.

Çelebi, M., 1994, Northridge (California) earthquake: Unique Ground Motions, IIIrd. Int'l Conf. on Recent Advances in Geotechnical Earthquake Engineering and Soil Dynamics, to be held in San Louis, Mo., April 1995.

Çelebi, M., and Luco, E., 1994, Recommendations for a soil-structure interaction experiment, IIIrd. Int'l Conf. on Recent Advances in Geotechnical Earthquake Engineering and Soil Dynamics, to be held in San Louis, Mo., April 1995.

Natural Frequencies of Highway Bridges in the New Madrid Region

1434-94-G-2491

Ralph Alan Dusseau, Ph.D., P.E.
Associate Professor
Wayne State University
Department of Civil and Environmental Engineering
Detroit, Michigan 48202
TEL: (313) 577-3842
FAX: (313) 577-3881

Project Objectives

The three principal objectives of this USGS-NEHRP project were as follows:

1. To develop a comprehensive computer database (the I-55 Bridge Database) containing geometric, geographic, and historic data for all 211 highway bridges along interstate highways I-55, I-57, and I-155 in southeastern Missouri. This includes all interstate highway bridges in southeastern Missouri from St. Louis, Missouri south through New Madrid, Missouri to the Missouri-Arkansas State Line near Blytheville, Arkansas.

2. To perform field ambient vibration measurements and laboratory data analyses on 20 to 25 typical highway bridge spans along I-55, I-57, and I-155 in southeastern Missouri in order to derive the fundamental natural frequencies of these spans.

3. To extrapolate the fundamental natural frequencies derived for 20 to 25 typical highway bridge spans to all of the highway bridge spans in the I-55 Bridge Database.

Bridge Spans Analyzed

The highway bridge spans that were analyzed were chosen to reflect, as closely as possible, the actual distribution of highway bridge span type and length for the 211 highway bridges along I-55, I-57, and I-155 in southeastern Missouri. In all, 25 typical spans from 12 different highway bridges were measured and analyzed. These 25 spans include 17 steel girder spans, six reinforced concrete slab spans, and two reinforced concrete box-girder spans. Table 1 lists the Missouri bridge number, the overall bridge length, the deck width, the maximum support height, the span number, the span length, and the span depth for each of these 25 typical highway bridge spans.

All 12 of the highway bridges that were measured were undercrossings, i.e. bridges that the main highway (I-55, I-57, or I-155) crosses under. The traffic along I-55, I-57, and I-155 was deemed to be too heavy to permit safe measurements on highway overcrossings, i.e. on bridges that the main highway crosses over. Only undercrossings with wide sidewalks or shoulders were

chosen for field ambient vibration measurement to facilitate safe access to each bridge without disruption of vehicular traffic.

Field Measurements and Laboratory Data Analyses

For each highway bridge span that was analyzed, field ambient vibration measurements were taken using eight seismometers. The signal output from each of these eight seismometers was amplified and then recorded on an FM tape recorder. For safety reasons, all eight seismometers were placed on only one of the bridge sidewalks or shoulders to avoid having the seismometer cables stretched across the roadway.

Laboratory analyses were conducted on each of the signal records that were taken in the field. In these analyses, the signal output that was recorded for each seismometer was played back through a spectrum analyzer and a fast Fourier transformation (FFT) was performed. The final results were plots of signal amplitude versus frequency from which the fundamental natural frequencies of the bridge span at the given location and in the given direction were read directly. These analyses also included comparisons of phase and coherence between pairs of seismometer signals. These comparisons aid in estimating the mode shape associated with each of the fundamental natural frequencies.

Project Results

Utilizing the plots of signal amplitude versus frequency that were derived for each seismometer record, the corresponding fundamental lateral, longitudinal, and vertical natural frequencies were derived for each bridge span. These fundamental natural frequencies are listed in Table 2. As noted in Table 2, the fundamental lateral and longitudinal frequencies were found to be unique values for each bridge as a whole, while the fundamental vertical frequencies were found to be unique for each individual bridge span.

The plots of amplitude versus frequency, phase versus frequency, and coherence versus frequency will all be presented in the Final Project Report which will be submitted by July 1, 1995. These plots will be contained in the following two volumes: Volume 1 which will include the results for the 17 steel girder bridge spans, and Volume 2 which will include the results for the eight concrete spans (six concrete slab and two concrete box-girder). Also included with the Final Project Report will be the I-55 Bridge Database which will contain the estimated fundamental natural frequencies for each bridge span. These estimated fundamental natural frequencies will be derived using empirical formulas which are currently under development. The I-55 Bridge Database will be stored on 3.5-inch IBM-compatible disks which will be formatted for use with the dBASE-V software package. All of the project results will be available for dissemination after July 1, 1995.

TABLE 1. BRIDGE SPANS ANALYZED BY AMBIENT VIBRATION MEASUREMENT

BRIDGE TYPE	MISSOURI BRIDGE NUMBER	BRIDGE LENGTH, meters	DECK WIDTH, meters	SUPPORT HEIGHT, meters	SPAN NO.	SPAN LENGTH, meters	SPAN DEPTH, meters
Steel Girder	A-593	61.93	9.98	9.15	1	8.82	0.91
					2	20.96	0.91
	A-618	73.05	11.51	9.46	1	15.19	1.03
					2	21.33	1.03
	A-2265R	75.75	11.20	9.73	1	10.75	0.78
					2	26.51	1.24
	A-2455R	77.80	11.20	10.62	4	10.56	1.26
					3	26.20	1.26
	A-2471R	91.99	12.42	10.20	4	12.40	1.49
					1	18.04	1.49
	A-2492R	97.29	11.20	9.45	1	14.81	0.86
					2	33.83	1.74
	A-1781R	111.97	13.03	10.66	1	16.54	0.91
					2	36.85	1.52
	A-2406R	113.74	14.25	12.72	4	15.87	0.88
					1	17.40	0.95
					2	40.23	1.97
Reinforced Concrete Slab	A-831R	64.17	13.41	9.23	1	12.58	0.65
					2	19.51	0.65
	A-1146	65.38	16.31	7.80	1	12.57	0.60
					2	20.12	0.60
	A-879	71.48	10.97	8.13	1	15.62	0.59
					2	20.12	0.59
Reinforced Concrete Box-Girder	A-1173	67.97	7.54	8.72	1	13.87	1.22
					2	20.12	1.22

TABLE 2. BRIDGE FUNDAMENTAL NATURAL FREQUENCIES

BRIDGE TYPE	MISSOURI BRIDGE NUMBER	FUNDAMENTAL LATERAL FREQUENCY	FUNDAMENTAL LONGITUDINAL FREQUENCY	SPAN NO.	FUNDAMENTAL VERTICAL FREQUENCY
Steel Girder	A-593	4.60 cps	8.80 cps	1	19.05 cps
				2	9.50 cps
	A-618	3.90 cps	4.85 cps	1	10.00 cps
				2	4.85 cps
	A-2265R	3.85 cps	11.35 cps	1	17.85 cps
				2	3.15 cps
	A-2455R	3.30 cps	4.20 cps	4	18.25 cps
				3	3.65 cps
	A-2471R	2.75 cps	3.75 cps	4	14.25 cps
				1	9.75 cps
	A-2492R	2.50 cps	4.05 cps	1	14.20 cps
				2	2.70 cps
	A-1781R	2.10 cps	4.00 cps	1	11.15 cps
				2	2.60 cps
	A-2406R	2.35 cps	11.80 cps	4	13.35 cps
				1	11.80 cps
				2	2.35 cps
Reinforced Concrete Slab	A-831R	5.30 cps	10.20 cps	1	13.40 cps
				2	4.85 cps
	A-1146	5.30 cps	4.95 cps	1	12.90 cps
				2	5.00 cps
	A-879	4.40 cps	10.70 cps	1	6.00 cps
				2	4.25 cps
Reinforced Concrete Box-Girder	A-1173	3.60 cps	10.35 cps	1	14.70 cps
				2	6.55 cps

Analysis of Digital Waveforms in the Northeastern U.S. for Source Depth and Strong Ground Motion Information

Award Number 1434-93-G-2349

John E. Ebel
Weston Observatory
Department of Geology and Geophysics
Boston College
Weston, MA 02193
(617) 552-8300
Fax: (617) 552-8388
EBEL@BCVMS.BC.EDU

Program Element: III.2 Predict Strong Ground Shaking

Investigations

The purpose of this research is to analyze the waveforms of locally recorded earthquakes in the northeastern U.S. to better determine the source depth and the propagation of strong ground motions across the region. The investigation involves three tasks: (1) searching for free-surface reflections in the local waveforms to help constrain the earthquake focal depths, (2) studying the amplitudes of P and S phases at about 100 km distance from the sources to see if any amplification due to post-critical Moho reflections may be present, and (3) studying the distance attenuation of the spectral components of the ground motions in the region with application to spectral seismic hazard maps. This research uses data from the New England Seismic Network operated by Weston Observatory of Boston College.

Data Analysis

The primary effort during the last year has been on research Tasks (2) and (3). Under Task (2) the waveforms recorded by the regional New England Seismic Network of Weston Observatory of five earthquakes from New England and vicinity were studied in detail. For each event, synthetic seismograms computed using the wavenumber-integration method were compared to observations of the events for epicentral distances ranging from about 100 km to 300 km. Indications of the focal depth of each event were sought in comparisons between the synthetics and the data. Under Task (3) regional network seismograms of ten earthquakes from

New England and vicinity were process to extract spectral ground acceleration information. As the events analyzed here were all small earthquakes (magnitudes ranging from m_{bLg} 2.7 to 4.5), the ground accelerations are low amplitude and spectrally limited. Nevertheless, they do contain information that can be compared to proposed strong ground motion distance-attenuation functions for the region.

Preliminary Results

The results of the event depth analysis (Task (2)) are encouraging although not definitive. Figure 1 show a suite of synthetic seismograms of the vertical component P-wave train for a thrust earthquake at focal depths of 2 km and 12 km at epicentral distances of 100 km to 300 km. The first arrivals in every case are head waves from the mid-crust (for the 100 km distance synthetics) or from the Moho (for the synthetics at distances of 200 km and beyond). The largest P-wave phases occur a few to several seconds after the first arrivals and are composed to post-critically reflected phases from the mid-crust and from the Moho. It is clear from an inspection of these seismograms that the timing of the largest P-wave amplitudes in these wavetrains relative to the first arrival time is a function of the source focal depth, with the deeper events generally having a larger time difference between the first and the maximum amplitudes for all epicentral distances studied. Thus, this aspect of the P waveforms can serve as a focal depth indicator at these near-regional distances.

Applications of these analysis ideas are applied to two earthquakes from this study in Figures 2 and 3. In Figure 2 synthetics and observations of the P waveforms from two stations for the June 17, 1991 m_{bLg}=4.5 earthquake at Summit, NY are compared. This earthquake has a well constrained focal depth of 12-13 km based on the hypocentral location of the mainshock and on the S-P times of two aftershocks recorded by portable seismographs which were deployed shortly after the occurrence of the mainshock. At station FLR the largest peak in the synthetic occurs at a time of about 8.5 seconds on the plot, very near to the time of the largest amplitude in the observation. There is also a good correspondence between the arrival times of several prominent phases between the synthetic and observation at times between 4 sec and 7.5 seconds, although the relative amplitudes of these phases is different between synthetic and observation. At station MD3 there also is a good correspondence between the arrival times of the phases on the synthetics and the observations for the first 5.5 seconds of the plot. However, at this station the largest observed amplitudes in this P-wave window occur at

about 8 sec, a time where the synthetic amplitudes are very small. This latter discrepancy notwithstanding, the 12 km focal depth synthetics generally are very consistent with the observations for this earthquake.

In Figure 3 synthetics and observations for the m_{bLg}=3.9 earthquake at Franklin Fall, New Hampshire on October 6, 1992 are compared. At station ECN the synthetic for a focal depth of 5 km seems to match the observation most closely, while at station MD3 it is the synthetic for a focal depth of 8 km which most closely resembles the observed waveform. All of the data from this earthquake best match the synthetic waveforms for a focal depth of 5 km, and a focal depth of 5-6 km is judged to be the best estimate for this event.

Some preliminary results are also available for Task (3). The spectral ground acceleration amplitudes for several earthquakes from New England and vicinity have been determined, and their decay with epicentral distance across the New England Seismic Network has been plotted. The distance decay for 3-Hz spectral acceleration for four events with m_{bLg} from 2.7 to 3.6 is shown in Figure 4, along with the expected distance-attenuation computed from the relations of Atkinson and Mereu (1992). The earthquakes have been normalized to a common magnitude (top plot) and a common seismic moment (bottom plot). There is a great amount of scatter in the data, and at distances of 100 km and greater most of the data points fall above the values predited by the Atkinson and Mereu (1992) relation. While not evident in these plots, there appears to be some systematic deviations relative to the mean for some of the stations.

Future Investigations

The work on Tasks (1) and (2) is nearing completion, and a paper describing the results of the research will be prepared for submission to a peer-reviewed scientific journal. The research on Task (3) is ongoing at present. In particular, the instrument deconvolutions to ground acceleration need to be checked further to ensure that there are no errors in that part of the analysis, and an event-by-event regression of the spectral amplitude attenuation needs to be made. The observations assembled in Task (3) will be compared to all of the published spectral attenuation curves for the northeastern United States.

References

Atkinson, G.M. and R.F. Mereu, The Shape of Ground Motion Attenuation Curves in Southeastern Canada, Bull. Seism. Soc. Am., 82, 2014-2031, 1992.

Publications - Abstracts

Ebel, J., Analysis of Spectral Attenuation Functions in New England for Seismic Hazard Analyses, EOS, Trans. Amer. Geophys. U., vol. 75, No. 44, p. 450, Supplement, 1994.

Ebel, J., Focal Depth Constraint of New England Earthquakes from Regional Seismic Network Seismograms, EOS, Trans. Amer. Geophys. U., vol. 74, No. 43, p. 401, Supplement, 1993.

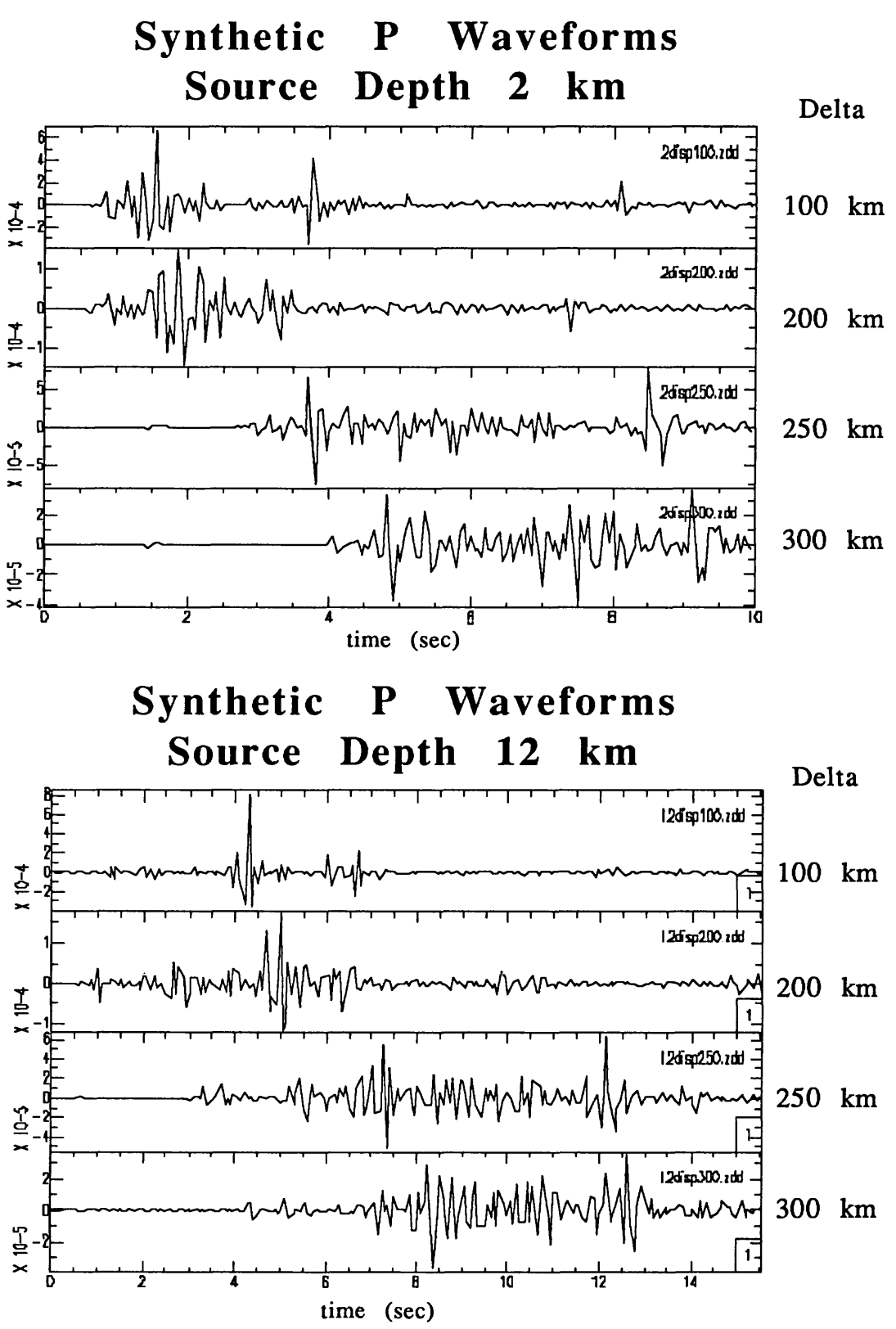

Figure 1. Synthetic P-wave seismograms for a 45° dip-slip earthquake at two different focal depths for several different epicentral distances. The synthetics have all been aligned with the first P-wave arrival occurring at 0.5 sec.

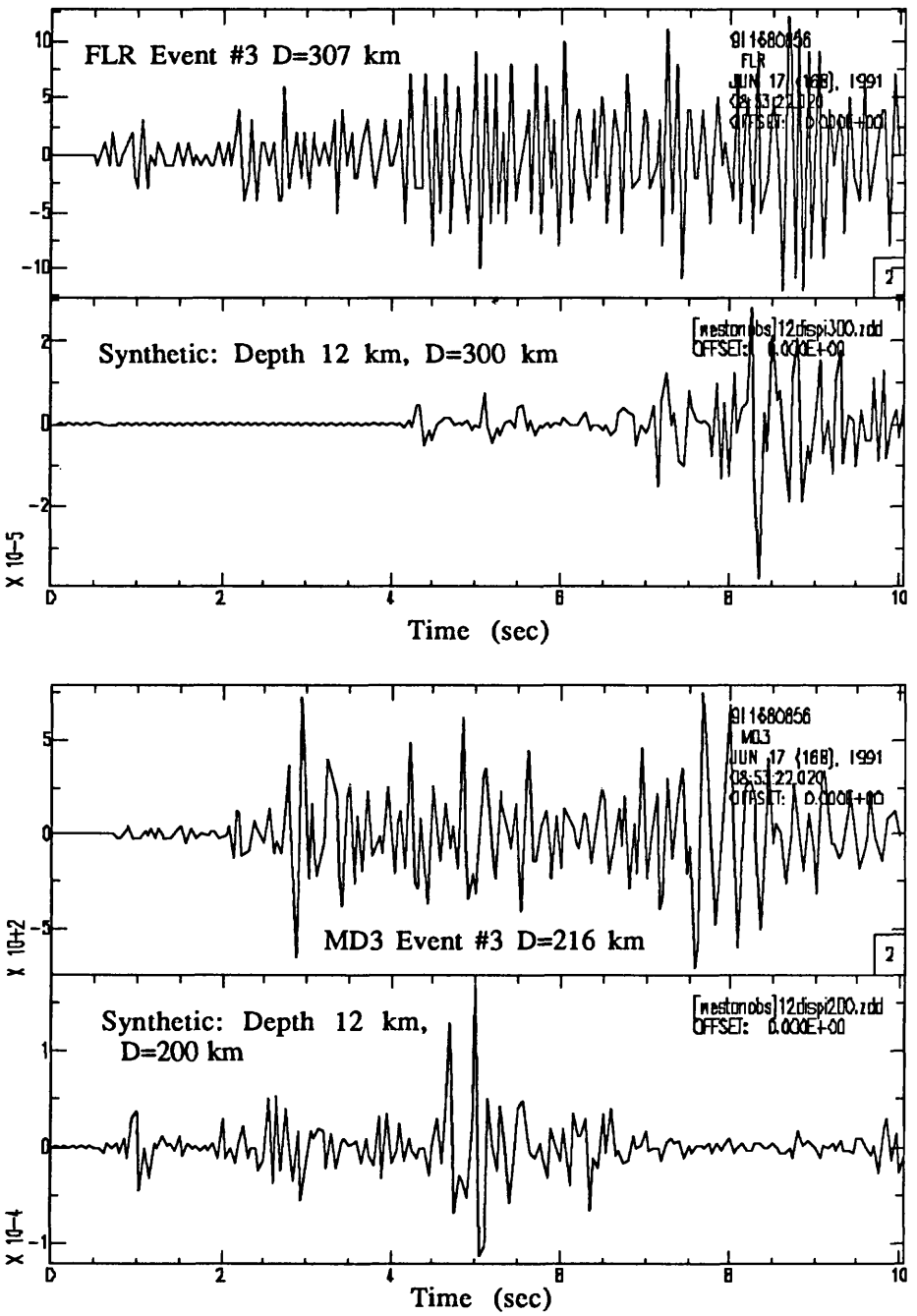

Figure 2. Observations (top) and synthetics (bottom) of the first 10 seconds of the P wavetrain for two recordings of the Summit, NY earthquake of June 17, 1991. The first arrivals of all of the waveforms are aligned at a time of 0.5 sec on the plots. The focal depth of the synthetics is indicated in each case, as is the epicentral distance (D) of the observation or synthetic.

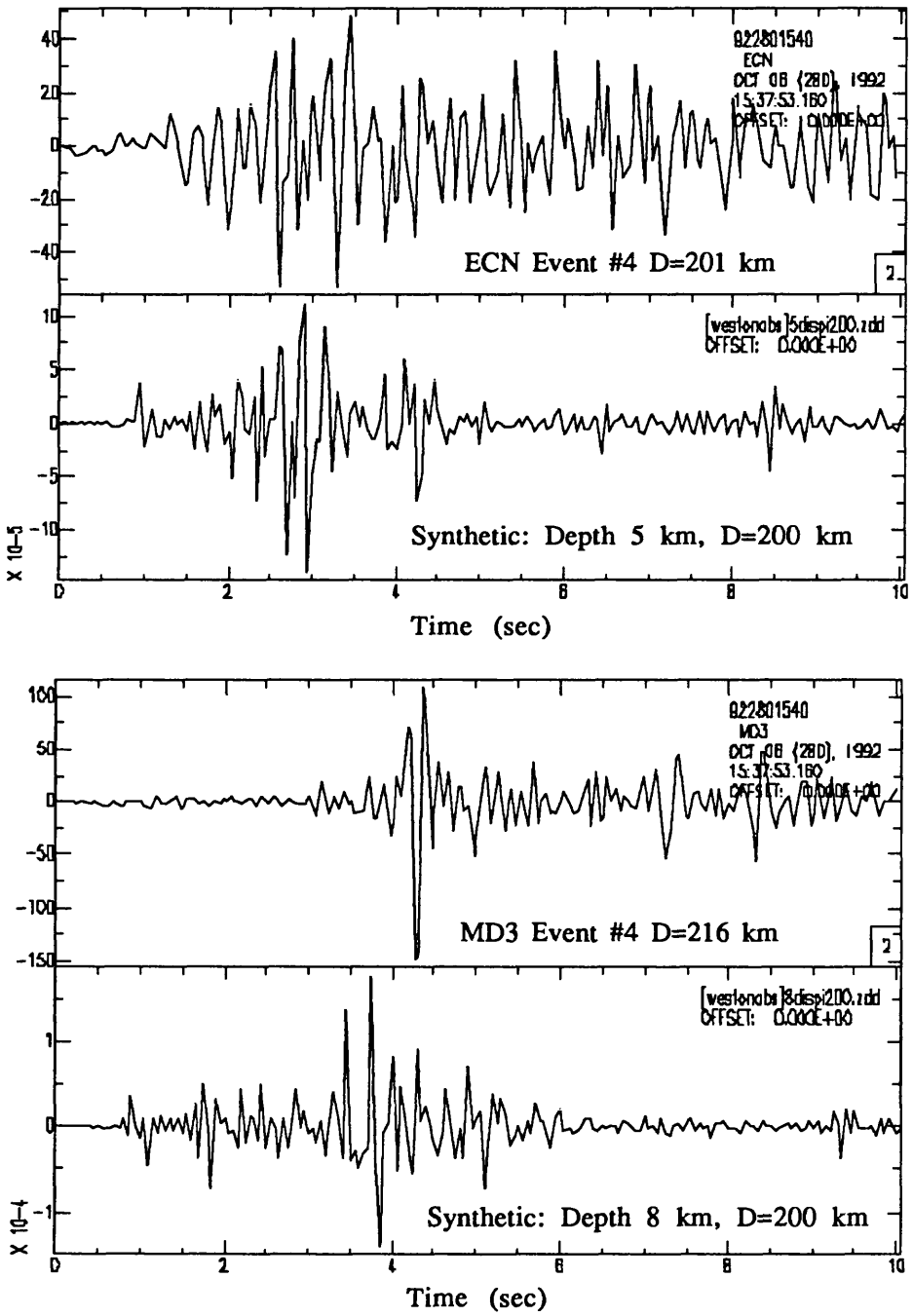

Figure 3. Observations (top) and synthetics (bottom) of the first 10 seconds of the P wavetrain for two recordings of the Franklin Falls, NH earthquake of October 10, 1992. The first arrivals of all of the waveforms are aligned at a time of 0.5 sec on the plots. The focal depth of the synthetics is indicated in each case, as is the epicentral distance (D) of the observation or synthetic.

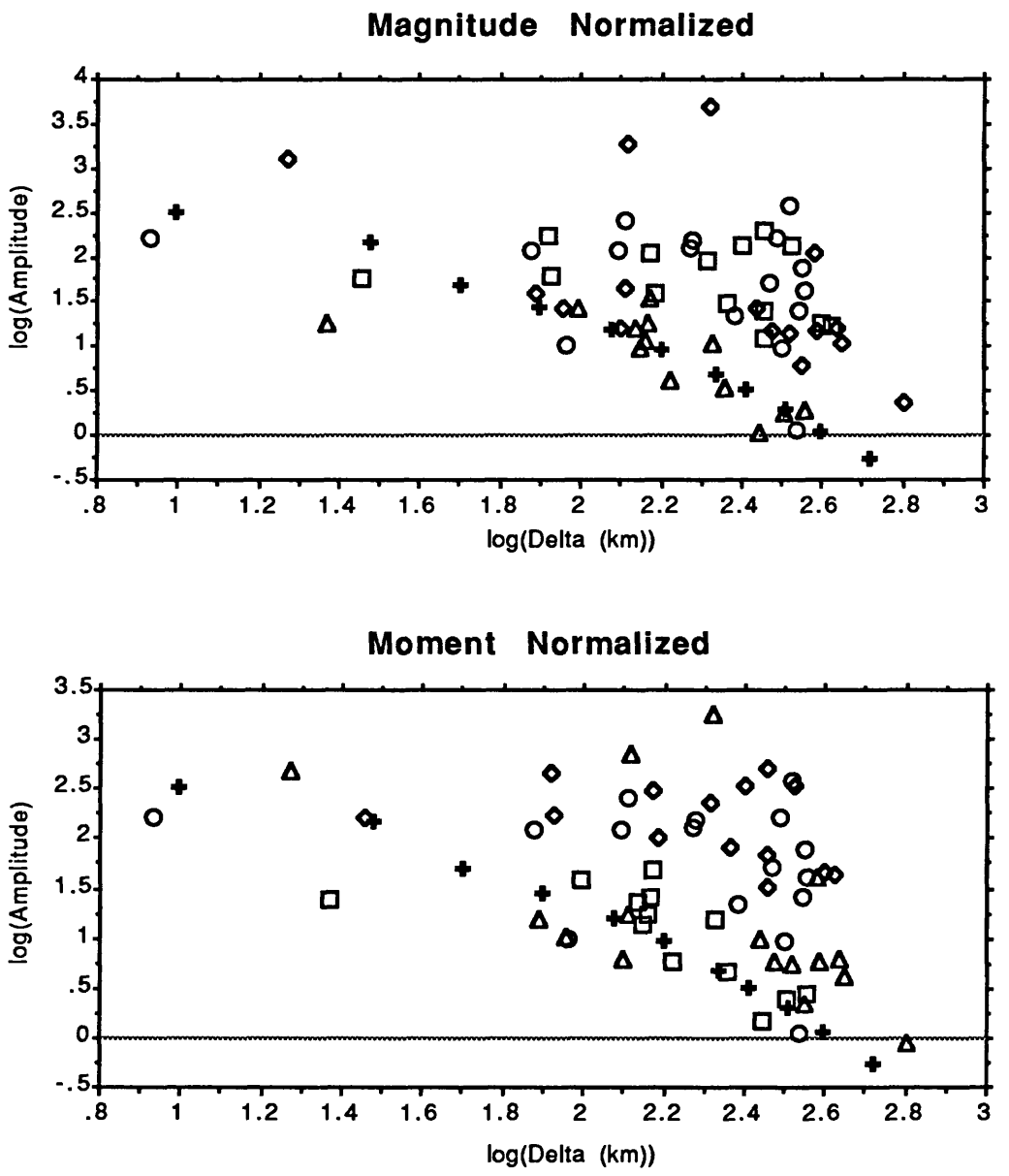

Figure 4. Preliminary results of the distance attenuation of 3-Hz spectral amplitudes for 4 earthquakes in New England (open symbols) compared to the predicted amplitude attenuation from the relation of Atkinson and Mereu (1992) (crosses). In the top plot the data points have been normalized to a common level based on the earthquake magnitude, while in the bottom plot the normalization was based on the earthquake moment.

Identification of Site Properties Using Earthquake Data Recorded By Downhole Arrays

Award No: 1434-94-G-2397

Ahmed-W. Elgamal[1] and Mourad Zeghal[2]

Civil and Environmental Engineering Department
Rensselaer Polytechnic Institute, Troy, NY 12180
Tel: (518) 276-2836

Program Element: III.3

Abstract

A general 2-dimensional system identification framework is developed to evaluate the mechanisms and parameters of site dynamic response from downhole seismic records. Investigations are focused on two unique sites instrumented with downhole arrays: (1) the US Wildlife refuge site (southern California), and (2) the Lotung site (Taiwan). The conducted analyses provide direct fundamental information on dynamic site response including soil liquefaction; and on the associated mechanisms of soil stiffness reduction, degradation and failure. For each soil layer located between downhole instruments, the recorded seismic data was employed to: (1) analyze the mechanisms of site dynamic response and seismic amplification, (2) evaluate soil shear stiffness and damping parameters as a function of shear strain amplitude, and (3) identify the mechanisms of soil softening, progressive loss of soil stiffness and strength, and accumulation of permanent deformation due to soil liquefaction (Wildlife site). The identified seismic response mechanisms and dynamic soil properties provided invaluable information directly estimated from the downhole seismic records. This information documented the actual seismic response characteristics of these two sites which represent typical near surface soft-soil profiles (loose saturated silty sand and liquefiable alluvial deposits). Results of this study are particularly useful for calibration of computational procedures; and for comparison with soil dynamic response data obtained by in situ/laboratory dynamic tests. These results also demonstrate the potential and worthiness of downhole arrays as a means of recovering seismic site response characteristics; and may be used to develop downhole instrumentation strategies so as to maximize the outcomes of invested capital and effort.

1 Introduction

The 1985 Mexico and the 1989 Loma Prieta earthquakes clearly demonstrated that local damage is greatly intensified by site characteristics and the resulting amplification (Mexico); and by liquefaction of loose saturated soil deposits (Loma Prieta [12]). Mitigation of the

[1]Associate Professor.
[2]Research Associate.

effects of site amplification and loss of stiffness requires a thorough understanding of the involved mechanisms.

In-situ investigations [13], laboratory tests [8, 10, 11], and centrifuge tests [1, 6], currently provide a means of evaluating seismic site response. However, due to limitations in reproducing in-situ stress-state, seismic loading histories, site stratification conditions, and appropriate boundary conditions, the results may not fully reflect the actual site behavior.

In order to develop a better understanding of seismic site response, soil dynamic characteristics may be inferred from actual downhole seismic records at different depths within the ground. Such records provide information on site seismic response that cannot be obtained from surface arrays only.

2 Objectives, Methodology and Scope

This study was aimed at utilizing downhole acceleration and pore pressure records to evaluate parameters and mechanisms of site shear stress-strain response during strong motion earthquakes; and to investigate the causes and effects of earthquake induced progressive loss of site stiffness due to soil liquefaction. Downhole earthquake records of sites in the United States and other locations of general relevance to the US seismic mitigation efforts were employed.

A two-dimensional (2D) system identification framework to analyze the mechanisms and properties of seismic shear response was developed. This framework consists of: (1) evaluation of site lateral shear stress-strain histories directly from seismic records, (2) identification of dynamic soil parameters (i.e., shear modulus and damping) as a function of shear deformation amplitude and pore pressure buildup, and (3) analyses of the mechanisms of progressive site stiffness degradation and accumulation of permanent deformation due to soil liquefaction.

A set of two unique sites instrumented with downhole arrays, namely Wildlife site in California, and Lotung site in Taiwan, were analyzed. These sites were selected because they represent two different dynamic response patterns, including a case of site liquefaction and progressive loss of soil stiffness at Wildlife. Wildlife refuge site, which was instrumented by USGS, is equipped with surface and a downhole accelerometers and pore pressure transducers [7]. It is unique in the sense that it had liquefied more than once in the recent past [15]. During the 1987 Superstition Hills earthquake, the recorded acceleration and pore water pressure data (and field observations) clearly indicated a case of site liquefaction and associated loss of soil stiffness. The Lotung site at Taiwan, which was instrumented by EPRI (Electric Power Research Institute) and TPC (Taiwan Power Company) is equipped with surface and downhole accelerometers [14]. A total of 18 earthquakes were recorded during 1985-1986 at Lotung (LSST1-LSST18). The behavior of this site is highly relevant to the seismic response of many soft soil sites in the United State and elsewhere worldwide.

The downhole records of a third site, namely Chiba in Japan, were also analyzed. This phase of research continues, and results will be available in the near future.

3 Analyses

3.1 Evaluation of site shear stress and strain histories

A nonparametric identification technique was employed to evaluate the actual 2-dimensional (2D) horizontal shear stress and strain histories for each site layer (between any two downhole stations) directly from the available downhole acceleration records [16, 17, 18], as described below.

Site seismic lateral shear vibrations are governed by the following equations (Fig. 2):

$$\frac{\partial \boldsymbol{\tau}}{\partial z} = \rho \mathbf{a}, \quad \text{subject to:} \quad \boldsymbol{\tau}(0,t) = \mathbf{0} \ \text{ and } \ \mathbf{u}(h,t) = \mathbf{u}_g \tag{1}$$

in which t is time, z is depth coordinate, x and y are coordinates in the horizontal plane, $\boldsymbol{\tau} = \{\tau_x,\ \tau_y\}^T$ is horizontal shear stress vector ($\tau_x = \tau_x(z,t)$ and $\tau_y = \tau_y(z,t)$ are horizontal shear stresses in the x and y directions respectively), $\mathbf{a} = \{a_x,\ a_y\}^T$ is horizontal absolute acceleration vector ($a_x = a_x(z,t)$ and $a_y = a_y(z,t)$ are horizontal absolute accelerations in the x and y directions respectively), $\mathbf{u} = \{u_x(z,t),\ u_y(z,t)\}^T$ is the corresponding displacement vector, $\mathbf{u}_g = \mathbf{u}_g(t)$ is input (or bedrock) horizontal displacement vector, h is site depth, and ρ is mass density.

Integrating Eq. 1 and using the surface stress free boundary condition, the horizontal shear stress vector at any level z may be expressed as:

$$\boldsymbol{\tau}(z) = \int_0^z \rho \mathbf{a}(z,t) dz. \tag{2}$$

If linear interpolation between adjacent downhole accelerations is utilized, the discrete counterpart of Eq. 2 reduces to:

$$\boldsymbol{\tau}_i = \sum_{k=1}^{i-1} \rho_k \frac{\mathbf{a}_k + \mathbf{a}_{k+1}}{2} \Delta z_k, \quad i = 2, 3, \cdots \tag{3}$$

where subscript i refers to the level z_i at which the stress is evaluated (Fig. 2), $\boldsymbol{\tau}_i = \boldsymbol{\tau}(z_i)$ is shear stress vector at level z_i, $\mathbf{a}_i = \mathbf{a}(z_i)$ is absolute horizontal acceleration vector at level i, and Δz_k is spacing interval as shown in Fig. 2.

These stress estimates (Eqs. 3 and 4) are second order accurate [16]. A corresponding second-order accurate shear strain $\boldsymbol{\gamma}_i$ at level z_i may be expressed as:

$$\boldsymbol{\gamma}_i = \frac{1}{\Delta z_{i-1} + \Delta z_i} \left((\mathbf{u}_{i+1} - \mathbf{u}_i) \frac{\Delta z_{i-1}}{\Delta z_i} + (\mathbf{u}_i - \mathbf{u}_{i-1}) \frac{\Delta z_i}{\Delta z_{i-1}} \right) \tag{4}$$

in which $\mathbf{u}_i = \mathbf{u}(z_i, t)$ is horizontal displacement vector at level i (obtained by double integration of the corresponding acceleration records).

Accuracy of shear stress $\boldsymbol{\tau}_i$ and shear strain $\boldsymbol{\gamma}_i$ estimates (Eqs. 3 and 4) is a function of acceleration wave length and spatial separation of the downhole accelerometers. Relative errors in estimating $\boldsymbol{\tau}_i$ and $\boldsymbol{\gamma}_i$ for the top 17 m layer at Lotung site [16] were found to be of the order of 3 % (for the significant frequency components of site response).

3.2 Soil stiffness and damping properties

3.2.1 Equivalent stiffness and damping

Soil stiffness and material damping properties were first assessed in terms of the conventional equivalent shear moduli and damping ratios, evaluated through measuring the secant stiffness and energy dissipated by selected stress-strain cycles [16].

3.2.2 System identification

A new algorithm that utilizes the nonparametric estimates of shear stress and strain histories was developed to estimate stiffness and damping properties. This algorithm is based on matching the actual stress-strain histories during seismic excitation rather than matching the recorded accelerations (conventional approach), and involves: (1) formulation of a class of constitutive models to idealize the observed (actual) seismic stress-strain histories, and (2) evaluation of the formulated constitutive model parameters as a function of strain amplitude.

Constitutive model. Linear and elasto-plastic models were employed to idealize the soil behavior. The linear and elasto-plastic relationships between horizontal shear stress and strain vectors may be expressed as [3]:

$$d\boldsymbol{\tau}^{l} = G^{l} d\boldsymbol{\gamma} + \eta^{l} d\dot{\boldsymbol{\gamma}} \tag{5}$$

$$d\boldsymbol{\tau}^{ep} = G_o d\boldsymbol{\gamma} - (G_o - G)\langle \boldsymbol{\tau}.d\boldsymbol{\gamma}\rangle \frac{\boldsymbol{\tau}}{||\boldsymbol{\tau}||} \tag{6}$$

respectively, G^l and η^l are linear stiffness and damping, $\langle\ \rangle$ are the McCaulay brackets (i.e., $\langle \boldsymbol{\tau}.d\boldsymbol{\gamma}\rangle = \boldsymbol{\tau}.d\boldsymbol{\gamma}$ if $\boldsymbol{\tau}.d\boldsymbol{\gamma} \geq 0$, otherwise $\langle \boldsymbol{\tau}.d\boldsymbol{\gamma}\rangle = 0$), $G = G(\boldsymbol{\gamma})$ is tangent shear modulus as a function of shear strain vector $\boldsymbol{\gamma}$, and G_o is initial tangent shear modulus at small strains.

Evaluation of soil model dynamic parameters. Shear stiffness and damping parameters were evaluated to minimize the difference between the actual (observed) shear stress histories $\boldsymbol{\tau}^{(o)}$ and those predicted by the selected models $\boldsymbol{\tau}^{(m)}$ using the actual shear strain histories. The optimality criterion was expressed as:

$$\mathcal{O}_\tau = \int_0^T ||\boldsymbol{\tau}^{(o)} - \boldsymbol{\tau}^{(m)}|| dt \tag{7}$$

in which $||\boldsymbol{\tau}^{(o)} - \boldsymbol{\tau}^{(m)}||$ refers to the Euclidean norm of $\boldsymbol{\tau}^{(o)} - \boldsymbol{\tau}^{(m)}$. The model optimal parameters are then given by:

$$\min_{G,\eta} \mathcal{O}_\tau \ \text{ such as : } \ G > 0 \text{ and } \eta > 0 \tag{8}$$

in which G and η are employed here to refer collectively to shear stiffness and damping parameters as described above.

4 Results

The following is a brief description of some of the retrieved dynamic soil response parameters and characteristics.

Lotung site: Acceleration records of DHB downhole array and FA1-5 surface station (Fig. 1) were utilized to estimate the Lotung site shear response characteristics during the 1985-1986 earthquakes, as described below:
(1) Shear stress and strain histories were evaluated at different locations within the instrumented zone. Fig. 3 depicts the LSST 16 NS (North-South) shear stress and strain histories at 6 m, 11 m and 17 m depths. The corresponding shear stress-strain histories revealed two salient response features: (a) stiffness reduction with the increase in shear strain amplitude, and (b) stiffness reduction due to pore pressure buildup [16].
(2) Equivalent shear moduli and damping ratios were evaluated from the estimated stress-strain histories, and were found to be in agreement with the stiffness properties estimated from laboratory triaxial and resonant colum tests of undisturbed Lotung sandy and clayey soil samples, as shown in Fig. 4.
(3) Optimal linear soil-model parameters were evaluated for two low-strain earthquakes (LSST 5 and 8 with peak accelerations of about 0.04 g). In general, linear constitutive models provided a good idealization of Lotung site stress-strain response during these low amplitude earthquakes. For instance, Fig. 5 exhibits the LSST8 EW stress histories estimated from acceleration records, along with the corresponding optimal linear soil-model estimates.
(4) Optimal elasto-plastic soil-model parameters were evaluated from the stress-strain histories of the relatively strong LSST 7, 12, and 16 earthquakes (at 3 m, 6 m, 8.5 m, 11 m and 14 m depths). As shown in Figs. 6 and 7, the stress histories predicted by the identified models closely matched those estimated directly from the acceleration records. The variations of the corresponding shear moduli as function of shear strain amplitude (for LSST 7, 12, and 16 at 3 m, 6 m, 8.5 m and 11 m depths) showed consistency and fell within a narrow band (Fig. 8). A single model representative of the site response during these earthquakes at all elevations is currently being finalized.
(5) Optimal parameters using an elasto-plastic soil model have also produced remarkable agreement with the recorded ground surface acceleration history (Figs. 9 and 10), when employed in a finite element 2D shear model of the top 6 m stratum. It is important to note that computational seismic response may be calculated through a sub-structuring approach. In this approach, the soil system above any downhole accelerometer may be isolated and modeled by finite elements. The recorded soil response at this substructure base, fully describes the boundary conditions, and qualifies as input to this substructure system. No approximations are involved in performing substructure computational analyses as verified by [9] within an illustrative framework.

Wildlife site: Seismic records of the 1987 Superstition Hills earthquake were utilized to estimate stress-strain histories (Fig. 11). The conducted 2D analysis, built on earlier 1D work and showed that soil progressively lost all stiffness due to liquefaction. After liquefaction, the site stress-strain relationship was characterized by cycles of large shear strain and very small shear stress. At these large strains, evidence of hardening response, possibly due to a dilative-type soil behavior, was observed (Fig. 11). Similar soil behavior is documented in controlled laboratory experiments [2]. A 2D constitutive model for dilative type soils with pore pressure generation capabilities, is being finalized and calibrated by the identified Wildlife stress and strain histories.

5 Achievements and Conclusions

The following has been achieved:
(1) A systematic methodology has been developed for evaluation of 2D shear stress and strain histories at downhole accelerometer locations and midway between these accelerometers. Stress-strain histories for Lotung (Taiwan), and Wildlife refuge (California) sites were identified.
(2) An elasto-plastic nonlinear soil model has been developed for identification of soil stiffness and damping properties. A pore pressure generation model is currently being finalized.
(3) A minimization algorithm has been developed in order to evaluate optimal soil model parameters.
(4) A 2D shear finite element model (with pore pressure generation capabilities) was adapted for computations of site response using the identified soil parameters [9]. The results were compared to the recorded site response.

This study has documented the potential of downhole array seismic records in providing direct information about soil stiffness and damping properties; and about mechanisms of progressive loss of soil stiffness during earthquake excitations [4, 16, 17, 18]. The findings provide a wealth of information about site amplification and soil failure due to liquefaction. Outcomes of these investigations may also be used in the development of strategies for deployment of downhole instrumentation at new sites, so as to maximize the outcome of invested capital and effort.

References

[1] Arulanandan, K. and Scott, R. F., *Proceedings of the International Conference on the Verification of Numerical Procedures for the Analysis of Soil Liquefaction Problems*, Vol. 1, Davis, CA, 1993.

[2] Arulmoli, K., Muraleetharan, K. K., Hossain, M. M. and Fruth, L. S., "Verification of Liquefaction Analyses by Centrifuge Studies Laboratory Testing Program Soil Data Report," Report, The Earth Technology Corporation, 1992.

[3] Elgamal, A.-W., Abdel-Ghaffar, A. M. and Prevost, J. H., "2-D Elasto-Plastic Seismic Shear Response of Earth Dams-I Theory," Journal of Engineering Mechanics Division, ASCE 113, 689-701 (1987).

[4] Elgamal, A.-W., Zeghal, M., . Tang, H. T and . Stepp, J. C, "Evaluation of Low-Strain Site Characteristics Using The Lotung Seismic Array" submitted for journal publication.

[5] *Guidelines for Determining Design Basis Ground Motions, Volume 1: Method and Guidelines for Estimating Earthquake Ground Motion in Eastern North America*, Report No. TR-102293, Electric Power Research Institute, Palo Alto, California, 1993.

[6] Hushmand, B., Crouse, C. B., Martin, G. and Scott, R. F., "Site Response and Liquefaction Studies Involving the Centrifuge: Structures and Methods," *Developments in Geotechnical Engineering 45*, A. S. Cakmak, ed., pp 3-24, 1987.

[7] Holzer, T. L., Youd, T. L. and Hanks, T. C., "Dynamics of Liquefaction During the 1987 Superstition Hills California Earthquake," Science, Vol 244, 56-59.

[8] *Liquefaction of Soils During Earthquakes*, National Research Council Committee on Earthquake Engineering, National Academy press, Washington D. C., 1985.

[9] Ragheb, A., "Computational Modeling of Soil Systems and Post Liquefaction Response," Ph.D. Thesis, Dept. of Civil Eng., Rensselaer Polytechnic Institute, Troy, NY, August, 1994.

[10] Seed, H. B., Wong, R. T., Idriss, I. M. and Tokimatsu, T., "Moduli and Damping Factors for Dynamic Analyses of Cohesionless Soils," Report EERC 84-14, Earthquake Research Center, University of California Berkeley, 1984.

[11] Seed, H. B. and Idriss, I. M., "Soil Moduli and Damping Factors for Dynamic Response Analyses," Report EERC 70-10, Earthquake Research Center, University of California Berkeley, 1970.

[12] Seed, R. B., Dickenson, S. E., Riemer, M. F., Bray, J. D., Sitar, N., Mitchell, J. K., Idriss, I. M., Kayen, R. E., Kropp, A., Hander, L.F. Jr. and Power, M. S., "Preliminary Report on the Principal Geotechnical Aspects of the October 17, 1989, Loma Prieta Earthquake," *Report No. UCB/EERC-90/05,* Earthquake Engineering Research Center, University of California Berkeley, April 1990.

[13] Stokoe, K. H. II and Woods, R. D., "In Situ Shear Wave Velocity by Cross-Hole Method," Journal of the Soil Mechanics and Foundation Division, ASCE, Vol. 98, No. SM5, pp. 442-460, May 1972.

[14] Tang, H. T., *Large-Scale Soil Structure Interaction*, Report No. NP-5513-SR, Electric Power Research Institute, Palo Alto, California, 1987.

[15] Youd, T. L. and Wieczorek, G. F., "Liquefaction During 1981 and Previous Earthquakes Near Westmorland California," *U.S. Geological Survey Open-File Report 84-680*, 1984.

[16] Zeghal, M. and Elgamal, A.-W., "Lotung Site: Downhole Seismic Data Analyses," *Report,* Civil and Environmental Engineering Department, Rensselaer Polytechnic Institute, Troy, NY, 1993 (in preparation as EPRI report).

[17] Zeghal, M., Elgamal, A.-W., "Analysis of Site Liquefaction Using Earthquake Records," Journal of Geotechnical Engineering, ASCE, Vol. 120, No. 6, June 1994.

[18] Zeghal, M., Elgamal, A.-W., Tang, H. T. and Stepp, J. C. , "Evaluation of Nonlinear Site Characteristics Using The Lotung Seismic Array," submitted for journal publication.

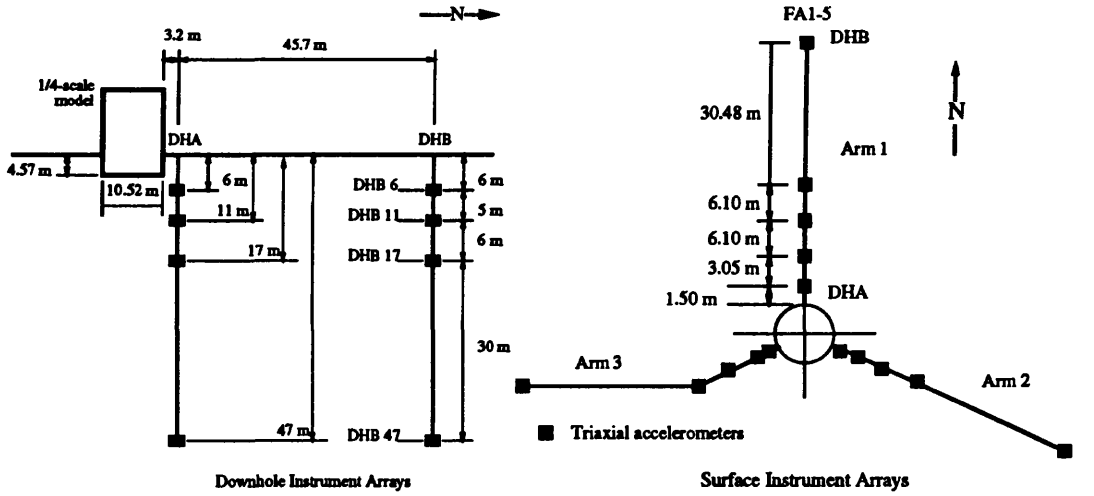

Figure 1: Instrumentation at Lotung experiment site.

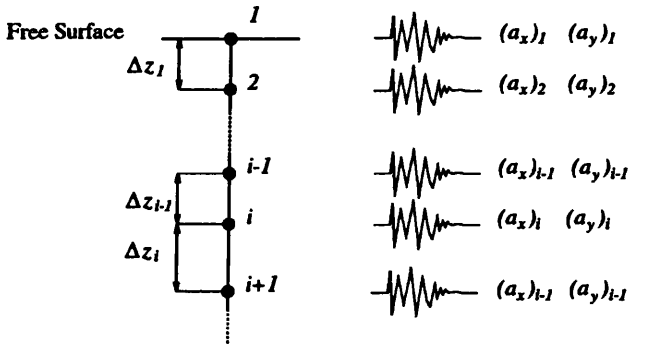

Figure 2: Geometrical model and discretization of site shear response.

Published Reports and Papers

• M. Zeghal and A.-W. Elgamal, "Identification of Site Dynamic Response Properties Using Downhole Seismic Records," Civil Engineering Department, Rensselaer Polytechnic Institute, Troy, NY (In preparation).

• Elgamal, A.-W., Zeghal, M., Tang, H. T. and Stepp, J. C., "Lotung Downhole Seismic Array: Evaluation of Site Dynamic Properties," submitted for journal publication.

• Zeghal, M., Elgamal, A.-W., Tang, H. T. and Stepp, J. C., "Lotung Downhole Seismic Array: Evaluation of Soil Nonlinear Properties," submitted for journal publication.

• A.-W. Elgamal and M. Zeghal, "Two-Dimensional Analysis of Wildlife Site 1987 Liquefaction," to be submitted for journal publication.

• A.-W. Elgamal and M. Zeghal, "Site Amplification Analyses Using Downhole Array Records," to be submitted to the 7th Canadian Conference on Earthquake Engineering, Canada.

• M. Zeghal and A.-W. Elgamal, "Downhole Arrays as a Tool for Seismic Zonation," to be submitted to the 5th International Conference on Seismic Zonation, France.

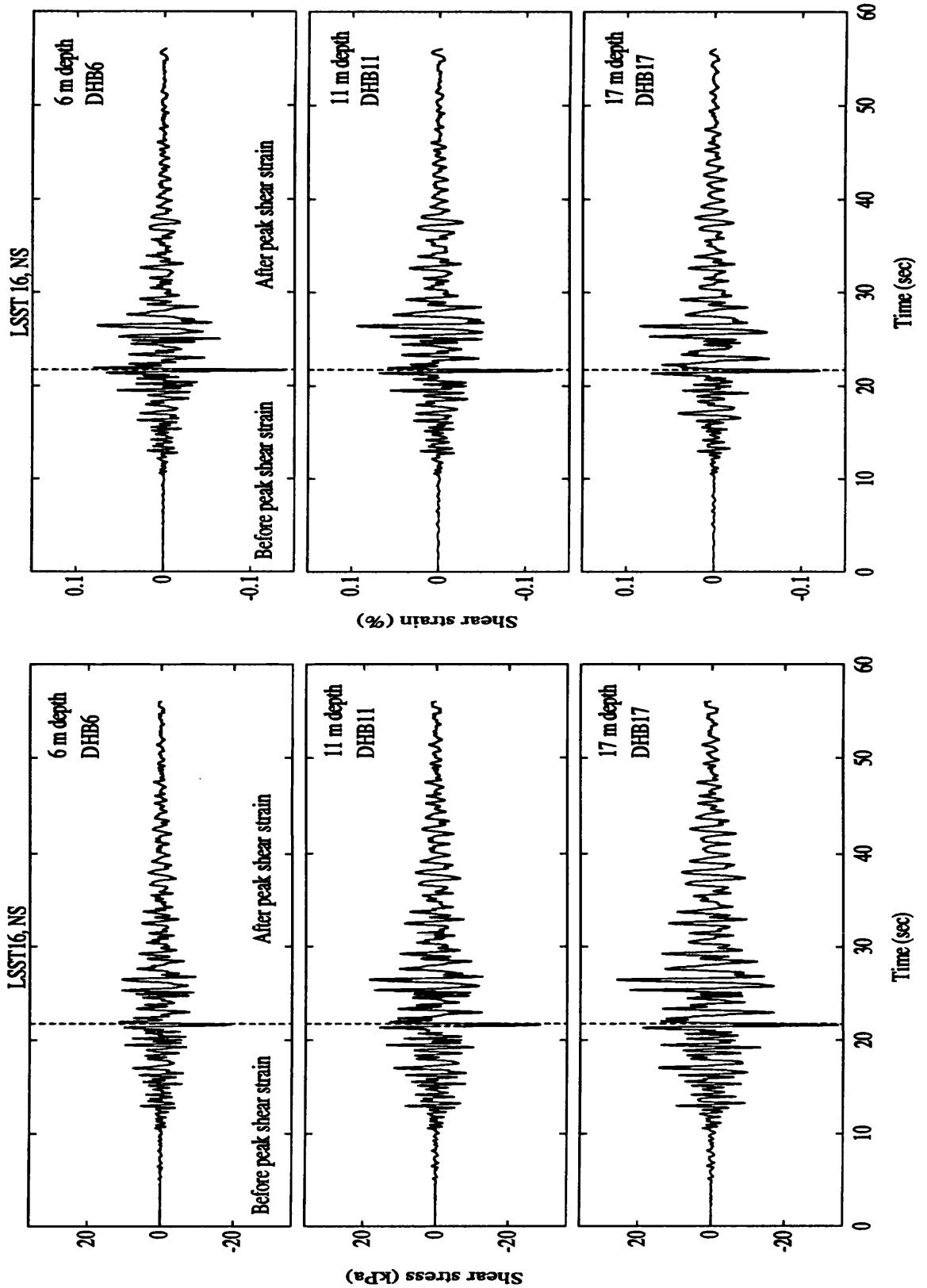

Figure 3: LSST 16 shear stress and strain histories at DHB6, DHB 11 and DHB17 (6m, 11 m, and 17 m depth).

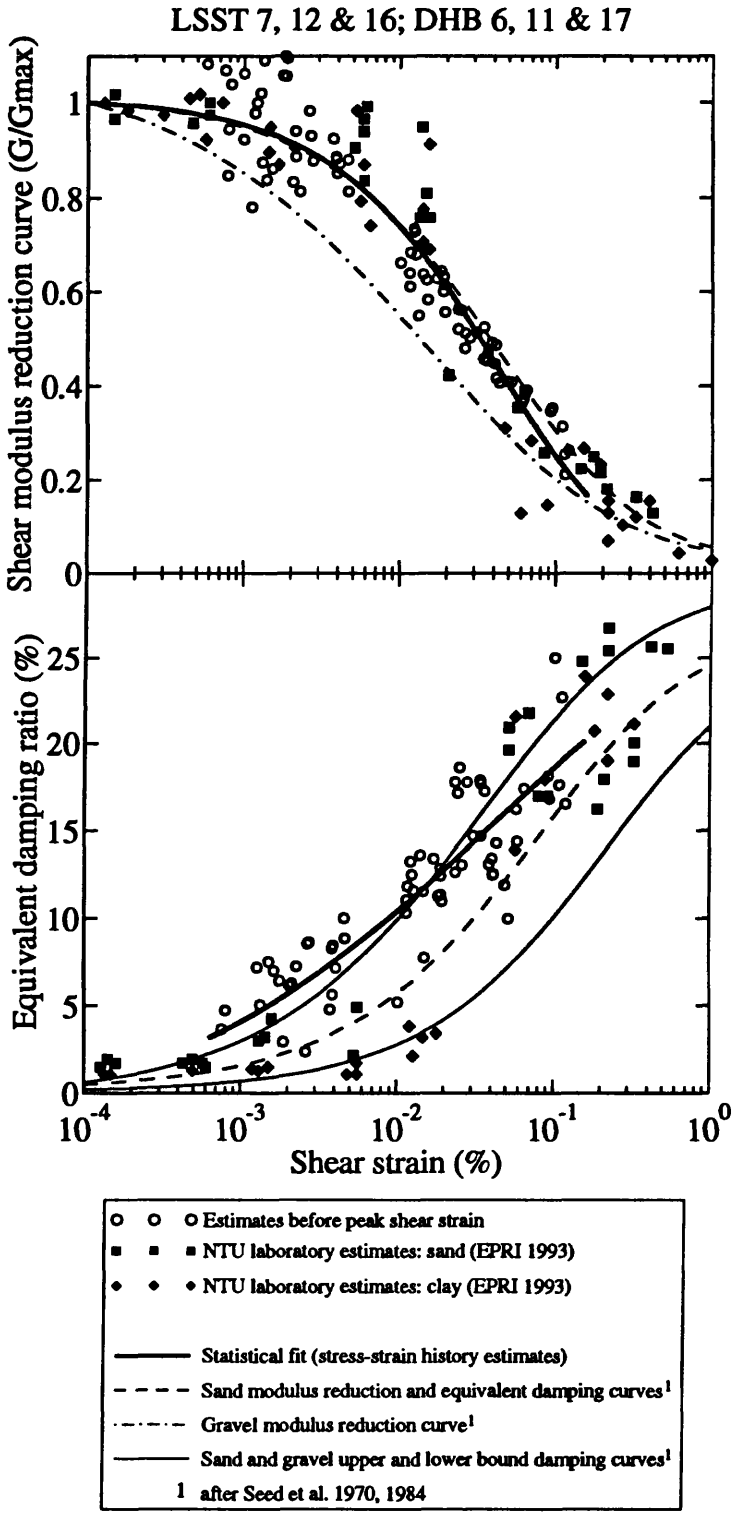

Figure 4: Comparison of equivalent shear moduli and damping ratios evaluated from stress-strain histories with those estimated from the National Taiwan University laboratory tests [5].

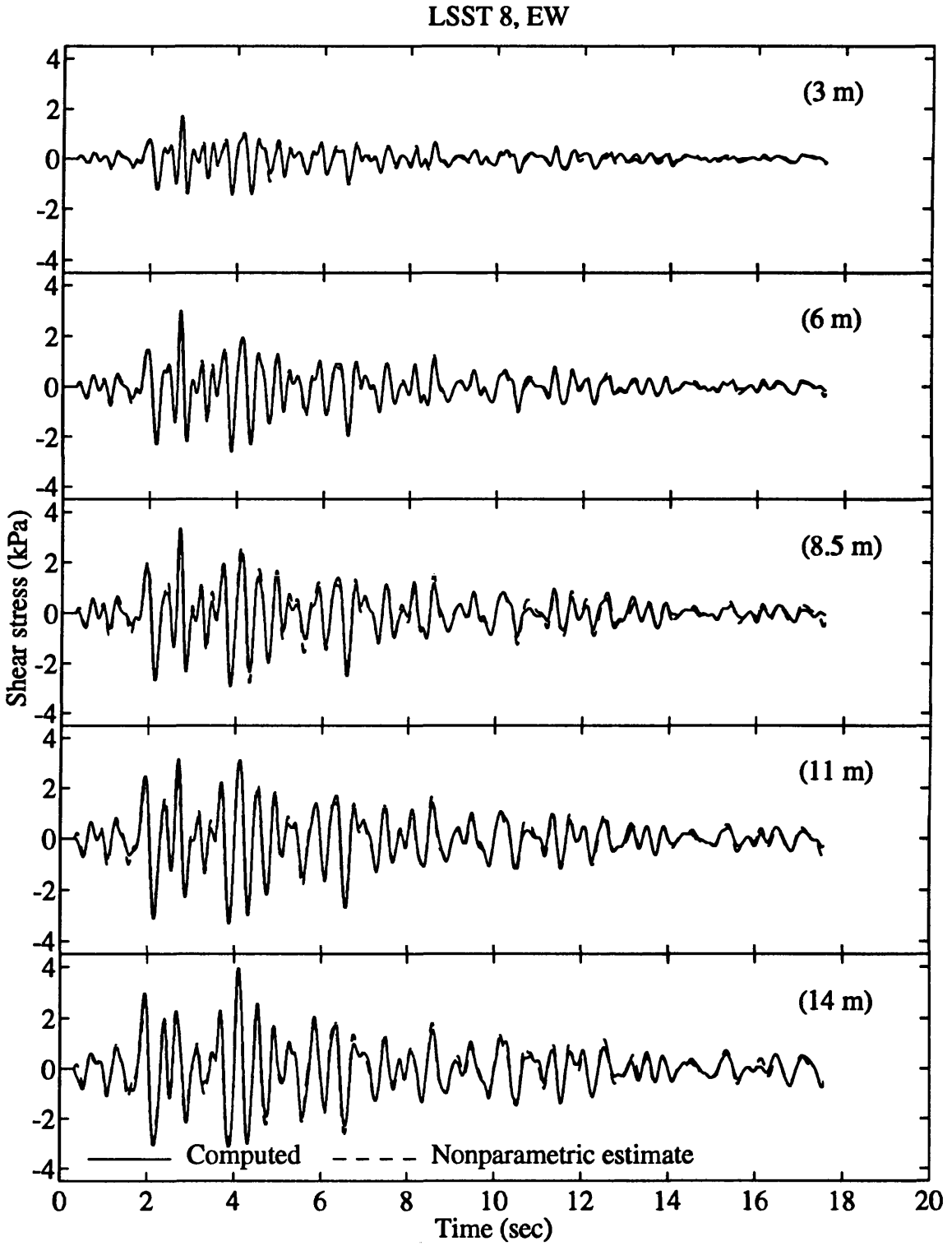

Figure 5: LSST 8 estimated and computed stress histories at 3 m, 6 m, 8.5 m, 11 m and 14 m depth (EW component).

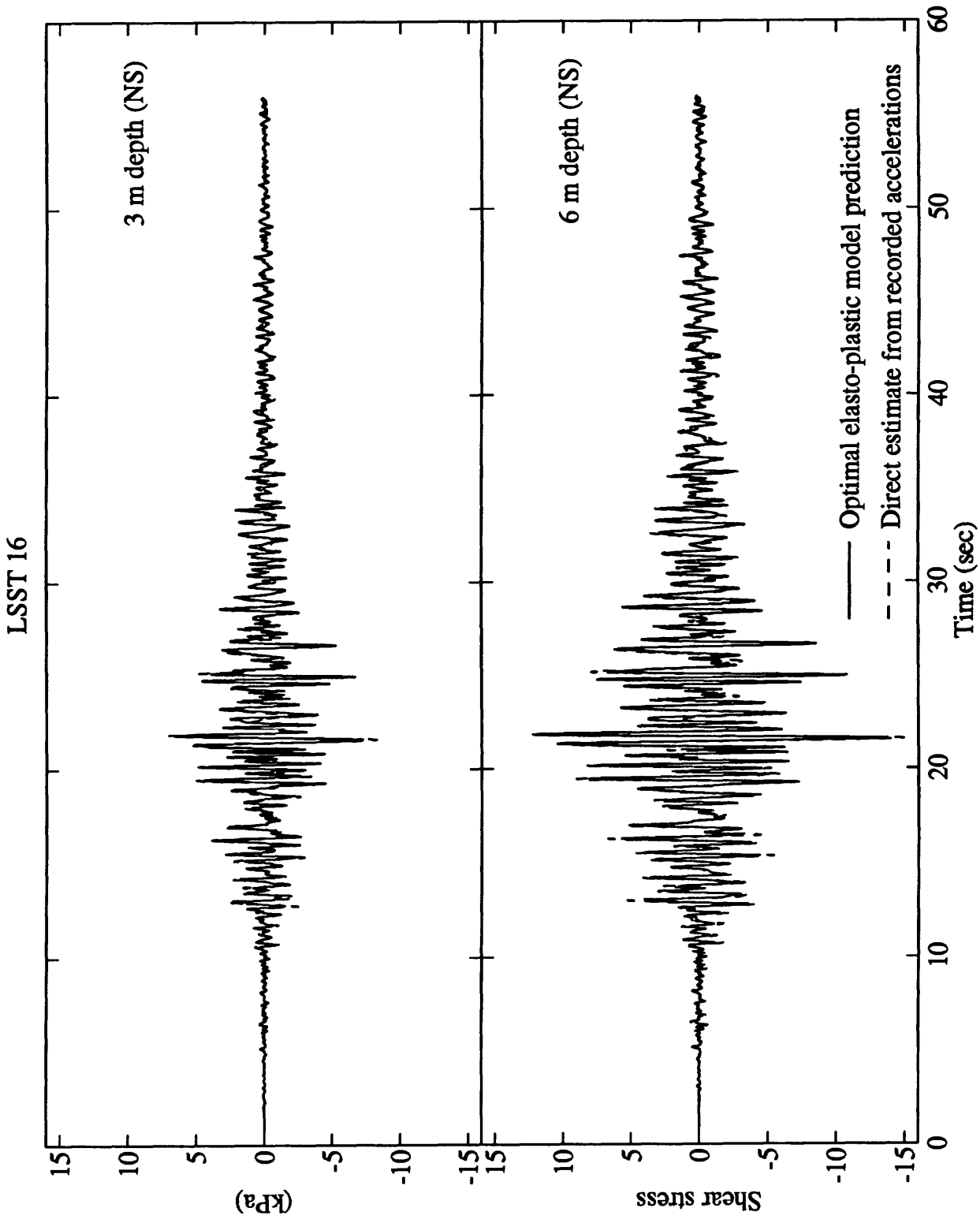

Figure 6: LSST 16 estimated and computed stress histories at 3 m and 6 m depth (NS).

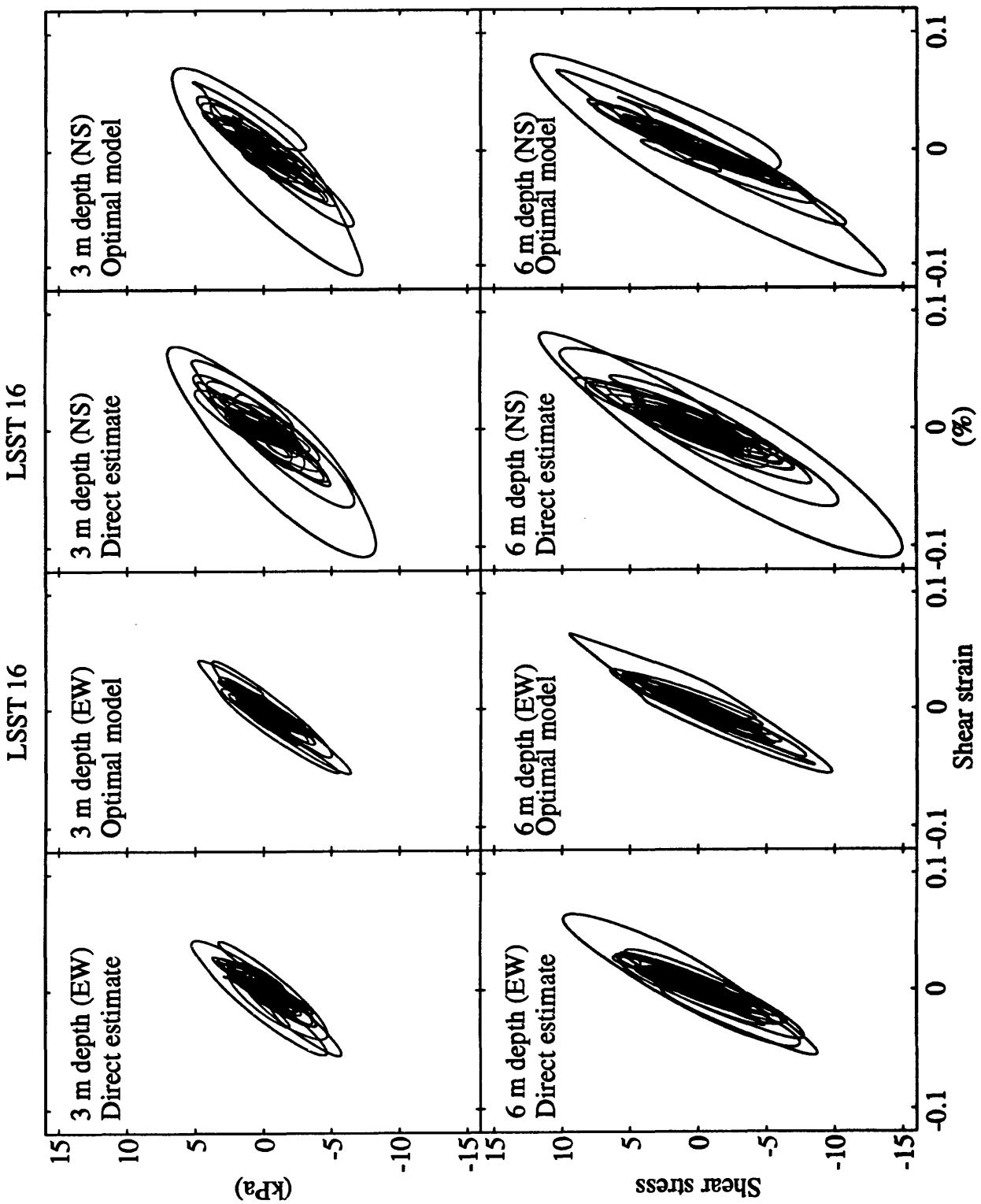

Figure 7: LSST 16 estimated and computed stress-strain histories at 3 m and 6 m depth (NS and EW).

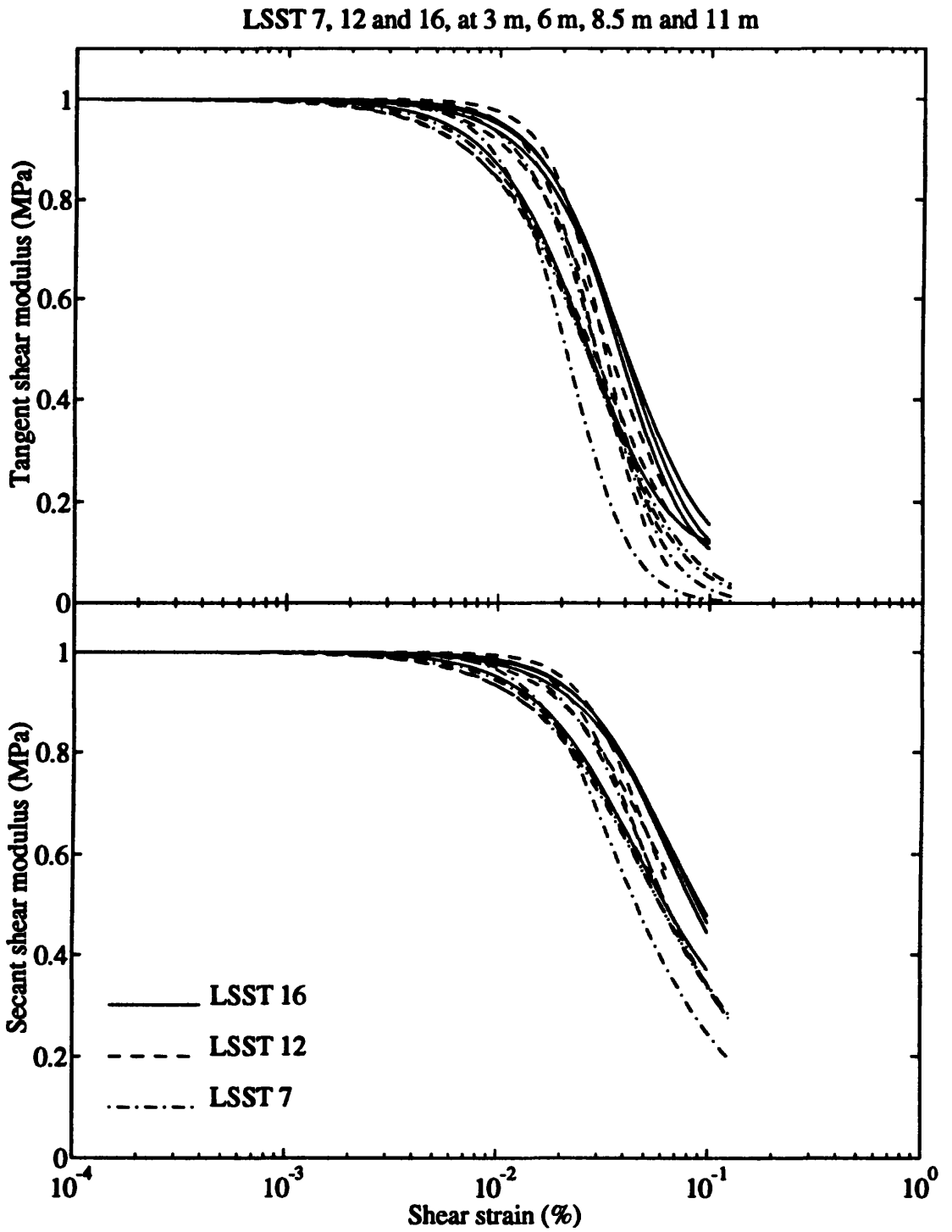

Figure 8: Lotung site shear moduli attenuation curves evaluated using the developed 2-D system identification framework.

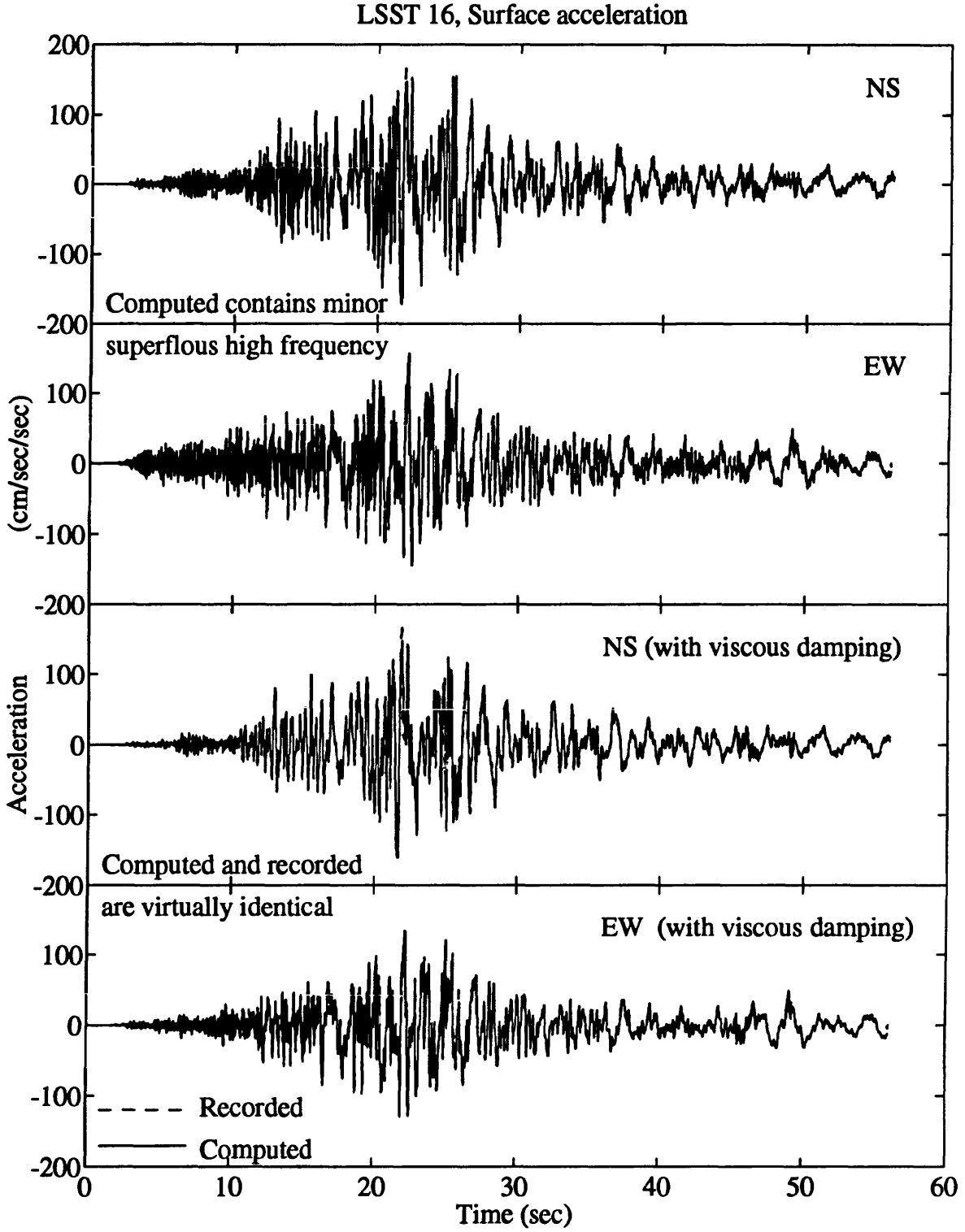

Figure 9: LSST 16 computed and recorded surface acceleration histories (NS and EW).

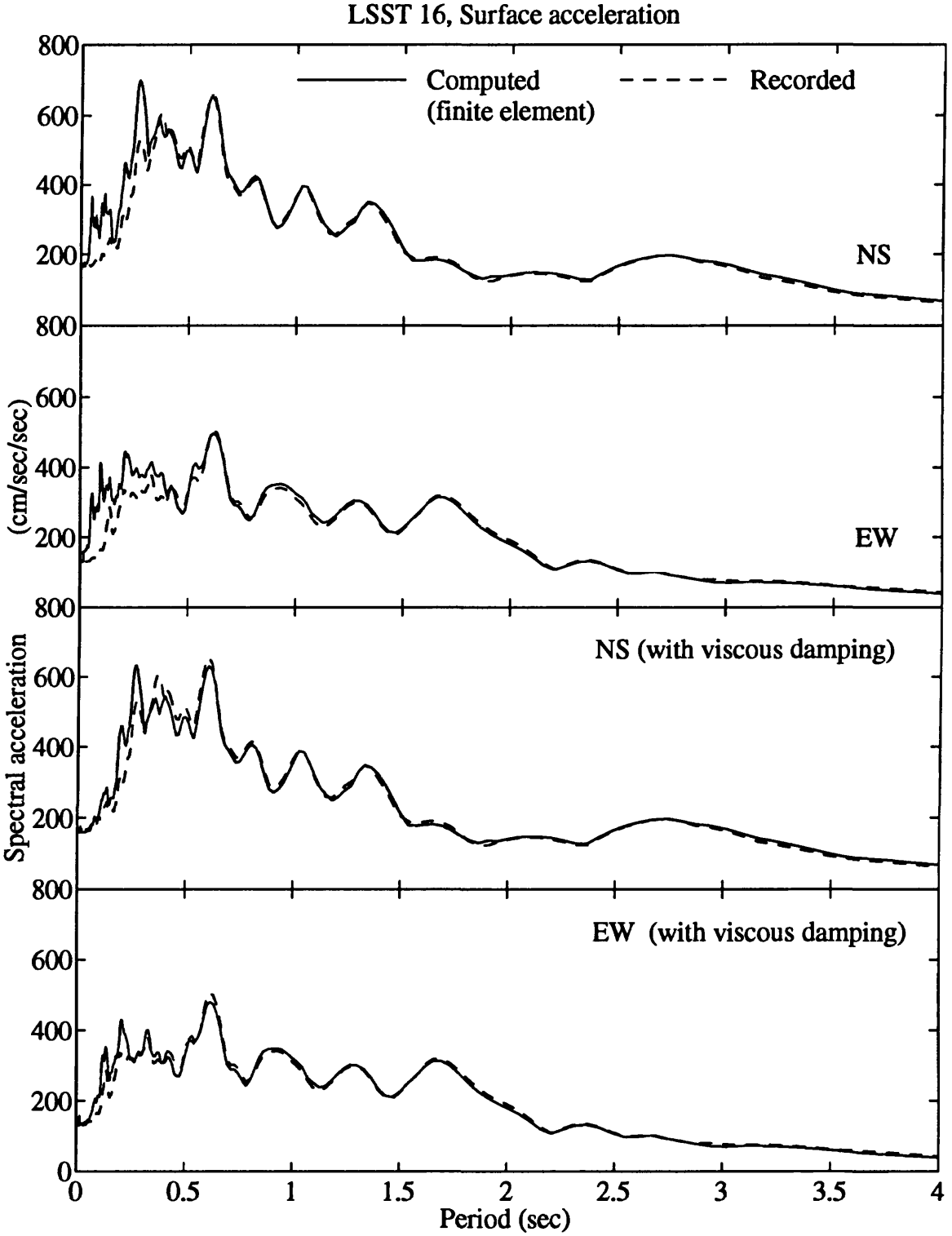

Figure 10: LSST 16 computed and recorded surface acceleration response spectra (NS and EW).

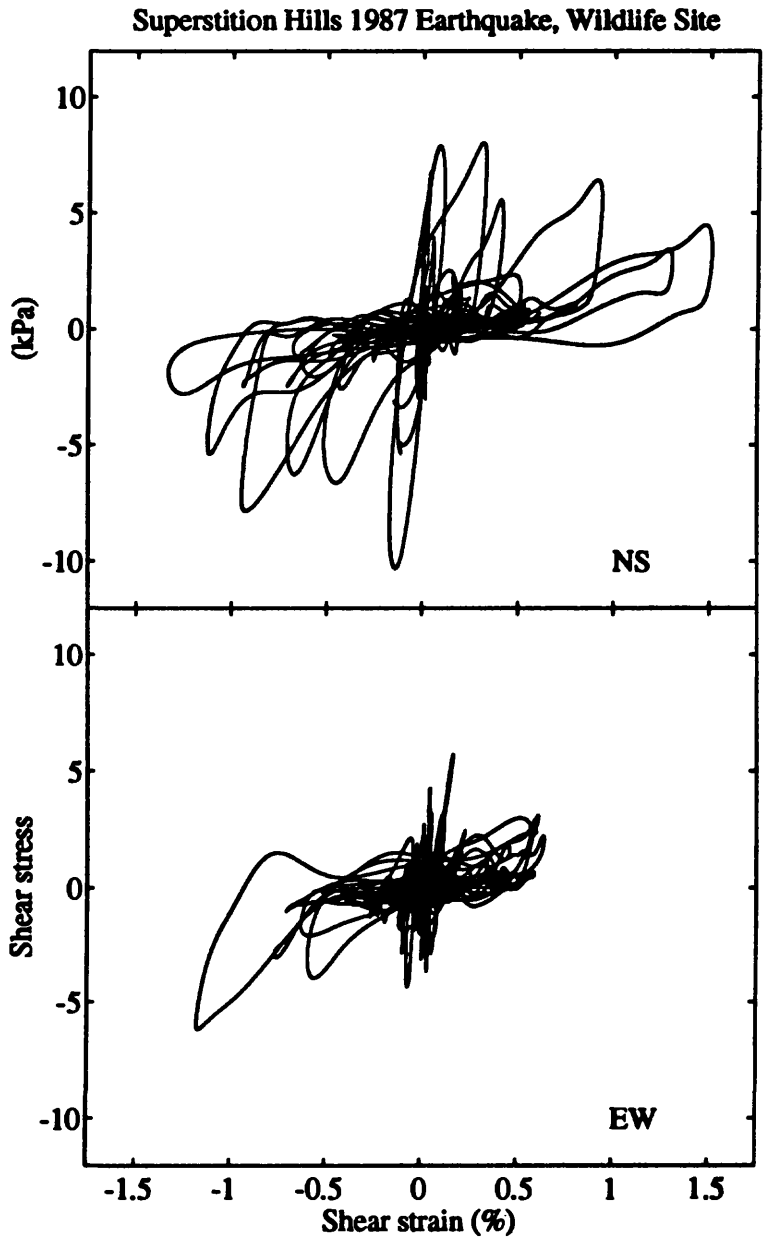

Figure 11: Wildlife site EW and NS shear stress-strain histories at 2.9 m depth during the 1987 Superstition Hills earthquake.

National and Regional Seismic Hazard Maps
9950-10025

A. Frankel, D. Perkins, E.V. Leyendecker, P. Thenhaus
S. Hanson, N. Dickman, M. Hopper

Branch of Earthquake and Landslide Hazards
U.S. Geological Survey
MS 966, Box 25046
Denver Federal Center
Denver, CO 80225
(303) 273-8556; email: afrankel@gldesg.cr.usgs.gov

Program goal: III

Investigations

1. We are preparing new national seismic hazard maps to be included in the 1997 edition of the NEHRP Recommended Provisions for the Development of Seismic Regulations for New Buildings. We are conducting a series of regional workshops to gather input for the new national maps and to get feedback on methodologies. These workshops are attended by USGS and non-USGS scientists as well as structural engineers and other users. We held workshops in the Pacific Northwest and the northeastern U.S. in FY 94.
2. We are preparing regional seismic hazard maps for selected urban areas.

Results

1. We developed a new methodology for constructing hazard maps for the central and eastern U.S. This methodology uses a multiple-model approach, where two of the models are based on spatially-smoothed representations of historical seismicity and the third model is a broad background zone. This methodology was endorsed by most participants of the northeastern U.S. workshop. Results from this new methodology were compared to results of the EPRI study for nuclear power plants. We found good agreement between the two methods, when the same attenuation relations were used for peak acceleration.

2. Preliminary hazard maps were produced for the central and eastern U.S. and northern California.

3. We prepared seismic hazard maps for the San Francisco Bay region and the San Bernardino Valley, incorporating site amplification based on surficial geology and recurrence rates based on fault slip rate data.

4. Interim seismic hazard maps were prepared for the 1994 edition of the NEHRP Provisions. These maps use the same source zones as the maps in the 1991 edition, except for a higher rate of M8.25 earthquakes along the Cascadia subduction zone. These interim maps assume that the Cascadia subduction zone is filled by M8.25 earthquakes every 500 years.

Reports

Frankel, A. and D. Perkins, Mapping seismic hazard in the central and eastern United States, abstract for eastern section meeting of the Seismological Society of America, Seismological Research Letters, in press, 1994.

Frankel, A., P. Thenhaus, D. Perkins, E.V. Leyendecker, Ground motion mapping--past, present, and future, in Proceedings of Seminar on New Developments in Earthquake Ground Motion Estimation and Implications for Engineering Design Practice, ATC 35-1, Applied Technology Council, Redwood City, CA, 40pp., 1994.

Frankel A., P. Thenhaus, D. Perkins, E.V. Leyendecker, New directions in the USGS national earthquake hazard assessment project, Proceedings of 5th U.S. National Conference on Earthquake Engineering, v. IV, pp. 599-608, 1994.

Frankel A. and P. Thenhaus, Regional seismic hazard maps incorporating linear and nonlinear site amplification, EOS, v. 75, p. 235, 1994.

Leyendecker, E.V., S.T. Algermissen, A. Frankel, Use of spectral response maps and uniform hazard response spectra in building codes, Proceedings of 5th U.S. National Conference on Earthquake Engineering, v. IV, pp. 379-388, 1994.

Perkins, D. and S. Hanson, Pacific Northwest probabilistic hazard maps for various recurrences of large subduction zone earthquakes, EOS, v. 74, p. 434, 1993.

Thenhaus, P., A. Frankel, S. Hanson, S.T. Algermissen, Ground-motion hazard in the San Francisco Bay area from models of fault segmentation and slip-based recurrence estimates, EOS, v. 74, p. 434, 1993.

Seismic Hazard Maps and Prediction of Ground Motions for the San Bernardino Valley

9950-11355

A. Frankel, P. Thenhaus, A. Rogers, S. Hanson, J. Tinsley, J. Gibbs,
L. Wennerberg, H. Benz

Branch of Earthquake and Landslide Hazards
U.S. Geological Survey
MS 966, Box 25046
Denver Federal Center
Denver, CO 80225
(303) 273-8556; email: afrankel@gldesg.cr.usgs.gov

Program goal: III

Investigations

1. Develop seismic hazard maps for the San Bernardino Valley incorporating site amplification.
2. Predict site-specific time histories of ground motions for hypothetical large earthquakes along the San Andreas fault.
3. Analyze seismograms of aftershocks of the Landers-Big Bear earthquakes recorded in the San Bernardino Valley by dense arrays.

Results

1. New probabilistic and deterministic seismic hazard maps were produced for the San Bernardino Valley, including site amplification. Recurrence rates of large earthquakes were based on geologic slip rates.
2. Time histories were determined for downtown San Bernardino for a magnitude 7 earthquake on the San Andreas fault, by summing and filtering recordings of an aftershock of the Big Bear earthquake using the procedure developed in Frankel (in press).
3. Landers-Big Bear aftershocks were analyzed to determine apparent velocity and direction of propagation using the dense array recordings. The analysis showed the presence of basin surface waves propagating in different directions across the Valley. These surface waves were modeled using 3-D simulations of seismic wave propagation in the San Bernardino Valley. In addition, SmS (critical reflection from crust-mntle interface) phases were analyzed from the aftershock recordings.

4. Acceleration recordings of the Landers mainshock were simulated by summing and filtering recordings of aftershocks using the procedure of Frankel (in press). The simulated and observed records showed good agreement, indicating that this method can be used to predict time histories of future large earthquakes using recordings of nearby small earthquakes.

Reports

Frankel, A., Dense array recordings in the San Bernardino Valley of Landers-Big Bear aftershocks: basin surface waves, Moho reflections, and three-dimensional simulations, Bull. Seism. Soc. Am., v. 84, pp. 613-624, 1994.

Frankel, A., P. Thenhaus, D. Perkins, E.V. Leyendecker, Ground motion mapping--past, present, and future, in Proceedings of Seminar on New Developments in Earthquake Ground Motion Estimation and Implications for Engineering Design Practice, ATC 35-1, Applied Technology Council, Redwood City, CA, 40 pp, 1994.

Frankel A., P. Thenhaus, D. Perkins, E.V. Leyendecker, New directions in the USGS national earthquake hazard assessment project, Proceedings of 5th U.S. National Conference on Earthquake Engineering, v. IV, pp. 599-608, 1994.

Frankel, A., Simulating strong-motion records of the Landers and Loma Prieta earthquakes using aftershock records and constant stress drop scaling, EOS, v. 74, p. 428, 1993.

Frankel A. and P. Thenhaus, Regional seismic hazard maps incorporating linear and nonlinear site amplification, EOS, v. 75, p. 235, 1994.

Frankel, A. and P. Thenhaus, Seismic hazard maps and prediction of time histories of strong ground motions for the San Bernardino Valley, California, Seism. Res. Letts., v. 65, p. 40, 1994.

Frankel, A., Simulating strong motions of large earthquakes using recordings of small earthquakes: the Loma Prieta main shock as a test case, Bull. Seism. Soc. Am., in press.

Earthquake Source Parameters, Site Response, and 3-D Basin Effects in the Portland region

9950-13375

A. Frankel, P. Thenhaus, M. Meremonte, S. Harmsen, L. Wennerberg

Branch of Earthquake and Landslide Hazards
U.S. Geological Survey
MS 966, Box 25046
Denver Federal Center
Denver, CO 80225
(303) 273-8556; email: afrankel@gldesg.cr.usgs.gov

Program goal: III

Investigations

1. Analyze recordings of Scotts Mills earthquake to determine source parameters and site effects.

2. Analyze recordings of aftershocks of the Scotts Mills earthquake to determine source, site, and path effects.

Results

1. Spectral ratios were calculated from seismograms recorded at a site in Portland for the Scotts Mills mainshock and an aftershock. Parameters derived from the spectral ratios at this site indicate a Brune stress drop of about 50 bars for the mainshock.
2. Waveforms of the Scotts Mills earthquake recorded at the Portland site were modeled with a reflectivity program. The recordings exhibit substantial long-period (1-3 sec) energy after the S-wave which is not present in the flat-layered synthetic seismograms. Therefore, this long-period energy probably represents basin surface waves produced by dipping structure at the edge of the Portland Basin.
3. Dense array recordings of Scotts Mills aftershocks were analyzed to determine apparent velocity and back-azimuth of propagation for arrivals in the seismograms.

Seismic Hazard Maps and Site Response Studies for the Central U.S.

9950-14365

A. Frankel, D. Perkins, P. Thenhaus, M. Meremonte, E. Cranswick, T. Bice, D. Overturf, S. Hanson, M. Hopper

Branch of Earthquake and Landslide Hazards
U.S. Geological Survey
MS 966, Box 25046
Denver Federal Center
Denver, CO 80225
(303) 273-8556; email: afrankel@gldesg.cr.usgs.gov

Program goal: III

Investigations

1. Develop new seismic hazard maps for the central U.S.

2. Conduct site response studies in the central U.S. to be used to incorporate site amplification into the seismic hazard maps.

Results

1. A new probabilistic ground-motion map was produced for the New Madrid region using areal source zones and a set of possible locations for the fault(s) that generated the 1811-1812 earthquakes. Seismic hazard curves were computed for Memphis using these new source zones. We also produced hazard maps for the region using a spatially-smoothed representation of the historical seismicity.

2. Three RefTek recorders were deployed in the Memphis region to determine site response on different geologic units. In FY 94, we recorded three earthquakes with magnitudes between about 1.5 and 3. These seismograms are being analyzed to determine site response and source parameters.

Reports

Frankel, A. and D. Perkins, Mapping seismic hazard in the central and eastern United States, abstract for eastern section meeting of the Seismological Society of America, Seismological Research Letters, in press, 1994.

Frankel, A., P. Thenhaus, D. Perkins, E.V. Leyendecker, Ground motion mapping--past, present, and future, in Proceedings of Seminar on New Developments in

Earthquake Ground Motion Estimation and Implications for Engineering Design Practice, ATC 35-1, Applied Technology Council, Redwood City, CA, 40 pp., 1994.

Frankel A. and P. Thenhaus, Regional seismic hazard maps incorporating linear and nonlinear site amplification, EOS, v. 75, p. 235, 1994.

Annual Project Summary

Title: Geotechnical Earthquake Hazard Analysis of the Evansville, Indiana Area.
Award Number: 1434-94-G-2476
Principal Investigator: J. David Frost
Institution: Georgia Institute of Technology
Address: School of Civil and Environmental Engineering, Atlanta, GA 30332
Phone Number: (404) 894-2280
Fax Number: (404) 894-2281
Email: dfrost@ce.gatech.edu
Program Element: III-3

INTRODUCTION

Seismic hazard and risk analyses play a major role in identifying the potential consequences of an earthquake both in relation to existing facilities as well as in the planning and location of new structures. Such analyses must include consideration of several geological and geotechnical hazards and thus of a large number of factors required to describe these hazards. The resulting large databases require an appropriate environment to optimize the evaluation procedures.

Recent advances in computer based Geographic Information Systems (GIS) have provided a technology which is ideally suited to fulfill the needs of earthquake hazard analyses. The overall objective of this ongoing research project is to integrate a variety of analysis procedures for identifying and mapping geotechnical hazards through the use of GIS. The focus of the work is on: (i) the selection and coding of hazard analysis procedures which incorporate the spatial nature of the subsurface data; (ii) the parallel usage of these procedures along with a range of spatial analysis systems in a comprehensive yet flexible framework; and (iii) implementation of the framework in a pilot study to assess the potential for a range of earthquake induced hazards in the Evansville, Indiana area. These phases complement the comprehensive GIS database efforts currently being undertaken by USGS for the New Madrid seismic zone and other areas. Further, the work is intended to build on recent efforts initiated by the Indiana Geological Survey, with support from the Indiana Department of Fire and Building Services, the City of Evansville and the State Emergency Management Agency, to study the soils in the Evansville, Indiana area and predict their likely response during seismic activity in the New Madrid Seismic Zone and the Wabash Valley Fault System.

INVESTIGATIONS UNDERTAKEN

A generalized framework which is reasonably independent of the geographic location is being developed. In this manner, the framework can be readily applied at any other location in the future without requiring the inclusion of significant additional constraints. The modular nature is attractive in that it can be readily updated as analytical procedures are modified and extended or as additional data concerning site and response characteristics becomes available. To date, software has been developed which integrates a GIS (ARC/Info), a geostatistical package (GeoEAS), visualization software (BOSS GMS) and custom algorithms to compute liquefaction potential using both deterministic and probabilistic routines. The structure of the integrated system for geotechnical earthquake/spatial analysis and a dataflow diagram are shown in Figures 1 and 2, respectively. Programming and integration of additional analytical routines to assess the potential for ground motion amplification and/or earthquake induced landsliding is currently being undertaken to extend the functionality of the system. Once the methodology framework has been fully established, a study will be performed at a regional level using a geological and geotechnical database for the Evansville, Indiana area. This area would be subjected to an estimated Modified Mercalli intensity as high as VIII to IX during the occurrence of an earthquake series similar to the 1811-1812 series in the New Madrid seismic zone.

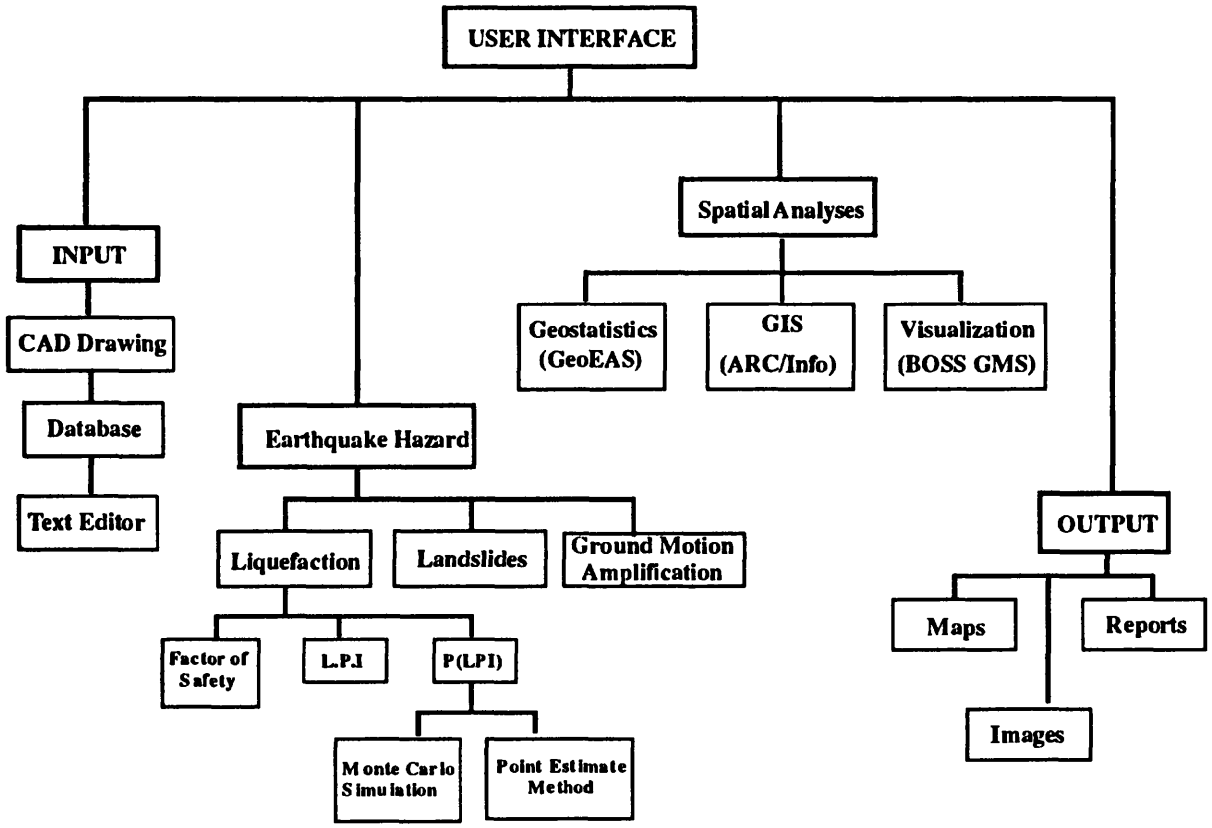

Figure 1 Overview of integrated system for geotechnical earthquake/spatial analysis

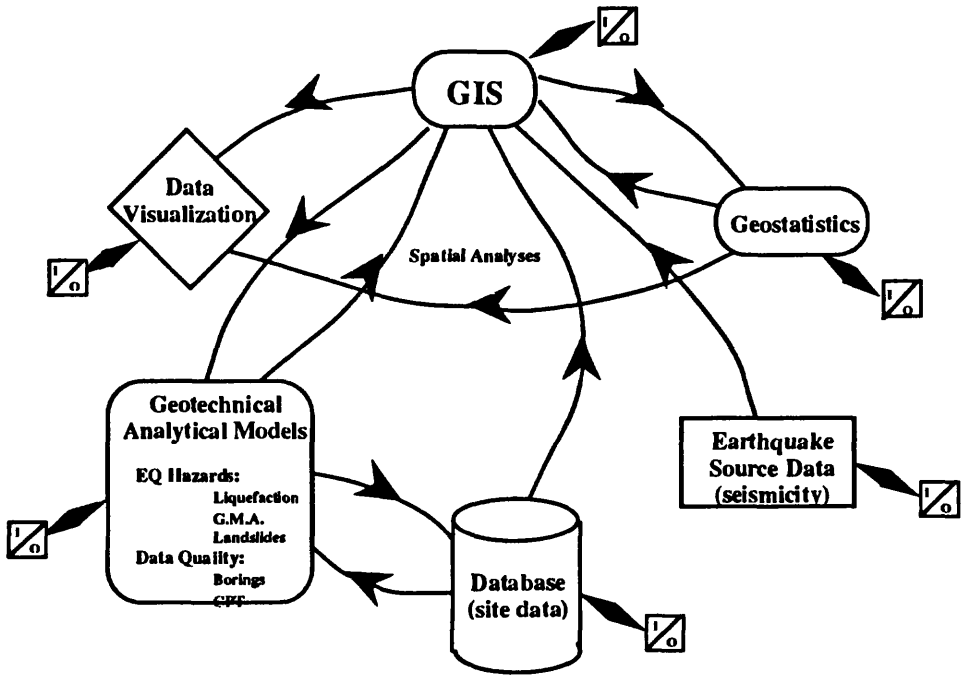

Figure 2 Dataflow in integrated system for geotechnical earthquake/spatial analysis

The geotechnical database is currently under development and is expected to contain some 1,000 individual geotechnical borings and in excess of 100 cone penetration test soundings when completed. These data sources are used to compute a Factor of Safety with respect to liquefaction at various elevations in the boring or sounding and following integration with an appropriate weighting factor, the liquefaction potential index (LPI) is computed as shown in Figure 3. The algorithm to compute a deterministic LPI (see Figure 4) as well as those to compute probabilistic values of LPI using either a Monte Carlo simulation based method or a Rosenbleuth Point Estimate based method have been programmed and verified.

Functionality has also been added to permit the geotechnical database to be queried by a variety of parameters ranging from date of boring to location to consultant. A procedure has been developed to quantify the quality of each boring log based on the information contained in it and any accompanying documentation provided with it. In this manner, it will be possible for future users of the database to make quality based queries about the information in the database also. The routines to quantify the quality of a boring log have been implemented in a spreadsheet for preliminary evaluation. This evaluation has been performed using about 200 borings. Results have indicated that, as expected, there is significant scatter in the quality of data available for use in a geotechnical database and that inclusion of this type of formal quality evaluation routine in the system is mandatory. Development and coding of an algorithm to allow for automated assessment of a boring log quality has been initiated.

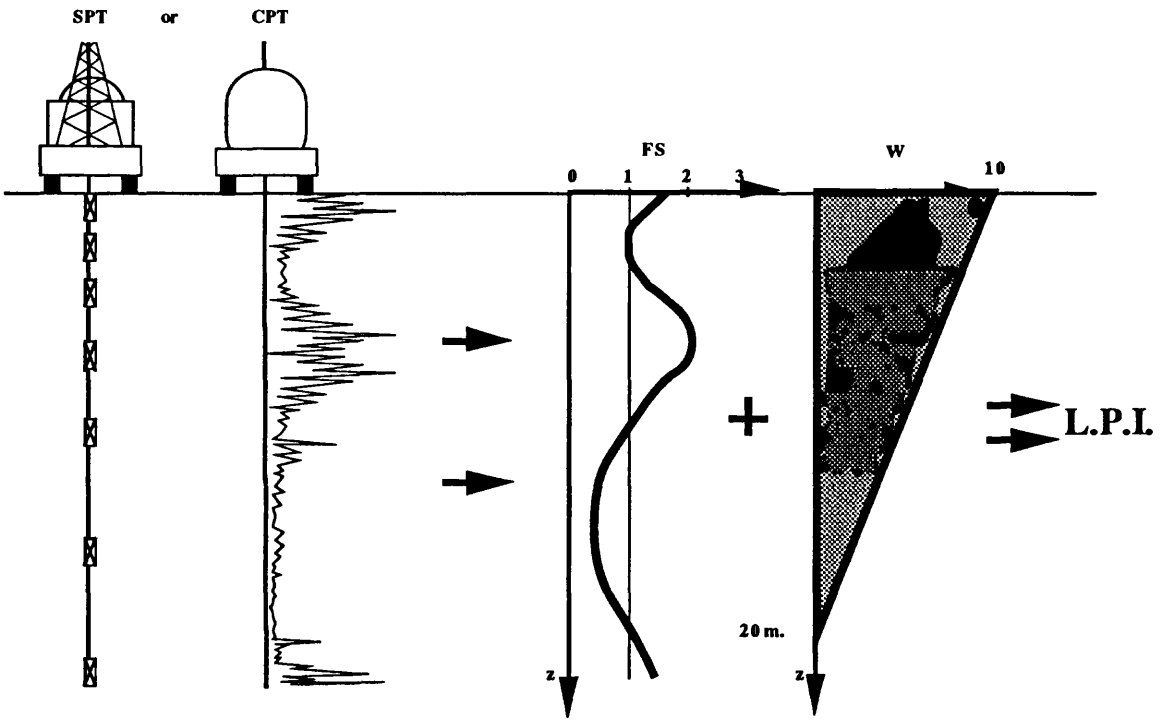

Figure 3 Conceptual graphic representation of Liquefaction Potential Index

REPORTS PUBLISHED

Consideration has been given throughout the development and execution of this project to ensure that the results can be easily disseminated and that the hazard analysis methodology will be readily and economically available to the various agencies which would benefit from

incorporating earthquake hazard analyses into their planning. The strong support expressed by City, County and State officials in the Evansville area for the proposed study, along with the cooperation and commitment of the Indiana Geological Survey attest to the likelihood of a successful transfer of information and technology. Accordingly, while no written reports have been prepared to date since the project is still in the initial development stage, significant effort has already been expended in meeting with representatives from the likely agencies that will benefit from and use the results of this study to solicit their input in designing the overall system and its capabilities and seek their assistance in identifying and accessing data for inclusion in the geotechnical database.

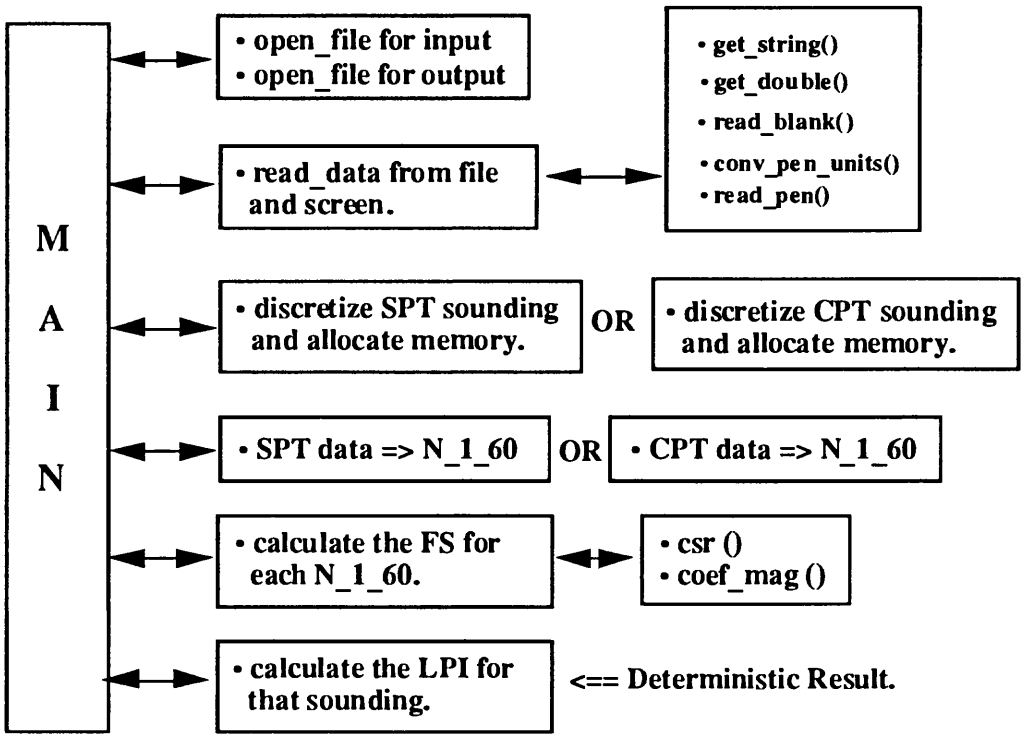

Figure 4 Algorithm to compute Liquefaction Potential Index

Near-Surface Lithologic and Seismic Properties

9930-12293

J.F. Gibbs
W.B. Joyner

Branch of Seismology
U.S. Geological Survey
345 Middlefield Road, MS 977
Menlo Park, California 94025
(415)329-5631 or (415)329-5640
Email Address: gibbs@samoa.wr.usgs.gov

Investigations:

Measurements of seismic velocity and attenuation to determine the effect of local geology on strong ground motion and to aid in the interpretation of seismic source parameters.

Results:

1. We have finished the interpretation of data (seimic velocities and geologic logs) from 30 boreholes drilled at strong-motion stations that recorded significant ground motions during the Loma Prieta Earthquake. These data and results are published in four U S Geological Survey Open-File Reports: Gibbs et al., 92-287, 93-376, 94-222 and 94-552. The last two Open-File Reports contain the results from 14 boreholes at strong-motion station operated by the U.S. Geological Survey.

2. We (with colleague Dave Boore) continue to refine our interpretation of shear-wave Q. A new system being tested at the present time includes a cross-correlation technique for verifying travel-times and using t^* values from observed and synthetic seismograms to determine corrections to be applied to the final Q_s values. We are optimistic that these changes (and perhaps others) will tighten the scatter and improve confidence in the determined values.

Reports:

Gibbs, J.F., D.M. Boore, W.B. Joyner, and T.E. Fumal, The attenuation of seismic shear waves in Quaternary Alluvium in Santa Clara Valley, California: ***Bull. Seis. Soc.*** *Am.* v. 84, no.1, p. 76-90, Feb. 1994.

Gibbs, J.F., T.E. Fumal, and T.J. Powers, Seismic velocities and geologic logs from borehole measurements at seven strong-motion stations that recorded the Loma Prieta, California Earthquake: U.S. Geological Survey *Open-File Report* 94-222.

Gibbs J.F., and T.E. Fumal, Seismic velocities and geologic logs from borehole measurements at seven strong-motion stations that recorded the 1989 Loma Prieta, California earthquake, Part IV: U.S. Geological Survey *Open-File Report* 94-552.

SIMULATING THE 3D BASIN RESPONSE IN THE PORTLAND AND PUGET SOUND REGIONS FROM LARGE SUBDUCTION ZONE EARTHQUAKES

ANNUAL PROJECT SUMMARY
AWARD: 1434-93-G-2327

Robert W. Graves
Woodward-Clyde Federal Services, 566 El Dorado St., Pasadena, CA 91101
PH: (818) 449-7650 / FAX: (818) 449-3536 / Email: rwgrave0@wcc.com

PROGRAM ELEMENT III.2: *Predict Strong Ground Shaking*

Investigations Undertaken

The objective of this project is to understand the effect of lateral variations in shallow crustal structure on expected strong ground motions in the Pacific Northwest from subduction zone earthquakes. This work begins with an analysis of strong motion recordings from the 25 April 1992 Cape Mendocino earthquake and its aftershocks as observed in the epicentral region. Although this event did not produce strong motions in Portland or Puget Sound, the fault geometry and slip mechanism are consistent with motion along the Cascadia plate interface, making it the first recorded subduction-type event in this region. In addition, the presence of strong motion recording stations within the Eel River basin provides the opportunity to test the procedure for modeling the long-period (1 to 10 sec) basin response for shallow subduction zone earthquakes.

Strong ground motions are simulated using an interfacing technique which couples the analytic response from a finite fault with a 3D finite-difference calculation for the basin response. The simulation technique has been tested against the Cape Mendocino earthquake data. Currently, we are calculating the long-period basin response in the Portland and Puget Sound regions from hypothetical earthquakes on the Cascadia subduction interface. Slip models and hypocenter locations will be varied to test the basin response to asperity distribution and directivity effects. The intended products of these simulations will include maps of the ground motion response throughout the Portland and Puget Sound regions for various earthquake scenarios, as well as maps showing the expected durations of strong ground motion in these regions for each of the simulated events.

Results

At long-periods ($T > 1$ sec), the strong ground motions in the epicentral region of large earthquakes are controlled primarily by deterministic features of the earthquake source and seismic wave propagation. Many times, earthquakes occur in regions of complicated geology and wave propagation through these variable geologic structures can significantly affect the observed strong ground motions, particularly at periods greater than 1 sec. For example, Vidale and Helmberger (1988) demonstrated that the long-period (1-10 sec) strong ground motions recorded in the Los Angeles region during the 1971 San Fernando earthquake were dominated by surface wave energy that was generated by seismic waves trapped within the San Fernando and Los Angeles basins.

In the case of the Cape Mendocino event, we face a similar problem in separating source and wave propagation effects in the observed data. Strong motion recording sites at Petrolia (petr), Cape Mendocino (capm), and Bunker Hill (bunk) are all located on hard rock directly above the fault plane (Figure 1), and much of the waveform information in these records is related to the details of the earthquake source. Further to the north, several other strong motion recording stations are located atop the sediments of the Eel River basin (Figure 1). This structure is a southeast-northwest trending river valley with sediments reaching depths of about 3 km. In general, the basin site recordings are richer in long-period and exhibit much longer durations of shaking than the hard rock recordings, as shown in the top right panel of Figure 1. In order to explain these data we have used a combination of numerical simulation and modeling techniques to derive a variable-slip rupture model of the event, and also investigate wave propagation effects related to the structure of the Eel River basin.

Cape Mendocino Variable-Slip Rupture Model

Based on the teleseismic focal mechanism and the distribution of aftershocks (see Oppenheimer et al., 1993), we have constrained our fault model to have a strike of 350°, a dip of 14° to the northwest, a rake of 105°, a length along strike of 32 km, a down-dip width of 32 km, and a depth to the top edge of the fault plane of 4.2 km. The midway point of the top edge is located at 40.357° N and 124.494° W. The surface projection of this fault area is shown by the shaded region in Figure 1. We have used a moment of 3.0×10^{26} dyne-cm (M_w=7) in our calculations. Given these constraints, our primary objective is to find the distribution of slip across the fault plane, which adequately explains the observed strong ground motions at stations bunk, capm, and petr.

Using a uniform slipmodel as a starting point, we used an iterative trial and error modeling procedure to obtain our preferred variable-slip rupture model, which is displayed in the bottom left panel of Figure 1. The ground velocities computed for this model are compared with the observed records in the bottom right panel of Figure 1. By using the variable-slip rupture model, we can produce ground motions which provide a very good match to the timing, waveform, and amplitude of most of the observed motions.

The variable-slip rupture model shown in Figure 1 is has a concentrated region of large slip located near the hypocenter. Maximum slip values are about 8.5 m and the distribution of slip is consistent with rupture directivity to the southwest as reported by Ammon et al. (1993). A significant amount of slip must occur near the hypocenter, in order to match the absolute timing of the records at capm and petr. In addition, the short duration, simple pulses observed at these sites also indicate that most of the energy was released from a single asperity location. The northern portion of the fault plane has relatively low slip values (less than 2 m of displacement), although this is somewhat less well constrained due to the lack of absolute timing at station bunk. We have assumed that the large arrivals observed at bunk originated near the hypocenter.

3D Numerical Simulations in the Eel River Basin

In order to model the seismic response of the basin structure, we use a hybrid simulation technique which couples the far-field, analytic S-wave response of a finite-fault with a 3D elastic, staggered-grid finite-difference (FD) modeling algorithm (Graves, 1994). The model space used in the FD computations is 20 km wide, 20 km long, and extends to a depth of 5 km. Using a grid spacing of 0.2 km, we obtain accurate results for frequencies up to 1 Hz in the lowest

velocity regions of the model. We have also included Q in the FD calculation, using the technique presented in Graves (1994). Shear wave Q values of 40 and 80, respectively, were used for the two layers of basin sediments, and a value of 150 was used for the basement rock.

The strong motion data for the Eel River basin sites (cent, fern, fort, frtn, lolt) appear to be richer in long period energy and shows longer durations than the data from the hard rock sites, indicating wave interactions with the structure of the basin. These effects are quite evident when the data is viewed along a profile extending to the north of the source region (Figure 2, top left panel). In this figure, the data are plotted as a function of increasing epicentral distance. The closest site (bunk) is located on hard rock, and the remaining sites extend across the basin. A series of large amplitude later arrivals, with slow apparent velocity are clearly seen in the basin site recordings. Timing lines have been superimposed on this figure to help facilitate identification of these arrivals and it is evident that these later arriving waves did not originate at the source, but were generated near station cent, at the near-source margin of the basin.

The bottom left panel of Figure 2 displays profiles of synthetic ground velocities calculated using the 3D model of the basin structure for the six recording sites. The timing lines superimposed on these profiles are the same as those shown for the observed data in the top left panel of this figure. It is clear from this simulation that the large amplitude, late arrivals observed at the basin sites are related to the 3D response of the basin structure. We interpret these arrivals to be surface waves which are generated from the conversion of body wave energy at the southern margin of the basin. These surface waves propagate northward across the basin with relatively slow apparent velocity, leading to the long durations and large amplitudes that are seen in the ground motion recordings.

A more detailed comparison between the simulated and observed ground motions is shown in the right panel of Figure 2. In general, the synthetic motions are in very good agreement with the amplitude, waveform, and duration of the observed records. The poorest fit is at station bunk; however, since this site is very close to the fault plane (see Figure 1), the far-field source representation used in the simulation is probably not appropriate. For the horizontal components of motion, the synthetics are in excellent agreement with the response recorded at the basin sites. In both the synthetic and observed records, the basin generated surface waves are more dominant on the east-west component of motion than on the north-south component. Due to the relative geometry of the source location with the structure of the basin, and the general northward propagation of energy across the basin, we conclude that these surface waves are primarily comprised of horizontally polarized shear waves (SH energy). Our technique tends to overpredict the amplitude of the vertical component records, probably as a result of using a relatively high near-surface shear velocity (v_s = 1.0 km/sec).

Puget Basin Simulations

Due to the lack of recorded strong motions for subduction events in the Puget Sound region, other means have been employed to derive estimates of expected ground motions for future large earthquakes. For example, empirical attenuation relations have been developed using data from other large subduction zone earthquakes (eg. Youngs et al., 1988; Crouse, 1991). However, using these relations to estimate ground motions in the Pacific Northwest requires the assumption that the source and wave propagation characteristics of the Cascadia region are similar to those of other subduction zones.

Long-period ground motions can be simulated in the basin environments of the Pacific

Northwest using the hybrid technique discussed in the previous section. As part of our first year's work, preliminary simulations have been performed in the Puget Sound region for a hypothetical M_w 8 subduction zone event. We have used the fault model which is shown in Figure 3. The fault is divided into 36 subfault elements, each with dimensions of 25 km × 20 km. Weights are applied to each of the subfaults to model the effects of heterogeneous slip across the fault plane. For these simulations, we have modeled a 40 km × 40 km area of the Puget basin centered on the city of Seattle (Figure 3). The basin reaches its maximum depth of just over 1 km near downtown Seattle.

Figure 4 compares synthetic ground velocities computed using our hybrid modeling technique for a plane-layer velocity model with those obtained using the basin velocity model. These motions are for a site located on the southeast margin of the basin structure. At very long periods (5-20 sec), the ground motions for both velocity structures are similar and are dominated by the earthquake source. However, at shorter periods (1-5 sec), the basin response shows much more complexity than the plane-layer response. These complex waveforms result from the trapping and focusing of 1-5 sec period energy within the basin structure. Due to the relatively shallow nature of the Puget basin, we expect that the ground motions in these structures will be most sensitive to these shorter periods. In addition, this suggests that the basin response will also be sensitive to source effects such as directivity, slip duration and rupture velocity, which are known to be important contributors to the ground motion response in this period range. These issues will be specifically addressed during the remainder of this project.

Reports Published

Graves, R. W. (1994). Simulating the 3D basin response in the Portland and Puget Sound regions from large subduction zone earthquakes, *USGS Annual Technical Report*, 35 pp.

References

Ammon, C. J., A. A. Velasco, and T. Lay (1993). Rapid estimation of rupture directivity: Application to the 1992 Landers (M_s=7.4) and Cape Mendocino (M_s=7.2), California earthquakes, *Geophys. Res. Lett.*, **20**, 97-100.

Crouse, C. B. (1991). Ground motion attenuation equations for earthquakes on the Cascadia subduction zone, *Earthquake Spectra*, **7**, 201-236.

Graves, R. W. (1994). Simulating wave propagation in 3D elastic media using staggered-grid finite-differences, *manuscript in preparation.*

Oppenheimer, D., G. Beroza, G. Carver, L. Dengler, J. Eaton, L. Gee, F. Gonzales, A. Jayko, W. H. Li, M. Lisowski, M. Magee, G. Marshall, M. Murray, R. McPerson, B. Romanowicz, K. Satake, R. Simpson, P. G. Somerville, R. Stein, and D. Valentine (1993). The Cape Mendocino, California earthquake sequence of April, 1992: Subduction at the triple junction, *Science*, **261**, 433-438.

Vidale, J. E., and D. V. Helmberger (1988). Elastic finite-difference modeling of the 1971 San Fernando, California earthquake, *Bull. Seism. Soc. Am.*, **78**, 122-141.

Youngs, R. R., S. M. Day and J. L. Stevens (1988). Near field ground motions on rock for large subduction earthquakes in *Proc. ASCE Conference on Earthquake Engineering and Soil Dynamics II: Recent Advances in Ground Motion Evaluation*, Geotechnical Special Publication 20, J. Lawrence von Thun (ed.), 445-462.

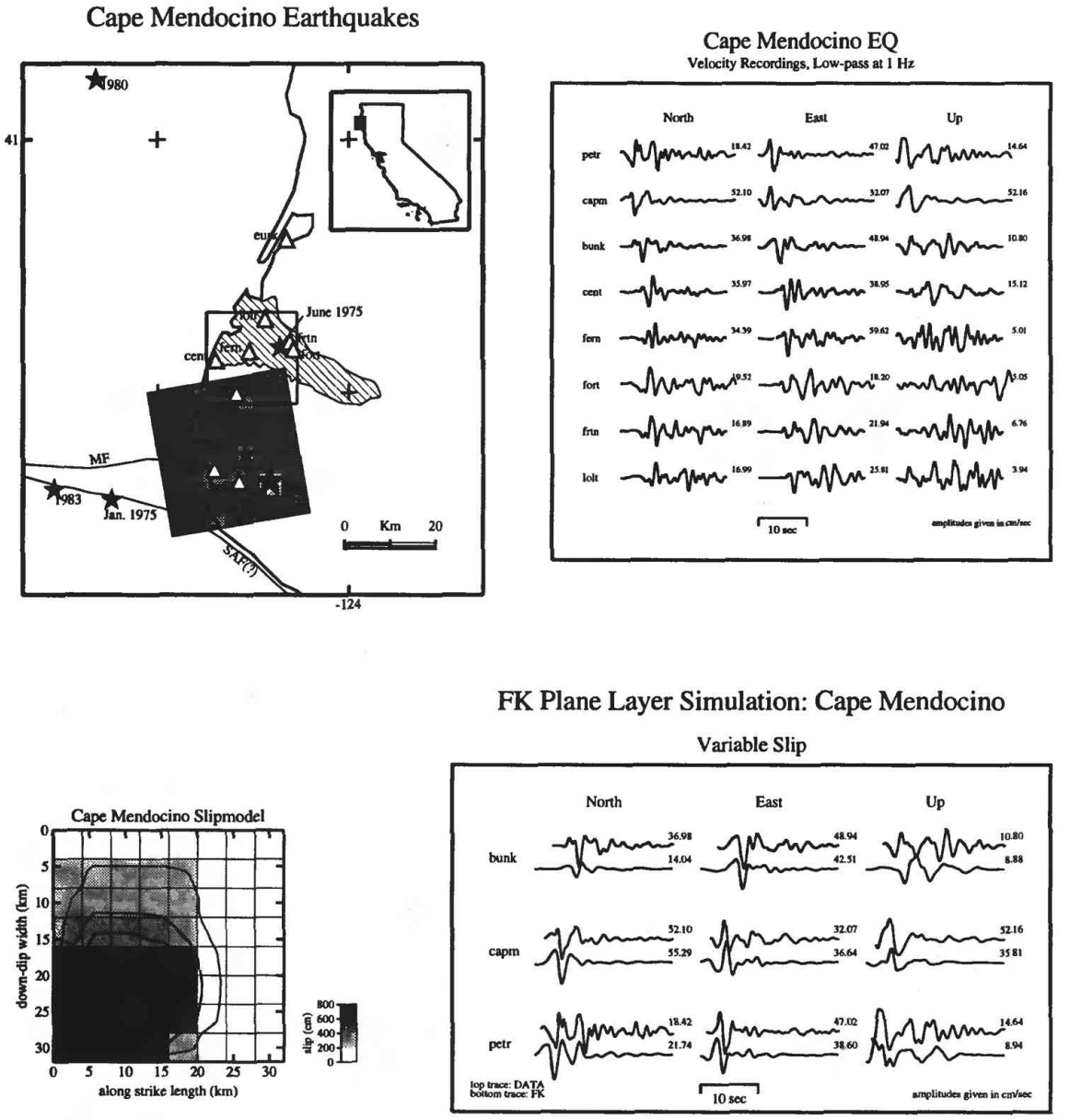

Figure 1: *Top left:* Map showing locations of USGS and CSMIP strong motion recording sites in the Cape Mendocino region. Large star and rectangular shaded region indicate the epicenter and rupture area, respectively, of the 1992 event. The hatched region to the north of the rupture area delineates the Quaternary sediments of the Eel River basin, where several of the strong motion sites are located. The box enclosing these sites depicts the areal extent of the finite-difference model space used in the numerical simulations. *Top right:* Ground velocities (integrated from recorded accelerations) for the strong motion recording sites. These motions have been bandpass filtered in the period range of 1-7 sec. *Bottom left:* Preferred rupture model of the Cape Mendocino earthquake determined from forward modeling. *Bottom right:* Comparison of ground velocities observed at the three near-fault strong motion sites for the Cape Mendocino earthquake with results simulated using the variable-slip rupture model. Both data and synthetics have been low-pass filtered at 1 Hz.

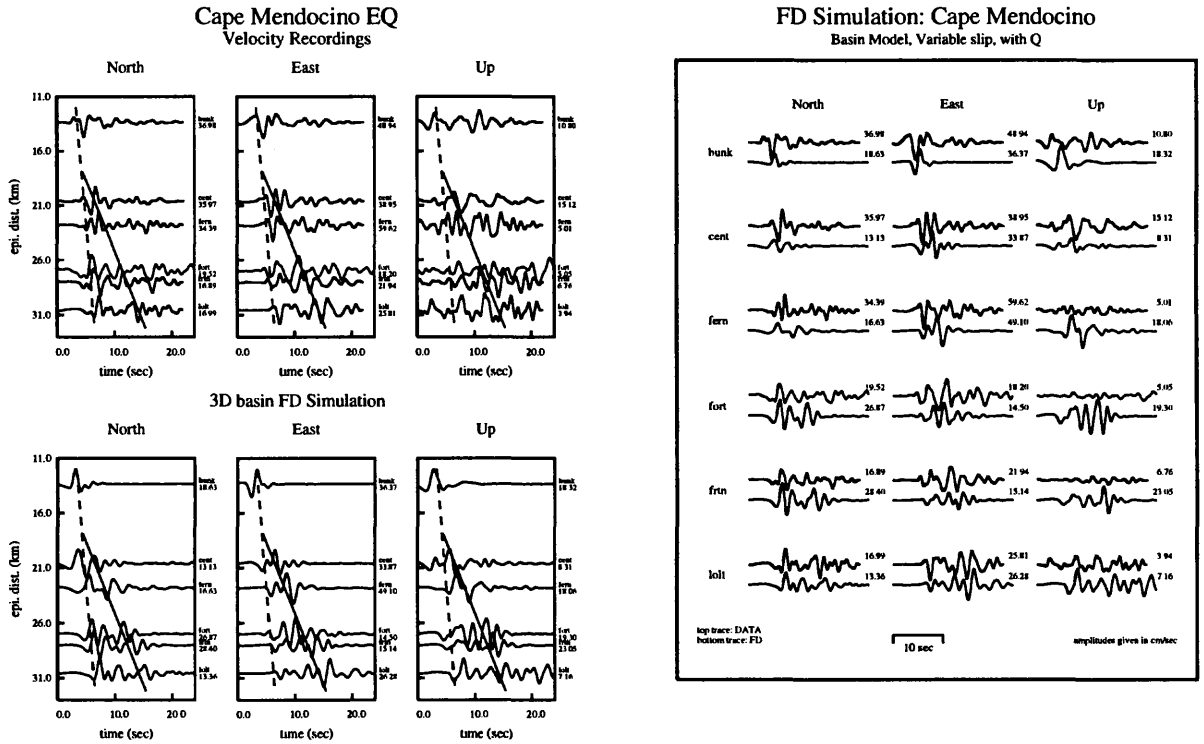

Figure 2: *Top left:* Three-component profiles of filtered ground velocity for the Eel River basin sites. The traces are plotted as a function of increasing epicentral distance. Superimposed on these profiles are timing lines indicating the approximate arrival of the direct S-wave (dashed line) and a later set of arrivals, which are thought to be basin generated surface waves (solid line). *Bottom left:* Three-component profiles of ground velocity computed for the Eel River basin sites using the hybrid FD simulation technique with the basin model shown in Figure 2.7. The traces are plotted as a function of increasing epicentral distance. Superimposed on these profiles are the same timing lines that are shown in the top panel of this figure. *Right panel:* Detailed comparison of observed and simulated ground velocities for the Eel River basin sites. For each pair of traces, the top trace is the data and the bottom trace is the synthetic response calculated for the 3D basin model. Each pair of traces is normalized to the same amplitude.

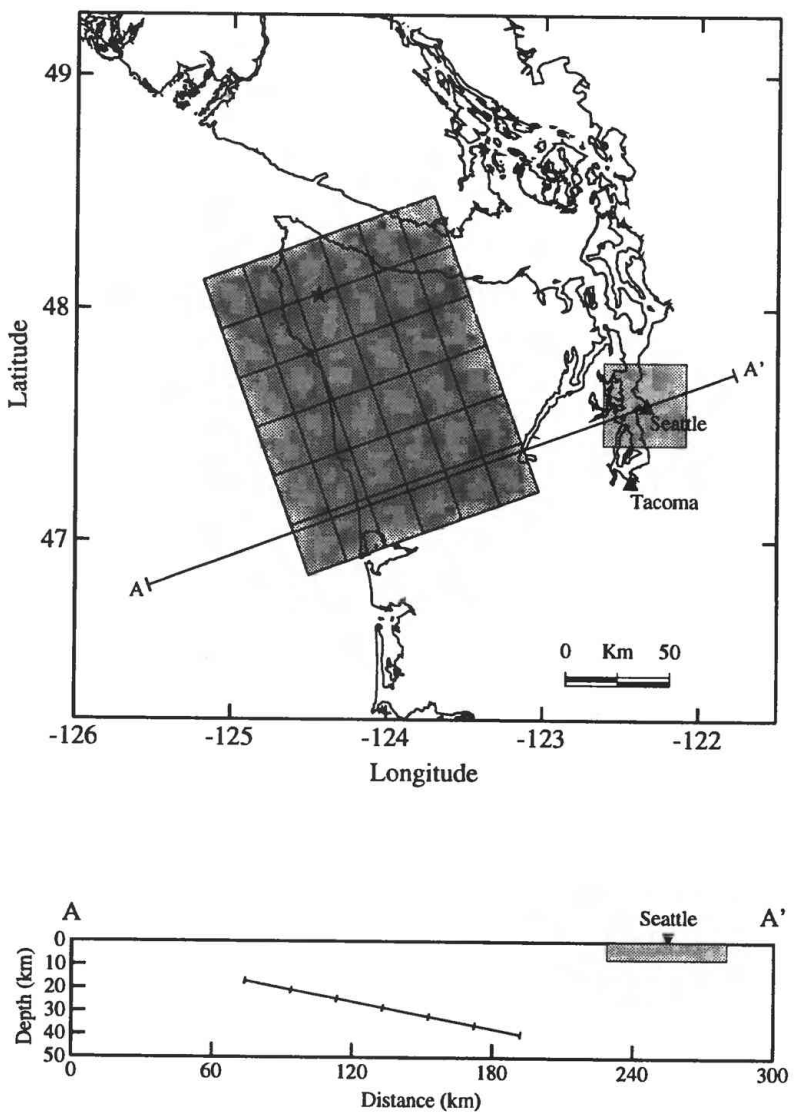

Figure 3: Fault model and geometry for a hypothetical M_w 8 subduction zone event on the Cascadia plate interface in the Puget Sound region.

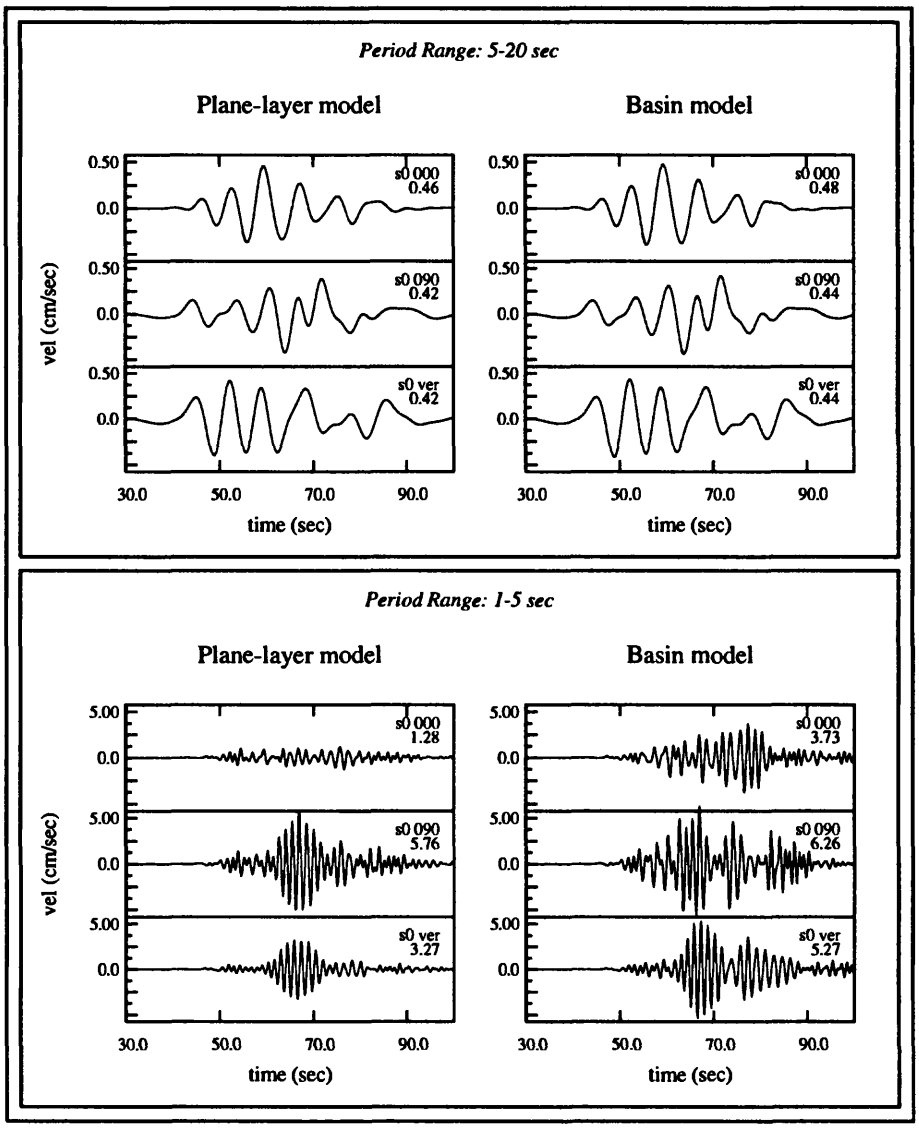

Figure 4: Simulation results for a site in the city of Seattle for the case of plane-layered structure and 3D basin structure. The top panels show the response in the period range 5-20 sec and the bottom panels show the response in the period range 1-5 sec.

LONG-PERIOD BASIN RESPONSE IN DOWNTOWN LOS ANGELES AND LONG BEACH FROM POSTULATED EVENTS ON THE ELYSIAN PARK THRUST AND PALOS VERDES/TORRANCE WILMINGTON FAULT SYSTEM

ANNUAL PROJECT SUMMARY
AWARD: 1434-94-G-2433

Robert W. Graves
Woodward-Clyde Federal Services, 566 El Dorado St., Pasadena, CA 91101
PH: (818) 449-7650 / FAX: (818) 449-3536 / Email: rwgrave0@wcc.com

PROGRAM ELEMENT III.2: *Predict Strong Ground Shaking*

Investigations Undertaken

Recent work has shown that the seismic potential of faults located within the Los Angeles basin is greater than was previously estimated. Many of these newly identified faults are blind thrusts, thus making their exact extent difficult to determine. However, it is reasonable to expect that these structures are capable of producing moderate to large-sized earthquakes. Hazard estimation in this region is further complicated by the presence of laterally varying geology in and around the Los Angeles basin. Previous work using data recorded from the 1971 San Fernando and the 1987 Whittier Narrows earthquakes has shown that wave propagation effects related to the geologic structure of the Los Angeles and San Fernando basins have a significant impact on the observed ground motions, particularly for periods longer than about 1 sec. These studies demonstrated that 2D models of the near-surface geology are required to explain the observed patterns of strong ground motions from these events. In many cases, these basin induced effects dominate the ground motions in the period range 1-10 sec. These effects cannot be reliably predicted using simple plane-layered (1D) models for the near-surface geology.

The aim of this study is to quantify the basin effects by simulating the strong ground motions that may be expected from large earthquakes occurring within the Los Angeles basin. We will concentrate our study on two paths for which strong motion data are available to constrain our calculations. The first involves rupture on the postulated Elysian Park Thrust, located along the northern edge of the Los Angeles basin, and its effects in the communities along the southern edge of the basin (eg., Long Beach). The second case involves rupture on the Palos Verdes Fault, located along the southwest margin of the basin, and its effects in the area near downtown Los Angeles. We consider these scenarios to be of primary importance for the following reasons: 1) both cases involve source/site geometries for which basin induced wave propagation effects should be quite significant; 2) both Long Beach and downtown Los Angeles are areas with large man-made structures (eg., tall buildings, highway bridges, etc.) that are particularly sensitive to long-period (1-10 sec.) ground motions; 3) the liquefaction potential of soils in Long Beach may be increased by the long durations of waves trapped in the basin; and 4) data are available for similar source/receiver geometries (1933 Long Beach and 1987 Whittier Narrows earthquakes), which can be used to validate the simulation procedure.

Ground motions will be simulated using a combination of 2D ray theory and finite-difference techniques, as well as fully 3D finite-difference calculations. The products of these simulations will be maps of the long period (1-10 sec) ground motion response (including wave field time-

slices illustrating complex wave propagation phenomena) and expected durations of shaking for the entire LA basin region. We will also provide a detailed comparison of the results for selected sites in downtown Los Angeles and the harbor area of Long Beach, which may be particularly sensitive to long period ground motions. We will characterize the calculated ground motions in terms of peak velocity, response spectral velocity in the period range of 1-10 sec, and duration of shaking. In addition, we will compare the values obtained from the 3D basin models with values calculated using a 1D velocity model of the Los Angeles basin, and evaluate the difference that inclusion of 3D effects makes to the ground motion estimates. These results will also be compared with ground motion values estimated from commonly used attenuation relations, as well as estimates of amplification factors derived from mapped variations in surface geology and microtremor analyses.

Results

Our work to date has concentrated on the analysis and modeling of data recorded from the 1994 Northridge earthquake. Although this event did not produce damaging motions in downtown Los Angeles or Long Beach, it is directly relevant to this project because the event occurred on a blind thrust fault located in the LA metropolitan region, and significant basin response effects are apparent in the ground motions recorded at sites in the Los Angeles basin. In addition, the abundance of high quality strong motion data from this event gives us the opportunity to test our procedures for modeling wave propagation within laterally varying media, as well as to develop and constrain structural models of the subsurface geology in the Los Angeles region.

The Northridge earthquake occurred on a blind thrust fault located beneath the San Fernando Valley, about 25 km northwest of downtown Los Angeles (Figure 1). This event was widely recorded at strong ground motion observation sites located throughout the Los Angeles metropolitan region. Figure 2 (left panel) shows a profile of strong motion velocity records from this event for sites along an azimuth extending to the southeast from the epicentral location. The nearest sites, shrm and scrs, are located at the margin of the San Fernando basin and in the Santa Monica Mountains, respectively, with the remainder of the sites extending across the Los Angeles basin. At the near-source locations, the strong motion records are dominated by two large S-wave arrivals (indicated by the dashed line pairs), which can be modeled as arrivals from separate source subevents. The recorded waveforms become increasingly more complex at greater distances (beyond about 25 km), showing multiple sets of arrivals with slow apparent velocities and extended durations. For periods greater than 1 sec, the peak recorded velocities at these sites occur well after the direct S-wave arrivals, and the nature of the recorded waveforms suggests that the ground motions are controlled by basin generated waves.

A significant amount of damage occurred in the northwestern portion of the Los Angeles basin during the Northridge earthquake. In this region, the nature of the recorded ground motions indicates that the basin effects are quite significant, as demonstrated in the right panel of Figure 2. The four sites shown in this figure are all within a few kilometers of one another, but the ground motions recorded at the three basin sites (bald, lacn, and smch) are quite different from the rock site recording (scrs). Ground motions at the basin sites are controlled by late-arriving phases, with extended durations of shaking, which are indicative of basin generated waves. It is quite possible that these large amplitude arrivals, as well as the extended durations, contributed to the structural damage at sites in Santa Monica and at the I-10 freeway collapse.

The map in Figure 1 shows the generalized geology of the Los Angeles region, along with contours indicating depth to crystalline basement within the basin structures. Both the San Gabriel and San Fernando basins reach depths greater than 3 km, and the Los Angeles basin extends past 9 km in depth (Davis et al., 1989). For our numerical calculations, we have taken a 2D cross-section through this model, running from northwest to southeast through the hypocenter of the Northridge earthquake. Since our primary interest is to investigate the ground motion response in the northwest portion of the Los Angeles basin, we have not included the structure of the San Fernando basin in this model. Due to the relatively deep location of the Northridge source, we anticipate that the structure of the San Fernando basin will probably have little effect on the response in the Los Angeles basin.

The basic structure of our model has two sedimentary layers overlying crystalline bedrock (Figure 3, top panel). Within the Los Angeles basin, the thickness of the sedimentary layers is allowed to vary in proportion to the depth of the underlying basement rock, which reaches a maximum depth of 4 km along this cross-section. In addition to this simple basin model, we have also considered a model which includes several small micro-basins located in the near-surface region of the large-scale basin structure (Figure 3, bottom panel). Although somewhat idealized in our model, these micro-basins are designed to represent near-surface geologic structures such as ancient stream channels or sediment filled depressions (old swamps or marshes), which are present throughout the LA basin. Previous work by Kawase and Aki (1989) and Saikia et al. (1994) have shown that these types of small-scale structures can significantly increase the duration and complexity of the ground motion response within larger sedimentary basins.

For our numerical simulations, we use a fourth-order, staggered-grid differencing algorithm which requires a minimum sampling of five grid points per seismic wavelength in order to avoid the generation of artifacts due to numerical grid dispersion (phase velocity error less than 1%) (Levander, 1988). The models were discretized with a grid spacing of 0.125 km, and using the above criterion, we have adequate grid sampling down to 1 sec period for energy propagating within the lowest velocity regions of the model (V_s = 0.65 km/s).

Figure 4 shows the computed SH response along a profile of stations for a flat-layer model (left panel), the simple basin model (middle panel) and the large-scale basin plus micro-basins model (right panel). The flat-layer model was designed to match the general nature of the geologic structure beneath the northwest portion of the LA basin (see Table 1). The calculated response for this model is dominated by the direct S arrival for all stations in the profile. Following the direct S wave, a series of lower amplitude arrivals are apparent, particularly for sites close to the epicenter. These later arrivals result from multiple reflections generated within the near surface layers of the model. Since the model is laterally homogeneous, these arrivals will always have lower amplitudes than the direct arrival. For the simplified basin structure (Figure 4, middle panel), the simulation consists of a single direct S arrival for sites out to about 16 km epicentral distance. Beyond this distance, the underlying sedimentary layers begin to change in thickness and the nature of the ground motion response becomes more complex. As the incident body waves enter the thickening edge of the basin margin, total internal reflection of energy can develop. In this process, the body waves are converted to surface waves which are trapped within the structure of the basin. These surface waves propagate across the basin with slow apparent velocity and little amplitude decay with distance. At sites within the basin, the largest ground motions are controlled by the basin generated waves and not the direct arrival from the source. By including the micro-basins within the large-scale basin structure, the

response becomes even more complicated at the basin sites (Figure 4, right panel). The primary effect of the micro-basin structures is to locally trap and focus seismic energy, generating a series of complex and delayed arrivals at sites near these structures. In addition, the amplitude response becomes quite variable, with differences up to a factor of four in peak response for sites just a few kilometers apart.

From these simulations, we have taken the ground motion response at sites located at the same closest distance from the source as the four west LA observations of the Northridge earthquake shown in Figure 1. These simulated responses are compared with the tangential component of recorded ground velocity in Figure 5. To facilitate comparison with the data, we have convolved each of the synthetics with the motion recorded at the hard rock site scrs. In general, both sets of synthetics from the 2D models match the gross features of the observed data; that is, amplified motions and extended durations at the basin sites relative to the rock site. These waveform features are not predicted by the 1D models because the wave energy incident from below cannot be trapped and amplified within the near-surface layers of the 1D model structure. Thus, the response computed for the 1D models will always be dominated by the direct S arrivals from the source.

In terms of matching the detailed phase and amplitude variations observed in the recorded ground motions, the synthetics from the 2D micro-basin simulation do much better than those computed from the simplified 2D basin model. This match may be somewhat fortuitous in light of the simplistic modeling approach that we have employed; however, it indicates that the presence of both large- and small-scale variations in geologic structure have a significant impact on the ground motion response at these basin sites.

Our preliminary analysis of long-period (1-10 sec) velocity recordings of the 1994 Northridge earthquake indicates the presence of significant basin induced effects in the observed patterns of strong ground motions. For sites located in the Los Angeles basin, the basin generated surface waves comprise the dominant features of the observed response. Numerical modeling of data from the northwest portion of the Los Angeles basin (Santa Monica and vicinity), indicates that a combination of large-scale (deep) and small-scale (shallow micro-basin) structures best explain the observed responses.

References

Davis, T. L. , J. Namson, and R. B. Yerkes, A cross-section of the Los Angeles area: seismically active fold and thrust belt, the 1987 Whittier-Narrows earthquake, and earthquake hazard, *J. Geophys. Res.*, **94**, 9644-9664, 1989.

Duke, C. M., J. A. Johnson, Y. Kharraz, K. W. Campbell, and N. A. Malpiede, Subsurface site conditions and geology in the San Fernando earthquake area, *UCLA-ENG-7260*, School of Engineering, UCLA, Los Angeles, California, 1971.

Fumal, T. E. and J. C. Tinsley, Mapping shear-wave velocities of near-surface geologic materials, *USGS Profess. Pap. 1360*, 127-149, 1985.

Jennings, C. W., R. G. Strand, and R. A. Rogers, Geologic map of California, scale 1:750,000, California Division of Mines and Geology, Sacramento, California, 1977.

Kawase, H. and K. Aki, A study on the response of a soft basin for incident S, P, and Rayleigh waves with special reference to the long duration observed in Mexico City, *Bull. Seism. Soc. Am.*, **79**, 1361-1382, 1989.

Levander, A. R., Fourth-order finite-difference P-SV seismograms, *Geophysics*, **53**, 1425-1436,

1988.

Saikia, C. K., D. S. Dreger, and D. V. Helmberger, Modeling of energy amplification recorded within greater Los Angeles using irregular structure, *Bull. Seism. Soc. Am.*, **84**, 47-61, 1994.

Wald, D. J. and T. H. Heaton, A dislocation model of the 1994 Northridge, California earthquake determined from strong ground motions, *USGS Open-file Report 94-278*, 54 pp., 1994.

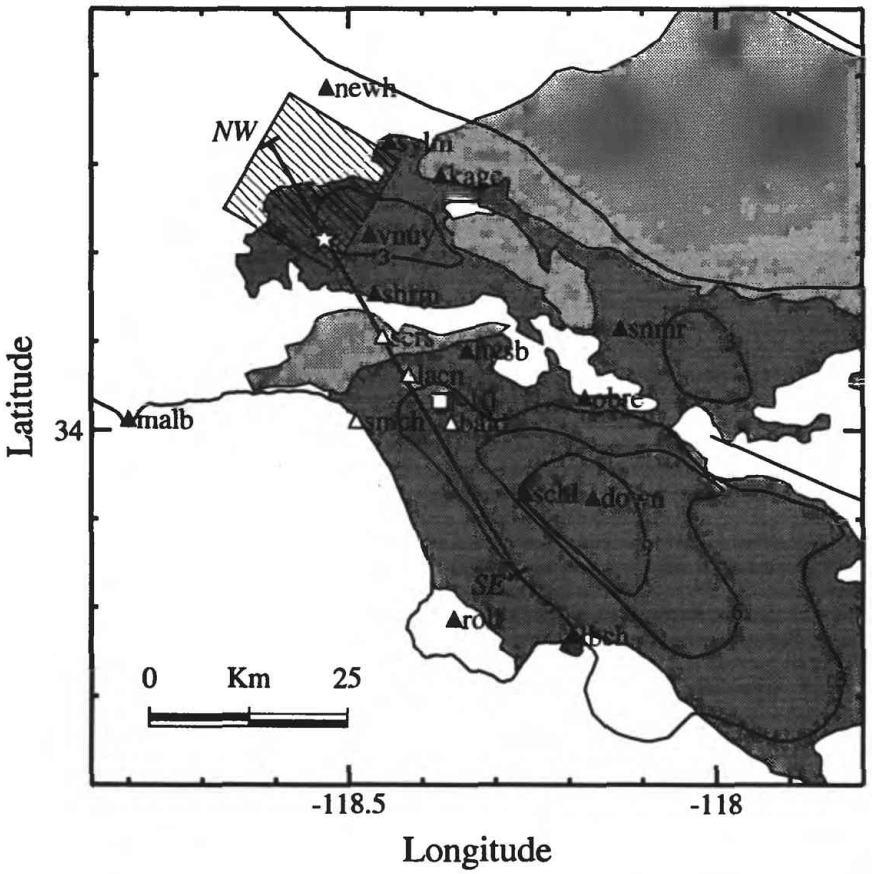

Figure 1: Generalized geologic map of Los Angeles region (after Jennings et al., 1977) showing the location of the strong motion recording sites for which digital data are presently available. Open triangles are sites in the northwest portion of the LA basin which are discussed in the text, and the open square indicates the location of the I-10 freeway collapse. The cross-hatched rectangle delineates the surface projection of the Northridge fault plane of Wald and Heaton (1994), with the open star at the epicentral location. Surface exposure of crystalline basement is shown by light shading; recent alluvial deposits are indicated by dark shading. Contours showing depth to crystalline basement (in km) within the basins are taken from Davis et al. (1989).

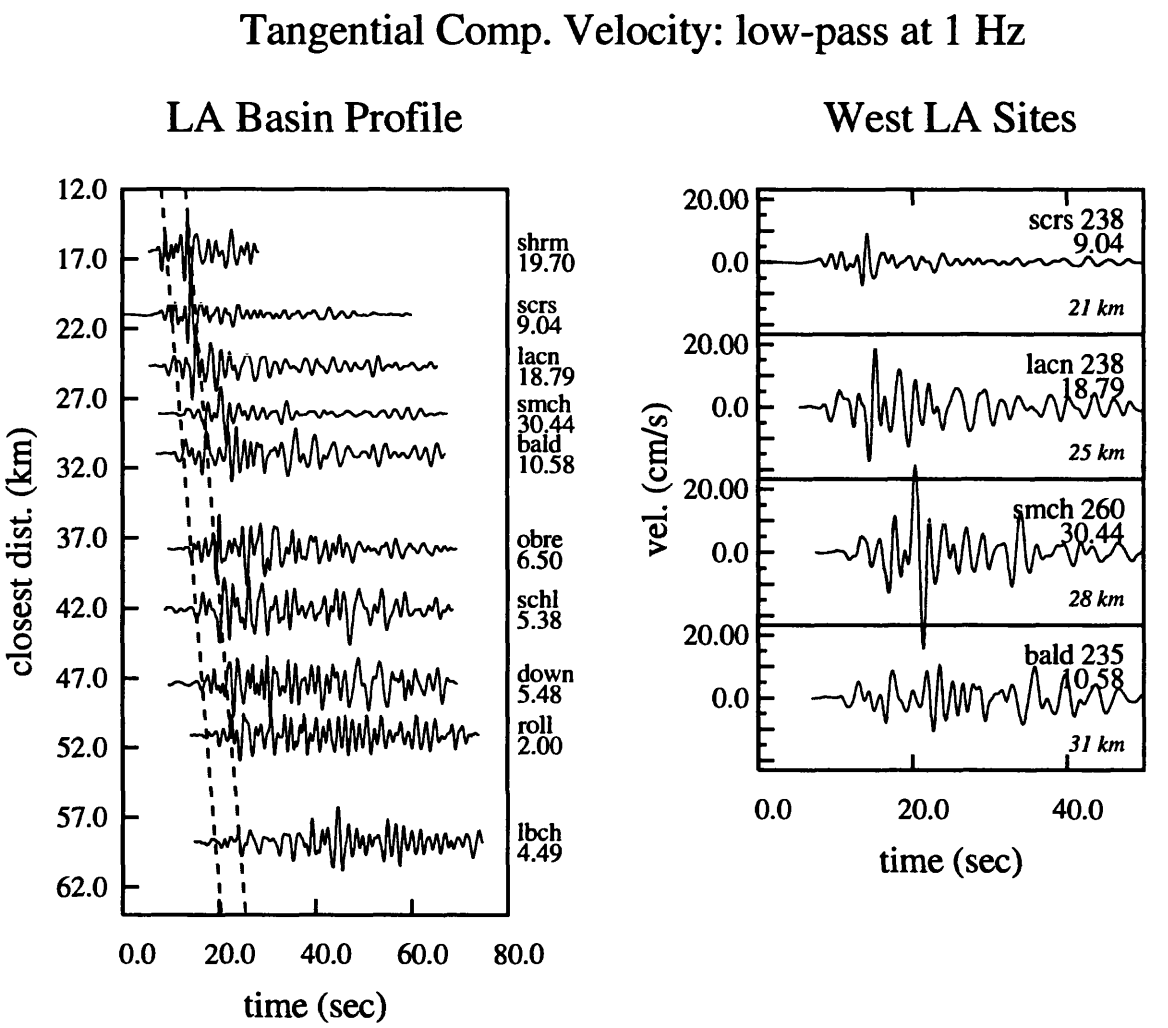

Figure 2: *Left panel:* Profile of tangential component strong motion velocity records for the Northridge mainshock, low-pass filtered at 1 Hz. Sites are located to the southeast of the epicenter, extending across the LA basin. Dashed line pairs indicate separate source subevent arrivals. *Right panel:* Observed velocity response at four sites located in west LA (open triangles in Figure 1). The closest distance to the rupture plane for each of the recording sites is indicated below each trace.

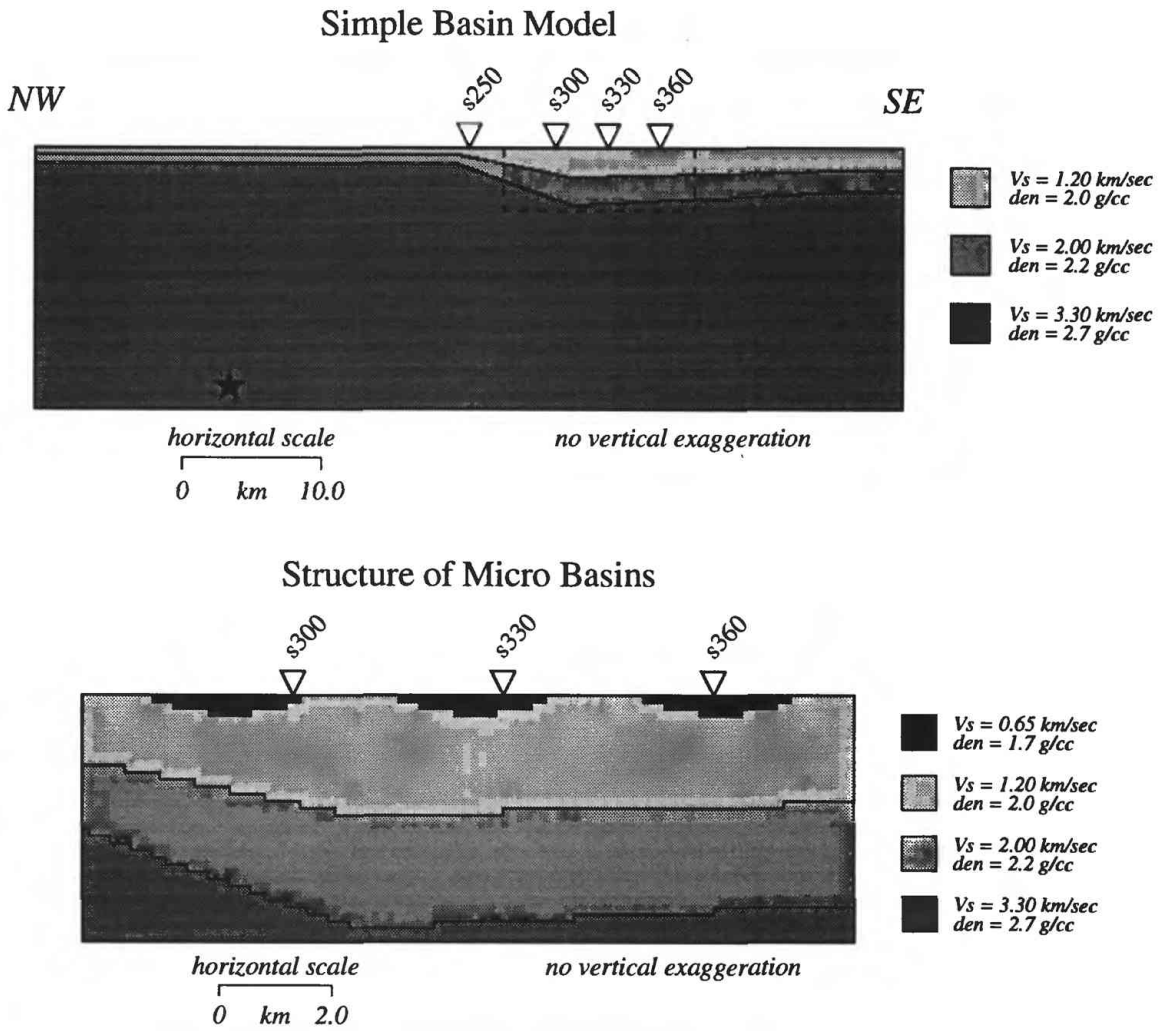

Figure 3: *Top panel:* 2D model cross-section taken along a NW-SE profile from the map shown in Figure 1. Stratigraphy and velocity structure are idealized from Duke et al. (1971) and Fumal and Tinsley (1985). *Bottom panel:* Detailed structure of the micro-basins used in this study. The shear velocity of 0.65 km/sec for the micro basins was chosen to be representative of the range of values (0.2 - 1.6 km/sec) found by Fumal and Tinsley (1985) for the soft, near-surface sediments.

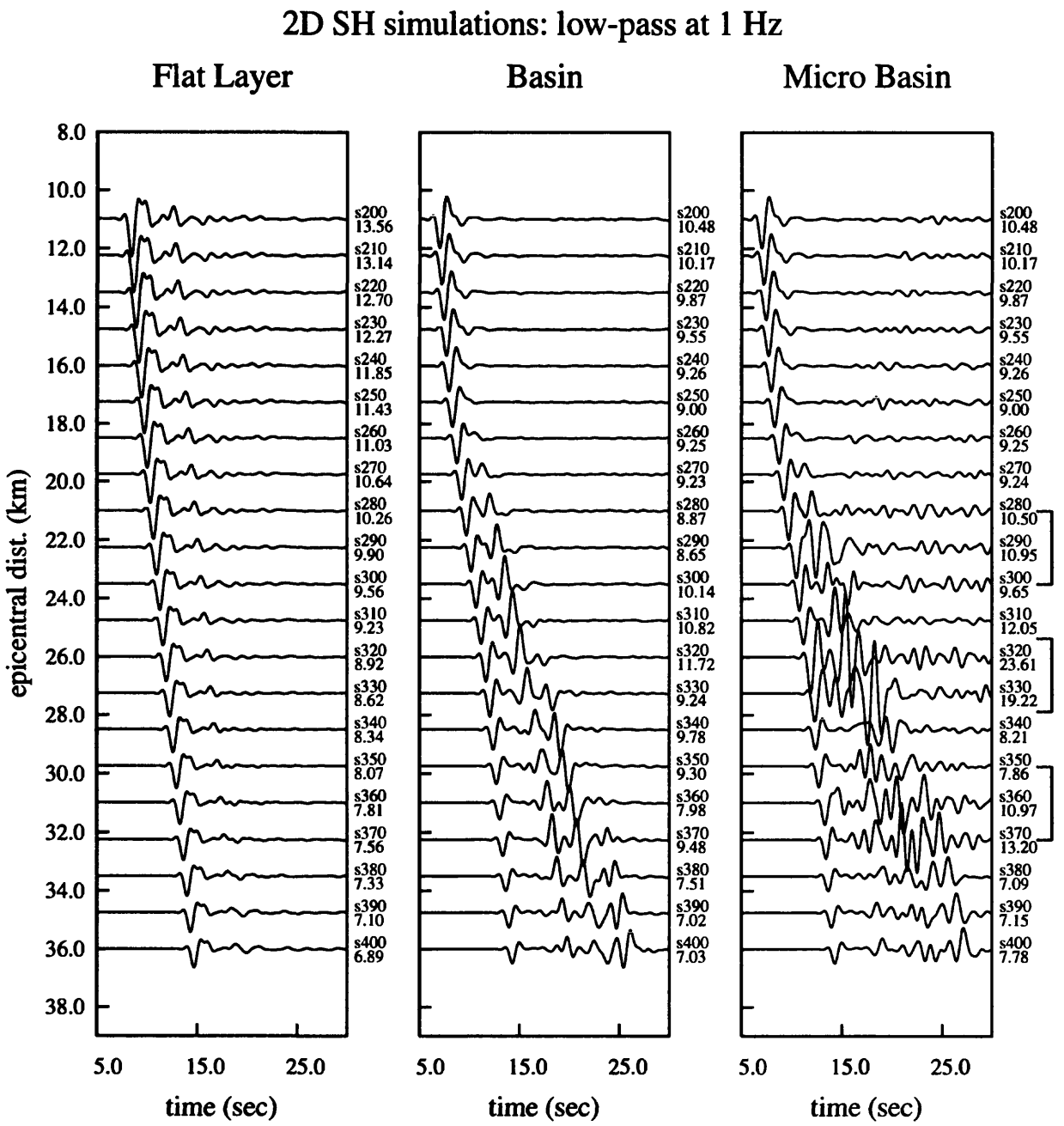

Figure 4: Left panel displays a profile of synthetic SH velocity ground motions computed for a plane-layered velocity structure (see Table 1), middle panel shows SH synthetics computed for the simplified 2D basin structure, and right panel shows SH synthetics computed for the 2D basin model containing small-scale (micro-basins) structural variations. Brackets along right margin of micro-basin profile indicate the surface locations of the three micro-basin structures.

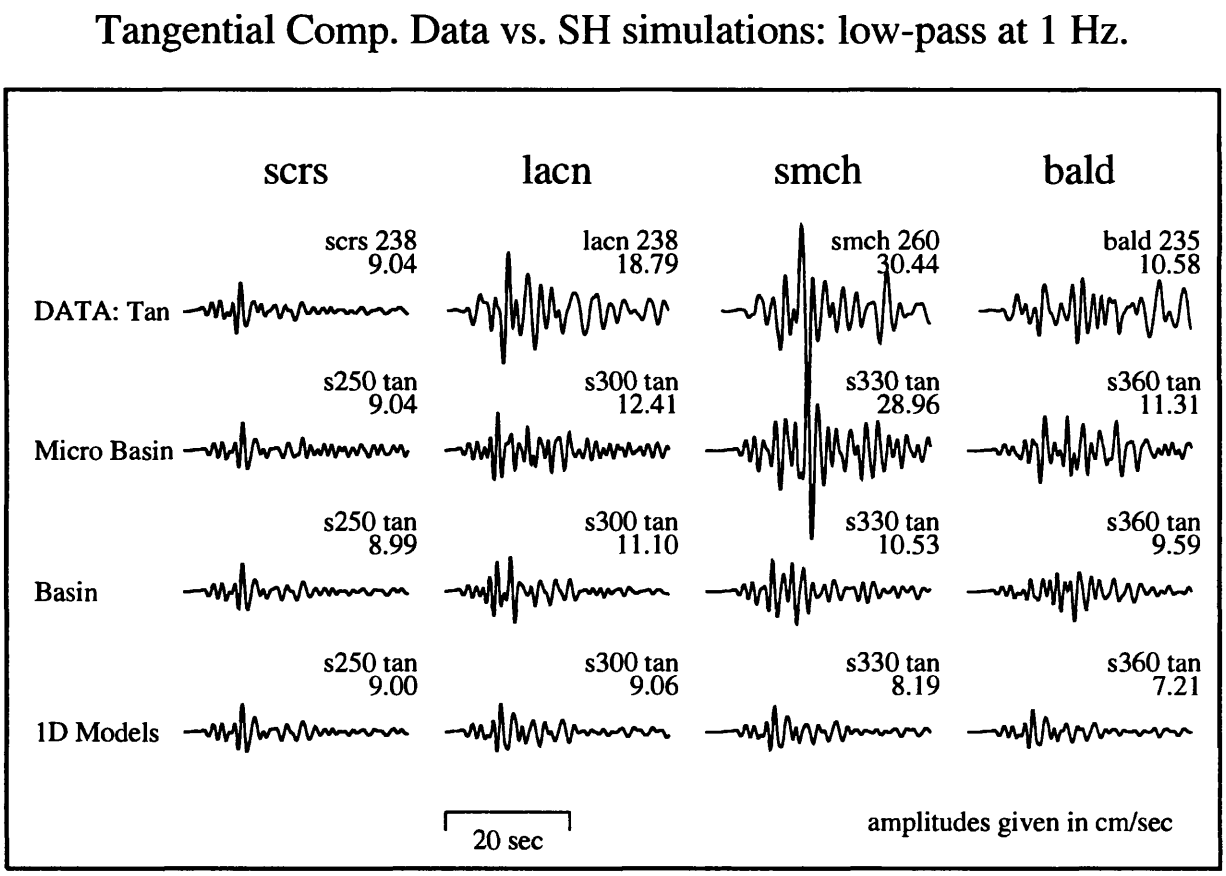

Figure 5: Comparison between the tangential component of velocity recorded during the Northridge earthquake at four sites located in west Los Angeles (top row) and the SH response simulated using the 2D basin models (middle two rows) and the 1D model (bottom row).

Seismic Landslide Instrument Array

9950-12075
9950-11075

Edwin L. Harp
Randall W. Jibson
Branch of Earthquake and Landslide Hazards
U.S. Geological Survey
Box 25046, MS 966
Denver, Colorado 80225
(303) 273-8557, Fax-(303)273-8600, harp@gldvxa.cr.usgs.gov
(303) 273-8577, Fax-(303)273-8600, jibson@gldvxa.cr.usgs.gov
NEHRP/SF/III.1&3; NEHRP/SC/III.1&3

Investigations Undertaken

Two sites, one in the San Francisco Bay area and one in the greater Los Angeles area have been instrumented to collect strong-motion, displacement, and pore-pressure data from active landslides likely to be reactivated in a future earthquake. Surface accelerometers have been installed both on and off the landslide masses, pore-pressure transducers (piezometers) within the slide masses below the water table, and extensometers across headwall scarps and lateral shear surfaces of the slides. During future earthquakes, surface accelerations, pore-water pressures, and displacements will be recorded simultaneously. The successful recording of such data will greatly enhance the understanding of the physics of the interaction between seismic inertial forces and the landslide-triggering and movement process.

A site in the Santa Cruz Range near La Honda, California has been instrumented to record future earthquake effects on a landslide within the San Francisco Bay area. The landslide selected was one that showed slight displacement (0.5 cm) along its lateral shear surfaces in response to the Loma Prieta earthquake. In southern California, a site at Chantry Flat north of Santa Anita Canyon on a deep-seated landslide mass that was reactivated ($\approx$ 15 cm displacement in its lower midsection) in the 1991 Sierra Madre earthquake has been instrumented. The site at Chantry Flat has been instrumented with three accelerometers, one on the landslide reactivated during the 1991 Sierra Madre earthquake, one on the ancient surrounding landslide mass, and one on stable bedrock. Two extensometers have been deployed across the 1991 scarp. Bedrock conditions at the site precluded installation of piezometers and inclinometer casing with existing in-house drilling capabilities.

The La Honda site has been instrumented with two surface accelerometers, one on the slide mass and one adjacent to it on stable ground, four piezometers at various depths, and two extensometers, all to be recorded simultaneously after being triggered by a seismic event. The piezometers and displacement meters are also recorded on a long term basis to provide displacement and pore-pressure data prior to an earthquake and for several hours or days after shaking stops.

Results

Sites have been instrumented in both the San Francisco Bay area and in southern California close to active faults likely to generate at least a magnitude 5-6 earthquake within the next ten years. The equipment was installed during summer 1992 and subsequently upgraded to measure long-term background data as well as that generated during an earthquake.

The accelerometers at Chantry Flat in southern California were triggered by the Landers, California, earthquake of June 28, 1992 and have all produced records. Ground motion at Chantry Flat during this earthquake was not sufficiently large to produce measurable displacements within the instrumented landslide mass. The Northridge, California earthquake triggered several millimeters of displacement across the same scarp produced in the Sierra Madre earthquake. Unfortunately, the recorders near the Chantry Flat helipad on the ancient landslide had been vandalized recently and did not record this event. The accelerometer at the upper helipad on bedrock did, however, produce a record of the ground motion that was obviously just above the threshold to trigger movement on the landslide so that, at least, an immediately adjacent set of records can be analyzed with respect to the landslide's threshold. The recorders at the lower helipad that were disturbed have been relocated to a more secure location within the Forest Service Fire Station compound.

Reports Published

Harp, Edwin L., and Jibson, Randall W., (in press), Seismic instrumentation of landslides: Building a better model of dynamic landslide behavior, Bulletin of the Seismological Society of America, 20 ms. p.

Heterogeneity of Rupture Processes in the New Madrid Seismic Zone

1434-94-G-2402
Robert B. Herrmann
Department of Earth and Atmospheric Sciences
Saint Louis University
3507 Laclede Avenue
St. Louis, MO 63103
(314) 977-3131
rbh@slueas.slu.edu

Introduction

This work uses the three component data set from the University of Memphis New Madrid deployment to study the earthquake process at some locations in the New Madrid seismic zone. In order to focus on the source and to reduce the effects of unknown site effects, events within swarms are used. To compare events within swarms by empirical Green's function studies, it is essential to know relative event locations and also event focal mechanisms. Thus this study involves both a search of the digital data of over 900 events for swarms, defined in terms of a narrow space/time window, from which a subset of events is subjected to detailed analysis.

Results

Figure 1 shows 76 events in the region of Ridgely, Tennessee, from 1989 - 1992, and the 21 events having similar waveforms for detailed analysis. Using a well recorded master event, a cross-correlation technique was applied to all other P and S wave arrivals and all events were relocated relative to the master event. Timing resolution limits the relative location precision to 30 m. The relocated events align in an approximate northeast-southwest direction, but in only three point event clusters.

Because of simple waveforms, focal mechanisms were determined using direct P, SH and SV arrivals. A simple earth structure was used, consisting of a thick layer of sediments overlying a crustal model. Figure 2 compares the observed waveforms and synthetics in the 1 - 20 km epicentral distance range. The focal mechanisms estimated using a search technique and moment tensor inversion is indicated.

The salient feature of the waveform solutions of Figure 1 is that none of the nodal planes strike northeast-southwest along the direction of apparent seismicity. A study of the temporal behavior of the swarm indicates a causal relationship. The group of locations are envisioned as a set of interacting *en echelon* cracks that interact with each other.

The success in waveform modeling means that many more of the events recorded by PANDA can be analyzed for focal mechanism. Together with the excellent PANDA locations, the detailed faulting process can be mapped in detail spatially. A total of 20 such events have been processed so far.

Publications

Liu, Z., J. Xie, and R. B. Herrmann (1994). Focal Mechanisms of Microearthquakes

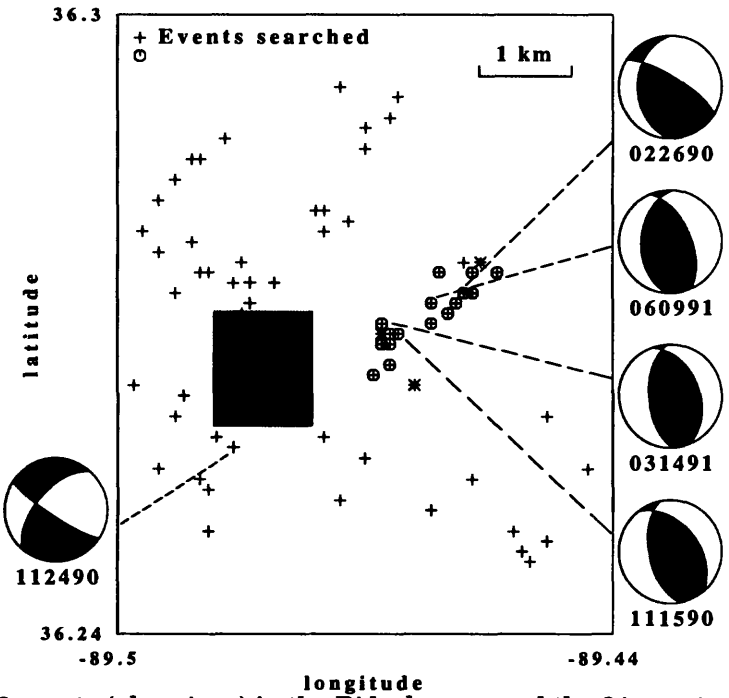

Fig. 1. Locations of 76 events (plus signs) in the Ridgely area and the 21 events studied in detail (circled events). The shaded rectangular region is the town of Ridgely. The focal mechanisms determined by waveform inversion are also indicated. These locations are single event locations.

in the Southern Junction of the New Madrid Seismic Zone, (draft).

Xie, J., Z. Liu, L. Cong, R. B. Herrmann, and J. M. Chiu (1994). Analyses of sesimic waveforms from clustered microearthquakes near the southern junction of the new Madrid seismic zone: I. Rupture properties and implications on fault weakening, (draft).

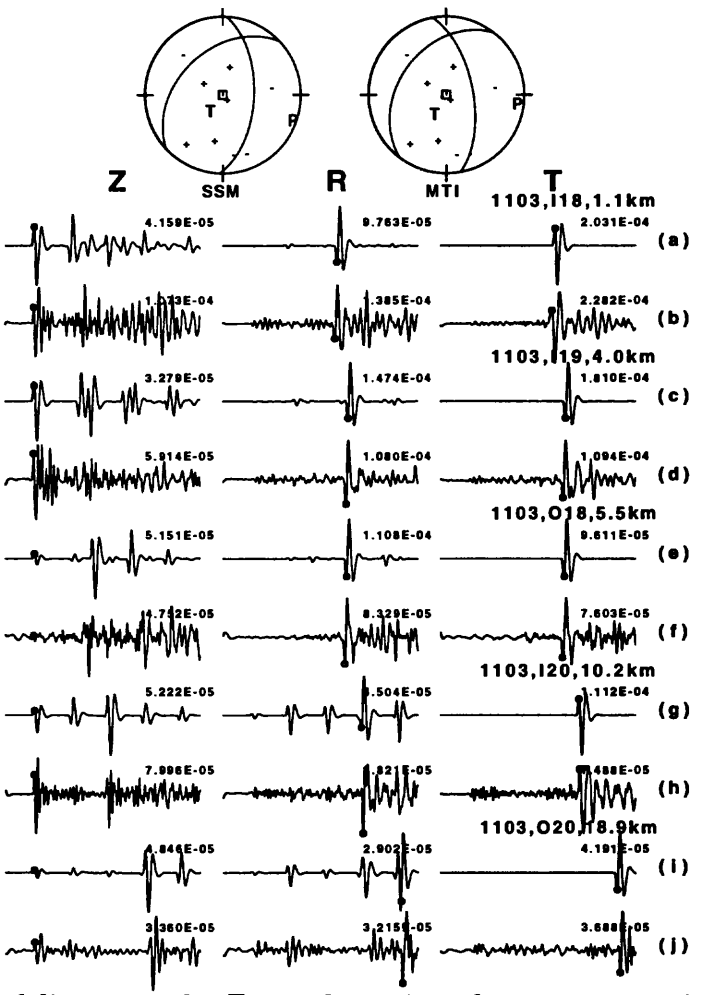

Fig. 2. Waveform modeling example. For each station, the upper trace is the low-pass filtered observed data and the lower is the synthetic. The amplitudes used in the inversion are indicated by the small circles. Even though the 8 observed P-wave first motions barely suffice to define the mechanism, the waveform fit requires the solutions shown.

Ground Motion Scaling from Earthquakes in the New Madrid Seismic Zone

1434-94-G-2403
Robert B. Herrmann
Department of Earth and Atmospheric Sciences
Saint Louis University
3507 Laclede Avenue
St. Louis, MO 63103
(314) 977-3131
rbh@slueas.slu.edu

Introduction

The objective of this work is to use regional seismic network data to define the scaling of earthquake ground motion in the distance range of 0 - 400 km. This entails separating the effects of source, site and crustal wave propagation. A typical scaling relation used is to relate the ground motion, A, to a source term, *Src*, a site term, *Site*, and a crustal spreading term, $G(r)$, by the relation

$$\log A = \log Src + \log Site + \log G(r)$$

Often $G(r)$ is approximated by $a + b \log r + cr$ over specified distance ranges.

The problem with such a formulation is the tradeoff between the various terms if site effects are severe and if the range of distances is narrow. In addition, poorly known instrument calibrations will map into all terms in a general regression. An alternative approach is given by Aki (1980) and used by Frankel et al (1990). The idea here is to use the seismic coda as a first order correction for the *Src* and *Site* terms. If t is the time after the origin, and if this time is at least twice the S-wave travel time, then the RMS coda amplitude $a(t)$ is modeled as

$$\log a(t) = \log Src_{coda} + \log Site_{coda} + \log C(t)$$

It is assumed that the coda shape function $C(t)$ is common to all stations. A multiple regression can be used to define each term as a function of frequency.

If at a common frequency, it is assumed that $Src_{coda} \approx Src$ and $Site_{coda} \approx Site$, then a normalization of the peak amplitude A by the coda will yield a first order approximation to the $G(r)$ term directly, without the tradeoffs with the source and site terms in the first equation. The assumption of proportionality between the source and site terms of the coda and peak amplitudes can be tested by direct comparison.

Results

To present results of interest to the engineering community, vertical component time histories from regional seismic network stations are filtered to produce the time histories used to five percent PSRV determination. Figure 1 shows the distance distribution of the stations used. Figure 2 shows the empirical coda shape, $\log C(t)$, at four different frequencies. Figure 3 shows the smoothed $\log G(r)$ over the observed distance range. The departure of the trends from simple r^{-1} spreading

is assumed to be related to predominant focal mechanism and crustal wave propagation, with the bump at 100 km due to supercritical crustal reflections. An interesting feature is that the decay of motion in the 0 - 40 km range is much more rapid than previously seen in eastern North America.

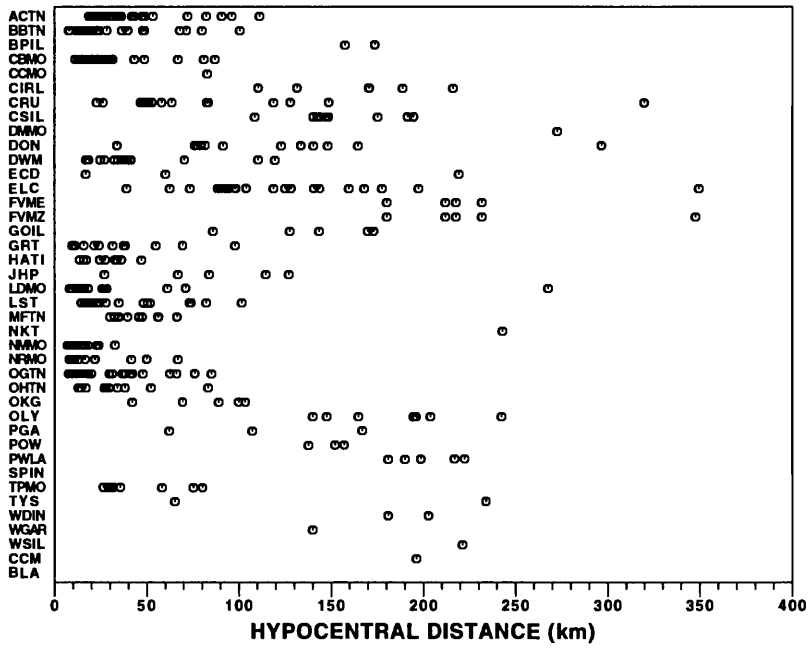

Fig. 1. Seismograph stations used and distribution of distances of observed peak motions. This presentation is required to understand potential biases in results.

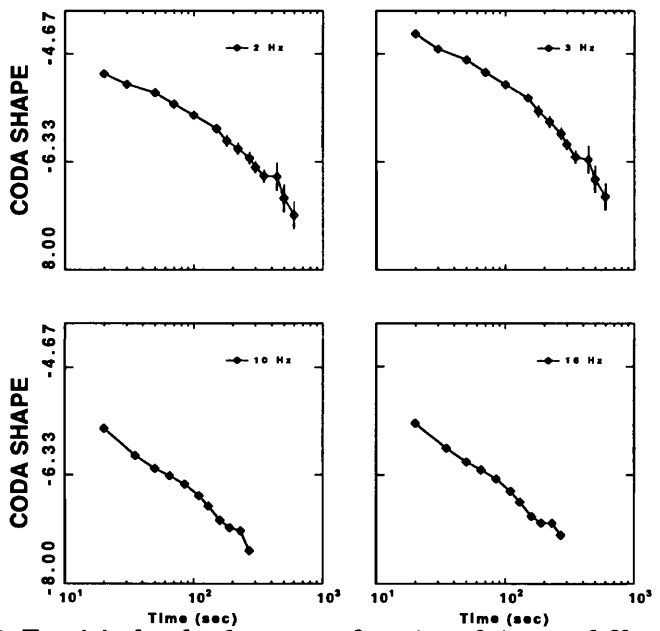

Fig. 2. Empirical coda shape as a function of time and filter frequency.

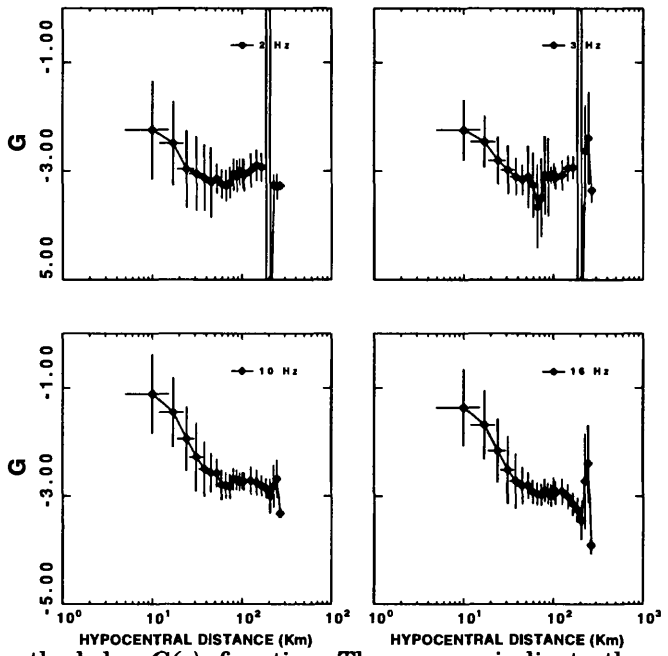

Fig. 3. Empirical smoothed log $G(r)$ function. The crosses indicate the one-sigma of the spread of individual log $G(r)$ estimates and the distance range over which each average is made.

Future Work

The preliminary results have several important implications. First, since the coda shape has been defined, the accelerograph data from small magnitude earthquakes can be now be incorporated since the coda can be used as a first order correction for source and site. Second, the $G(r)$ of horizontal motions must be determined. This is possible using the PANDA (University of Memphis) New Madrid data set. However, because of short 60 second triggers, the assumption that the vertical component coda shape is the same as that of the horizontal will have to be tested. Finally, the empirical coda shape functions can be used to understand the effects of intrinsic and scattering Q on high frequency motions.

High frequency peak motion modeling will be used to understand the results in terms of crustal structure and source mechanism. Initial modeling shows that the distance decay of vertical motion is much more rapid than for tangential motion. In order to calibrate a forward model, the scaling of horizontal motion with distance is a necessary next step. For the results to be acceptable,

References

Aki, K. (1980). Attenuation of shear waves in the lithosphere for frequencies from 0.05 to 25 Hz, *Phys. Earth Planet. Inter.* **21,** 50-60.

Frankel, A., A. McGarr, J. Bicknell, J. Mori, L. Seeber and E. Cranswick (1990). Attenuation of high-frequency shear waves in the crust: measurements from New York state, South Africa, and southern California, *J. Geophys. Res.* **95,** 17,441-17,457.

LIQUEFACTION RESEARCH

4-9960-12286

THOMAS L. HOLZER AND MICHAEL J. BENNETT
BRANCH OF EARTHQUAKE GEOLOGY AND GEOPHYSICS
345 MIDDLEFIELD ROAD MS-977
MENLO PARK, CALIFORNIA 94025-3591
415/329-5637 OR 415/329-4890

JOHN C. TINSLEY III
BRANCH OF WESTERN REGIONAL GEOLOGY
345 MIDDLEFIELD ROAD MS-975
MENLO PARK, CALIFORNIA 94025-3591
415/329-4928

CHARLES S. MUELLER
BRANCH OF SEISMOLOGY
345 MIDDLEFIELD ROAD MS-977
MENLO PARK, CALIFORNIA 94025-3591
415/329-5646

PROGRAM ELEMENT III

Investigations

1. A compilation of property losses by earthquake hazard during the 1989 Loma Prieta earthquake.
2. Compilation and analysis of geotechnical data collected by the USGS at 1989 liquefaction sites in the Monterey Bay area. This includes a field deployment of portable seismographs to improve ground motion estimates at sites that experienced liquefaction during the 1989 Loma Prieta earthquake. The goal of the deployment is to permit rigorous testing of the simplified procedure for predicting liquefaction with geotechnical data collected following Loma Prieta.
3. An evaluation of a retrievable pore-pressure transducer for installations at special arrays to monitor strong motion and pore pressure response at sites susceptible to liquefaction.
4. Cooperative agreement with the Applied Technology Council to transfer USGS results from engineering seismology research to the practicing design engineer (ATC-35).

Results

1. A method was developed to assign property losses caused by the 1989 Loma Prieta, California, earthquake to specific earthquake hazards - ground shaking, liquefaction, landslides, tectonic ground rupture, and tsunami. It was found that approximately 98%

of the $5.9 billion in property damage from the 1989 Loma Prieta earthquake was caused directly by ground shaking. Moreover, approximately two-thirds of the losses were caused by enhanced ground shaking, that is ground shaking that was higher than normally expected. Permanent ground deformation accounted for only 2% of the total property loss. These results indicate that earthquake hazard reduction efforts in the United States would benefit from improved understanding of phenomena that enhance ground shaking; mapping areas susceptible to enhanced ground shaking; and delineating seismogenic geologic structures at greater distances from urban areas with soft soil conditions (Holzer, 1994a,b).

2. A total of 150 cone penetration tests and 334 standard penetration tests in 58 borings have now been conducted at 18 sites, 14 of which displayed liquefaction-related ground failure in the Monterey Bay area. Index properties of soils sampled in the areas of ground failure have been determined for comparison with soil properties in areas where ground failure did not occur. Supporting soils data and penetration test data have been entered into a geotechnical database using GTGS® software (Bennett, 1994b). Analysis of a 2-km-long lateral spread south of Watsonville indicates liquefaction occurred in a 5-m-thick sand layer in the younger floodplain facies. The top of the liquefied layer was about 5 m from the ground surface. Observed settlements and lateral spreading displacements did not agree with those predicted by standard engineering methods. The field study clarified the mechanism of lateral deformation and developed a new technique that places an upper limit on permanent ground displacement by inertial movement of soil blocks above liquefied layers (Holzer, Tinsley, Bennett, and Mueller, 1994).

   Beginning in August 1993, portable digital seismographs were deployed at seven sites in the Monterey Bay area. The purpose of the deployment was to improve estimates of ground motion during the Loma Prieta earthquake at sites that experienced liquefaction. The August 11, 1993, Hall's Valley M4.9 earthquake was recorded at several of the sites and the recordings permit an evaluation of localized variations in site response. The January 11, 1994, Simas Lake M4.2 earthquake was recorded at all of the sites and permits estimates of the attenuation of mainshock ground motion to be made at all of the geotechnical drilling sites.

3. Field testing in collaboration with the California Institute of Technology was conducted in Spring 1994 with a retrievable pore pressure transducer system. The system permits easy retrieval of pore pressure transducers permanently installed at liquefaction arrays. We also conducted CPT and SPT investigations on at the test site determine liquefaction resistance of the hydraulic fill (Bennett, 1994a). The data are being analyzed. We also published an analysis of the pore pressure transducers at the Wildlife liquefaction array (Youd and Holzer, 1994).

4. Two seminars series were sponsored. The first seminar, *New developments in earthquake ground motion estimation and implications to engineering design practice*, was held in January-February 1994 in Los Angeles, Memphis, New York, San Francisco, and Seattle. It was attended by 1200 practicing design engineers. A second seminar on regional earthquake potential was held as part of the 5th National

Earthquake Engineering Conference in Chicago, July 14. It was attended by approximately 100 engineers.

Reports

Bennett, M.J., 1994a, Sand boils and their source beds during the Loma Prieta earthquakes of October 17, 1989 [abs.]: Association of Engineering Geologists, 37th Annual Meeting, Wlliamsburg, Virginia, p. 39.

Bennett, M.J., 1994b, Geotechnical investigation in Pajaro, California: U.S. Geological Survey Open-File Report 94-279, 10 p.

Holzer, T.L., 1994a, Loma Prieta damage largely attributed to enhanced ground shaking: Transactions, American Geophysical Union, EOS, v. 75, no 26, p. 299-301. (Reprinted in Oregon Geology, v. 56, no. 5, p. 111-113, 1994)

Holzer, T.L., 1994b, Predicting earthquake effects - Learning from Northridge and Loma Prieta: Science, v. 265, p. 1182-1183.

Holzer, T.L., and Bennett, M.J., 1994, Searching for a paleoliquefaction signature in geotechnical borings in sands [abs.]: Geological Society of America Abstracts with Programs, v. 26, no. 7, p. A252 - A253

Holzer, T.L., and Bennett, M.J., 1994, A paleoliquefaction signature in natural sand deposits? [abs.]: EOS, Transactions, American Geophysical Union, v. 75, no. 44 (Fall Meeting Supplement), p. 452.

Holzer, T.L., Tinsley, J.C., III, and Bennett, M.J., 1994a, Field measurements and prediction of ground deformation: Miller Farm Lateral Spread, Watsonville, California [abs.]: Abstracts: 5th U.S.-Japan Workshop on Earthquake Resistant Design of Lifeline Facilities and Countermeasures Against Soil Liquefaction, Snowbird, Utah, p. 2.

Holzer, T.L., Tinsley, J.C., III, Bennett, M.J., and Mueller, C.S., 1994b, Observed and predicted ground deformation - Miller Farm lateral spread, Watsonville, California: 5th U.S. - Japan workshop, 26 pages, 3 tables, 10 figs.

Kayen, R.E., Mitchell, J.K, and Holzer, T.L., 1994, Ground motion characteristics and their relation to soil liquefaction at Wildlife liquefaction array [abs.]: Abstracts: 5th U.S.-Japan Workshop on Earthquake Resistant Design of Lifeline Facilities and Countermeasures Against Soil Liquefaction, Snowbird, Utah, p. 2.

Kayen, R.E., Mitchell, J.K., and Holzer, T.L., 1994, Ground motion characteristics and their relation to soil liquefaction at the Wildlife liquefaction array, Imperial Valley, California: Proceedings, 5th U.S. - Japan workshop, 17 pages, 8 figs.

Youd, T.L., and Holzer, T.L., 1994, Piezometer performance at the Wildlife liquefaction site, California: American Society of Civil Engineers, Journal of Geotechnical Engineering, v. 120, no. 6, p. 975-995.

HAZARD POTENTIAL, FAILURE TYPE, AND TIMING OF LIQUEFACTION-INDUCED LANDSLIDING IN THE FARMINGTON SIDING LANDSLIDE COMPLEX, WASATCH FRONT, UTAH

1434-94-G-2498
Program Element III.3

M.D. Hylland and Mike Lowe
Utah Geological Survey
2363 South Foothill Drive
Salt Lake City, Utah 84109-1491
(801) 467-7970

INVESTIGATIONS

The purpose of this study is to date movement on the liquefaction-induced Farmington Siding landslide complex, infer the geologic and hydrologic conditions under which landsliding originally occurred, evaluate the failure type (lateral spread versus flow failure) and extent of internal deformation, and assess the potential for movement of the landslides and for failure in landslide-crown areas above main scarps during future earthquakes. Assessment of failure type and extent of internal deformation will aid in predicting the amount of ground displacement during future liquefaction-induced landsliding. Depending on the accuracy with which the landslide events can be dated, it may be possible to better constrain the timing of specific paleoseismic events on the nearby Wasatch fault zone.

A major goal of this project is to assess the potential hazards presented by the landslide complex, both on the landslide and in crown areas, and the need for consideration of such hazards in land-use planning. In addition to helping reduce the loss of life and property in the Farmington area as a result of earthquakes, hazard-evaluation methods developed during this study may prove valuable for evaluating similar problems on other landslides along the Wasatch Front and elsewhere.

Geologic and geomorphic mapping of the Farmington Siding landslide complex has been completed previously (Van Horn, 1975; Miller, 1980; Anderson and others, 1982; Nelson and Personius, 1990; Harty and others, 1993). Subsurface exploration will be conducted during this study within the boundaries of the landslide complex to determine failure type, extent of internal deformation, and relative timing of landslide events. Radiocarbon dating and correlations with well-documented Holocene Great Salt Lake and late Pleistocene Lake Bonneville lake-level chronologies and associated stratigraphy will provide additional means of determining the approximate ages of the landslides. Ground-water conditions in crown areas will be evaluated to determine the potential for future flow failures in these areas.

PROJECT STATUS

As of October 1994, we are in the process of compiling available borehole, water-well,

and test-pit logs from the area of the landslide complex, and field-checking and obtaining clearance for proposed trenching sites. We expect to complete the trenching and sample collection by December 1995.

REFERENCES

Anderson, L.R., Keaton, J.R., Aubry, Kevin, and Ellis, S.J., 1982, Liquefaction potential map for Davis County, Utah: Utah State University Department of Civil and Environmental Engineering and Dames & Moore Consulting Engineers unpublished Final Technical Report for the U.S. Geological Survey, 50 p.

Harty, K.M., Lowe, Mike, and Christenson, G.E., 1993, Hazard potential and paleoseismic implications of liquefaction-induced landslides along the Wasatch Front, Utah: Utah Geological Survey unpublished Final Technical Report for the U.S. Geological Survey, 57 p.

Miller, R.D., 1980, Surficial geologic map along part of the Wasatch Front, Great Salt Lake Valley, Utah: U.S. Geological Survey Miscellaneous Field Investigations Map MF-1198, scale 1:100,000.

Nelson, A.R., and Personius, S.F., 1990, Preliminary surficial geologic map of the Weber segment, Wasatch fault zone, Weber and Davis Counties, Utah: U.S. Geological Survey Miscellaneous Field Studies Map MF-2132, scale 1:50,000.

Van Horn, Richard, 1975, Largest known landslide of its type in the United States - A failure by lateral spreading in Davis County, Utah: Utah Geology, v. 2, no. 1, p. 83-87.

Seismic Slope Stability
9950-10075

David K. Keefer
Branch of Earthquake and Landslide Hazards
U.S. Geological Survey
345 Middlefield Rd., MS 998
Menlo Park, CA 94025
(415) 329-4893 FAX (415) 329-5390
dkeefer@mojave.wr.usgs.gov

Edwin L. Harp and Randall W. Jibson
Branch of Earthquake and Landslide Hazards
U.S. Geological Survey MS 966
P. O. Box 25046
Denver Federal Center
Denver, Colorado 80225
(303) 273-8557 and (303) 273-8577
FAX (303) 273-8600
harp@gldvxa.cr.usgs.gov and jibson@gldvxa.cr.usgs.gov

Program Elements: Process and Theory Elements III.1 and III.3

Investigations

- Research continued on defining relations between seismic shaking severity (as measured by Arias intensity) and landslide concentrations, using data gathered from the recent Loma Prieta, Sierra Madre, and Northridge, California earthquakes.

- Correlations have been established between "rock-mass-quality" (Q), a measure of rock-mass fracture characteristics, and concentrations of earthquake-induced rock falls and rock slides. Additional data are being analyzed to refine statistical correlations between Q and rock-slope failure concentrations and thresholds.

- Analysis of the Springdale, Utah, landslide, which was triggered at a great distance from a moderate earthquake is being completed. This landslide and others triggered at great epicentral distances in Colorado Plateau earthquakes suggest that attenuation of ground failures may differ among regions.

- The Newmark seismic slope-stability analysis is being refined and improved to facilitate regional assessment of seismic slope-stability, using design strong-motion records. The analysis is being calibrated using data from slope failures triggered by the Loma Prieta earthquake adjacent to the Corralitos strong motion-station.

- The landslide distribution produced by the 1989 Loma Prieta, California, earthquake has been recorded in map form. This distribution has been digitized and is being analyzed in a GIS system to determine if significant correlations exist between the landslide distribution, on the one hand, and geology, strong-motion parameters, and topography, on the other.

- Modeling was undertaken on the long-term effects of major episodes of earthquake-induced landsliding coupled with sediment transport during El Niño-generated floods in causing a complex sequence of hazards in coastal Peru. Modeling was calibrated with data from both the historic and archaeological records.

- Developed a model to predict quantitatively the component of earthquake-generated landslides in overall long-term slope erosion and slope-failure potential in seismically active regions. Model was applied to 12 regions, including the San Francisco Bay, Sierra Nevada-Great Basin, and Transverse Range regions of California and to the island of Hawaii.

Results

- Published a paper that provides a practical documentation of how to apply Newmark's seismic slope-stability analysis to predict the seismic performance of natural or engineered slopes. The paper contains a general model based on Newmark's method that predicts landslide displacement as a function of slope stability and shaking intensity and thus provides a widely applicable tool for seismic hazard analysis.

- Documented landslides triggered by the Northridge earthquake and began acquiring strong-motion records; analysis of these data sets will facilitate quantification of the relations between strong shaking, slope stability, and landslide distribution.

- Entered data on landslide locations from the Loma Prieta earthquake into GIS system and began analysis of landslide concentrations as function of geologic materials, and epicentral and source distances.

- Used quantitative method to determine contribution of earthquake-induced landslides to slope-failure and erosion potential regions in US and abroad. Determined long-term absolute component of erosion from earthquake-induced landslides and rate relative to other slope-erosion and fluvial processes. Determined that rate of earthquake-induced landsliding is high on the island of Hawaii and in the San Francisco Bay region and is low to moderate in the Sierra Nevada-Great Basin and Transverse Range regions of California.

- Determined that seismically generated landsliding in Peru is a major, ongoing, and catastrophic hazard, which can be detected both in the recent record and in the prehistoric (archaeological) record. Identified at least three major episodes--one recent and two prehistoric--in which a series of events, beginning with earthquake-generated landslides have had catastrophic economic and social consequences. The entire hazards processes includes earthquake-generated landslides, transport of the resulting anomalous sediment loads by El Niño-generated floods, coastal progradation, longshore transport, and subsequent inland aeolian transport of sediment, which buries dwellings and infrastructure.

- Developed a method and published a paper on use of landslides as paleoseismic indicators and applied method to large landslides in the New Madrid seismic zone.

- Compiled Arias intensity values from strong-motion recordings of Loma Prieta, Whittier Narrows, and Superstition Hills earthquakes to compare their spatial

variation with landslide distributions, concentration attenuations, and distance limits from these earthquakes.

- Correlated additional data on rock-failure distributions and "rock-mass-quality" (Q), from the Whittier Narrows, Sierra Madre, and Northridge earthquakes in southern California. This data will permit extension of pre-existing correlations of Q with rock-failure concentrations and limits to a greater range of earthquake magnitudes.

Reports Published

Harp, E. L., and Jibson, R. W., 1993, The Springdale, Utah, landslide: An extraordinary event: Japan Landslide Society, Landslide News, No. 7, p. 16-19.

Harp, E.L., and Jibson, R.W., Instrumentation of landslides for dynamic response during earthquakes: Bulletin of the Seismological Society of America (technical note), 20 ms p. [In press]

Harp, E. L., Jibson, R. W., and Keefer, D. K., 1993, Seismically induced landslides triggered at extraordinary distances: evidence from the Springdale, Utah, landslide: Geological Society of America Abstracts with Programs, v. 25, no. 6, p. A32.

Harp, E. L., Jibson, R. W., Keefer, D. K., and Wilson, R. C., Landslides triggered by the January 17, 1994, Northridge, California earthquake: implications for future hazards: Geological Society of America Annual Meeting, Abstracts with Programs, vol. 26, no. 7, p. A217.

Harp, E. L., and Noble, M. A., 1993, An engineering rock classification to evaluate seismic rock-fall susceptibility and its application to the Wasatch Front: Bulletin of the Association of Engineering Geologists, vol. 30, no. 3, p. 293-319.

Harp, E.L., and Wilson, R.C., Shaking intensity thresholds for rock falls: Evidence from 1987 Whittier Narrows and Superstition Hills earthquake strong-motion records: Bulletin of the Seismological Society of America, 35 ms. p. [Submitted for publication].

Jibson, R.W., 1993, Predicting earthquake-induced landslide displacements using Newmark's sliding block analysis: Transportation Research Record, No. 1411, p. 9-17.

Jibson, R.W., and Harp, E.L., 1993, The Springdale, Utah, landslide, *in* Christensen, G.E., ed., The St. George, Utah earthquake of September 2, 1992: Utah Geological Survey Bulletin, 21 p.

Jibson, R.W., and Harp, E.L., 1993, How to build a better model of the seismic behavior of landslides: Catch them in the act: Geological Society of America Abstracts with Programs, v. 25, no. 6, p. A32.

Jibson, R.W., Harp, E.L., Keefer, D.K., and Wilson, R.C., 1994, Landslides triggered by the 1994 Northridge earthquake [abs.]: Southern California Academy of Sciences, Annual Meeting, May 6-7 1994, Irvine, California, Proceedings, p. 10.

Jibson, R.W., Harp, E.L., Keefer, D.K., and Wilson, R.C., 1994, Landslides triggered by the 17 January 1994 Northridge, California earthquake: Japan Landslide Society, Landslide News, No. 8, p. 7-10.

Jibson, R.W., Harp, E.L., Keefer, D.K., and Wilson, R.C., 1994, Landslides triggered by the 17 January 1994 Northridge, California earthquake: U.S. Geological Survey, Earthquakes and Volcanoes, 13 ms. p. [Submitted for publication].

Jibson, R. W., Harp, E. L., Speigel, R. A., Hajjeh, R. A., Schneider, E. E., Marshall, G. A., and Stein, R. S., 1994, Landslides can be hazardous to your health: an outbreak of Coccidioidomycosis (Valley Fever) caused by landslides triggered by the 1994 Northridge, California, earthquake: Geological Society of America Annual Meeting, Abstracts with Programs, vol. 26, no. 7, p. A318.

Jibson, R. W., and Keefer, D. K., 1993, Analysis of the seismic origin of landslides: examples from the New Madrid seismic zone: Geological Society of America Bulletin, v. 105, no. 4, p. 521-536.

Jibson, R. W., and Keefer, D. K., 1994, Analysis of the origin of landslides in the New Madrid seismic zone, *in* Johnston, A. C., and Shedlock K. M., eds., Investigations of the New Madrid seismic zone: U. S. Geological Survey Professional Paper 1538, p. D1-D23.

Keefer, D. K., 1993, The susceptibility of rock slopes to earthquake-induced failure: (Technical Note) Bulletin of the Association of Engineering Geologists, vol. 30, no. 3, p. 353-361.

Keefer, D. K., 1993, Contribution of earthquakes to long-term slope evolution [abs.]: EOS, vol. 74, no. 43, 1993/supplement, p. 300.

Keefer, D. K., 1994, The importance of earthquake-induced landslides to long-term slope erosion and slope-failure hazards in seismically active regions: Geomorphology, v. 10, p. 265-284.

Keefer, D. K., and Moseley, M. E., Catastrophic Effects of combined seismic landslide generation and El Niño flooding on prehispanic and modern populations in Peru: Geological Society of America Annual Meeting, Abstracts with Programs, vol. 26, no. 7, p. A342.

Keefer, D. K., and Schuster, R. L., 1993, Landslides generated by the Klamath Falls earthquakes of September 20, 1993: Earthquakes and Volcanoes, v. 24, no. 3, p. 140-146.

Norris, R. D., Walter, S. R., Clynne, M. A., Keefer, D. K., Muffler, L. J. P., Harp, E. L., and Knight, B., 1993, Seismic and field observations of the 26 August 1993 rockfall at Lassen Peak, California [abs.]: EOS, vol. 74, no. 43, 1993/supplement, p. 649.

Wiley, T. J., Sherrod, D. R., Keefer, D. K., Qamar, A., Schuster, R. L., Dewey, J. W., Mabey, M. A., Black, G. L., and Wells, R. E., 1993, Klamath Falls earthquakes, September 20, 1993: Oregon Geology, vol. 55, no. 6, p. 127-134.

Youd, T. L., and Keefer, D. K., 1994, Liquefaction during the 1977 San Juan Province, Argentina earthquake (M_S = 7.4): Engineering Geology, vol. 37, p. 211-233.

p. 956 follows

Earthquake Induced Landslides, East San Francisco Bay Hills
9950-12505

David K. Keefer
Branch of Earthquake and Landslide Hazards
U.S. Geological Survey
345 Middlefield Rd., MS 998
Menlo Park, CA 94025
(415) 329-4893 FAX (415) 329-5390
dkeefer@mojave.wr.usgs.gov

Program Elements: Northern California Elements III.3 and III.4

Investigations

The East San Francisco Bay Hills lie immediately east of the northern East Bay and southern East Bay segments of the Hayward fault, which have high probabilities of producing an M=7 earthquake within in the next 30. This region, which includes some of the most rapidly developing parts of the San Francisco Bay urban area, also has a history of landslide problems. The combination of landslide-prone terrain, proximity to the Hayward and other active faults, such as the Calaveras, and rapid population growth give this area a high priority for evaluation of earthquake-induced landslide hazard and risk.

The purpose of this project is to develop an updated method for producing hazard and risk maps and to use that method to produce maps of the area. The method is based on the analytical slope-stability method developed by Newmark. In this method, the inherent stability of a particular slope, which depends on material properties, hydrologic conditions, and geometry, is characterized by its critical acceleration, a_c, which is related to the static factor of safety, FS, by the relation:

$$a_c = (FS-1)g\sin\theta$$

where g is the acceleration due to gravity and θ is the slope angle.
The Newmark method calculates the dynamic displacement of a slope with a given a_c by performing a step-wise double integration of the quantity, $a(t) - a_c$ where a(t) is the acceleration at any time, t, on a given strong-motion record.

The Newmark method has been adapted for use in evaluating and mapping hazard on a regional scale. The method requires input on expected levels of seismic shaking, topography, geologic and geotechnical properties of the slope materials, and hydrologic conditions. Expected levels of seismic shaking are being modeled for several earthquake scenarios, with initial concentration on M=7 events on the Hayward fault. This initial modeling uses existing attenuation relations for landslides, but additional relations involving other parameters, which are currently under development, will also be evaluated for possible use. Attenuation relations will be calibrated using data on landslide concentrations in several historical earthquakes, including the 1989 Loma Prieta earthquake.

Title Assessment of Soil Slope Stability during Earthquakes using Manifold Method
Award Number 1434-94-G2434
Investigator Jeen-Shang Lin
Institution Department of Civil and Environmental Engineering, University of Pittsburgh
Address Pittsburgh, PA 15261
Phone (412)624-8158 **Fax** (412)624-0135
Program Element Element III, Component III.3: Predict Ground Failure

INTRODUCTION

The main objective of this research is to develop the manifold method, an innovative computational methodology, in assessing stability of slopes during earthquakes. In particular, this study is to develop a computational tool, to improve on the computation of the permanent displacement of slopes, and to investigate key questions in the displacement computation for the seismic hazard assessment of slope lands.

For the present study, the manifold method formulation can be viewed as a combination of the finite element method and the discrete element method. It is well suited for analyzing interactions between continuum and discontinuum. The method is particularly useful for tackling dynamic problem that involves lightly constrained components which may become unstable during the course of an excitation, and eventually become detached from the main structure.

METHODOLOGY

The framework of the Manifold Method" was proposed by Shi (1991). The term "manifold" is a generalization of the "differential manifold" in differential geometry and topology.

Suffice it to say that for the present study, a manifold represents the collection of all the descriptions, or **atlases**, that define a problem. In theory, there is no limit to the number of atlases that can be used for a given problem. For this study only two atlases are employed: a **base mathematical atlas** and **physical atlas**. A mathematical atlas, can be a grid, or a template that at least covers a problem domain. It may be chosen according to a problem geometry, solution accuracy requirements, and physical property zoning. A physical atlas, on the other hand, should follow the physical boundaries of a problem, and should include all discontinuities.

Central to the manifold method is the idea of "generalized element." It utilizes the concept of finite covers from topology. The use of finite covers avoids confusion when many discontinuities are present within a continuum. To explain this central concept, a continuum block marked by a discontinuity is discussed here. Fig. 1(a) shows a rather arbitrary mathematical atlas that consists of 12 nodes. On the other hand, the physical atlas is dictated by the problem at hand which is shown as Fig. 1(b). Fig. 1(c) shows the manifold of the

problem which is a combination of these two atlases.

A **chart** associated with a node is a region influenced by the movement of the node. For instance, the chart associated with node 7 is the hatched area shown in Fig. 2. Physical discontinuities may cut a chart into subregions known as covers. Fig. 2(b) shows that the physical atlas divides chart 7 into two covers, 7_1 and 7_2. Similarly, chart 8 in Fig. 1(c) is divided into covers 8_1 and 8_2. Each of the cover numbers is used as a generalized node in the manifold method. Fig. 3 shows the 22 generalized nodes for the example; they are:

chart no.	covers formed	chart no.	covers formed
1	1_1, 1_2	7	7_1, 7_2
2	2_1, 2_2	8	8_1, 8_2
3	3_1, 3_2	9	9_1
4	4_1	10	10_1, 10_2
5	5_1, 5_2	11	11_1, 11_2
6	6_1, 6_2	12	12_1, 12_2

Each generalized element in the manifold method is an area common to a fixed number of generalized nodes. This number is a function of the order of the approximation function, or interpolation function. For the depicted problem this number is four. Thus, there are 10 generalized elements as labeled in Fig. 4. It is interesting to note that a generalized element in the manifold method may have an arbitrary geometric shape defined by a number of vertices. This is a distinct characteristics of the manifold method. In this example, elements 3 and 4 have three vertices, element 5 has 6 vertices and the rest of the elements all have 4 vertices.

A manifold analysis starts by obtaining the generalized elements and nodes from the mathematical and physical atlases. Then, it keeps track at each time step if any of the bounded objects comes into contact. If so, which kind of contacts it is-- is it newly formed or a continuation from previous time steps? Contact produces coupling between objects are translated into coupling in the governing equation. The kinematic constraints that different objects must not penetrate each other is implemented through penalty functions. This together with the use of the minimum potential energy principle give the governing simultaneous equation for the problem. Graph theory is then used to allocate computer memory for solving the equations. At the end of each time step, the problem geometry is updated. The computation continues until a desired time is reached.

RESEARCH IN PROGRESS

The research focus since it was started in June, 1994, has been on formulation and code development. To summary the progress, an example problem involving an unstable slope is analyzed here using the code developed so far. First, the example slope, as depicted in Fig. 5, is modeled with three slices. This figure is the physical atlas of the problem. The slope is modeled as elastic, while its base rigid. A triangular grid as shown in Fig. 6 is adopted as the mathematical atlas. The manifold for this analysis is the superposition of both graphs as depicted in Fig. 7. To show the strength of the manifold method, a very large slope

movement is created by using a very low strength for the soil. Fig. 8 is slope configuration sometimes after the failure takes place as obtained by the manifold method. Fig. 9 shows what the configuration may look like if the slope is, instead, modeled as one piece. Results such as these clearly demonstrate the potential use of the manifold method in seismic hazard mitigation planning involving slope lands.

The work that are still to be carried out include further debugging the code, assessing the current methods used in practice and the determination of slope movement with respect to earthquake magnitudes.

REFERENCES

1. Shi, G. H., "Manifold Method of Material Analysis", Proc. Ninth Army Conf. on Applied Mathematics and Computing, 1991.

FIGURES

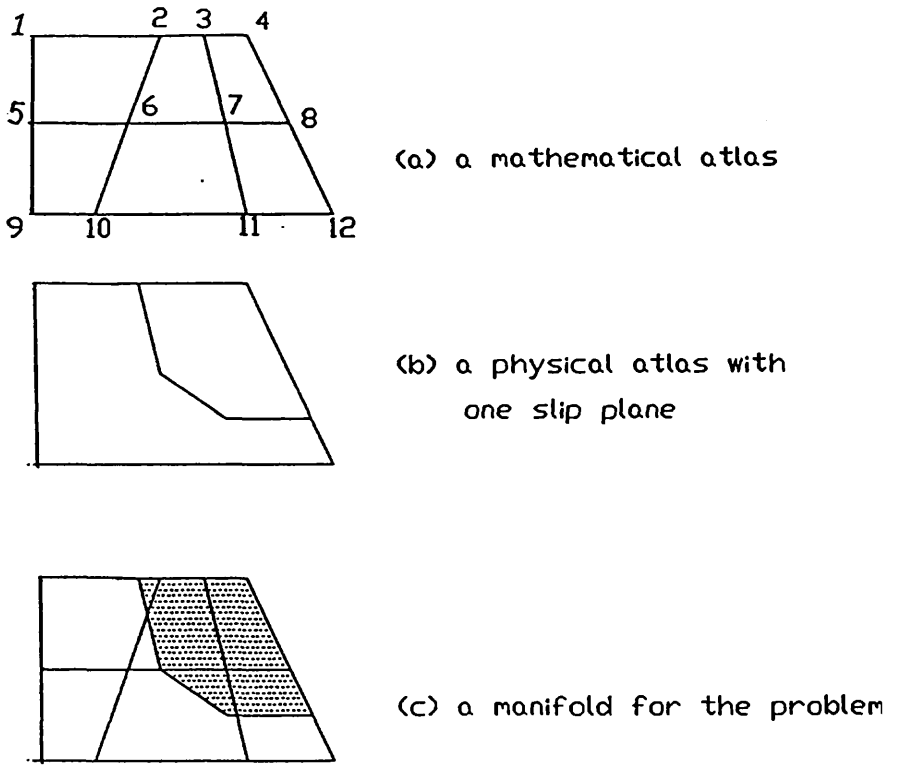

Figure 1 A simple manifold for a continuum with a discontinuity

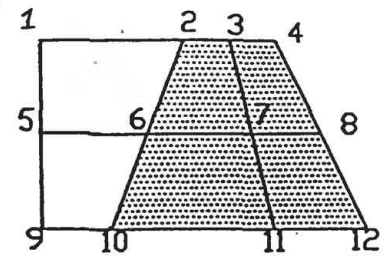

(a) a chart associated with node 7

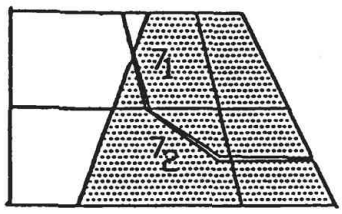

(b) two covers 7_1 and 7_2 formed by Chart 7 and the physical atlas

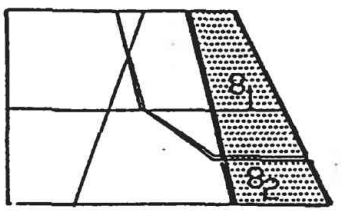

(c) two covers 8_1 and 8_2 formed by Chart 8 and the physical atlas

Figure 2 The concept of chart and covers

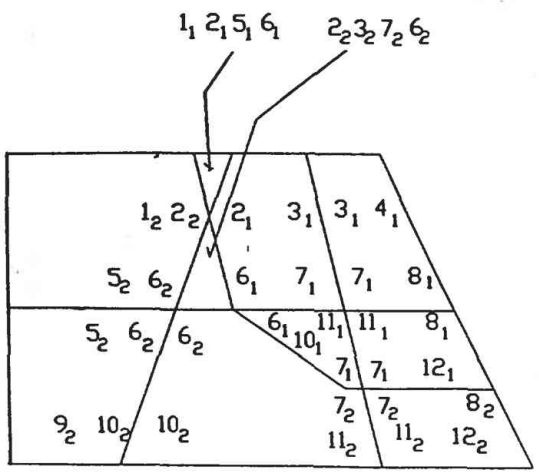

Figure 3 Finite covers and generalized nodes

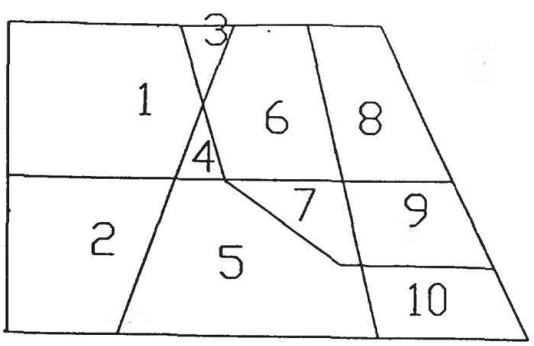

Figure 4 Generalized elements as determined by finite covers

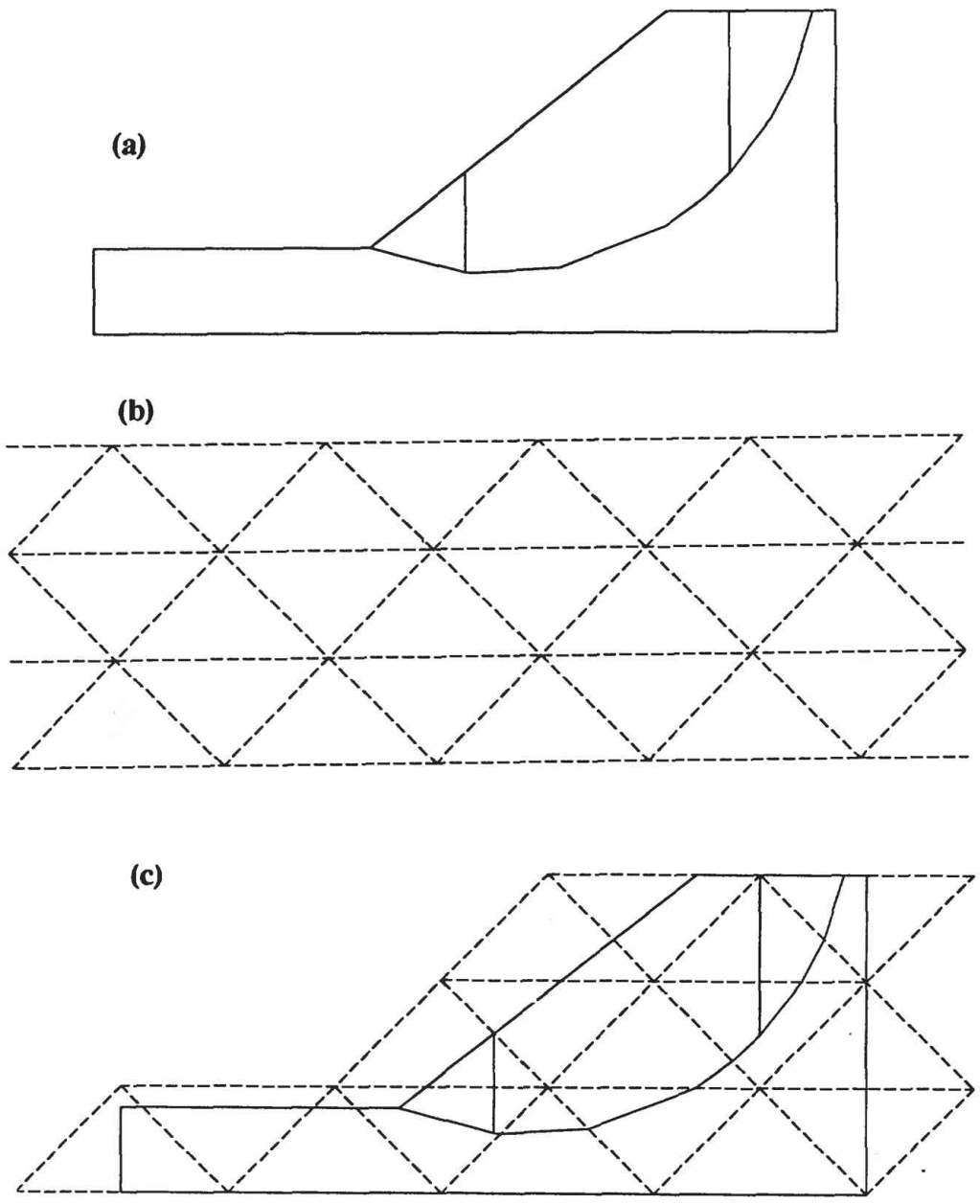

Figure 5 A manifold for slope stability analysis (a)Physical atlas (b)Mathematical atlas (c) A manifold

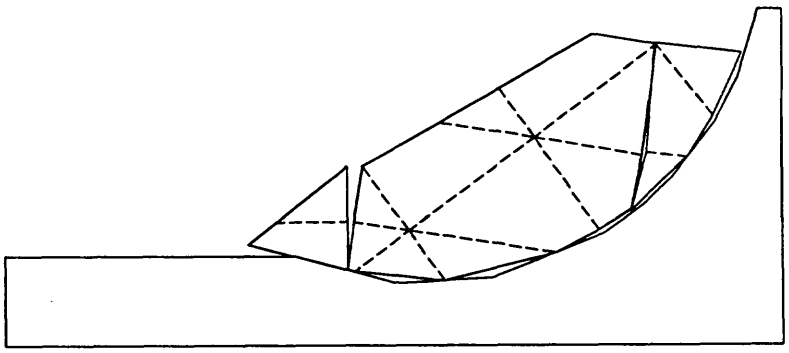

Figure 6 A post-failure configuration of the slope as obtained by the manifold method

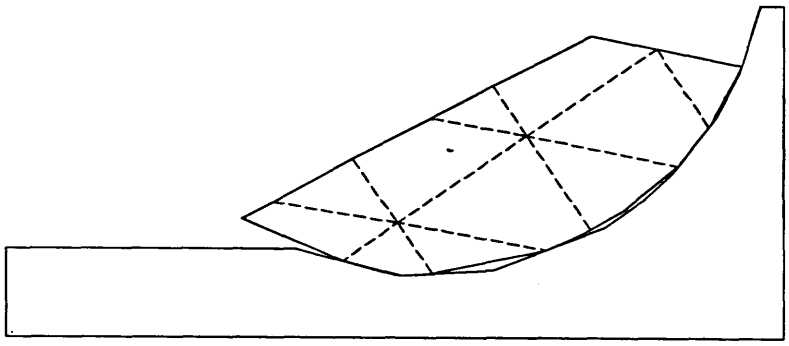

Figure 7 The post-failure configuration if slope moves as one piece.

Small Borehole Locking Seismometer

4-9540-10090

Hsi Ping Liu, Robert L. Maier
Branch of Seismology
345 Middlefiled Road MS-977
Menlo Park, California 94025-3591
415-329-5643

John C. Tinsley
Branch of Western Regional Geology
345 Middlefiled Road MS-975
Menlo Park, California 94025-3591
415-329-4928

Investigations:

1. The quantitative characterization of site-dependent conditions that contribute to enhanced ground motion requires knowledge of the shear-wave velocity of earth materials beneath the site. In order to facilitate making these measurements at as many locations as possible, without having to drill and case our own holes at each site (a burdensome expense), we are designing and building equipment suitable for working in existing small diameter. cased holes drilled for other geological or geophysical purposes. Most of these holes are used for monitoring purposes and commonly use a 2-inch ID casing. To take advantage of these existing holes, we are constructing a small-borehole locking seismometer suitable for use in existing 2-inch diameter cased holes. The prototype instrument or probe is 4.0 ft long and measures 1.75 in. O.D. (outside diameter). The principal technological achievement has been the successful design and manufacture of the locking device that secures the device inside the casing while the measurements are being made.

The instrument is fabricated with an external shell of stainless steel tubing, with internal housings of aluminum used to support and seal all geophones and the gears and motor of the locking device. Among the key components are Oyo Geospace GS-14-L9, 28Hz natural frequency geophones used to sense the horizontal component and a Mark Products L-410 geophone for vertical component of the down-hole seismic waves.

Results:

1. A prototype has been fabricated and presently is awaiting testing. It is noteworthy that one of us (Maier) is a retired mechanical engineer, who contributed significantly to the design and fabrication of the instrument.

Reports:

A summary report containing engineering drawings and a parts list will be filed upon successful testing of the device.

Note: Use of brand names is for informational purposes only and does not constitute an endorsement by the U. S. Geological Survey.

SITE CHARACTERIZATION FOR EARTHQUAKE ENGINEERING STUDIES

9930-14333

Hsi-Ping Liu
Branch of Seismology
U. S. Geological Survey
345 Middlefield Road, MS 977
Menlo Park, California 94025
(415) 329-5643; liu@esg.wr.usgs.gov
Element III. Predicting the Effects of Earthquakes

Investigations

The current aim of this project is, in cooperation with scientists from Center of Earthquake Research and Information (CERI) of the University of Memphis, to measure shear-wave velocity and attenuation in shallow unconsolidated sediments. The 1994 project objectives and work plans are: (1) improvement of our air-powered shear-wave generator in order to ensure the quality of field data acquisition for experiments in the New Madrid Seismic Zone; (2) downhole shear- and compressional-wave velocity measurements in a 58-m deep borehole at Shelby Forest State Park, Tennessee (the soil column consists of loess, sands, and clay); in a 38-m deep borehole at Marked Tree, Arkansas (the soil column consists of unconsolidated fluvial sand deposits); and in a 28-m deep borehole at Risco, Missouri (the soil column consists of fluvial sand and gravel deposits); and (3) incorporating shear-wave velocities in shallow sediments into information for ground-motion amplification in the New Madrid Seismic Zone.

Results

1. One shortcoming existed with our air-powered shear-wave source—a forerunning signal is generated by reaction to the rapid acceleration of an inertial mass when a poppet valve controlling the compressed air is opened. The forerunners limit the accuracy in determining the arrival time and waveform of the shear waves generated when the inertial mass impacts an anvil attached to the baseplate. We have improved that *SH*-wave source, reducing the forerunner amplitude to a negligible amount, by replacing the poppet valve with a ball valve. When a ball valve is opened by turning its stem at a constant angular speed, its flow capacity increases gradually, resulting in a smooth and gradual acceleration of the inertial mass. To compensate for the slower acceleration of the inertial mass, the double-acting air cylinder of the previous design has been replaced by a longer-stroke single-acting air cylinder. The longer stroke allows velocity of the inertial mass to build up before impacting the anvil.

2. Downhole shear- and compressional-wave velocity measurements have been carried out in a 58-m deep borehole at Shelby Forest State Park, Tennessee; in a 38-m deep borehole

at Marked Tree, Arkansas; and in a 28-m deep borehole at Risco, Missouri. Measurements at 3-feet intervals from surface to the bottom of each hole were made and records with high signal-to-noise ratio have been obtained in digital form.

3. Following the Northridge, California earthquake, we side-tracked from the work for the New Madrid Seismic Zone to provide support for the post-earthquake response in the San Fernando Valley, California. We constructed and tested three three-component borehole seimsmometers using Mark Products L-22 geophones as sensing elements. These three borehole seismometers have been successfully deployed in three boreholes (of 242-m, 109-m, and 50-m depths) in San Fernando Valley.

4. In preparation for attenuation measurements in the New Madrid Seismic Zone, the following research has been carried out to improve the methodology of seismic data interpretation in highly-attenuative materials such as loess and sands in the New Madrid Seismic Zone. I resolved some analytical difficuties associated with applying physical anelastic models to the calculation of wave propagation in highly-attenuative media. It is shown that, for a given set of relaxation mechanisms, a lower limit exists for $Q(\omega)$, the seismic quality factor at angular frequency ω. In conformity with field observations that $Q(\omega)$ is approximately constant over a wide frequency renge, a band-limited, six-parameter anelastic model that yields a nearly-constant midband Q for such media has been devised.

Reference cited

Liu, H.-P., R. E. Warrick, R. E. Westerlund, J. B. Fletcher, and G. L. Maxwell (1988). An air-powered impulsive shear-wave source with repeatable signals, *Bull. Seismol. Soc. Am.* **78**, 355-369.

Reports

Liu, H.-P. (1994). Application of band-limited anelastic models to wave propagation in highly-attenuative media, *Bull. Seism. Soc. Am.*, submitted.

EXPERIMENTAL AND THEORETICAL ROCK MECHANICS

9960–10036/12036

D. Lockner, J. Byerlee, D. Moore, C. Morrow, R. Summers
Branch of Earthquake Geology and Geophysics
U.S. Geological Survey
345 Middlefield Road, MS/977
Menlo Park, California 94025
(415) 329-4826
email: dlockner@isdmnl.wr.usgs.gov

In cooperation with:[1]

Investigations

Laboratory experiments are being carried out to study the physical properties of rocks at elevated confining pressure, pore pressure and temperature. The goal is to obtain data that will help us to determine what causes earthquakes and how to predict them. The relevant investigations cover a broad range of conditions. Stick-slip instabilities, which are the laboratory counterpart to earthquakes, are studied to understand both the dynamics of rupture and the processes leading to fault instability. Additional studies of permeability and chemical reactions that can occur in the crust at seismogenic depths are conducted to understand the large crustal system that loads earthquake-prone faults. Investigations are also underway to study conditions of borehole stability to aid in the interpretation of field data related to crustal stress measurements.

Results

The Earthquake Cycle for Fluid-Filled Faults

The San Andreas fault appears to be weak in both an absolute and relative sense. To explain this low strength, it has been proposed that large strike-slip faults contain water in seal-bounded compartments. We propose that a relatively small number of

[1] M. Blanpied and S. Hickman, U.S. Geological Survey, Menlo Park, California; D. Scott and and C. Sammis, University of Southern California, Los Angeles, California; L. Vernik, Stanford University, Stanford, California; M. Rusanov, Nedra Enterprise, Yaroslavl, Russia; T. Röckel, KTB Oberfalz, Windisch-eschenbach, Germany; J. Ma, Institute of Geology, State Seismological Bureau, Beijing, China; B. Armstrong, formerly I.B.M., Palo Alto, California; R. Kerrich, University of Saskatchewan, Saskatoon, Saskatchewan, Canada; S. Stanchits, Ioffe Physical-Technical Institute, St. Petersburg, Russia; A. Ponomarev, Institute of Physics of the Earth, Russian Academy of Sciences, Moscow, Russia.

compartments establish impermeable seals to the surrounding country rock late in the phase of compaction and crack healing between large earthquakes. As a result, the fault zone material in these compartments becomes compacted and lithified and fluid pressure remains near hydrostatic. Consequently, in the interval before an earthquake the undisturbed strength of these compartments is high. By contrast, most compartments in the fault zone establish impermeable seals soon after each earthquake, so that with a small amount of compaction fluid pressure rises to nearly lithostatic levels. Material in these high fluid pressure compartments remains underconsolidated since consolidation is retarded by the low effective confining pressure. When one of the locked sections eventually fails, the system adjoining high and low pressure compartments can become unstable. As slip occurs, the underconsolidated material in the shear zone tends to compact, causing fluid pressure to rise and the gouge to weaken even more. In the low fluid pressure compartments, the material is initially overconsolidated so that when slip occurs the material dilates and reduces pore pressure. This effect leads to 'dilatancy-hardening' of the fault gouge which is expected to suppress the developing earthquake instability. However, the increase in strength due to the drop in fluid pressure is more than offset by the accompanying decrease in strength due to displacement-weakening (failure) of the fault (i.e., the drop from peak to residual strength). If the surrounding rock mass is sufficiently compliant to drive an instability, slip will propagate along the fault until the shear fracture runs into a low stress or high strength region. Frictional heating and the accompanying increase in fluid pressure that are suggested to occur during shearing of the fault zone will act as an additional destabilizing process. However, significant heating occurs only after a finite amount of slip and therefore is more likely to contribute to the energetics of rupture propagation than to the initiation of the instability.

In this model, a number of significant changes occur coseismically that are an integral part of the earthquake cycle. First, a net reduction in shear stress in the region surrounding the earthquake provides the energy for the instability. Second, a net increase in porosity occurs within the fault zone as a result of the rapid coseismic deformation. Since the dominant processes occurring in the interseismic period result in compaction and porosity loss, the coseismic dilatancy is essential to allow for repeated earthquakes. Third, seals that separate fluid pressure compartments are shattered during the earthquake, allowing fluids to move relatively freely between the fault and the surrounding country rock until new seals are formed.

Permeability Loss in Granite Under Hydrothermal Conditions

The earthquake cycle model just described requires the formation of low-permeability mineral seals in or around faults in the intervals between earthquakes. The sealing rate of a given rock type potentially could depend on the degree to which it has been physically disrupted during an earthquake. To test this effect, we measured the high-temperature permeability of Westerly granite in three sample configurations; an intact cylinder, a cylinder containing a throughgoing tensile fracture; and a layer of gouge sandwiched between intact granite pieces. In order to accelerate mineral reactions, the experiments were run at 400°C, with 150 MPa confining pressure and 100 MPa pore pressure.Deionized water was the starting pore fluid; the same fluid was in contact with the sample throughout

an experiment. Permeability decreased over time in all 3 experiments, but in different ways. The permeability of the intact sample decreased uniformly from 1.4×10^{-19}m^2 to 1.8×10^{-20}m^2 over a 45-day period. The rate of permeability reduction of the gouge-bearing sample was initially high but declined over the first 10 to 12 days, after which it stabilized at the same rate of decrease as the intact sample. After 10 days of uniformly high flow rate through the fractured sample, the flow rate decreased rapidly over the next 7 days and then levelled off when it reached the same permeability as the intact sample.

The two halves of the fractured sample were sealed together by mineral deposits. Quartz and K-feldspar crystals on the fracture surface show evidence of dissolution, but at least some quartz and many K-feldspar crystals were redeposited elsewhere along the fracture. Plagioclase reacted with biotite to form numerous albite and actinolitic amphibole crystals. Similar crack-filling mineral deposits were also identified in the other two samples. Our results suggest that both the gouge generated within a fault zone and the fractured country rock surrounding a fault may be subject to rapid sealing by solution-transfer processes and fluid-enhanced mineral reactions. In addition, the high initial rate of permeability decrease in gouge may be caused by increased reactivity of the fines, which are preferentially dissolved and redeposited. The presence of gouge may thus enhance the initial rates of permeability reduction in a fault zone.

Permeability of Sealed Fault Rocks From Yellowknife, Northwest Territories

Studies of the Con Shear Zone near Yellowknife, Northwest Territories suggest that the vein systems were formed by hydrofracturing during past episodes of open system hydrothermal discharge, consistent with fault-valve models in which pore fluids reach supra-lithostatic values under low permeability conditions prior to fault instability (*Sibson*, 1977; *Byerlee*, 1993). Accordingly, the gold-bearing massive silicified basalts and chloritic schists collected from the shears have been identified as possible "sealed-fault rocks" representing the low permeability phase of the fault-valve cycle. Laboratory permeability studies of the rocks were carried out in order to compare field evidence with current fault models. Permeabilities ranged from 10^{-21} to 10^{-23} m^2 at confining pressures up to only a few tens of MPa. These values are exceedingly low on an absolute scale compared to most other deeply buried rocks. Petrographic observations show that extensive hydrothermal activity has sealed and healed pre-existing fractures. This, together with the fine grain size leads to the low hydraulic conductivity of the samples. While these permeability tests are not indicative of supra-hydrostatic conditions *in situ*, the very low permeability values and petrographic evidence are consistent with the theory that the Con Shear Zone rocks are examples of "sealed-fault rocks" in which post-failure hydrothermal precipitation has decreased permeability to very low values, in accordance with current models of fault-valve mechanics.

Effects of Fluids on Fault Strength and Stability

We have conducted triaxial measurements demonstrating that shear-rate-dependent dilatancy observed in dry fault gouge has a strong stabilizing influence when the gouge is saturated and hydraulically isolated from its surroundings. In this case, a pore volume increase results in lowered pore pressure and therefore increased effective normal stress

and shear strength. When applied to crustal faults, this effect would suppress rupture nucleation in favor of slow creep. In one experiment, we sheared a 1-mm-thick layer of quartz gouge in an undrained condition at a nominal pore pressure of 50 MPa and confining pressure of 100 MPa. Slip rate cycling between 0.01 and 10 μm/s resulted in an apparent rate-dependent frictional variation of 0.060 (i.e. (a-b) $\approx$ +0.009). This value is 2 to 10 times greater than (and opposite in sign to) typical rate-weakening values reported for dry bare-rock surfaces. A second experiment in which a drillhole allowed direct communication rate dependence and measurable rate-dependent pore volume variations similar to those reported by *Morrow and Byerlee* (1989), *Marone et al.* (1990) and *Marone and Kilgore* (1993). From our observations we infer that fault zone fluid pressure dropped 14% in our first experiment, resulting in an increase in effective normal stress and the observed increase in shear strength.

If large crustal strike-slip faults are weak due to entrapment of pore fluid at superhydrostatic pressure, this same rate-dependent dilatancy mechanism could be expected to operate. In this case, dilatancy-strengthening effects acting through an increase in effective pressure are expected to more than offset rate-weakening effects reported for bare dry rocks. Laboratory measurements of gouge-filled faults, which would seem a better analog for crustal fault systems than bare rock, generally report neutral to rate-strengthening friction. Thus it would appear that a model based solely on rate-dependent friction would be insufficient, by itself, to result in an earthquake triggering mechanism.

P-wave Velocity and Amplitude Transients due to Fluid Infiltration in Granite

Numerous models have been proposed for the temporal variation of seismic velocities expected to occur prior to an earthquake. Many of these models (e.g., the dilatancy-diffusion model) are based on the observation that brittle failure of rock involves opening of cracks and volumetric strain leading to an under-saturation of the nucleation zone followed by re-saturation due to the influx of water from the surrounding rock. While precursory velocity changes have not been identified in field measurements, neither do we know of laboratory measurements that explicitly show the sequence of velocity decrease and then recovery predicted to occur when fluid diffuses into a stressed rock. At the same time, dilatancy during failure of brittle rock remains an experimental fact.

Therefore, we have performed a laboratory simulation to measure the magnitude and duration of velocity and attenuation changes that can be produced as a rock is deformed to failure. A cylindrical sample of Westerly Granite, 190.5 mm long by 76.2 mm in diameter was deformed at constant confining pressure of 50 MPa. Thirteen piezoelectric transducers (5 transmitters and 8 receivers) with a frequency range of 200 to 1200 kHz were epoxied to the surface of the rock. Constant pore pressure of 1.0 MPa was applied to the ends of the sample. During the experiment discrete axial strain steps were applied to the sample and velocity and attenuation were monitored as the sample adjusted. We show results from two stages of loading (referred to as A and B), at 86 and 95% of peak stress, respectively. Each step lasted 48 hours during which digitized waveform data were periodically collected for 23 ray paths. Strong anisotropy and heterogeneity developed in both velocity and attenuation of P-waves during stages A and B. Both strain steps were characterized by

an initial drop in transverse P-wave velocity, $V_{p\perp}$, of as much as 15% accompanied by an increase in attenuation of 4 to 7 dB. We interpret these changes as resulting from opening of unsaturated microcracks within the rock. As water flowed into the sample, $V_{p\perp}$ in all parts of sample began to increase, and after 48 hours, $V_{p\perp}$ had recovered to within 6% of its initial value. At the same time, however, attenuation continued to increase. Symmetry of the orientation of newly formed microcracks results in anisotropic velocity and attenuation fields which systematically evolve in response to changes in stress, strain and influx of water. These measurements provide constraints on the magnitude and duration of velocity and attenuation transients that can be expected to accompany the nucleation of earthquakes in the Earth's crust.

High Frequency Acoustic Emission Monitoring Near Parkfield, California

An array of four high frequency transducers (30 kHz resonance) has been deployed in shallow holes adjacent to the Varian well near Parkfield, California to monitor naturally occurring acoustic emissions. We will attempt to relate these signals to tidal strains, creep events and strains associated with nearby earthquakes. A recent experiment at the San Francisco Presido (*Valdes-Gonzalez et al.*, 1992] demonstrated that naturally occurring AE were generated in response to both diurnal thermoelastic heating and earth tides. Correlation of the AE signals with nearby strain measurements indicated that the AE is sensitive to local strains on the order of 10^{-9}. Thus, AE monitoring (in the 10 to 60 kHz range) may be of potential use as a local strain monitoring device. Since the acoustic signals in this frequency range suffer rapid attenuation, devices of this type must be responding to strains within a few tens of meters of the transducer. We have now deployed our shallow transducer array and are collecting long-term ambient AE rate data. Preliminary results show strong diurnal and semi-diurnal fluctuations in AE rate. We are in the process of comparing these AE time series to Earth tide and local strainmeter data. The successful correlation of AE with earth tides is considered the most important objective since this will provide a measure of the sensitivity of AE to local strain changes.

Articles and Reports

Blanpied, M. L., J. D. Byerlee, and D. A. Lockner, Effects of temperature and P_{H_2O} on frictional strength of granite, *U.S. Geological Survey Open File Report, 94-228*, in press, 1994a.

Blanpied, M. L., D. A. Lockner, and J. D. Byerlee, Frictional slip of granite at hydrothermal conditions, *J. Geophys. Res.*, submitted, 1994b.

Blanpied, M. L., C. J. Marone, D. A. Lockner, and J. D. Byerlee, Friction constitutive parameters for sliding granite at dry vs. hydrothermal conditions or - Quantitative measure of the variation in fault rheology due to fluid-rock interactions, *J. Geophys. Res.*, in preparation, 1994c.

Fenoglio, M. A., M. J. S. Johnston, and J. D. Byerlee, Magnetic fields associated with changes in high pore pressure in fault zones - application to the Loma Prieta ULF emissions, *J. Geophys. Res.*, in press, 1994.

Johnston, M. J. S., M. A. Fenoglio, and J. D. Byerlee, Strain, magnetic and electric fields associated with changes in pore pressure within fault zones, *U.S. Geological Survey Open File Report*, in press, 1993.

Kuksenko, V., N. Tomilin, E. Damaskinskaya, and D. Lockner, A two-stage model of fracture of rocks, *Pure Appl. Geophys.*, submitted, 1994.

Lockner, D., and B. Evans, Densification of quartz powder and reduction of conductivity at 700°C, *J. Geophys. Res.*, in press, 1994.

Lockner, D. A., The role of acoustic emission in the study of rock fracture, *Int. J. Rock Mech. Min. Sci. & Geomech. Abstr., 30*, 883–899, 1993.

Lockner, D. A., Rock failure, in *AGU Handbook of Physical Constants*, edited by T. J. Ahrens, in press, 1994.

Lockner, D. A., and J. D. Byerlee, Dilatancy in hydraulically isolated faults and the suppression of instability, *Geophys. Res. Lett.*, in press, 1994a.

Lockner, D. A., and J. D. Byerlee, Precursory AE patterns leading to rock fracture, in *Proceedings, Fifth Conference on Acoustic Emission/Microseismic Activity in Geological Structures and Materials*, edited by H. R. Hardy, Trans-Tech Publications, Clausthal-Zellerfeld, Germany, 14 (in press), 1994b.

Lockner, D. A., and J. D. Byerlee, An earthquake instability model based on faults containing high fluid-pressure compartments, *Pure Appl. Geophys. (ISMPG mtg. Beijing, Sept. 1994)*, submitted, 1995.

Lockner, D. A., S. A. Stanchits, J. D. Byerlee, and A. V. Ponomarev, Anisotropic changes in P-wave velocity and attenuation during deformation and fluid infiltration of granite, *Internat. J. Rock Mech. and Min. Sci. Abst.*, in preparation, 1995.

Moore, D. E., and D. A. Lockner, The role of microcracking in shear-fracture propagation in granite, *J. Struct. Geol.*, in press, 1994.

Moore, D. E., D. A. Lockner, and J. D. Byerlee, Reduction of permeability in granite at elevated temperatures, *Science, 265*, 1558–1561, 1994.

Morrow, C., D. A. Lockner, S. Hickman, M. Rusanov, and T. Röckel, Effects of lithology and depth on the permeability of core samples from the Kola and KTB drill holes, *J. Geophys. Res., 99*, 7263–7274, 1994.

Morrow, C. A., and D. A. Lockner, Permeability differences between surface-derived and deep drillhole core samples, *Geophys. Res. Lett., 21*, 2151–2154, 1994.

Reches, Z., and D. A. Lockner, Nucleation and growth of faults in brittle rocks, *J. Geophys. Res., 99*, 18,159-18,173, 1994.

Scott, D. R., D. A. Lockner, J. D. Byerlee, and C. G. Sammis, Triaxial testing of Lopez fault gouge at 150 MPa mean effective stress, *Pure Appl. Geophys., 142*, 749–775, 1994.

Vernik, L., S. Hickman, D. Lockner, and M. Rusanov, Ultrasonic velocities in cores from the Kola superdeep well and the nature of subhorizontal seismic reflections, *J. Geophys. Res.*, in press, 1994.

Abstracts:

Blanpied, M. L., J. D. Byerlee, and D. A. Lockner, Effect of temperature and P_{H_2O} on slip of granite, in USGS Red Book Conference on the Mechanical Involvement of Fluids in Faulting, Fishcamp, Calif., 1993.

Byerlee, J. D., The role of water in the evolution of large strike-slip faults, in *SGTSG Conference*, 1994.

Byerlee, J. D., and D. A. Lockner, The earthquake instability on faults containing water in seal-bound compartments, *Eos (Amer. Geophys. Union Transactions), 75*, 425–426, 1994a.

Byerlee, J. D., and D. A. Lockner, The earthquake instability on faults containing water in seal-bounded compartments, in *IUTAM Symposium on Mechanics Problems in Geodynamics*, Beijing, China, edited by R. Wang, Intern. Union of Theor. Appl. Mech., 1994b.

Fenoglio, M. A., M. J. S. Johnston, and J. D. Byerlee, Magnetic fields associated with changes in high pore pressure in fault zones - application to the Loma Prieta ULF emissions, *Eos, Trans. American Geophys. Union, 74*, 441, 1993.

Lockner, D. A., and J. D. Byerlee, An earthquake instability model based on faults containing high fluid pressure compartments, in *ASME 1994 International Mechanical Engineering Congress and Exposition*, Chicago, IL, edited by R. C. Batra and H. Zbib, 1994.

Lockner, D. A., D. E. Moore, and J. D. Byerlee, Rate of permeability reduction in granite at elevated termperatures, in *Chapman Conference: Hydrothermal Processes: Building and Testing Atomistic- to Basin-Scale Models, June 6-9, 1994, Loon Mtn., Lincoln, New Hampshire*, edited by T. Torgersen, AGU, 1994.

Lockner, D. A., S. A. Stanchits, J. D. Byerlee, and A. V. Ponomarev, P-wave velocity and amplitude transients due to fluid infiltration in granite, *Eos (Amer. Geophys. Union Transactions), 75*, 615, 1994.

Moore, D. E., and D. A. Lockner, Quantitative analysis of the process zone of a propagating shear frature in granite, *GSA Abstracts with Programs*, 1994.

Moore, D. E., D. A. Lockner, R. Summers, and J. D. Byerlee, Permeability changes in intact, fractured and crushed granite under hydrothermal conditions, *Eos (Amer. Geophys. Union Transactions), Fall Mtg.*, 1994.

Morrow, C., R. Kerrich, D. Lockner, and J. Byerlee, Permeability of sealed fault rocks from Yellowknife, Northwest Territories, *Eos (Amer. Geophys. Union Transactions), 75*, 637, 1994.

Stanchits, S. A., D. A. Lockner, A. V. Ponomarev, and J. D. Byerlee, Anisotropic changes in P-wave velocity and attenuation during deformation and fluid infiltration of granite, in *Second Internat. Conference on Mechanics of Jointed and Faulted Rock*, Vienna, Austria, edited by H. P. Rossmanith, Balkema, A. A., 1995.

Vernik, L., S. Hickman, D. Lockner, and M. Rusanov, Ultrasonic velocity in cores from the Kola superdeep well and the nature of subhorizontal seismic reflections, *Eos (Amer. Geophys. Union Transactions), 75*, 676, 1994.

Reassessment of Seismic Sources and their Earthquake Recurrence Rates for Use in Probabilistic Ground Motion Mapping in the Pacific Northwest
9950-13425

David M. Perkins, Paul C. Thenhaus
Branch of Earthquake and Landslide Hazard
US Geological Survey
Mail Stop 966 Box 25046
Denver Federal Center
Denver, CO 80225

Ph: (303) 273-8554; Fx (303) 273-8600; perkins@gldvxa.cr.usgs.gov

Program Element: III.4

This purpose of the project: Convoke a workshop to obtain information to be used by USGS staff to define new source zones and source faults for probabilistic ground motion maps and building code zonation for the Pacific Northwest. Demonstrate how geoscience information relates to the needs of the engineers and hazard analysts. The workshop was held at the University of Washington on June 7 and 8th, 1994 at the University of Washington student union. Attendance was about 60, half researchers funded under NEHRP and half university, consultant, and user professionals

Investigations and Issues

Major elements scheduled for discussion at the Workshop:

Past and current hazard work: zonations, maps and expression of maps in codes. Zonation and fault modeling alternatives. Probabilistic and deterministic ground motions in building codes.

Brief statements of items of outstanding concerns held by individual attendees.

Cascadia subduction zone. Landward boundary of plate interface, width of interface. Uniformity of seismic potential along the plate interface. Various maximum magnitudes and their recurrences.

Active slab-bend region. Extent of the intermediate-focus earthquakes. Recurrence rates south of Puget Sound.

Mount St. Helens seismicity trend. Extent, spatial extrapolation, and maximum magnitude. Do the data support extrapolation of low-magnitude recurrence rates to rates for damaging magnitudes?

Issues related to fault models. Comparison of alternate methods for establishing recurrence rates for known Holocene faults. Is inventory of these faults complete? Should all Quaternary faults be represented? What are their activity rates? Are all Quaternary faults known? How should a seismic source model account for possible unknown Quaternary faults? Where could areal fault zones and random fault rupture be used in lieu of modeled faults?

Puget Sound. Modeling the surface seismicity in the area: The hazard of the Seattle Fault. Should other transverse, high-gravity gradient features be treated as analogs of the Seattle fault, and what should their recurrences be?

Portland Vicinity. Bases for detailed source models in the vicinity. Should there be a Scotts Mills source zone? Are there other fault analogs to this source near Portland?

Northern and Southern Cascade Mountains region. Candidate individual fault sources. Alternative areal source zones. Recurrence for a Klamath Mountains source zone.

Accretionary wedge. Seismic potential of continental-shelf faults and possible on-shore extensions.

Columbia plateau. How to model earthquake potential? Olympic-Wallowa lineament (OWL). Depth of faulting along the OWL. Depth of faulting in fault-cored folds of the Yakima fold belt.

Consensus and conflicts. Can a consensus zonation be developed? Comments on the "consensus" issues of application to engineering and codes. Implications for research priorities.

Results.

The following represent salient observations, but should not be taken as established results.

Concerns: Disagreement as to whether all significant crustal faults could have been delineated by now. Wide range of hazard estimates from a subduction earthquake. Desirability of detailed source descriptions being made available. Desire to continue use of peak acceleration rather than only spectral ordinates, inasmuch as conversion to spectral base design amongst practicing engineers may take 10 years, and peak acceleration is more intuitively understood. Use of deterministic earthquakes to set floors for ground motions. Need for map to reflect consensus of experts.

Cascadia subduction zone. A subduction zone capable of producing large, damaging earthquakes is well-established. There is still prevailing disagreement on maximum magnitudes and recurrences. A maximum magnitude of 8.25–8.5 is too small because a long length of sites investigated for marsh subsidence show near-synchronous events. Lack of widespread paleo-liquefaction evidence does not rule out a maximum magnitude as large as 9, because the distance from the subduction rupture to most inland sites is large, and few sites have readily liquefiable sediments.

Active slab-bend region. The north-south extent over which intermediate-depth magnitude 7 events might extend is obvious between 47 and 49 degrees latitude. Small magnitude events are found at intermediate depths north and south of these limits at very low seismic rates, making a magnitude 7 possible under Portland, though not likely, and may be impossible all the way to California.

Mount St. Helens seismicity trend. Activity analogous to the NNW linear trend now seen in the vicinity of Mount St. Helens could occur throughout the Cascades.

Issues related to fault models. Strong consensus that faults should be modeled individually where known and that recurrence be estimated slip rates. A characteristic earthquake model is generally preferred, but not a definitive model for all faults. The fault inventory is about 80 percent complete for Oregon. Some significant problems remain: Slip-rate based recurrences predict too frequent recurrences in southern Oregon (though the difference may not be very significant for probabilistic ground motion). A large percent of Holocene faults have no geologic evidence of earlier Holocene or even late Quaternary movement. Maximum magnitude is crucial for determining recurrence for the characteristic earthquake model, demonstrating a need for constraint on this parameter. Fault length alone is not sufficient. A method was demonstrated for determining the maximum magnitude using the thickness of the crust down to the brittle ductile boundary and the dip of the rupture plane. Also, historical seismicity can provide a crucial constraint since low maximum

magnitudes generate much too high recurrences. High maximum magnitudes, on the other hand, may produce recurrences so long as to produce very low probabilistic ground motion hazard for short return periods (e.g., 500 years).

Puget Sound. A ramp fault model may explain zones of uplift and subsidence in Puget Sound estuaries. Parameters in this model suggest long recurrences for magnitude 7 events. Uplift on the Seattle fault is 0.2 to 0.4 mm/year. Focal mechanisms are generally in agreement with the ramp model, but seismicity patterns show little difference between 10–20 km slices and 20–30 km slices, indicating that some ramp-associated features may descend below the presumed ramp surface. At one location, coal data suggest uplift as much as 1 mm/yr.

Portland Vicinity. The Scotts Mills earthquake could reasonably be associated with the Bright Angel Fault, and there are other analogous faults in the vicinity of Portland. However, individual researchers dispute best focal mechanism orientations, making association of hazard with individual faults difficult.

Northern and Southern Cascade Mountains region. Great reluctance was expressed to attaching seismicity to individual hypothetical faults in the the Cascades. Generally a diffuse areal zonation is preferred.

Accretionary wedge. Although definite fault-like features are found in offshore sediments, there was general reluctance to modeling individual source faults.

Columbia plateau. Maximum magnitudes could be as high as 7.3 for the Topponish Ridge feature, but if faulting is associated only with basalts the maximum magnitude may be as low as 6. Focal mechanism do not support treating the Olympic-Wallowa lineament as a distinct feature.

Consensus. Using the Pezzopane-Weldon Quaternary fault map as a base, Ray Wells attempted a sketch map representing both map area discriminations suggested in the workshop and his own ideas of zonation based on domains of different styles of tectonic expression. This map was well received, because it summarized so neatly many of the points made in the workshop, although there was reservation that the zones went beyond what was scientifically established.

Residual concerns. Two largest historic Vancouver Island earthquakes do not appear to be associated with the Nootka fault zone. Indeed, the three largest shallow events in the Pacific Northwest do not seem to be associated with known faults. Hence one should be reluctant to associate hazard only with known faults.

Strain rates for the entire pacific Northwest may be ten times smaller than those of California, arguing significantly lower hazard from crustal earthquakes.

Continued disagreement remains both on whether to model individual faults in the western Puget lowlands and on discriminating the eastern lowland from the western on the basis of seismic rate.

National Earthquake Information Service

9920–10022

Waverly J. Person
Branch of Earthquake and Geomagnetic Information
U.S. Geological Survey
Denver Federal Center
Box 25046, Mail Stop 967
Denver, Colorado 80225
(303) 273–8500

Investigations and Results

The Quick Epicenter Determinations (QED) continues to be available to individuals and groups having access to a 1200- or 2400-baud terminal or computer with dial-up capabilities to a toll-free WATS number or a commercial telephone number in Golden, Colorado. It is also accessible via BBS. The QED has become one of our most popular ways of making near real-time earthquake information available to the general public and scientists throughout the world. The time period of data available in the QED is approximately three weeks (from about two days behind real time to the current PDE in production). With the exception of any earthquake that is released to the press (felt earthquakes in the United States, magnitude 6.5 or greater anywhere in the world or potentially damaging), the parameters of these earthquakes will be on the computer for our users within one hour after the release. The QED program is available on a 24-hour basis, 7 days a week. From October 1, 1993 through September 30, 1994, there were 64,044 logins to the On-Line Information System, which includes the QED, earthquake lists, and a geomagnetic field values program to generate QED programs. A daily QED message, 7 days behind real time, is transmitted to many different agencies and individuals in the United States and throughout the world via electronic mail, over 800. The daily QED message is also distributed to another 32 agencies via U.S. government communications (VADATS/DTS/AUTODIN), including worldwide distribution on the communications system of the World Meteorological Organization.

NEIS is making extensive use of electronic mail for data acquisition. Data are now being received via GEONET, TYMNET, internet, BITnet, DECNET/SPAN and uucp on a regular basis from several dozen agencies. Some of the agencies sending data to the NEIS via electronic mail include the following:

Universidad Nacional Autonoma de Mexico, Mexico City
Istituto Nazionale di Geofisica, Rome, Italy
Centre Seismologique Euro-Mediterranean, Bruyeres-le-Chatel, France
Kandilli Observatory, Istanbul, Turkey
Harvard University, Cambridge, MA (Centroid, Moment Tensor Solutions)
Graefenberg Observatory, Germany

Icelandic Meteorological Institute, Reykjavik, Iceland
Central Seismological Observatory, Obninsk, Russia
Seismological Survey, Ljubljana, Slovenia
Inst. of Seismology, Helsinki, Finland
Australian Geological Survey Organization
Institute of Geological and Nuclear Sciences, Ltd.
Universidad Nacional de la Plata, Argentina
INSIVUMEH, Guatemala City, Guatemala
Bureau Central Seismologique Francaise, Strasbourg, France
Universidad de Chile, Santiago, Chile
Geofyzikalni ustav CSAV, Prague, Czech Republic
Slovak Academy of Sciences, Bratislava, Slovakia
USGS Guam Observatory, Mariana Islands

In addition, the following agencies contribute data to the PDE program by computer file transfer or remote login via the computer networks:

USGS Calnet and Alaska Seismic Projects, Menlo Park
USGS/California Institute of Technology, Pasadena
USGS Fredericksburg Observatory, Corbin, Virginia
University of California, Berkeley
University of Southern California, Los Angeles
University of Washington, Seattle
Oklahoma Geophysical Observatory, Leonard

Over 700 receive the earthquake release which is put on QED messages via e-mail.

The following organizations are now receiving automatic notification messages about earthquakes located by the NSN system when an earthquake meets their notification criteria:

Recipient		Event Criteria	
S. Sipkin, USGS/NEIC		≥5.5	worldwide
T. Heaton, CalTech, Pasadena, CA		≥5.5	worldwide
	or	≥2.5	in CA or NV
Duty Officer, PTWC, Honolulu, HI		≥5.5	worldwide
USGS CalNet Duty Officer, Menlo, CA		≥4.0	in CA or NV
Union Pacific Railroad, Omaha NE		≥4.5	in contig. US
T. Ahern, IRIS/DMC, Seattle, WA		≥5.5	worldwide
B. Hammond, AEIC, Fairbanks, AK		≥2.5	in AK
S. Malone, Univ. of Washington		≥2.5	in WA or OR
B. Herrmann, St. Louis University		≥3.0	in Central U.S.
S. Davis, CERI, Memphis State		≥3.0	in Central U.S.
Weatherdata, Inc., Wichita, KS		≥4.5	in contig. U.S.

L. Gomez, INDRHI, Dominican Republic	≥4.8	in/near Dom. Rep.
W. Hanke, GFZ, Potsdam, Germany	≥5.5	worldwide
M. Henger, BGR, Hanover, Germany	≥5.5	worldwide
G. Schweitzer, GERESS, Bochum, Germany	≥5.5	worldwide & others
G. Malave, INTEVEP, Venezuela	≥5.0	in/near Venezuela
J. Mejia, OSSO, Cali, Colombia	≥5.0	in/near Colombia
INGEOMINAS, Bogota, Colombia	≥5.0	in/near Colombia
Univ. of West Indies, Trinidad	≥5.0	in eastern Caribbean
G. Smriglio, ING, Rome, Italy	≥5.5	worldwide
J. Fyen, NORSAR, Norway	≥5.5	worldwide
Inst. of Geophysics, UNAM, Mexico	≥4.8	in/near Mexico
U. Kradolfer, ETH, Zurich, Switz.	≥5.5	worldwide
Japan Meteorological Agency, Tokyo	≥5.5	worldwide
Duty Officer, CSEM, Bruyeres-le-Chatel, France	≥5.5	worldwide
Duty Officer, ReNass, Strasbourg, France	≥5.5	worldwide

Recipient		Event Criteria	
M. Villagran, INSIVUMEH, Guatemala		≥4.8	in/near Guatemala
J. Mendoza, FUNVISIS, Venezuela		≥5.0	in/near Venezuela
E. Norabuena, IGP, Lima, Peru		≥5.5	in/near Peru
FEMA, Washington, DC		≥4.5	in contig. US, HI, or central or SE AK
D. Rosen, UN Radio Readiness Group, NY		≥5.5	worldwide
Duty Officer, IGN, Madrid, Spain		≥5.5	in/near Spain
USGS Calnet Computer, Menlo Park		≥2.5	in CA or NV
	or	≥4.5	in contig. US
	or	≥5.5	worldwide

Telegraphic data are now being exchanged with Russia on most larger earthquakes. The data from the countries of the former Soviet Union are being received from the Central Seismological Observatory, Obninsk, under the auspices of the World Data Center system. Our designation as World Data Center A for Seismology played a key role in permitting this exchange to be established.

Data from the People's Republic of China via the American Embassy continue to be received in a very timely manner and in time for the PDE publication. We continue to receive four stations on a weekly basis from the State Seismological Bureau of the People's Republic of China. The Bulletins with additional data are not being received at the present time. We are in the process of establishing routine data exchange by electronic mail.

Special efforts are being made to receive more data from the Latin American countries on a more timely basis. The increased availability of telefax and electronic mail is permitting much more interaction with Latin American countries than in

the past, but there are still problems getting data on a timely basis for many large earthquakes.

We have rapid data exchange (alarm quakes) with Centre Seismologique Euro-Mediterranean (CSEM), France and Istituto Nazionale de Geofisica, Rome, Italy, and Sicily, and data by telephone from Mundaring Geophysical Observatory, Mundaring, Western Australia and Pacific Tsunami Warning Center in Honolulu. The geophysical laboratory in Papeete, French Polynesia contributes a single-station estimate of seismic moment within about 24 hours of a large event in the Pacific region. We also have the capability to dial into computers at the EMSC Australian Geological Survey Organization, Canberra, Australia, and Swiss Seismic Services at Zurich, Switzerland, and collect data on recent earthquakes. The Monthly Listing of Earthquakes is up to date. As of September 30, 1994, the Monthly Listing and Earthquake Data Report (EDR) have been completed through May 1994. The total number of events located for 1993 was 21,476, the largest number for any given year. Radiated energy, moment tensor, P-wave first-motion and broadband depth solutions continue to be determined by the USGS when possible and published in the Monthly Listing and EDR for any earthquake having an m_b magnitude ≥ 5.8. Moment tensor solutions are being computed by the NEIC, and centroid, moment tensor solutions contributed by Harvard University are being published in the Monthly Listing and EDR. Moment tensor solutions and broadband depths are being published in the QED for selected events. Also, the M_W magnitude is being published on a routine basis in the QED, PDE, and Monthly Listing for most earthquakes of magnitude 5.5 and above.

The Earthquake Early Alerting Service (EEAS) continues to provide information on recent earthquakes on a 24-hour basis to the Office of Earthquakes, Volcanoes, and Engineering; scientists; news media; other government agencies; foreign countries; and the general public.

One-hundred and eighteen releases were made from October 1, 1993 through September 30, 1994. The most significant earthquakes in the United States were as follows:

- November 19, 1993, a magnitude 6.5 Mw in Unimak Island region. Slight damage occurred at False Pass.
- December 4, 1993, a magnitude 5.4 Mw in Oregon. Damage at Klamath Falls and slight damage at Tulelake, California.
- January 17, 1994, a magnitude 6.7 Mw in southern California (Northridge). Sixty people were killed; more than 7,000 were injured, and maybe as much as 20 billion dollars in damage.
- January 17, 1994, an aftershock of magnitude 5.9 Mw. Additional damage in the epicentral area. Altogether there were 10 aftershocks having magnitudes of 5.0 or greater.

- September 1, 1994, a magnitude 7.1 Mw occurred off the cost of northern California. It was felt throughout much of northern California and parts of southern Oregon. Local tsunami generated maximum wave height (peak-to-trough) of 14 cm at Crescent City.

The most significant foreign earthquakes were as follows:

- October 13, 1993, a magnitude 7.0 Ms, in eastern New Guinea region, Papua, New Guinea.
- October 25, 1993, a magnitude 7.0 Ms, in eastern New Guinea region, Papua, New Guinea.
- November 13, 1993, a magnitude 7.0 Ms near east coast of Kamchatka. It was felt at Petropavlovsk-Kamchatskiy and Severo-Kurilsk.
- January 21, 1994, a magnitude 7.2 Ms in Halmahera, Indonesia. Seven people were killed, 40 injured, and 550 houses damaged in the Kau area.
- February 5, 1994, a magnitude 6.2 Mw in Uganda. At least two people were killed, several injured, and most buildings damaged in the Fort Portal area. Two people were killed and one injured by a landslide in Kasese.
- February 12, 1994, a magnitude 7.1 Ms in the Vanuatu Islands and was felt at Port-Vila.
- February 15, 1994, a magnitude 7.0 Ms in southern Sumatera, Indonesia at least 207 people were killed, more than 2,000 injured, and 75,000 were left homeless. There was extensive damage from landslides, mudslides, and fires in Lampung Province. Much of the damage and loss of life occurred in the Liwa area. Damage was estimated to be about 169 million in U.S. dollars.
- February 23, 1994, a magnitude 6.1 Ms in northern Iran. Six people were killed and many injured in the Sistan region.
- March 1, 1994, a magnitude 6.0 Mw in southern Iran. At least two people were killed, 50 injured and reports of damage in the Firuzabad area.
- March 2, 1994, a magnitude 5.1 Ms in Haiti region. Four people were killed and there was damage to houses in the St. Luis du Nord area.
- March 9, 1994, a magnitude 7.5 Mw in Fiji Islands region. It was felt at Suva and Lautoka Viti Levu.
- March 14, 1994, a magnitude 7.0 Mw on the central Mid-Atlantic Ridge.
- June 2, 1994, a magnitude 7.7 Mw south of Jawa, Indonesia. At least 250 people were killed, 27 were missing, 423 injured, and 1,425 houses were damaged or destroyed, leaving many people homeless. Approximately 278 boats sank or were damaged by the tsunami along the southeast coast of Jawa. Tsunamis of 5 meters occurred in some places.
- June 6, 1994, a magnitude 6.8 Mw in Colombia. At least 295 people were killed, 27 were missing, 423 were injured, and 1,426 houses were damaged or destroyed. Another 500 were missing and 13,000 left homeless. Severe damage to houses, highways, and bridges by the earthquake and ensuing landslides in Cauca and Huila Department. Moderate structural damage occurred at Bogota and Cali.

- June 9, 1994, a magnitude 8.2 Mw in northern Bolivia. Five people were reported killed in Peru. Three people were killed in Arequipa Province by a landslide collapsing their house and two were killed in Cuzco Province—one by falling debris and the other by a heart attack. It was felt at many locations in North America including Los Angeles, California; Renton, Washington; Omaha, Nebraska; Sioux City, Iowa; Minneapolis, Minnesota; La Crosse, Wisconsin; Chicago, Illinois; Parkersburg, West Virginia; Norwich, Connecticut; Boston, Massachusetts; and Toronto, Canada. This is the first earthquake from this part of South America believed to have been felt in North America and is also believed to be the largest ever recorded in this general area.
- July 13, 1994, a magnitude 7.4 Ms in Vanuatu Islands. It was felt on Ambrym, Aoba, Efate, Epi, Erromongo, Espiritu Santo, Maewo, Malakula, and Pentecost.
- August 18, 1994, a magnitude 5.9 Ms in northern Algeria. At least 159 people were killed, 289 were injured, 8,000 to 10,000 were left homeless, and thousands of structures were destroyed in Mascara Province.

Reports

Monthly Listing of Earthquakes, in Seismological Research Letters, Eastern Section, SSA, v. 65, no. 2, January-March 1993; v. 65, no. 3 and no. 4, April-June 1993 and July-September 1992; v. 65, no. 1, October-December 1992. Compilers: Jacobs, W., Chang, P., Koyanagi, S., Lavonne, C., Minsch, J., Needham, R., Person, W., Presgrave, B., Schmieder, W., Tatalaski, P.

Monthly Listing of Earthquakes and Earthquake Data Reports (EDR); 12 publications from July 1993 through May 1994. Compilers: Jacobs, W., Chang, P., Koyanagi, S., Lavonne, C., Minsch, J., Needham, R., Person, W., Presgrave, B., Schmieder, W., Tatalaski, P.

Person, Waverly J., Earthquakes, in Earthquakes and Volcanoes, v. 24, no. 1, November–December 1992, January-February 1993; Global Distribution of Earthquakes with M≥7.0 in 1992, v. 24, no. 2., March-April 1993; v. 24, no. 3, Earthquakes, May-June 1993; v. 24 no. 4, Earthquakes, July-August 1993.

Person, Waverly J., Seismological Notes: Bulletin of the Seismological Society of America, v. 83, no. 6, January–February 1993; v. 84, no. 1, March–April 1993; v. 84, no. 2, May–June 1993; v. 84, no. 3, July–August 1992; v. 84, no. 4, September–October 1993; v. 84, no. 5, November–December 1993.

Preliminary Determination of Epicenters (PDE); 52 weekly publications from October 1, 1993 through September 29, 1994, numbers 36–93 through 36–94. Compilers: Jacobs, W., Chang, P., Koyanagi, S., Minsch, J., Person, W., Presgrave, B., Schmieder, W., Tatalaski, P.

Additional Outreach

Number of calls received on 24-hour answering machine for earthquake information	39,371
Number of requests received from the public for earthquake information	4,009
Number of visitors that have taken tours or received invited talks	8,452
Number of outside presentations by Waverly Person	42
Number of tours given by the NEIS staff	411
Number of Tremor 2 calls (Aug.–Sept.)	155

Significant Earthquakes of the World (October 1, 1993 — September 30, 1994)

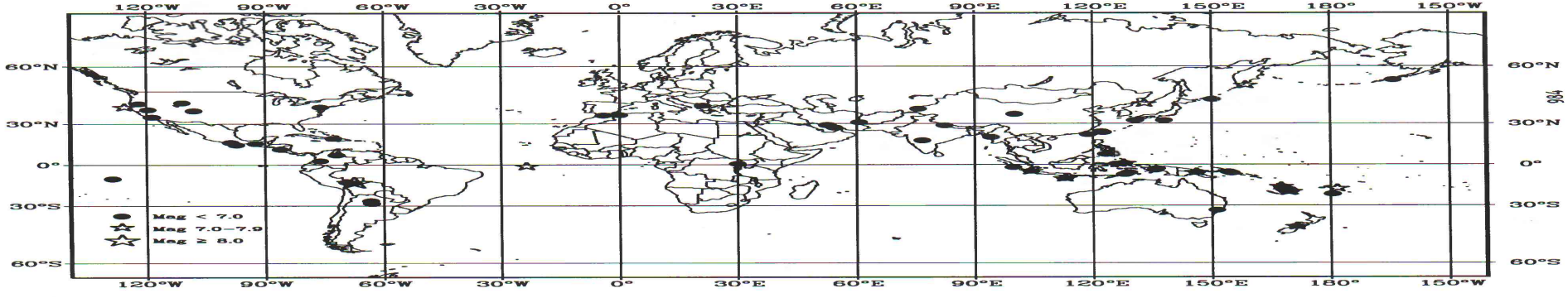

Significant Earthquakes of the Contiguous United States
(October 1, 1993 — September 30, 1994)

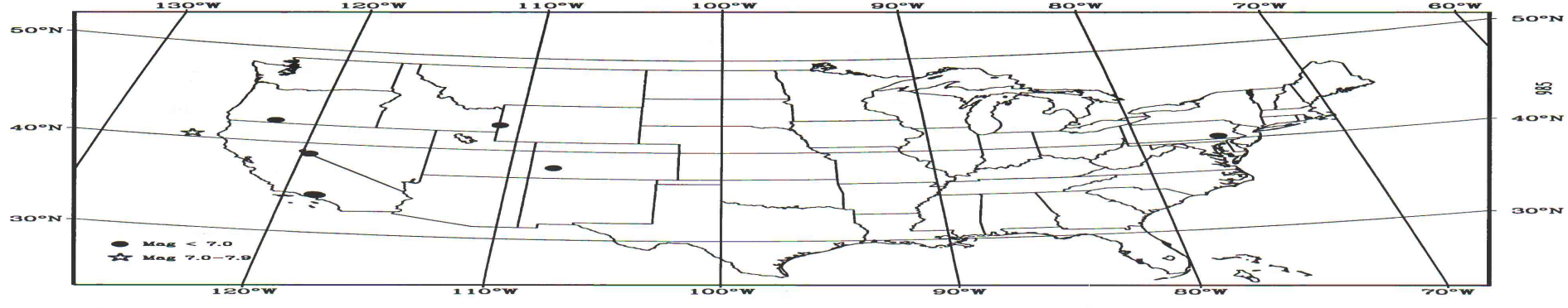

Developing Ground-shaking Site Factors for Applications in Hazard Mapping in Los Angeles Basin

Project No.: 9950-11455
Project Chief: A. M. Rogers
S.C. Harmsen
D.M. Perkins
Branch of Earthquake and Landslide Hazards
U.S. Geological Survey
Box 25046, MS 966
Denver, CO 80225
303-272-8553
Program Task/Subtask: III.2, III.4

Investigations Undertaken

1.) We have begun comparisons of spectral ratios derived directly from soil-rock ratios with those obtained from direct linear least squares inversion assuming a Brune source function. This technique, which is based on the work of Andrews (1986), Anderson and Humphrey (1991), and Hartzell (1984), permits us to obtain the site response function without a reference site. If this technique can be shown to be valid, much more data will be available for site response studies than would be otherwise possible.

2.) We have evaluated the scaling of peak accelerations with magnitude and distance using a finite-fault earthquake source that incorporates isochron addition, extremal statistical properties, and sampling bias caused by instrument triggering levels.

3.) We have begun installation of two borehole strong-motion seismograph stations in downtown San Bernardino and in Cerritos, Ca. These stations will be used to study non-linear site response for typical Los Angeles basin site conditions.

Results

1.) Strong-motion data for approx. 105 sites that recorded the 1 Oct. 1987 Whittier Narrows earthquake have been analyzed in three primary ways, (1) spectral ratios with reference site, (2) removal of ω^2 source and predetermined geometric and anelastic attenuation to yield site functions, and (3) separation of arbitrary source and site functions based on method of Andrews (1986) and Hartzell (1994). Aftershock data collected by our branch following the Whittier Narrows earthquake have been analyzed using methods (1) and (2). These data consist of about 10 earthquakes and 10 sites occupied by S6000 instruments.

Strong-motion data for approx. 28 CDMG sites that recorded the 17 Jan. 1994 Northridge Calif. earthquake have been analyzed using methods 1 through 3 above. In a separate investigation, Hartzell has analyzed data from about 90 sites that recorded about 60 aftershocks of the Northridge mainshock using method (3). We have compared inferred site functions from the mainshock and aftershock studies for those sites that are collocated or nearly collocated.

Strong-motion data for approx. 6 CDMG sites that recorded the 28 June 1991 Sierra Madre, Calif. earthquake have been analyzed using methods 1 through 3 above. The data from the three mainshocks have been analyzed simultaneously using method (3) to determine if a "stable" site function is obtained. However, the large dataset available for Whittier Narrows is not yet available for the other mainshocks, thus, this analysis has not yet been completed.

CDMG station data for the Landers, Calif. earthquake of 28 June 1992 have been examined. Comparisons with Whittier Narrows mainshock records at the same given sites indicate that for the

LA basin and vicinity, spectral energy is relatively strong at about 2 seconds for the Landers mainshock, whereas Whittier Narrows' data indicate little energy at this period.

The primary source of data for strong motion in the San Fernando Valley is the University of Southern California, which provided about 10 3-component accelerograms for the Whittier Narrows earthquake. Neither the USGS nor CDMG have strong-motion sites within the San Fernando Valley, although records from a few sites at the edge of the valley, such as Tarzana and Sylmar Olive View Hospital, have been processed by CDMG and have been examined by us. The validation of methods that use aftershock records to infer mainshock site response functions will be greatly strengthened by data for the Northridge mainshock when these data are released by USC and other institutions.

The Whittier Narrows mainshock appears to conform better to the ω^2 source model than does the Northridge mainshock, at least as recorded by the limited set of stations now available (all CDMG). In general, the Northridge records decay more rapidly with frequency (i.e., have greater κ) than do the Whittier Narrows records at a given site This difference may be in part due to source differences and in part to propagation or azimuthally dependent site differences. The CDMG Northridge records also are very deficient in low frequency energy, based on the predicted scalar moment obtained by fitting the spectral data to an ω^2 point-source using method 2 above. The predicted scalar moment is about 8×10^{25} dyne-cm, about 8 times that predicted for Whittier Narrows mainshock. The USGS Preliminary Determination of Epicenters lists the Northridge moment as 3×10^{26} dyne-cm, thus, the local data prediction for Northridge is a factor of 4 low. For Whittier Narrows, the scalar moment predicted is in excellent agreement with various investigators' estimates (10^{25} dyne-cm). In spite of the above differences, many details of site transfer functions determined from analysis of the various mainshock data are in good agreement, as are many features between mainshock and collocated-site aftershock data for Northridge and Whittier Narrows. For example, in the 2 to 5 Hz range, a given site generally displays about the same amplification (to within about a factor of 2) for S-waves regardless of the source size or location. Exceptional sites, such as Tarzana, display very different response to Whittier Narrows versus Northridge, however. The cause of these differences is not yet known.

2.) The major effects on the scaling of peak accelerations with magnitude and distance are expected to be isochron pulse addition and the statistical properties of extreme values. A peak acceleration is an extreme value because it is the largest pulse selected from a distribution of recorded pulses. Additional factors, such as instrument triggering level, fault finiteness, fault dip, and rupture propagation direction, are also expected to be important. We examine the predictions produced by a fault model that includes all these features. This model assumes that the fault is composed of elemental patches that rupture as the rupture front passes. Each patch generates a peak acceleration sampled from a statistical distribution. Computationally, the model allows inclusion of either extreme sampling, isochron effects, or both. Isochron addition is the increase in peak amplitude that occurs at the station because contributions from two or more points on a propagating rupture arrive at the station at the same time. Magnitude scaling occurs because isochrons lengthen as fault size increases, and hence more contributions are available to add. Magnitude scaling produced by extreme sampling occurs because as fault size increases the number of random-amplitude, non additive contributions at the station increases, leading to increased likelihood of sampling a larger value.

The model results show that isochron addition and extreme sampling each produce distance-dependent magnitude scaling that saturates with increasing magnitude. The extreme sampling method permits the model parameters to be adjusted to fit smoothed worldwide peak-acceleration data. The isochron addition method is more difficult to parameterize, thus complicating the fitting of the data. The method produces peak acceleration scaling that is dependent on patch pulse shape and pulse width relative to the patch rupture time. Scaling due to isochron effects is excessive for a square pulse shape with width equal to the rupture time across a patch. Scaling is too little for pulse widths that are effectively a fraction of the patch rupture time. Although the scaling due to extreme

sampling alone is sufficient to fit the smoothed data, it is likely that both isochron and extreme sampling effects are present in the data. When fitting the data with a model that includes both effects, however, the predicted scaling of peak acceleration is primarily produced by extremal part of the model.

Reports

Rogers, A.M. and Perkins, D.M., (submitted), Monte Carlo simulation of peak acceleration attenuation using a finite-fault uniform-patch model, 26 ms. p.

Perkins, D.M., Rogers, A.M., and Campbell, K.W., (submitted), Limitations of the world-wide strong-motion data base: effects on peak acceleration regression analysis, 26 ms. p.

Rogers, A.M. and Perkins, D.M., (1994), Peak acceleration scaling produced by isochron pulse addition and extreme sampling, EOS, Transactions of the American Geophysical Union, v.75, no. 44, p. 448.

Analyses of Structural Response to Earthquakes

9920-10282

Erdal Şafak
Branch of Earthquake and Geomagnetic Information
U.S. Geological Survey
922 National Center
12201 Sunrise Valley Drive
Reston, Virginia 22092
(703)-648-6534

Investigations

The feasibility of predicting structural response to large earthquakes by using recorded responses from co-located smaller earthquakes is investigated. It was shown that records from large earthquakes can be approximated as linear combinations of records from smaller earthquakes. This allows development of methods to scale seismic structural response, and to predict main shock response from aftershock recordings. The accuracy of the methods are tested by applying them to recorded data from structures.

Results

Two methods are introduced to predict structural response to large earthquakes by using recorded responses from co-located smaller earthquakes: the constant scaling method and the recursive filtering method. The first method uses the moment magnitudes of the large and small earthquakes for scaling, whereas the second method uses the moment magnitudes of the large and small earthquakes and the corner frequency of the small earthquake. Both methods assume constant stress drop. The accuracy of the methods are tested by applying them to data sets from a highway overpass in Rio Dell, California, recorded during two co-located earthquakes. The methods are also used to predict the main shock response of the collapsed I5-I14 interchange during the Northridge earthquake of January 17, 1994 by scaling the aftershock recordings from the interchange. Both applications gave satisfactory results.

Reports

1. Şafak, E. (1994). Prediction of structural response to large earthquakes by using recordings from smaller earthquakes, *Proceedings*, ASCE Structures Congress XII, April 24-28, 1994, Atlanta, Georgia, Vol. 2, pp.1391-1396.

2. Şafak, E. (1994). Scaling of seismic structural response, ASCE, Journal of Structural Engineering (submitted for publication).

FAULT PATTERNS AND STRAIN BUDGETS

9960-11176, 9960-12176

Robert W. Simpson
Branch of Earthquake Geology and Geophysics
U.S. Geological Survey
345 Middlefield Road, MS/977
Menlo Park, California 94025
(415) 329-4865
simpson@gold.wr.usgs.gov

Program Element: III

Investigations

The goal of this project is to better understand how faults interact and how earthquakes on one fault might trigger or delay earthquakes on another fault. The approach is to calculate the static stress changes generated by large earthquakes using dislocation theory in an elastic half-space. Surprisingly small changes in the static stress field seem able to affect the spatial distribution and timing of aftershocks and subsequent large earthquakes on nearby faults.

In Southern California, working in collaboration with Ruth Harris and Paul Reasenberg, we calculated the stress changes on faults within several hundred kilometers of the Northridge earthquake in an effort to try to identify which faults might have become more stressed as a result of the earthquake. We also looked at changes in seismicity rates in the region after the earthquake to see if any correlation could be found between rate changes and calculated stress changes.

In Northern California, for a CONCERT workshop on faults in San Francisco bay, I investigated the behavior that might be expected from faults under the bay if they were to slip in response to large earthquakes on the San Andreas and Hayward faults. In collaboration with Ken Lajoie and Dave Oppenheimer, I have also been trying to use average topography data for the San Francisco bay region in conjunction with focal mechanisms and geodetic data to search for blind thrusts that might be capable of producing Northridge-type earthquakes.

Results

Southern California: After the Northridge earthquake, we attempted to calculate how stresses had changed on faults within several hundred kilometers of the hypocenter. The nearest part of the San Andreas fault got a small amount of stress added, probably equivalent to 1 or 2 years of normal tectonic loading. Most faults in our models that were within the zone of aftershocks got more stressed, as did parts of the San Gabriel fault, the Santa Monica fault and the Newport-Inglewood fault. Although seismicity subsequently increased on some of these faults, the correspondence between calculated stress changes and seismicity rate changes does not appear to be as well defined as it was in the San Francisco Bay region after the 1989 Loma Prieta earthquake. All M>5 aftershocks of the Northridge earthquake were calculated to have been

encouraged by the Northridge rupture, and 70% of the M>3 aftershocks were calculated to have been encouraged, so the stress calculations seem consistent with aftershock occurrence.

We observed that if stress changes for all pairs of M>5 earthquakes in Southern California since 1968 are calculated, there is an increased likelihood of a second M>5 earthquake within the two year period after the first earthquake in the pair. The second earthquake occurred on a fault that was more stressed by the first earthquake in 15 out of 16 cases. In order to arrive at this result, only pairs with stress changes greater than 0.1 bar on the second fault plane were considered (based on our study of significant stress levels after the Loma Prieta earthquake). Pairs closer than 5 km were not considered, because our abilty to correctly calculate stress changes for such closely spaced faults becomes very poor, given the lack of detailed information about slip distributions for most of these earthquakes. This result suggests that static stress change calculations can help to identify faults that have come closer to failure after an earthquake. It also suggests that present hazard estimates of M>5 aftershocks may be low, because some of these pairs would probably not have been included in the empirical determination of aftershock parameters.

Northern California: The so-called "mud faults" in San Francisco bay seemed likely to be capable of secondary slip after earthquakes on the San Andreas or Hayward faults, especially in light of the ground deformation produced on secondary structures surrounding the Landers and Northridge earthquakes in Southern California. Re-interpretation of the seismic data has called into question the existence of most of these proposed faults, although aeromagnetic data still suggest the presence of at least one old fault under the bay. Stress calculations show that if such old faults are capable of slipping in response to applied earthquake-induced stresses, they might slip by as much as several tens of centimeters, posing a possible hazard for pipelines and other man-made structures crossing the bay.

The possibility of Northridge-type earthquakes occurring on blind thrusts in the San Francisco bay region has led to an effort to identify such faults. Ken Lajoie suggested using regional-scale topography data to get an overview of possible areas of hazard, and to see if features in the topography could be used to identify target study areas. By comparing topography with focal mechanisms calculated by Dave Oppenheimer, we hoped to be able to correlate active reverse faulting with topographic features. Inherent ambiguities in many of the focal mechanisms have made this more difficult than anticipated. It appears that the majority of reverse mechanisms fall to the south of a northeast trending line at about 37.5N latitude; many of them are Loma Prieta aftershocks. To the north of this line, the topography as seen on averaged maps is quite subdued up to about 38.5N latitude, with scattered normal and reverse mechanisms, suggesting a change in the stress field or tectonic regime in the low-lying region. We are investigating the possibility that this region is undergoing extension at about N30W, as well as strike-slip deformation.

Reports

Harris, R.A., and Simpson, R.W., 1994, Earthquake interactions among moderate and large earthquakes in the Landers region: Seismological Research Letters, v. 65, p. 54.

Harris, R.A., and Simpson, R.W., and Reasenberg, P.A., 1994, Static stress changes influence future earthquake locations in southern California: Eos, Transactions, American Geophysical Union, v. 75, p. 169.

Olson, Jean, Zoback, Mary Lou, Simpson, R.W., and Marlow, M.S., 1994, Deformation in the San Francisco bay block?: Eos, Transactions, American Geophysical Union, v. 75, p. 683.

Scientists of the U.S. Geological Survey and the Southern California Earthquake Center, 1994, The magnitude 6.7 Northridge, California, earthquake of 17 January 1994: Science, v. 266, p. 389-397.

Simpson, R.W., Castillo, D.A., Harris, R.A., Hutton, L.K., and Jones, L.M., 1994, Faults in Southern California with increased Coulomb failure load after M_L>5 earthquakes are more likely to have M_L>5 events in the year following: Seismological Research Letters, v. 65, p. 63.

Simpson, R.W., Harris, R.A., and Reasenberg, P.A., 1994, Stress changes caused by the 1994 Northridge earthquake: Seismological Society of America, Program for Northridge Abstracts, abstract #3.

Simpson, R.W., Lajoie, K.R., and Oppenheimer, D.H., 1994, Inferring blind thrusts in the San Francisco bay region from earthquake focal mechanisms and averaged topography: Eos, Transactions, American Geophysical Union, v. 75, p. 681.

Simpson, R.W., and Reasenberg, P.A., 1994, Earthquake-induced static stress changes on central California faults, *in* Simpson, R.W., ed., The Loma Prieta, California, earthquake of October 17, 1989 -- tectonic processes and models: U.S. Geological Survey Professional Paper 1550-F.

NEAR-FAULT GROUND MOTION ESTIMATES INCLUDING DIRECTIVITY EFFECTS FROM LARGE STRIKE-SLIP EARTHQUAKES IN THE SAN FRANCISCO BAY AREA

Award No. 1434-93-G-2314

Investigator: Paul G. Somerville

Woodward-Clyde Federal Services
566 El Dorado St., Pasadena, CA 91101
Tel: (818) 449-7650 Fax: (818)449-3536 Email: pgsomer0@wcc.com

Program Element: III.3

INVESTIGATIONS

At long periods (longer than about 1 second), ground motions are strongly influenced by the earthquake faulting mechanism (the orientation of the fault and the direction of slip on the fault); the location of the earthquake hypocenter; and the location of the recording station in relation to the fault. A particularly important effect at long periods is the rupture directivity effect in near-fault strong ground motion, which is due to propagation of the rupture toward the recording site and fault slip occurring in the direction toward the site. This causes a large long-period pulse of motion in the direction normal to the fault that occurs near the beginning of the record. The qualitative effects of rupture directivity on long-period ground motions have been described by Somerville and Graves (1993). In the work reported on here, this description has been extended (Somerville et al., 1994) to include quantitative adjustments to empirical attenuation relations to account for these effects.

We have developed methods to account for near-fault rupture directivity effects (sometimes referred to as "fling") in the development of ground motions for seismic design. Two kinds of modification to average horizontal response spectral attenuation relations to account for rupture directivity effects are described. The first, developed from an empirical analysis of near-fault data, describes modifications to average horizontal values to obtain fault-normal and fault-parallel components, which differ at periods longer than one second in a manner that is both magnitude- and distance-dependent. The second, based on comparison of current empirical attenuation relations with recent data and with simulations of strong ground motions, describes modifications of current empirical attenuation relations for average horizontal motions to account for near-fault effects. Not all near-fault recordings contain forward rupture directivity effects; they only occur when rupture propagates toward the site and when the fault slip direction is also toward the site. In order to facilitate the selection of time histories that represent near-fault ground motion conditions in an appropriate manner, we provided a table of near-fault records indicating the nature of the rupture directivity effects that each contains.

In the top part of Figure 1, we show the acceleration, velocity and displacement time histories of a strong motion record close to a large strike-slip earthquake. The time history, which includes a preliminary correction for instrument response, was recorded 1.8 km from the surface rupture and 45 km from the epicenter of the M 7.3 Landers earthquake of 1992, and contains the forward directivity effect. There is a large difference between fault-normal and fault-parallel motions at long periods (peak velocity and displacement), but this difference vanishes at short periods (peak acceleration).

To supplement the relatively sparse set of strong motion recordings close to large earthquakes, we have used a broadband strong motion simulation procedure to generate suites of near-fault time histories. We have used these large suites of near-fault time histories to examine the characteristsics of near-fault groud motions. An example of a broadband time history generated by this procedure is shown in the lower part of Figure 3. It represents the ground motions at a rock site located 10 km from the rupture surface and 50 km from the epicenter of a M 7.5 strike-slip earthquake. The overall characteristics of this time history, which contains forward rupture directivity effects, resemble those of the Lucerne recording of the Landers earthquake shown above. In both cases, the peak fault normal velocity is much larger than the peak fault parallel velocity, while the peak accelerations of the fault normal and fault parallel components are comparable.

RESULTS

Adjustment for difference between fault-normal and fault-parallel components

We quantified the difference between the fault-normal and fault-parallel motions as a function of wave period, earthquake magnitude and distance to the fault. Design ground motions which reflect this difference can be developed from empirical attenuation relations that contain this modification, using either deterministic or probabilistic seismic hazard analyses.

Our quantification of differences between long-period fault-normal and fault-parallel motions is based on regression analysis of a data set of strong motion records. The earthquakes selected for this study include all California crustal earthquakes with magnitudes of 6 or larger for which digital strong motion data and faulting mechanism are available, together with selected crustal earthquakes from other regions to augment the data set for larger magnitudes. The data set provides a fairly uniform sampling of the magnitude range of 6.0 to 7.5 and the distance range of 0 to 50 km.

The dependence of the ratio of fault-normal to fault-parallel response spectral acceleration on magnitude, distance, style of faulting, and site category was examined by means of a regression analysis of the data using the random effects method (Abrahamson and Youngs, 1992). This method provides a means of partitioning random variability in ground motion amplitudes into inter-event and intra-event terms, and ensures that the results of the regression are not unduly influenced by events having large numbers of recordings.

The fault-normal to fault-parallel ratio data were fit using an equation of the form:

$$y = C1 + C2*\ln(R+1) + C3*(M-6) + C4*F + C5*S \qquad \text{for } M > 6$$

where y is the natural logarithm of the fault-normal to fault parallel ratio at a given period, R is closest distance, M is moment magnitude, F is style of faulting (1 for strike-slip; 0 for oblique and reverse), S is site category (1 for rock; 0 for soil), and C1 through C5 are period dependent coefficients.

The values of the coefficients of the resulting model of the fault-normal to average ratio are listed as a function of period in Table 1. The magnitude and distance dependence of the fault-normal to average horizontal ratio for this model are shown as a function of period in Figure 2. The fault-normal motion is obtained by multiplying the attenuation relation value by the fault-normal to average horizontal ratio shown in Figure 2 and tabulated in Table 1. Similarly, the fault-parallel motion is obtained by dividing the attenuation relation value by this ratio.

The uncertainty in the model of the fault-normal to average ratio consists of two terms: one due to variability from one earthquake event to another (the inter-event variability, tau), and another due to variability from one recording of an earthquake to another (the intra-event variability, sigma). The overall variability is the combination of these two components. These two uncertainties and their combined value are shown as a function of period in Figure 2 and listed in Table 1. The inter-event variability is much lower than the intra-event variability, and dominates the total variability.

Adjustment of Average Ground Motion Levels in Empirical Attenuation Relations

In the preceding empirical analysis of the data, we did not address the question of absolute ground motion levels; we developed an adjustment that modifies the partition of amplitude among the fault-normal and fault-parallel components without changing their average value. However, since the data set that we analyzed contains recordings from recent events that are not widely represented in empirical attenuation relations, we checked the absolute ground motion levels of our data set with those of empirical attenuation relations. We used strong motion simulations, generated using the method described above, to further evaluate whether the empirical attenuation relations may be underpredicting the average long period ground motions of large earthquakes. Ground motion simulations for rock sites in the magnitude range 6.5 to 7.5 and the distance range 0 to 50 km, were compared with the predictions of the empirical attenuation relations.

We found that both the augmented data and the simulations are underpredicted by the attenuation relations for periods longer than 1 to 2 seconds. The simulations thus have trends with respect to the attenuation relations that are similar to those of the data set, and thus appear to model the data well at periods longer than 1 second. Based on these analyses, we conclude that the strong motion data from recent earthquakes, as well as strong motion simulations that we have performed, suggest that current empirical attenuation relations based on less current data may underpredict the average ground motions for periods longer than 1 second on rock. In order to address the possibility that additional data may confirm this trend, we suggest that it may be

appropriate to modify the empirical attenuation relations at the longer periods. An appropriate modification is to increase the attenuation relations by 50% for periods of 3 seconds and longer, and to taper this modification to unity at 1 second.

Catalog of Near-Fault Strong Motion Records Describing the Nature of Directivity Effects They Contain

As described above, forward rupture directivity effects occur when the rupture propagates toward a site and when the fault slip direction is also in the direction toward the site. This means that forward rupture directivity effects are present in some but not all near-fault strong motion recordings. As a guide to the selection of time histories for use in design and evaluation of structures that are sensitive to long-period ground motions, we listed a set of near-fault strong motion recordings and indicated the nature of the rupture directivity effects that they contain. Since the response spectrum developed for design or evaluation of a near-fault site will be influenced by forward rupture directivity effects at most sites, especially if the adjustments described above are implemented, it is important to select an appropriate proportion of time histories that include forward rupture directivity effects if time histories are being used in conjunction with the response spectrum. This is true even if the time histories are to be spectrally matched to the response spectrum, since the spectral matching process cannot build a rupture directivity pulse where none is present to begin with.

The catalog of records includes those whose closest distance to the fault rupture is 10 km or less in the data set that was used in the analysis of fault-normal and fault parallel motions described above. The catalog contains records only for crustal earthquakes, but it could be extended to include subuction earthquakes. The influence of rupture directivity effects on each record is indicated, based on the geometrical relationships between the recording site, the fault rupture, the epicenter, and the direction of slip on the fault. Forward directivity occurs when the rupture propagates toward the site and the direction of slip on the fault is also toward the site. Most near-fault strike-slip recordings, and many near-fault reverse fault recordings, are influenced by forward directivity. Backward directivity occurs when the rupture propagates away from the site. Recordings near the epicenters of strike-slip earthquakes, a relatively small group, fall in the backward directivity category. There are no reverse-fault recordings in this category because none of the reverse faults in our data set ruptured in the downdip direction away from surface stations. Recordings that do not clearly belong in either of these categories are grouped in a neutral category. This category includes sites located fairly close to the epicenters of strike-slip earthquakes, sites located off the end of the updip projection of reverse faults, and sites for which the geometrical orientation of the rupture surface is poorly known.

REPORTS PUBLISHED

Somerville, P.G. and R.W.Graves (1993). Conditions that give rise to unusually large long period ground motions, The Structural Design of Tall Buildings 2, 211-232.

Somerville, P.G., N.F. Smith, R.W. Graves, and N.A. Abrahamson (1994). Accounting for near-fault rupture directivity effects in the development of design ground motions. Paper submitted to the 1995 ASMA/JSME PVP Conference, Hawaii, July 23-27.

Table 1. Coefficients of the Model for the Fault-Normal to Average Horizontal Ratio

PERIOD (SEC)	C_1 (CONSTANT)	C_2 (DISTANCE)	C_3 (MAGNITUDE)	SIGMA	TAU	TOTAL ERROR
1.0	0.0000	0.00000e-00	0.000000	0.2633	0.0559	0.2692
1.5	0.1061	-1.37253e-02	0.000000	0.2493	0.0774	0.2611
2.0	0.1219	-2.34635e-02	0.000000	0.2428	0.0621	0.2506
2.5	0.1587	-3.10171e-02	0.000000	0.2320	0.0585	0.2392
3.0	0.1876	-3.71888e-02	0.000000	0.2376	0.0619	0.2456
3.5	0.2102	-4.24070e-02	0.062189	0.2460	0.0815	0.2592
4.0	0.2195	-4.69270e-02	0.078486	0.2436	0.0726	0.2542
4.5	0.2285	-5.09140e-02	0.105138	0.2353	0.0776	0.2477
5.0	0.2384	-5.44805e-02	0.123672	0.2339	0.0801	0.2472
6.0	0.2393	-6.06525e-02	0.131424	0.2448	0.0558	0.2511

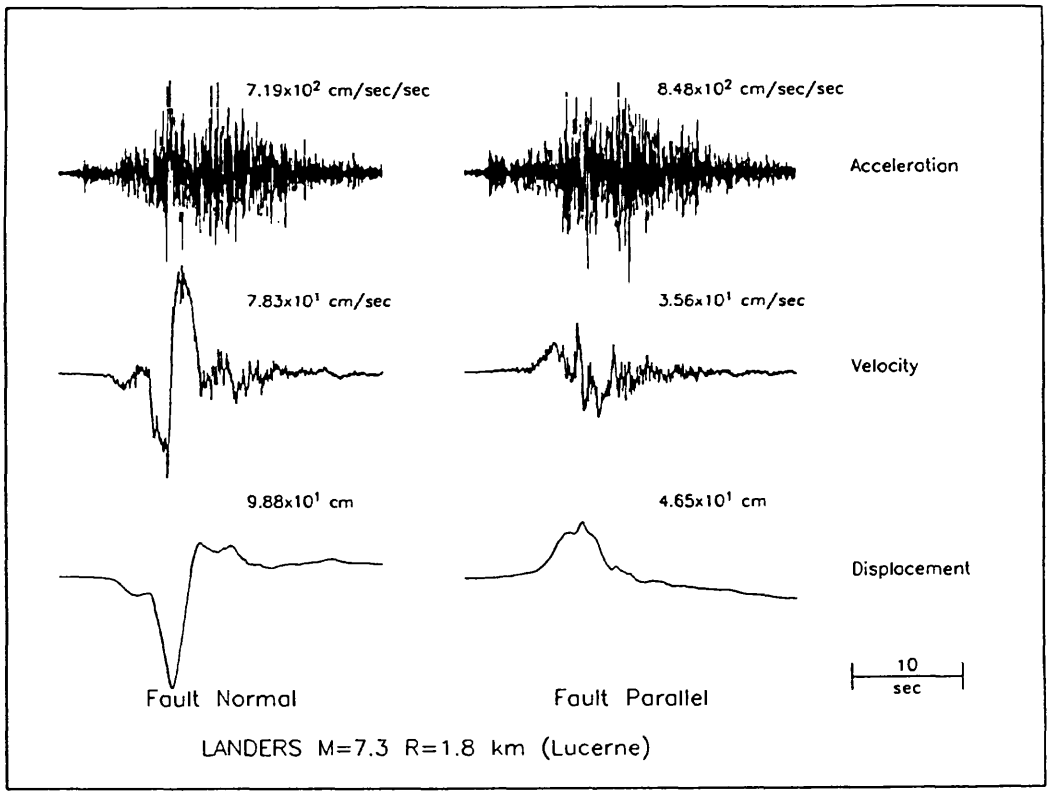

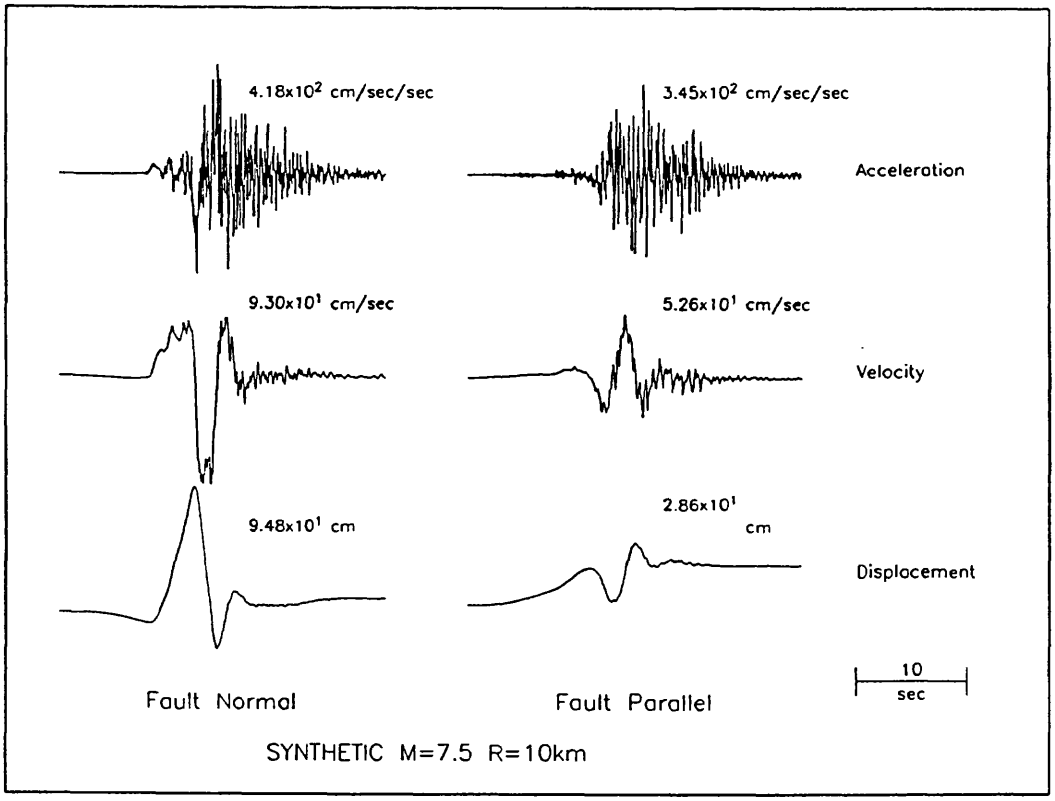

Figure 1. Above: acceleration, velocity and displacement time histories of the fault-normal and fault-parallel components of horizontal motion, with preliminary correction for instrument response, at the Lucerne site recorded from the 1992 Landers earthquake. Below: broadband simulated time histories for a magnitude 7.5 earthquake at a closest distance of 10 km.

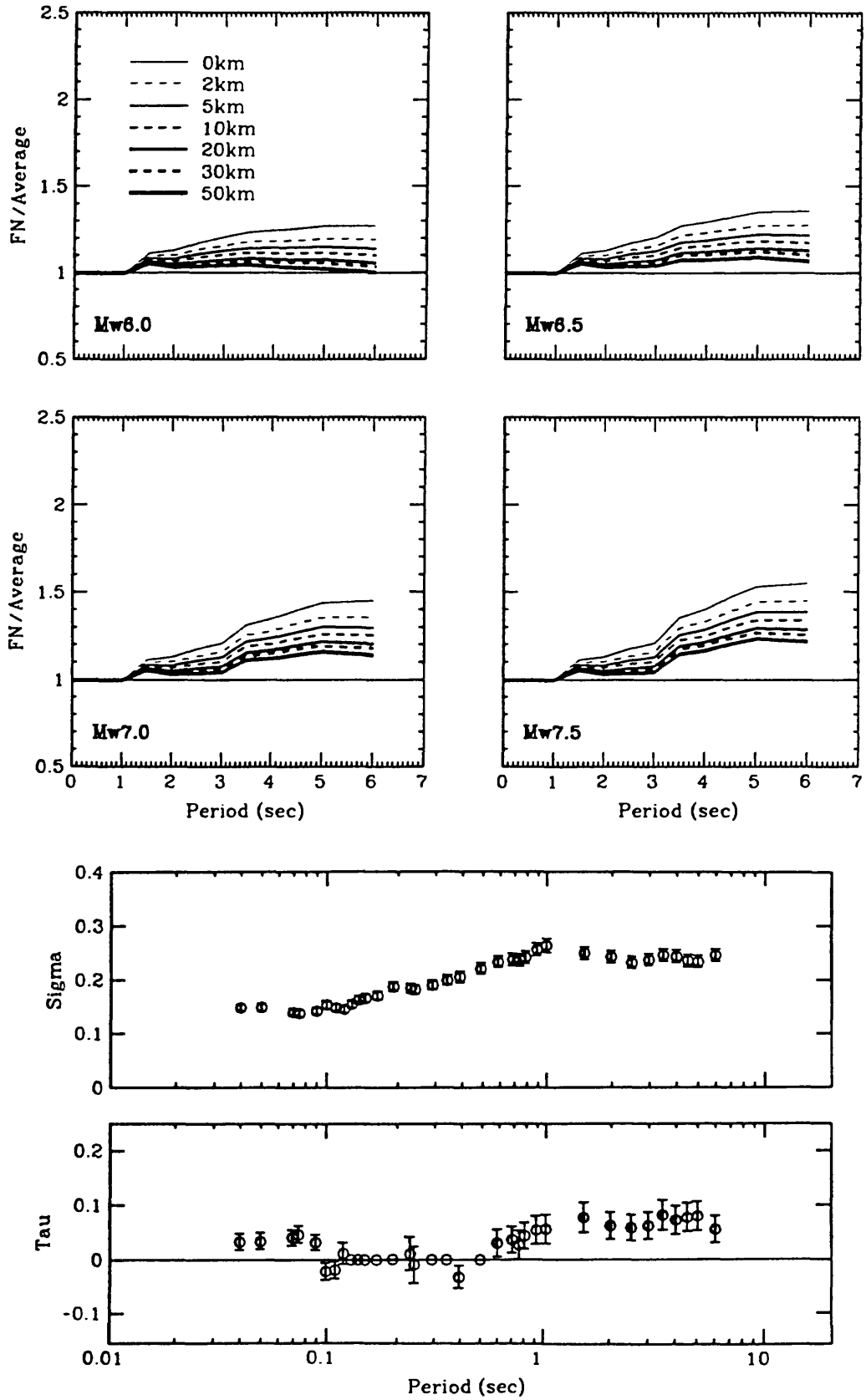

Figure 2. Empirical model of the magnitude and distance dependence of the fault-normal to average horizontal response spectral ratio, together with its intra-event variability (sigma) and inter-event variability (tau).

Strong Motion Instrumentation for the San Francisco Bay Region
9930-12373

Paul Spudich† and Edwin Etheredge°
†Branch of Seismology and ° Branch of Earthquake and Geomagnetic Information
U.S. Geological Survey
Mail Stop 977
345 Middlefield Road
Menlo Park, CA 94025

(415) 329-5654 (voice), (415) 329-5163 (fax), spudich@samoa.wr.usgs.gov

Program Element III.1

Investigations Undertaken

This is a continuing project initiated after the 1989 Loma Prieta earthquake to augment and upgrade strong motion instrumentation in the San Francisco Bay region. Over the last several years the goals of this project have been the following:

1) to colocate digital strong motion instruments with digital weak motion instrumentation being installed as part of the Hayward Fault Telemetered Digital Network,
2) to colocate digital strong motion instrumentation with upgraded 3-component Northern California Seismic Network (NCSN) stations,
3) to colocate digital or analog strong motion instumentation with existing vertical NCSN stations, and
4) to add WWVB time receivers to existing strong motion instruments lacking them.

During FY91 we acquired 10 Kinemetrics SSA-2 digital accelerographs that were customized to have an external signal output plug to allow both internal and external recording of the accelerometer (the external output going to NCNS or HFTDN telemetry, as appropriate). We also acquired 3 Kinemetrics SSA-1 digital accelerographs, and 31 Kinemetrics WWVB-PCB time receivers. During FY92 and FY-93 we acquired miscellaneous fiberglass huts, solar panels, battery boxes, memory expansions, and other items needed for installation or maintenance of the purchased instrumentation. WWVB receivers were added to many instruments, primarily along the Calaveras Fault.

Results of FY94 Activities

During FY94 additional hardware was acquired (solar panels, battery boxes, and a contract for concrete pads) and many digital instruments were installed. Instrumentation status, as of 12/1/94, is shown in Tables 1 and 2. We anticipate completion of the installation of existing equipment in FY95.

Reports Published:

None.

Table 1: Status of accelerograph installations:

		Intended	Status
Hayward Fault Telemetered Digital Network			
	Garin Regional Park	SSA-2 + wwvb/pcb	installed
	Coyote Hills Regional Park	SSA-2+ wwvb/pcb	installed
	Mills Creek, Fremont	SSA-2+ wwvb/pcb	installed
NCSN 3-component			
	Volmer Peak	SSA-2+ wwvb/pcb	installed
	Point Molate	SSA-2+ wwvb/pcb	installed
	San Leandro Hills	SSA-2+ wwvb/pcb	installed
	Hamilton Air Force Base	SSA-2+ wwvb/pcb	installed
	San Bruno Mountain	SSA-2+ wwvb/pcb	installed
	Pacific Park Plaza, Emeryville	SSA-2+ wwvb/pcb	temporary SMA-1 installed
Standard NCSN station			
	NCF - west of Cotati	SSA-2+ wwvb/pcb	hardware acquired
	JEG - near El Granada	SSA-1+ wwvb/pcb	hardware acquired
	JGB - near San Gregorio	SSA-1+ wwvb/pcb	hardware acquired
	NBR - Beebe Ranch, Sta Rosa	SMA-1+ wwvb/pcb	hardware acquired
	CMC - Mills College, Oakland	SMA-1+ wwvb/pcb	hardware acquired
	JRG - Rodeo Creek, Sta Cruz	SMA-1+ wwvb/pcb	hardware acquired
	NTY - Taylor Mtn, Sta Cruz	SMA-1+ wwvb/pcb	hardware acquired
Misc			
	Oakland, downtown	SSA-1+ wwvb/pcb	hardware acquired
	Oakland - downtown	SMA-1+ wwvb/pcb	hardware acquired
	Richmond, Mira Vista CC	SMA-1+ wwvb	installed
	Union City, Masonic Home	SMA-1+ wwvb/pcb	hardware acquired

Table 2: Status of clock upgrades:

station	WWVB-PCB status
APEEL #6	installed
Calaveras Reservoir	installed
Danville, 800 San Ramon Vy	installed
Dublin, 7494 Donahue Dr	installed
Pleasant Hill, 2212 Geary Rd	installed
Sunol, Ohlone Wilderness	installed
Emeryville,Pacific Park Plaza	installed
Foster City, 335 Menhaden Ct	installed
Larkspur, Ferry Terminal	installed
Los Gatos, 14750 Skyline Blv	installed
Stanford/SLAC ground station	installed

Simulation of Strong Ground Motion From the 1992 Cape Mendocino/Petrolia Earthquakes"

Contract No. 1434-94-G-2446

Jeffry L. Stevens and Keith L. McLaughlin
S-CUBED, A Division of Maxwell Laboratories
P. O. Box 1620, La Jolla, CA 92038

stevens@scubed.com, 619-587-8442
scatter@scubed.com, 619-587-8436
FAX: 619-755-0474

Steven M. Day
Department of Geological Sciences
San Diego State University, San Diego, CA 92182
day@moho.sdsu.edu, 619-594-2663

Technical Project Summary

Investigations Undertaken

1. Simulation of the ground motion from the 1992 Cape Mendocino/Petrolia earthquakes using two subevent superposition methods.

2. Comparison of the simulated ground motion with observed ground motion at CSMIP stations.

3. Simulation of the ground motion from a hypothetical M_W 8.1 earthquake with the same hypocenter as the 1992 main shock, but with a rupture 50 km wide and 140 km long.

Results

We model the strong ground motion from the 1992 Cape Mendocino/Petrolia earthquakes by superposition of ground motion from a large number of subevents on the fault. The location of these events and their aftershocks is shown in Figure 1. Two subevent distribution models are used: the first uses a fixed subevent radius of 1.3 km and Brune stress drop of 100 bars; with variability modeled through stochastic variations in both the radius and stress drop. In earlier studies (Stevens, *et al.*, 1994; Stevens, *et al.*, 1988; Youngs, *et al.*, 1988) these parameters were found to work well for simulation of ground motion for the 1983 Coalinga earthquake and the 1989 Loma Prieta earthquake. The second model is the fractal distribution of Zeng, Anderson, and Yu (1994), in which the number of events increases according to a power law with

decreasing size, and the largest subevents may be as large as a fraction of the smallest fault dimension. These two subevent models are shown schematically in Figure 2. For our simulations we restricted the largest event to less than 50% of the minimum dimension. The subevent source model is derived from finite difference simulations of earthquakes. The moment and geometry of the fault are constrained to the observed values. Wave propagation is modeled using geometric ray theory for each subevent to receiver path. Simulations included the direct P and S rays and mantle reflections. Mantle reflections become important at distances greater than about 50 km.

For the fixed size subevent model, ground motion simulations for the 4/25/92 Petrolia M_W 7.1 main shock agree fairly well with the observed ground motion. Simulations with the fractal subevent distribution generate larger ground motions, and simulations using a subevent stress drop of 50 bars produce ground motions similar to those of the fixed size subevent model with a 100 bar stress drop. Both the fixed size subevent and fractal subevent models reproduce the peak acceleration and peak velocity measurements quite well out to a distance of 100 km (Figures 3 and 4). Distance refers to the distance to the closest point on the fault rupture. The simulations match the waveforms and response spectra at individual stations reasonably well on an average basis, however the details of the spectra at individual stations show more variation than the simulations. Figure 5 shows the calculated and observed response spectra at Cape Mendocino and Rio Dell. At Cape Mendocino, calculated peak accelerations are more persistent than observed, with multiple peaks near the maximum value rather than a single large peak as was observed. Consequently, the calculated response spectrum is slightly higher at all frequencies. At Rio Dell, on the other hand, there is a strong site effect that amplifies the observed spectrum, making it larger than the simulation in the 0.1-2 hz frequency band.

Simulations of the two large (M_W 6.5 and 6.6) Cape Mendocino aftershocks using the same parameters used for the main shock underpredict the observed ground motion, indicating that these smaller events have a higher stress drop than the main shock. These events were not located on the same fault as the M_W 7.1 main shock, and were deeper and further offshore.

Figure 6 shows the location of the rupture used for our simulation of an M_W 8.1 earthquake in this area. We used the same hypocenter, and the same fault orientation (strike, dip, and rake) as the Cape Mendocino main shock, but extended the width to 50 km and the length to 140 km. Since the fault dips to the east, the depth increases on the eastward extension of the fault. In Figure 7, we show the predicted peak accerations and velocities for this event. The main effect is that because of the much larger extent of the fault, many of the CSMIP stations are much closer to the fault, and therefore see higher ground motion. As a function of distance from the fault, however, peak accelerations are only slightly higher than for the 1992 Cape Mendocino earthquake, and peak velocities are about a factor of 2 higher than for the 1992 M_W 7.1 event.

References

Stevens, J. L., S. M. Day, and T. G. Barker (1988), "Simulation of Strong Ground Motion from Earthquakes," S-CUBED scientific report SSS-TR-89-9988, September.

Stevens, J. L. and S. M. Day (1994), "Simulation of Strong Ground Motion," in '"The Loma Prieta, California, Earthquake of October 17, 1989 - Strong Ground Motion," *U. S. Geological Survey Professional Paper 1551*-A, R. Borcherdt, editor, p. A53-A60.

Youngs, R. R., S. M. Day, and J. L. Stevens (1988), "Near Field Ground Motions on Rock for Large Subduction Earthquakes," *Proceedings of Earthquake Engineering & Soil Dynamics II*, GT Div/ASCE Park City, Utah, June 27-30, 1988.

Zeng Y., J. G. Anderson, and G. Yu (1994), "A Composite Source Model for Computing Realistic Synthetic Strong Ground Motions," *Geophysical Research Letters, v. 21*, pp. 725-728.

Reports Published

Stevens, J. L., K. McLaughlin, and S. M. Day (1994), "Simulation of Strong Ground Motion From the Cape Mendocino/Petrolia Earthquakes", *Transactions of the American Geophysical Union, v 75, no. 44*, p. 440.

Stevens, J. L. and S. M. Day (1994), "Simulation of Strong Ground Motion," in "The Loma Prieta, California, Earthquake of October 17, 1989 - Strong Ground Motion," *U. S. Geological Survey Professional Paper 1551*-A, R. Borcherdt, editor, p. A53-A60.

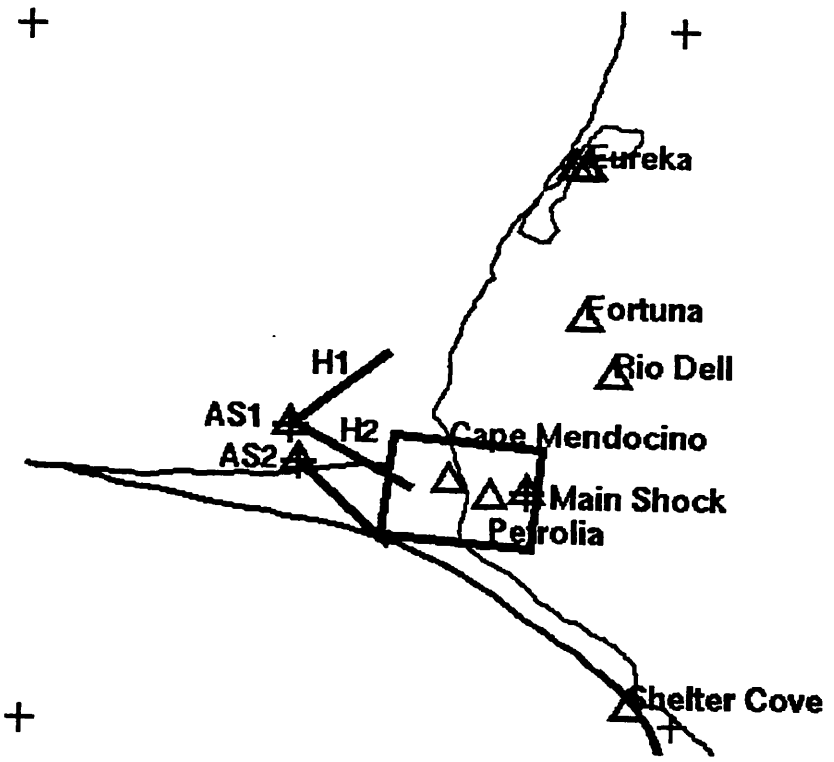

Figure 1. Map showing the location of the Cape Mendocino main shock (rectangle) and aftershocks AS1 and AS2. H1 and H2 are two different orientations for aftershock 1 which have been proposed.

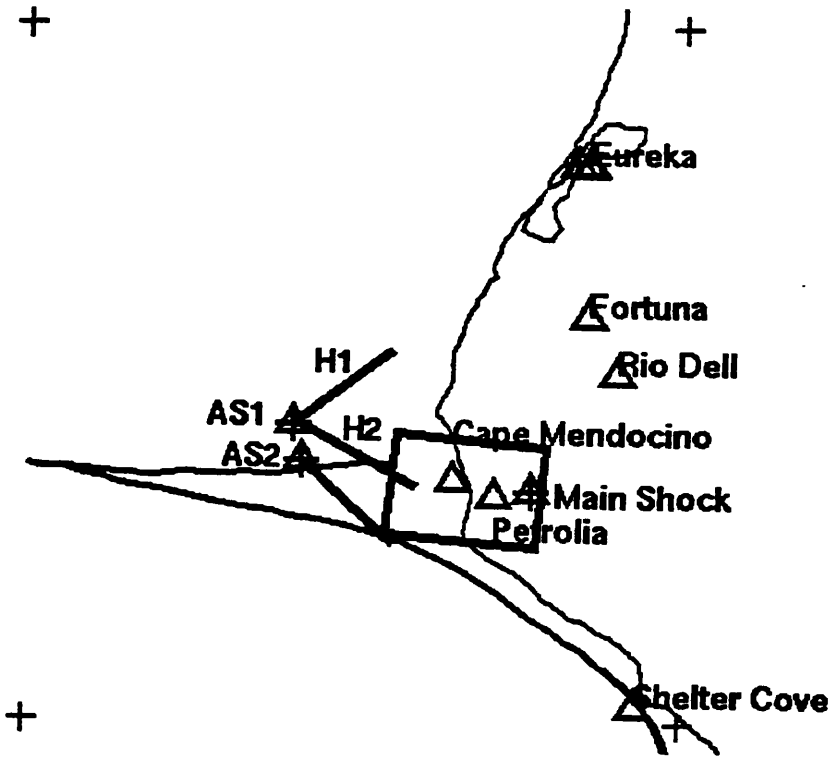

Figure 1. Map showing the location of the Cape Mendocino main shock (rectangle) and aftershocks AS1 and AS2. H1 and H2 are two different orientations for aftershock 1 which have been proposed.

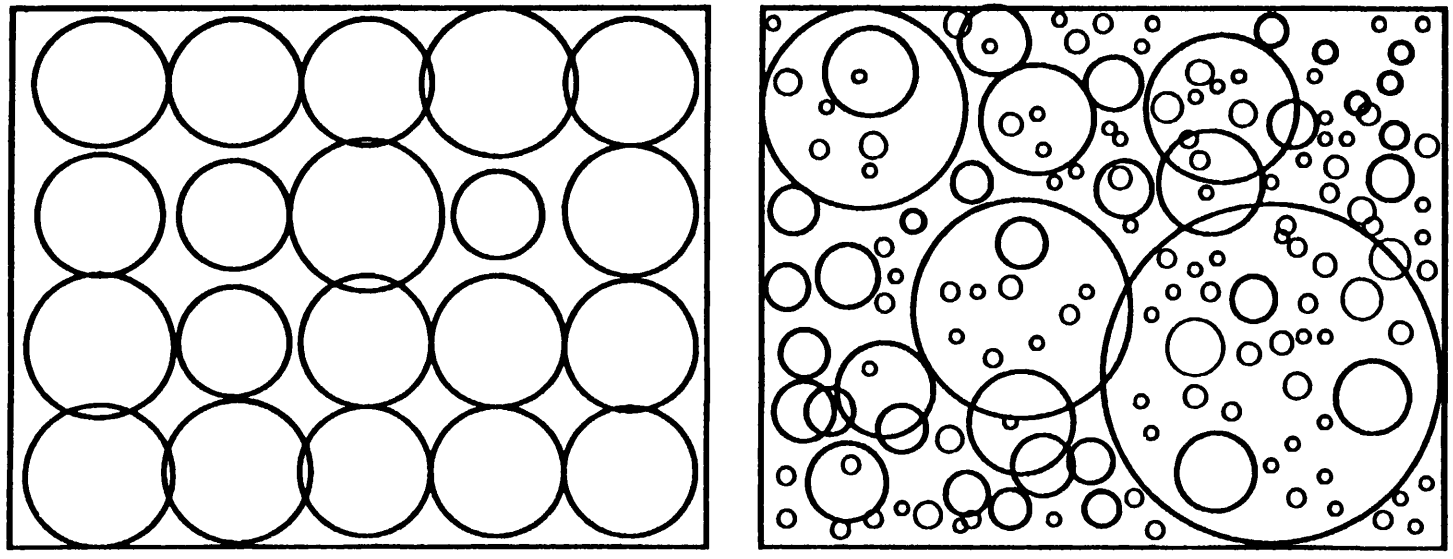

Figure 2. The fixed size model has fixed size subevents with stochastic size variations. The subevent size and stress drop are variables to be constrained by comparison with observed ground motion. Previous simulations show that large events require a larger subevent size and lower stress drop. The fractal model has a fractal distribution of subevent sizes. Subevent size scales naturally with event size. Stress drop is a variable that must be constrained by observations.

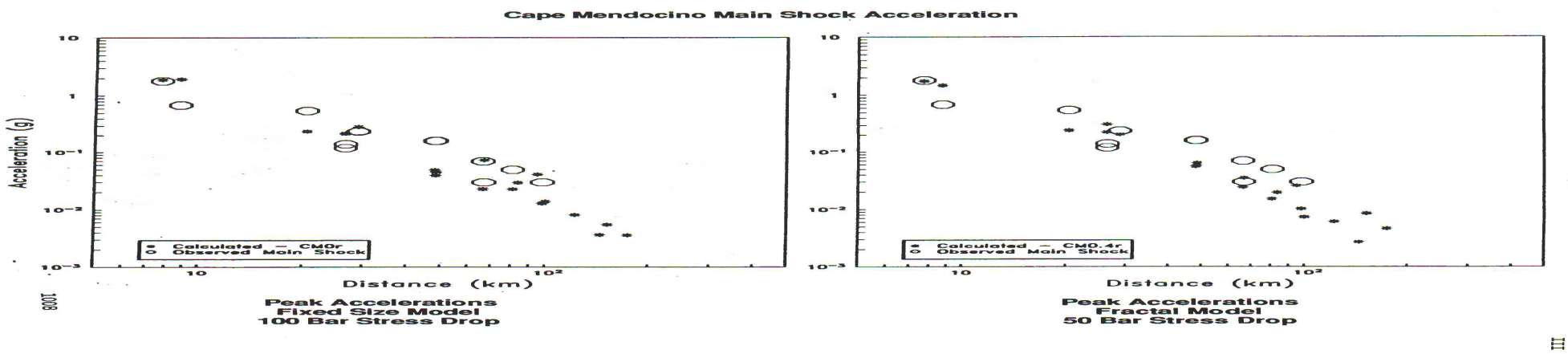

Figure. 3. Cape Mendocino main shock simulated and observed peak accelerations for the fixed size and fractal subevent models.

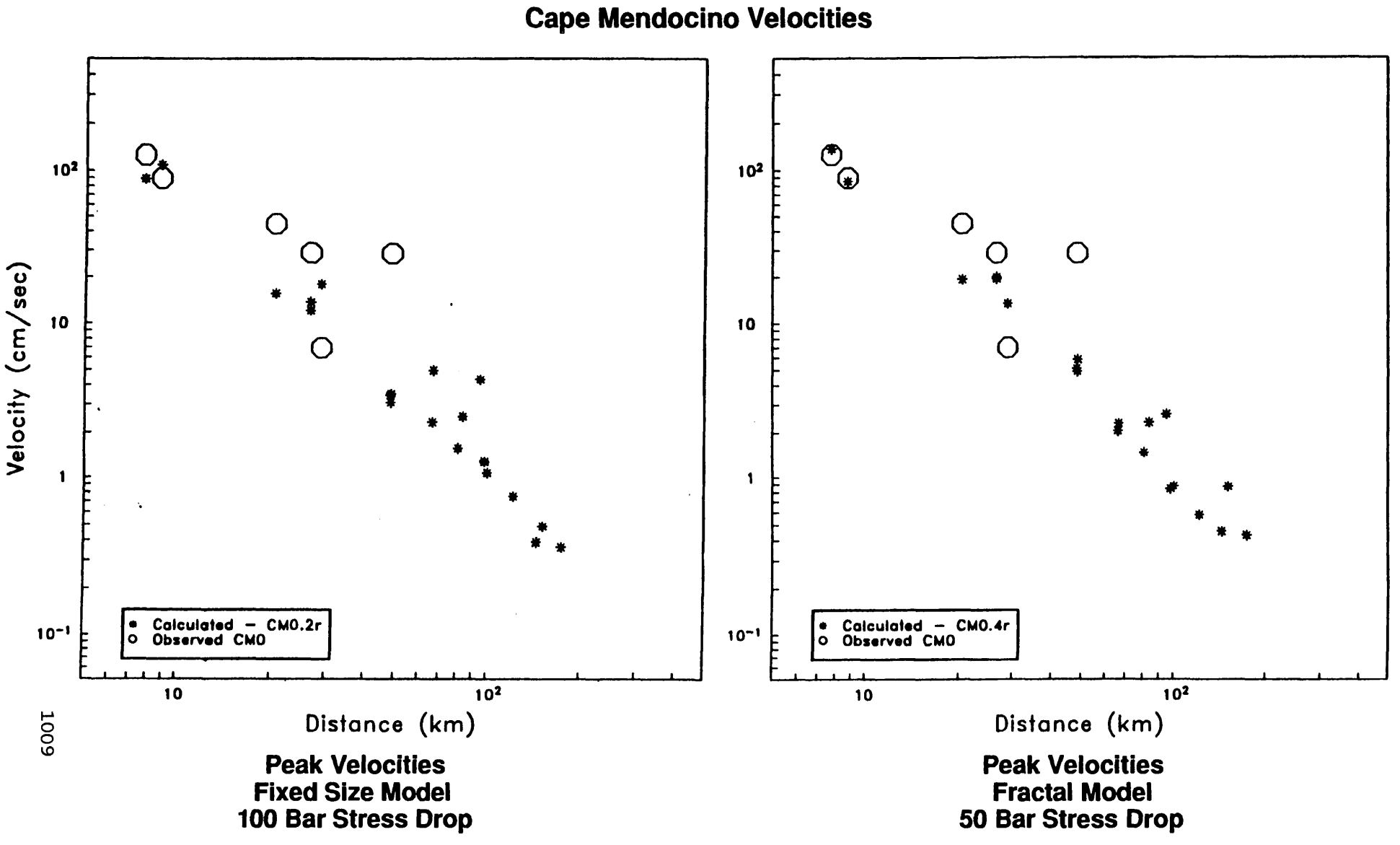

Figure 4. Cape Mendocino main shock simulated and observed peak velocities for the fixed size and fractal subevent models.

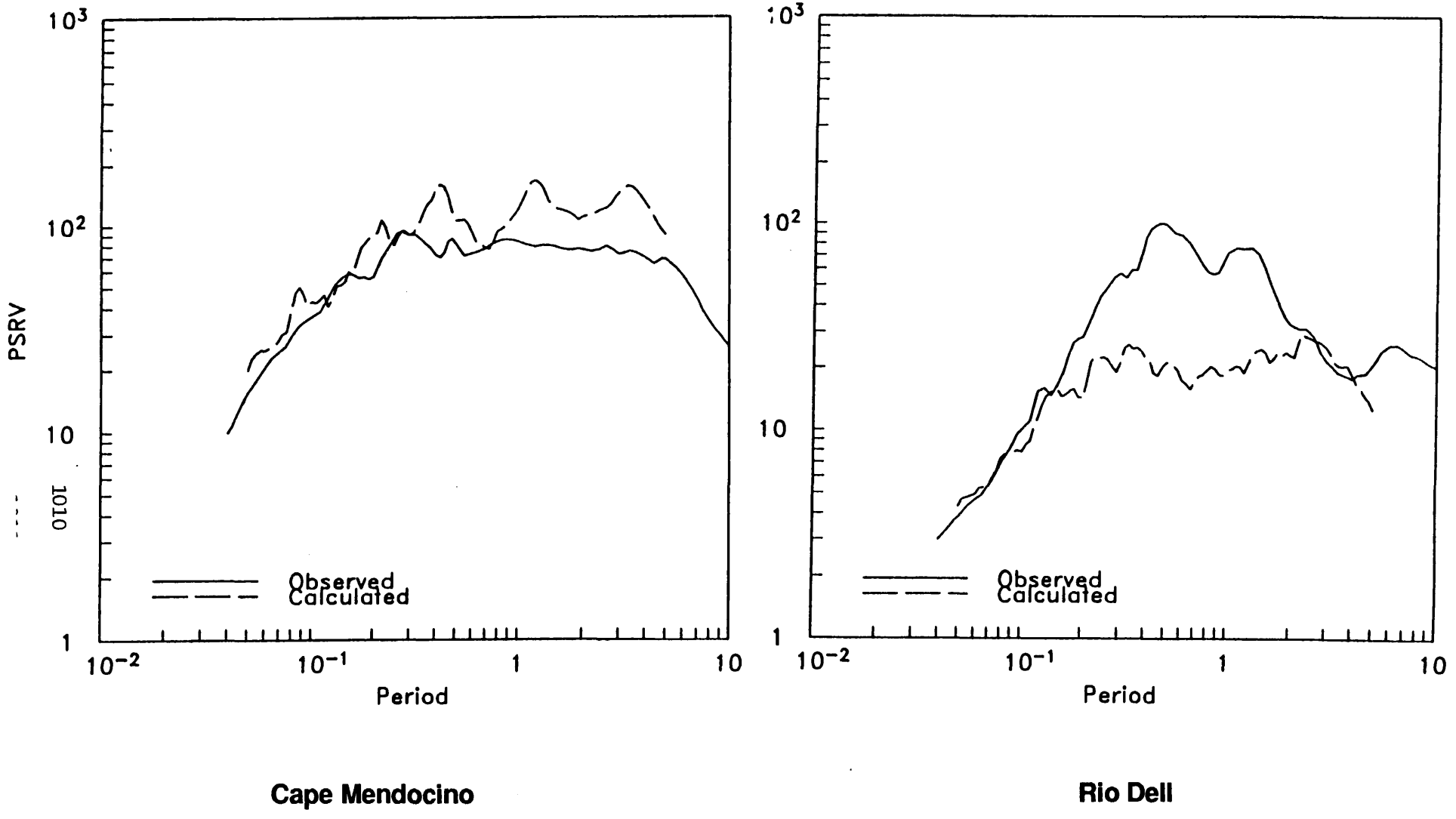

Figure 5. Simulated and observed response spectra from the Cape Mendocino main shock at the Cape Mendocino and Rio Dell CSMIP stations.

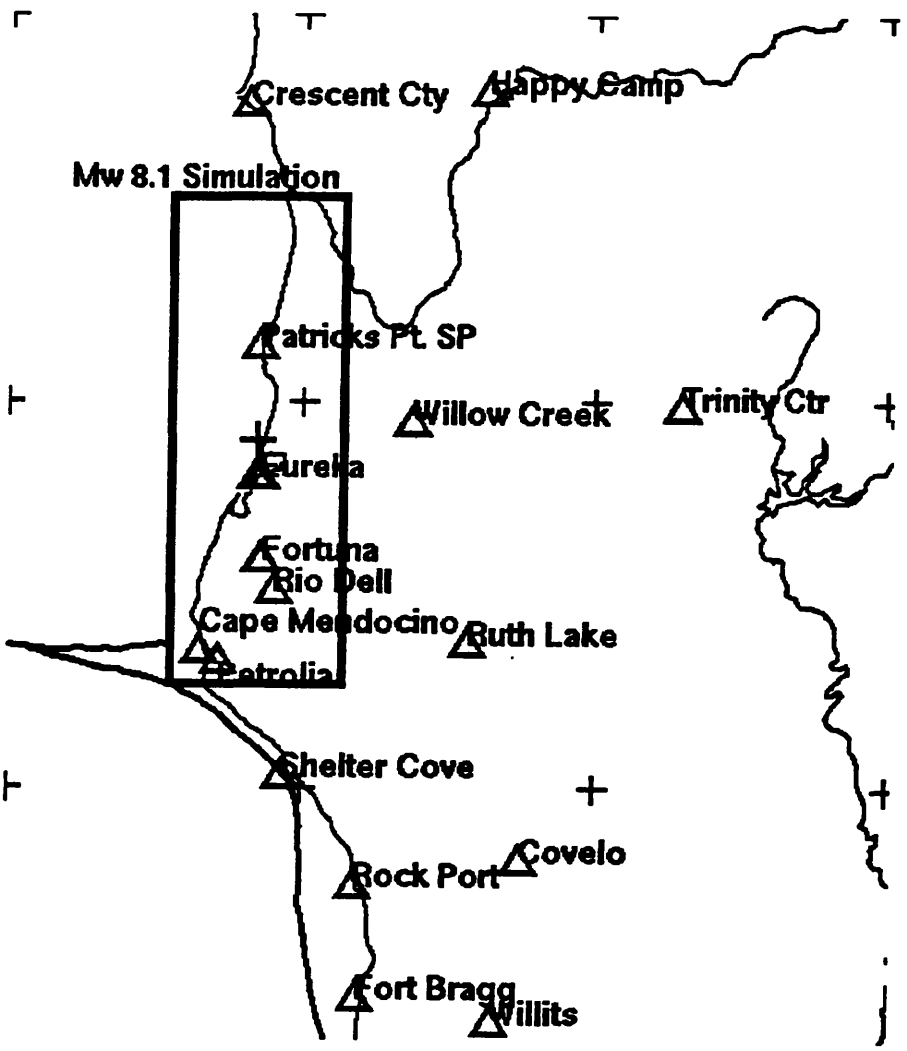

Figure 6. Map showing the location of the fault rupture in the M_w 8.1 event simulation and nearby CSMIP strong motion stations.

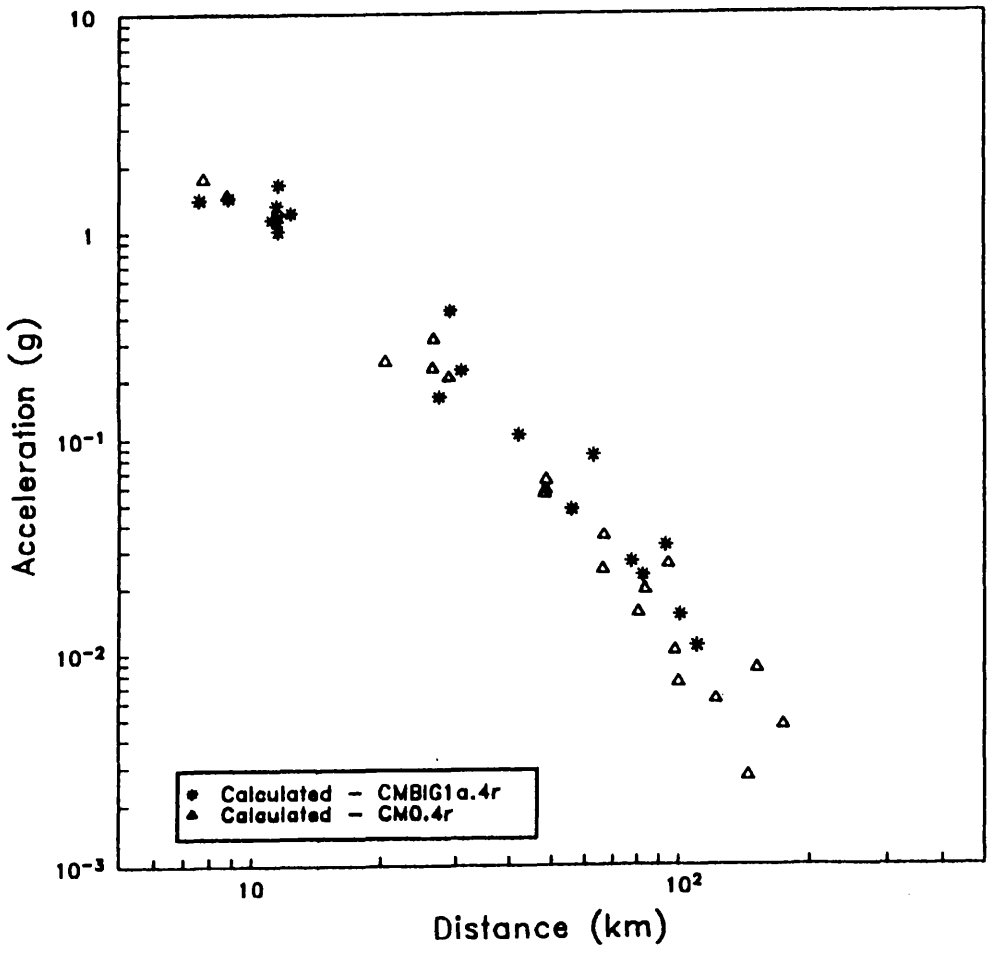

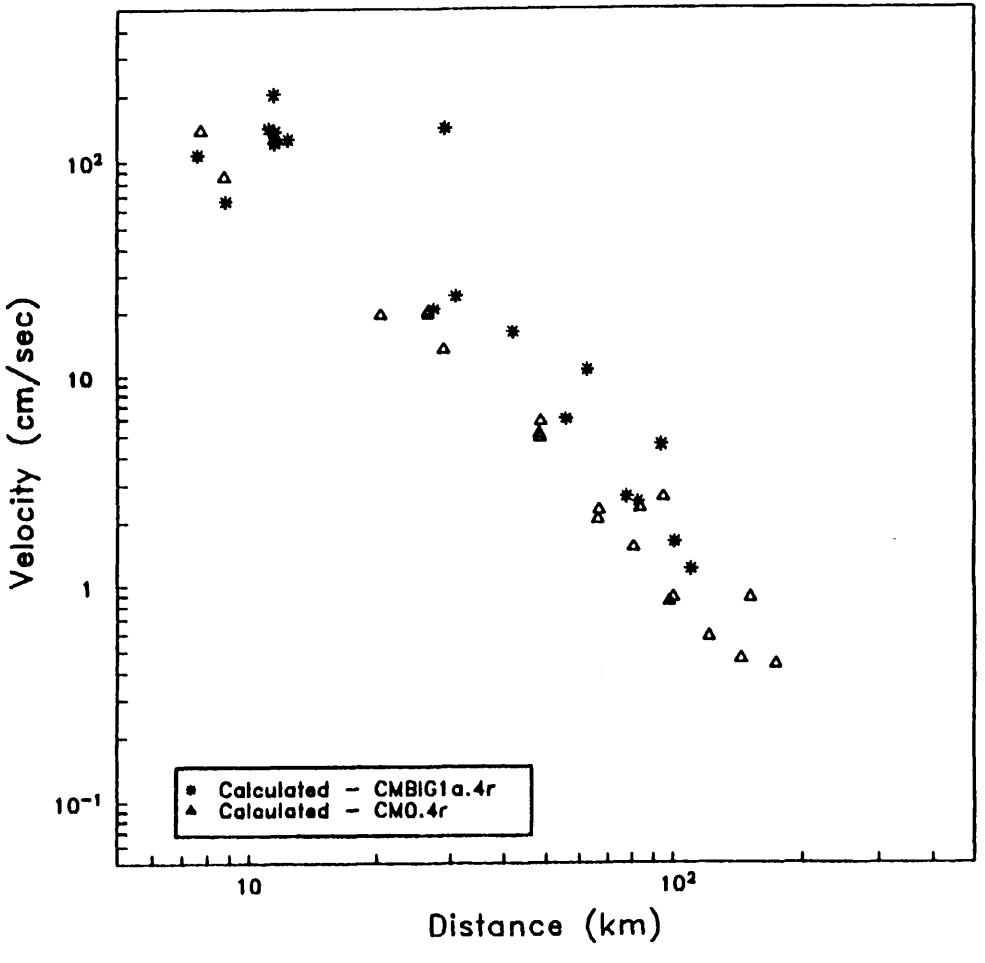

1012

111

Accelerations **Velocities**

Figure 7. Predicted peak accelerations and velocities from the M_W 8.1 simulation (*), compared with the predicted peak accelerations and velocities from the Cape Mendocino main shock (Δ).

A COMPREHENSIVE GEOTECHNICAL AND SEISMIC INVESTIGATION OF SITE EFFECTS AT REPRESENTATIVE STRONG-MOTION STATIONS IN THE NEW MADRID SEISMIC ZONE

Award Number 1434-94-G-2441

Ron Street
University of Kentucky
Department of Geological Sciences
Lexington, Kentucky 40506-0053

(606) 257-4777
FAX: (606) 323-1938
E-mail: geo151@ukcc.uky.edu

Program Element III

Investigation Undertaken

Geotechnical holes, near the strong-motion stations HIKY in Hickman, Kentucky, and RIDG in Ridgely, Tennessee, are being drilled as part of a program to compare results obtained from high-resolution SH- and P-wave seismic profiling to SPT, resonant column tests of Shelby tube samples, and other soil column parameters. The two strong-motion station sites were chosen for the study because they represent the two predominant geomorphic terrains found in nearby vicinity of the New Madrid seismic zone. Station HIKY is located on a loess bluff in the southwestern corner of Kentucky. The site conditions at Hiky are typical of site conditions found at many of the communities located along the Chickasaw bluffs of western Kentucky and western Tennessee. Station RIDG is located in the flood plain of the Mississippi river in northwestern Tennessee, and is typical of the site conditions found at communities in that terrain.

Results

A 24 m geotechnical hole near HIKY was completed in July. The hole, located approximately 1 km northeast of the existing strong-motion station, is on state property at a highway garage. Shelby tube samples were obtained from the hole at 9.1 (30 ft) and at intervals of 3.05 m thereafter to a depth of 18.2 m (60 ft), where refusal was encountered. Blowcounts were logged at 3.05 m intervals for the entire depth of the hole. Table 1 summarizes the properties of the soils in the drill hole as determined in the Soils Laboratory at the University of Kentucky.

The 24 m hole is scheduled to be instrumented with a Kinemetrics FBA-23DH accelerometer in February, 1995. At the that time the strong-motion station at HIKY will be closed and the free-field Kinemetrics FBA-23 accelerometer presently at HIKY will moved to the site where the 24 m hole was drilled. The 12-bit Kinemetrics SSA-1 presently being used at HIKY will be replaced at the new site by a 6-channel, 24-bit, Kinemetrics K-2 accelerograph equipped with a GPS receiver. The long-term goal of the vertical accelerometer installation is to test our ability to account for the near-surface, low-velocity soils in our modeling, and to further our understanding of weak- and moderate-strain on site effects.

Depth (m)	Shelby Tube	SPT (blows)	USCS Class.	LL-PL (%)	Gs	Wc (%)	Vs (m/s)
3.0-3.5	No	1-1-3	CL	27-24	2.75	31.7	157
6.1-6.6	No	1-1-1	CL	26-22	2.70	29.2	157
9.10-10.2	Yes	3-3-4	CL	29-23	2.72	28.6	157
12.2-13.3	Yes	2-3-7	CL	54-38	2.71	60.4	594
15.2-16.3	Yes	2-6-12	CL	42-36	2.69	52.2	594
18.2-18.9	Yes (poor)	11-17-35	CL	41-35	2.62	43.5	594
21.3-21.8	No	7-10-16	CL	35-33	2.58	39.9	594

The geotechnical hole at RIDG is to be drilled by early December. Delays were encountered in getting this hole drilled sooner because the initial bids for the drilling were too high. As with the geotechnical hole near HIKY, Shelby tube samples will be collected where possible, samples of the soils will be analyzed in the Soils Lab, and the hole will be instrumented with a Kinemetrics FBA-23DH accelerometer. Resonant column tests will be done on all of the Shelby tube samples once the hole at RIDG is completed.

Results Published

Street, R., E. Woolery, Z. Wang, and J. Harris (1995). Shear-wave velocities and other site conditions at selected strong-motion stations in the New Madrid seismic zone, Seismological Research Letters 66(1), in press.

Basic Earthquake Hazards Studies in Hawaii

Award No. 1434-94-G-2488
Clifford H. Thurber and Clifford G. Munson
Department of Geology and Geophysics
University of Wisconsin-Madison
Madison, WI 53706
608-262-6027, FAX 608-262-0693, email clifft@geology.wisc.edu
Program Element NI

Investigations undertaken

We are analyzing 3-component digital seismic data recorded by the 1990 PASSCAL experiment (Project ALOHA) and the USGS strong motion array to investigate attenuation, peak ground acceleration (PGA), and site response characteristics on the Island of Hawaii. At present, knowledge of attenuation, PGA, and site response in Hawaii is quite limited. The current project directly addresses this knowledge gap. We model attenuation using the approach of Anderson, Hough, and coworkers, with a site component and a distance-dependent path component for the spectral decay parameter We are employing a new nonlinear least squares method that includes estimates of parameter uncertainties to determine "optimal" and "constrained" estimates of the spectral decay parameter (κ) using microearthquakes in south-central Hawaii (magnitude up to about 3) from the PASSCAL data and larger earthquakes (moment magnitude up to 6.8) island-wide from USGS strong motion data. We are also working to derive a PGA versus distance and magnitude relation for Hawaii using strong motion data and the multiple-regression approach of Joyner and Boore [1993, 1994]. The regression model includes a site term for strong motion stations on ash. The third component of our work involves multiple methods for estimating site response, including shallow seismic profiling, spectral ratios, a generalization of Nakamura's horizontal-to-vertical spectral ratio method, and microearthquake receiver function modeling. The result of these efforts will be the first thorough analysis of attenuation, peak ground acceleration, and site response in Hawaii for the purposes of earthquake hazard evaluation.

Results

Our derived values for the spectral decay parameter (κ) for Hawaii are plotted as a function of epicentral distance in Figure 1, along with values for Imperial Valley and Pinyon Flat from Anderson [1986]. Our values for κ overlap those for Imperial Valley. In particular, the site terms for Hawaii and Imperial Valley are comparable and are significantly greater than that for Pinyon Flat. However, unlike the Imperial Valley values, the Hawaii κ values do not show a significant increase with increasing epicentral distance. This implies that the bulk of the attenuation takes place in the near surface. This finding is consistent with the results of Munson et al. [1993] that the anisotropy causing observed shear wave splitting in southern Hawaii is also

mainly restricted to the near surface (uppermost 4 km or less). The high attenuation values are also consistent with the strong shear wave velocity anisotropy observed [Munson et al., 1993].

We derive a horizontal PGA predictive equation for the island of Hawaii using the Joyner and Boore [1993 and 1994] two-step linear regression method. Our data set consists of 56 horizontal PGA values from 13 events (Figure 2) including six subevents of the 1975 Kalapana main shock (moment magnitudes M_w = 6.1, 6.1, 6.1, 6.4, 6.8, and 6.6), the 1983 Kaoiki event (M_w = 6.5), and two 1989 South Flank subevents (M_w = 6.1 and 6.0). Epicentral distances vary from 0 to 98 km and event depths vary from 8 to 16 km. We use records from instruments triggered before the S-wave arrival. Moment magnitudes and additional earthquake source parameters are determined by a theoretical fit to the observed Fourier spectra using the method of Anderson and Humphrey [1991]. Our resulting equation is

$$\log PGA = 0.910 + 0.286 (M_w - 6) - 6.792 \times 10^{-3} r - \log r + 0.422 G_{HC}$$

where PGA is in units of g, $r = (d^2 + h^2)^{1/2}$ with d = fault distance and h = average depth, and G_{HC} is 1 for Hamakua Coast ash sites and 0 otherwise. The standard deviation for our attenuation curve ($\sigma_{\log Y}$ = 0.182) is comparable to that of Joyner and Boore [1981] ($\sigma_{\log Y}$ = 0.260) and Boore et al. [1993] ($\sigma_{\log Y}$ = 0.205). Klein [1994] modifies the Boore et al. [1993] attenuation curve to approximately fit the Hawaii PGA data by shifting the curve upwards by a factor of 1.2. Our attenuation curve decays more gradually than this modified Boore attenuation curve for distances less than 20 km while beyond 20 km our curve decays much more rapidly. Figure 3 (a to c) shows the fit of our curve to data from 3 events and (d) a comparison of our curve to those of Boore and Klein (that is, modified Boore). Three Quaternary ash sites on the Hamakua coast display horizontal PGA amplifications as high as 4.8 relative to lava sites, generating a significant site term in our attenuation curve.

Work on site response is in progress. We are taking a multi-faceted approach to the problem of site response estimation. Pseudo-acceleration response spectra (PARS) for three events are shown in Figure 4 (a to c) along with a summary plot in Figure 4d comparing average spectra on lava to that on two ash areas (Hamakua Coast and Wood Valley). Site response variations are clearly substantial, especially the short period amplifications at Hamakua Coast sites, as discussed above. Ongoing efforts include using a generalization of Nakamura's method (horizontal to vertical single-station spectral ratios), microearthquake receiver functions, and forward modeling of spectra to investigate the role of the very shallow structure in site response. Shallow seismic profiling at strong motion station sites was carried out in the summer of 1994 to test these estimates of shallow structure. Initial results indicate a good correspondence between profile structure and prior estimates of the structure.

References

Anderson, J. G., Implication of attenuation for studies of the earthquake source, in Earthquake Source Mechanics, AGU Monograph 37, 311-318, 1986.

Anderson, J. G. and J. R. Humphrey, A least-squares method for objective determination of earthquake source parameters, Seismol. Res. Lett. 62, 201-209, 1991.

Boore, D. M., W. B. Joyner, and T. E. Fumal, Estimation of response spectra and peak acceleration from western North American earthquakes: An interim report, USGS Open File Rep. 93-509, 72 pp., 1993.

Joyner, W. B. and D. M. Boore, Peak horizontal acceleration and velocity from strong-motion records including records from the 1979 Imperial Valley, California earthquake, Bull Seismol. Soc. Am 71, 2011-2038, 1981.

Joyner, W. B. and D. M. Boore, Methods for regression analysis of strong-motion data, Bull Seismol. Soc. Am 83, 469-487, 1993.

Joyner, W. B. and D. M. Boore, Methods for regression analysis of strong-motion data, ERRATA, Bull Seismol. Soc. Am 84, 955-956, 1994.

Klein, F. W., Seismic hazards at Kilauea and Mauna Loa volcanoes, Hawaii, USGS Open File Rep. 94-216, 94 pp., 1994.

Munson, C. G., C. H. Thurber, and Y. Li, Observations of shear wave splitting on the southeast flank of Mauna Loa volcano, Hawaii, Geophys. Res. Lett. 20, 1139-1142, 1993.

Reports Published:

Munson, C. G., and C. H. Thurber, Spectral modeling of Hawaiian earthquakes: source parameters, attenuation, and site response, Seismol. Res. Lett. 65, 34, 1994.

Munson, C. G., C. H. Thurber, and A. D'Silva, A peak-ground-acceleration predictive equation for Hawaii, EOS, Trans. Am. Geophys. Un. Suppl. 75, 448, 1994.

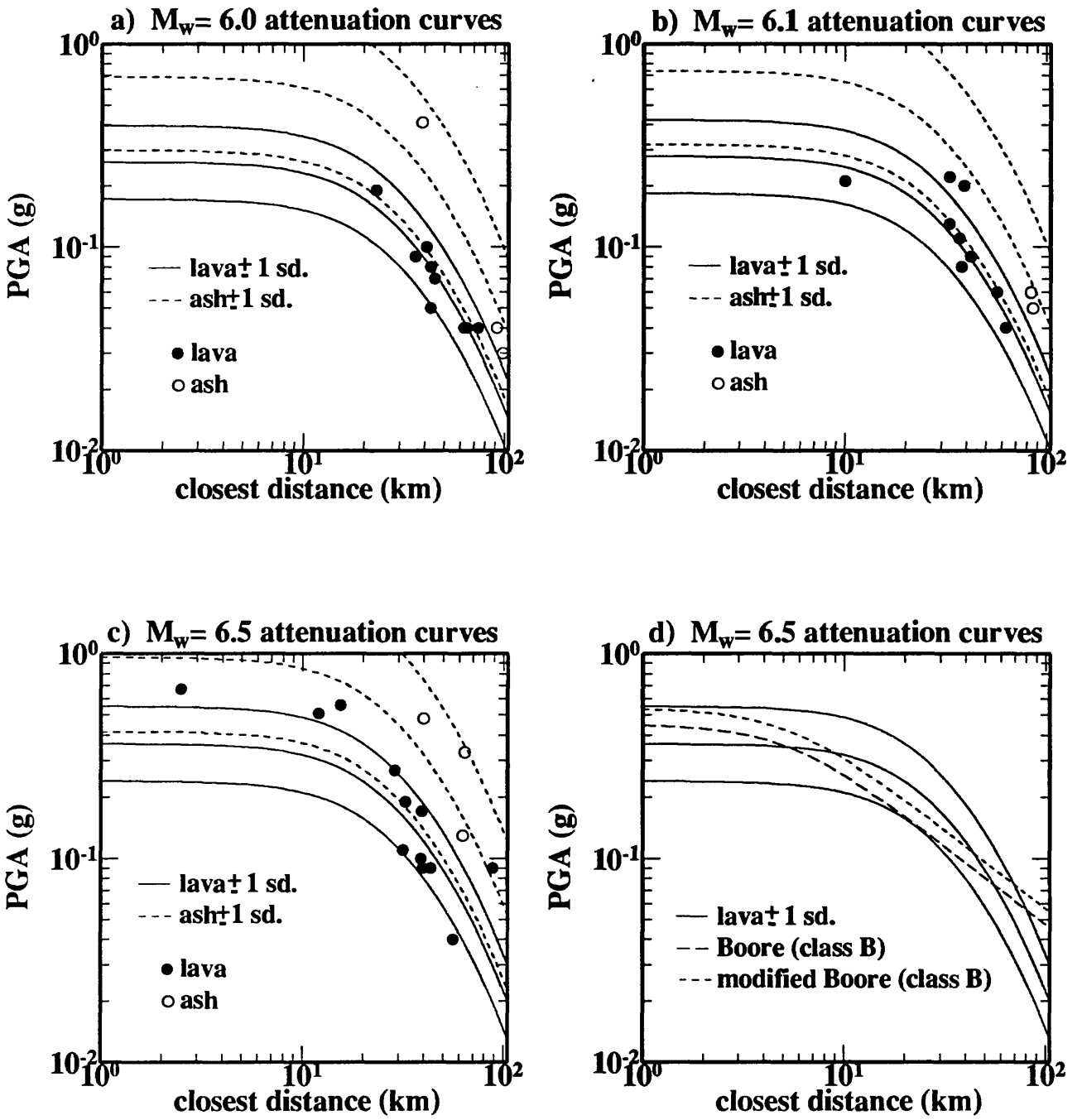

Figure 3. (a-c) Fit of data from 3 different magnitudes to our PGA versus distance curves, showing both lava (solid) and ash (dashed/open) predicted and observed values. (d) Comparison of our PGA curve to the Boore and Klein (modified Boore) curves for M_w = 6.5.

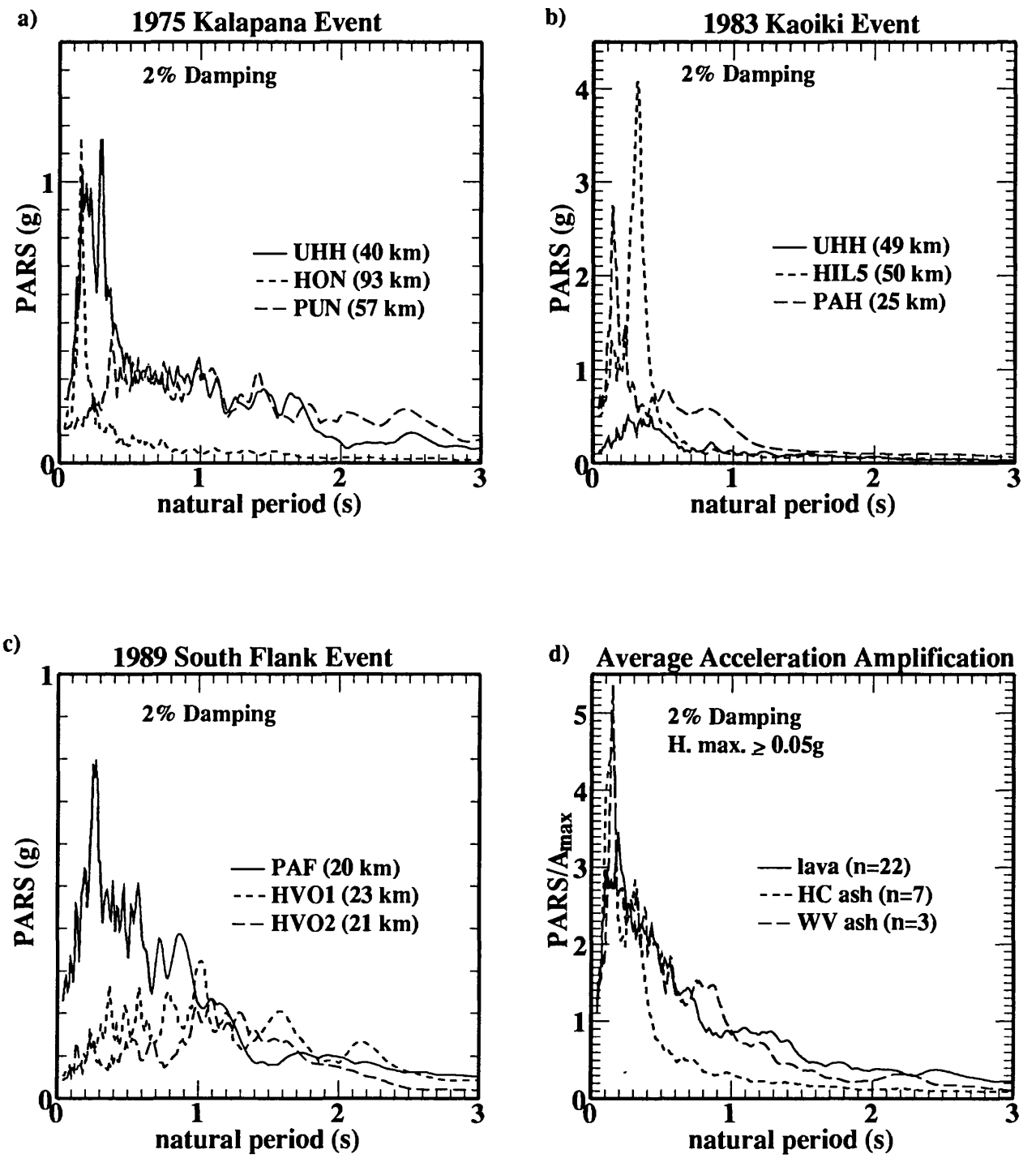

Figure 4. (a-c) Pseudo-acceleration response spectra (PARS) for three events, and (d) summary plot comparing average spectra on lava to that on two ash areas (Hamakua Coast and Wood Valley).

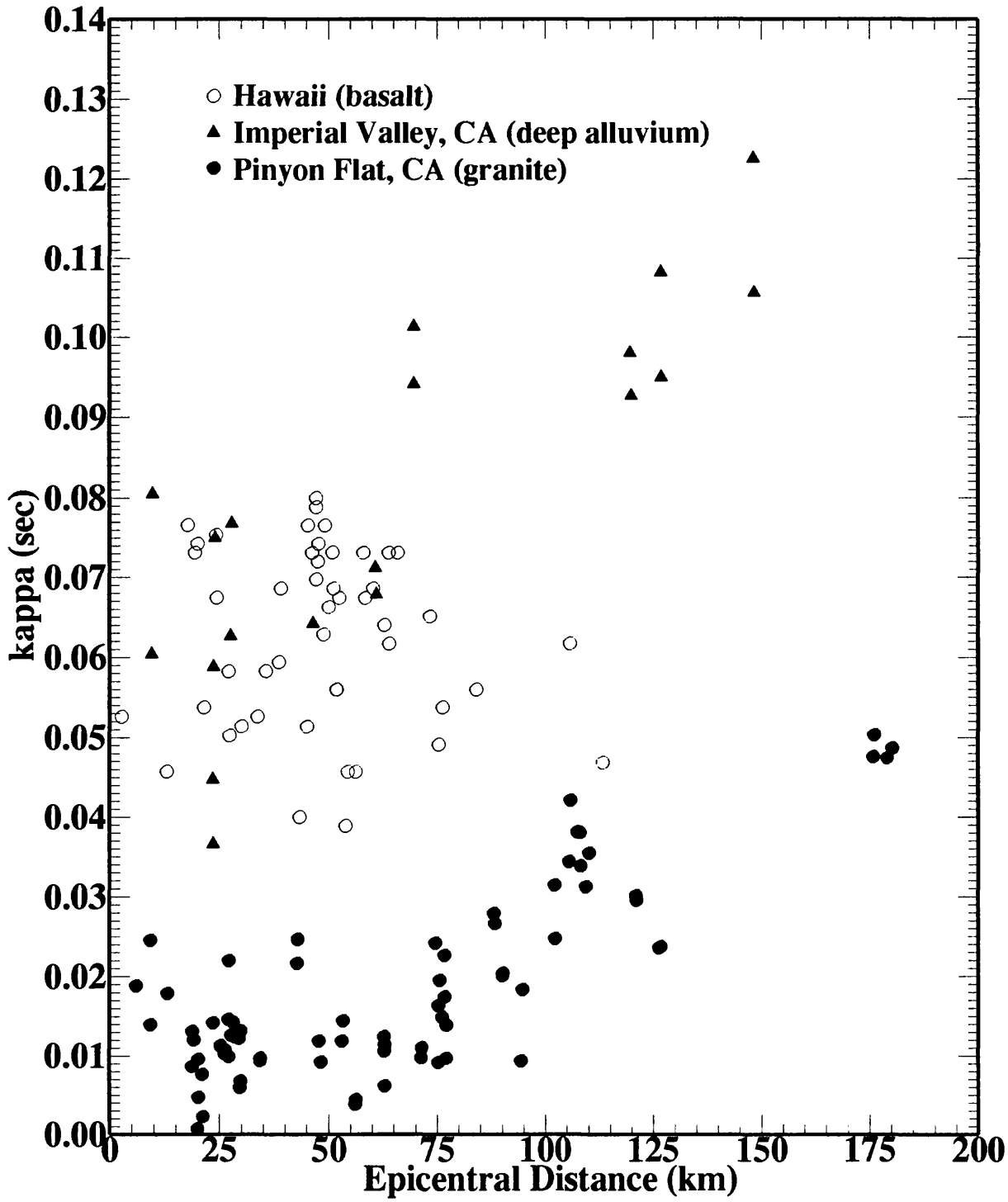

Figure 1. Spectral decay parameter (κ) values as a function of distance for Hawaii (open circles) compared to Imperial Valley (triangles) and Pinyon Flat (filled circle) values from Anderson [1986]. The Hawaii values substantially overlap the Imperial Valley values.

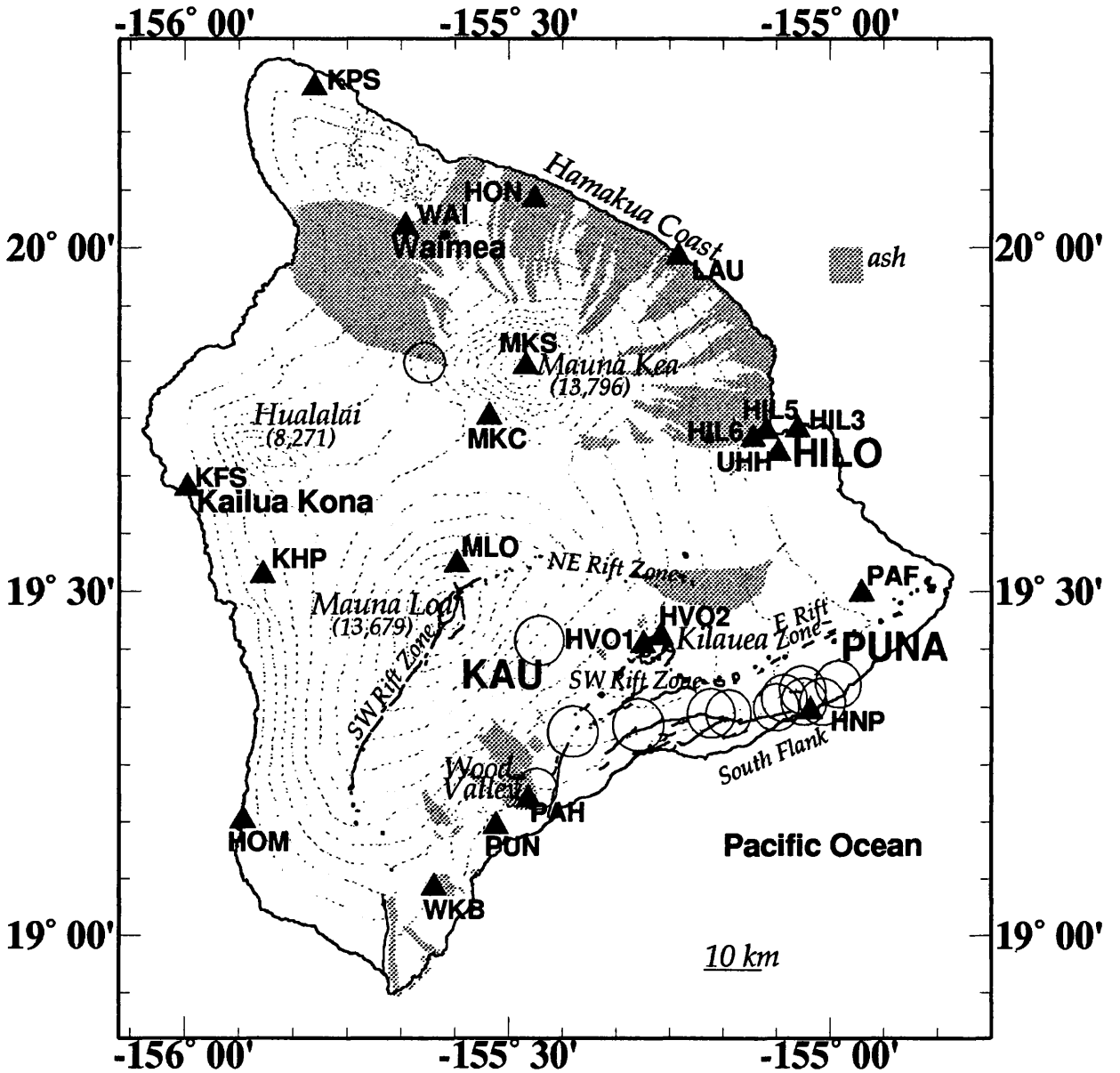

Figure 2. Location map for Hawaii showing events (open circles) and strong-motion stations (solid triangles) used in the PGA analysis. Areas of significant ash thickness are shaded.

Quaternary Framework for Earthquake Studies, California

4-9540-10010

John C. Tinsley
Branch of Western Regional Geology
345 Middlefield Road MS-975
Menlo Park, California 94025-3591
415-329-4928

Investigations:

1. Identification of areas susceptible to lateral spread ground failure was achieved during 1994 by statistically combining geologic, hydrologic, and topographic information within a geographical information systems (GIS) framework. The approach is interesting in that it substitutes generalized geologic, hydrologic, and topographic information for the detailed geotechnical measures customarily employed to make site-specific work and regional assessments of susceptibility to liquefaction and lateral spreading. The geologic map data were assembled as digital map files of six 7.5' quadrangles of the Monterey Bay area (750 sq. km.) and prepared in digital format by Tinsley and Geoff Phelps (USGS, Menlo Park). Statistical manipulations were conducted within a GIS framework at a grid resolution of 100m. Susceptibility was estimated in a 2-step procedure using threshold criteria and then using multiple linear (probit) regression techniques.

2. Pursuant to the Northridge earthquake, digital files of the regional geologic mapping published as page-size (1:250,000 scale) maps in the USGS Professional Paper 1360 edited by J. I. Ziony (Evaluating earthquake hazards in the Los Angeles region—an earth science perspective) are being prepared for use by interested investigators.

Results:

1. In summary, there were 49,654 1-hectare parcels comprising the 6 quadrangles used in the study. Those parcels (1) located in bedrock areas, (2) pre-Holocene sediments adjudged to be unlikely to liquefy owing to age (>10,000 yr. old) or diagenesis, and those in areas too steep for lateral spreading (slopes >3%) were assigned susceptibility values of zero. All but 12 of the area's 36 mapped geologic units were eliminated. For the remaining 12 map units, relative susceptibility (S_R) is defined operationally as the chance that each of the 25,508 hectare cells is located in 1 or 2 geologic units (late Holocene flood plain deposits, map unit Qyf; Holocene channel fill deposits, map unit Qcf) judged by an expert as most likely to liquefy. The regression relation is expressed as follows:

$$S_R = 4.8\% \text{ sand} - 0.56 \ln \text{distance} - 0.95 \log \text{age} - 0.28 \ln \text{slope}$$

where sand is the sand content of the map unit, age is the geologic age of the deposit, distance is the horizontal distance from nearest surface water, and slope is the ground slope derived from digital elevation models of the quadrangles studied. The regression is dominated by sand content and then age is statistically significant at the 1% level and explains 76% of the variance. The map generated by these statistical manipulations makes geological sense in that the highest S_R values commonly coincide with the most susceptible unit (Qyf, mean $S_R = 0.98 \pm 0.03$) and with the 363 hectare parcels within

which lateral spreading was observed following the 1989 Mw 6.9 Loma Prieta earthquake.

2. This mapping was published initially in USGS Professional Paper 1360; it has been used widely by the public and private sector in earth science applications. Most recently, the mapping has been used by the California Division of Mines and Geology along with additional sources of geologic and hydrologic information to compile maps showing liquefaction hazard maps, presently being prepared under the authority of the California Seismic Hazards Mapping Act of 1990 .

Reports:

Pike, R. J., Bernknopf, R. L., Tinsley, J. C., III, and Mark, R. K., 1994, Hazard of earthquake-induced lateral spread ground failure on the Central California coast modeled from earth-science map data in a geographic information system: U.S. Geological Survey Open-File Report 94-662, 46 p., 1 plate (scale 1:62,500).

Scientists of the U.S. Geological Survey and the Southern California Earthquake Center, 1994, The magnitude 6.7 Northridge, California, earthquake of 17 January 1994: Science, v. 266, p. 389-397.

Additional project-related activities and reports are cited in the report by T. H. Holzer and others, Liquefaction Research, this volume.

New Methods of Empirical Spectral Prediction

Award Number: 1434-94-G-2461
Investigators: Alexei G. Tumarkin and Ralph J. Archuleta
Institution: Institute for Crustal Studies,
University of California at Santa Barbara
Address: Santa Barbara, CA 93106-1100
Telehone: (805) 893-8446
Fax: (805) 893-8649
E-mail: alexei@quake.crustal.ucsb.edu
Program Element: III. PREDICTING THE EFFECTS OF EARTHQUAKES

INTRODUCTION

We developed new empirical methods of ground motion prediction based on multiple source models. The idea of many empirical Green's functions methods (Hartzell, 1978) is to utilize the observed small earthquakes originating within the rupture area of the simulated large earthquake as its subsources, representing heterogeneities, asperities, etc. For the validity of this approach all subevents should have focal mechanisms similar to that of the simulated main event. Suppose that we have a good coverage of the anticipated main event rupture area by observed subevents. Then we may try to simulate the large earthquake as a subsequent rupture of properly scaled and lagged subevents. Such procedure will account for the source-receiver geometry by virtue of the initial choice of only those subevents, which are co-located with the main event. Directivity effects can be taken into consideration by determining rupture times of subevents according to both their position on the fault with respect to the main event hypocenter and the azimuth between the site and the direction of rupture propagation.

The important features of our approach are the following:

- It is completely empirical.
- It allows one to use all the available records at a site. Thus a prediction is not biased by a single record, and different possible source-receiver paths are taken into account.
- It requires the following input parameters for the simulated large event:
  i) target seismic moment M_0;
  ii) location of the seismogenic zone, in particular its size R_0;
  iii) direction of rupture propagation;
  iv) location of the hypocenter (not required for the spectral prediction method).

  There are no other free parameters.
- By applying the method to all three components of ground motion we can predict simultaneously the three components of ground motion at a site.
- It exploits the established connection of the basic scaling relations (Aki, 1967; Brune, 1970; Kanamori and Anderson, 1975) between large and small earthquakes to parameters of the seismic source spectrum. This results in a flexibility of the method with respect to different observed seismic parameters' scaling and spectral falloffs.

- It produces a ground motion prediction in the whole frequency range avoiding deficiency in spectral amplitudes near the target corner frequency.

Any method of adding subevents in the time domain requires knowledge (or determination) of rupture times of subevents. We show that it is possible to perturb rupture velocity in a multiple source model consisting of identical constant stress drop subevents in order to produce an arbitrary target source. The idea of adjusting rupture times of identical subevents was suggested by Wennerberg (1990). However he used a non-causal subevent-to-main event transfer function that resulted in unrealistic negative rupture times on the fault. By using both the amplitude and the phase of the Brune's source spectral model (Dan *et al.*, 1990) our model develops only positive rupture times.

A new method of empirical spectral prediction, which uses only observed amplitude spectra of small earthquakes co-located with the predicted large earthquake, was also developed. This new method does not require the knowledge of details of seismic rupture and is theoretically capable of predicting ground motion spectra in the whole frequency range of analyzed subevents.

The principal difference between these two approaches is that the time-domain approach requires both the amplitude and phase information to produce time-series predictions, while the spectral approach uses only amplitude spectra of subevents to predict the amplitude spectrum of the target earthquake. On the other hand the time-domain additions of subevents can be equally well performed in the spectral domain by considering simultaneously the amplitude and phase spectra. At the same time our spectral methods are capable of producing time-series by associating either subevents phase information or random phase with the amplitude spectral prediction.

Empirical Green's functions methods

The general concept of the Empirical Green's Functions Method (EGFM) is to account for realistic path and site effects by using observed records of the so-called subevents — small earthquakes located within the rupture area of the simulated large earthquake (main event). The idea of EGFM (Hartzell, 1978; Wu, 1978) was extensively used for synthesizing strong ground motions as well as for inverting for source properties of seismic ruptures (Joyner and Boore, 1988; Aki and Irikura, 1991).

The major and the most difficult part of this approach is deciding how to sum the subevents' records to obtain the prediction (Hartzell, 1978; Irikura, 1983; Joyner and Boore, 1986; Heaton and Hartzell, 1989). We study this problem in both the time and the frequency domains by providing general methods of adding arbitrary sets of observations for site-specific ground motion simulations of scenario earthquakes. A different EGFM approach based on a kinematic modeling of the seismic rupture process (Hutchings, 1994) lies beyond the scope of this paper.

Often, EGFM considers a single observed subevent in order to simulate the ground motions for an anticipated main event. This subevent is replicated many times to obtain a distribution of similar subevents covering the expected rupture area of the main event. Using only one initial record for EGFM allows the predictions to have a strong dependence on characteristics of the input record.

Consequently, there is a large variation in predictions simply due to the choice of a subevent (Dan *et al.*, 1990).

In order to match the seismic radiation for both lowest and highest frequencies a subevent's waveform might be appropriately filtered in the time or frequency domains (Irikura, 1983; Boatwright, 1988; Heaton and Hartzell, 1989), or it might be specifically scaled and replicated (Joyner and Boore, 1986). Also, a satisfactory fit in the whole frequency range can be achieved by choosing an appropriate probability distribution of time delays between these identical subevents (Wennerberg, 1990). Another approach is to use EGFM to predict ground motions in a limited frequency range, say, above a certain frequency (Heaton and Hartzell, 1989) and then combine the results with a deterministic modeling at low frequencies (Somerville, 1993).

Joyner and Boore (1988) were the first to notice another major problem. The common methods that provide a satisfactory simultaneous fit to the lowest and highest frequencies of the target spectrum (Irikura, 1983; Joyner and Boore, 1986; Boatwright, 1988) are all based on a uniform distribution of rupture times of subevents, i.e., a constant rupture velocity over the fault. However this natural assumption leads to a significant underestimation of the main event's spectrum in the vicinity of the target corner frequency. This problem can not be overcome by allowing for different size subevents.

Source time functions and spectra

We use a functional description of the *S*-wave radiation that was suggested and verified against observations and physical models in pioneering works of K. Aki and J. Brune (Aki, 1967; Brune, 1970, 1971). The ω-γ spectral model with three parameters: M_0 - the seismic moment of the event, ω_0 - corner frequency (associated with the event's linear dimension and duration), and γ - high-frequency decay rate, has been widely used to study radiation of seismic sources (Joyner and Boore, 1988; Aki and Irikura, 1991). Different functional models of seismic sources (e.g., Randall, 1973) as well as the *P*-wave radiation can be treated along the same lines.

According to the classic ω-squared model (Aki, 1967; Brune, 1970, 1971), it is assumed that the shape of displacement amplitude spectrum $|S(\omega)|$ of a seismic event is

$$|S(\omega)| = C_s \frac{M_0}{1 + \left(\frac{\omega}{\omega_0}\right)^2} \qquad (1)$$

where $\omega=2\pi f$ is frequency, and C_S is a constant independent of M_0 and ω_0. This amplitude spectrum corresponds to the source time function, known as "Brune's pulse" (Brune, 1970):

$$S(t) = \sqrt{2\pi} C_s M_0 \omega_0^2 t e^{-\omega_0 t} H(t) \qquad (2)$$

where $H(t)$ is the Heavyside function. The behavior of the Brune's pulse at $t=0$, i.e., the first-order discontinuity of its derivative, controls the high-frequency behavior of the Aki-Brune's spectrum (1) which decays as ω^{-2} (Randall, 1973).

If we consider a more general source time-function

$$S(t) = \frac{\sqrt{2\pi}}{\Gamma(\gamma - 1)} C_s M_0 \omega_0^{\gamma} t^{\gamma-1} e^{-\omega_0 t} H(t) \qquad (3)$$

($\Gamma(\gamma-1)$ is the Gamma-function: $\Gamma(\gamma-1)=(\gamma-2)!$ for integer values of γ), then its Fourier transform has the form:

$$S(\omega) = C_s \frac{M_0}{\left(1 + i\frac{\omega}{\omega_0}\right)^{\gamma}} \qquad (4)$$

(for $\gamma=2$ see Dan *et al.* (1990)); and the corresponding *S*-wave amplitude spectrum is a familiar $\omega^{-\gamma}$-model

$$|S(\omega)| = C_s \frac{M_0}{\left(1 + \left(\frac{\omega}{\omega_0}\right)^2\right)^{\frac{\gamma}{2}}} \qquad (5)$$

in a form considered, for example, by Chael and Kromer (1988).

Multiple source models

It is well known that simple fault models (point-source, double-couple, Haskell-type rupture, etc.) produce accelerograms, that contradict the observed high-frequency complexity of radiated acceleration. There are different ways of introducing heterogeneity into the source models, thus enhancing radiated high frequencies. One of the most promising and widely used methods is to represent a heterogeneous rupture (main event) as a multiple source, i.e., as a composite of discrete subsources (subevents). These multiple source earthquake models include various self-similar models of complex earthquake rupture (Boatwright, 1988), the specific barrier model of Papageorgiou and Aki (1983), as well as some empirical Green's functions methods (Joyner and Boore, 1988). In a general sense every finite-element (or any other discrete) model of a seismic rupture can be viewed as a

multiple source model, although often the term "composite earthquake" is reserved for the specific case when each subevent is a small earthquake by itself (Frankel, 1991; Zeng *et al.*, 1994). Such composite earthquake models have inherent limitations (Tumarkin *et al.*, 1994).

At the same time site-specific predictions of ground motions should utilize all the available information contained in observations of earthquakes at the particular site. Uncertainties in the predicted path and site effects can be reduced by examining data from past earthquakes that originate within the rupture area of the anticipated large earthquake (e.g., Joyner and Boore, 1988). If more subevents are simultaneously included as a basis for a prediction, the results are less dependent on characteristics unique to a single seismic record.

Suppose that we have observations of N earthquakes (subevents) having the same focal mechanism and all located within the rupture area of an anticipated large earthquake. The most natural and simple idea is to simulate the radiation from the large earthquake as a linear combination of subsources – scaled and lagged small earthquakes (Heaton and Hartzell, 1989). The source time function $S_0(t)$ of the simulated earthquake is represented as a linear combination of source time functions $S_j(t)$ of subevents:

$$S_0(t) = \sigma_1 S_1(t-\tau_1) + \sigma_2 S_2(t-\tau_2) + \ldots + \sigma_N S_N(t-\tau_N) \qquad (6)$$

where τ_j denotes the rupture time of the jth subevent, and σ_j are scaling coefficients for the jth source $S_j(t)$. Allowing for σ_j to be free parameters of the model means that we are permitting arbitrary changes of stress drops of subevents in order to fit the target earthquake (variable stress drop model). Similarly variations of τ_j result in a variable rupture velocity over the fault plane.

Assuming that the source time functions $S_0, S_1, \ldots, S_N$ have the functional form (3), we can rewrite (6) as:

$$\begin{aligned} M_0\omega_0^\gamma t^{\gamma-1} e^{-\omega_0 t} H(t) \approx\ & \sigma_1 M_{01}\omega_1^\gamma (t-\tau_1)^{\gamma-1} e^{-\omega_1(t-\tau_1)} H(t-\tau_1) + \\ & \sigma_2 M_{02}\omega_2^\gamma (t-\tau_2)^{\gamma-1} e^{-\omega_2(t-\tau_2)} H(t-\tau_2) + \ldots + \\ & \sigma_N M_{0N}\omega_N^\gamma (t-\tau_N)^{\gamma-1} e^{-\omega_N(t-\tau_N)} H(t-\tau_N) \end{aligned} \qquad (7)$$

where $M_0, M_{01}, \ldots, M_{0N}$ are the seismic moments of the target event and subevents; $\omega_0, \omega_1, \ldots, \omega_N$ are their corner frequencies; and γ is the common spectral falloff.

Parameters σ_j and τ_j can be determined as solutions of a non-linear least-squares problem (7). It is possible to consider a minimization problem with constraints on values of σ_j and t_j forcing them to lie within the physical limits on stress drops and rupture velocity. If the rupture times τ_j of subevents are postulated (e.g., by assuming a constant rupture velocity), then the coefficients σ_j can be found as a

solution of a linear least squares problem. However the problem of determining the best fitting rupture times τ_j is severely non-linear. Nonetheless there is a way of explicitly resolving for τ_j in the framework of the approach proposed by Wennerberg (1990), which is developed in the next section. The relation (7) is satisfied by varying only τ_j while keeping σ_j=*const*. This approach corresponds to a constant stress drop model with a variable rupture velocity.

If the coefficients σ_j and τ_j are found from the relation (7), the ground motion $U_0(t)$ from the large earthquake at any site can be approximated as the linear combination of observed ground motions $U_j(t)$ from the subevents:

$$U_0(t) \approx \sigma_1 U_1(t-\tau_1) + \sigma_2 U_2(t-\tau_2) + \ldots + \sigma_N U_N(t-\tau_N), \qquad (8)$$

which follows from (6) and the representation theorem for seismic sources (Aki and Richards, 1980).

Directivity

Radiation from extended seismic sources often has a distinct asymmetric structure. At the same distance from the seismogenic area in the direction of the rupture propagation higher amplitudes are accompanied by shorter durations, while in the back-azimuth lower amplitudes and long durations are observed. This effect was discovered by Benioff (1955) and was named "directivity" by Ben-Menahem (1961). Directivity is closely related to the Doppler effect (Douglas *et al.*, 1988). Earlier theoretical and laboratory studies (Archuleta and Brune, 1975; Boore and Joyner, 1978) as well as observations of moderate and large earthquakes (e.g., Boatwright and Boore, 1982; Kanamori *et al.*, 1992) emphasize the importance of accounting for rupture directivity in ground motion prediction algorithms.

The apparent *S*-wave spectrum $S_\theta(\omega)$ of a seismic source moving with constant speed v observed at a site located at an angle θ from the direction of rupture is given by:

$$S_\theta(\omega) = S\left(\frac{\omega}{D}\right), \qquad (9)$$

where D is the directivity factor:

$$D = \frac{1}{1 - \frac{v}{\beta}\cos\theta}$$

(Aki and Richards, 1980; Douglas *et al.*, 1988; Joyner, 1991). Thus the directivity factor D is controlled by both the azimuth θ and the Mach number $M=v/\beta$, where β is the shear wave velocity. Directivity effects increase with an increase of the Mach

number M.

Assuming the Aki-Brune spectral source model the relation (9) is equivalent to the shift of the apparent source corner frequency $\omega_{0\theta}$:

$$\omega_{0\theta} = \frac{\omega_0}{1 - \frac{v}{\beta}\cos\theta}. \qquad (10)$$

Assuming that $v=0.85\beta$ (Kostrov, 1964; see also below), we find that the apparent source corner frequency is greatly augmented in the forward direction — $\omega_{0\theta}=6.67\omega_0, \theta=0$; unchanged in the direction perpendicular to the fault — $\omega_{0\theta}=\omega_0, \theta=90°$; and reduced by almost a factor of 2 in the back azimuth — $\omega_{0\theta}=0.54\omega_0$, $\theta=180°$. This angular variation of corner frequency explains the focusing of seismic energy in the direction of rupture propagation. Consequently directivity results in a dramatic azimuthal dependence of the shape of ground motion spectrum and the total radiated energy for unilateral seismic ruptures (Boore and Joyner, 1978; Boatwright and Boore, 1982; Kanamori *et al.*, 1992). It is worth noting that heterogeneous ruptures (and thus multiple source models) may have even stronger directivity effects than uniform ruptures (Boore and Joyner, 1978; Joyner, 1991).

TIME-SERIES PREDICTION

First we consider an elegant, though particular, approach to solution of the problem (6), initiated by Wennerberg (1990). The Brune's source time function (2) is approximated by adjusting rupture times but not the stress drops of subevents. The general case (3) is treated analogously, but explicit expressions for the rupture velocity can be obtained only for particular values of γ, such as $\gamma=3$.

The final result is an algorithm for time-series prediction that allows for an arbitrary number of observed empirical Green's functions.

Methods based on an appropriate choice of time delays between subevents

A number of studies (Irikura, 1983; Joyner and Boore, 1986; Boatwright, 1988; Heaton and Hartzell, 1989) proposed methods for adding identical subevents with uniformly distributed rupture times. These methods succeeded in matching both the low- and high-frequency radiation from simulated earthquakes. At the same time Joyner and Boore (1986, 1988) found that their procedure resulted in a deficit of energy in the intermediate frequency range of the simulated spectrum (especially, in the vicinity of the corner frequency ω_0 of the main event). This fact is an inherent feature of all methods assuming a uniform distribution of rupture times of subevents, i.e., a constant rupture velocity (Joyner and Boore, 1988) (Fig. 2). The underestimation of the energy poses the problem of how to lag small earthquakes, other than uniformly distributing their rupture times, in order to simulate radiation from a large earthquake for the whole frequency range.

The importance of an adequate fit to the target spectrum in the vicinity of the corner frequency ω_0 is driven by both seismological and engineering applications of EGFM. The spectral corner frequency ω_0 acts as a resonant frequency of the source energy since the velocity amplitude spectrum of a seismic source is peaked at ω_0 for the common ω-squared model (Aki, 1967; Brune, 1970, 1971). Therefore any misfit to the target spectrum in the vicinity of its corner frequency severely affects the total energy.

Wennerberg (1990) suggested an approach to eliminate this deficit by determining an appropriate distribution of rupture times of subevents. Wennerberg assumed that the phase spectrum between a small and a large earthquake is preserved. That assumption results in a non-causal transfer function for small-to-large earthquake scaling leading to unrealistic negative rupture times for one half of the subevents.

We eliminate the negative rupture times in the Wennerberg's method by using the complex form of the Aki-Brune's spectral model (4). Rather than treating the distribution of rupture times of subevents as some transformation of a uniformly distributed random variable (Wennerberg, 1990), we consider rupture time as a function of the position on the fault. This allowed us to study the rupture front velocity in this model and to propose non-instantaneous kinematic source models with Brune-type spectra (Tumarkin and Archuleta, 1994).

Algorithm for time-series prediction

Suppose that at a given site we have observations $U_j(t)$, $j=1,...,N$ of N small earthquakes originating within the rupture area of an anticipated large earthquake. We assume that these earthquakes have the same focal mechanism as the large event. If the observations cover the anticipated main event rupture area, we try to simulate the large earthquake as the sum of subevents generated from the properly scaled and lagged observed small earthquakes. Meanwhile we account for the source-receiver geometry by choosing only those subevents that are co-located with the main event. We account for directivity effects by determining rupture times of subevents according to both their position on the fault with respect to the main event hypocenter and their azimuth between the site and the direction of rupture propagation.

In practice the number of observations is usually small, they are distributed non-uniformly between the hypocenter and the boundary of the anticipated rupture area, and they have different sizes. The following simple procedure allows to overcome the first two problems. We choose a new number of subevents N_0 that is assumed to be sufficiently large to mimic a continuous uniform distribution of subevents on the fault. Testing on data shows that N_0=100 works quite well. Then we uniformly distribute N_0 subevents on the fault, for example, by assigning

$$R_j = \frac{j}{N_0} R_0,$$

where R_j is the distance between the hypocenter of the main event and the j-th subevent, and R_0 denotes the size of the main event. Now we take the observed small earthquake closest to the main event's hypocenter. All subevents located closer to the main event's hypocenter than this small earthquake are assumed to have waveforms similar to that from this observed small earthquake. Subevents positioned further than the first observed small earthquake but closer than the second from the origin small earthquake are assumed to be similar to the latter one, etc. This procedure divides the whole set of N_0 subevents into n_1 subevents similar to the observed small earthquake closest to the main event's hypocenter, n_2 subevents similar to the second closest observed earthquake, etc. Thus after arranging the observed small earthquakes according to their distances to the main event's hypocenter, the numbers $n_1, n_2,..., n_N$ are proportional to the difference between hypocentral distances of two successive small earthquakes. There are many other possible ways to redistribute subevents, in particular in a more accurate manner accounting for the source-receiver geometry, and/or making $n_1=n_2=...=n_N$.

If subevents' corner frequencies are sufficiently large, we can use the limiting case $\omega_{0e}=\infty$ to determine their rupture times. The resulting algorithm for time-series prediction, based on this approach, has the following steps:

1) Estimate the total rupture duration T_0 by dividing the fault size R_0 by the average rupture velocity v (e.g., $v=0.85\beta$). Calculate the target corner frequency $\omega_0=2\pi/T_0$.

2) Determine the apparent source corner frequency $\omega_{0\theta}$ at the site according to the directivity factor D:

$$\omega_{0\theta} = \frac{\omega_0}{1-\frac{v}{\beta}\cos\theta}$$

(relation (10)).

3) Calculate the seismic moment M_{0j} (or estimate moments from the catalog magnitudes) for each observed subevent;

4) Determine the rupture time τ_j of the jth subevent:

$$\rho_j = 1-\left[1+\omega_{0\theta}\tau_j\right]e^{-\omega_{0\theta}\tau_j},$$

where ρ_j is the distance between the main shock's and subevent's hypocenters normalized by the size R_0 of the main fault plane (e.g., $\rho_j=1/j$);

5) Determine coefficients σ_j. This can be done, for example, by adjusting subevents to a common seismic moment M_0/N_0, then $\sigma_j = \frac{1}{N_0}\frac{M_0}{M_{0j}}$; or, more

naturally, use the same normalization $\sigma_j=\sigma$ of the stress drop for all subevents:

$$\sigma = \frac{M_0}{n_1 M_{01}+n_2 M_{02}+...+n_N M_{0N}};$$

6) Add observed subevents' waveforms according to (8).

SPECTRAL PREDICTION

In this section we describe an alternative approach to ground motion prediction (Archuleta and Tumarkin, 1994). We consider only the amplitude spectra. Fourier amplitude spectrum is a measure of ground motion that (i) is related to both the earthquake source and propagation/site effects; (ii) covers the entire seismic bandwidth; (iii) directly applies to earthquake engineering; and (iv) is a robust measure of the total ground motion. At the same time phase spectra carry the most uncertainty and variability, being influenced by details of the rupture nucleation and propagation, size and location of asperities, etc.

Joyner and Boore (1986) considered the case of a number of identical subevents with uniformly distributed rupture times (see also Heaton and Hartzell, 1989). We generalize their results for an arbitrary distribution of small earthquakes by using a slightly different approach that is based on a direct comparison of levels of the target and added spectra at the lowest and the highest frequencies. In our method the summation of subevents amplitude spectra is controlled by a frequency-dependent partial coherence exponent. This novel approach allows to avoid the deficit of the resulting spectral prediction in the vicinity of the target corner frequency.

Algorithm for spectral prediction

Here we describe a new general algorithm for empirical spectral prediction (Archuleta and Tumarkin, 1994). This approach utilizes only amplitude spectra of subevents, thus it does not require any phase information (such as location of the hypocenter, time delays between subevents, etc.).

Suppose that at a given site you have N records of earthquakes, located within the prospective rupture area of a large earthquake with the seismic moment M_0 and the corner frequency ω_0. The idea of the algorithm, common for all EGFM approaches, is that the observed records already contain information on the propagation path from the simulated source to the studied station and on the local geology beneath the station. Moreover, if there is a way to use as many recorded events, as possible, then the possible dependence of the simulated spectrum on peculiarities of a single record is significantly reduced. Also, different path effects are taken into account by spanning a majority of the anticipated fault plane. This is especially important in case of larger earthquakes where rupture lengths of tens kilometers are comparable to the distance between source and site.

The proposed algorithm includes the following steps:

1) Calculate the seismic moment M_{0j}; S-wave corner frequency ω_j; and the source

spectral falloff γ for each jth subevent. This can be done, for example, on the basis of existing automated methods of fitting observed spectra (e.g., Fletcher and Boatwright, 1991; Lindley and Archuleta, 1992).

2) Determine the scaling exponent δ for the seismic moment. This is done by applying regression analysis to logarithms of values of the seismic moment and of corner frequencies, calculated in step 1.

3) Determine the apparent source corner frequency $\omega_{0\theta}$ at the site according to the directivity factor D controlled by the azimuth θ from the rupture direction to the given site:

$$\omega_{0\theta} = \frac{\omega_0}{1 - \frac{v}{\beta}\cos\theta}$$

(relation (10)).

4) Multiply each observed amplitude spectrum $|U_j(\omega)|$ by $(\omega_{0\theta}/\omega_j)^{2\gamma-\delta}$:

$$|\tilde{U}_j(\omega)| = \left(\frac{\omega_{0\theta}}{\omega_j}\right)^{2\gamma-\delta} |U_j(\omega)|$$

5) Calculate the normalizing constant C for the observed distribution of subevents:

$$C = \frac{\omega_{0\theta}{}^{-2\gamma}}{\omega_1{}^{-2\gamma} + \omega_2{}^{-2\gamma} + \ldots + \omega_N{}^{-2\gamma}}$$

6) Determine the partial coherence exponent $\varepsilon(\omega)$:

$$\varepsilon(\omega) = \frac{1}{1 - \frac{\ln\left[1 + \left(\frac{\omega}{\omega_{0\theta}}\right)^2\right] - \ln\left[1 + \left(\frac{\omega}{\omega_{min}}\right)^2\right]}{4\ln\left(\frac{\omega_{min}}{\omega_{0\theta}}\right)}},$$

where ω_{min} is the smallest corner frequency of subevents, i. e., the corner frequency of the largest subevent.

7) Raise the normalized amplitude spectra $|\tilde{U}_j(\omega)|$ to the power $\varepsilon(\omega)$ and add them together, taking each normalized spectrum C times. The resulting spectral

prediction $|U_0(\omega)|$ is expressed by:

$$|U_0(\omega)| = C^{\frac{1}{\varepsilon(\omega)}} \left\{ \left|\tilde{U}_1(\omega)\right|^{\varepsilon(\omega)} + \left|\tilde{U}_2(\omega)\right|^{\varepsilon(\omega)} + \ldots + \left|\tilde{U}_N(\omega)\right|^{\varepsilon(\omega)} \right\}^{\frac{1}{\varepsilon(\omega)}} .$$

8) Scale the resulting spectrum $|U_0(\omega)|$, accounting for a possible difference between the average stress drop of subevents and the stress drop of predicted main event. Technically this is achieved by comparing the given value of the seismic moment M_0 for the simulated event with the result of extrapolation of the regression relation, obtained in Step 2, to the value $\omega_{0\theta}$ of the apparent source corner frequency. The ratio between the target and extrapolated seismic moments gives the scaling multiplier to be applied to predicted spectrum $U_0(\omega)$, accounting for the difference in stress drops.

TESTING ON DATA

We have tested the time series and spectral algorithms on data from the Joshua Tree earthquake sequence. Results from a retrospective "prediction" of the M_W6.1 Joshua Tree mainshock using 5 smaller earthquakes (Table 1) are presented. The source parameters of the used subevents were taken from (Lindley, 1994). In order to obtain S-wave corner frequencies we divided P-wave corner frequencies from Table 1 by $\sqrt{3}$. For example, for the main event we get f_0=0.29 Hz. The main event is an almost purely strike-slip rupture with a roughly 12 km square fault-plane striking N10°W. For a rupture velocity 3 km/s that would imply a total rupture duration of 4 s and the source corner frequency 0.25 Hz, which is consistent with the above mentioned value. The rupture propagated unilaterally from the hypocenter to the North (Kanamori *et al.*, 1993).

The studied site is the Garner Valley Downhole Array (GVDA) (Archuleta *et al.*, 1992, 1993) located at an epicentral distance of 45 km and an azimuth 226° from the mainshock. Therefore the angle θ for calculating the directivity factor is 124°. Consequently $D=0.68$ assuming $v=0.85\beta$. We used digital acceleration records from the downhole three-component, dual-gain Kinemetrics force balance accelerometer, located 220 m below the surface in a competent rock (shear wave velocity 3.15 km/s), and from a similar surface instrument. Upper 18 m are comprised of recent alluvial deposits forming a lakebed valley (shear wave velocity between 280 and 90 m/s) (Archuleta *et al.*, 1992). The water table is about 1 m (during winter rainy season it reaches the surface). Thus we can test the performance of the algorithms applied to a rock site and a soft soil liquefiable site.

We first show the time-series predictions using the algorithm with a constant stress drop scaling. We rearrange small earthquakes according to their distances 1, 2.9, 5.3, 9.5, 10.1 km from the mainshock's hypocenter (Table 1). Having only 5 subevents and consequently only 5 time-delays will provide a very poor fit to the target source function. Thus we have taken 100 subevents uniformly located at

hypocentral distances 0-12 km, i.e., $\rho_j=j/100$, j=1,...,100. For subevents located at less than 1 km we assume that their waveforms are similar to the small earthquake closest to the mainshock's hypocenter (M_L 4.6 foreshock), subevents positioned between 1 and 2.9 km are assumed to be similar to the second from the origin small earthquake (M_L 3.3 aftershock), etc. The simulated time series are shown in Figure 1 (bottom traces).

Although there is a scatter in the seismic moment scaling for subevents, it is reasonably well described by the value $\delta = 3$. The source spectral falloff γ was assumed to be 2 (Lindley, 1994). At the same time the stress drop of the Joshua Tree main shock was approximately 10 times greater than its aftershocks (Kanamori *et al.*, 1993; Lindley, 1994). By multiplying the main event corner frequency by the directivity factor 0.68 we are already producing a seismic moment that is 0.68^{-3}=3.3 times larger. Therefore to account for the difference between the stress drops of the main event and subevents we need to multiply our predictions from Step 6 of the spectral algorithm by an additional factor of 3 (Step 8). Figure 2 shows comparisons of predicted whole record amplitude spectra (dotted lines) with observations (solid lines).

Using random vibration theory (e.g., Joyner and Boore, 1988) we obtain estimates of the response spectrum from the Fourier amplitude spectrum without using any phase information. The only additional parameter needed for such an estimate is the duration of the record. The shorter the duration used for such an estimate, the higher the predicted response spectrum. The explanation is simple: releasing the same amount of energy (as the amplitude spectrum is preserved) in a shorter time produces higher amplitudes of the signal. Thus the underestimation of the duration in this approach will result in an overestimation of the response spectrum. For the duration we used the value 12 seconds, which corresponds to the average Trifunac-Brady duration (Trifunac and Brady, 1975) of downhole and surface horizontal components of acceleration. For a forward prediction it is possible to use an empirical estimate of the duration T in terms of the earthquake's corner frequency f_0 and epicentral distance r, e.g., $T=1/f_0+0.05r$ (Joyner and Boore, 1988).

Comparisons of observed response spectra (solid lines) with predictions obtained from time-series (dotted lines) and spectral (dashed lines) methods are shown in Figure 3. The overall quality of predictions by the both the time-domain and spectral approaches is very good, although the spectral method tends to slightly overestimate observed spectral ordinates at longer periods.

TABLE 1.
Source parameters of the Joshua Tree earthquake sequence. Listed are the main event and 5 subevents, used in the present study.

Earthquake	Latitude N (degrees minutes)	Longitude W (degrees minutes)	Depth (km)	Distance# (km)	M_L	Seismic moment (dyne-cm)	P-wave corner frequency (Hz)	Stress drop (bars)
4/23 02:25:30	33 57.37	116 19.05	11.5	1.0	4.6	$1.2\ 10^{23}$	1.47	31
4/23 04:50:23	33 57.67	116 19.05	12.38	0.0	6.1	$1.9\ 10^{25}$	0.51	203
4/23 18:56:03	33 59 47	116 17.06	3.49	10.1	4.4	$3.1\ 10^{22}$	1.91	17
4/26 03:07:58	33 59.59	116 19.94	8.73	5.3	3.6	$7.9\ 10^{21}$	3.17	20
5/02 12:46:41	33 59.36	116 17.21	3.97	9.5	4.2	$2.6\ 10^{22}$	2.69	41
5/17 06:21:32	33 57.60	116 18.97	9.44	2.9	3.3	$1.9\ 10^{21}$	4.78	17

Earthquake locations are taken from the Caltech catalog. The seismic moment of the Joshua Tree main shock is taken from (Kanamori *et al.*, 1993). Seismic moments and P-wave corner frequencies of earthquakes were then determined by the spectral ratio method by Lindley (1994). The ratio of P-wave to S-wave corner frequencies is assumed to be $\sqrt{3}$.
Distance is measured between the hypocenters of the main event and the aftershock.

RESULTS

We have developed and validated empirical ground motion prediction algorithms satisfying three critical conditions:

- The prediction is consistent with the entire observed seismic spectrum from the lowest to the highest frequencies.
- Our source models incorporate the basic scaling relations between source parameters and spectral parameters.
- Our methods allow for any subset of the available data, i.e., for any number of recorded empirical Green's functions.

With these conditions met the ground motion prediction is internally self-consistent. It accounts for the complexity of the source while maintaining the basic seismic scaling relations and the complexity of the path/site effects without being dependent on the characteristics of a single empirical Green's function.

Our time-series prediction algorithm is based on determination of a non-uniform distribution of rupture times of subevents (Wennerberg, 1990). By introducing a specific rupture velocity we avoid the major problem of deficiency of predictions in the vicinity of the main event's corner frequency. This problem is an inherent feature of methods based on a uniform distribution of subevents' rupture times (Irikura, 1983; Joyner and Boore, 1986; Boatwright, 1988).

We have proposed a new alternative approach to the problem of simulation of a large earthquake by adding co-located subevents. By introducing a novel notion of a partial coherence we were able to sum subevents' amplitude spectra directly without using any information on their rupture times and phase histories. Predictions by this method are not dependent on details of the rupture nucleation and propagation, location of asperities and other predominantly phase-affecting factors that are responsible for the most uncertainty of the time-domain methods.

PUBLICATIONS

Archuleta, R. J., and A. G. Tumarkin (1994). Empirical prediction of site-specific ground motion spectra. In "*Proceedings of the International Workshop on Strong Motion Data, December 13-17, 1993, Menlo Park*", Vol.2, Port and Harbor Research Institute, Yokosuka, Japan, 301-316.

Tumarkin, A. G., Archuleta, R. J. and R. Madariaga (1994). Scaling relations for composite earthquake models, *Bull. Seismol. Soc. Am.*, **84**, 1279-1283.

Tumarkin, A. G., and R. J. Archuleta (1994). Empirical ground-motion prediction, *Annali di Geofisica (Special Issue"Proceedings of the International School on Earthquake Source Mechanics, September 1-7, Erice, Sicily")*, (in press).

REFERENCES

AKI, K. (1967): Scaling law of seismic spectrum, *J. Geophys. Res.*, **72**, 1217-1231.

AKI, K. and P. G. RICHARDS (1980): *Quantitative Seismology. Theory and Methods. Vol. 1,2* (W. H. Freeman and Company, San Francisco), 932 pp.

AKI, K. and K. IRIKURA (1991): Characterization and mapping of earthquake shaking for seismic zonation, in *Proceedings of the Fourth International Conference on Seismic Zonation, Vol. I*, (EERI, Oakland), pp. 61-110.

ARCHULETA, R. J., SEALE, S. H., SANGAS, P. V., BAKER, L. M. and S. T. SWAIN (1992): Garner Valley downhole array of accelerometers: instrumentation and preliminary data analysis, *Bull. Seismol. Soc. Am.*, **82**, 1592-1621. (Correction, *Bull. Seismol. Soc. Am.*, **83**, 2039, 1993).

BENIOFF, H. (1955): Mechanism and strain characteristics of the White Wolf fault as indicated by the aftershock sequence, in *Earthquakes in California during 1955*, edited by G. B. OAKESHOTT (Calif. Div. Mines, Bull. 171), pp. 199-202.

BEN-MENAHEM, A. (1961): Radiation of seismic surface-waves from finite moving sources, *Bull. Seismol. Soc. Am.*, **51**, 401-435.

BOATWRIGHT, J., and D. M. BOORE (1982): Analysis of the ground accelerations radiated by the 1980 Livermore Valley earthquakes for directivity and dynamic source characteristics, *Bull. Seismol. Soc. Am.*, **72**, 1843-1865.

BOATWRIGHT, J. (1988): The seismic radiation from composite models of faulting, *Bull. Seismol. Soc. Am.*, **78**, 489-508.

BOORE, D. M., and W. B. JOYNER (1978): The influence of rupture incoherence on seismic directivity, *Bull. Seismol. Soc. Am.*, **68**, 283-300.

BRUNE, J. (1970): Tectonic stress and the spectra of seismic shear waves from earthquakes, *J. Geophys. Res.*, **75**, 4997-5009. (Correction, *J. Geophys. Res.*, **76**, 5002, 1971)

CHAEL, E. P. and R. P. KROMER (1988): Teleseismic time functions for large shallow subduction zone earthquakes, *Bull. Seismol. Soc. Am.*, **78**, 561-570.

DAN, K., WATANABE, T., TANAKA, K. and R. SATO (1990): Stability of earthquake ground motion synthesized by using different small-event records as empirical Green's functions, *Bull. Seismol. Soc. Am.*, **80**, 1433-1455.

DOUGLAS, A., HUDSON, J. A., and R. G. PEARCE (1988): Directivity and the Doppler effect, *Bull. Seismol. Soc. Am.*, **78**, 1367-1372.

FLETCHER, J. B. and J. BOATWRIGHT, Source parameters of Loma Prieta aftershocks and wave propagation characteristics along the San Francisco Peninsula from a joint inversion of digital seismograms, *Bull. Seismol. Soc. Am.*, **81**, 1783-1812.

FRANKEL, A. (1991): High-frequency spectral falloff of earthquakes, fractal dimension of complex rupture, *b* value, and the scaling of strength on faults, *J. Geophys. Res.*, **96**, 6291-6302.

HARTZELL, S. H. (1978): Earthquake aftershocks as Green's functions, *Geophys. Res. Lett.*, **5**, 1-4.

HEATON, T. H. and S. H. HARTZELL (1989): Estimation of strong ground motions from hypothetical earthquakes on the Cascadia subduction zone, Pacific Northwest, *PAGEOPH*, **129**, 131-201.

HUTCHINGS, L. (1994): Kinematic earthquake models and synthesized ground motion using empirical Green's functions, *Bull. Seismol. Soc. Am.*, **84**, 1028-1050.

IRIKURA, K. (1983): Semi-empirical estimation of strong ground motions during large earthquakes, *Bull. Disast. Prev. Res. Inst., Kyoto Univ.*, **33**, 63-104.

JOYNER, W. B., and D. M. BOORE (1986): On simulating large earthquakes by Green's-function addition of smaller earthquakes, in *Earthquake Source Mechanics*,

edited by S. DAS, J. BOATWRIGHT and C. H. SCHOLZ (A.G.U., Geoph. monogr. 37, M. Ewing Vol. 6), pp. 269-274.

JOYNER, W. B., and D. M. BOORE (1988): Measurement, characterization, and prediction of strong ground motion, in *Earthquake Engineering and Soil Dynamics II- Recent Advances in Ground-Motion Evaluation*, edited by J. L. VON THUN (A.S.C.E., N.Y.), pp. 43-102.

JOYNER, W. B. (1991): Directivity for nonuniform ruptures, *Bull. Seismol. Soc. Am.*, **81**, 1391-1395.

KANAMORI, H. and D. L. ANDERSON (1975): Theoretical basis of some empirical relations in seismology, *Bull. Seismol. Soc. Am.*, **65**, 1073-1096.

KANAMORI, H., MORI, J., HAUKSSON, E., HEATON, T. H., HUTTON, L. H. and L. M. JONES (1993): Determination of earthquake energy release and M_L using TERRAscope, *Bull. Seismol. Soc. Am.*, **83**, 330-346.

KOSTROV, B. V. (1964): Self-similar problems of propagation of shear cracks, *J. Appl. Math. Mech. (PMM)*, **28**, 1077-1087.

LINDLEY, G. T. (1994): Source parameters of the 23 April 1992 Joshua Tree, California, earthquake, its largest foreshock, and aftershocks, *Bull. Seismol. Soc. Am.*, **84**, 1051-1057.

LINDLEY, G. T. and R. J. ARCHULETA (1992): Earthquake source parameters and the frequency dependence of attenuation at Coalinga, Mammoth Lakes and the Santa Cruz Mountains, California, *J. Geophys. Res.*, **97**, 14,137-14,154.

MADARIAGA, R. (1976): Dynamics of an expanding circular fault, *Bull. Seismol. Soc. Am.*, **66**, 636-666.

MADARIAGA, R. (1983): High frequency radiation from dynamic earthquake fault models, *Ann. Geophys.*, **1**, 17-23.

PAPAGEORGIOU, A. and K. AKI (1983): A specific barrier model for the quantitative description of inhomogeneous faulting and the prediction of strong ground motion. Part I. Description of the model, *Bull. Seismol. Soc. Am.*, **73**, 693-722.

RANDALL, M. J. (1973): The spectral theory of seismic sources, *Bull. Seismol. Soc. Am.*, **63**, 1133-1144.

SOMMERVILLE, P. G. (1993): Engineering applications of strong ground motion simulation, *Tectonophysics*, **218**, 195-219.

TRIFUNAC, M. D. and A. G. BRADY (1975): A study of the duration of strong earthquake ground motions, *Bull. Seismol. Soc. Am.*, **65**, 581-626.

TUMARKIN, A. G., ARCHULETA, R. J. and R. MADARIAGA (1994): Scaling relations for composite earthquake models, *Bull. Seismol. Soc. Am.*, **84**, 1279-1283.

WENNERBERG, L. (1990): Stochastic summation of empirical Green's functions, *Bull. Seismol. Soc. Am.*, **80**, 1418-1432.

WU, F. (1978): Prediction of strong ground motion using small earthquakes, in *Proceedings of the 2nd International Conference on Microzonation, Vol. II* (San Francisco), pp. 701-704.

ZENG, Y., ANDERSON, J. G., and G. YU (1994): A composite source model for computing realistic synthetic strong ground motions, *Geophys. Res. Lett.*, **21**, 725-728.

GVDA 220 m Downhole EW
Acceleration [cm/s/s]
observation.DOWNHOLE EW
prediction.DOWNHOLE EW
Time [s]
GVDA 220 m Downhole NS
Acceleration [cm/s/s]
observation.DOWNHOLE NS
prediction.DOWNHOLE NS
Time [s]
GVDA Surface EW
Acceleration [cm/s/s] X 10+2
observation.SURFACE EW
prediction.SURFACE EW
Time [s]
GVDA Surface NS
Acceleration [cm/s/s] X 10+2
observation.SURFACE NS
prediction.SURFACE NS
Time [s]

Figure 1

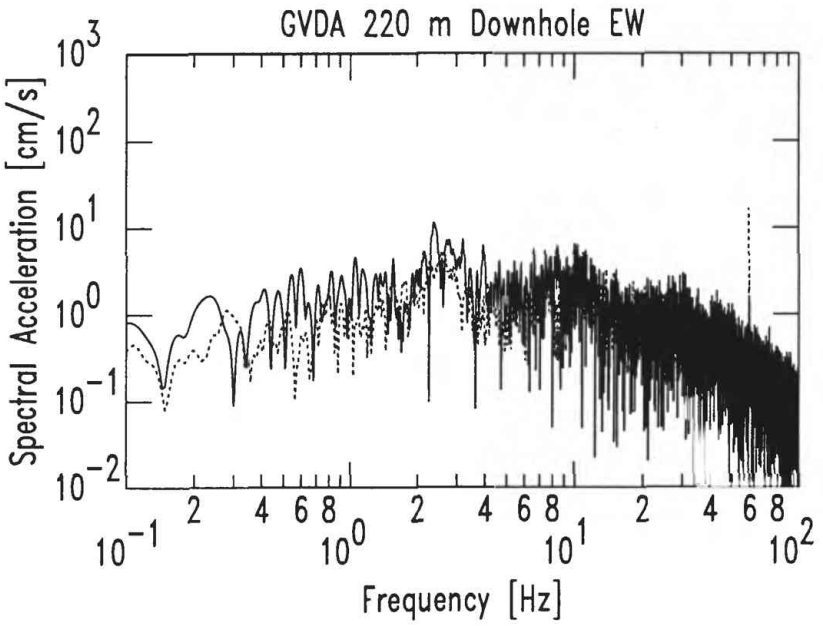
GVDA 220 m Downhole EW
Spectral Acceleration [cm/s]
Frequency [Hz]

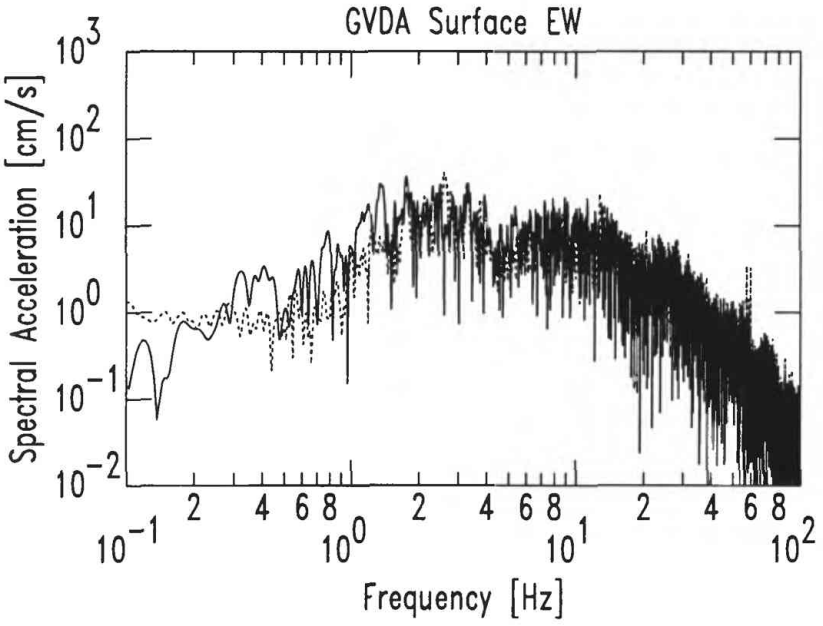
GVDA Surface EW
Spectral Acceleration [cm/s]
Frequency [Hz]

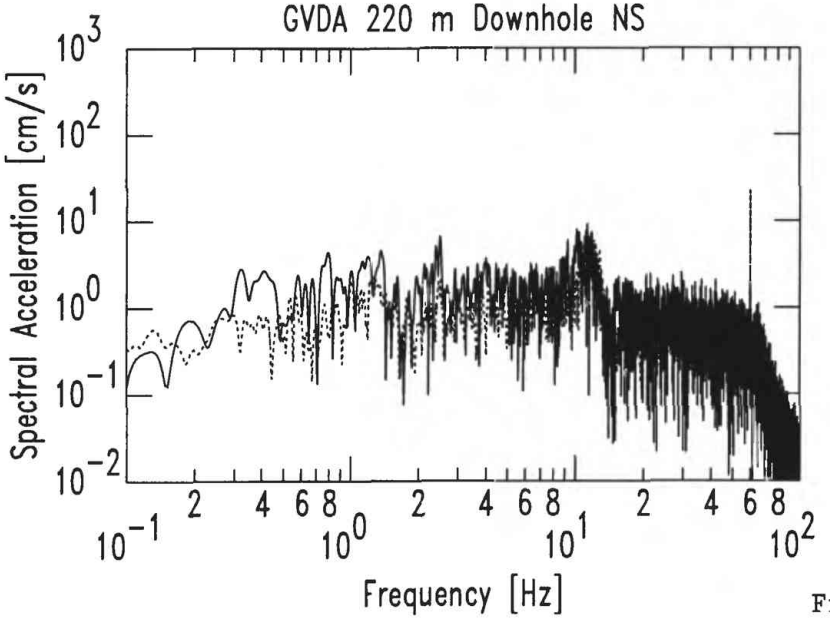
GVDA 220 m Downhole NS
Spectral Acceleration [cm/s]
Frequency [Hz]

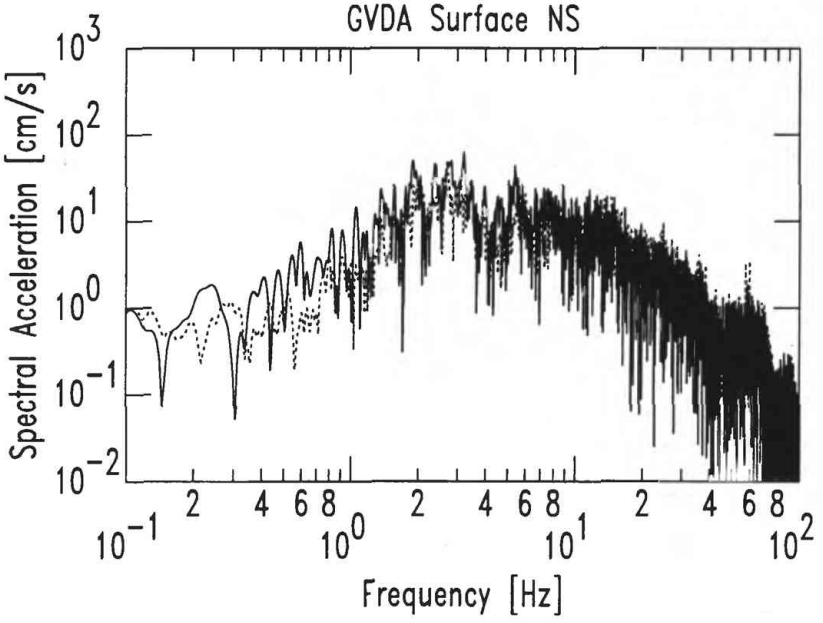
GVDA Surface NS
Spectral Acceleration [cm/s]
Frequency [Hz]

Figure 2

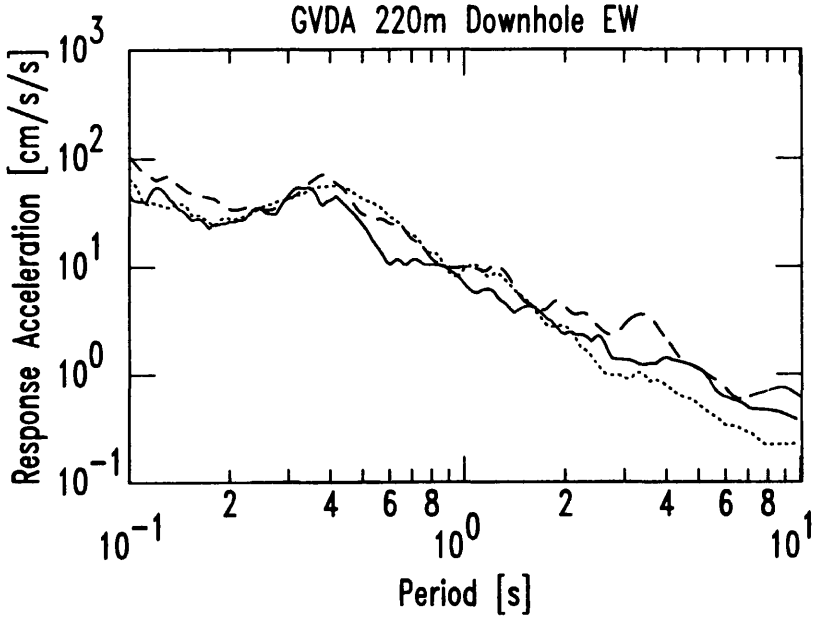
GVDA 220m Downhole EW
Response Acceleration [cm/s/s]
Period [s]

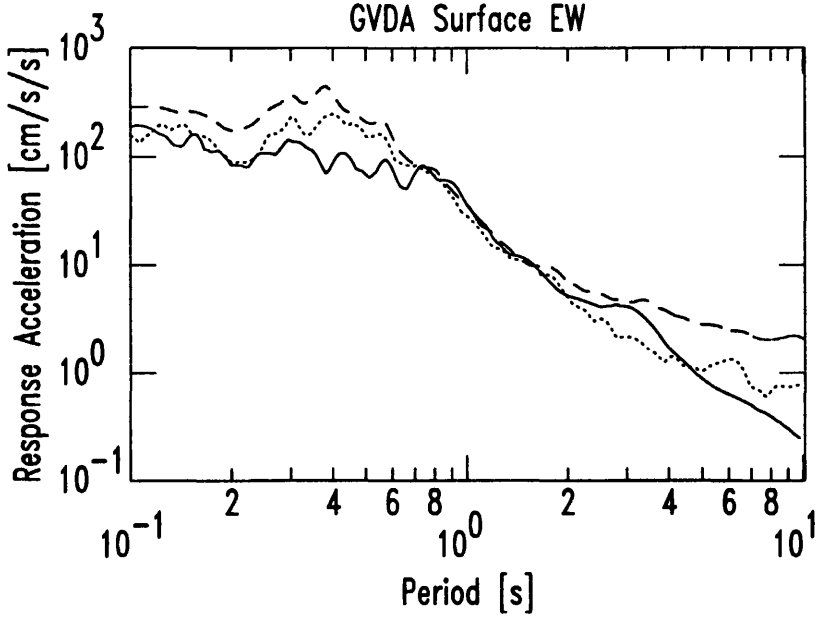
GVDA Surface EW
Response Acceleration [cm/s/s]
Period [s]

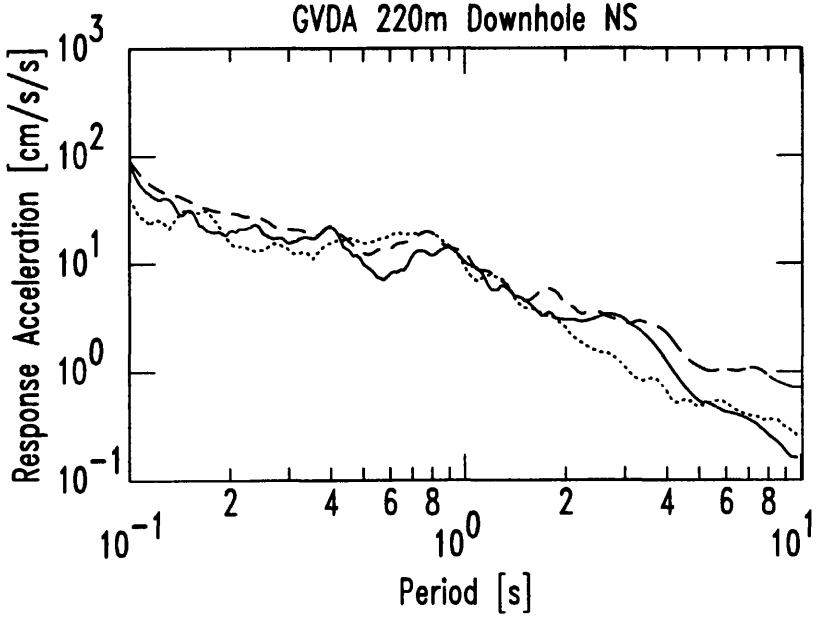
GVDA 220m Downhole NS
Response Acceleration [cm/s/s]
Period [s]

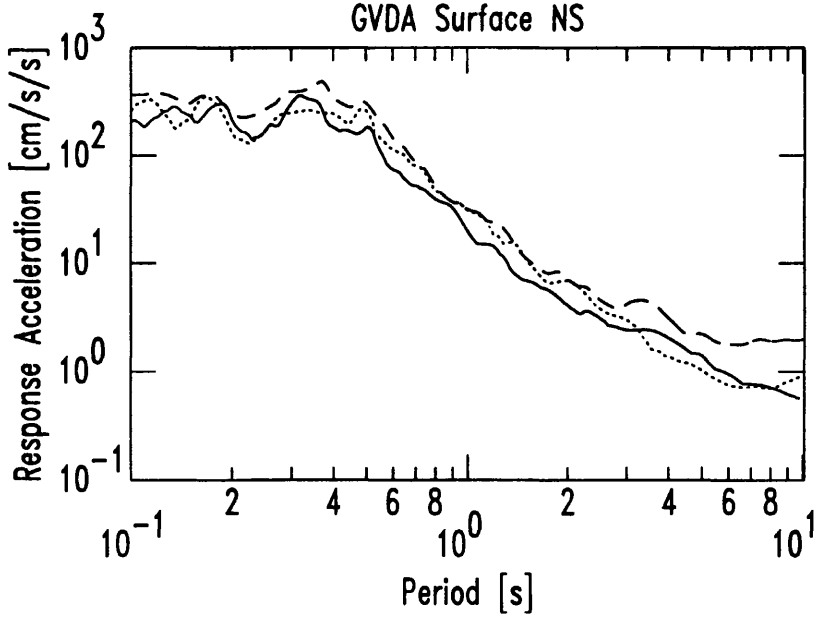
GVDA Surface NS
Response Acceleration [cm/s/s]
Period [s]

Figure 3

Title: Model Land Use and Development Regulations for Mitigating Seismic Risks in the Portland Metropolitan Area

Award Number: 1434-94-G-2448

Investigators: O. Gerald Uba, Ph.D., Metro
George Mader, AICP, President, Spangle Associates

Institution: Metro

Address: 600 NE Grand Avenue
Portland, OR 97232

Telephone: (503) 797-1737
Fax: (503) 797-1794

Recent earthquake studies reveal that the Portland metropolitan area is in an active seismic zone and very vulnerable to earthquakes. In 1993, Oregon had more significant earthquakes than any state in the nation, and the only earthquake related death. In the same year, the Oregon Department of Geology and Mineral Industries prepared a series of earthquake hazards maps which show the distribution of liquefaction, landslide, and ground motion amplification hazards in the Portland area. The availability of the information raised question of how the maps can be used to mitigate the impact of major earthquakes in the metropolitan region. Land use planning and building regulation were considered as key tools that could be developed with the earthquake hazard maps. The focus of this study is on land use regulations.

Metro (a regional planning agency in the Portland metropolitan area) and Spangle Associates (a land use consulting firm based in California) teamed up to figure out how the hazard maps could be used in local land use planning.

There are three phases of this project. In the phase 1, the interdisciplinary team of land use planners, structural and geo-technical specialists who have studied the earthquake hazard maps from their perspectives recommended correlations between land uses, earthquake performance objectives, and acceptable risks. These correlations helped in establishing a reasonable procedure for justifying why and how earthquake hazard maps should be included in the range of multiple factors considered by land use planners in the distribution of land uses. The fundamental concept that guided the team is as follows:

seismic hazard + land use = risk

In order words, the risk of loss or damage from an earthquake depends on the presence of hazardous land (i.e., land subject to failure or strong effects from an earthquake) and land use (land plus its infrastructure, buildings, building content and function). Risk may be reduced by avoiding or modifying the land in hazardous areas or by constructing buildings and facilities to withstand the effects of earthquakes.

The first step in the correlation exercise was to use the conventional method of classifying land uses into common uses to develop a classification that is based on common tolerance for risk. Under such classification, the following grouping of land uses according to vulnerability to earthquake damage was developed:

Land Uses with Potentially Catastrophic Consequences of Damaged
Land Uses with High Occupancy and Involuntary or Dependent Occupants
Land Uses with Essential for Emergency Response
Land Uses Critical to Functional of the Metro Region
Land Uses with High Occupancy
Land Uses with Important Local Impacts if Damaged
Land Uses with Moderate Occupancy
Land Uses with Low Occupancy

Typical land uses under each category was developed as shown in Table 1. These land uses can be refined to fit the goal of a local community.

The second step in the correlation exercise was to establish earthquake performance objectives for buildings and facilities (or acceptable levels of damage from an earthquake) for each category of land use. The result is in Table 2. Products of the above two steps will help local communities to develop comprehensive plan policies that addresses the questions of life-safety and extent of damage acceptable in their areas.

Finally, the third step in the correlation process was to look at location as a key variable in earthquake vulnerability (or in reaching earthquake performance objectives and acceptable level of risk). In this process, a rating of acceptable (Y), probably acceptable (Y*), probably not acceptable (N*) and not acceptable (N) was used to correlate each category of land use with the four hazard zones (greatest hazard to least hazard) shown in the earthquake hazard maps.

The first product of this project is the draft Phase 1 Report: ***"Using Earthquake Hazard Maps For Land Use Planning"*** that is being reviewed by the Metro's Advisory Committee for Mitigating Earthquake Damage. The committee is composed of land use planners, building engineers, geologist, lawyer, emergency planner, and insurance and developer's representatives.

The functional areas identified in the phase 1 report that the maps are useful include urban growth boundary, comprehensive plans, zoning regulations, infrastructure plans, subdivision regulations, grading regulations, parks and greenspace plans, public and private facility locations, building standards, retrofit programs, redevelopment planning and emergency management.

In the second phase of the study, the correlations from the first phase will be translated into model regulations that local governments can adopt to their local needs. Major features of these regulations will include provisions and guidelines for actions such as adoption of hazard maps as accepted maps of earthquake hazards for a local government, adoption of earthquake performance objectives and acceptable risks levels and matrices correlating land uses to hazard zones, refinement of hazard maps by property owners as required by a local community, and funding local government review of geologic and geotechnical reports through applicant fees.

In the third phase of the study, other key variables in earthquake vulnerability, such as structural design and construction will be used to develop specific recommendations related to the earthquake hazard information.

Table 1. LAND USES GROUPED BY SEISMIC RISK

Land Uses with Potentially Catastrophic Consequences if Damaged
Dams impounding large amounts of water
Nuclear power plants
Facilities using or storing large quantities of hazardous materials (defined by Oregon State law)

High-Occupancy Land Uses with Involuntary or Dependent Occupants
Day care centers
Public and private schools K-12
Convalescent homes
Jails and retention facilities

Land Uses Critical to the Functioning of the Metro Region
Power plants, power intertie, sewage treatment plants, water plants
Regional highways, bridges, rail lines, overpasses, tunnels, airports, port facilities
Major communications facilities, telephone exchanges, radio and TV stations
Major industries and employers

High-Occupancy Land Uses
Apartments with 25 or more units
Buildings with more than 150 employees
Buildings with more than 10 stories
Public and private colleges and universities
Public assembly places with capacity of 300 or more
Hotels and motels with more than 50 rooms

Land Uses with Important Local Impacts if Damaged
Facilities using, storing, transporting small quantities of hazardous materials
Small dams whose failure would expose downstream population to flooding
Gas stations
Health care clinics
Local highways, streets, and bridges
Local utility lines and substations, gas and water mains, communication lines
Industries and business important to the local economy

Moderate-Occupancy Land Uses
Apartments with 9 to 25 units
Buildings with 50-150 employees
Buildings with 4 to 10 stories
Public assembly places with capacity between 50-300
Hotels and motels with fewer than 50 rooms

Low-Occupancy Land Uses
Apartments with 2 to 8 units
Buildings with fewer than 50 employees
Buildings with 1 to 3 stories
Single-family houses
Mobile homes

Table 2. EARTHQUAKE PERFORMANCE OBJECTIVES AND ACCEPTABLE RISK

Categories of Land Uses	Earthquake Performance Objectives*	Acceptable Risk
Potential Catastrophe if Damaged	Fully Functional	near zero
High Occupancy with Involuntary or Dependent Occupants	Immediate Occupancy	very low
Essential for Emergency Response	Immediate Occupancy	very low
Critical to the Functioning of the Region	Immediate Occupancy	very low
High-Occupancy	Damage Control	low
Important Local Impacts if Damaged	Damage Control	low
Moderate-Occupancy	Substantial Life-Safety	low
Low-Occupancy	Substantial Life-Safety	moderate

Table 3. LAND USES ACCEPTABLE IN HAZARD ZONES SHOWN ON THE REHM

Land Uses	*A-Red*	*B-Orange*	*C-Yellow*	*D-White*
Potential Catastrophe if Damaged	N	N*	N*	Y*
High Occupancy with Involuntary and Dependent	N	N*	Y	Y
Essential for Emergency Response	N*	N*	Y*	Y
Critical to the Functioning of the Metro Region	N*	N*	Y*	Y
High Occupancy	N*	Y*	Y*	Y
Important Local Impacts if Damaged	N*	Y*	Y*	Y
Moderate Occupancy	N*	Y*	Y*	Y
Low Occupancy	N*	Y*	Y	Y

Data Processing Section

9920-10142

Robert L. Woodward
Branch of Earthquake and Geomagnetic Information
U. S. Geological Survey
Building 10002, Kirtland AFB-East
Albuquerque, New Mexico 87115-5000
phone: (505)846-5646, FAX: (505)846-6973, E-mail: woodward@asl.cr.usgs.gov

Investigations

1. Data Collection. The Incorporated Research Institutions for Seismology (IRIS) have designated the Albuquerque Seismological Laboratory (ASL) to be a Data Collection Center (DCC) for a global network of digitally recording seismograph systems (the Global Seismograph Network or GSN). Some 76 seismograph stations around the world send data (typically via magnetic computer tape) directly to the ASL for processing.

2. Data Processing. All of the data received from stations of the GSN and other contributing networks is read, reviewed, checked for quality, and archived at the ASL.

3. Data Distribution. After the data collection and quality review, all of the data are assembled into network volumes which are distributed to regional data centers and other government agencies.

Results

1. Data Collection. IRIS has an ongoing program to deploy over 100 seismograph stations around the world. The USGS has been assigned the task of installing and maintaining many of these stations and processing the digital data they produce. At present, the ASL maintains and receives data from roughly 41 IRIS stations. The ASL will install roughly 10 to 20 new stations per year, for at least the next two years. In addition to the 41 IRIS stations, the ASL DCC receives data from 8 stations of the Global Telemetered Seismograph Network, 10 stations of the China Digital Seismograph Network, and 17 stations from the TERRAscope network in Southern California. Thus the total number of stations for which the ASL has direct responsibility includes some 76 stations. At present, each of the IRIS stations produces roughly 5 to 8 megabytes of compressed seismic data per day. In addition to the 76 stations for which the ASL has primary responsibility, data is received from 22 stations of the IRIS/IDA network (supported by the University of California, San Diego). The IRIS/IDA data arrives pre-processed by the IRIS/IDA DCC, so this data is ready to be archived, with little intervention by the ASL DCC.

2. Data Processing. The current data flow into the DCC amounts to a daily total of approximately 600 to 700 megabytes. This data is reviewed for quality, which primarily consists of checking for timing and hardware problems. When problems are detected, the appropriate ASL Field Engineers or station personnel are notified, so that the problem may be rectified. After quality control, the data are reformatted into a uniform format and are stored on optical disks. In addition to our own quality control program, the DCC also responds to any data problems reported by seismologists who are using the data.

3. Data Distribution. For data distribution, the ASL DCC acts much like a data wholesaler, by delivering data to regional data centers. The regional centers act much like data retailers, by distributing data to individual seismologists. The primary means of delivering data to the regional data centers is via SEED (Standard for the Exchange of Earthquake Data) format network volumes. The network volume program is a continuing program which assembles all of the data recorded by all of the above listed networks for a specific calendar day (or days) onto one magnetic tape. This tape includes all of the auxiliary information (station parameters, calibration data, transfer functions, time corrections) for each station on the tape. All of the data on these network volumes are written in SEED format (a standard format developed by the USGS in cooperation with other organizations) and copies are distributed to several university and government research groups for detailed analysis and further distribution. These network volume tapes are assembled approximately 60 days after real time in order to provide sufficient time for the data to be recorded at the station, mailed to the ASL, and processed at the DCC.

In addition to the network volumes, special data volumes are created several times per week which contain all recently arrived data. These special volumes are sent to the IRIS Data Management Center (DMC) where the data is freely accessible to scientists all over the world with the minimum possible delay.

The ASL DCC is also involved in two special data distribution projects. In the first project, data collected by the ASL in the time period 1980-1987 are being reformatted and re-released in the modern SEED format. Republishing this data in a modern format will facilitate the use of this data by many seismologists. In the second project, the ASL is cooperating with the USGS National Earthquake Information Center, the IRIS DMC, and the Federation of Digital Seismograph Networks, to publish on CD-ROM the data from the most important earthquakes throughout the world. Publication on CD-ROM will make this data even more accessible to the international seismological community.

Earthquake Hazard Studies, Metropolitan Los Angeles-Western Transverse Ranges

R. F. Yerkes
5-9540-70050
Branch of Western Regional Geology
345 Middlefield Road, MS 975
Menlo Park CA 94025
415-329 4946; FAX 415-329 4936

R. H. Campbell
Office of Earthquakes Volcanoes and Engineering
922 National Center
Reston, VA 22092
703-648 6784; FAX 703-648 6908

INVESTIGATIONS AND RESULTS

Completed and released in open files full-color digital geologic map of Topanga 1;24,000 quadrangle, one of 16 in preparation for the west half of the Los Angeles 1;100,000 quadrangle geologic map; completed and field-checked Fillmore, Piru, Point Dume, Triunfo Pass, and Val Verde 1:24,000 quadrangles. Prepared preliminary full-color digital version of the 1;100,000 map, which was exhibited at the 1994 Cordilleran Section GSA and Pacific Section AAPG meetings. Outside requests for release of this and 1;24,000 quadrangles in digital format being received. Continuing compilation and revision of 1;24,000 quadrangles after field checking; continuing preparation of 1:100,000 map for release. Compiling additional quadrangles that include Quaternary geology of San Fernando Valley (site of 1994 Northridge earthquake): Van Nuys essentially completed, San Fernando well started.

REPORTS

Yerkes, R. F., and Campbell, R. H., 1994, preliminary geologic map of the Topanga 7.5' quadrangle, southern California: U. S. Geological Survey Open File Report 94-266.

Urban Seismic Hazard Mapping Using Spatial Database Management Tools

DR. EARL J. BELL

A Report on the activities of the University of Washington, Cascadia Center for Interdisciplinary Studies, Center for Sustainable Settlements[1] funded by USGS Award 1434-94-G-2408

October 24, 1994

Introduction

This project, begun in January, 1994, is investigating the potential for using Geographic Information Systems (GIS) to identify and regulate hazardous areas. The goal of the project is to develop methods to identify seismically-hazardous areas and to investigate ways this information may be used within the land use planning process toward effective hazard mitigation.

The effectiveness of this approach depends critically upon the ability of planners and decision-makers to make sense of spatial hazards data, and to relate this data to a dynamic, ever-changing local planning process. We believe that the best way to convey this information to these parties is through the use of spatial database management tools -- essentially, desktop versions of existing high-end GIS products, such as ESRI's ArcView.

Such desktop GIS capability will undoubtedly reform the planning process. Our goal is to present an example wherein the use of GIS is transformed from its contemporary use in planning -- that of a graphics tool, after the fact -- to a more fundamental decision support system that can be used "up front" in the planning process. To this end, our project is critically dependent on the availability of these tools, and the expertise to use them, within the seismic hazard community.

Accomplishments to Date

During the period January 1, 1994 to October 24, 1994, we have accomplished the following tasks toward fulfilling our obligations to the United States Department of Interior, Geological Survey:

1. We have identified and collected geographic, seismic, lifeline, housing and population data for the City of Seattle. This information has been converted to ARC/INFO format and resides on the Cascadia Institute's SUN Workstation. The attached "Data Dictionary" lists and sources this data.

---

[1] Earl J. Bell, Ph.D., Principal Investigator.

2. We performed preliminary tests combining the collected data using vector-based spatial overlay techniques. Reviewing this analysis, we concluded that large portions of our study area were not being determined 'hazardous' at all. We revised our approach, and compiled a preliminary relative hazard determination for the City of Seattle using raster-based methods.

3. The results of our data collection and raster analysis were presented to an advisory committee composed of local planners, seismologists, and emergency management personnel at the Federal, State, and local levels on April 27, 1994. The committee suggested areas of improvement to the application, and have been supportive throughout the process. A second committee meeting is tentatively planned for December 1, 1994.

4. An internal draft report describing the project has been completed and under revision.

Areas where progress has been stalled

The following issues have forestalled us in the completion of the project to date:

1. Because of the dependency of our project on the availability of spatial database management tools described above, we have been unable to make substantial process on the completion of the final "view" that will be distributed to end users at the conclusion of the project. We received ArcView 2 from ESRI in mid-October, 1994. We had anticipated receiving this software package sometime in the spring, but release dates were repeatedly delayed. As a result, we are just now grappling with the difficulties of learning new software and applying it to existing data.

2. We have undergone one staff change. A critical graduate research assistant graduated in August. He was replaced by a new research assistant in October. We have experienced a slight delay in bringing new staff to the task, and anticipate the necessity to replace another assistant in December.

This project has contributed substantially to many external gains for some of the student researchers involved, including summer employment with the Federal Emergency Management Agency, and a nearly-complete Master's Thesis on seismic hazard mitigation in the land use planning process.

Data Dictionary for USGS Project on Earthquake Hazard Mapping

Coverage Name	Coverage Type	Description	Data Source
blockgroup	polygon	census blockgroups with demographic information	Washington Redistricting File (WRF)
city	vector	cities within King County (KC)	KC
county	vector	KC boundary	WRF
hydro	vector & polygon	streams, lakes, and Puget Sound	WRF
kerosion	polygon	KC erosion hazard areas from Comprehensive Plan	KC
kflood	polygon	KC flood hazard areas from Comprehensive Plan	KC
kparks	polygon	KC parks from Comprehensive Plan	KC
kseismic	polygon	KC seismic hazard areas from Comprehensive Plan	KC
kslide	polygon	KC landslide hazard areas from Comprehensive Plan	KC
llnz	text	converts latitude and longitude to north zone projection	Jeff Henderson (JH)
llutm	text	converss latitude and longitude to UTMS	JH
log	text	Arc/Info record of your commands	
medhugr		median year housing built grid (median year housing built from the census blockgroup coverage was isolated and gridded)	WRF, JH and John Davies (JD) additions
mmi49gr	grid	point coverage of the MMI survey in 1949 converted to 325' by 325' grid cells	UW Geophysics, JH
mmi65gr	grid	point coverage of the MMI survey in 1965 converted to 325' by 325' grid cells	UW Geophysics, JH
outgrid	grid	result of hazard "index" calculation	JH, JD
outpoly	polygon	outgrid in polygon format	JH, JD
pls	vector?	Public Land Survey: KC township and range sections	WRF
rails	vector	major rail lines	WRF
readme.grids	text	description of grids	JH, JD
rechyr	grid	reclassified housing year grid (pre-1946 = 10, 1946-1953 = 6, 1953-1964 = 3, post-1964 = 0)	JH
remap2.rm	text	remap file for housing ranges above	JH
roads1	vector	major highways and freeways (no addresses)	WRF
roads2	vector	arterials and minor roads (no addresses)	WRF
s49m71	point	MMI readings for 1949 earthquake of magnitude 7.1 on Richter scale	UW Geophysics
s49mmi.csv	ASCII	comma delimited ASCII files containing a unique number and MMI for 1949 earthquake	UW Geophysics
s65m65	point	MMI readings for 1965 earthquake of magnitude 6.5 on Richter scale	UW Geophysics
s65mmi.csv	ASCII	comma delimited ASCII files containing a unique number and MMI for 1965 earthquake	UW Geophysics
seabg	polygon	census blockgroup coverage clipped for Seattle	WRF, JH,RK
seattle	vector	city reselected for seattle	WRF, JH
sliqgrid	grid	Seattle liquefaction grid (1 = liquefaction, 0 = no liquefaction)	City of Seattle
sliqzones	polygon	polygon version of sliqgrid	City of Seattle, JH
sparks	polygon	Seattle parks	City of Seattle

Coverage Name	Coverage Type	Description	Data Source
blockgroup	polygon	census blockgroups with demographic information	Washington Redistricting File (WRF)
sslgr	grid	Seattle landslide grid (9 = landslide, 0 = no landslide)	City of Seattle
sslide	polygon	sslgr converted to polygon coverage	City of Seattle, JH
ssteep_b	polygon	Seattle steep slopes south (below) of Ship Canal	City of Seattle
ssteep_t	polygon	Seattle steep slopes north (top) of Ship Canal	City of Seattle
sznz.prg	text	projection file: Washington (WA) plane south zone feet to WA plane north zone feet	JH
tract	polygon	census tract geography with attributes	WRF
utmnz.prj	text	conversion from UTM to WA north zone projection	JH
village	vector	Seattle urban village boundaries	City of Seattle

Probabilistic Earthquake Assessment
9920-80832

Charles G. Bufe, Stuart P. Nishenko, James W. Dewey
Branch of Earthquake and Geomagnetic Information
U. S. Geological Survey
Box 25046, MS 967
Denver Federal Center
Denver, CO 80225
(303) 273-8413
FAX (303) 273-8450
cbufe@gldfs.cr.usgs.gov
OP 91010

Investigations

1. Definition of the seismic cycle

Stuart Nishenko and Chuck Bufe are developing a universal or generic model of the seismic cycle, based on earthquake data from Alaska, paleoseismic data from California and Utah, and M≥7 data from other plate boundaries that are either more active than those in the United States or have longer historic records. Analysis of multiple cycles from these regions can not only shed light on the distribution of seismicity within a single cycle, but also on the variability of moment release from cycle to cycle (e.g., how repeatable are "characteristic" earthquakes?). Stuart Nishenko was a 1994 G.K. Gilbert Fellow with C. Barton (USGS, Denver), conducting research on scaling laws for natural disasters and the application of fractal statistics to life and economic loss data. Nishenko is also working with J. P. McCalpin, GEO-HAZ Consulting, Estes Park, CO, to improve previously published forecast models for large earthquakes along the Wasatch Fault Zone in Utah.

2. Application of nonlinear dynamics to earthquake recurrence

In application of previous G.K. Gilbert Fellowship research (with Dave Varnes, USGS, Golden), Chuck Bufe will examine implications of chaos theory and nonlinear dynamics for earthquake recurrence models. Nearly periodic recurrence patterns (e.g., Parkfield) of characteristic earthquakes, and the ephemeral regularities of regional or global large earthquake occurrence, may be manifestations of deterministic chaos. Implications regarding the predictability of earthquake recurrence patterns in a chaotic or near-chaotic recursive system will be assessed, as will earthquake triggering and periodicity or log-periodicity in earthquake sequences.

3. Test of M8 algorithm

Jim Dewey continued his participation with J. Healy and V. Kossobokov in the forward test of algorithm M8. This implementation of M8 is directed to the prediction of earthquakes of magnitude 7.5 or greater. M8 is being applied to 147 circles of investigation located in the circum-Pacific belt and Indonesia. Each circle has a radius of 427 km. The algorithm identifies Times of Increased Probability (TIPS) within which there is hypothesized to be an increased probability for the occurrence of shocks of magnitude 7.5 or larger. M8 is evaluated against the null hypothesis that TIP's randomly distributed in the 147 circles of investigation are as effective as M8. The test will run through 1997.

4. Intermediate-term forecasts for Alaska-Aleutian region

Chuck Bufe, Stu Nishenko, and Dave Varnes continued to work on the long- and intermediate-term forecasts for large and great earthquakes along selected segments of the Alaska-Aleutian seismic zone.

Results

1. Definition of the seismic cycle

At the 1994 SUBCON meeting, Nishenko (Nishenko and Bufe, 1994) presented a composite of normalized time and magnitude data for intra-cycle seismicity on individual segments of circum-Pacific plate boundaries and also examples of periodic clustering on the plate boundary scale for central and southern Chile [from 1500 to 1990] and in the SW Pacific [from 1900 to 1990].

2. Application of nonlinear dynamics to earthquake recurrence

David Varnes and Chuck Bufe have completed analysis of interevent time data for a cyclic and fractal foreshock sequence in the Virgin Islands (Varnes and Bufe, 1994). Clusters within the sequence (see Table 1) occur at nearly log-periodic intervals which become shorter as the time of the main shock approaches. These intervals are multiples of a period near the fortnightly tidal period. However, comparison with computed and observed ocean tidal data indicates that the inherent fractal periodicities observed in the earthquake sequence cannot be explained entirely by tidal triggering. The episodic, accelerating sequence and mainshock are well described by the nonlinear time- and slip-predictable model for foreshocks of Bufe, Varnes, and Nishenko (1994). Bufe also continued to perfect software to determine temporal and spatial fractal dimensions, interevent-time spectra, and interevent-time ratio spectra for earthquake sequences.

TABLE 1. Lengths of the intervals between larger, clustered earthquakes in the Virgin Islands foreshock sequence. The average of ratios of successive intervals is close to 3/4. Times of events are in days from January 1, 1979, 00 hr, 00 min. t_f-t is the remaining time to failure (i.e., time to main shock). m_b is body-wave magnitude.

Event number	m_b	Time (days)	Interval number	Interval length	Ratio I_{i+1}/I_i	t_f - t
7=t_1	2.5	131.41				278.31
			I_1	97.27		
14=t_2	3.1	228.68			0.8566	181.04
			I_2	83.32		
23=t_3	3.3	312.00			0.6779	97.72
			I_3	56.48		
30=t_4	3.0	368.48			0.7302	41.24
			I_4	41.24		
37=t_5	4.8	409.72				00.00

				Average	0.7549	

3. Test of M8 algorithm

Jim Dewey continued his participation with J. Healy and V. Kossobokov in the forward test of algorithm M8, evaluating results against the null hypothesis that TIP's randomly distributed in the 147 circles of investigation are as effective as M8.

4. Intermediate-term forecasts for Alaska-Aleutian region

Analysis of seismicity patterns in the Alaska-Aleutian seismic zone (Bufe, Nishenko, and Varnes, 1994) has indicated zones characterized by cycles of accelerating seismic release and others by cycles of decelerating seismic release. In the latter zones, large earthquakes are often preceded by quiescence. Zones of acceleration include the Shumagin, Alaska Peninsula, Delarof, and Kommandorski segments. Extrapolation of these trends using time-to-failure analysis indicates probable rupture of one or more of the zones within a 3-yr period (1994-1996). The M_S 6.9 Shumagin and M_S 6.7

Delarof Islands earthquakes of 13 and 15 May, 1993, continued the previously observed patterns of accelerating seismic release in two of these zones. The projected failure windows for the zones are indicated in Table 2.

TABLE 2. Estimated times of failure for segments with accelerating seismic release in the Alaska-Aleutian seismic zone. Dates are inclusive.

Segment	Estimated t_f	Estimated M_W
Kommandorski Islands	1995-2003	7.5-8.5
Delarof Islands	1994-1996	7.3-7.7
Shumagin Islands	1994-1996	7.3-7.7
Alaska Peninsula	1994-1996	7.3-8.7
Shumagin+Alaska Peninsula	1994-1996	7.5-8.2

Reports

Bufe, C. G., Varnes, D. J., and Nishenko, S. P, 1993, A nonlinear time- and slip-predictable model for foreshocks [abs.]: EOS (American Geophysical Union, Transactions), v. 74, p. 437.

Bufe, C. G., Nishenko, S. P., and Varnes, D. J., 1994, Seismicity trends and the potential for large earthquakes in the Alaska-Aleutian region: Pure and Applied Geophysics, v. 142, Special Issue on Shallow Subduction Zones, R. Dmowska and G. Ekstrom, eds., pp. 83-99.

Bufe, C. G., Varnes, D. J., and Nishenko, S. P., 1994, Long-term seismicity patterns and pre-earthquake failure processes [invited abs.]: EOS (American Geophysical Union, Transactions), v. 75, no. 44, p. 434.

Nishenko, S. and Barton, C., 1993, Scaling laws for natural disasters: An application of fractal statistics to life and economic loss data [abs.]: 1993 Annual Meeting, Geological Society of America, Oct 25-28, 1993, Boston, MA, pp. A-412.

Nishenko, S. P, Ebel., J., and Perkins, D., 1993, New England earthquake hazard estimates [abs.]: EOS(Trans. Amer. Geophys. Union), v. 74, p. 288.

Nishenko, S. and Barton, C., 1994, Scaling laws for natural disasters: An application of fractal statistics to life and economic loss data [abs.]: Santa Fe Institute Workshop on Natural Hazards Reduction, Jan 5-9, 1994, Santa Fe, New Mexico.

Nishenko, S. P., and Bufe, C. G., 1994, The seismic cycle in space and time -- some circum-Pacific examples: in Proceedings, SUBCON, An Interdisciplinary Conference on the Subduction Process, June 12-17, 1994, Catalina Island, CA, pp. 271-274.

Nishenko, S. P., and Bufe, C. G., 1994, Testing the seismic cycle [invited abs]: EOS (American Geophysical Union, Transactions), v. 75, no. 44, p. 453.

Varnes, D.J., and Bufe, C.G., 1994, The cyclic and fractal seismic series preceding the magnitude 4.8 earthquake on 14 February 1980 near the Virgin Islands, Director's approval January 1994.

Earth Structure and Source Parameters
9920-10102

George L. Choy
Branch of Global Seismology and Geomagnetism
U. S. Geological Survey
Denver Federal Center
Box 25046, Mail Stop 967
Denver, Colorado 80225
(303) 273-8424
FAX (303) 273-8450
choy@neis.cr.usgs.gov
OP 91010

Investigations

1. NEIC reporting services. The NEIC now uses broadband data to routinely compute source parameters of earthquakes. These parameters include depth of nucleation from differential arrival times, focal mechanism from broadband waveforms, source complexity and radiated energy. Arrival times of late-arriving phases are digitally enhanced and also reported. The information is published in the Monthly Listing of the Preliminary Determination of Epicenters and in the Earthquake Data Report. Algorithms have been developed so that these source parameters can be accomplished rapidly enough for public dissemination through the Quick Epicenter Determination and the Preliminary Determination of Epicenters.

2. Manual of broadband seismogram interpretation. A manual on seismogram interpretation was last produced by a government agency in 1966. The techniques described in that manual have since been outdated by advances in source theory, wave propagation and instrumentation. Work is progressing on a new manual which would describe modern practices of seismogram interpretation, especially the full waveform analysis adopted by the NEIC to derive source parameters from broadband digital data.

3. Effects of earth structure on source parameters. To improve the accuracy of source parameters derived from waveform analysis, we are developing corrections for the effects of wave propagation in the earth.

- **A. Body wave interactions with upper mantle structure.** With the proliferation of digitally recording broadband networks around the world (including the USNSN), new techniques must be developed for the interpretation of seismic phases recorded at regional distances.
- **B. Effects of attenuation on the computation of source parameters.** We are developing techniques to determine the depth- and frequency-dependence of attenuation in the earth. Resolution of this frequency dependence requires analysis of a continuous frequency band from several Hz to tens of seconds. It also requires consideration of the contributions of scattering and slab diffraction to apparent broadening of a pulse.

4. Rupture process of large- and moderate-sized earthquakes.

A. Radiated energy provides a fundamentally different measure of earthquake size than either moment or magnitude. Using spectral analysis of broadand digital data, the NEIC has computed direct (rather than empirical) estimates of radiated energy for more than 679 earthquakes of magnitude $\geq$ 5.8 that occurred between 1986-1992. We are mapping these energies as a function of seismic region, tectonic environment, focal mechanism and depth to determine patterns of stress release.

B. To better understand the earthquake cycle in subduction zones, we are studying the seismicity before and following the M_W 8.7, 1957 Aleutian arc earthquake, and the M_S 8.1, 1974 Peru earthquake. The interpretation of seismicity patterns can be used to infer the probable mode of stress accumulation, main-shock size, main-shock rupture characteristics, and stress redistributions following large earthquakes at subduction zones.

C. To evaluate seismic risk in the western United States, we are performing a comparative study of the 1882 Colorado and 1984 Wyoming earthquakes.

Results

1. Reporting Services. The NEIC now uses broadband waveforms routinely: (1) to resolve depths of all earthquakes with $m_b > 5.8$; (2) to constrain first-motion focal-mechanism solutions; (3) to present as representative digital waveforms in the Monthly PDE's; and (4) to compute the energy radiated by earthquakes. In the Monthly Listings of the PDE covering the interval August 1993 to May 1994, depths using differential arrival times from broadband waveforms were computed for 114 earthquakes; radiated energies were computed for 130 earthquakes. An algorithm for rapid retrieval of data from the USNSN and selected GSN stations now permits broadband depths and energies to be computed in times for inclusion in the QED and the PDE.

2. Manual of broadband seismogram interpretation. An essential element in full-waveform analysis of body waves is an understanding of various modes of rupture. We are accumulating and cataloging a data base of broadband displacement and velocity seismograms of body waves that demonstrate the hierarchy of source complexity.

3. Effects of Earth structure on source parameters.

A. Body wave interactions with upper mantle. Synthetic seismograms generated for P and S waves interacting with the upper mantle are sensitive to differences in velocity contrasts, velocity gradients and attenuation at the 420- and 670-km discontinuities. Major contributions to waveform shape come from later arrivals such as interference head waves and cusp-diffracted waves. In waveform data with sufficient broad bandwidth, these features can be identified and used to infer acceptable models of the upper mantle. A Langer locked-mode method of synthesizing seismograms for local distances is being adapted for computation of synthetics out to regional distances.

B. Attenuation in the earth. We are attempting to separate intrinsic attenuation from scattering in waveforms. We synthesize waveforms using a method

that simultaneously models causal attenuation and source finiteness. Under the assumption that intrinsic attenuation can be described by minimum phase operators, we can attribute discrepancies in the waveforms to scattering.

3. Rupture process of large- and moderate-sized earthquakes.

A. Radiated energy has now been computed for over 400 shallow earthquakes at subduction zones, oceanic ridges and intraplate environments. The scatter of energy and moment, while large, is not random. The release of energy and apparent stress is a strong function of faulting type and tectonic setting. Most seismic regions can be associated with a characteristic apparent stress. As global correlations between energy and moment become more precise, they can be applied to improving the estimation of seismic hazard potential.

B. Earthquakes along the Aleutian arc before and after the great 1957 Aleutian Islands and 1986 Andreanof Islands earthquakes have been relocated and catalogued. The earthquake catalog is complete down to magnitude 5.5 from 1957 to 1989, and down to 4.7 from 1964 to 1989. The aftershock distributions of the 1957 and 1986 earthquakes indicate that the moment distributions are spatially anticorrelated. This observation suggests that mechanically strong portions of the fault (asperities) cannot be identified by simply mapping the moment distribution of the most recent great earthquake. Contrary to the supposition of the asperity model, the moment distribution from earthquakes occurring during the present cycle may not be reflective of what the moment distribution will look like for the next earthquake cycle.

We have completed an investigation of aftershocks, relocated with data from an 11-station temporary network, for the October 3, 1974, Peru earthquake (M_W 8.1). The characteristics of the main-shock rupture and aftershock distribution can be related to the broad influence of the Nazca ridge. Preseismicity was concentrated at the downdip edge of the main-shock rupture and in the steeper plate region, which is consistent with the loading of asperities of the main shock by sinking of the Nazca plate. The spatio-temporal interplay between clusters of aftershocks reflect loading of the asperities by the continued sinking of the Nazca plate.

C. The Wyoming earthquake of 1882, thought to have a magnitude of about 6.0, occurred about 50 km north of a 1984 earthquake in Colorado with a magnitude of 5.4. The 1984 earthquake occurred in a structure analogous to the 1882 earthquake. A re-evaluation of the intensity pattern for the 1882 earthquake indicates that the shape of the intensity pattern of 1882 earthquake can be reasonably interpreted to be similar to that of the recent 1984 earthquake. For the 1984 earthquake we have determined aftershock locations and focal mechanisms for main shock and aftershocks. The 1984 earthquake has an anomalous large felt area and a mid-crustal focal depth of about 22 km. Parallels between the 1882 and 1984 earthquakes suggest that the 1882 earthquake also had a mid-crustal depth. The predominantly NE-SW, shallow-dipping direction of the tension axes of the focal mechanisms are representative of the regional stress field.

Reports

Boyd, T.M., Engdahl, E.R., and Spence, W., 1994, Seismic cycles along the Aleutian arc–Analysis of seismicity from 1957 through 1991: Journal of Geophysical Research (in press).

Choy, G.L. and Boatwright, J.L., 1994, Global patterns of radiated energy release: submitted, Journal of Geophysical Research.

Choy, G.L., LaVonne, C.K., and Needham, R.E., 1994, Processing and analysis of broadband seismograms at the U. S. G. S. National Earthquake Information Center [abs.]: Abstracts of the 24th General Assembly of ESC, p. 46.

Engdahl, E.R., Kirby, S.H., Okal, E.A., Choy, G.L., and Bergman, E. A., 1994, High-resolution seismological characteristics of the Arca Elbow region and the June 1994 Deep Earthquake [abs.]: EOS, (American Geophysical Union, Transactions), v. 75, no. 44, p. 467.

Langer, C.J. and Spence, W., 1994, The 1974 Peru earthquake series: Bulletin of the Seismological Society of America (in press).

Spence, W. and Langer,C.J., 1994, Similarities among significant earthquakes in the Front Range, Colorado and in the Laramie Mountains, Wyoming [abs.]: EOS, (American Geophysical Union, Transactions), v. 75, no. 16, p. 241.

United States Earthquakes

9920–10042

J. W. Dewey
Branch of Earthquake and Geomagnetic Information
U.S. Geological Survey
Denver Federal Center
Box 25046, Mail Stop 967
Denver, Colorado 80225
(303) 273–8419

Investigations

During the period October 1, 1993 through September 30, 1994, we conducted canvasses by mail questionnaire for information on damages and felt effects from 262 earthquakes. One of these shocks occurred in Alabama, 77 in Alaska, 96 in California, 5 in Canada near the United States border, 5 in Colorado, 1 in Georgia, 1 in Hawaii, 16 in Idaho, 3 in Illinois, 1 in Kentucky, 2 in Maine, 1 in Michigan, 1 in Montana, 1 in North Carolina, 1 in Nebraska, 8 in Nevada, 1 in New Mexico, 1 in New York, 1 in Ohio, 1 in Oklahoma, 9 in Oregon, 3 in Pennsylvania, 4 in or near Puerto Rico, 1 in Tennessee, 3 in Utah, 4 in Washington, and 14 in Wyoming. A survey of seismologists around the country was conducted to determine the extent of felt shaking from the deep-focus Bolivian earthquake of June 9, 1994.

A field survey of damage from the January 17, 1994, Northridge, California earthquake was conducted by Jim Dewey and Glen Reagor.

We continue to update data bases on the Earthquake Data Base System (EDBS) and to furnish seismic data to engineers, land-use planners, architects, oil company geophysicists, insurance companies, university programs, and private citizens.

Results

Fourteen earthquakes caused damage (MM VI or greater) in the United States and its dependencies during the period covered by this report. Two of these shocks were in Alaska, 6 in California, 1 in Nevada, 2 in 0regon, 1 in Pennsylvania, and 2 in Wyoming.

The magnitude (MW) 6.7 Northridge, California, earthquake of January 17, 1994, caused billions of dollars of damage, directly caused the deaths of 33 people, and was felt over approximately 214,000 square kilometers of the land area of the U. S. Intensities of IX were assigned to the communities of Northridge, Granada Hills, and Sherman Oaks, to an area along the Interstate-5 corridor at the east edge of the Santa Susana Mountains, and to small sections of Santa Monica and west-central Los Angeles. Intensity VIII was assigned to many communities in the San Fernando

Valley, and to some communities north of the Santa Susana Mountains or south of the Santa Monica Mountains. Shaking was generally perceived as strong out to 100 km from the epicenter, although damage was light at distances of more than 50 km from the epicenter.

Approximately 50 preliminary isoseismal maps (Dewey, Reagor, and Dengler, 1994) were mailed to people who requested them: recipients were mostly consulting engineers, but also included were earth scientists, educators, and interested members of the general public. An early version of the isoseismal map was rendered in color by staff artists of the Los Angeles Times and published with accompanying text in the March 5, 1994 issue.

The felt reports associated with the Bolivian earthquake of June 9, 1994, are interesting because the epicentral distances at which the quake was felt were the largest known to have been associated with any earthquake. The strongest shaking in the United States occurred in the upper midwest—central and southern Minnesota, northwestern Iowa, northeastern Nebraska, and southeastern South Dakota. These locations were approximately 7,000 kilometers from the earthquake's epicenter. The most distant report received was from the Puget Sound area, at an epicentral distance of 8,700 kilometers. On the other hand, seismographic centers in many states received no felt reports, although these centers are normally inundated by calls after minor local shocks. Many, but not all, of the reports came from upper stories of multistory buildings, and observers specifically noted that some of these buildings are situated on loose sedimentary deposits. Most of the reports describe effects typical of Modified Mercalli I or II. A few reports describe effects that would be rated at III if the effects could be considered representative of an entire community.

The third version of the Global Hypocenter Data Base CD-ROM was released in September 1994. Six additional catalogs have been added; the PDE and EPB were updated through 1992. The EPIC retrieval software has been modified so that the data on the CD-ROM can be augmented by non-CD-ROM quarterly updates after 1992.

During this reporting period, 577 seismicity searches were conducted on the EDBS. 375 of these were made for USGS personnel or visiting scientists; 62 for universities, foreign governments, schools, and local, state, or outside federal agencies. 140 searches were conducted for commercial entities or individuals.

The following catalogs in the EDBS (listed by the abbreviation with which they are accessed in the EDBS) were added or updated during the 1993 fiscal year:

ARIEH	–	Israel and adjacent areas, 1903–1963.
DOYLE	–	Australia, 1899–1966.
EPB	–	Canada, 1568–1992.

p. 1067 follows

GER	–	Earthquake catalog for Germany, 823–1992. GOUIN – Ethiopia and the Horn of Africa, 1400–1977. INDIA – Peninsular India, 1939–1984.
ISC	–	World-wide earthquakes located by the International Seismological Center, 1964–1991.
ISN	–	Israel, 1900–1993.
LIBYA	–	Libya, 1903–1975.
PDE	–	Epicenters located worldwide by the National Earthquake Information Center. Updated weekly and monthly.
SAFR	–	South Africa, 1620–1970.

Reports

Dewey, J.W., 1993, Damages from the 20 September earthquakes near Klamath Falls, Oregon: Earthquakes and Volcanoes, v. 24, no. 3, p. 121 - 128.

Dewey, J.W., and Pitt, A.M., 1994, Redetermination of locations and magnitudes of earthquakes in northern Yellowstone Park, Wyoming, and adjacent Montana and Idaho [abs.]: Seismological Research Letters, v. 65, no. 1, p. 67.

Dewey, J.W., Reagor, B.G., and Dengler,L., 1994, Isoseismal map of the Northridge, California, earthquake of January 17, 1994 [abs.]: Poster talk presented at the 89th Annual Meeting of the Seismological Society of America, April 5 - 7, Pasadena, California, abstract 24 in the Program for Northridge Abstracts.

Dewey, J.W., Reagor, B.G., Johnson, Dennis, Choy, G.L., and Baldwin, Frank, 1994, The Scotts Mills, Oregon, earthquake of March 25, 1993: intensities, strong-motion data, and teleseismic data: U. S. G. S. Open-File Report 94-163, 26 p.

Stover, C.W., and Brewer, L.R., 1994, United States earthquakes, U. S. Geological Survey Bulletin 2089, 240 p. (in press).

U. S. Geological Survey—National Earthquake Information Center, 1994, Global Hypocenter Data Base, Version 3.0 (CD-ROM).

New England Seismic Information System

Award Number 1434-94-G-2400

John E. Ebel
Weston Observatory
Department of Geology and Geophysics
Boston College
Weston, MA 02193
(617) 552-8300
Fax: (617) 552-8388
EBEL@BCVMS.BC.EDU

Program Element: IV.2 Transfer hazards information and assessment methods to users.

Investigations

The purpose of this project is to provide for an easy-to-use dekstop information system (running under Windows on a PC using ARCVIEW) that will present seismicity from throughout the northeastern United States and adjoining Canada. The system, called the New England Seismic Information System (NESIS), will provide a basis for viewing, interrogating, and accessing earthquake epicenter data in relationship to regional geology, infrastructure (roads, political boundaries, and population centers), regional gravity and magnetics, and major water boundaries. The research work involved is to assemble the requisite datasets, to construct ARCVIEW maps from the datasets, and to test out the resulting information system. We plan to make NESIS available to the general public for those who are interested in doing computer interrogations of regional earthquake information.

Data Acquisition and NESIS Assembly

The major work in this project is to acquire the various data sets from federal and state agencies. While each of the New England states has its own GIS center housing the datasets of interest to this project, accessing and acquiring the datasets has proven far from straightforward. The details of ordering datasets from the various GIS centers have been very confusing in many cases, and the average order has taken about 2 months to fill. Each of the New England states makes their data available through a different physical transfer medium (e.g., floppy disk, 9-track tape, PC

back-up tapes, etc.), making it a great challenge in some cases to find a convenient way to put the data onto the machine upon which we are constructing the NESIS. Furthermore, the available datasets span a range of map scale, level of detail, and dataset size. Many of the datasets proved so large that they did not fit onto a new 512 Mbyte hard disk we purchased to complete this project. As of November, 1994 there are still several outstanding datasets that we have yet to finish transferring onto our PC upon which ARCVIEW resides.

Preliminary Results

Due to the unexpectedly large size of the datasets being assembled, a number of hardware and software upgrades were required to ensure successful completion of the project. Manipulation of the GIS datasets is being done in the program AUTOCAD through the program ARCCAD. An upgrade of AUTOCAD was purchased to better handle the demands of this project. Some datasets have been successfully imported into ARCVIEW and displayed with the software. Nuances of the ARVIEW software necessary to optimally construct the NESIS have been learned and will be incorporated into the final NESIS system. It is our goal to have a working version of the NESIS available for display at the Northeastern GSA meeting in Harford, Connecticut in March, 1995.

Future Work

The primary work still to be done is to finish the assembly of the datasets into the final version for distribution. Editing of the datasets will be necessary in many cases, and a selection of the final set of layers to be included in the NESIS will depend on both the utility of the information presented and the work involved in getting the data layer into the ARCVIEW system.

Publication - Abstract

Lazarewicz, A., J.E. Ebel, and Y. Zhou, New England Seismic Information system, EOS, Trans. Amer. Geophys. U., vol. 75, No. 44, p. 450, Supplement, 1994.

PREPARATION OF PUBLIC-INFORMATION PRODUCTS FROM NEHRP RESEARCH RESULTS, WASATCH FRONT, UTAH

Sandra N. Eldredge
Utah Geological Survey
2363 South Foothill Drive
Salt Lake City, Utah 84109-1491
1434-93-G-2342
Program Element IV.2

After nearly a decade of intensive research under the National Earthquake Hazards Reduction Program (NEHRP) in Utah, much new information is now available for use in public policy-making, reducing geologic hazards and risk, and increasing public awareness. The most effective way to get the appropriate information to specific user groups is to produce publications tailored to their needs. The objective of the project is to provide publications for the general public, including homebuyers and real-estate agents.

The Utah Geological Survey (UGS) is producing four public-information products: (1) a homebuyer's guide to earthquake hazards, (2) a full-color brochure describing and illustrating Utah's most active fault, the Wasatch fault, (3) a pamphlet "translating" information on the ground-shaking hazard in Utah, and (4) a series of page-size liquefaction-potential maps for Wasatch Front counties. These products will be published in the UGS public information series, and distributed free-of-charge. The UGS will also publish as contract reports, the NEHRP-funded liquefaction-potential maps and reports prepared by Utah State University and Dames and Moore, Inc., that are complete but not widely available.

Published in October 1994 were: the four page-size liquefaction-potential maps, in color, as UGS Public Information Series 24, 25, 27, and 28; and Contract Reports 94-1, 94-2, 94-3, 94-4, and 94-5, which are the 1:48,000-scale liquefaction-potential maps accompanied by a six-page "non-technical" summary. As of mid-October 1994, the "technical" contract reports and the ground-shaking pamphlet are in press. The homebuyer's guide and the Wasatch fault brochure are in the review process.

RAPID EARTHQUAKE DATA INTEGRATION

Award Number: 1434-94-G-2399

Lind S. Gee, Douglas S. Neuhauser, Barbara Romanowicz
Seismographic Station
475 McCone Hall
UC Berkeley
Berkeley CA 94720-4760
510-642-3977

and

Jack Moehle
Earthquake Engineer Research Center
Richmond Field Station
UC Berkeley
Berkeley CA 94720
510-231-9554

The availability of reliable earthquake information and accurate estimates of regional damage within minutes of a major seismic event is of fundamental importance to the emergency operations and disaster response teams of the federal, state, and local governments. The mobilization of an emergency response can be greatly enhanced by dependable near real-time estimates of earthquake location, magnitude, and extent of strong-ground shaking, contributing significantly to the mitigation of hazard and the assurance of public safety.

Investigations Undertaken

Efforts to design and implement systems to provide rapid earthquake information have expanded over the last five years [Hauksson et al., 1992; Buland & Person, 1992; Romanowicz et al., 1992; Ekström, 1992; Ammon et al., 1993], motivated by recent developments in seismic instrumentation and digital data acquisition and telemetry. In the last year, the UC Berkeley Seismographic Station and the Earthquake Engineering Research Center combined their efforts to develop a system to provide useful and rapid information on potentially damaging earthquakes in northern and central California. With support from the NEHRP program, the first phase of the Rapid Earthquake Data Integration (REDI) project has been implemented.

Results Obtained

Over the past year, we have made significant progress in the development of the Rapid Earthquake Data Integration (REDI) project toward the goal of providing rapid and reliable earthquake information. We have collaborated with scientists at Caltech and the USGS to coordinate our research effortt. For example, the Caltech-USGS Broadcast of Earthquakes (CUBE) project utilizes the Southern California Seismic Network (SCSN) and the TERRAscope network to provide rapid notification for earthquakes in southern California. Due to the differences in the type and geometry of our networks, we were unable to employ the software developed by Caltech for event association and processing and have designed our own system. However, we have coordinated broadcast regions with Caltech in order to provide uniform coverage for the state and have adopted their end-user software for the graphical display of earthquake information. We are also working with Caltech to establish a redundancy of coverage between REDI and CUBE. This redundancy will be critical in ensuring fail-safe communications during a large earthquake in either northern or southern California.

The REDI system is comprised of five major elements: phase association; event declaration; event scheduling; event processing; and event notification (Figure 1).

Phase association
The REDI system receives phase picks from the Northern California Seismic Network (NCSN) and event detections from the Berkeley Digital Seismic Network (BDSN) (Figure 2). The NCSN picks presently originate from the three hardware Real-Time-Picker (RTP) systems [Allen, 1978; 1982] in Menlo Park and are transmitted to UC Berkeley through an Internet link. The BDSN event detections are generated by the Quanterra data loggers using the Murdock-Hutt algorithm [Murdock & Hutt, 1983] and are transmitted through continuous telemetry links to UC Berkeley. The input phase arrivals are formed into "events" using the phase associator algorithm developed by Dr. Carl Johnson of University of Hawaii [Johnson et al., 1993]. As phase picks arrive in the shared memory region created by the associator, the program compares them with a list of known events. If a phase pick satisfies the residual criteria, it is associated with an event and the earthquake is relocated. If a pick remains unassociated after this comparison, the program evaluates the list of independent picks to form possible new events. Both the USGS Menlo Park and the Seismographic Station are collaborating with Dr. Johnson on the continued development of the phase associator.

Event declaration
The main task of the associator is to analyze phase picks as they are received and combine them into probable events. Because phase information is acquired continuously, the associator's "view" of an event is never static. The task of event declaration is carried out by a separate process referred to as the watch dog program. This program "watches" a shared memory region created by the associator and keeps track of when an event is created, when its most recent modification occurred, and the number of phases currently associated with the event. The program uses these parameters to determine when an event should be "declared." In the present implementation, the software imposes some delays before deciding to process an event. While event detections from the BDSN system may be received within 7 to 10 s of their occurrence, the hardware RTPs trigger for 180 s before the phase information becomes available. Rather than declare an event based on only BDSN phases, the watchdog program waits at least 180 s before declaring an event, in order to insure that the RTP picks have arrived. With the completion of the Earthworm system at Menlo Park [Bittenbinder et al., 1994], it will be possible to relax this 180 s delay and reduce the overall time required to process an earthquake.

Event scheduling
Once an event is declared, it is queued for processing by the event scheduler. This program allows up to m events to be analyzed simultaneously. The scheduler is given the task of overseeing the event processing, from initiation to notification. The scheduler is also charged with deleting an event, if more recent information received by the associator has destroyed the phase grouping. The scheduler prioritizes events by preliminary magnitude, rather than origin time, to avoid potential overloading during an energetic sequence.

Event processing and notification
The phase associator program determines a preliminary location and magnitude for each group of associated phases. The magnitude estimate is based on the first few swings of the P-wave arrival (Pmag) [Hirshorn et al., 1993] and may be inaccurate, while the preliminary location is generally quite good, although we have observed some cases where the associator will capture stray picks and group them with an event which is unrelated, mislocating the resulting earthquake.

Rather than proceed with preliminary information which may be inaccurate, the REDI system contains an event processing step (Figure 3). In this procedure, events are relocated and magnitudes are recomputed. The first step in the event processing software is the decision to extracting BDSN waveforms. For events with preliminary magnitudes greater than 3.0 or events

with no magnitude information, the processing software extracts waveforms from the continuous 20 samples per second BDSN archive, based on the initial location and magnitude. Only stations which are predicted to have a Wood-Anderson amplitude greater than .5 mm are extracted (events without preliminary magnitudes are assumed to be at least a 3 for this purpose). While the waveforms are being extracted, the event processing program generates revised location using the standard 1-D location program of the Seismographic Station.

When the relocation and the waveform extraction (if any) is complete, the event processor computes a new magnitude. If waveforms were not extracted or if the extraction did not complete normally, the Pmag magnitude is recalculated. If waveforms were extracted, the broadband records are convolved with the Wood-Anderson instrument response in order to estimate local magnitude [Anderson et al., 1993]. Thus, for larger events (M > 3.0) the magnitude is determined using the high dynamic range, broadband records of the BDSN.

After the revised location and magnitude are determined, the event scheduler dispatches the appropriate notifications. REDI uses both a commercial paging system and electronic mail to notify state and federal agencies of earthquake occurrence. We have coordinated with Caltech to format messages identical to those generated by the CUBE system and are using the Qpager software developed by Peter German to display earthquake location and magnitude on a personal computer.

We have completed the preliminary development of the REDI project. The current scheme provides for the automatic notification of earthquake origin time, location, and magnitude. Within a few months, we will be supplementing this basic information for larger events with parameters useful for characterizing earthquake damage potential.

References cited

Allen, R. V., Automatic earthquake recognition and timing from single traces, *Bull. Seis. Soc. Am.*, *68*, 1521-1532, 1978.

Allen, R. V., Automatic phase pickers: Their present use and future prospects, *Bull. Seis. Soc. Am.*, *72*, S225-S242, 1982.

Ammon, C. J., A. A. Velasco, and T. Lay, Rapid estimation of rupture directivity - application to the 1992 Landers (Ms = 7.4) and Cape Mendocino (Ms = 7.2), California, earthquakes, *Geophys. Res. Lett.*, *20*, 97-100, 1993.

Anderson, G. J., S. J. Loper, R. Uhrhammer, and B. Romanowicz, Synthetic Wood-Anderson records at the University of California, Berkeley, *Seis. Res. Lett.*, *64*, 51, 1993.

Bittenbinder, A. N., B. M. Bogaert, C. E. Johnson, and S. D. Malone, Earthworm: A modular distributed processing approach to seismic network processing, *Seis. Res. Lett.*, *65*, 51, 1994.

Buland R., and W. Person, Earthquake early alerting service, *EOS*, *73*, 69, 1992.

Ekström, G., A system for automatic earthquake analysis, *EOS*, *73*, 70, 1992.

Hauksson, E., H. Kanamori, S. Bryant, J. Hockwald, T. Heaton, and D. Given, *CUBE*, *EOS*, *73*, 69, 1992.

Hirshorn, B., A. G. Lindh, R. V. Allen, and C. Johnson, *Seis. Res. Lett.*, *64*, 48, 1993.

Johnson, C. E., A. Bittenbinder, and B. Hirshorn, Auryn: A stacking method for the rapid association of multiple earthquake phases, *EOS*, *74*, 394, 1993.

Murdock, J. N., and C. R. Hutt, A new event detector designed for the Seismic Research Observatories, *USGS Open File Report 83-0785*, 39p., 1983.

Romanowicz, B., G. Anderson, L. Gee, R. McKenzie, D. Neuhauser, M. Pasyanos, and R. Uhrhammer, Real-time seismology at UC Berkeley, *EOS*, *73*, 69, 1992.

Reports

Anderson, G. J., S. J. Loper, R. Uhrhammer, and B. Romanowicz, Synthetic Wood-Anderson records at the University of California, Berkeley, *Seis. Res. Lett.*, *64*, 51, 1993.

Gee, L. S., D. S. Neuhauser, D. S. Dreger, M. E. Pasyanos, B. Romanowicz, and R. A. Uhrhammer, Real-time seismology at UC Berkeley, *EOS*, *75*, 1994.
Gee, L. S., D. S. Neuhauser, D. S. Dreger, M. E. Pasyanos, B. Romanowicz, and R. A. Uhrhammer, Rapid Earthquake Data Integration, manuscript in preparation, 1994.
Romanowicz, B., G. Anderson, L. Gee, R. McKenzie, D. Neuhauser, M. Pasyanos, and R. Uhrhammer, Real-time seismology at UC Berkeley, *EOS*, *73*, 69, 1992.

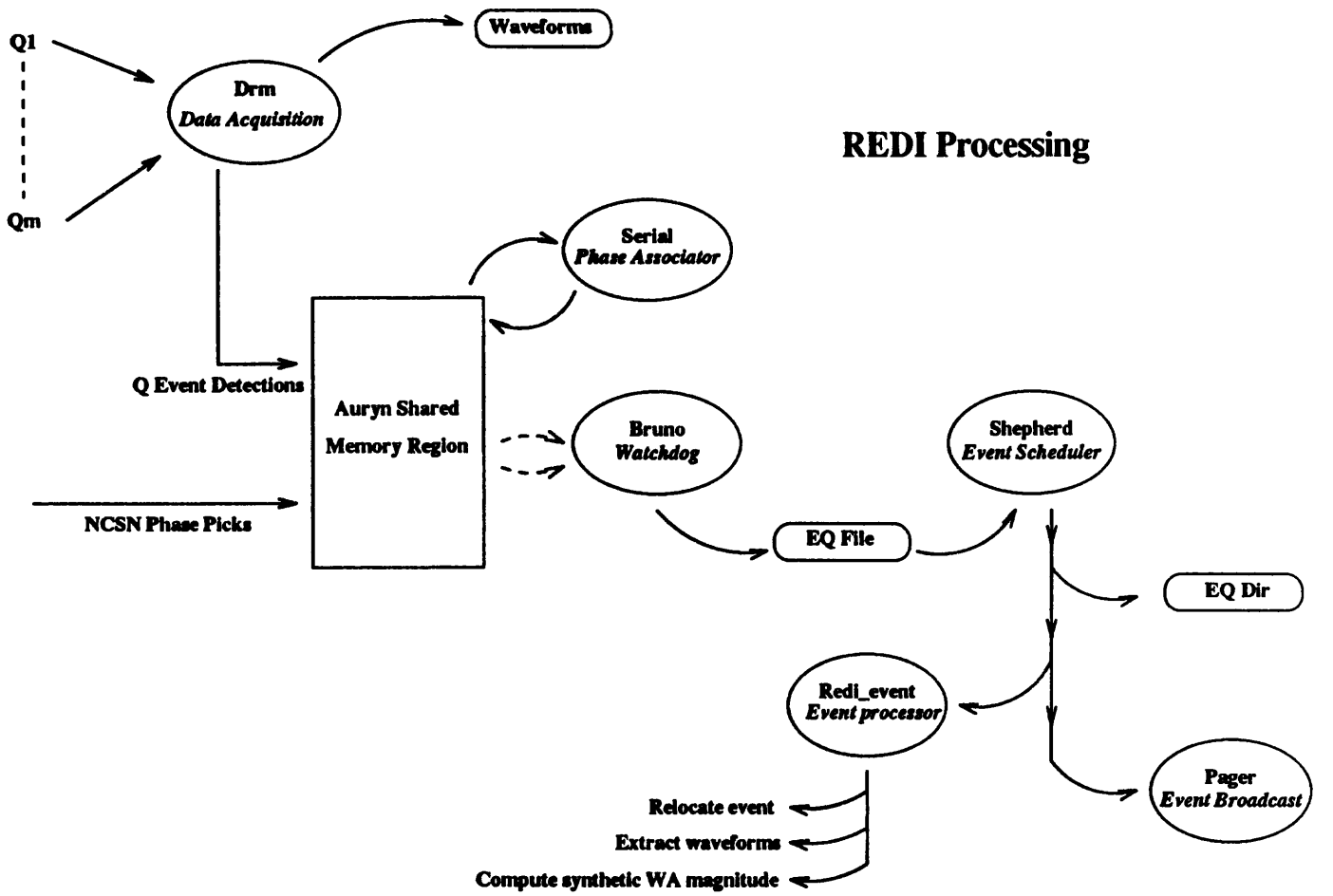

Figure 1: Schematic diagram illustrating REDI processing. NCSN picks and Quanterra event detections are associated into events by serial. Bruno, the watchdog program, declares an event ready for analysis based on the number of picks and the length of time an event has been associated. Once declared, an event is queued for processing by shepherd, the event scheduler. Individual event processing is performed by redi_event.

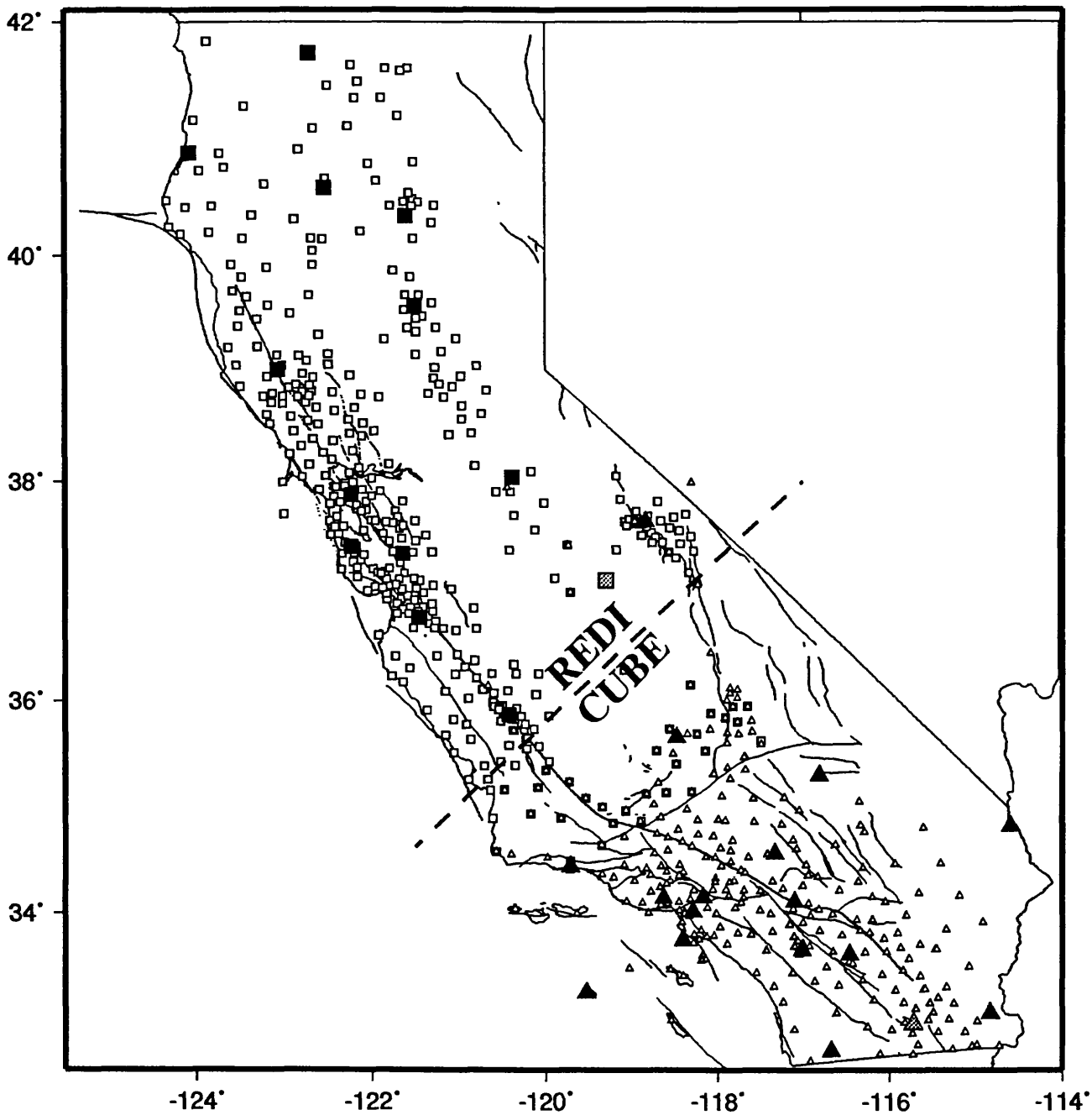

Figure 2: Map illustrating the regions covered by the REDI and CUBE projects. Smaller open squares indicate the location of NCSN stations; larger filled squares indicate the position of BDSN instrumentation (stippled symbols are future sites). Smaller open triangles indicate the location of SCSN stations while the larger filled triangles indicate the position of TERRAscope instrumentation. Some stations are common to the NCSN and the SCSN.

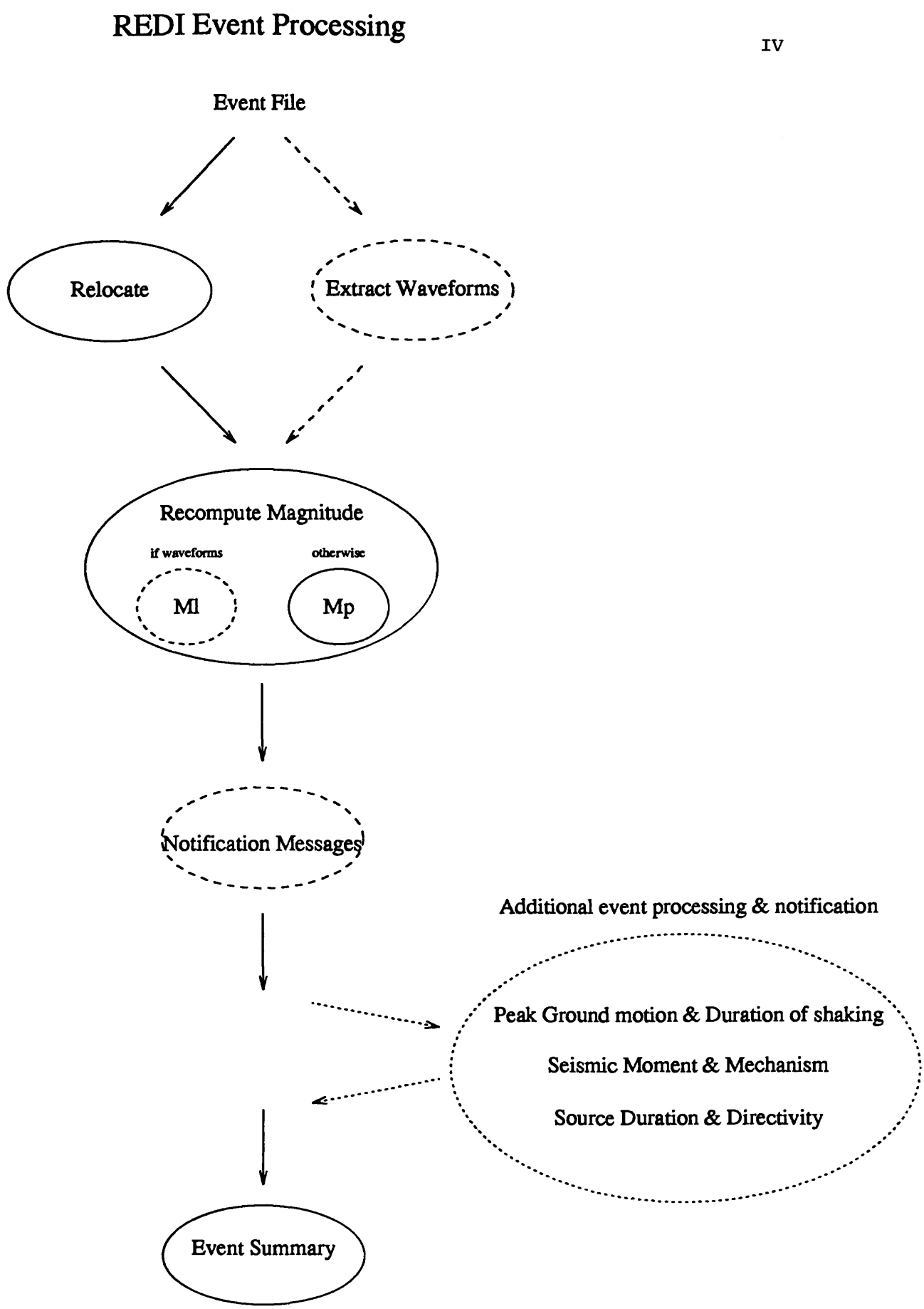

Figure 3: Schematic diagram illustrating REDI event processing. Long dashed lines indicate processing which is undertaken when an event meets certain criteria (for example, BDSN waveforms are extracted if the preliminary magnitude estimate is greater than 3 or if no estimate exists). Short dashed lines illustrate the planned "additional processing" queue for events with magnitudes greater than 5.0.

EFFECTIVE DISSEMINATION OF NEHRP RESEARCH RESULTS IN UTAH--CONNECTING RESEARCHERS AND PRACTITIONERS

1434-94-G-2486
Program Element IV.1

Janine L. Jarva and Gary E. Christenson
Utah Geological Survey
2363 South Foothill Drive
Salt Lake City, Utah 84109-1491

PURPOSE OF THE PROJECT

In 1983 the National Earthquake Hazards Reduction Program (NEHRP) targeted the Wasatch Front for five years of support under the Regional and Urban Earthquake Hazards Evaluation program element. The Wasatch Front NEHRP initially focused on research to accelerate the development of the knowledge base on the causes and effects of earthquakes, and then emphasized implementation activities to facilitate use of research results to reduce losses. The Utah Geological Survey (UGS) has continued an active program to translate scientific research results into products useful to a diverse community of end-users, and to forge strong partnerships between the research community (universities, the private sector, and state and federal agencies) and those who ultimately use the information to implement hazard-reduction policies (local government, engineers, architects, planners, and emergency planners and responders). The purpose of this project is to develop and apply new geographic information systems (GIS) methods to the recently completed Quaternary Tectonics of Utah (Hecker, 1993) database and to expand and update two other ongoing projects, the Geologic Hazards Bibliography of Utah (Harty and others, 1992) and the *Fault Line Forum* (formerly called the *Wasatch Front Forum*), to more effectively disseminate earthquake-hazards information.

INVESTIGATIONS

The Geologic Hazards Bibliography of Utah was created to identify existing information related to earthquakes and other geologic hazards in Utah, especially information released in formats that may not be widely available or distributed to a non-technical audience, that can be used by decision makers, the public, and researchers. The computerized database currently contains over 3800 references which have been assigned geographical and geologic-hazards key words. Over half of all the references have more than one of the earthquake-related key words associated with them. These key words allow searches and inquiries of the database to be tailored to the needs of the user. Although it is kept current to the extent possible, it has not had a comprehensive update of published literature since 1990. UGS will formally update the bibliography for published literature through December, 1993. We estimate that about half of the added references will be directly related to new and continuing earthquake research and implementation studies in Utah supported by NEHRP grants.

The *Fault Line Forum* is a quarterly newsletter published by the UGS to inform the Utah earthquake community and others of earthquake-related activities and information. It began with the Wasatch Front NEHRP in 1983 and has remained available free of charge to all those interested in Utah earthquake information since that time. The *Fault Line Forum* was originally prepared from materials submitted by Wasatch Front NEHRP participants and published in conjunction with the U.S. Geological Survey (USGS). It contained information that was not published elsewhere or information that was in a preliminary form. In 1987, when the emphasis of the Wasatch Front NEHRP shifted from scientific research aimed at evaluating earthquake hazards to implementation activities aimed at reducing earthquake risk, the *Fault Line Forum* evolved to reflect this change. Its audience was broadened to target people responsible for planning and implementing risk-assessment and loss-reduction programs in local government, business, utility, transportation, communication, economic, and social arenas. We have expanded coverage from the Wasatch Front to the entire state and broadened our coverage of earthquake issues, particularly those which are significant in translating and transferring complex scientific and technical information to non-technical users. The *Fault Line Forum* continues to inform readers of new and ongoing scientific research, especially if the results will not be formally published until much later.

The Quaternary Tectonics of Utah database provides a comprehensive, up-to-date summary of information on fault-specific seismic sources and Quaternary surface fault rupture which can be used to evaluate earthquake hazards in Utah. Digitally compiled, 1:500,000-scale maps show all known Quaternary tectonic features in Utah. The digital geographic files have been converted into an ARC/INFO GIS system. Tables summarize significant paleoseismic data on the activity of mapped features necessary to assess space-time distributions of large-magnitude paleoearthquakes and to estimate regional probabilities of future earthquakes. We are converting these tectonic-activity parameter data from the tables and attaching them as attributes to the spatial geographic data in the ARC/INFO files. When completed, this comprehensive ARC/INFO database will allow easy access, query, and display, as well as the ability to continually update the data. Once implemented, advanced analysis can be performed. For example, map and attribute data will be generated to display faults with specific recurrence intervals and slip rates for specific geographic areas of interest. In addition, these data can be combined with other digital data that now exist or are being converted, to create derivative maps from overlay analysis of tectonic data with lifeline or critical-facility data to assess risk.

RESULTS

As of September 1994, the search of published literature from 1990 through 1993 is nearly complete, and approximately 500 new references have been added to the Geologic Hazards Bibliography of Utah.

Two issues of the *Fault Line Forum* (volume 10, numbers 1 and 2) have been completed and mailed out. Volume 10, number 3 is in press. The format and layout of the publication have been significantly improved. We have received positive feedback from many readers. The expanded breadth of coverage has reached new audiences, and the Federal Emergency Management Agency recently requested permission to reprint an article from the *Fault Line Forum* (v. 10, no. 1; Jarva, 1994) in an emergency management and mitigation guide that they are developing for state legislators.

We have developed the ARC/INFO database for the Quaternary tectonics of Utah in conformance with the database being developed by the USGS for their maps of major active faults of the United States and the western hemisphere. The tectonic-activity-parameter data that are currently being prepared for import into our database includes: (1) timing of the most recent surface-rupturing event on a fault (age), (2) the length of time between successive events (recurrence interval), (3) the amount of displacement during individual events, (4) the length of surface fault ruptures, and (5) fault slip rates. This information is necessary to assess space-time distributions of large-magnitude paleoearthquakes and to estimate regional probabilities of future earthquakes. When the map and database are complete, overlay analysis of the geologic information with lifeline, critical facility, and other coverages to assess risk will be possible. We will provide the finalized ARC/INFO database to the USGS for use in their map compilations mentioned above, in support of the Global Seismic Hazards Assessment Program.

REPORTS

Jarva, J.L., editor, 1994, *Fault Line Forum*, v. 10, no. 1: Utah Geological Survey, 16 p.

Jarva, J.L., editor, 1994, *Fault Line Forum*, v. 10, no. 2: Utah Geological Survey, 16 p.

REFERENCES

Harty, K.M., Hecker, Suzanne, and Jarva, J.L., 1992, Geologic hazards bibliography of Utah: Utah Geological Survey Open-File Report 264-DF, 21 p. plus floppy diskette.

Hecker, Suzanne, 1993, Quaternary tectonics of Utah with emphasis on earthquake-hazard characterization: Utah Geological Survey Bulletin 127, 157 p., scale 1:500,000.

Jarva, J.L., 1994, Earthquakes and politics--get involved!: *Fault Line Forum*, v. 10, no. 1, p. 3-4.

Collaborative Research Oregon Department of Geology and Mineral Industries (DOGAMI), and Washington Division of Geology and Earth Resources (DGER): Relative Earthquake Hazard Map of the Clark County Urban Area, Washington

Award #1434-93-G-2318
Ian. P. Madin, Dr. Matthew A. Mabey, Oregon Department of Geology and Mineral Industries
800 NE Oregon St. # 28
Portland, OR 97232

Dr. S. Palmer
Washington Division of Geology and Earth Resources
P.O. Box 47007
Olympia, WA 98504-7007

ELEMENT IV.1

Investigations

The purpose of this project was to use an existing database of subsurface geology (Madin and Swanson, 1992), and an established hazard mapping methodology (Mabey and others 1993) to produce 1:24,000 scale earthquake hazard maps for the Orchards and Vancouver Washington quadrangles, which cover most of urban Clark County Washington.

Progress

The drilling and cone penetrometer profiling, shear wave velocity logging and data reduction, digital geologic modelling and amplification, liquefaction, slope hazard, and composite hazard analysis are all complete. The maps have been submitted to the DGER cartography shop and should be released in January of 1995. Preliminary Relative Amplification (Figure 1), Relative Slope Stabilty (Figure 2), Relative Liquefaction (Figure 3) and Relative Earthquake Hazard (Figure 4) maps are presented below.

References

Mabey, M.A., Madin, I.P., Youd, T.L., Jones, C.F., 1993, Lateral Spread Displacement, Relative Ground Motion Amplification and Relative Dynamic Slope Instability maps of the Portland Quadrangle, Oregon; In Earthquake Hazard Maps of the Portland Quadrangle, Multnomah and Washington Counties, Oregon. Oregon Department of Geology and Mineral Industries GMS-79

Madin, I.P., and Swanson, R.S., 1992 Earthquake-Hazard Geology maps of southwestern Clark County: Intergovernmental Resource Center, Vancouver, Washington

FIGURE 1.
Preliminary Relative Amplification Map of Central Clark County, Washington

Greatest Hazard Least Hazard

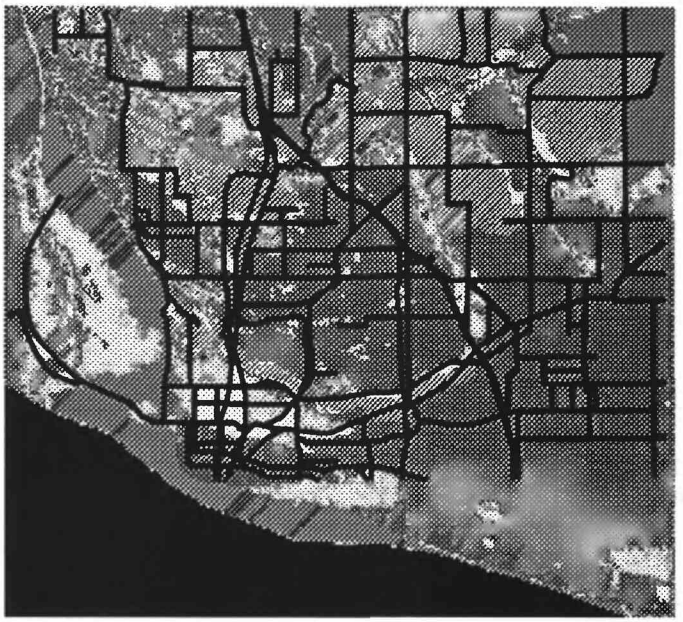

FIGURE 2.
Preliminary Relative Slope Stabilty Map of Central Clark County, Washington

Greatest Hazard Least Hazard

FIGURE 3.

Preliminary Relative Liquefaction Map of Central Clark County, Washington

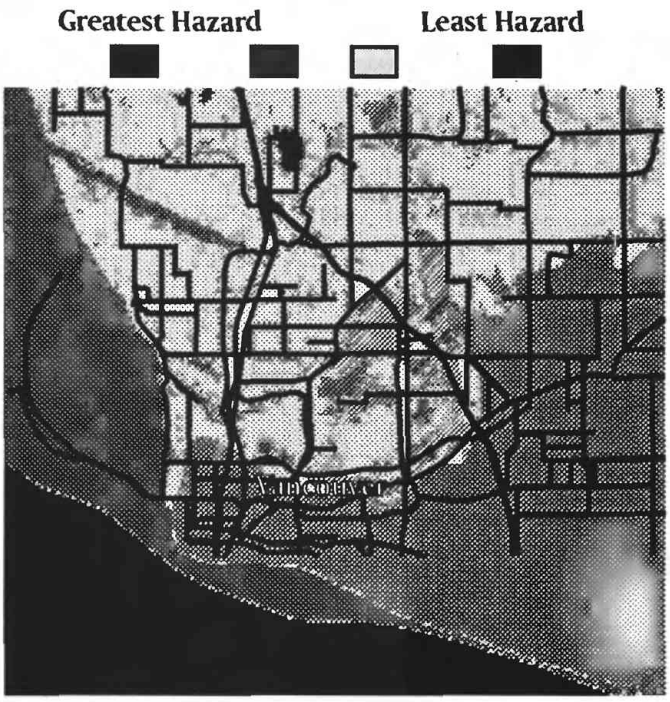

FIGURE 4.

Preliminary Relative Earthquake Hazard Map of Central Clark County, Washington

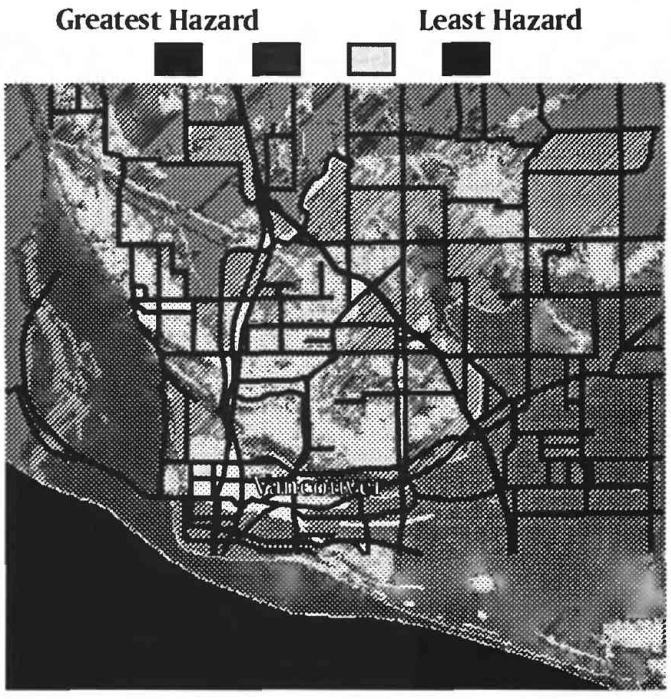

Global Seismicity Mapping

9920–10242

Robert P. Massé
Branch of Earthquake and Geomagnetic Information
U.S. Geological Survey
Denver Federal Center
Box 25046, Mail Stop 967
Denver, Colorado 80225
(303) 273–8480

Investigations

Regional/Global Seismicity Maps. Produce and distribute seismicity maps on shaded map bases.

Results

Seismicity Maps. The aim of the seismicity maps is to provide the most complete picture possible of where earthquakes have occurred historically in relation to geographic, geomorphic and cultural features. This is accomplished by selecting or compiling an earthquake database that is then plotted and printed on a shaded base map.

Since this project began in 1988, seismicity maps have been completed for Alaska, California, Hawaii, Utah, Southern California, Nevada, Oregon/Washington, and the U.S. A global seismicity poster has also been prepared.

The maps resulting from this project are distributed to the research community worldwide, as well as to numerous educational institutions in the U.S. They are also available for public purchase. The results of this project form a significant part of the outreach program of the National Earthquake Information Center.

Geotechnical Information in Emergency Management

9960-12126

C.E. Mortensen
Branch of Earthquake Geology and Geophysics
U.S. Geological Survey
345 Middlefield Road, MS 977
Menlo Park, California 94025
(415) 329-4856
Program Element IV

Investigations

1. Served as USGS Liaison (with Mike Blanpied) to FEMA/OES Disaster Field Office (DFO) during response to Northridge earthquake, supporting the Emergency Support Function for Information and Planning (ESF-5). Provided real-time seismic and geological information relevant to disaster management planning, resource allocation , and decision making.

2. Represented USGS at the Northridge Hazard Mitigation Workshop (with Bill Bakun). Provided recommendations to FEMA and OES officials regarding priorities for Northridge Hazard Mitigation Grant program.

3. Conducted advisory activities for the Regional Interagency Steering Committee (RISC), which is convened bimonthly by FEMA to accomplish and coordinate regional planning for earthquake preparedness and response. Met with the Governor's Office of Emergency Services to discuss the use of seismological and geotechnical data in emergency management, the use of Geographic Information Systems technology for that purpose, and formalizing the establishment of an OES-CDMG Clearinghouse during future earthquake disasters. Participated in CONCERT (Coordinating Organizations for Northern California Earthquake Research and Technology) workshop and other activities.

4. The Governor's Office of Emergency Services has installed an OASIS (Operational Area Satellite Information System) station at USGS Menlo Park Headquarters to facilitate rapid delivery of seismological, geological and geotechnical data and information to emergency managers in the event of a damaging earthquake anywhere in California. System was used to capture Emergency Data and Information System (EDIS) messages during Northridge earthquake response.

5. Contributed to a draft Branch plan for post-earthquake investigations to facilitate coordination and logistics following large earthquakes. Executed the plan in response to the Northridge earthquake.

6. Worked on developing the capability to rapidly summarize and transfer earth science information to emergency managers using the MapInfo GIS, desk-top mapping software.

Results

1. Organized and conducted a conference on Earth Science Information and GIS Technology in Emergency Management, June 14, 1994. Conference was sponsored by the Coordinating Organizations for Northern California Earthquake Research and Technology (CONCERT) and the American Society of Photogrammetry and Remote Sensing (ASPRS).

2. Represented USGS on advisory panel for Association of Bay Area Governments that provides recommendations on application of regional hazard mapping projects.

3. Presented White Paper on Information and Planning functions in the Federal Response to the Northridge earthquake at the FEMA-sponsored Disaster Operations Review for the Northridge Earthquake, conducted during July 27-29, 1994, in Newport Beach, CA.

Reports

Mortensen, C.E., M.L. Blanpied, and E.A. Wegenka, 1994, Scientific information in emergency management, *in* Program for Northridge Abstracts, 89th Annual Meeting of the Seismological Society of America, #29.

Buika, James A., Carl E. Mortensen, and Elizabeth A. Wegenka, 1994, Toward the development of a rapid earthquake-damage intelligence system for emergency response to a catastrophic earthquake, *in* Proceedings of the Fifth U.S. National Conference on Earthquake Engineering, July 10-14, Chicago Illinois, v. II, p. 5-15.

DEVELOPMENT AND EVALUATION OF ALTERNATIVE METHODS TO PROVIDE EARTHQUAKE MAPS AS GIS DATA TO USER COMMUNITIES -- SAN FRANCISCO BAY AREA

1434-94-G-2394
Jeanne B. Perkins
Association of Bay Area Governments (ABAG)
P.O. Box 2050 -- Oakland, CA 94604
(510) 464-7934 -- FAX (510) 464-7970 -- jeannep@abag.ca.gov
Program Element -- IV

PROJECT BACKGROUND AND OBJECTIVES

Since the mid-1970s, ABAG has had extensive involvement in earthquake hazard mapping for the nine-county San Francisco Bay Area. This work has been funded by the U.S. Geological Survey and the National Science Foundation. ABAG, using a geographic information system (GIS), has developed a number of ground shaking hazard maps and maps of other hazards associated with earthquakes.

Following the 1989 Loma Prieta earthquake, ABAG has evaluated these maps. We discovered that there were two very different problems with the maps. ***First***, although the maps were, in general, reasonably accurate, the maps needed to be updated using more recent information to more accurately model the distribution of ground shaking problems which occurred during the Loma Prieta earthquake. During the last two years, many of those maps have been revised as part of a National Science Foundation-funded project. ***Second***, the maps had not been used to the extent they could have been. The primary goal of this project is to address this second problem.

The objectives of this project are to:

- establish priorities for developing ways to increase use of earthquake hazard maps;
- develop a variety of model applications programs for local governments and other community organizations to use computer data files, rather than the printing of large numbers of hard copies of maps covering the entire region;
- evaluate the successes and problems with these applications to provide guidance to others looking at ways to improve implementation of earthquake hazard research and make that implementation effort self-supporting; and
- ensure that the results of this applied research have wide distribution.

AVAILABLE MAPS AND SOFTWARE CAPABILITIES

The earthquake hazard map files currently (or soon to be) available include:

- fault traces;
- fault study zones;
- individual "scenario" ground shaking intensity maps from earthquakes on the San Gregorio fault; the Loma Prieta segment of the San Andreas fault; the peninsula segment of the San Andreas fault; the entire Bay Area segment of the San Andreas fault (similar to 1906); the southern segment of the Hayward fault (south of San Leandro); the northern segment of the Hayward fault

(north of San Leandro); the entire Hayward fault; the entire Healdsburg-Rodgers Creek fault; the Bay Area segment of the Maacama fault; part of the southern Calaveras fault (similar to the Morgan Hill earthquake); the northern segment of the Calaveras fault (north of Calaveras Reservoir); the entire Greenville fault; the entire Concord-Green Valley fault; the West Napa fault;

- susceptibility of various geologic units to ground shaking;
- dam failure inundation areas; and
- tsunami inundation areas.

In addition, several ABAG maps that will be revised in the next few months (if enough interest is expressed) include:

- maximum ground shaking intensity;
- risk of ground shaking damage for most wood-frame dwellings;
- risk of ground shaking damage for concrete and steel buildings; and
- risk of ground shaking damage for poorly designed tilt-up or unreinforced masonry buildings;
- liquefaction susceptibility; and
- liquefaction potential.

In addition, the TIGER files from the U.S. Bureau of the Census can be combined with these files. The TIGER files include:

- streets (including street address ranges which can be used in address matching routines);
- city boundaries (as of the 1990 census);
- county boundaries; and
- 1990 census tract boundaries.

The other major ABAG files are 1985 and 1990 existing land use.

MAJOR TASKS AND STATUS

Major tasks of this project include:

- conducting an "interest" survey (completed);
- setting priorities for project products (completed);
- modifying software and/or files to meet the needs of those users (on-going);
- evaluating the extent to which the resulting products and capabilities meet the needs of local governments (based on a second survey and documentation of actual use);
- documenting this research effort; and
- holding a workshop to demonstrate and highlight potential uses for other local governments in the Bay Area.

Interest Survey

The project "interest" survey was mailed to approximately 566 local government staff members. Of these, 150 were returned. No follow-up phone calls were made to increase the response rate for we

assumed that those not returning the survey were not highly interested in the project. The number of surveys mailed and the response rate for each group is shown below.

TYPE	NUMBER MAILED / RETURNED	PERCENT RESPONDING
County Office of Emergency Services Chiefs	3/19	15.8%
Local Administrative Agencies (for hazmat)	4/24	16.7%
County Congestion Management Agencies	5/9	55.6%
Chief Building Inspectors	22/90	24.4%
City Managers/County Administrators	25/109	22.9%
Planning and Community Development Dirs.	42/108	38.9%
Public Works Directors	32/107	29.9%
Fire Chiefs	17/100	17.0%

At least one survey was returned from all nine counties and 80 of the 100 cities.

Twenty five people indicated that they were so interested in this project that they were willing to participate on the project Review Committee. Only 28 of the 150 people indicated that they had no interest. However, as mentioned earlier, most of those with no interest probably did not respond to the survey. Of the remaining 99 people, 58 had specific interests in software, data files and maps, while 41 were only interested in further information at some future time.

Priorities for Sample Projects

These participants set project priorities (in order of highest to lowest) as:

1) development of appropriate guidelines for use of the files
2) development of "turn-key" software so that files can easily be formatted for other software packages, probably as DXF polygon files registered to latitude-longitude coordinates;
3) documentation and distribution of MapFrame software to local governments in the Bay Area;
4) development of non-GIS computer files (such as pict files to be used on Macs with Hypercard, or pcx files that can be viewed with graphics software such as Harvard Graphics or Power Point on PCs)
5) "hard copy" maps for local areas
6) integration of more accurate street network files (beyond TIGER)

Delivery of information in computer form is quick, but must be accompanied by innovative ways of ensuring that the information is understood and not misused, one priority of this effort. For example, one potential problem with retrieving hazard data by "address" is the potential for obtaining information out of context and the possible belief that the data are "site specific." Care is being taken to prevent such misuse.

Another product of this project will be the "speeding up" of the transfer process to other GIS software formats. Both U.C. Berkeley and the U.S. Geological Survey have successfully imported ABAG's files

into ArcInfo. However, this process is not straightforward. ArcInfo can, in turn, export the raster files as polygons for importing into other software packages.

These BASIS (Bay Area Spatial Information System) files can be viewed using software from MapFrame Corporation. MapFrame's president, Paul Wilson, is a former ABAG employee specializing in custom GIS software. The MapFrame "package" has been specifically designed to work with the raster-based earthquake files from ABAG. The MapFrame viewing software can be used for address matching, address displays, and overlaying of streets, zip codes or city boundaries on the ABAG BASIS files. One of the major disadvantages of this software is that because it was specifically designed for ABAG's needs, the documentation is quite sketchy. One of the products of this effort will be improved documentation of this "in-house" software for those local government users without existing software packages.

A potential product with a lower priority is to improve the street network files. BASIS currently uses the TIGER files from the U.S. Bureau of the Census. The major problems with the TIGER street, city and zip code layers are their positional accuracy (because they are randomly misregistered by up to 300 meters) and the lack of 10% to 30% of the addresses in the region (depending on the area). This work received the lowest priority because local governments with existing GIS software already have street network files in their systems.

Other Tasks

In the future, Review Committee participants will be encouraged to provide input into pilot applications projects priorities:

- Risk Management Prevention Programs (RMPPs) for hazardous materials;
- emergency response exercises and planning;
- design and implementation of priorities for hazardous building mitigation (such as non-ductile concrete, poorly designed tilt-up and unreinforced masonry commercial and industrial structures); and
- housing rehabilitation and recovery planning.

Transportation planning may need to be added to this list. However, at the present time, we are hopeful that we will be working on a cooperative project with CalTrans. The funding from the federal Department of Transportation has been approved, but the cooperative agreement with CalTrans is still pending. ABAG currently expects a start date of Spring 1995.

A sample Internet pilot Internet project will be added to this list, assuming that funding for this project (which has tentatively been approved by USGS with a start date of February 1995) is funded in a timely manner. This Internet project will also be integrated into ABAG's Internet project, abagOnLine, which is being funded, in part, by the National Technical Information Service.

Historic Catalog
1434-93-G-2323 A.I. Qamar, P.I.

A.I. Qamar and R.S. Ludwin
Geophysics Program
University of Washington
Seattle, WA 98195
(206) 543-8020
e-mail: tony or ruth@geophys.washington.edu
Oct. 1, 1993 - Sept. 30, 1994

Investigations

We are compiling an improved catalog of historic felt and damaging earthquakes in Washington and Oregon based on existing earthquake catalogs (published or unpublished), supplemented by contemporaneous newspaper clippings, diary entries, references to articles in scientific journals, and other available information. Our new catalog takes advantage of powerful relational data-base features to store extensive information on each event and to allow the user to view the information in various ways; from a single-line summary to a complete report including all available sources of information for an earthquake.

Progress

During this contract period, we completed entering and tabulating our collection of existing catalogs and newspaper articles. We are now compiling tabulated entries by earthquake, reviewing our compilation of materials for each earthquake, selecting preferred values of time, location etc., and flagging earthquakes for which additional information might be available.

The catalog is being constructed using Microsoft ACCESS, a PC data-base product. The design of the data-base includes 3 main tables; a "Scrapbook" of original source materials, a "Tabulation" of selected information about earthquakes mentioned in the source materials, and a "Cardfile" of earthquakes which gives an interpretation of the various sources of original information (which are sometimes conflicting), and includes the preferred time, location, etc. for each earthquake.

We have developed data-base tools that allow us to view the data in ways which facilitate each step of the development of the three tables. We have used ACCESS "Forms" to allow us to view information from one, two, or all three of our tables. We have a "Scrapbook entry" form which uses the the Scrapbook table only; "Tabulate" and Compile" forms which use both the Scrapbook and Tabulation tables; and a "Prefer" form which uses the Cardfile and Tabulation tables to display the current preferred date/time, location etc. and all available choices for an individual event. The "Prefer" form also draws on the Scrapbook table to display all of the underlying information available for that event.

We are now considering distribution and publication options. The data-base will be available via Internet **ftp** as an ACCESS data-base and also in a more universal data-base format so that it can be imported into other data-bases. We plan to publish a companion report through the Washington State Dept. of Natural Resources which will include a catalog of events and a source list for each event, as well as a full description of the data-base fields, and instructions on the ACCESS implementation.

Annual Project Summary

Title: Geologic Map of Cascade Range
Project No.: 13198
Investigator: David R. Sherrod
Institution: U.S. Geological Survey
5400 MacArthur Blvd.
Vancouver, WA 98661
ph.: 206-696-7995 fax: 206-696-7863
e-mail: dsherrod@pwavan.wr.usgs.gov

Program element: IV, Application and utilizing research results

Investigations undertaken:

This project was funded by NEHRP outside the conventional project-proposal mechanism and was in response to a pair of ~M-6 earthquakes that struck Klamath Falls in September 1993. Scientific investigations consisted of searching for ground rupture and other geologic effects of the earthquakes.

Substantially more time was spent in outreach-related activities. For example, a project member participated as geologic consultant for an American Society of Civil Engineers facilities review field trip, in which we examined the structural integrity and adequacy of measures that might prevent failures at telephone and power companies, hospitals, transportation systems, and 911 headquarters.

The most significant contribution centered on a three-day series of public seminars and emergency services-oriented workshops, in cooperation with colleagues from Cascades Volcano Observatory and the USGS Geophysics group at Univ. of Washington. Project members were invited to perform this service by the Klamath Basin chapter of the American Red Cross following three months of aftershocks and amid increasing rumors of devastation (the Northridge earthquake occurred the week before our workshops).

Financial support provided for 3.3 pay periods but no operating expenses. Time actually spent was 5 or 6 pay periods; operating expenses amounted to nearly $1k The deficit was met at expense of other programmatic funding under project's control.

Results

The earthquakes were too small to produce surface rupture. Building damage and a deadly rockfall produced the lasting evidence of the earthquake.

The outreach was successful. The ASCE facilities review must have alerted supervisors and public officials of the inadequate preparation at all critical facilities. A larger quake would have toppled storage batteries or snapped fuel lines that start and feed emergency power generators at every facility we visited.

During the January seminars we addressed and answered questions for ~600 people . The first public lecture was taped by the local TV station and replayed three times the following week; total TV viewing is uncertain but it probably added at least another 500 people.

Reports published

Wiley, T.J., Sherrod, D.R., Keefer, D.K., Qamar, Anthony, Schuster, R.L., Dewey, J.W., Mabey, M.A., Black, G.L., and Wells, R.E., 1993, Klamath Falls earthquakes, September 20, 1993—including the strongest quakes ever recorded in eastern Oregon: Oregon Geology, v. 55, no. 6, p. 127-134.

Sherrod, D.R., 1994, Historic and prehistoric earthquakes near Klamath Falls, Oregon: Earthquakes and Volcanoes, v. 24, no. 3, p. 106-120.

Project Summary: Grant No. 1434-94-G4255

Post-Earthquake Monitoring and Analysis of Landslides Triggered by the 1989 Loma Prieta Earthquake, Central Santa Cruz Mountains, California

P. O. Shires, D. R. Marcum and W. F. Cole

William Cotton and Associates, Inc.
330 Village Lane
Los Gatos, California 95030
(408) 354-5542

Element III.3

This study involves post-earthquake monitoring, and resulting analysis, of large, pre-existing landslides that moved in response to the 1989 Loma Prieta earthquake. The in-place borehole instrumentation provides an opportunity to acquire data pertaining to post-earthquake activity of large bedrock landslide and re-examine these landslides. This instrumentation, consisting of 15 inclinometer casings and 45 piezometers, was installed at considerable expense soon after the earthquake (October 17, 1989) under the direction of the Federal Emergency Management Agency, U. S. Army Corps of Engineers, and Santa Cruz County. Although the instruments were monitored for about one year after installation, monitoring activities ceased in early 1991. Thus, the piezometers only provided information on ground water levels following several years of drought, and the inclinometers did not demonstrate conclusive evidence of movement with which to establish depths of landsliding. Although there was considerable speculation regarding the potential for additional movement in the event of increased ground water levels, the effects of several periods of rainfall on displacement of these landslides is not known.

No indication of obvious ground deformation has been observed in several field reconnaissances of the landslides. Comparison of new instrumentation readings with the initial readings will enable us to determine whether or not these landslides have experienced any measurable deformation or movement due to post-earthquake rainfall, as well as to define the depth and magnitude of such movement if it has occurred. If the landslides show no signs of additional movement under higher ground water levels, then this information will provide another calibration point with respect to the average shear strength of the basal landslide rupture surfaces. In addition, if the monitoring data confirm that the landslides have not have moved significantly since the earthquake despite periods of elevated ground water conditions, then such information would be useful to stability assessments of other bedrock landslides in this region. The new ground water data will allow us to conduct supplemental analyses that incorporate long-term variations in ground water and better constrained shear strength values. Our current plan is to continue monitoring through the Spring of 1995 in order to bracket the period of ground water levels through one complete winter.

Digital Data Analysis

9920–10112

Stuart A. Sipkin
Branch of Earthquake and Geomagnetic Information
U.S. Geological Survey
Box 25046, Mail Stop 967
Denver Federal Center
Denver, Colorado 80225

Phone: [303] 273-8415
Fax: [303] 273-8450
email: sipkin@gldfs.cr.usgs.gov

Program Element: IV – Using research results

Investigations undertaken

1. Moment Tensor Inversion. Apply methods for inverting body phase waveforms for the best point-source description to research problems.

2. Other Source Parameter Studies. Apply methods for inverting body phase waveforms for distributed kinematic and dynamic source properties.

3. Earth Structure. Use long-period and broadband body phases to study lateral heterogeneity, attenuation, and scattering in the crust and mantle.

4. Network Activity. Participate in international endeavors aimed at increasing the installation, deployment, and operation of modern worldwide digital seismic networks, especially within areas where seismic-station coverage is poor, for the routine reporting of earthquake arrival-time information.

5. Data Services. Provide seismological data and information services to the public and to the seismological research community, particularly data from the Global Digital Seismograph Network (GDSN) on SEED tapes, Network-Day tapes, Network-Event tapes, and Network-Event CD-ROMs.

6. NEIC Monthly Listing. Contribute both fault-plane solutions (using first-motion polarity) and moment tensors (using long-period body-phase waveforms) for all events of magnitude 5.8 or greater when sufficient data exists. Contribute waveform/focal-sphere figures of selected events.

Results

1. Moment Tensor Inversion. A paper listing the moment-tensor solutions for 133 moderate-to-large size earthquakes occurring in 1992 has been published and a paper listing the moment-tensor solutions for 130 moderate-to-large size earthquakes occurring in 1993 is in press. We have implemented a procedure, now in routine use, for the near-real-time estimation of moment-tensor solutions using USNSN, GTSN, and IRIS/GSN data. The moment tensors are decomposed to yield estimates of moment magnitude and earthquake source geometry. On the order of 12 earthquakes per month are being analyzed using this new system. These solutions are sent by e-mail to over 200 investigators worldwide. A paper describing this procedure and analyzing the results has been published. A paper describing a useful new method for displaying and comparing earthquake mechanisms and assessing and quantifying their similarities and differences has been published.

2. Other Source Parameter Studies. Linear and nonlinear methods of waveforms inversion are being implemented to derive the distributions of fault slip and rupture time as a function of position on the earthquake fault. These methods have been applied mostly to teleseismic and strong-motion body-wave data although other seismic-wave types can be easily incorporated into the inversion scheme. An analysis of the local strong ground motions, teleseismic body waves, and long-period Rayleigh waves recorded for the 1985 Chile earthquake has been published. These data allow a complete derivation of the temporal evolution of the coseismic rupture. A similar study using teleseismic body waves has been conducted for intraplate North American earthquakes and is currently in press. Results of an inversion of the short-period, broadband, and long-period P waves recorded for the 1979 Petatlan, Mexico, earthquake are also in press. The results obtained for these three events have been included in a summary of the inversion procedure written in Spanish that is to be published in a special issue of Fisica de la Tierra. In addition, an examination of the results obtained for subduction-zone earthquakes has been presented at the Seismological Society of Japan Annual Meeting, and a study of the teleseismic broadband P waves and the near-source strong motions recorded for the 1993 Hokkaido, Japan, earthquake is currently in progress.

3. Earth Structure. Data sets of long-period and broadband shear-wave data have been assembled for the purpose of studying lateral heterogeneity, attenuation, and deep discontinuities in the earth. A paper describing regional variation of attenuation and shear velocity beneath China has been published. In this paper we show that the crust and upper mantle beneath China are not in thermal equilibrium and hypothesize that this is due to strain heating resulting from the collision of the Indian sub-continent with Eurasia. One companion paper detailing mantle discontinuity structure beneath China has been published, another is in press. One of the more remarkable results of these two studies is that, beneath the Sea of Japan, the Yellow Sea, and easternmost Asia, a layer of negatively buoyant silicate melt lies above the 410-km discontinuity.

4. Network Activity. Participation in the Middle America Seismograph (MIDAS) program continues, including collaboration with the Universidad Nacional Autonoma de Mexico in the installation of the Mexican national network of digital seismograph stations.

5. Data Services. The Albuquerque Seismological Laboratory produces and distributes digital seismic data, from 1988 to present in Standard for the Exchange of Earthquake Data (SEED) format. FORTRAN software to read and extract the digital data from SEED tapes and files has been developed and distributed to the research community worldwide, with support on a variety of platforms. Event CD-ROMs are produced containing the relevant digital waveform data. The time windows are calculated based upon magnitude of the earthquake, epicentral distance to the station, and channel. Ten volumes have been produced, covering 1980 through June 1987. The CD-ROMs are distributed to over 220 universities across the United States and geophysical research institutions worldwide. The first Federation of Broadband Digital Seismograph Network (FDSN) CD-ROM, containing data from thirty-nine earthquakes occurring in January and February 1990, has been produced and distributed. There were special requests for waveform data from over 100 earthquakes in FY 1994. The digital data from these events were either mailed on floppy diskette or transferred via e-mail. Fault motion color plots are produced for all large or otherwise significant earthquakes.

6. NEIC Monthly Listing. Since January 1981, first-motion fault-plane solutions for all events of magnitude 5.8 or greater have been contributed to the Monthly Listings. Since July 1982, moment-tensor solutions and waveform/focal-sphere plots have also been contributed. In the last year solutions for 166 events have been published. Seismicity maps are prepared for the Office of Earthquakes, Volcanoes, and Engineering and for other Offices and federal agencies on request.

Reports published

Ahern, T.K., Skjellerup, K., Astiz, L., Sipkin, S.A., and Woodward, R.L., 1994, IRIS-USGS Activities within the FDSN [abs.]: Abstracts, 27th IASPEI General Assembly, Wellington, New Zealand.

Bergman, E.A., and Sipkin, S.A., 1994, Measurement protocols for routine analysis of digital data [abs.]: Abstracts, 27th IASPEI General Assembly, Wellington, New Zealand.

Hartzell, S., Langer, C., and Mendoza, C., 1994, Rupture histories of eastern North American earthquakes: Bulletin of the Seismological Society of America, in press.

Mendoza, C., 1994, Finite-fault analysis of the 14 March 1979 Petatlan, Mexico, earthquake using teleseismic P waveforms: Geophysical Journal International , in press.

Mendoza, C., 1994, Modelado cinematico de fuentes sismicas en una falla finita: Aplicaciones: Fisica de la Tierra, in press.

Mendoza, C., 1994, Subduction-zone asperities: Observations from finite-fault analysis [abs.]: Abstracts, Japan Earth and Planetary Science Joint Meeting, Sendai, Japan.

Mendoza, C., and Fukuyama, E., 1994, Finite-fault source analysis of the 1993 Hokkaido-Nansei-Oki, Japan, Earthquake [abs.]: EOS (American Geophysical Union, Transactions), v. 75, p. 427.

Mendoza, C., Hartzell, S., and Monfret, T., 1994, Wide-band analysis of the 3 March 1985 central Chile earthquake: Overall source process and rupture history: Bulletin of the Seismological Society of America, v.84, p. 269–283.

Revenaugh, J., and Sipkin, S.A., 1994, Evidence of silicate melt atop the 410-km discontinuity: Nature, v. 369, p. 474–476.

Revenaugh, J., and Sipkin, S.A., 1994, Mantle discontinuity structure beneath China: Journal of Geophysical Research, in press.

Sipkin, S.A., 1993, Display and assessment of earthquake focal mechanisms by vector representation: Bulletin of the Seismological Society of America, v. 83, p. 1871–1880.

Sipkin, S.A., 1994, Fast USGS moment-tensor solutions [abs.]: Abstracts, 27th IASPEI General Assembly, Wellington, New Zealand.

Sipkin, S.A., 1994, Rapid determination of global moment-tensor solutions: Geophysical Research Letters, v. 21, p. 1667–1670.

Sipkin, S.A., and Needham, R.E., 1994, Moment tensor solutions estimated using optimal filter theory: Global seismicity, 1992: Physics of the Earth and Planetary Interiors, v. 82, p. 1–7.

Sipkin, S.A., and Needham, R.E., 1994, Moment tensor solutions estimated using optimal filter theory: Global seismicity, 1993: Physics of the Earth and Planetary Interiors, in press.

Sipkin, S.A., and Revenaugh, J., 1993, Regional variation of attenuation in China from analysis of multiple-ScS phases: Journal of Geophysical Research, v. 99, p. 2687–2699.

Zirbes, M.D., Sipkin, S.A., and Woodward, R.L., 1994, The "Federation" CD-ROM [abs.]: EOS (American Geophysical Union, Transactions), v. 75, p. 431.

COMPUTER GRAPHICS LABORATORY

9950-10225, 9950-13225, 9950-14225, 9950-16225

A. C. Tarr
Branch of Earthquake and Landslide Hazards
U. S. Geological Survey
MS 966, Box 25046, Denver Federal Center
Denver, CO 80225
(303) 273-8570
FAX: (303) 273-8600
E-Mail: atarr@gldrtv.cr.usgs.gov
Program Element IV

Investigations

The objective of this project is to provide computer graphics services (such as access to Geographic Information System (GIS) software) to USGS geological hazards investigators. These services include (1) consultation on digital spatial data base design and data acquisition, (2) training in the use of GIS methods, (3) assistance in the assembly of large spatial data sets, and (4) research into advanced spatial data analysis topics. In addition, the Laboratory manages a large Geological Hazards Data Base and assists in producing outreach products that require advanced graphics technologies. Personnel associated with this project are: S. R. Brockman, J. A. Michael, and A. Tarr.

Specific investigations conducted during Fiscal Year 1994 were (1) Geologic Hazards Data Base, (2) Central U.S., Pacific Northwest, and southern California earthquake hazards data, (3) Quaternary faults, and (4) Laboratory expansion.

Results

Geologic Hazards Data Base -- During FY 1994, the Geologic Hazards Data Base was managed and maintained by the Computer Graphics Laboratory in Golden, Colorado for the benefit of projects supported by the National Earthquake Hazards Reduction and Landslide Hazards Programs in the Central U.S., Pacific Northwest, California, and Colorado. The data in the Data Base consist principally of on-line ARC/INFO coverages and off-line native format data tapes containing USGS Digital Line Graph (DLG), Digital Elevation Model (DEM) files, and SPOT image files. The on-line data consist of working ARC/INFO coverages (approximately 1800 MB) and archived ARC/INFO coverages (approximately 500 MB). The archived coverages have been released by authors for informal distribution to other researchers while the working data are subject to revision and are only available by agreement with the authors. The on-line ARC/INFO data are accessible to local researchers over a LAN and to authorized remote users over Internet; in addition, the archived data sets are available to other research groups via anonymous ftp. For security reasons,

the on-line data backup tapes and all the off-line data tapes are stored in a vault at the Central Region GIS Lab at the Denver Federal Center.

It is planned that in FY 1995 parts of the Geologic Hazards Data Base will become available as part of the National Spatial Data Infrastructure (NSDI), a major initiative proposed by the Federal Geographic Data Committee. The Data Base will be indexed by Wide-Area Information Service (WAIS) software; a WAIS and a Mosaic server will be installed on one of the Laboratory's workstations. Most of the WAIS implementation in the Laboratory in FY 1994 was done by S. Brockman.

Central U.S.-- During FY 1994, digital spatial data sets for eleven new 30- by 60-minute (1:100,000-scale) quadrangles encompassing the Wabash Valley supplemented base data layers for ten topographic quadrangles encompassing the New Madrid seismic zone. The base layers are hydrography, roads and trails, railroads, airports, pipelines, and power transmission lines. Additional thematic data layers for New Madrid include isoseismals of damaging shocks (MM intensity > 6), updated earthquake catalogs, MiniSosie lines, and Mississippi River reflection lines. The source data for the new thematic data layers were provided by M. Hopper, J. Odum, Memphis State University, and St. Louis University. All of the new data sets were added to the Geologic Hazards Data Base.

Numerous maps and illustrations were produced in the Laboratory for use by various workers. Notable among these were a five-sheet two-color seismotectonic map (MF-Map series) of the New Madrid region, full-color seismotectonic map (I-Map series), and a three-sheet map of infrastructure elements at risk prepared by R. Wheeler and S. Rhea. The seismotectonic maps will show new geologic and geophysical information collected in the decade and a half since the previous seismotectonic map of the area. The Professional Paper chapter (Wheeler, Rhea, and Tarr, in press) describes the data sets, notes spatial relations among them, and suggests likely social and economic impacts of a large New Madrid earthquake. All of these maps were produced digitally, including color separations for the printed maps

Pacific Northwest -- During FY 1994, new thematic data supplemented digital data base layers for 32 30- by 60-minute (1:100,000-scale) topographic quadrangles encompassing western Washington and Oregon; these included faults off the Oregon coast, instrumentally-located hypocenters and historical epicenters for the entire Pacific Northwest, and volcanic centers. All these data layers were added to the Geologic Hazards Data Base. Numerous illustrations, poster graphics, and maps were prepared for C. Weaver, T. Yelin (Yelin and others, 1994), R. Bucknam, S. Personius, and T. Pratt using data from the Geologic Hazards Data Base.

Southern California -- The Laboratory provided GIS support to numerous USGS studies mounted in response to the January 17, 1994 Northridge earthquake. Activities included acquiring digital spatial base data for the Los Angeles area to be used for the construction of base maps and digital thematic data sets, such as

intensity contours (J. Dewey, USGS), building damage (California Office of Emergency Services), landslides (E. Harp and R. Jibson, USGS), acceleration contours (C. Wentworth, USGS, and portable seismic array data (E. Cranswick, A. Frankel).

Quaternary Fault Map of North America-- The Computer Graphics Laboratory assisted in providing facilities, consultation, and cartographic services for acquisition of digital fault data for this project under the direction of M. Machette. Most of the compilation and digitization of faults in western States has been completed and presented as maps to an international team of collaborators. The most challenging task thus far was attributing a scanned version of the complex California State fault map. The completed digital fault data sets are expected to be extremely useful to numerous other projects.

Laboratory Expansion -- The number of projects requesting services from the Computer Graphics Laboratory increased substantially during the fiscal year, resulting in contention for the available hardware and software resources in the Laboratory. At the end of FY 1994, Laboratory computer resources consisted of two Sun Microsystems 4/75GX workstations, two Sun 3/60 workstations, 14.3 GB hard disk on-line storage, HP 650C color plotter, two single-seat (Rev. 6.1.1) ARC/INFO license and one six-seat node-locked (Rev. 6.1.1) license, an Exabyte 8mm tape drive for data base backups and data exchange, a Tektronix XP356 X-terminal, and an Altek AC40 digitizing tablet (36" by 48").

Reports Published

Rhea, Susan, Wheeler, Russell L., and Tarr, Arthur C., 1994, Map showing seismicity and sandblows in the vicinity of New Madrid, Missouri: U.S. Geological Survey Miscellaneous Field Investigations Map MF-2264-A, 1 sheet, scale 1:250,000.

Wheeler, Russell L., Rhea, Susan, and Tarr, Arthur C., in press, Elements of infrastructure and seismic hazard in the central United States, in Shedlock, Kaye M. and Johnston, Arch C., eds., Investigations of the New Madrid seismic zone: U.S. Geological Survey Professional Paper 1538-M, 61 ms. p., 3 folded plates, scale 1:2,500,000.

Yelin, Thomas S., Tarr, Arthur C., Michael, John A., and Weaver, Craig S., 1994, Washington and Oregon earthquake history and hazards: U. S. Geological Survey Open-File Report 94-226B, 10 p.

Title: Fifth National Conference on Earthquake Engineering, dated April 11, 1994
Project Number: 1434-94-G-2506
Investigator: Susan K. Tubbesing
Institution: Earthquake Engineering Research Institute
Address: 499 14th Street, Suite 320, Oakland, CA, 94612
Telephone Number: (510) 451-0905 Fax: (510) 451-5411
E-mail: susant@rock.eerc.berkeley.edu

The Conference, 5NCEE, was the fifth in a series of national conferences on earthquake engineering. Previous conferences have been held in Ann Arbor, Michigan, Stanford, California, Charleston, South Carolina, and Palm Springs, California. They are held at four-year intervals, halfway in time between the World Conferences on Earthquake Engineering. All of the conferences have been sponsored by EERI, the Earthquake Engineering Research Institute.

The conference provided a valuable means for research workers and practitioners in the several technical disciplines involved in earthquake hazard reduction to come together and exchange research results and professional ideas and techniques. The Proceedings of the conference provided a valuable repository of information and a useful basis for future advances in this field.

SEISMOTECTONIC MAPS OF THE CENTRAL U.S.

9950-14295

Russell L. Wheeler, Susan Rhea
Branch of Earthquake and Landslide Hazards
U.S. Geological Survey
Box 25046, MS 966, Denver Federal Center
Denver, CO 80225
(303) 273-8589; FAX (303) 273-8600; wheeler@gldvxa.cr.usgs.gov
Program Element IV.I

Investigations undertaken

(1) In FY 1994 we completed production of (1) a three-sheet infrastructure map of the central U.S. with accompanying text, showing main lifelines, critical structures, and urban areas that could be at risk from large earthquakes in the New Madrid seismic zone, (2) a five-map folio of two-color seismotectonic maps of the New Madrid, Missouri, area with accompanying texts, and (3) a full-color map summarizing the main features of the five New Madrid seismotectonic maps. We continued to put the maps and associated digital data bases into the hands of the target audiences by showing the maps at scientific meetings, distributing draft copies, and disseminating parts of the data bases electronically on request. We also did preliminary planning to produce similar seismotectonic maps of the lower Wabash Valley (parts of Illinois, Indiana, and Kentucky) during FY 1995 and FY 1996, and of New England beyond FY 1996.

(2) Wheeler continued, as map making allowed, to prepare and revise mss. that suggest improvements to the geologic foundations of probabilistic hazard mapping in the East. This work supports the USGS national probabilistic-hazard maps that are due by April, 1996. One ms. is in journal review and a second is ready to submit.

Results

(1) No new findings from the central U.S. We spent most of the year revising draft maps in response to review and editing, and producing materials needed for production and publication of the maps.

(2) Earthquakes at three and perhaps five locales in the northwestern part of the Appalachians have been attributed by operators of local networks to compressional reactivation of Iapetan extensional faults. The faults formed during Late Proterozoic to early Paleozoic continental rifting that formed the northeast trending Iapetan passive margin. The faults and earthquakes occur beneath overlying Paleozoic thrust sheets of the Appalachians. If some Iapetan faults are presently

seismogenic, then for the purpose of probabilistic-hazard mapping all are suspect in the long term. Therefore, hazard assessment requires delineating the area in which Iapetan faults exist. The northeast-trending area is delineated by identifying its northwestern and southeastern boundaries. First, published geologic mapping and results of petroleum exploration identify the northwestern boundary; it coincides approximately with the boundary between the seismically quiet Precambrian craton of eastern North America, on the northwest, and the diffuse belt of seismicity that covers the Phanerozoic rim of eastern North America, on the southeast. Second, interpretation of 8 published, Moho-imaging, seismic-reflection profiles identifies the southeastern boundary; it coincides with the Appalachian gravity gradient. Thus, Iapetan faults are inferred to be seismogenic or potentially seismogenic throughout a source zone 100-400 km wide and 3700 km long from Alabama to the Labrador Sea.

Reports published

Powell, Christine A., Bollinger, G.A., Chapman, Martin C., Sibol, Matthew S., Johnston, Arch C., and Wheeler, Russell L., 1994, A seismotectonic model for the 300-kilometer-long eastern Tennessee seismic zone: Science, v. 264, p. 686-688.

Rhea, Susan, and Wheeler, R.L., 1994a, New Madrid, Mo., seismotectonic maps [abs.]: EOS, Transactions of the American Geophysical Union, v. 75, no. 16 (Supplement), p. 236.

Rhea, Susan, and Wheeler, Russell L., 1994b, Map showing large structures inferred from geophysical data in the vicinity of New Madrid, Missouri: U.S. Geological Survey Miscellaneous Field Investigations Map MF-2264-B, 1 sheet, scale 1:250,000.

Rhea, Susan, and Wheeler, Russell L., 1994c, Map showing locations of geophysical survey and modeling lines in the vicinity of New Madrid, Missouri: U.S. Geological Survey Miscellaneous Field Investigations Map MF-2264-C, 1 sheet, scale 1:250,000.

Rhea, Susan, and Wheeler, Russell L., in press, Map showing synopsis of seismotectonic features in the vicinity of New Madrid, Missouri: U.S. Geological Survey Miscellaneous Investigations Map I-2521, scale 1:250,000.

Rhea, Susan, Wheeler, Russell L., and Tarr, Arthur C., 1994, Map showing seismicity and sand blows in the vicinity of New Madrid, Missouri: U.S. Geological Survey Miscellaneous Field Investigations Map MF-2264-A, 1 sheet, scale 1:250,000.

Wheeler, Russell L., in press, Southeast boundary of seismogenic Iapetan faults under the Appalachians [abs.]: Seismological Research Letters, v. 65.

Wheeler, R.L., and Rhea, Susan, 1994a, Central U.S. infrastructure maps [abs.]: EOS, Transactions of the American Geophysical Union, v. 75, no. 16 (Supplement), p. 236.

Wheeler, Russell L., and Rhea, Susan, 1994b, Seismotectonic maps of the New Madrid area -- A model for maps of the lower Wabash Valley [abs.], in Ridgley, Jennie L., Drahovzal, James A., Keith, Brian D., and Kolata, Dennis R., eds., Proceedings of the Illinois Basin energy and minerals workshop, September 12-13, 1994, Evansville, Indiana: U.S. Geological Survey Open-File Report 940298, p. 45-46.

Wheeler, Russell L., and Rhea, Susan, 1994c, Map showing surficial and hydrologic features in the vicinity of New Madrid, Missouri: U.S. Geological Survey Miscellaneous Field Investigations Map MF-2264-E, 1 sheet, scale 1:250,000.

Wheeler, Russell L., Rhea, Susan, and Dart, Richard L., 1994, Map showing structure of the Mississippi Valley graben in the vicinity of New Madrid, Missouri: U.S. Geological Survey Miscellaneous Field Investigations Map MF-2264-D, 1 sheet, scale 1:250,000.

Wheeler, Russell L., Rhea, Susan, and Tarr, Arthur C., in press, Elements of infrastructure and seismic hazard in the central United States, in Shedlock, Kaye M., and Johnston, Arch C., eds., Investigations of the New Madrid seismic zone: U.S. Geological Survey Professional Paper 1538-M, 61 ms. p., 3 folded plates, scale 1:2,500,000.

INDEX 1

INDEX ALPHABETIZED BY PRINCIPAL INVESTIGATOR

Tarr, A. C.	U.S. Geological Survey	1097
Teng, T.	Southern California, University of	195
Thorson, R. M.	Connecticut, University of	763
Thurber, C. H.	Wisconsin-Madison, University of	767
Thurber, C. H.	Wisconsin-Madison, University of	1015
Tinsley, J. C.	U.S. Geological Survey	1022
Toksoz, M. N.	Massachusetts Institute of Technology	201
Toksoz, M. N.	Massachusetts Institute of Technology	771
Tubbesing, S. K.	Earthquake Engineering Research Institute	1100
Tullis, T. E.	Brown University	208
Tumarkin A. G.	California, University of, Santa Barbara	1024
Tuttle, M.	Maryland, University of	782
Tworzydlo, W. W.	The Computational Mechanics Company	216
Uba, O. G.	Spangle Associates	1044
Unruh, J. R.	William Lettis & Associates, Inc.	794
VanArsdale, S.	Memphis, University of	221
VanSchaack, J.	U.S. Geological Survey	797
Vernon, F.	California, University of, San Diego	798
Walsh, T. J.	Washington Geology and Earthe Resources	799
Weaver, C. S	U.S. Geological Survey	800
Weber, G. E.	Weber, Hayes and Associates	805
Weber, G. E.	Weber, Hayes and Associates	808
Wentworth, C. M	U.S. Geological Survey	810
Wesnousky, S. G.	Nevada, University of, Reno	813
Wesnousky, S. G.	Nevada, University of, Reno	815
West, M. W.	Michael West & Associates, Inc.	817
Wheeler, R. L.	U.S. Geological Survey	1101
Williams, C.	U.S. Geological Survey	223
Woodward, R. L.	U.S. Geological Survey	1048
Wyatt, F. K.	California, University of, San Diego	828
Wyatt, F. K.	California, University of, San Diego	832
Yeats, R. S	Oregon State University	838
Yerkes, R. F.	U.S. Geological Survey	1050
Zoback, M. D.	Stanford University	846
Zoback, M. L.	U.S. Geological Survey	852

INDEX 2

INDEX ALPHABETIZED BY INSTITUTION

U.S. Geological Survey	McCrory, P. A.	571
U.S. Geological Survey	McLaughlin, R. J.	586
U.S. Geological Survey	Mortensen, C. E.	94
U.S. Geological Survey	Mortensen, C. E.	1085
U.S. Geological Survey	Nelson, A. R.	595
U.S. Geological Survey	Obermeier, S. F.	606
U.S. Geological Survey	Oppenheimer, D. H.	144
U.S. Geological Survey	Perkins, D. M.	974
U.S. Geological Survey	Person, W. J.	977
U.S. Geological Survey	Ponti, D. J.	623
U.S. Geological Survey	Potter, C. J.	627
U.S. Geological Survey	Pratt, T. L.	631
U.S. Geological Survey	Prentice, C.	634
U.S. Geological Survey	Roeloffs, E.	646
U.S. Geological Survey	Rogers, A. M.	986
U.S. Geological Survey	Rymer, M. J.	681
U.S. Geological Survey	Safak, E.	989
U.S. Geological Survey	Sarna-Wojcicki,A. M.	684
U.S. Geological Survey	Sato, M.	687
U.S. Geological Survey	Schultz, A.	692
U.S. Geological Survey	Shaw, H. R.	710
U.S. Geological Survey	Sherrod, D. R.	1092
U.S. Geological Survey	Silverman, S.	722
U.S. Geological Survey	Simpson, R. W.	990
U.S. Geological Survey	Sipkin, S. A.	1094
U.S. Geological Survey	Spudich, P.	739
U.S. Geological Survey	Spudich, P.	1000
U.S. Geological Survey	Stein, R. S.	741
U.S. Geological Survey	Swanson, D. A.	756
U.S. Geological Survey	Tarr, A. L.	1097
U.S. Geological Survey	Tinsley, J. C.	1022
U.S. Geological Survey	Van Schaack, J.	797
U.S. Geological Survey	Weaver, C. S.	800
U.S. Geological Survey	Wentworth, C. M.	810
U.S. Geological Survey	Wheeler, R. L.	1101
U.S. Geological Survey	Williams, C.	223
U.S. Geological Survey	Woodward, R. L.	1048
U.S. Geological Survey	Yerkes, R. F.	1050
U.S. Geological Survey	Zoback, M. L.	852
Utah Geological Survey	Black, B. D.	257
Utah Geological Survey	Eldredge, S. N	1070
Utah Geological Survey	Harty, K. M.	399
Utah Geological Survey	Jarva, J. L.	1078
Utah, University of	Arabasz, W. J.	4
Utah, University of	Forster, C. B.	71
Utah, University of	Hylland, R. D.	948

☆ U.S GOVERNMENT PRINTING OFFICE: 1995 – 387 - 088 / 44062